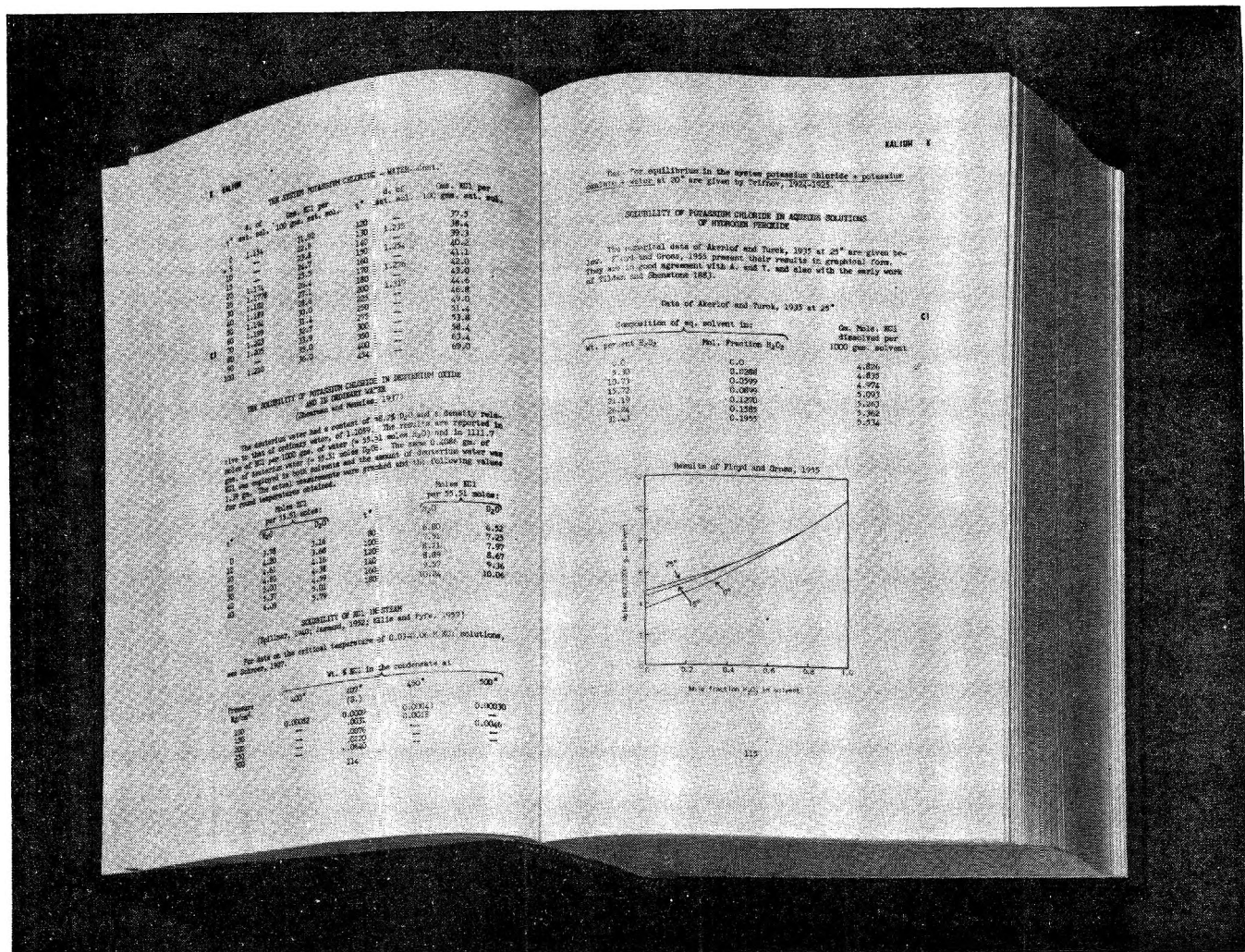


THE JOURNAL OF PHYSICAL CHEMISTRY

Volume 74, Number 4 February 19, 1970

Temperature Dependence of $\Delta\bar{C}_p^\circ$ for the Self-Ionization of Water and for the Acid Dissociation of Acetic Acid and Benzoic Acid in Water	Constance S. Leung and Ernest Grunwald	687
Temperature Dependence of $\Delta\bar{C}_p^\circ$ for the Self-Ionization of Methanol and for the Acid Dissociation of Benzoic Acid in Methanol	Constance S. Leung and Ernest Grunwald	696
Dissociation Constant of Protonated 2,2-Bis(hydroxymethyl)-2,2',2''-nitrilotriethanol (Bis-tris) and Related Thermodynamic Functions from 0 to 50°	Maya Paabo and Roger G. Bates	702
Deuterium Isotope Effects and the Dissociation of Deuteriophosphoric Acid from 5 to 50°	Maya Paabo and Roger G. Bates	706
The Intrinsic Viscosity of Polyelectrolytes	Ichiro Noda, Takeaki Tsuge, and Mitsuru Nagasawa	710
Thermochemistry of Simple Alkylsilanes	P. Potzinger and F. W. Lampe	719
Thermal Conductivity of Binary Mixtures of Alkali Nitrates	John McDonald and H. Ted Davis	725
The Electrical Conductance of Molten Lead Chloride and Its Mixtures with Potassium Chloride	A. J. Easteal and I. M. Hodge	730
Mass Transport in Ionic Melts at Low Temperatures. Chronopotentiometric Diffusion Coefficients of Silver(I), Cadmium(II), and Thallium(I) in Calcium Nitrate Tetrahydrate	C. T. Moynihan and C. A. Angell	736
Proton Magnetic Resonance Study of Aluminum Chloride and Aluminum Perchlorate in Acetonitrile	James F. O'Brien and Mohammed Alei, Jr.	743
The Importance of the Effect of the Solvent Dielectric Constant on Ion-Pair Formation in Water at High Temperatures and Pressures	W. R. Gilkerson	746
Molecular Complexes of Iodine with Pyrone-(4) and 1-Thiopyrone-(4)	N. Kulevsky and G. K. Liu	751
A Bromine-79 Nuclear Magnetic Resonance Study of the Structure of Aqueous Solutions of Mono-, Di-, and Trialkylammonium Bromides	Björn Lindman, Håkan Wenneström, and Sture Forsén	754
Variation of Osmotic Coefficients of Aqueous Solutions of Tetraalkylammonium Halides with Temperature. Thermal and Solute Effects on Solvent Hydrogen Bonding	S. Lindenbaum, L. Leifer, G. E. Boyd, and J. W. Chase	761
Diffraction Pattern and Structure of Aqueous Ammonium Halide Solutions	A. H. Narten	765
The Crystal Structure of 1-Phenyl-3-(2-thiazolin-2-yl)-2-thiourea	J. L. Flippen and I. L. Karle	769
Charge Transfer to Molecules on the Surface of Irradiated Porous Glass	P. K. Wong and A. O. Allen	774
Effect of Hydrogen Chemisorption on the Electrical Conductivity of Zinc Oxide Powder	D. Narayana, V. S. Subrahmanyam, Jagdish Lal, M. Mahmood Ali, and V. Kesavulu	779
Infrared Spectroscopic Study of Carbon Monoxide Adsorption on Hydrogen and Oxygen Treated Silver Surfaces	George W. Keulks and A. Ravi	783
Magnetic Resonance Studies of Aromatic Hydrocarbons Adsorbed on Silica-Alumina. III. Chemical Exchange Effects	G. M. Muha	787
Interactions between Sulfur Hydroxyl Groups and Adsorbed Molecules. I. The Thermodynamics of Benzene Adsorption	J. A. Cusumano and M. J. D. Low	792
Rotational Isomerism in Dichloroacetyl Halides	A. J. Woodward and Neville Jonathan	798
An Electron Spin Resonance Study of Several Purine and Pyrimidine Radical Anions	Michael D. Sevilla	805
Substituent Effects on Aromatic Proton Chemical Shifts. VII. Further Examples Drawn from Disubstituted Benzenes	William B. Smith, Arthur M. Ihrig, and James L. Roark	812
A Nuclear Magnetic Resonance Study of the Effect of Hydrogen Bonding and Protonation on Acetone	W. H. de Jeu	822



NOW AVAILABLE FROM THE AMERICAN CHEMICAL SOCIETY

A valuable, new edition of an essential chemical reference—

Volume II of the Fourth Edition of Seidell's

SOLUBILITIES OF INORGANIC AND METAL ORGANIC COMPOUNDS

Illustrated above are two of the 57 pages of data on solubilities of only *one* inorganic compound, potassium chloride, in various solvents and with various compounds. Volume II has a total of 1,914 pages of critically evaluated data, with tables, values at various temperatures, and melting point references . . . all systematically arranged for quick reference. And data are given for 1,281 other compounds besides potassium chloride and for 26 elements as well, covering the elements with symbols from K through Z.

Volume I appeared in 1959. With the appearance of Volume II in 1966 the data for inorganic and metal organic compounds in the Fourth Edition is now complete . . . a painstaking revision by Dr. William F. Linke, American Cyanamid

Company, continuing the compendium started by the late Dr. Atherton Seidell.

The book is a time-saving work aid, clearly indexed, and carefully cross-referenced with Volume I in terms of subject matter and literature cited in both volumes.

Seidell-Linke, "Solubilities of Inorganic and Metal Organic Compounds," Fourth Edition, Vol. II. iii 1,941 pages. Cloth bound. (1966) . . . \$32.50

Order from:

Special Issues Sales

AMERICAN CHEMICAL SOCIETY

1155 Sixteenth Street, N.W.

Washington, D. C. 20036

On the Oxyiodine Radicals in Aqueous Solution	O. Amichai and A. Treinin	830
The Flash Photolysis of Mercaptans in Aqueous Solution	Günter Caspari and Albrecht Granzow	836
Ionization of Liquids by Radiation Studied by the Method of Pulse Radiolysis. III. Solutions of Galvinoxyl Radical	C. Capellos and A. O. Allen	840
Photoreduction of 1-Nitronaphthalene by Protonation in the Excited State	W. Trotter and A. C. Testa	845
The Radiolysis of Gaseous Trifluoriodomethane in the Presence of Nitric Oxide	I. McAlpine and H. Sutcliffe	848
Mechanism of Reaction of Hydroxyl Radicals with Benzene in the γ Radiolysis of the Aerated Aqueous Benzene System	I. Balakrishnan and M. P. Reddy	850
Dye-Sensitized Photopolymerization in the Presence of Reversible Oxygen Carriers	Nan-Loh Yang and Gerald Oster	856
On the Mechanism of Decomposition of Dithiocarbamates	Serge J. Joris, Keijo I. Aspila, and Chuni L. Chakrabarti	860
Comparison of the Reactions of Atomic and Molecular Halogens with Silver	R. J. McIntyre and F. K. McTaggart	866
Mass Spectrometric Investigation of the Fragmentation Pattern and the Pyrolysis of Borane Carbonyl	O. Herstad, G. A. Pressley, Jr., and F. E. Stafford	874
The Hydrogen-Deuterium Exchange of Benzene at a Fuel Cell Electrode	H. J. Barger, Jr., and A. J. Coleman	880
Tautomeric and Protolytic Properties of <i>o</i> -Aminobenzoic Acids in Their Lowest Singlet and Triplet States	A. Tramer	887
A Calculation of the Energy Barriers Involved in the Isomerization Processes of Ethylene in Its Excited and Ionized States	A. J. Lorquet	895
Determination of the Equilibrium Constants of Associating Protein Systems. V. Simplified Sedimentation Equilibrium Boundary Analysis for Mixed Associations	P. W. Chun and S. J. Kim	899
Estimation of the Excess Thermodynamic Functions of Nonelectrolyte Solutions from the First-Order Perturbation of a Hard-Sphere System	T. Boublik and G. C. Benson	904
Coal-Like Substances from Low-Temperature Pyrolysis at Very Long Reaction Times	R. A. Friedel, J. A. Queiser, and H. L. Retcofsky	908
Carbon-13 Nuclear Magnetic Resonance Spectroscopy. Solvent Effects on Chemical Shifts	Robert L. Lichter and John D. Roberts	912
The Decay of Radicals in Ammonia-Oxygen-Nitrogen Flames	Melvin P. Nadler, Victor K. Wang, and Walter E. Kaskan	917
Isotopic Exchange Reactions in Nitrogen Oxides	H. D. Sharma, R. E. Jarvis, and K. Y. Wong	923
Conductance of Lanthanum Hexacyanoferrate(III) Tetrahydrate in Dioxane-Formamide and Acetone-Formamide Mixtures at 25°	Gyan P. Johari	934

NOTES

Alkyl Radical Disproportionation	R. L. Thommarson	938
The Photolysis of Aqueous Solutions of Cystine in the Presence of Benzyl Chloride	C. J. Dixon and D. W. Grant	941
The Osmotic Pressure of Polyelectrolyte in Neutral Salt Solutions	Akira Takahashi, Narundo Kato, and Mitsuru Nagasawa	944
Activity Coefficients of $[\text{Co}(\text{NH}_3)_4(\text{NO}_2)_2][\text{Co}(\text{NH}_3)_2(\text{NO}_2)_4]$ in Divalent Metal Perchlorate and Other Salt Media	Zofia Libuś	947
Kinetics of the Gas Phase Pyrolysis of Chlorine Pentafluoride	A. E. Axworthy and J. M. Sullivan	949
Calculation of Photodissociation Quantum Yields for Azoethane	P. G. Bowers	952
The Oxidation of Hypophosphorous Acid by Chromium(VI)	J. N. Cooper	955
Medium Effects on Hydrogen-1 Chemical Shift of Benzene in Micellar and Nonmicellar Aqueous Solutions of Organic Salts	John E. Gordon, J. Colin Robertson, and Robert L. Thorne	957
A Convenient Method for Obtaining Free Energies of Activation by the Coalescence Temperature of an Unequal Doublet	H. Shanani-Atidi and K. H. Bar-Eli	961
Conductance Measurements of Thallium Perchlorate and Fluoroborate in Acetonitrile	Howard L. Yeager and Byron Kratochvil	963

COMMUNICATIONS TO THE EDITOR

Comments on "Onsager's Reciprocal Relation. An Examination of Its Application to a Simple Process"	J. A. M. Smit and A. J. Staverman	966
Reply to Communication of Smit and Staverman	R. P. Wendt and E. H. Bresler	967

AUTHOR INDEX

- Alei, M., Jr., 743
 Ali, M. M., 779
 Allen, A. O., 774, 840
 Amichai, O., 830
 Angell, C. A., 736
 Aspila, K. I., 860
 Axworthy, A. E., 949

 Balakrishnan, I., 850
 Bar-Eli, K. H., 961
 Barger, H. J., Jr., 880
 Bates, R. G., 702, 706
 Benson, G. C., 904
 Boublik, T., 904
 Bowers, P. G., 952
 Boyd, G. E., 761
 Bresler, E. H., 967

 Capellos, C., 840
 Caspari, G., 836
 Chakrabarti, C. L., 860
 Chase, J. W., 761
 Chun, P. W., 899
 Coleman, A. J., 880
 Cooper, J. N., 955
 Cusumano, J. A., 792

 Davis, H. T., 725
 de Jeu, W. H., 822
 Dixon, C. J., 941

 Easteal, A. J., 730

 Flippen, J. L., 769
 Forsén, S., 754
 Friedel, R. A., 908

 Gilkerson, W. R., 746
 Gordon, J. E., 957
 Grant, D. W., 941
 Granzow, A., 836
 Grunwald, E., 687, 696

 Herstad, O., 874
 Hodge, I. M., 730

 Ihrig, A. M., 812

 Jarvis, R. E., 923
 Johari, G. P., 934
 Jonathan, N., 798
 Joris, S. J., 860
 Karle, I. L., 769

 Kaskan, W. E., 917
 Kato, N., 944
 Kesavulu, V., 779
 Keulks, G. W., 783
 Kim, S. J., 899
 Kratochvil, B., 963
 Kulevsky, H., 751

 Lal, J., 779
 Lampe, F. W., 719
 Leifer, L., 761
 Leung, C. S., 687, 696
 Libus, Z., 947
 Lichter, R. L., 912
 Lindenbaum, S., 761
 Lindman, B., 754
 Liu, G. K., 751
 Lorquet, A. J., 895
 Low, M. J. D., 792

 McAlpine, I., 848
 McDonald J., 725
 McIntyre, R. J., 866
 McTaggart, F. K., 866
 Moynihan, C. T., 736
 Muha, G. M., 787

 Nadler, M. P., 917
 Nagasawa, M., 710, 944
 Narayana, D., 779
 Narten, A. H., 765
 Noda, I., 710

 O'Brien, J. F., 743
 Oster, G., 856

 Paabo, M., 702, 706
 Potzinger, P., 719
 Pressley, G. A., Jr., 874

 Queiser, J. A., 908

 Ravi, A., 783
 Reddy, M. P., 850
 Retcofsky, H. L., 908
 Roark, J. L., 812
 Roberts, J. D., 912
 Robertson, J. C., 957

 Sevilla, M. D., 805
 Shanani-Atidi, H., 961
 Sharma, H. D., 923
 Smit, J. A. M., 966

 Smith, W. B., 812
 Stafford, F. E., 874
 Staverman, A. J., 966
 Subrahmanyam, V. S., 779
 Sullivan, J. M., 949
 Sutcliffe, H., 848

 Takahashi, A., 944
 Testa, A. C., 845
 Thommarson, R. L., 938
 Thorne, R. L., 957
 Tramer, A., 887
 Treinin, A., 830
 Trotter, W., 845
 Tsuge, T., 710

 Wang, V. K., 917
 Wendt, R. P., 967
 Wennerström, H., 754
 Wong, K. Y., 923
 Wong, P. K., 774
 Woodward, A. J., 798

 Yang, N.-L., 856
 Yeager, H. L., 963

Temperature Dependence of $\Delta\bar{C}_p^\circ$ for the Self-Ionization of Water and for the Acid Dissociation of Acetic Acid and Benzoic Acid in Water¹

by Constance S. Leung and Ernest Grunwald

Chemistry Department, Brandeis University, Waltham, Massachusetts 02154 (Received June 26, 1969)

A calorimeter is described that can measure heats of reaction in dilute solution with an accuracy approaching 0.1% between -95 and 75° . $\Delta\bar{H}^\circ$ was obtained for the reaction of hydrochloric acid, acetic acid, and benzoic acid with sodium hydroxide in water at 0, 5, 15, 25, 35, 45, and 55° . $\Delta\bar{C}_p^\circ$ was derived for these reactions and also for the acid dissociation of these acids. For the self-ionization of water, $\Delta\bar{C}_p^\circ$ goes through a pronounced maximum near 35° . For acid dissociation of acetic acid and benzoic acid, $\Delta\bar{C}_p^\circ$ goes through a minimum. The discussion considers how maxima or minima in the formal heat capacity can arise from real or seeming endothermic processes of a solvated solute. According to that theory the data suggest that the hydrated hydroxide ion undergoes a process with $\Delta H^* = 8.8$ kcal and $\Delta S^* = 28.1$ gibbs.

Some years ago, Feates and Ives² measured the acid dissociation constant, K_A° , for cyanoacetic acid in water with such high accuracy that the temperature dependence of $\Delta\bar{C}_p^\circ$ could be established. They found that $\Delta\bar{C}_p^\circ$ goes through a maximum near 25° . More recently, Marsden and Ives³ reexamined those data and confirmed that the maximum is real, with a statistical probability of greater than one-half. They also measured K_A° for diisopropylcyanoacetic acid and calculated $\Delta\bar{C}_p^\circ$.³ In that case there was no maximum; instead, $\Delta\bar{C}_p^\circ$ appeared to decrease gently with increasing temperature.

Independent evidence that \bar{C}_p as a function of temperature can go through a maximum comes from heat capacity measurements for aqueous electrolyte solutions and from heats of solution of solid salts at various temperatures.^{4,5} Maxima of \bar{C}_p were found for NaOH, NaCl, HCl, BaCl₂, and the sodium salts of several carboxylic acids.^{4,5}

A maximum in the formal partial molal heat capacity of a solute can be interpreted as follows. The solute is an equilibrium mixture of two molecular species that differ in enthalpy. \bar{C}_p goes through a maximum near that temperature at which the two species are

present in equal amounts.^{6,7} For electrolytes at moderate concentrations in water, the two species in equilibrium might be free ions and ion pairs.^{6,7} However, for electrolytes at infinite dilution, they must be different species of the solvated free ions. If we theorize further and consider the free ions to be solvation complexes and if the formal ion is known to be thermally stable, then a maximum in \bar{C}_p must indicate an endothermic change in the solvent shell. On that basis, \bar{C}_p° might prove to be a sensitive probe for studying the nature of solvent shells.

When making plans to study $\Delta\bar{C}_p^\circ$ as a function of temperature, we thought it might be easiest to measure heats of reaction in dilute solution. Extrapolation of $\Delta\bar{H}$ to infinite dilution should not be too

(1) We gratefully acknowledge support of this work in part by the National Science Foundation under Grant GP-7381X.

(2) F. S. Feates and D. J. G. Ives, *J. Chem. Soc.*, 2798 (1956).

(3) D. J. G. Ives and P. D. Marsden, *ibid.*, 649 (1965).

(4) T. Ackermann, *Z. Elektrochem.*, 62, 411 (1958); T. Ackermann and F. Schreiner, *ibid.*, 62, 143 (1958).

(5) C. M. Criss and J. W. Cobble, *J. Amer. Chem. Soc.*, 83, 3223 (1961).

(6) M. Eigen and E. Wicke, *J. Phys. Chem.*, 58, 702 (1954).

(7) E. Wicke and M. Eigen, *Z. Elektrochem.*, 57, 319 (1953).

difficult, and a single differentiation would yield $\Delta\bar{C}_p^\circ$. In this paper we describe a calorimeter that is capable of giving accurate results over a wide temperature range. We also report measurements of $\Delta\bar{H}^\circ$ and derived values of $\Delta\bar{C}_p^\circ$, for the reaction of NaOH with HCl, acetic acid, and benzoic acid in water between 0 and 55°. Our results provide further evidence that heat capacity maxima at infinite dilution can be real.

Experimental Section

Calorimeter. We hoped to design a calorimeter that would measure heats of reaction in an inert atmosphere over a wide temperature range, from -95 to 75°. The calorimeter was therefore set up inside a dewar flask, the temperature of which was controlled by a flow of nitrogen at constant temperature.

A schematic diagram of the calorimeter-dewar assembly is shown in Figure 1. The calorimeter is somewhat unusual because it is neither isothermal nor adiabatic.^{8,9} We thought that an isothermal titration calorimeter^{10,11} might be difficult to manipulate much below room temperature, that an adiabatic calorimeter¹² might take an inconveniently long time to reach the temperature, and that the heat of stirring might become a problem. Our calorimeter actually has a half-time on the order of 20 min for coming to temperature equilibrium with its constant-temperature environment. This time is long compared to other time intervals that are relevant to the measurement: mixing of reactants, production of reaction heat, and attainment of a new even temperature, about 3 sec; response half-time of the thermometer probe, about 5 sec; heating time in the measurement of heat capacity, about 60 sec; half-time for heat exchange between heater and solution, about 9 sec.

Returning to Figure 1, the calorimeter sits on a small Teflon stand that leaves most of it exposed to the nitrogen atmosphere. It consists of two coaxial beakers (outer beaker, 6.4-cm o.d. \times 7.4-cm height, wall thickness 2.4 mm; inner beaker 5.1-cm i.d., wall thickness 0.8 mm), fused at the top and separated by an annular space of about 3 mm. The outer beaker has two glass side arms that terminate in 1-mm capillary tubing of 1-cm length. The top is covered with a Teflon lid that has holes to accommodate a stirrer shaft, heater, thermometer probe, and liquor mixing bottle.

The calorimeter is designed for experiments involving about 50 ml of liquid. To bring the liquid to the desired temperature, a gentle stream of nitrogen is pumped through the annular space *via* the capillary side arms. When pumping is stopped, the capillaries effectively seal off the gas remaining in the annular space.

The temperature outside the calorimeter is sensed and regulated by means of a copper-constantan ther-

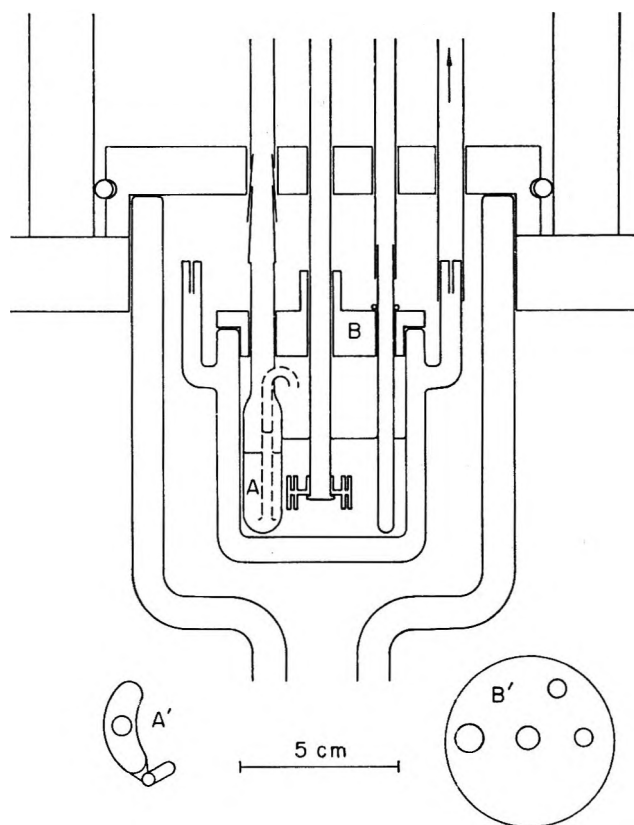


Figure 1. Schematic diagram of calorimeter-dewar assembly. Liquor bottle: A, cross section; A', top view. Lid: B, cross section; B', top view.

mal junction placed just below the calorimeter. The reference junction sits in an ice bath. The thermal emf is compared with the output of a potentiometer. Any difference in the two voltages is sensed and brought to zero by a servomechanism that controls the voltage to a small heater.

A steady flow of nitrogen is maintained in the dewar by boiling liquid nitrogen with a small heater at a constant heating rate of about 100 W. The cold gas is preheated, if necessary, before it enters the dewar at the bottom, where it flows first over a 5.5-ohm heater whose voltage is controlled by the servomechanism, then through a space packed with steel wool to make the temperature quite homogeneous, and finally into the widened space around the calorimeter shown in Figure 1.

(8) J. M. Sturtevant in "Physical Methods of Organic Chemistry," A. Weissberger, Ed., Interscience Publishers, New York, N. Y., 1949, Chapter 14.

(9) C. M. Herzfeld, Ed., "Temperature, Its Measurement and Control," Reinhold Publishing Corp., New York, N. Y., 1962.

(10) J. J. Christensen, R. M. Izatt, and L. D. Hansen, *Rev. Sci. Instrum.*, **36**, 779 (1965).

(11) J. J. Christensen, H. D. Johnston, and R. M. Izatt, *ibid.*, **39**, 1356 (1968).

(12) E. M. Arnett, W. G. Bentrude, J. J. Burke, and P. McC. Dugleby, *J. Amer. Chem. Soc.*, **87**, 1541 (1965); E. M. Arnett and J. W. Larsen, *ibid.*, **90**, 791, 792 (1968).

The dewar is covered at the top with a Teflon lid with appropriate holes for stirrer shaft, wire, and tubings. The lid is cut into two pieces to permit assembly. A polyethylene foam box is built to insulate the top of the dewar and the lid assembly from drafts and temperature fluctuations in the laboratory.

Thermometer Probe. Two kinds of temperature must be measured: the absolute temperature, with an accuracy of 0.1° or better, and the temperature rise, with an accuracy approaching 0.0001° . On the basis of previous experience we thought that both requirements could be met by the copper-constantan thermocouple. We therefore fabricated¹³⁻¹⁵ a five-junction thermopile from a wire (Leeds and Northrup copper-constantan duplex wire, Type T, Gauge No. 38) that was known to give thermal emf's in close agreement with standard reference tables¹⁶ over the entire temperature range.¹⁷

The reference junctions were kept in a thermally insulated ice bath that opened into the same polyethylene foam box as the dewar-calorimeter. To construct the temperature-sensing junctions, the glass wrap and enamel coating were stripped off the final 2-3 mm of each wire. The wires were then twisted in pairs and each pair was soldered to make a proper junction. The thermopile was assembled in a thin-walled (0.25 mm), 5-mm o.d., precision glass tubing, 9.5 cm long and fused into a test tube bottom at one end. A solid glass rod (2-mm o.d. \times 1-cm length) was held at the center of this glass tubing and surrounded by glass wool, and the thermocouple tips were jostled into the space between the glass rod and the inner wall of the glass tubing with the help of a sharpened birchwood applicator. The tips were then pressed against the inner wall of the glass tubing with plugs of glass wool. Finally, the point of exit of the thermocouple wires from the glass tubing was sealed with Teflon tape and wrapped with aluminum foil.

The wires connecting the reference and temperature-sensing junctions were tied together with Teflon ribbon, enclosed in plastic tubing, and wrapped with aluminum tape. The copper leads to the potentiometer were treated similarly.

The thermal emf was compared with a standard emf, obtained from a Leeds and Northrup Type K-5 potentiometer, and the difference, after linear amplification, was recorded on a Varian G-10 recorder. The gain was adjusted so that $1 \mu\text{V}$ corresponded to 1 cm. The noise level of the recorder was then about 0.02 cm. For a five-junction copper-constantan thermopile, dE/dT varies from $220 \mu\text{V}/\text{deg}$ at 70° to $140 \mu\text{V}/\text{deg}$ at -100° . Absolute temperature accuracy is about 0.05° .

Small temperature changes, $T_2 - T_1$, were measured with our instrumentation to better than 0.0002° . To calculate the temperature from the thermal emf, we

applied the power series (1a) and evaluated the required derivatives from the empirical eq 1b. Of course, some of the figures in (1b) are insignificant guard figures, but the equation reproduces the data in the standard reference table¹⁶ between -100 and $+75^\circ$ with remarkable accuracy, even unto the last digit. To calculate T_1 , we obtain from the standard reference table the emf E_0 at the nearest temperature T_0 and apply eq 1, with the derivatives evaluated at T_0 . To calculate $T_2 - T_1$, we apply eq 1 again, with the derivatives evaluated at T_1 .

$$\delta T = \left(\frac{dT}{dE}\right) \delta E + \left(\frac{d^2T}{dE^2}\right) \frac{(\delta E)^2}{2} + \left(\frac{d^3T}{dE^3}\right) \frac{(\delta E)^3}{6} \quad (1a)$$

$$dT/dE = 9.0476 + 4619.9/T \quad (\text{for a single copper-constantan thermocouple}) \quad (1b)$$

In the measurements of ΔH , one compares the temperature rise produced by an unknown amount of heat with a subsequent temperature rise produced by a known amount of heat. Since the calculation of ΔH involves the ratio of two δT 's, any systematic errors inherent in (1b) will tend to cancel out. Moreover, by basing the calculation on a nonlinear function, (1a), with temperature-dependent derivatives, we eliminate errors that might arise when the two δT 's or initial temperatures are not precisely equal.

Heater and Stirrer. Because of limited space, the electrical heater had to be more compact than usual in macrocalorimetry. We modified the usual bifilar winding of the resistance wire so that it would fit into a thin-walled 5-mm o.d. glass tubing of the same type used to house the thermopile. The heater resistance was made from two 6-ft pieces of No. 40 Formvar-insulated manganin wire (30.36 ohms/ft) which, when connected in parallel, give about 90 ohms. The two pieces were wound side by side on a strand of glass wool into three concentric noninductive coils (about 6 mm long), glass wool was packed tightly between the layers of wire, and the ends were soldered to two 1.5-ft copper leads so as to combine the resistances in parallel.

To make a housing for the heater, one end of a 9.5 cm length of thin-walled, 5-mm o.d. glass tubing was fused into a test tube bottom. The heater assembly was then shoved gently into the tubing from the top with the aid of a birchwood applicator, with

(13) J. A. Hall, "Fundamentals of Thermometry," Reinhold Publishing Corp., New York, N. Y., 1953.

(14) J. A. Hall, "Practical Thermometry," Reinhold Publishing Corp., New York, N. Y., 1953.

(15) E. Calvet, H. Prat, and H. A. Skinner, "Recent Progress in Microcalorimetry," The Macmillan Co., New York, N. Y., 1963.

(16) H. Schenker, J. I. Lauritzen, R. J. Corruccini, and S. T. Lonberger, "Reference Tables for Thermocouples," National Bureau Standards Circular 561, U. S. Government Printing Office, Washington, D. C., 1955.

(17) We thank Dr. S. Meiboom of Bell Telephone Laboratories for the calibrated wire.

the solder joints well separated and inserted first, until the solder joints touched the test tube bottom. Finally, glass wool was stuffed tightly into the space extending 5 mm above the coil.

To mount the heater in the calorimeter, the glass tubing is inserted through a hole in the Teflon lid and held in place with a rubber ring. The heater bottom sits about 2 mm above the bottom of the liquid, and the heating coil and superposed glass wool are well immersed in the liquid. The glass wool produces somewhat better heat exchange than the more conventional paraffin oil; it is less messy and will not freeze at low temperature.

The temperature rise of the calorimeter in control experiments depended only on the amount of electrical energy supplied to the heater and was independent of the wattage. The heater resistance was measured at each temperature after completion of the experiment. A small correction was made for the resistance of the copper leads.

The stirrer is driven by a synchronous motor at 150 rpm and provides smooth agitation, apparently without spray, and with barely a vortex. The Teflon impellor—a light, wheellike object of 2-cm o.d. and 1-cm height—is made with two concentric bands of blades, one facing outside and the other inside. The outside-facing blades drive liquid toward the bottom of the calorimeter while the inside-facing ones drive it upward through the openings in the impellor wheel, which is located about 1 cm above the bottom of the liquid.

Electrical Measurements. Other components and operating procedures were fairly standard and need not be described in detail. The electrical engineering was of such quality that the electrical measurements did not add significantly to experimental error from other sources. Stable dc voltages for the operation of the K-5 potentiometer and other electrical measuring instruments were supplied by three solid-state regulated power supplies, which in turn received their power from a stabilized 115-V ac supply. The high stability of these dc sources was a marked improvement over that of storage batteries and contributed to the accuracy of the measurements.

Sample Introduction Device. Before mixing, the reactant in excess (usually 5.0 ml of 0.22 *N* NaOH) is separated from the other (usually 50.00 ml of 0.02 *N* acid) by placing it in a 6-ml thin-walled glass liquor bottle.¹⁸ The bottle is oval in cross section, to fit into the narrow space, and has a gooseneck leading from its lowest point to a point near the center of, and a short distance above the liquid level in, the calorimeter (Figure 1). After a steady state of temperature has been reached, the solution in the liquor bottle is forced under gentle pressure through the gooseneck into the calorimeter. To make that delivery virtually quantitative, the bottle is made so that the

glass at any point slants down toward the point of attachment of the gooseneck.

The preceding method is convenient but must be applied with care, because we found it impossible to design the liquor bottle so that the temperature of the solution inside would be precisely the same as that of the solution outside in the steady state before mixing. This temperature difference was small at room temperature but increased progressively at higher and lower temperatures and amounted to several hundredths of 1° at the extremes. To attain high accuracy, we developed precise, reproducible techniques and measured the combined effect, of temperature difference in the steady state and heat of dilution, in a series of control experiments in which the sodium hydroxide solution in the liquor bottle was added to pure solvent. To test whether these controls are valid, we duplicated the measurements in a scrambled sequence, on various days, and obtained good reproducibility. To make a still more sensitive test of reproducibility and constancy, we studied the heat exchange between the calorimeter and its surroundings.

The liquor bottle is connected to a 10-ml syringe through a length of Tygon tubing. To force the liquid out of the liquor bottle, the syringe is advanced at a constant speed by a motor-driven "push wheel" such that 8 cm³ of gas is pumped out in 2 sec. The temperature of the gas entering the calorimeter is controlled by having much of the Tygon tubing sit inside the polyethylene foam box around the top of the calorimeter-dewar.

Heat Exchange with Surroundings. Corrections for heat exchange amounted to several per cent. Since we were aiming at 0.1% accuracy, we made a kinetic study of heat exchange between the calorimeter and its surroundings, so that these corrections might be made by objective analytical methods. The results also provide us with a sound estimate of the experimental error.

Before reporting the results of this study, we wish to review the relationship between the temperature *T* of the stirred solution in the calorimeter and the temperature Θ of the thermometer immersed in it. The relationship between *T* and Θ is stated in eq 2, where *t* is the time, α is a characteristic "rate constant" for heat exchange between thermometer and solution, $s = dT/dt$, and $m = -ds/dT$. At time t_0 , these variables

$$\frac{d\Theta}{dt} = -\alpha(\Theta - T) \quad (2a)$$

$$T = T_0 + s_0(t - t_0) - [(ms)_0(t - t_0)^2/2] + \dots \quad (2b)$$

are T_0 , Θ_0 , s_0 , and m_0 , respectively. We shall assume that the series (2b) may be terminated at the quadratic

(18) F. Daniels, J. W. Williams, P. Bender, R. A. Alberty, and C. D. Cornwell, "Experimental Physical Chemistry," McGraw-Hill Book Co., Inc., New York, N. Y., 1962.

term. Solution under those conditions leads to (2c)

$$s = s_0(1 - m[t - t_0]) \quad (2c)$$

$$T = \theta + \frac{s}{\alpha} \left(1 + \frac{m}{\alpha}\right) - \left(\theta_0 - T_0 + \frac{s_0}{\alpha} \left[1 + \frac{m}{\alpha}\right]\right) e^{-\alpha(t-t_0)} \quad (2d)$$

and (2d). In the steady state, the exponential term in (2d) has become negligible, and T and s are given for the following conditions: if $\alpha(t - t_0) \gg 1$

$$T = \theta + [s(\alpha + m)/\alpha^2] \quad (3a)$$

$$s = (d\theta/dt)(\alpha^2)/(\alpha + m)^2 \quad (3b)$$

if both $\alpha(t - t_0)$ and $\alpha/m \gg 1$

$$T = \theta + (s/\alpha); \quad s = d\theta/dt \quad (3c)$$

We shall find that $\alpha \gg m$. In the following, we shall therefore use (3c).

To evaluate α , we measured θ under conditions where T is a known function of time and fitted to eq 2d. We found that α increases slowly with T —it nearly doubles between -95 and 55° —and is slightly smaller for aqueous solutions than for solutions in methanol. A typical value for α is 0.134 sec^{-1} for aqueous solutions at 25° . Heat exchange between the calorimeter and its surroundings was always measured under conditions where eq 3 apply.

The relationship between s and the other variables is stated in eq 4. In that equation, T_{surr} is the temperature outside the calorimeter, κ the heat-transfer

$$s = [-\kappa(T - T_{\text{surr}})/C_p] + [h/C_p] \quad (4)$$

coefficient, C_p the effective heat capacity, and h the rate of generation of heat in the calorimeter. In testing eq 4, we measured s under conditions where heat is generated only by stirring. If the variables in (4) are controlled adequately, certain experimental quantities must be constant. We shall now examine whether these quantities are in fact constant.

For definiteness, consider a series of experiments involving aqueous solutions at 5° . In each experiment, 50.00 ml of 0.02 N acid is placed in the calorimeter proper, 5.00 ml of 0.22 N NaOH is placed in a separate liquor bottle inside the calorimeter, and the system is brought into thermal equilibrium with its surroundings at 5° such that s_1 at θ_1 is close to zero. The reactants are then mixed, the temperature rises, and s_2 is measured at θ_2 after the solution, and the thermometer are again in steady-state equilibrium. Some time later, s_3 is measured at an intermediate temperature θ_3 , a known quantity of heat is introduced electrically, and finally s_4 is measured at θ_4 . This sequence of operations is then repeated in a control experiment in which 50.00 ml of pure water is used in place of the 0.02 N acid. We shall use primed symbols (s_1' to s_4' , θ_1'

to θ_4') to denote results obtained in the control experiment. All temperatures (θ_1 to θ_4 , θ_1' to θ_4') are within 0.5° of the nominal temperature of 5° .

In applying eq 3c and 4 to represent s as a function of θ , it is helpful to introduce the parameters m and b , as in (5a). The relationship of s to θ is then (5b). On

$$m = \kappa/(C_p + \alpha^{-1}\kappa); \quad b = (\kappa T_{\text{surr}} + h)/C_p \quad (5a)$$

$$s = -m\theta + b \quad (5b)$$

differentiating and applying (3c), we find that $m = -ds/dT$, the same variable that appears in eq 2-3b.

We expect that the effective values for κ , C_p , and h might change somewhat when the contents of the liquor bottle are introduced into the calorimeter proper. Two sets of values for the parameters are therefore required: m_i and b_i , to apply before mixing (at θ_1 and θ_1'); and m_f and b_f , to apply after mixing (at θ_2 to θ_4 and θ_2' to θ_4'). Equation 5a evaluates m_f from data before and after the electrical heating, and (5b) evaluates it from data before and after the mixing of the reactants. In deriving (5b), we make use of the experimental fact that $s_1 \approx s_1' \approx 0$.

$$m_f = -(s_4 - s_3)/(\theta_4 - \theta_3) = -(s_4' - s_3')/(\theta_4' - \theta_3') \quad (6a)$$

$$m_f = -\frac{(s_2 - s_1) - (s_2' - s_1')}{(\theta_2 - \theta_1) - (\theta_2' - \theta_1')} \quad (6b)$$

For the standard procedure described above, m_f should be the same, at a given nominal temperature, for all experiments involving dilute aqueous solutions. We can therefore judge the reproducibility of the technique. However, m_f should vary with the nominal temperature and with the solvent. Averaged results for two solvents are listed in Table I. Values computed from eq 6a and 6b are listed separately so that their agreement may affirm the validity of the

Table I: Heat Exchange between Calorimeter and Surroundings

Temp. °C	— $10^4 m_f, \text{sec}^{-1}$ —		Temp. °C	— $10^4 m_f, \text{sec}^{-1}$ —	
	Eq 6a	Eq 6b		Eq 6a	Eq 6b
For Aqueous Solutions					
0	3.5	3.6	35	4.6	4.5
5	3.7	3.7	45	5.15	5.2
15	3.9	4.1	55	5.7	5.8
25	4.1	4.2			
For Methanol Solutions					
-95	5.5	4.1	-15	7.1	6.8
-85	5.2	4.6	-5	7.4	7.0
-75	5.1	4.9	5	8.0	7.6
-65	6.05	5.6	15	7.7	7.8
-55	5.9	5.9	25	8.9	9.4
-45	6.2	6.05	30	9.9	10.1
-35	6.4	5.9	35	10.2	10.85
-25	6.8	7.0			

control experiments. The agreement is excellent for aqueous solutions and quite good for methanol solutions even at the lowest temperatures.

The mean standard deviation of a single m_f measurement in water is about 5% in each case and corresponds to an 0.2% standard error in ΔH . However, these figures are upper limits because we actually used two calorimeters, with very similar properties, but failed to record which of them was used in a particular experiment. The 5% standard deviation of m_f therefore includes a small but real difference between the two calorimeters. The actual reproducibility of ΔH is $\pm 0.1\%$.

We shall digress briefly to discuss the physical mechanism of the heat exchange. Since $m \ll \alpha$, it follows from (5a) that $\kappa \approx m_f C_p$, both of which are available for the calorimeter after the reactants are mixed. We expect, from the dimensions and materials of the calorimeter, that heat exchange is largely by thermal conduction, with conduction through the nitrogen-filled annular space being rate determining. κ by that mechanism should vary as $T^{1/2}$, where T is the absolute temperature. At lower temperatures, a square-root relationship can indeed reproduce the data for each solvent, but at higher temperatures, κ increases faster. Guessing that the excess heat exchange might be proportional to the solvent vapor pressure, p (in atmospheres), we fitted the data for each solvent¹⁹ to eq 7 by the method of least squares. The guess was quite

$$\kappa \approx m_f C_p = A\sqrt{T} + Bp \quad (7)$$

successful: the fit is good and the values of A and B are plausible. $A = 0.00137$ for water and 0.00125 for methanol; $B = 0.0750$ for water and 0.0509 for methanol. Thus A appears to be independent of the solvent, so that $A\sqrt{T}$ can indeed represent thermal conduction through a layer of nitrogen gas. B , as it turns out, is closely proportional to $\lambda M^{1/2}$, where λ is the specific heat of vaporization (582 cal/g for water and 285 cal/g for methanol¹⁹) and M is the molecular weight. At the conclusion of an experiment, we usually find that the surface of the calorimeter above the level of the solution is covered with a light fog of liquid. It is possible that this minute amount of condensate first forms while the system is being brought to the desired temperature, during which operation there are substantial temperature gradients. After a steady state is reached, distillation takes place very slowly along the steady temperature gradient.

Calculation of Temperature Rise. On the recorder trace of Θ vs. time for a rapid temperature rise, there are two regions in which the solution temperature T is known with good accuracy: in the initial steady state before the temperature rise and some time later when thermometer and solution are again in steady-state equilibrium. In Figure 2, these regions are shown by solid lines. To calculate the temperature

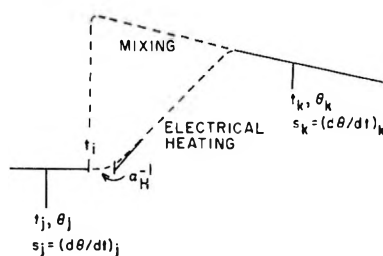


Figure 2. Calculation of temperature rise. Explanation of variables in eq 8.

rise, we must extrapolate the solid lines to some time, t_0 , chosen so that the effect of heat exchange with the surroundings is nullified exactly. In a typical experiment, we might measure Θ_j and s_j at t_j , and Θ_k and s_k at t_k —see Figure 2. We can then construct the required extrapolation functions (8) by applying eq 2b, 2c, and 3c.

$$T_2 = \Theta_k + s_k \left\{ (t - t_k) \left(1 - \frac{m}{\alpha} - \frac{m}{2} [t - t_k] \right) + \frac{1}{\alpha} \right\} \quad (8a)$$

$$T_1 = \Theta_j + s_j \left\{ (t - t_j) \left(1 - \frac{m}{\alpha} - \frac{m}{2} [t - t_j] \right) + \frac{1}{\alpha} \right\} \quad (8b)$$

$$\delta T = T_2 - T_1 \quad (\text{at } t_0) \quad (8c)$$

The values of m required to reproduce the gentle curvature of the extrapolation functions were taken from Table I. Values of t_0 were obtained as follows. For the mixing of two solutions, prior analysis indicated that lags inherent in the transfer from the liquor bottle and distribution of the resulting heat by stirring should be about 3 sec. We decided, however, to approach the problem empirically by measuring the time lag between the start of mixing and the temperature rise of the thermometer, which should be a good model for t_0 . Estimates obtained by this method decreased smoothly from 2.2 sec at 0° to 1.2 sec at 55° for aqueous solutions, and from 3.9 sec at -95° to 2.4 sec at 35° for methanol solutions. An error of 1 sec in t_0 would cause 0.04% error in ΔH .

In the measurement of the heat capacity, an electric heater operates with constant power output from t_i to t_f . (See Figure 2.) However, the temperature of the solution lags behind that of the heater. In eq 4, the term h/C_p now takes the form (9), where Θ_H is the temperature of the heater, α_H is the characteristic rate constant for heat exchange, and the constant term C represents the effect of stirring. It

$$h/C_p = \alpha_H(\Theta_H - T) + C \quad (9)$$

acteristic rate constant for heat exchange, and the constant term C represents the effect of stirring. It

(19) Data from "Handbook of Chemistry and Physics," Chemical Rubber Publishing Co., Cleveland, Ohio, and from D. F. Dever, A. Finch, and E. Grunwald, *J. Phys. Chem.*, 59, 668 (1955).

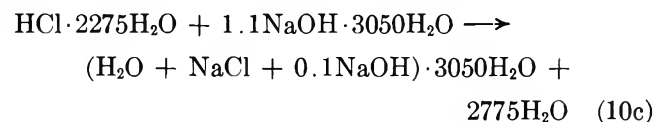
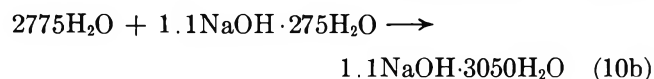
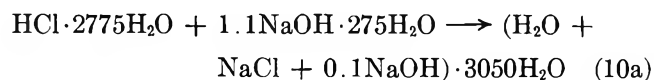
can be shown that under these conditions, eq 8 must be solved at $t_0 = \frac{1}{2}(t_i + t_f) + \alpha_H^{-1}$. Although the heater lag, α_H^{-1} , cannot be measured by itself, the combined lag of heater and thermometer, $\alpha_H^{-1} + \alpha^{-1}$, can be measured easily; it is equal to the length of the induction period that precedes the rise in Θ after the heater is switched on. $\alpha_H^{-1} + \alpha^{-1}$ was measured with best accuracy toward the end of the heating period, when Θ_H and Θ increase at the same rate. After subtracting α^{-1} , we found that α_H^{-1} is nearly constant at 13 ± 1 sec in all experiments.

Materials. Distilled water was redistilled twice before use. HCl-water solutions were prepared from constant-boiling HCl. NaOH solutions were prepared carbonate free from sodium metal and water. To avoid violent reaction, the sodium metal was contained in a small glass tubing and reaction took place only at the open ends. Acetic acid was purified by partial freezing in an ice bath. Benzoic acid primary standard was purchased from the National Bureau of Standards.

To test the calorimeter at low temperatures, heats of neutralization were measured in methanol solution. Purification of and preparation of solutions in methanol followed previous practice.²⁰ Definitions: 1 cal = 4.1840 J; $0^\circ = 273.16^\circ\text{K}$.

Results

Averaged heats of neutralization are listed in Table II and are taken as the difference of heats of neutralization and control experiments, as shown for HCl in (10a) and (10b). The net process is therefore the reaction of *ca.* 0.02 *N* acid with 10% excess of *ca.* 0.02 *N* NaOH, *e.g.*, eq 10c. The reproducibility of



these results is $\pm 0.1\%$. The accuracy, according to careful error analysis, should be better than 0.25%. The results were corrected to infinite dilution on the basis of the Debye-Hückel limiting law for apparent partial molal enthalpies.²¹ The corrections were less than 110 cal. Errors due to the use of the limiting law were well within the experimental error because the deviations from the limiting law tend to cancel.²¹ In the case of acetic and benzoic acid, the data were corrected also for acid dissociation in the initial state. The heats of neutralization at infinite dilution were then used to calculate heats of acid dissociation. Results are listed in Table III.

Table II: Enthalpy Change for the Reaction of 0.02 *F* Acids with Excess 0.02 *F* Sodium Hydroxide in Water^a

Temp, °C	ΔH , kcal/mol, for		
	HCl	HAc	HBz
0	-15.038	-14.217	...
5	-14.600	-13.918	-13.877
15	-13.922	-13.600	-13.432
25	-13.401 ^b	-13.467	-13.223
35	-13.008	-13.346	-13.184
45	-12.561	-13.119	-13.087
55	-12.059	-12.826	-12.922

^a See, for example, eq 10. ^b HCl at 25°: -13.404 kcal/mol at 0.01 *F*; -13.410 kcal/mol at 0.04 *F*.

Table III: Enthalpy Change for Acid Dissociation in Water, at Infinite Dilution

Temp, °C	$\Delta\bar{H}^\circ$, kcal/mol, for acid dissociation of		
	H ₂ O ^a	HAc ^b	HBz ^b
0	14.998	0.804	...
5	14.555	0.657	0.736
15	13.866	0.275	0.460
25	13.334 ^c	-0.137	0.118
35	12.928	-0.430	-0.272
45	12.467	-0.671	-0.657
55	11.950	-0.901	-1.029

^a The data in Table II were corrected to infinite dilution on the basis of the Debye-Hückel limiting law. The ionic strength was about 0.02 *M*. ^b For this charge type, correction to infinite dilution is zero, according to the Debye-Hückel limiting law. In calculating $\Delta\bar{H}^\circ$, a correction was made for the acid dissociation of the carboxylic acid in the initial 0.02 *F* state. ^c At 25°, $\Delta\bar{H}^\circ = 13.354$ kcal/mol from extrapolation of the data at 0.01 *M* ionic strength, and $\Delta\bar{H}^\circ = 13.315$ kcal/mol from extrapolation of those at 0.04 *M* ionic strength.

$\Delta\bar{C}_p^\circ$ for acid dissociation was calculated for each acid as the temperature derivative of $\Delta\bar{H}^\circ$. Results are listed in Table IV. The accuracy of $\Delta\bar{C}_p^\circ$ is better than ± 4 cal/mol deg at 10–50° and better than ± 8 cal/mol deg at 2.5°. The maximum in $\Delta\bar{C}_p^\circ$ for the ionization of water is therefore highly significant. The minima for the carboxylic acids are less certain but are probably real also.

The agreement of our results with previous work is in most cases satisfactory. For the ionization of water at 25°, our value of 13.334 kcal for $\Delta\bar{H}^\circ$ is in good agreement with recent calorimetric determinations of 13.335, 13.336, and 13.350 kcal.^{22–24} The dis-

(20) E. Grunwald, C. F. Jumper, and S. Meiboom, *J. Amer. Chem. Soc.*, **84**, 4664 (1962).

(21) H. S. Harned and B. B. Owen, "The Physical Chemistry of Electrolytic Solutions," Reinhold Publishing Corp., New York, N. Y., 1943.

(22) J. D. Hale, R. M. Izatt, and J. J. Christensen, *J. Phys. Chem.*, **67**, 2605 (1963).

(23) C. E. Vanderzee and J. A. Swanson, *ibid.*, **67**, 2608 (1963).

(24) R. N. Goldberg and L. G. Hepler, *ibid.*, **72**, 4654 (1968).

Table IV: $\Delta\bar{C}_p^\circ$ for Acid Dissociation in Water at Infinite Dilution

Temp., °C	$\Delta\bar{C}_p^\circ$, cal/mol deg., for acid dissociation of		
	H ₂ O	HAc	HBz
2.5	-88.6	-29.4	...
10	-68.9	-38.2	-27.6
20	-53.2	-41.2	-34.2
30	-40.6	-29.3	-39.0
40	-46.1	-24.1	-38.5
50	-51.7	-23.0	-37.2

crepancy between values of $\Delta\bar{H}^\circ$ by direct calorimetry and those derived from the temperature derivative of potentiometric values for K_w are thus confirmed.²⁴ For acetic acid at 25°²⁵⁻²⁷ and for benzoic acid at several temperatures between 10 and 40°,²⁸⁻³⁰ our values are in very good agreement with all but two of the previously reported numbers and deviate seriously only in one case.²⁷ Our values for $\Delta\bar{C}_p^\circ$ for the ionization of water agree with values derived by Ackermann⁴ from specific heats of fairly concentrated aqueous solutions up to about 25° but begin to deviate at higher temperatures.

Discussion

Table V lists values of \bar{C}_p° for various formal species in water. The striking maximum for H₃O⁺ + OH⁻ seems to come from the hydroxide ion rather than the hydronium ion, because neither H₃O⁺ + Ac⁻ nor H₃O⁺ + Bz⁻ behave at all similarly.

Table V: \bar{C}_p° for Various Formal Species in Water

Temp., °C	H ₂ O ^a	HAc ^b	H ₃ O ⁺ + OH ^{-c}	H ₃ O ⁺ + Ac ^{-d}	OH ⁻ - Ac ⁻
2.5	18.11	41	-52.4	30	-82
10	18.04	42.5	-32.8	22	-55
20	17.99	43.5	-17.2	20	-37
30	17.98	44.5	-4.6	33	-38
40	17.98	45.5	-10.1	38	-48
50	17.99	44.5	-15.7	40	-56

^a N. S. Osborne, H. F. Stimson, and D. C. Ginnings, *J. Res. Nat. Bur. Stand.*, **23**, 238 (1939). ^b Reference 5. ^c $\Delta\bar{C}_p^\circ + 2C_{p,H_2O}^\circ$. ^d $\Delta\bar{C}_p^\circ + \bar{C}_{p,H_2O}^\circ + \bar{C}_{p,HAc}^\circ$.

It has been stated in the introductory section that a maximum in the formal \bar{C}_p° for a pair of thermally stable free ions can be ascribed to an endothermic change in the solvent shell around one of the ions. However, the physical description of that change can cover a wide range of phenomena. At one extreme, the change might be a genuine chemical reaction: for instance, an octahydrate becomes a hexahydrate. At the other extreme, it might be merely an artifact resulting from a peculiar energy level diagram for a single species.

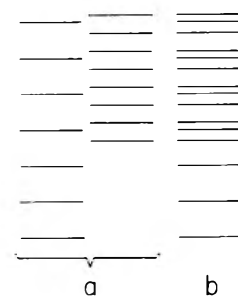


Figure 3. Alternate representation of a set of energy levels: (a) two species; (b) single species with a marked increase in the density of energy levels above a critical energy.

In Figure 3, a set of energy levels is displayed in two ways: (a) as two subspecies and (b) as a single species. Figure 3a is appropriate when the two subsets of levels are separated by a potential barrier and represents the case of a genuine chemical transformation. Figure 3b is appropriate in the absence of a potential barrier and represents a single chemical species for which the density of energy levels increases markedly above a certain critical value. Of course, the two descriptions lead to the same thermodynamic consequences. Thus the single species represented in Figure 3b is indistinguishable, on the basis of thermodynamic data, from an equilibrium mixture of two subspecies.

The point is worth making, because energy-level diagrams of the sort of Figure 3b may not be so unusual for solvated species in the liquid phase. A marked increase in energy-level density might arise, for instance, when the energy becomes sufficient to permit rotation in place of libration.

Suppose, then, that the formal solute may be treated as an equilibrium mixture of the sort $A \rightleftharpoons B$. Let x denote the fraction of solute molecules belonging to the species B, $K = [B]/[A]$, $\Delta H^* = \bar{H}^\circ_B - \bar{H}^\circ_A > 0$, and $\Delta S^* = \bar{S}^\circ_B - \bar{S}^\circ_A$. $\bar{H}^\circ_{\text{formal}}$ for the formal solute, $A + B$, is then given by (11), and $\bar{C}_p^\circ_{\text{formal}}$ by (12). To

$$\bar{H}^\circ_{\text{formal}} = (1 - x)\bar{H}^\circ_A + x\bar{H}^\circ_B \quad (11)$$

$$d\bar{H}^\circ_{\text{formal}}/dT = \bar{C}_p^\circ_{\text{formal}} = (1 + x)\bar{C}_p^\circ_A + x\bar{C}_p^\circ_B + \Delta\bar{H}^*(dx/dT) \quad (12)$$

solve for dx/dT , we write (13) and make the usual assumption that over a limited temperature range, ΔH^* and ΔS^* are constant; that is $\Delta\bar{C}_p^* = 0$. The result is

(25) H. S. Harned and R. W. Ehlers, *J. Amer. Chem. Soc.*, **55**, 652 (1933).

(26) J. J. Christensen, R. M. Izatt, and L. D. Hansen, *ibid.*, **89**, 213 (1967); J. J. Christensen, J. L. Oscarson, and R. M. Izatt, *ibid.*, **90**, 5949 (1968).

(27) I. Wadso, *Acta Chem. Scand.*, **16**, 479 (1962).

(28) L. P. Fernandez and L. G. Hepler, *J. Phys. Chem.*, **63**, 110 (1959).

(29) T. L. Cottrell, G. W. Drake, D. L. Levi, K. S. Tully, and J. A. Wolfenden, *J. Chem. Soc.*, 1016 (1948).

(30) W. J. Canady, H. M. Pappee, and K. J. Laidler, *Trans. Faraday Soc.*, **54**, 505 (1958).

first (14a), then (14b). In (14a), the sum of the first

$$\begin{aligned}\ln K &= \ln[x/(1-x)] \\ &= (\Delta S^*/R) - (\Delta H^*/RT); \quad \Delta C_p^* = 0\end{aligned}\quad (13)$$

$$\bar{C}_p^\circ \text{ formal} = (1-x)\bar{C}_p^\circ \text{ A} + x\bar{C}_p^\circ \text{ B} + [x(1-x)(\Delta H^*)^2/RT^2] \quad (14a)$$

$$= \bar{C}_p^\circ \text{ A} + [x(1-x)(\Delta H^*)^2/RT^2] \quad (\text{if } \Delta C_p^* = 0) \quad (14b)$$

two terms on the right will show the normal gentle increase of heat capacity with temperature. The last term, however, will go through a maximum at a temperature, T_{\max} , at which $x = 1/2 - (RT_{\max}/\Delta H^*)$. If, at that temperature, $\Delta H^* \gg RT_{\max}$, x will be approximately $1/2$ and the "abnormal" last term will be $(\Delta H^*)^2/4RT_{\max}^2$. Whether or not the "abnormal" term can be distinguished from experimental error will depend not only on its magnitude, which is proportional to $(\Delta H^*)^2$ but also on its sharpness (or inverse half-width on the plot vs. T) which, owing to (13), is also quite sensitive to ΔH^* . As a result, the detection of the term is extremely sensitive to ΔH^* . Some sample calculations, based on (13) and (14b), are plotted in Figure 4.

Having a mechanism by which $\bar{C}_p^\circ \text{ formal}$ can go through a maximum, there are now several ways for obtaining a minimum. As T increases above T_{\max} , the "abnormal" last term in (14) becomes progressively smaller while the two other terms together become larger. If ΔH^* is large enough, a minimum will result. A probable example is \bar{C}_p° for water, which goes through a minimum at about 35° (Table V). That interpretation is probable because certain other properties of liquid water are also consistent with the $A \rightleftharpoons B$ model.³¹

If the solute undergoes consecutive or parallel (in case of a pair of ions) endothermic changes, it is possible for the corresponding contributions to the formal heat capacity to give well-resolved maxima on the plot vs. T . If the measurements happen to fall into the temperature range between two maxima, \bar{C}_p° will appear to go through a minimum. Probable examples are furnished by \bar{C}_p° for $\text{H}_3\text{O}^+ + \text{Ac}^-$ (Table V) and by $\Delta\bar{C}_p^\circ$ for the acid dissociation of acetic acid (Table IV), benzoic acid (Table IV), and diisopropylcyanoacetic acid.³

The maximum in \bar{C}_p° for $\text{H}_3\text{O}^+ + \text{OH}^-$, which has been ascribed to the hydroxide ion, gives best fit to the $A \rightleftharpoons B$ model if ΔH^* is 8.8 kcal—see Figure 4. If that model can be accepted, then the relatively high value of ΔH^* suggests that the real or seeming process associated with ΔH^* is a cooperative process affecting a number of molecules in the solvation shell. We favor that interpretation, but to gain a better perspective, we wish to consider one alternative model.

Suppose that the endothermic transformation of the solvation shell takes place in n equal and independent steps, each with an enthalpy change of $\Delta H'$. These

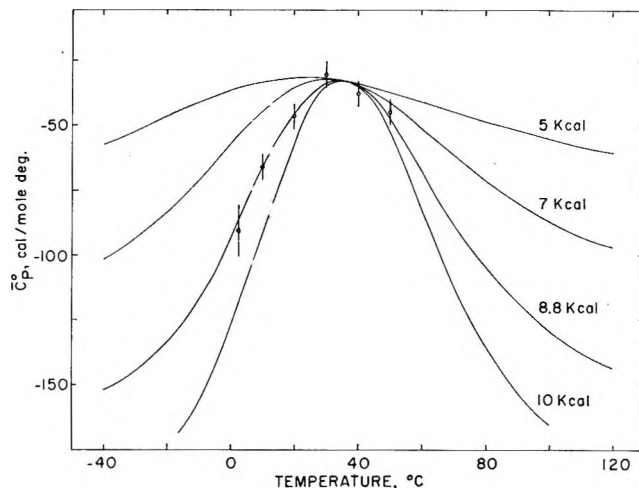


Figure 4. Sample calculations based on eq 11-14. The scale of the ordinate is chosen in each case so that the maximum falls in the experimental range. Circles indicate experimental values of $\bar{C}_p^\circ \text{ formal}$ for $\text{H}_3\text{O}^+ + \text{OH}^-$.

steps might be the successive "loosening" of n independent and equivalent water molecules. Let x' be the fractional completion of the process at the given temperature, and let $K' = x'/(1-x')$. The enthalpy of the formal species is then given by (15), where $\bar{H}^\circ \text{ A}$ is the enthalpy of the original low-temperature form.

$$\bar{H}^\circ \text{ formal} = \bar{H}^\circ \text{ A} + nx'\Delta H' \quad (15)$$

Differentiation with respect to T yields (16). On expressing x' as a function of K' and assuming constant $\Delta H'$ ($\Delta C_p' = 0$), we obtain (17). Note that this model accommodates eq 14 as a special case with $n = 1$.

$$\bar{C}_p^\circ \text{ formal} = \bar{C}_p^\circ \text{ A} + nx'\Delta C_p' + [nx'(1-x')(\Delta H')^2/RT^2] \quad (16)$$

$$\bar{C}_p^\circ \text{ formal} = \bar{C}_p^\circ \text{ A} + [nK'(\Delta H')^2/RT^2(1+K')^2] \quad (17a)$$

$$\ln K' = (\Delta S'/R) - (\Delta H'/RT) \quad (17b)$$

The fit of (17) was tested for $n = 1, 3$, and 4 and was equally satisfactory for each. "Best fit" was obtained with the following parameters: $n = 1$, $\Delta H' = 8.8$ kcal, $\Delta S' = 28.1$ gibbs, $\bar{C}_p^\circ \text{ A} = -107$ cal/deg; $n = 3$, $\Delta H' = 6.4$ kcal, $\Delta S' = 20.0$ gibbs, $\bar{C}_p^\circ \text{ A} = -163$ cal/deg; $n = 4$, $\Delta H' = 6.0$ kcal, $\Delta S' = 18.7$ gibbs, $\bar{C}_p^\circ \text{ A} = -191$ cal/deg. In each case, $\bar{C}_p^\circ \text{ A}$ was assumed to be constant. By comparison, for pure liquid water the two-state model gives "best fit" if $\Delta H' = 2.55$ kcal and $\Delta S' = 3.9$ gibbs.³¹ For the freezing of water, $\Delta C_p^\circ = -9$ cal/mol deg at 0° .

In our opinion, the only plausible set of parameters is that for $n = 1$. In particular, $\bar{C}_p^\circ \text{ A}$ strikes us as

(31) See, for example, C. E. Walrafen, *J. Chem. Phys.*, **48**, 244 (1968).

unreasonably negative when n is assumed to be 3 or 4. If we assume a molar heat capacity of 18 cal/deg for $\text{H}_3\text{O}^+ + \text{OH}^-$ (2 mol of frozen water) and an increment of -9 cal/deg for each mole of water that becomes frozen in solvation shells, then even the fairly modest -107 cal/deg obtained for \bar{C}_p° when $n = 1$ already implies the freezing of 14 water molecules. The value of 8.8 kcal obtained for $\Delta H'$ when $n = 1$ seems plausible if the process is a manifestation of the same hydrogen-bonding phenomenon that gives a $\Delta H'$ of 2.55 kcal in pure water but requires the concerted action of three or four water

molecules that are hydrogen bonded to the hydroxide ion.

Values of $\Delta \bar{H}^\circ$ and of $\Delta \bar{C}_p^\circ$ for the analogous reactions of HCl and benzoic acid with sodium methoxide in methanol are being reported in an accompanying paper.³² In methanol, the values of $\Delta \bar{C}_p^\circ$ do not show any maxima or minima of the sort observed in water, even though the experimental temperature range, -95 to $+35^\circ$, is much wider.

(32) C. S. Leung and E. Grunwald, *J. Phys. Chem.*, **74**, 696 (1970).

Temperature Dependence of $\Delta \bar{C}_p^\circ$ for the Self-Ionization of Methanol and for the Acid Dissociation of Benzoic Acid in Methanol¹

by Constance S. Leung and Ernest Grunwald

Chemistry Department, Brandeis University, Waltham, Massachusetts 02154 (Received June 26, 1969)

$\Delta \bar{H}$ was measured with an accuracy of 0.2% for the reaction of HCl and of benzoic acid with sodium methoxide in methanol at 10° intervals from -95 to $+35^\circ$. The ionic strength of the solutions was about 0.015 M . The dielectric constant of methanol was measured between -95 and 25° , so that interionic effects could be corrected for. $\Delta \bar{H}^\circ$ was calculated for the self-ionization of methanol and for the acid dissociation of benzoic acid. Using known pK° values for these processes at 25° , $\Delta \bar{H}^\circ$ was used to derive pK° over the entire liquid range of methanol, such that the accuracy of pK° was limited by that of pK° at 25° . The resulting values can serve as a basis for pH and $p\text{OCH}_3$ standards in methanol. $\Delta \bar{C}_p^\circ$ was derived from $\Delta \bar{H}^\circ$ and compared with $C_p^\circ(l)$ for liquid methanol. For both processes, $\Delta d\bar{C}_p^\circ/dT = -k dC_p^\circ(l)/dT$ in good approximation, where k is about 15 for self-ionization of methanol and 16 for acid dissociation of benzoic acid. A theory is proposed in which k is simply related to the number of methanol molecules that become "frozen" in the solvation shells of the ionic products. There is no evidence for endothermic changes of these solvation shells over the entire temperature range.

It has been shown²⁻⁴ that $\Delta \bar{C}_p^\circ$ for acid-base reactions in water can be a sensitive and complex function of the temperature, exhibiting maxima and minima that can be attributed to endothermic changes in the hydration shells surrounding molecules of the reactive species.⁴ Wishing to know whether this phenomenon is characteristic of hydroxylic solvents in general or of water in particular, we have measured $\Delta \bar{H}^\circ$ and $\Delta \bar{C}_p^\circ$ for some acid-base reactions in methanol. The results of that study are reported in this paper.

Methanol is a good solvent for our purpose. It has a wide liquid range, from -97.8 to 64.7° , and a fairly high dielectric constant.^{5,6} It is readily prepared anhydrous and in a high state of purity.

Our calorimetry covers the temperature range from -95 to $+35^\circ$. $\Delta \bar{H}$ was measured for the reaction of methyloxonium chloride (HCl in methanol) with sodium methoxide and of benzoic acid with sodium methoxide, at ionic strengths on the order of 0.015 M . The calorim-

eter⁴ was set up in a temperature-controlled atmosphere of dry nitrogen, from which moisture was excluded. Results were reproducible to better than 0.2% in $\Delta \bar{H}$ and are believed to be similarly accurate. The

(1) We gratefully acknowledge support of this work in part by the National Science Foundation under Grant GP-7381X.

(2) F. S. Feates and D. J. G. Ives, *J. Chem. Soc.*, 2798 (1956); D. J. G. Ives and P. D. Marsden, *ibid.*, 649 (1965).

(3) T. Ackermann, *Z. Elektrochem.*, **62**, 411 (1958); T. Ackermann and F. Schreiner, *ibid.*, **62**, 1143 (1958).

(4) C. S. Leung and E. Grunwald, *J. Phys. Chem.*, **74**, 687 (1970).

(5) P. S. Albright and L. J. Gosting, *J. Amer. Chem. Soc.*, **68**, 1061 (1946); E. C. Evers and C. A. Kraus, *ibid.*, **70**, 3049 (1948); T. T. Jones and R. M. Davies, *Phil. Mag.* (VII), **28**, 307 (1939); N. Koizumi and T. Hanai, *Bull. Inst. Chem. Res. Kyoto Univ.*, **33**, 14 (1955). Values reported for ϵ at 25° are 32.66, 32.6, 32.61, and 32.31, respectively; F. E. Critchfield, J. A. Gibson, and J. L. Hall, *J. Amer. Chem. Soc.*, **75**, 1991 (1953), have obtained a value within 0.1% of 32.66.

(6) J. Juillard, Sc.D. Thesis, University de Clermont-Ferrand, Sept 1968, pp 128, 197. Here 32.63 is listed for ϵ of methanol at 25° . J. Juillard, *Bull. Soc. Chim. Fr.*, 1727 (1966).

dielectric constant of methanol was redetermined in this temperature range to permit more accurate extrapolation of our results to infinite dilution.⁷

Values of $\Delta\bar{C}_p^\circ$ were calculated for (A) the self-ionization of methanol, (B) the acid dissociation of benzoic acid, and (C) the reaction of benzoic acid with sodium methoxide. All three are smooth functions of the temperature and can be scaled to be superimposable almost exactly on the heat capacity curve of pure liquid methanol.^{8,9} In reactions A and B, in which dissociated ions are produced, the temperature dependence of $\Delta\bar{C}_p^\circ$ is quite large. However, the temperature dependence of $C_p^\circ(l)$ for pure methanol is relatively large also, and the data permit the interpretation that a number of methanol molecules become "frozen" in the solvent shells around the ions. The number of methanol molecules so "frozen" appears to be about the same as the number of water molecules immobilized around similar ions in their low-temperature form in aqueous solution.⁴

There is nothing in the data to indicate any endothermic changes in the solvation shells around the ions, of the sort inferred for aqueous solutions. We conclude, therefore, that the peculiar temperature dependence of $\Delta\bar{C}_p^\circ$, which indicates that such changes take place in water,²⁻⁴ results from specific properties of the water molecules.

The new values of $\Delta\bar{H}^\circ$, in conjunction with equilibrium constants for reactions A to C at 25°,^{6,10-13} enable us to obtain accurate equilibrium constants for those reactions over the entire liquid range of methanol, thus filling a need for pH standards¹⁴ in methanol at temperatures other than room temperature.

Experimental Part

Materials. Reagent grade methanol (spectral grade) was treated with magnesium and distilled twice, the second time with a trace of benzoic acid in the distilling flask.¹⁵ Methanol used in the dielectric constant measurements was redistilled five times, until the conductivity was acceptably low.

Hydrogen chloride was prepared by addition of concentrated sulfuric acid to sodium chloride. The HCl gas was allowed to bubble through concentrated sulfuric acid before being dissolved in methanol. A solution of sodium methoxide in methanol was prepared by the reaction of clean sodium metal with the pure solvent.

Benzoic acid primary standard was purchased from the U. S. National Bureau of Standards.

All solutions were prepared and stored under an atmosphere of dry nitrogen. Acid-base titers were checked periodically and were known to 0.1%. As a final check, titers were proved with potassium acid phthalate primary standard from the U. S. National Bureau of Standards. Where appropriate, solute concentrations were corrected for the change in density¹⁶ with temperature.

Calorimetry. The calorimeter and measuring procedure were essentially those described in the preceding paper.⁴ For experiments at and below -55° , the polyethylene foam box around the top of the calorimeter-dewar assembly was sealed and "leak-proofed" with masking tape around the edges, to assure that the nitrogen gas would emerge from the box through the opening for the stirrer shaft at the top, and a 2 in. taller dewar flask was used. Proper protection (in the form of a small paper cylinder) was made to prevent frost formation on the stirrer shaft.

In the experiments involving HCl and NaOCH₃, 50.00 ml (at 23°) of freshly prepared 0.015 *N* acid was placed in the calorimeter, and 5.00 ml of 0.26 *N* methoxide was placed in the liquor bottle. In the experiments involving benzoic acid and NaOCH₃, a similar procedure, with methoxide in excess, was used at -15° and above. At lower temperatures there seemed to be a problem with some of the benzoic acid creeping up the glass walls of the calorimeter and then not reacting immediately when excess methoxide was added. The problem was overcome by making benzoic acid the reagent in excess. At -35° and -55° , 50.00 ml (at 23°) of 0.02 *N* methoxide was placed in the calorimeter and 5.00 ml of 0.26 *N* benzoic acid was placed in the liquor bottle. At still lower temperatures these concentrations were reduced somewhat because of solubility limitations for benzoic acid. It was found, in separate experiments at 25°, that $\Delta\bar{H}$ is independent of which reagent is in excess: with methoxide in excess, $\Delta\bar{H} = 5.930 \pm 0.009$ kcal; with benzoic acid in excess, $\Delta\bar{H} = 5.935 \pm 0.010$ kcal.

The reproducibility of $\Delta\bar{H}$ was generally 0.2% or better. The precision of the temperature measurements approached 0.0001°. The absolute accuracy of the temperature at which $\Delta\bar{H}$ is measured should be better than 0.1°. The ohmic resistance of the standard heater was measured in each experiment and varied by about 1% between 35 and -95° . To detect errors that might vary systematically with time, the measurements were made in a jumbled sequence, especially with respect to temperature. The smooth variation of the

(7) Measurements of ϵ for methanol below 0° have been reported by R. Abegg and W. Seitz, *Z. Phys. Chem.*, **29**, 242 (1899). Our new values are substantially higher.

(8) K. K. Kelley, *J. Amer. Chem. Soc.*, **51**, 180 (1929).

(9) L. A. K. Staveley and A. K. Gupta, *Trans. Faraday Soc.*, **45**, 50 (1949).

(10) A. L. Bacarella, E. Grunwald, and E. L. Purlee, *J. Org. Chem.*, **20**, 747 (1955).

(11) M. Kilpatrick, *J. Amer. Chem. Soc.*, **75**, 584 (1953).

(12) I. D. Tabagua, *Russ. J. Phys. Chem.*, **37**, 828 (1963). This value was not included in the average.

(13) J. Koskikallio, *Suomen Kemistilehti*, **B**, **30**, 111 (1957).

(14) R. G. Bates, *Anal. Chem.*, **40**, 28A (1968).

(15) E. Grunwald, C. F. Jumper, and S. Meiboom, *J. Amer. Chem. Soc.*, **84**, 4664 (1962).

(16) "International Critical Tables," Vol. 3, E. W. Washburn, Ed., McGraw-Hill Book Co., Inc., New York, N. Y., 1926, p 27.

final results with temperature suggests that time-dependent errors were absent. Definitions: 1 cal = 4.1840 J; $0^\circ = 273.16^\circ\text{K}$.

The titer of the standard HCl decreased by about 0.6% during the period of the measurements, consistently with the known rate of the reaction of $\text{Cl}^- + \text{CH}_3\text{OH}_2^+ \rightarrow \text{CH}_3\text{Cl} + \text{HOH}$ at room temperature.¹⁷ It was judged that the small quantity of water produced would not cause serious error.¹⁸ The titers of the standard benzoic acid and sodium methoxide remained constant.

Dielectric Constants. The three-terminal stainless steel dielectric cell was manufactured by Balsbaugh Laboratories, South Hingham, Mass. Before use it was dismantled and treated with boiling perchloroethylene, boiling water, and finally boiling methanol. It was then set up in the same thermostated dewar container that had been used for the calorimetry, filled with low-conductivity methanol, and brought to the desired temperature.

The capacitance and dissipation factor of the cell were measured at a frequency of 10 kHz with a General Radio Type 1615 A capacitance bridge. There was no difficulty in detecting the bridge balance to 0.1%. Dielectric constants, ϵ , were calculated from the effective parallel capacitance. The air capacitance of the cell was 58.27 pF at 25° , and the dielectric constant of air was taken to be 1.00054. A small correction was made for the contraction of the stainless steel concentric cylindrical measuring electrodes below 25° .

The temperature inside the cell was measured to better than 0.1° with a calibrated copper-constantan thermocouple, one glass-sheathed junction of which was immersed in ice, the other being immersed in methanol in the cell at a point guarded from the electrical measuring region. Results of the measurements are listed in Table I.

Table I: Dielectric Constant of Methanol

Temp, $^\circ\text{C}$	$1000d \ln(\epsilon T)/dT$	
-95.21	73.16	
-85.80	67.94	-2.37
-74.19	62.11	-2.56
-64.94	58.07	-2.37
-45.76	50.88	-2.30
-24.81	44.32	-2.40
-5.82	39.30	-2.44
14.03	34.86	-2.44
25.38	32.57	-2.58

In the following, we shall need to know $d \ln(\epsilon T)/dT$. Average values of that derivative are given for each temperature interval in Table I. Within their experimental error, these values could be constant. However, the slight indication of a shallow minimum near -50°

appears to be correct. If we assume a linear relationship between $\ln(\epsilon T)$ and T , we predict that $\epsilon = 27.64$ at 55° , whereas a reliable experimental value is 27.21 at that temperature.⁵ However, if we fit a parabola according to eq 1, we predict that $\epsilon = 27.33$, in much better agreement. Integration of (1), change to de-

$$-1000 \frac{d \ln(\epsilon T)}{dT} = 2.37 + 4.26 \times 10^{-4}(T - 225.9)^2 \quad (1)$$

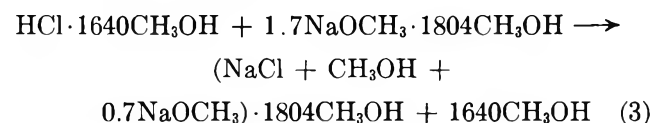
cadic logarithms, and evaluation of the constant of integration leads to (2), which fits our data well within 0.1%. Equation 2 predicts a dielectric constant of

$$\log(\epsilon T) = 4.2970 - 1.029 \times 10^{-3}T - 6.16 \times 10^{-9}(T - 225.9)^3 \quad (2)$$

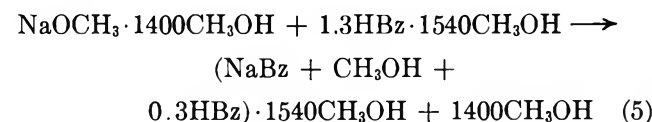
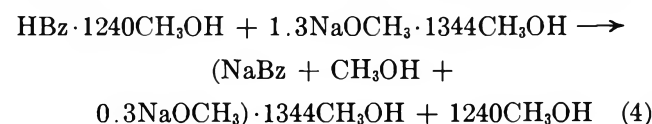
32.62 for methanol at 25° , in almost perfect agreement with the mean of several recent measurements.^{5,6}

Results

Average values of $\Delta\bar{H}$ are listed in Table II. Each $\Delta\bar{H}$ is the difference between a heat of reaction and the corresponding heat of dilution ("the control," as described in the preceding paper⁴), computed per mole of reaction. For the reaction of HCl with excess NaOCH_3 , the typical thermochemical process to which $\Delta\bar{H}$ refers is shown in eq 3. For the reaction of benzoic



acid with excess NaOCH_3 , the typical process is shown in (4), and for the reaction of NaOCH_3 with excess benzoic acid, it is shown in (5). In each of those proc-



esses, three of the entities involved are solutions, and the fourth is pure solvent.

To correct $\Delta\bar{H}$ to infinite dilution,¹⁹ let φ_L denote the relative apparent molal enthalpy of a solute and n the number of formula weights. Let $\Sigma n_R \varphi_{L,R}$ and $\Sigma n_P \varphi_{L,P}$ denote, respectively, the sum of such enthalpy terms for

(17) W. Voss and W. Wachs, *Ann.*, **522**, 253 (1936); C. N. Hinshelwood, *J. Chem. Soc.*, 600 (1935).

(18) For data concerning the basicity of water in methanol, see J. Koskikallio, *Suomen Kemistilehti*, **B**, **30**, 43 (1957); I. M. Kolthoff and L. S. Guss, *J. Amer. Chem. Soc.*, **62**, 1494 (1940).

(19) See, for example, H. S. Harned and B. B. Owen, "The Physical Chemistry of Electrolytic Solutions," Reinhold Publishing Corp., New York, N. Y., 1943, sections 3(8), 5(2), and 8(2).

Table II: Enthalpy Changes (in kcal/mol) for Acid-Base Reactions in Methanol

Temp., °C	S_H (eq 8)	HCl + NaOCH ₃		FBz + NaOCH ₃	HBz + CH ₃ OH → Bz ⁻ + CH ₃ OH ₂ ⁺
		$-\Delta\bar{H}$	$-\Delta\bar{H}^\circ$	$-\Delta\bar{H}, -\Delta\bar{H}^\circ$	$\Delta\bar{H}^\circ$
-95	0.551	14.463	14.369	8.061	6.308 ^b
-85	0.630	14.234	14.127	7.846	6.281
-75	0.720	14.005	13.882	7.659	6.223
-65	0.818	13.761	13.626
-55	0.930	13.507	13.349	7.300	6.049
-45	1.052	13.231	13.059
-35	1.190	12.938	12.743	6.938	5.805
-25	1.346	12.612	12.394
-15	1.523	12.288	12.039	6.581	5.458
-5	1.728	11.917	11.638	6.431	5.207
5	1.962	11.524	11.208	6.266	4.942
15	2.233	11.107	10.748	6.127	4.621
25	2.542	10.634	10.227	5.933	4.294
30	2.715	10.365	9.932	5.860	4.072
35	2.899	10.070	9.611	5.808	3.803

^a Temperature $\pm 0.05^\circ$. ^b Column 5 minus column 4.

the two reactant solutions and the product solution. The enthalpy change at infinite dilution, $\Delta\bar{H}^\circ$, is then given by

$$\Delta\bar{H}^\circ = \Delta\bar{H} - \sum n_P \varphi_{L,P} + \sum n_R \varphi_{L,R} \quad (6)$$

To estimate φ_L , we used the Debye-Hückel limiting law,¹⁹ expressed conventionally in the form of (7), where S_H is the limiting slope for relative partial molal enthalpy, z_i the charge number of the i th ionic species, and μ the ionic strength. If φ_L is expressed in kilocalories per mole and μ in moles per liter, S_H is given by (8), where ρ is the density

$$\varphi_{L,i} = (2/3)z_i^2 S_H \mu^{1/2} \quad (7)$$

$$S_H = \frac{12.53 \times 10^3 T^2}{(\epsilon T)^{3/2}} \left[\frac{1}{3} \left(\frac{d \ln \rho}{dT} \right) - \frac{d \ln (\epsilon T)}{dT} \right] \quad (8)$$

Table III: pK° and $\Delta\bar{C}_p^\circ$ for Self-Ionization and Heat Capacity of Liquid Methanol

Temp., °C	pK° (<i>m</i> scale) ^a	$\Delta\bar{C}_p^\circ$		$C_p^\circ(l)$ eq 10 ^{b,d}
		Obsd ^b	Calcd ^c	
-90	22.61	-24.2	-25.0	16.78
-80	21.74	-24.5	-25.1	16.81
-70	20.97	-25.6	-25.7	16.87
-60	20.28	-27.7	-26.8	16.97
-50	19.67	-29.0	-28.4	17.11
-40	19.12	-31.6	-30.5	17.28
-30	18.63	-34.9	-33.1	17.48
-20	18.19	-35.5	-36.3	17.72
-10	17.79	-40.1	-40.0	17.99
0	17.44	-43.0	-44.1	18.30
10	17.12	-46.0	-48.8	18.64
20	16.84	-52.1	-54.0	19.01
25	(16.71) ^e	...	-56.8	19.21
27.5	16.65	-59.0	-58.3	19.32
32.5	16.53	-64.2	-61.3	19.53

^a $K^\circ = (m_{H^+})(m_{OCH_3^-})/\gamma_{\pm}^2$. ^b In cal/mol deg. ^c Equation 10. ^d Based on ref 8 and 9. ^e Reference 13.

On applying these equations, $d \ln (\epsilon T)/dT$ was calculated from eq 1, $d \ln \rho/dT$ from data in ref 16, and φ_L for a univalent electrolyte ($= 4S_H \mu^{1/2}/3$). There is considerable cancellation of φ_L terms between reactant and product solutions. Thus in (3), $\Delta\bar{H}^\circ = \Delta\bar{H} + \varphi_{L,HCl}$; while in (4) and (5), the difference between $\Delta\bar{H}^\circ$ and $\Delta\bar{H}$ may be neglected in this approximation. Results obtained for ΔH° are included in Table II.

Table IV: Thermodynamic Data for Acid-Base Reactions of Benzoic Acid in Methanol

Temp., °C	pK_A° (<i>m</i> scale)	Acid dissociation $\Delta\bar{C}_p^\circ$		HBz + NaOCH ₃ $\Delta\bar{C}_p^\circ$ (obsd ^a)
		Obsd ^a	Calcd ^{a,b}	
-90	11.93	-2.7	-4.9	21.5
-80	11.54	-5.8	-5.3	18.7
-65	11.04	-8.7	-6.8	18.0
-45	10.48	-12.2	-10.8	18.1
-25	10.03	-17.4	-17.1	17.9
-10	9.75	-25.1	-23.3	15.0
0	9.60	-26.5	-28.1	16.5
10	9.46	-32.1	-33.5	13.9
20	9.34	-32.7	-39.4	19.4
25	(9.28) ^c
27.5	9.25	-44.2	-44.3	14.6
32.5	9.21	-53.8	-47.6	10.4

^a In cal/mol deg. ^b Equation 10. ^c Based on ref 6, 10, and 11.

Values of pK° and $\Delta\bar{C}_p^\circ$ derived from the $\Delta\bar{H}^\circ$ data are listed in Tables III and IV. Regarding $\Delta\bar{C}_p^\circ$, we computed $\delta\Delta\bar{H}^\circ/\delta T$ for each temperature interval in Table II and report the result as $\Delta\bar{C}_p^\circ$ at the mean temperature of the interval. Standard errors of $\Delta\bar{C}_p^\circ$ should be within $15/\delta T$ cal/mol deg; that is, the error in $\delta\Delta\bar{H}^\circ$ is within 15 cal/mol and the error in δT is relatively negligible. For most of the data, δT is 10° .

Of course, the errors for adjacent intervals are not independent.

Regarding pK° , we selected a value of 16.71, based on the work of Koskikallio,¹³ for the self-ionization of methanol at 25°, and a value of 9.28, the mean of several quite concordant values,^{6,10,11} for the acid dissociation of benzoic acid at 25°. Values at other temperatures were then obtained by integration according to (9), using relevant data in Table II. All pK values are on

$$pK^\circ_T = pK^\circ_{298.16} - \int_{298.16}^T (T^{-2}\Delta\bar{H}^\circ dT)/2.303R \quad (9)$$

the m (molal concentration) scale.

According to eq 9, the error of pK°_T is the sum of independent errors in $pK^\circ_{298.16}$ and in the magnitude of the integral, which in turn depends on the error in $\Delta\bar{H}^\circ$. The error in $pK^\circ_{298.16}$ is probably no less than 0.02 unit, judging by the reproducibility of the published data. Compared to that error, we now wish to show that the error in the magnitude of the integral is relatively small, even at the extreme of the temperature range. The maximum difference between pK°_T and $pK^\circ_{298.16}$ in Tables III and IV is 4.90 units. On estimating the error in $\Delta\bar{H}^\circ$ as 0.2% and neglecting the error of extrapolation to infinite dilution (a similar extrapolation, employing the Debye-Hückel theory, is used in obtaining pK° from pK at 298.16°, so at least there is no error owing to lack of consistency), we estimate an *upper limit* to the error in that difference of 0.2% of 4.90, or 0.01 pK unit. This estimate is conservative if the individual errors in $\Delta\bar{H}^\circ$ are random, because then their effects will tend to cancel in the integration.

Because of current research interest in the physical organic chemistry of polar nonaqueous solvents including methanol,²⁰ there is some need for reliable pH standards, especially at temperatures far removed from room temperature. On the basis of the preceding analysis and having demonstrated that accurate thermochemical measurements can be made over a wide temperature range, we believe that the best experimental approach may be to measure pK° directly only at one, preferably optimum, temperature and to derive pK° at other temperatures from measurements of $\Delta\bar{H}^\circ$. The pK° values in Tables III and IV will permit the preparation of solutions of known pH and $pOCH_3$ in methanol, especially if the ionic strength is kept near 0.015 M and activity coefficients are estimated by the Debye-Hückel theory.

Previous less accurate measurements of $\Delta\bar{H}^\circ$ for the reaction of hydrogen ion with methoxide ion in methanol near room temperature²¹ are in substantial agreement with ours.

Discussion

The data in Tables II to IV permit the tabulation of $\Delta\bar{G}^\circ$, $\Delta\bar{H}^\circ$, $\Delta\bar{S}^\circ$, and $\Delta\bar{C}_p^\circ$ for the given reactions over a

wide temperature range. Such information should be useful for testing diverse theories of solvation effects in ionic reactions, and we hope to publish on that subject at a future date. The present discussion will be limited to the temperature dependence of $\Delta\bar{C}_p^\circ$. Is there evidence for any abnormal absorption of heat, of the sort that can be ascribed to endothermic processes involving the solvated ions?

In the preceding study of $\Delta\bar{C}_p^\circ$ for acid-base reactions in water,⁴ the most revealing evidence was found in the self-ionization of water, where $\Delta\bar{C}_p^\circ$ went through a maximum near 35°. That maximum was sufficiently sharp so that $\Delta\bar{C}_p^\circ$ clearly became less than the maximum within about 10°.

In the present study, if we discount random fluctuations, $\Delta\bar{C}_p^\circ$ in Tables III and IV reaches a stationary value only at the lowest temperatures: for all three reactions, the change in $\Delta\bar{C}_p^\circ$ becomes quite gradual below about -65°. A similar approach to a stationary value near -90° has been observed in the case of $C_p^\circ(l)$ for liquid methanol, where precise and generally concordant data from two laboratories^{8,9} are available between -93 and 20° (Table III).

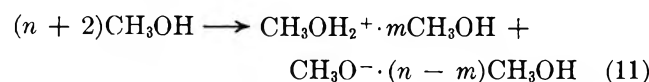
We find that the heat capacity data can be represented in each case by a quadratic equation, which fits over the entire temperature range with apparently random deviations. Because of our interest in stationary values, we shall write the quadratic equation in the form (10), where a , b , and θ are adjustable parameters and T is the absolute temperature. Thus θ is

$$\Delta\bar{C}_p^\circ \text{ (or } C_p^\circ(l)) = a + b(T - \theta)^2 \quad (10)$$

the temperature at which $\Delta\bar{C}_p^\circ$ or $C_p^\circ(l)$ is stationary.

Least-squares values of the parameters are listed in Table V, where the parameters are given with at least one insignificant guard figure. The quality of the fit is illustrated in Tables III and IV. The reaction of HBz with $NaOCH_3$ is not included in this treatment because the temperature dependence of $\Delta\bar{C}_p^\circ$ is too slight to support the use of a three-parameter equation. However, $\Delta\bar{C}_p^\circ$ for that reaction must be the difference of $\Delta\bar{C}_p^\circ$ for reactions B and A.

The θ values in Table V are remarkably similar and fall just above the melting point of methanol, 175.3°K. To interpret the near coincidence, we recall that ionic charge is produced in reactions A and B, and we therefore assume that a number of methanol molecules become immobilized. For example, self-ionization (reaction A) might be formulated as in



(20) See, for example, C. W. Clare, D. Cook, E. C. F. Ko, Y. C. Mac, and A. J. Parker, *J. Amer. Chem. Soc.*, **88**, 1911 (1966); C. D. Ritchie and R. E. Uschold, *ibid.*, **90**, 2821 (1968).

(21) J. H. Wolfenden, W. Jackson, and H. B. Hartley, *J. Phys. Chem.*, **31**, 850 (1927); J. Koskikallio *Suomen Kemistilehti*, **B**, **30**, 155 (1957).

Table V:^a Fit of $C_p^\circ(l)$ and of $\Delta\bar{C}_p^\circ$ for Reactions in Methanol to Eq 10

	Variable		$\theta, ^\circ K$
	a	$10^6 b$	
$C_p^\circ(l)$ for MeOH	16.773	1.716	178.87
$\Delta\bar{C}_p^\circ$ for A	-25.0	-25.7	186.78
$\Delta\bar{C}_p^\circ$ for B	-4.9	-28.0	182.24

^a MeOH is liquid methanol; data of ref 8 and 9. A is the self-ionization of methanol; data in Table III. B is the acid dissociation of HBz; data in Table IV.

On that basis, $\Delta\bar{C}_p^\circ = \bar{C}_p^\circ(\text{solv ions}) - (n + 2)C_p^\circ(l)$.

We shall further assume that in the absence of endo-thermic processes in the solvation shells, $\bar{C}_p^\circ(\text{solv ions})$ will increase with temperature only gently. (The heat capacity of solid methanol, which perhaps is a model for the heat capacity of methanol "frozen" in a solvation shell around an ion, has a Debye temperature of 138°K.) However, if $d\bar{C}_p^\circ(\text{solv ions})/dT \approx 0$, then $d\Delta\bar{C}_p^\circ/dT \approx -(n + 2)dC_p^\circ(l)/dT$; that is, the plots of $\Delta\bar{C}_p^\circ$ vs. T and of $C_p^\circ(l)$ vs. T differ only by a scaling factor of $-(n + 2)$, and the near equality of θ is accounted for.

To make the analysis more quantitative, we assume that the heat capacity of the solvated ions can be represented by a quadratic equation and write

$$\bar{C}_p^\circ(\text{solv ions}) = \alpha + \beta T + \gamma T^2 = \Delta\bar{C}_p^\circ + (n + 2)C_p^\circ(l) \quad (12)$$

On substituting numerical values from Table V for the quantities on the right in (12) and the solving for α , β , and γ , we obtain eq 13 for the self-ionization (reaction A). If β and γ are indeed small, as assumed, then

$$\alpha = -114.6 + 22.263(n + 2) \quad (13a)$$

$$\beta = (95.7 - 6.14(n + 2)) \times 10^{-2} \quad (13b)$$

$$\gamma = (-25.7 - 1.716(n + 2)) \times 10^{-4} \quad (13c)$$

$n + 2 \approx 95.7/6.14 = 15.6$ from (13b), $n + 2 \approx 1.716 = 15.0$ from (13c). Although exact equality is not to be expected, the discrepancy is small enough to support the assumption. For acid dissociation of benzoic acid (reaction B), $n + 1$ is found by the same method to be 16.7 by setting $\beta = 0$ and 16.4 by setting $\gamma = 0$.

As with most estimates of solvation numbers, the present values can be relied upon only as to order of magnitude. However, this method represents an improvement over some earlier methods because we show (within the framework of our assumptions) that the number of solvent molecules that becomes frozen does not change with the temperature. In water, where the solvated ions are found, by the same approach, to undergo endothermic processes, the estimation of solvation numbers from thermodynamic data is far more difficult. As reported in the preceding paper,⁴ our best estimate of a hydration number for the low-temperature form of $H_3O^+ + OH^-$ is 14, in close agreement with the preceding estimates of solvation numbers for similar ions in methanol.

Dissociation Constant of Protonated

2,2-Bis(hydroxymethyl)-2,2',2''-nitrilotriethanol (Bis-tris)

and Related Thermodynamic Functions from 0 to 50°

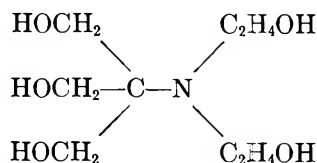
by Maya Paabo and Roger G. Bates

National Bureau of Standards, Washington, D. C. 20234 (Received August 11, 1969)

The acidic dissociation constant of protonated 2,2-bis(hydroxymethyl)-2,2',2''-nitrilotriethanol (bis-tris) has been determined at 11 temperatures from 0 to 50° by emf measurements of hydrogen-silver chloride cells without liquid junction. At 25°, pK_a is 6.483, and consequently buffer solutions of the base and its hydrochloride are useful for pH control in the region pH 5.5 to 7.5. The values of pK_a over the temperature range studied are given as a function of the thermodynamic temperature (T) by the equation $pK_a = 1287.855/T + 2.7905 - 0.00210396T$. Standard thermodynamic functions for the acidic dissociation process have been derived. At 25°, $\Delta H^\circ = 28,238 \text{ J mol}^{-1}$ (6749 cal mol⁻¹), $\Delta S^\circ = -29.4 \text{ J K}^{-1} \text{ mol}^{-1}$ (-7.0 cal deg⁻¹ mol⁻¹), and $\Delta C_p^\circ = 24 \text{ J K}^{-1} \text{ mol}^{-1}$ (5.7 cal deg⁻¹ mol⁻¹). Conventional p_{aH} values for five equimolar buffer solutions composed of bis-tris and its hydrochloride have been calculated.

Introduction

The control of pH in the physiologically important range of acidities is rendered difficult by the scarcity of weak acid-base systems with pK between 6 and 8. Tris(hydroxymethyl)aminomethane, known variously as "THAM" or "tris," has been shown to be a useful biochemical buffer in the range pH 7 to 9,¹⁻⁴ and the pK of the protonated base has been carefully measured over the range 0 to 50°.^{5,6} Attention has recently been focused on the N,N-bis(2-hydroxyethyl) derivative of tris, termed "bis-tris," which, with a pK_a of 6.46, promises to make possible the control of pH between 5.5 and 7.5 at 25°.⁷ The free base is named 2,2-bis(hydroxymethyl)-2,2',2''-nitrilotriethanol and has the formula

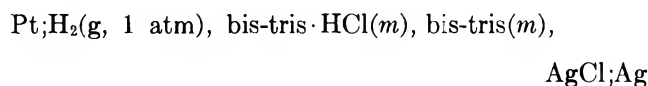


It is not difficult to prepare⁷ and is now available commercially.

In an extension of our studies of the thermodynamics of the dissociation of protonated weak bases,⁸ we have now determined the pK_a of bis-tris at 11 temperatures from 0 to 50°. From the data, the standard enthalpy, entropy, and heat capacity changes for the dissociation process have been evaluated. In addition, conventional p_{aH} values for equimolar buffer solutions composed of bis-tris and its hydrochloride have been calculated.

Method

The emf method used is essentially that of Harned and Ehlers,⁹ and the procedures were the same in nearly all respects as in the study of other bases.^{5,8,10} The cell, which had no liquid junction, can be represented by



The molalities (m) of bis-tris and its hydrochloride were equal in all of the buffer solutions.

The solubility of silver chloride in a 0.1 M solution of bis-tris was found to be about 0.0003 mol l.⁻¹. Since this value is so low, a correction to the molality of chloride ion in the solution is unnecessary.¹⁰ Furthermore, the pH of all of the cell solutions was so close to neutrality that the buffer ratio remained at unity, no corrections for hydrolysis being needed.

- (1) G. Gomori, *Proc. Soc. Exptl. Biol. Med.*, **62**, 33 (1946).
- (2) H. Stormorken and T. F. Newcomb, *Scand. J. Clin. Lab. Invest.*, **8**, 237 (1956).
- (3) G. G. Nahas and H. Rosen, *Fed. Proc.*, **18**, 111 (1959).
- (4) R. G. Bates and V. E. Bower, *Anal. Chem.*, **28**, 1322 (1956).
- (5) R. G. Bates and H. B. Hetzer, *J. Phys. Chem.*, **65**, 667 (1961).
- (6) S. P. Datta, A. K. Grzybowski, and B. A. Weston, *J. Chem. Soc.*, 792 (1963).
- (7) J. C. Lewis, *Anal. Biochem.*, **14**, 495 (1966).
- (8) See H. B. Hetzer, R. A. Robinson, and R. G. Bates, *J. Phys. Chem.*, **72**, 2081 (1968), and citations to earlier work given there.
- (9) H. S. Harned and R. W. Ehlers, *J. Amer. Chem. Soc.*, **54**, 1350 (1932).
- (10) R. G. Bates and G. D. Pinching, *J. Res. Nat. Bur. Stand.*, **42**, 419 (1949).

Table I: Electromotive Force of the Cell Pt;H₂(g, 1 atm), Bis-tris·HCl(*m*), Bis-tris (*m*), AgCl;A₂ from 0 to 50° (in V)

<i>m</i>	0°	5°	10°	15°	20°	25°	30°	35°	40°	45°	50°
0.009032	0.72776	0.72899	0.73005	0.73091	0.73159	0.73210	0.73244	0.73255	0.73270	0.73250	0.73235
0.01328	0.71964	0.72070	0.72160	0.72231	0.72283	0.72320	0.72338	0.72345	0.72335	0.72309	0.72270
0.01884	0.71240	0.71334	0.71411	0.71468	0.71507	0.71530	0.71536	0.71528	0.71505	0.71467	0.71416
0.02707	0.70506	0.70585	0.70648	0.70691	0.70716	0.70725	0.70719	0.70698	0.70660	0.70609	0.70547
0.02868	0.70394	0.70471	0.70530	0.70571	0.70592	0.70599	0.70591	0.70556	0.70527	0.70473	0.70408
0.03851	0.69814	0.69879	0.69927	0.69956	0.69968	0.69964	0.69943	0.69910	0.69859	0.69795	0.69717
0.04634	0.69451	0.69508	0.69550	0.69572	0.69577	0.69566	0.69538	0.69494	0.69436	0.69366	0.69284
0.04776	0.69394	0.69451	0.69490	0.69511	0.69514	0.69502	0.69474	0.69432	0.69374	0.69302	0.69216
0.05298	0.69198	0.69250	0.69284	0.69300	0.69299	0.69280	0.69251	0.69204	0.69142	0.69067	0.68978
0.05698	0.69062	0.69110	0.69144	0.69156	0.69151	0.69132	0.69100	0.69051	0.68987	0.68909	0.68818
0.06490	0.68816	0.68858	0.68886	0.68895	0.68886	0.68863	0.68822	0.68758	0.68699	0.68617	0.68521
0.06634	0.68775	0.68819	0.68844	0.68852	0.68843	0.68818	0.68775	0.68720	0.68649	0.68565	0.68468
0.07323	0.68595	0.68633	0.68654	0.68656	0.68642	0.68614	0.68570	0.68511	0.68437	0.68350	0.68250
0.07936	0.68453	0.68479	0.68498	0.68499	0.68482	0.68450	0.68402	0.68340	0.68264	0.68173	0.68071
0.08593	0.68301	0.68333	0.68348	0.68345	0.68325	0.68289	0.68239	0.68174	0.68094	0.68001	0.67895
0.08738	0.68273	0.68303	0.68317	0.68313	0.68291	0.68255	0.68205	0.68140	0.68060	0.67966	0.67860
0.09843	0.68055	0.68080	0.68090	0.68081	0.68056	0.68016	0.67961	0.67889	0.67805	0.67708	0.67625

The data for the emf (*E*) were used to derive acidity functions $p(a_{\text{H}\gamma\text{Cl}})$ for each of the cell solutions at all 11 temperatures by the equation

$$p(a_{\text{H}\gamma\text{Cl}}) \equiv -\log(m_{\text{H}^+}\gamma_{\text{H}^+}\gamma_{\text{Cl}^-}) = \frac{E - E^\circ}{(RT \ln 10)/F} + \log m \quad (1)$$

where E° is the standard emf of the cell.¹¹ With the use of the mass law and the Debye-Hückel equation, the "approximate" dissociation constant K_a' was derived from the activity function

$$pK_a - \beta m = p(a_{\text{H}\gamma\text{Cl}}) - \frac{2Am^{1/2}}{1 + B\tilde{a}m^{1/2}} \equiv pK_a' \quad (2)$$

where *A* and *B* are constants of the Debye-Hückel theory and \tilde{a} and β are empirical parameters, the former being the ion-size parameter and the latter the slope parameter. The intercept of pK_a' at $m = 0$ is pK_a . Values of pK_a , β , and \tilde{a} for the 11 temperatures were found by the method of nonlinear least squares using the relation set forth in eq 2.

Experimental Section

A commercial sample of bis-tris was purified by repeated recrystallization from absolute ethanol. The product had a melting point of 104.0–104.5°; it assayed 99.98% (std dev = 0.01) when titrated with a standard solution of hydrochloric acid under carbon dioxide-free conditions to a calculated end point of pH equal to 3.74 (0.1 *M* solution).

Attempts to prepare bis-tris hydrochloride by passing dry hydrogen chloride gas into a solution of bis-tris in methanol yielded a product which assayed only 99.8% by determination of its chloride content. For this reason, the solutions used for the emf measurements were made by dissolving the crystalline base in a standard solution of hydrochloric acid prepared from twice-distilled 6 *M* acid. The acid solution was standardized

by gravimetric determination of chloride (weighed as silver chloride).

The preparation of cell solutions and electrodes followed the usual procedures of this laboratory. Seventeen different buffer concentrations were studied in three different series of measurements. The molality *m* was varied between 0.009 and 0.1. The emf readings were made between 0 and 50° over a 3-day period. Initial and final measurements were made at 25°. The cells showed excellent stability, the initial and final emf readings agreeing well within 0.05 mV.

Results

The emf data, corrected to a hydrogen partial pressure of 1 atm, are summarized in Table I. The values of pK_a and \tilde{a} derived from the experimental data are listed in Table II. The estimated uncertainties in pK_a are given in the third column. They are approximately two standard deviation limits. These standard deviations were estimated from the last iteration of a nonlinear fitting procedure based on a Taylor series expansion about the estimated values.

Table II: pK_a of Protonated Bis-tris from 0 to 50°

<i>t</i> , °C	pK_a^a	Estimated uncertainty	pK_a , calcd ^b	\tilde{a} , Å
0	6.9314	0.0010	6.9306	1.9
5	6.8344	0.0007	6.8353	2.0
10	6.7429	0.0006	6.7431	2.2
15	6.6536	0.0005	6.6536	2.5
20	6.5665	0.0005	6.5669	2.6
25	6.4835	0.0006	6.4827	2.8
30	6.4013	0.0006	6.4009	2.8
35	6.3212	0.0008	6.3215	2.9
40	6.2441	0.0008	6.2442	3.2
45	6.1690	0.0008	6.1691	3.2
50	6.0959	0.0022	6.0959	3.4

^a Derived from the experimental data by eq 2. ^b pK_a (calcd) = 1287.855/*T* + 2.7905 - 0.00210396*T*.

(11) R. G. Bates and V. E. Bowser, *J. Res. Nat. Bur. Stand.*, **53**, 283 (1954).

Table III: Thermodynamic Functions for the Acidic Dissociation of Bis-tris·H⁺ at 15, 25, and 35°

	15°	25°	35°
ΔH° , J mol ⁻¹	28,001 (6692) ^a	28,238 (6749)	28,482 (6807)
ΔS° , J K ⁻¹ mol ⁻¹	-30.2 (-9.5)	-29.4 (-7.0)	-28.6 (-6.8)
ΔC_p° , J K ⁻¹ mol ⁻¹	23 (5.5)	24 (5.7)	25 (6.0)

^a Values in parentheses are in calories (1 cal = 4.184 J).

The calculated values of pK_a given in the fourth column were computed from the equation

$$pK_a = 1287.855/T + 2.7905 - 0.00210396T \quad (3)$$

where T is the thermodynamic temperature in Kelvins. The constants in eq 3 were estimated by the method of least squares from the pK_a values in second column using the OMNITAB computer program. The residual standard deviation of the fit was 0.0007. The pK_a value reported in Table II (6.483) at 25° is slightly higher than that quoted by Lewis⁷ (6.46).

Thermodynamic Functions

The standard thermodynamic functions characterizing the dissociation of protonated bis-tris were calculated by the usual thermodynamic formulas from the constants of eq 3. The values for 15, 25, and 35° are listed in Table III. The estimated uncertainties in these values at 25° are ΔH° , 37 J mol⁻¹ (8.8 cal mol⁻¹); ΔS° , 0.1 J K⁻¹ mol⁻¹ (0.1 cal deg⁻¹ mol⁻¹); ΔC_p° , 5 J K⁻¹ mol⁻¹ (1.2 cal deg⁻¹ mol⁻¹). These uncertainties represent approximately two standard deviation limits obtained using the method of propagation of error.

pa_H Values

Conventional pa_H values for equimolar buffer solutions composed of bis-tris and its hydrochloride were calculated from the acidity functions $p(a_{H\gamma_{Cl}})$. The convention used for the evaluation of the activity coefficient of chloride ion was the same one on which the NBS standard pH scale is based¹²

$$pa_H \equiv p(a_{H\gamma_{Cl}}) - \frac{Am^{1/2}}{1 + 1.5m^{1/2}} \quad (4)$$

The values of the Debye-Hückel constant A at the 11 temperatures are listed elsewhere.¹³

Bis-tris buffers should prove useful in controlling pH near the neutral point for equilibrium and kinetic studies. The values given in Table IV show that the dilution or concentration effect on pa_H is small but that dpH/dt amounts to about 0.016 pH K⁻¹ near room temperature.

Inasmuch as the convention on which these pa_H values are based is presumed to be exact by definition, the uncertainty in pa_H arises solely from uncertainties in E , E° , and the natural constants on which the acidity function $p(a_{H\gamma_{Cl}})$ is based. The total error in the pa_H

Table IV: Conventional pa_H Values for Equimolar Bis-tris Buffer Solutions: Bis-tris·HCl (m), Bis-tris (m) from 0 to 50°

t , °C	Molality (m)				
	0.02	0.04	0.06	0.08	0.1
0	7.000	7.029	7.050	7.067	7.082
5	6.905	6.932	6.953	6.969	6.983
10	6.812	6.839	6.859	6.876	6.889
15	6.722	6.748	6.767	6.783	6.796
20	6.635	6.662	6.681	6.696	6.710
25	6.551	6.577	6.595	6.610	6.623
30	6.469	6.495	6.513	6.528	6.540
35	6.390	6.415	6.434	6.448	6.460
40	6.312	6.336	6.353	6.367	6.378
45	6.237	6.262	6.280	6.294	6.306
50	6.165	6.190	6.208	6.222	6.235

values is therefore about 0.002 to 0.004 unit, the highest uncertainties being at the extreme temperatures of 0 and 50°. It must be cautioned, however, that residual liquid-junction potentials may lead to discrepancies greater than 0.01 unit when bis-tris buffer solutions are compared with the primary pH standard solutions in a pH assembly with liquid junction. Similar (but smaller) differences have been observed with tris buffers and other buffer mixtures of the charge type R·NH₃⁺, RNH₂. The departures are in the same direction as are found for solutions with pH in excess of 11.¹⁴ This similarity suggests that the mobility of the anion (chloride) is markedly greater than that of the cation (protonated bis-tris). The lowered mobility is consistent with the highly hydrophilic character imparted to the ion by the five terminal OH groups.

Discussion

The pK_a and thermodynamic functions for the dissociation of protonated bis-tris are compared in Table V with the corresponding values for other compounds (R·NH₃⁺) structurally related to bis-tris·H⁺. As Timimi and Everett¹⁶ have pointed out, hydroxymethyl or hydroxyethyl substitution uniformly results in a lowering of pK_a , ΔG° , and ΔH° . It seems likely that

(12) R. G. Bates and E. A. Guggenheim, *Pure Appl. Chem.*, **1**, 163 (1960).

(13) R. G. Bates, "Determination of pH," John Wiley & Sons, Inc., New York, N. Y., 1964, p 406.

(14) Reference 13, Chapter 3.

Table V: Thermodynamic Functions at 25° for the Dissociation of Protonated Bases Structurally Related to Bis-tris·H⁺

Acid	pK _a	ΔH° J mol ⁻¹	ΔS° J K ⁻¹ mol ⁻¹	ΔC _p ° J K ⁻¹ mol ⁻¹	Ref.
(CH ₃) ₃ C·NH ₃ ⁺	10.685	60,070 (14,508) ^a	-3.1 (-0.7)	15 (3.6)	15
(CH ₃) ₂ (CH ₂ OH)C·NH ₃ ⁺	9.694	53,948 (12,894)	-4.6 (-1.1)	-19 (-4.5)	16
CH ₃ (CH ₂ OH) ₂ C·NH ₃ ⁺	8.797	49,794 (11,901)	-1.3 (-0.3)	-45 (-10.7)	16, 17
(CH ₂ OH) ₂ C·NH ₃ ⁺	8.072	47,488 (11,350)	4.8 (1.2)	-78 (-18.6)	5, 6
(CH ₂ OH) ₃ C·NH(C ₂ H ₄ OH) ₂ ⁺	6.483	28,238 (6749)	-29.4 (-7.0)	24 (5.7)	This work

^a Values in parentheses are in calories (1 cal = 4.184 J).

these relatively bulky hydrophilic substituent groups partially shield the basic nitrogen and make the interaction with hydrogen ions more difficult. This is especially true of N substitution. The effect on ΔS° of the first hydroxyl substitution in the radical R is small, but N substitution of either alkyl groups¹⁶ or hydroxyethyl groups (Table V) results in rather appreciable negative entropy effects. Increased ordering is implied, and it may indicate a stabilization of the solvent structure in the vicinity of the molecules of uncharged base.

The contrary variation of ΔS° and ΔC_p°, apparent in Table V, has long been difficult to explain. Electrostatic interactions with charged species lead to an orientation of polar solvent molecules in the vicinity of the ions and presumably lower both the entropy and

heat capacity of the system. However, the current view is that other "hydrophobic interactions" between uncharged molecules and the water structure may lead to both a decrease in entropy and an increase in heat capacity.¹⁸ The nature of these interactions is not yet fully understood.

Acknowledgment. The authors are indebted to Brian L. Joiner for assistance in the statistical analysis of the data.

- (15) H. B. Hetzer, R. A. Robinson, and R. G. Bates, *J. Phys. Chem.*, **66**, 2696 (1962).
 (16) B. A. Timimi and D. H. Everett, *J. Chem. Soc., B*, 1380 (1968).
 (17) H. B. Hetzer and R. G. Bates, *J. Phys. Chem.*, **66**, 308 (1962).
 (18) M. C. Cox, D. H. Everett, D. A. Landsman, and R. J. Munn, *J. Chem. Soc., B*, 1373 (1968).

Deuterium Isotope Effects and the Dissociation of Deuteriophosphoric Acid from 5 to 50°

by Maya Paabo and Roger G. Bates

National Bureau of Standards, Washington D. C. 20234 (Received August 11, 1969)

The first dissociation constant of deuteriophosphoric acid in deuterium oxide has been determined over the temperature range 5 to 50° from emf measurements of cells using deuterium gas electrodes and silver-silver chloride electrodes, with the following results: $pK_1 = 843.979/T - 4.5714 + 0.0139555T$, where T is the thermodynamic temperature. The changes of enthalpy, entropy, and heat capacity characterizing the dissociation process have been derived from pK_1 and its temperature coefficient. By comparison of the results with similar data for protiophosphoric acid in water, the deuterium isotope effects on pK_1 and the thermodynamic functions have been evaluated. The isotope effect $pK_1(\text{in D}_2\text{O}) - pK_1(\text{in H}_2\text{O})$ is 0.272 unit and almost unchanged over the temperature range studied. This value confirms a linear relationship between the isotope effect for inorganic acids and pK (in H_2O).

Introduction

A recent paper¹ has focused attention once again on the relationship between acidic strength and the deuterium isotope effect on the dissociation as measured by $pK(\text{in D}_2\text{O}) - pK(\text{in H}_2\text{O})$. It was shown that this difference, or ΔpK , is not uniformly a linear function of $pK(\text{in H}_2\text{O})$ in spite of earlier evidence supporting a linear variation.²⁻⁵ As a group, inorganic acids fell close to a single straight line, especially those with pK greater than 7. However, a critical examination of the data for a considerable number of organic acids, both carboxylic acids and substituted ammonium ions, led to ΔpK in the vicinity of 0.5 to 0.6, even though the corresponding pK values in water ranged from 0 to 6.

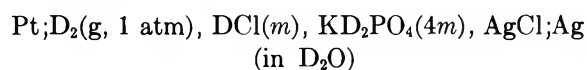
To make the situation still more complex, the points for the two strongest inorganic acids that have been studied (bisulfate ion and phosphoric acid) fell near, but not exactly on, the straight line fixed by the data for the inorganic acids of pK greater than 7. Because of the high degree of dissociation of these acids, accurate pK values are difficult to obtain. Nevertheless, it has been shown that reliable values for the first dissociation constant of phosphoric acid can be determined by confining the measurements to buffer mixtures in which the concentration of dihydrogen phosphate ion considerably exceeds that of the phosphoric acid.⁶ A similar procedure has now been applied to a determination of the pK of deuteriophosphoric acid in deuterium oxide. From the results and those for the pK in water, a new value of ΔpK which lies almost exactly on the straight line passing through the ΔpK values for other inorganic acids of higher pK has been obtained.

The pK_1 for deuteriophosphoric acid in deuterium oxide was determined at ten temperatures from 5 to 50° by the analysis of emf data for cells without liquid junction containing deuterium gas electrodes and silver-silver chloride electrodes. The thermodynamic func-

tions—enthalpy, entropy, and heat capacity—characterizing the dissociation of deuteriophosphoric acid in D_2O have been derived from pK_1 and its temperature coefficient. The deuterium isotope effect, namely $pK_1(\text{in D}_2\text{O}) - pK_1(\text{in H}_2\text{O})$, was found to be 0.272 unit and to remain almost unchanged between 5 and 50°.

Method

The cell can be represented



where m is the molality in mol kg^{-1} . The standard emf (E°) of this cell being known,⁷ the pK_1 for deuteriophosphoric acid in D_2O can be related to the emf (E) by

$$pK_1 = \frac{(E - E^\circ)F}{(RT \ln 10)} + \log m + \log \frac{m_{\text{D}_3\text{PO}_4}}{m_{\text{D}_2\text{PO}_4^-}} + \log \frac{\gamma_{\text{D}_3\text{PO}_4} \gamma_{\text{Cl}^-}}{\gamma_{\text{D}_2\text{PO}_4^-}} \quad (1)$$

The last term of eq 1 is expected to be small in very dilute solutions and to vary linearly with ionic strength (I) at higher concentrations. Hence

$$pK_1' = pK_1 - \beta I = \frac{(E - E^\circ)F}{(RT \ln 10)} + \log \frac{m \cdot m_{\text{D}_3\text{PO}_4}}{m_{\text{D}_2\text{PO}_4^-}} \quad (2)$$

(1) R. A. Robinson, M. Paabo, and R. G. Bates, *J. Res. Nat. Bur. Stand.*, **73A**, 299 (1969).

(2) R. P. Bell, "The Proton in Chemistry," Cornell University Press, Ithaca, N. Y., 1959, Chapter 11.

(3) P. Ballinger and F. A. Long, *J. Amer. Chem. Soc.*, **82**, 795 (1960).

(4) N. C. Li, P. Tang, and R. Mathur, *J. Phys. Chem.*, **65**, 1074 (1961).

(5) See also E. Högfeldt and J. Bigeleisen, *J. Amer. Chem. Soc.*, **82**, 15 (1960).

(6) R. G. Bates, *J. Res. Nat. Bur. Stand.*, **47**, 127 (1951).

(7) R. Gary, R. G. Bates, and R. A. Robinson, *J. Phys. Chem.*, **68**, 1186 (1964).

where pK_1' , the approximate value of pK_1 at finite I , becomes equal to pK_1 on linear extrapolation to $I = 0$.

The deuteriophosphoric acid is rather extensively ionized, even though the stoichiometric ratio of $D_2PO_4^-$ to D_3PO_4 was kept at a high value (3) to repress ionization. Consequently, estimation of m_{D^+} was necessary in order to calculate the second term on the right of eq 2 with the required accuracy

$$\frac{m \cdot m_{D_2PO_4}}{m_{D_2PO_4^-}} = \frac{m(m - m_{D^+})}{3m + m_{D^+}} \quad (3)$$

It was evaluated from the acidity function $p(a_D\gamma_{Cl})$, together with values of the mean activity coefficient of deuterium chloride calculated by a Debye-Hückel formula

$$\begin{aligned} -\log m_{D^+} &= p(a_D\gamma_{Cl}) + 2 \log \gamma_{\pm} (DCl) \\ &= \frac{(E - E^\circ)F}{RT \ln 10} + \log m - \frac{2A(I d_0)^{1/2}}{1 + B\hat{a}(I d_0)^{1/2}} \end{aligned} \quad (4)$$

In eq 4, A and B are the Debye-Hückel constants for the appropriate temperature and solvent dielectric constant,⁷ \hat{a} is the ion-size parameter, and d_0 is the density of the solvent.⁸ The ionic strength is given by

$$I = 4m + m_{D^+} \quad (5)$$

It was shown earlier⁶ that the estimation of m_{D^+} (or m_{H^+}) introduces the major uncertainty into the determination of pK values for moderately strong acids by the emf method. In the present work, a computer program combining eq 2, 3, 4, and 5 was written. Values of the ion-size parameter \hat{a} were selected, and corresponding values of pK_1' were computed. The intercept pK_1 was obtained by the method of least squares, and the standard deviation of the intercept was derived. The value of the ion-size parameter which yielded the smallest standard deviation for pK_1 was judged to be the best choice. The \hat{a} values all fell in the range 4.5 to 5.5 Å, showing no dependence on temperature. It is noteworthy that this is of the same order (4.3 to 5.0 Å) found for HCl in water⁹ and for DCl in deuterium oxide⁷ over this temperature range. However, in the present procedure, \hat{a} enters only indirectly in a correction term (eq 4).

Experimental Section

Materials. Potassium dihydrogen phosphate, NBS Standard Reference Material 2186I, was used. It was heated at 120° for 2 hr. The salt was converted into KD_2PO_4 upon solution in deuterium oxide; the resulting contamination of the solvent (0.4 atom % hydrogen in the most concentrated of the cell solutions) was too slight to be of concern.

The deuterium oxide used had an isotopic purity of 99.8% and a conductivity of $9 \times 10^{-7} \Omega^{-1} \text{cm}^{-1}$ at

25°. Deuterium gas, obtained commercially, was analyzed by mass spectrometry at intervals during the course of the work. The results uniformly indicated a hydrogen content less than 0.5 atom %. The stock solution of deuterium chloride was prepared by diluting a commercial sample of the acid (20% DCl in D_2O) with deuterium oxide. Its molality was determined by coulometric analysis.

Cells and Procedures. The cells were of all-glass construction except for the Teflon stopcock plugs. These cells have been described in ref 7. The procedures differed slightly from those followed earlier, in that the vacuum treatment of the electrodes was omitted. Instead, the solutions were saturated with deuterium gas, and the cell vessels were flushed with deuterium before the solutions were admitted. The measurements at the ten temperatures extended over a period of 3 days. A comparison of the initial and final emf at 25° indicated excellent stability during this period, the average change for all cells during the course of the run being only 0.05 mV. To conserve deuterium gas, the flow was interrupted during the night when measurements were not being made.

Results

The observed emf values recorded at a total pressure (deuterium gas plus solvent vapor) equal to the atmospheric pressure were corrected in the usual way to a deuterium partial pressure of 1 atm. The corrected values are summarized in Table I. In the analysis of the data, a range of values of the ion-size parameter \hat{a} was chosen, and the corresponding intercepts (pK_1) were obtained in the manner already described, together with the standard deviations of the intercepts. The best estimates of \hat{a} and pK_1 were assumed to be those for which the standard deviation was at a minimum. This criterion, adopted in the analysis of the data for the standard emf of the hydrogen-silver chloride cell in ordinary water,⁹ has proved useful in many other similar studies in this laboratory.

The values of pK_1 and the corresponding standard deviations of the intercepts are listed in Table II. The dissociation constants are based on the molal scale. The experimental values of pK_1 can be expressed by the equation

$$pK_1 = 843.979/T - 4.5714 + 0.0139555T \quad (6)$$

where T is the thermodynamic temperature, $t(^{\circ}\text{C}) + 273.15$. The standard deviation of the ten pK_1 values from those calculated by this equation is 0.0003. The constants of eq 6 were found by the method of least squares with the aid of the OMNITAB program. The pK_1 in water is listed in the next to the last column and

(8) T. L. Chang and L. H. Tung, *Chinese J. Phys.*, **7**, 230 (1949).

(9) R. G. Bates and V. E. Bower, *J. Res. Nat. Bur. Stand.*, **53**, 283 (1954).

Table I: Electromotive Force of the Cell Pt;D₂(g, 1 atm), DCl(*m*), KD₂PO₄(4*m*), AgCl;Ag from 5 to 50° (in V)

<i>m</i>	5°	10°	15°	20°	25°	30°	35°	40°	45°	50°
0.003416	0.52942	0.53258	0.53564	0.53865	0.54161	0.54444	0.54725	0.54997	0.55269	0.55537
0.004754	0.51898	0.52200	0.52495	0.52785	0.53069	0.53347	0.53616	0.53887	0.54149	0.54408
0.008000	0.50347	0.50629	0.50904	0.51164	0.51431	0.51700	0.51957	0.52207	0.52454	0.52697
0.01044	0.49570	0.49841	0.50106	0.50362	0.50621	0.50880	0.51125	0.51372	0.51611	0.51844
0.01448	0.48642	0.48901	0.49153	0.49399	0.49646	0.49888	0.50125	0.50355	0.50585	0.50811
0.01976	0.47793	0.48039	0.48280	0.48520	0.48755	0.48987	0.49211	0.49437	0.49655	0.49863
0.02496	0.47164	0.47402	0.47633	0.47861	0.48090	0.48312	0.48533	0.48745	0.48956	0.49163
0.02946	0.46716	0.46946	0.47172	0.47395	0.47615	0.47835	0.48046	0.48258	0.48462	0.48662
0.03467	0.46279	0.46506	0.46724	0.46940	0.47155	0.47365	0.47574	0.47774	0.47975	0.48166
0.03936	0.45951	0.46171	0.46386	0.46588	0.46796	0.47022	0.47222	0.47425	0.47618	0.47808
0.04487	0.45597	0.45813	0.46021	0.46227	0.46431	0.46636	0.46835	0.47026	0.47216	0.47403
0.04876	0.45368	0.45580	0.45787	0.45990	0.46191	0.46395	0.46587	0.46781	0.46966	0.47149

Table II: Dissociation Constant of Deuteriophosphoric Acid in Deuterium Oxide from 5 to 50° and Related Isotope Effect

<i>t</i> , °C	p <i>K</i> ₁ , D ₂ O, exptl	Std dev ^a	p <i>K</i> ₁ (H ₂ O) ^b	Δ <i>pK</i>
5	2.3445	0.0007	2.071	0.273
10	2.3610	0.0007	2.088	0.273
15	2.3788	0.0007	2.106	0.273
20	2.3981	0.0005	2.127	0.271
25	2.4202	0.0005	2.148	0.272
30	2.4437	0.0007	2.171	0.273
35	2.4677	0.0007	2.196	0.272
40	2.4939	0.0008	2.222	0.272
45	2.5211	0.0007	2.249	0.272
50	2.5501	0.0008	2.278	0.272

^a At each temperature, *n* = 12. ^b Reference 6.

the isotope effect, Δ*pK* = p*K*₁(in D₂O) - p*K*₁(in H₂O), in the last column.

To provide a further confirmation of the magnitude of the isotope effect, a series of measurements of p*K*₁ in ordinary water was also made, following exactly the same procedure as for the measurements in deuterium oxide. The values of p*K*₁(in H₂O) so obtained agreed very well with those found earlier by Bates,⁶ the average difference at the ten temperatures being only 0.0019 unit.

The value of p*K*₁ at 25° given in Table II (2.420 on the molal scale) can be compared with 2.362 (molar scale) obtained from conductance measurements by McDougall and Long.¹⁰ Inasmuch as the scalar difference is log *d*₀ (0.043 at 25°), the latter value becomes 2.405 on the molal scale. The agreement is therefore seen to be quite satisfactory, particularly so in view of the difficulties encountered in measuring the p*K* of an acid as strong as phosphoric.

The thermodynamic functions enthalpy, entropy, and heat capacity for the dissociation of deuteriophosphoric acid in heavy water at 25° have been calculated in the usual way from the temperature coefficient of p*K*₁ using the constants of eq 6. They are given in Table III

Table III: Thermodynamic Functions for the Dissociation of Phosphoric Acid in Deuterium Oxide and Water at 25°

	In D ₂ O	In H ₂ O ^b
Δ <i>H</i> ^o , J mol ⁻¹	-7593 (-1815) ^a	-7650 (-1828)
Δ <i>S</i> ^o , J K ⁻¹ mol ⁻¹	-71.8 (-17.2)	-66.8 (-16.0)
Δ <i>C</i> _p ^o , J K ⁻¹ mol ⁻¹	-159 (-38)	-154 (-37)

^a Values in parentheses are in calories (1 cal = 4.184 J). ^b Reference 6.

and compared with the corresponding quantities for the dissociation of phosphoric acid in ordinary water.⁶ The uncertainties in the thermodynamic functions estimated from the variances of the least-squares constants of eq 6 are as follows: Δ*H*^o, 12 J mol⁻¹ (3 cal mol⁻¹); Δ*S*^o, 0.1 J K⁻¹ mol⁻¹ (0.1 cal deg⁻¹ mol⁻¹); Δ*C*_p^o, 2 J K⁻¹ mol⁻¹ (0.5 cal deg⁻¹ mol⁻¹).

Discussion

Six weak acids have now been studied in both water and deuterium oxide by thermodynamically rigorous methods utilizing cells without liquid junction. The p*K* values for these acids in the two solvents are compared in Table IV. The isotope effect Δ*pK*, that is, p*K*(in D₂O) - p*K*(in H₂O), is given in the last column. The acids are arranged in order of decreasing strength in water. It can be seen in Figure 1, where Δ*pK* is plotted as a function of p*K*(in H₂O), that Δ*pK* for phosphoric acid now lies on the straight line fixed by the isotope effects for the three inorganic acids with p*K* greater than 7. The point marked "AcOD" represents the Δ*pK* value for both acetic acid and acetic acid-*d*₃. Its departure from the line is too large to be attributed to experimental error. Taken with other data summarized elsewhere,¹ it supports the conclusion that the isotope effect is different for organic and inorganic (mineral) acids below p*K* = 7. It cannot be said, however, that a clear difference between carboxylic acids, phenols, and anilinium acids exists.¹ The charge

(10) A. O. McDougall and F. A. Long, *J. Phys. Chem.*, **66**, 429 (1962).

Table IV: Deuterium Isotope Effects on pK at 25°

Acid	pK (in D_2O)	pK (in H_2O)	ΔpK	Ref ^a
Phosphoric	2.420	2.148	0.272	This work, 6
Acetic	5.312	4.756	0.556	11, 12
Acetic- d_3	5.326	4.771	0.553	13, 14
Primary phosphate ion	7.780	7.200	0.580	15, 16
Bicarbonate ion	11.077	10.329	0.748	17, 18
Solvent	14.955	13.997	0.958	19, 20

^a The first reference is to the pK (in D_2O), the second to the pK (in H_2O).

Table V: Deuterium Isotope Effect on the Thermodynamic Functions for the Dissociation of Weak Acids at 25°^a

Acid	$\Delta H^\circ(d) - \Delta H^\circ(h)$, J mol ⁻¹	$\Delta S^\circ(d) - \Delta S^\circ(h)$, ^a J K ⁻¹ mol ⁻¹	$\Delta C_p^\circ(d) - \Delta C_p^\circ(h)$, ^a J K ⁻¹ mol ⁻¹
Phosphoric	57 (13) ^b	-5.0 (-1.2)	-4 (-1)
Acetic	1561 (373)	-5.4 (-1.3)	-8 (-2)
Acetic- d_3	1456 (348)	-5.4 (-1.3)	-17 (-4)
Primary phosphate ion	1628 (389)	-5.9 (-1.4)	-18 (-4)
Bicarbonate ion	2564 (613)	-5.9 (-1.4)	+15 (+4)
Solvent	3284 (785)	-7.3 (-1.7)	-34 (-8)

^a d = in D_2O ; h = H_2O . ^b Values in parentheses are in calories (1 cal = 4.184 J).

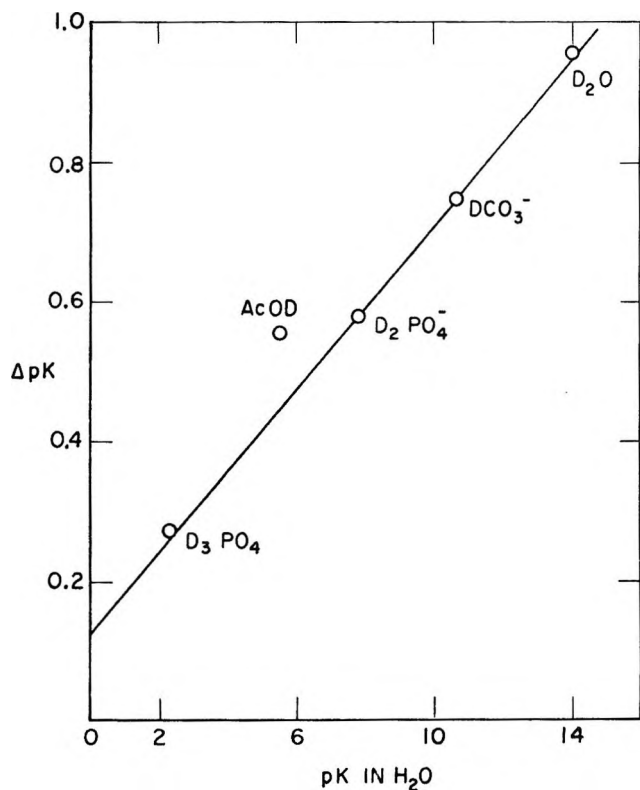


Figure 1. Deuterium isotope effects (ΔpK) for some weak acids plotted as a function of pK (in H_2O) at 25°.

type thus appears to be of secondary importance, in agreement with the conclusion of Martin.²¹

The pK values of a sufficient number of weak acids have now been determined over a range of temperatures

in both water and deuterium oxide to make worthwhile a comparison of the enthalpy, entropy, and heat capacity effects of changing solvent. Such a comparison is made in Table V; the acids are again arranged in order of increasing pK (decreasing strength).

The figures given in each column represent the excess of the indicated thermodynamic function (ΔH° , ΔS° , or ΔC_p°) in deuterium oxide over the value in water. The differences in enthalpy and heat capacity are seen to increase as the acid becomes weaker, but the isotope effect on the entropy change appears to be nearly independent of the acid's strength.

The very slight decrease in ΔpK from 5 to 50° apparent in Table II is consistent with the small positive

(11) R. Gary, R. G. Bates, and R. A. Robinson, *J. Phys. Chem.*, **69**, 2750 (1965).

(12) H. S. Harned and R. W. Ehlers, *J. Amer. Chem. Soc.*, **55**, 652 (1933).

(13) M. Paabo, R. G. Bates and R. A. Robinson, *J. Phys. Chem.*, **70**, 2073 (1966).

(14) M. Paabo, R. G. Bates, and R. A. Robinson, *ibid.*, **70**, 540 (1966).

(15) R. Gary, R. G. Bates, and R. A. Robinson, *ibid.*, **68**, 3806 (1964).

(16) R. G. Bates and S. F. Acree, *J. Res. Nat. Bur. Stand.*, **34**, 373 (1945); F. Ender, W. Teltschik, and K. Schäfer, *Z. Elektrochem.*, **61**, 775 (1957); A. K. Grzybowski, *J. Phys. Chem.*, **62**, 555 (1958).

(17) M. Paabo and R. G. Bates, *ibid.*, **73**, 3014 (1969).

(18) H. S. Harned and S. R. Scholes, Jr., *J. Amer. Chem. Soc.*, **63**, 1706 (1941).

(19) A. K. Covington, R. A. Robinson, and R. G. Bates, *J. Phys. Chem.*, **70**, 3820 (1966).

(20) H. S. Harned and R. A. Robinson, *Trans. Faraday Soc.*, **36**, 973 (1940).

(21) R. B. Martin, *Science*, **139**, 1198 (1963).

values of $\Delta H^\circ(\text{d}) - \Delta H^\circ(\text{h})$ given in Table V. The two quantities are related by

$$-\frac{d(\Delta pK)}{dT} = \frac{\Delta H^\circ(\text{d}) - \Delta H^\circ(\text{h})}{RT^2 \ln 10} \quad (7)$$

The enthalpy differences listed in the second column of Table V show that the isotope effect on pK decreases

uniformly with increasing temperature and that the decrease is greater the weaker the acid.

Acknowledgment. The authors are indebted to C. E. Champion and W. D. Dorko of the Analytical Chemistry Division for the coulometric analyses of the DCl solution and the mass spectrometric examination of the deuterium gas.

The Intrinsic Viscosity of Polyelectrolytes

by Ichiro Noda, Takeaki Tsuge, and Mitsuru Nagasawa

Department of Synthetic Chemistry, Nagoya University, Chikusa-ku, Nagoya, Japan (Received July 28, 1969)

The intrinsic viscosity of sodium poly(acrylate) was determined in sodium bromide solutions of various concentrations C_s as a function of molecular weight M and degree of ionization i . It was found experimentally that the electrostatic part of the expansion factor, which is defined as the ratio of the intrinsic viscosity to its value at infinite ionic strength, can be expressed in terms of a reduced parameter $(M/C_s)^{1/2}$ at all degrees of neutralization if the molecular weight is lower than 10^6 . On the other hand, in almost all theories so far published, the electrostatic part of the expansion factor is given as a function of $M^{1/2}/C_s$ if the charge density of the polyion is low enough.

Introduction

Among various characteristic properties of linear polyelectrolyte solutions, the intrinsic viscosity may be one of the most important problems remaining unsolved. In spite of a vast number of publications on this problem, the following features of the intrinsic viscosity of linear polyelectrolytes have not yet been explained.

(1) *Molecular Weight Dependence of Intrinsic Viscosity.* The theories on the expansion factor of *nonionic* polymers can be, roughly speaking, divided into two types. The representative of the first type is the well known theory of Flory¹ which gives

$$\alpha^5 - \alpha^3 = 2.60z \quad (1)$$

where α^2 represents the ratio of the mean-square end-to-end distance of polymer perturbed by the excluded volume effect to that of the unperturbed polymer and z is proportional to the square root of molecular weight such as

$$z = (3/2\pi)^{3/2} BA^{-3} M^{1/2} \quad (2a)$$

and

$$A^2 = \langle h_0^2 \rangle / M \quad (2b)$$

$$B = \beta / m_s^2 \\ = (4\pi / m_s^2) \int_0^\infty \{1 - \exp[-u(r)/kT]\} r^2 dr \quad (2c)$$

Here, $\langle h_0^2 \rangle$ is the mean end-to-end distance of unperturbed polymer, M and m_s are the molecular weights of the polymer and a segment, β is the excluded volume characterizing the interaction between a pair of segments, and $u(r)$ is the potential of average force between two segments at distance r apart. The other representative is the theory of Stockmayer and Fixman² which gives

$$\alpha^3 - 1 = 2z \quad (3)$$

The recent experimental results of light scattering from *nonionic* polymer solutions appear to show that eq 1 agrees with experimental results better than eq 3.^{3,4} However, the conclusion cannot always be valid if we compare the theories with experimental data of intrinsic viscosity by assuming the Flory-Fox relationship¹ that

$$[\eta] / [\eta]_\theta = \alpha_\eta^3 \quad (4)$$

$$\alpha_\eta^3 = \alpha^3 \quad (5)$$

(1) P. J. Flory, "Principles of Polymer Chemistry," Cornell University Press, Ithaca, N. Y., 1953, Chapter XIV.

(2) W. H. Stockmayer and M. Fixman, *J. Polym. Sci. Part C*, **1**, 137 (1963).

(3) G. C. Berry, *J. Chem. Phys.*, **44**, 4550 (1966); **46**, 1338 (1967).

(4) T. Norisuye, K. Kawahara, A. Teramoto, and H. Fujita, *ibid.*, **49**, 4330 (1968); K. Kawahara, T. Norisuye, and H. Fujita, *ibid.*, **49**, 4339 (1968).

where $[\eta]$ and $[\eta]_\theta$ are the intrinsic viscosities in non- θ and θ solvents, respectively. If the molecular weights are low or if the expansion factor α^2 is not high, eq 3 appears to be in better agreement with experimental data of intrinsic viscosity of both nonionic and ionic polymers than eq 1.⁵ The reason for the discrepancy between the experimental results on viscosity and expansion factor at low molecular weights is not fully clear, though there are some speculations.^{3,4}

Concerning the molecular weight dependence of the intrinsic viscosity of polyelectrolytes, moreover, there are more ambiguous points. It has not yet been confirmed that the experimental expansion factor of polyion α ,³ can be explained by eq 1 when the molecular weights are high. The relationship of eq 5 should also be examined more carefully for polyions than for nonionic polymers since the effect of drainage on intrinsic viscosity may not be neglected because of their high expansion.⁶ In any case, the molecular weight dependence of the expansion factor of the polyion is not necessarily expressed by the same equation as used for nonionic polymers since the distribution function of segments inside a polyion coil may be different from that inside a nonionic polymer coil.

(2) *Ionic Strength Dependence of Intrinsic Viscosity.* If the molecular weight is kept constant, the intrinsic viscosity of a polyion is experimentally found, with no exception, to be linear with respect to the reciprocal square root of ionic strength ($1/\sqrt{C_s}$).^{7,8} The linearity was first found and explained by Pals and Hermans.⁷ The theory of Flory⁹ also gives the linear relationship if the molecular weight is kept constant. As shown later, however, neither theory can explain the molecular weight dependence of intrinsic viscosity of low molecular weight samples, for which, too, the linearity of $[\eta]$ against $1/\sqrt{C_s}$ holds well.^{10,11} Therefore, the agreement between the theories and experimental results may be fortuitous. Beside these two theories, several theories (Fixman,¹² Kurata,¹³ Alexandrowicz¹⁴) were published to explain both the molecular weight and ionic strength dependences consistently. It is one of our purposes to examine these theories using the experimental data covering wider conditions than before.

(3) *The Effective Charge Density (Ion-Binding).* In all theories so far published, it is assumed that the effective charge density of the polyion is lower than the analytical charge density due to binding of counterions on the macro-ion. The origin of this ion binding is believed to be that the counterions are attracted closely to the polymer skeleton by the high charge density of the polyion so that the ionic atmosphere around the fixed charges may be quite different from that of the Debye-Hückel type. One of the most important assumptions concerning ion binding is that the degree of ion binding is assumed to be independent of both added-salt and polymer concentrations. This assumption appears to be permissible for studies on the thermody-

amic properties of polyelectrolyte solutions such as the osmotic pressure coefficient and ionic activity coefficient.¹⁵⁻¹⁸ To discuss the expansion of the polyion, however, the assumption cannot be accepted without re-examination since only a slight change in the degree of ion binding causes a great change in the expansion factor calculated. Before we can understand the ion-binding phenomenon precisely, it may be desirable to avoid the use of the assumption of ion binding by comparing the theories with experimental data at the limit of negligible charge density where no ion bonding can be assumed.

In the present work, the intrinsic viscosities of poly(acrylic acid) (PAA) with various degrees of ionization are determined in the solutions of various ionic strengths. Then, the dependence of the intrinsic viscosity on molecular weight, ionic strength, and charge density are experimentally established. The data, particularly the data at low charge density, are compared with the theories so far published. From the comparison, it will be pointed out that all theories so far published are not satisfactory.

Experimental Section

Samples. The high molecular weight samples of poly(sodium acrylate) (NaPA) were obtained from the samples supplied from Tokai Gosei Co., Ltd. by fractionation, while the samples of low molecular weights were separated from the samples which were prepared by polymerization with $(\text{NH}_4)_2\text{S}_2\text{O}_8$ as a catalyst in NaOH aqueous solution under nitrogen gas atmosphere at 55°. The samples of poly(methacrylic acid) (PMAA) were also prepared by polymerization with H_2O_2 in aqueous solutions. The unfractionated samples were purified three times by precipitation and then fractionated in methanol-water mixtures in the presence of NaOH for NaPA or in hexane-isopropyl alcohol mixtures for PMAA. The fractions were first freeze-dried and then completely dried under vacuum at 65°.

(5) M. Kurata and W. H. Stockmayer, *Fortschr. Hochpolym. Forsch.*, **3**, 196 (1963).

(6) M. Nagasawa and Y. Eguchi, *J. Phys. Chem.*, **71**, 880 (1967).

(7) D. T. F. Pals and J. J. Hermans, *Rec. Trav. Chim.*, **71**, 433 (1952).

(8) R. A. Cox, *J. Polym. Sci.*, **47**, 41 (1960).

(9) P. J. Flory, *J. Chem. Phys.*, **21**, 162 (1953).

(10) A. Takahashi and M. Nagasawa, *J. Amer. Chem. Soc.*, **86**, 543 (1964).

(11) S. Lapanje and S. Kovac, *J. Macromol. Sci. (Chem.)*, **A1(4)** 707 (1967).

(12) M. Fixman, *J. Chem. Phys.*, **41**, 3772 (1964).

(13) M. Kurata, *J. Polym. Sci. Part C*, **15**, 347 (1966).

(14) Z. Alexandrowicz, *J. Chem. Phys.*, **46**, 3789, 3800 (1967); **47**, 4377 (1967).

(15) R. Mock and C. A. Marshall, *J. Polym. Sci.*, **13**, 263 (1954).

(16) M. Nagasawa, M. Izumi, and I. Kagawa, *ibid.*, **37**, 375 (1959).

(17) M. Nagasawa, A. Takahashi, M. Izumi, and I. Kagawa, *ibid.*, **38**, 213 (1959).

(18) Z. Alexandrowicz, *ibid.*, **43**, 337 (1960).

Molecular weights of NaPA and PMAA were determined from their intrinsic viscosities using for NaPA

$$[\eta] = 12.4 \times 10^{-4} M_w^{1/2} \text{ in } 1.5 N \text{ NaBr at } 15^\circ 10$$

and for PMAA

$$[\eta] = 6.6 \times 10^{-4} M_w^{1/2} \text{ in } 0.002 N \text{ HCl at } 30^\circ 19$$

The molecular weights of the fractionated samples thus determined are shown in acid forms in Table I. Since, in the present work, attention is focused on the comparison between the intrinsic viscosities of the samples having different molecular weights, we prefer the viscosity method rather than the light-scattering method to determine the molecular weights of the samples. The viscosity equation for NaPA was previously determined by a light-scattering method using the same series of NaPA.¹⁰

Table I

		Poly(acrylic acid)							
$M_v \times 10^{-4}$		PAA1	PAA2	PAA3	PAA4	PAA5	PAA6	PAA7	PAA8
		80.4	53.2	22.4	12.3	3.53	3.77	1.91	0.962
		Poly(methacrylic acid)							
$M_v \times 10^{-4}$		PMAA1	PMAA2	PMAA3	PMAA4				
		65.5	32.3	24.1	10.6				

These fractions of NaPA were converted into acid forms by passing through a mixed bed ion-exchange resin column (Amberlite IR-120 and IR-400). The partially neutralized samples were prepared by adding calculated amounts of NaOH in the presence of added salt of various concentrations. The added salts were sodium bromide and sodium chloride of a special grade of Katayama Chemical Co. The salt concentrations used were 0.5, 0.1, 0.025, and 0.01 mol/l. of NaBr for PAA and 0.1 mol/l. of NaCl for PMAA. Other concentrations were also used to determine the unperturbed dimension of PAA at each charge density.

Intrinsic Viscosity Measurements. Intrinsic viscosities of partially neutralized samples were determined at $25 \pm 0.01^\circ$ in an atmosphere of nitrogen gas with capillary viscometers of the modified Ubelohde type, which have three or four bulbs to give the rate of shear corrections. The kinetic energy correction factors of the three viscometers were not more than 0.8%. The constants K in the equation for the average rate of shear ($\dot{\gamma} = K/v_{rel}$) were between 99 and 557 sec^{-1} . The rate of shear dependence of viscosity was observed for the samples having high molecular weights but was found to be negligible at salt concentrations higher than 0.025 N . Typical examples of polymer concentration dependence of viscosity at various charge densities are shown in Figure 1. The reduced viscosity was

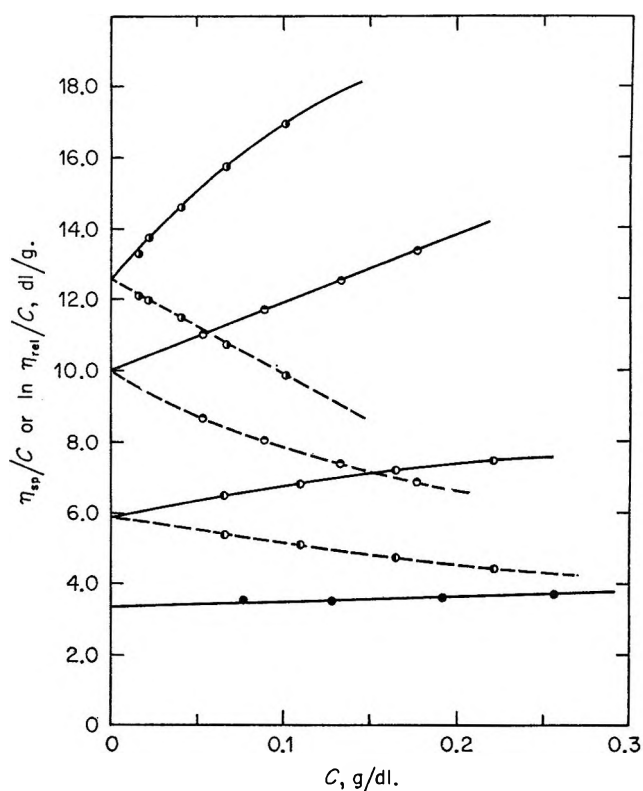


Figure 1. Selected viscosity vs. concentration plots for sample PAA2 with various degrees of ionization; concn of NaBr, 0.025 N ; degrees of ionization, 0.103, 0.200, 0.600, and 1.0 from bottom to top.

found to increase with decreasing polymer concentration if the degree of neutralization i is 0.1 and the polymer concentration is lower than 0.1 g/dl. Since this is caused by dissociation of unneutralized carboxyl groups, the intrinsic viscosity was obtained by extrapolating the viscosity data at concentrations higher than about 0.1 g/dl to zero polymer concentration. The actual degree of dissociation at $i = 0.1$ is 0.103 if a correction for the hydrogen ion concentration in the solutions is calculated from the pH.²⁰ At a degree of neutralization higher than 0.2, the correction is negligible and the degree of dissociation is equal to the degree of neutralization.

Results

Examples of the variation of intrinsic viscosity with charge density are given in Figure 2. A remarkable difference between the behaviors of PAA and PMAA is observed in the region of low charge density. The intrinsic viscosity of PAA increases with increasing charge density smoothly, whereas that of PMAA is constant at low charge density but begins to increase when the charge density reaches a certain value. That is, the radius of gyration of PMAA coil does not in-

(19) A. Katchalsky and H. Eisenberg, *J. Polym. Sci.*, 145 (1950).

(20) M. Nagasawa and I. Noda, *J. Amer. Chem. Soc.*, 90, 7200 (1965).

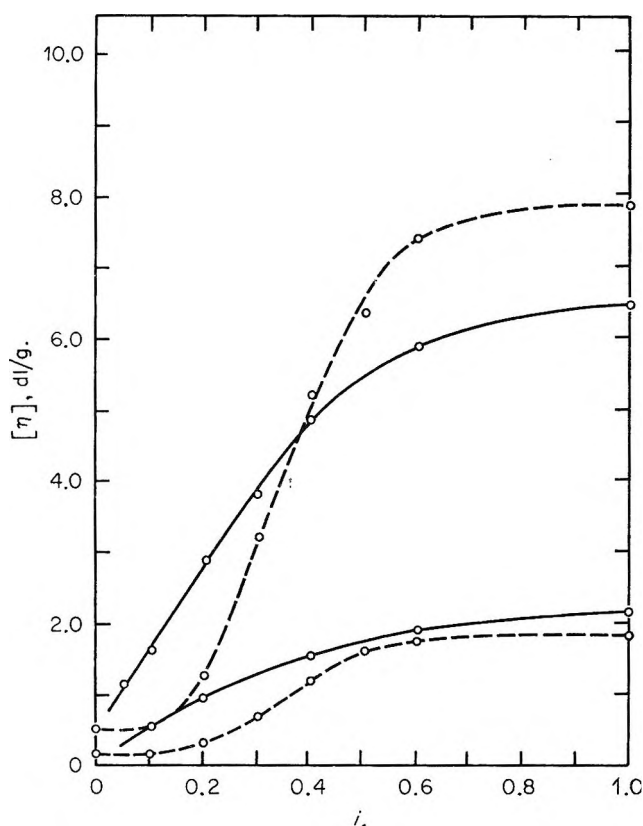


Figure 2. Typical examples of the relationship between intrinsic viscosity and degree of ionization; concn of NaBr, 0.1 *N*; solid lines denote the data of PAA4 and PAA2 and broken lines denote the data of PMAA4 and PMAA1 from bottom to top.

crease with increasing electrostatic repulsive force until the repulsive force reaches a certain value. This unusual behavior is believed to be due to the hydrophobic interaction of methyl group of PMAA which keeps the compact structure of PMAA coil. Similar behavior of PMAA is also observed in the potentiometric titration data.^{21,22} Therefore, most of the present experiments were carried out by using PAA which does not show such unusual behavior. Except at low charge density, however, there is no qualitative difference between the behavior of both polyacids.

Examples of the relationship between $[\eta]$ and the molecular weight of PAA are shown in a logarithmic scale in Figure 3. The values of K and ν in the Mark-Houwink-Sakurada equation, $[\eta] = KM^\nu$, are given in Table II as a function of both added salt concentration and charge density. The coefficient ν increases more rapidly at low charge density than at high charge density.

If we assume that a polymer coil is nondraining for solvent flow, we have the following type of equation for intrinsic viscosity in the framework of two-parameter theory²³

$$\alpha_\eta^3 = 1 + az + (\text{higher terms of } z) \quad (6)$$

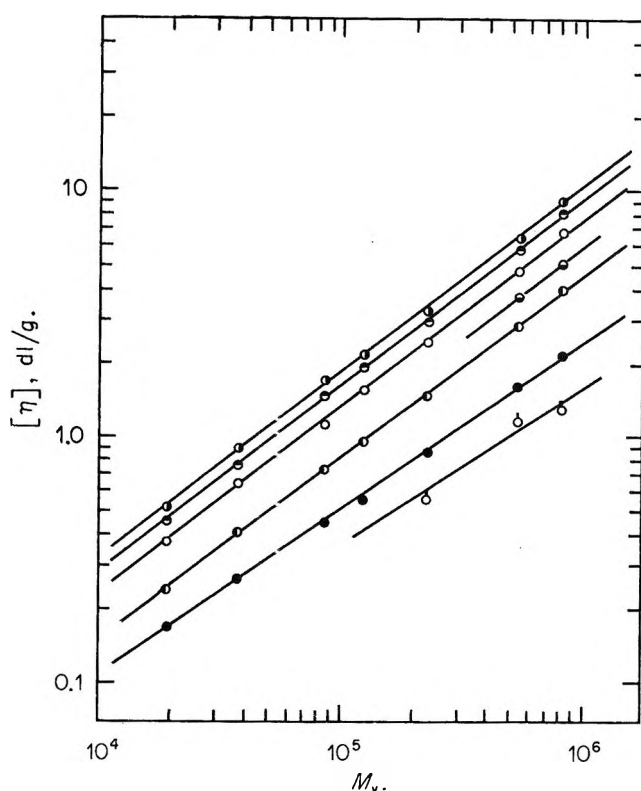


Figure 3. Viscosity equations of poly(acrylic acid) with various degrees of ionization; concn of NaBr, 0.1 *N*; degree of ionization, 0.005, 0.1, 0.2, 0.3, 0.4, 0.6, and 1.0 from bottom to top.

Table II: Dependence of K and ν in Viscosity Equation on Ionic Strength and Charge Density at 25°

i	C_s				
	0.5	0.1	0.025	0.01	
$K \times 10^4$	0.103	23.7	2.07	1.04	0.356
	0.200	9.28	1.61	0.942	0.515
	0.400	3.69	1.93	1.085	1.00
	0.600	3.74	2.35	1.38	1.34
	1.0	5.06	3.12	1.76	1.32
ν	0.103	0.384	0.679	0.785	0.909
	0.200	0.521	0.743	0.838	0.926
	0.400	0.655	0.743	0.867	
	0.600	0.675	0.768	0.860	0.898
	1.0	0.656	0.755	0.850	0.910

though no definite conclusion has yet been obtained on the validity of a power series expansion of α_η^3 in terms of z . The value of a is a numerical constant depending on the theory adopted. If we neglect the higher terms of z , eq 6 reduces to the well known theory

(21) J. G. Leyte and M. Mandel, *J. Polymer Sci., Part A*, **2**, 1879 (1964).

(22) M. Nagasawa, T. Murase, and K. Kondo, *J. Phys. Chem.*, **69**, 4005 (1965).

(23) M. Kurata and H. Yamakawa, *J. Chem. Phys.*, **16**, 565 (1948).

of Stockmayer and Fixman,² eq 3, which can be transformed into

$$[\eta]/M^{1/2} = K_0 + 0.51\Phi_0BM^{1/2} \quad (7)$$

Here, Φ_0 is the well known Flory constant¹ at the θ temperature (2.87×10^{21}) and K_0 is also a constant related to the unperturbed dimension of the polymer by

$$K_0 = \frac{\Phi_0 \langle h_0^2 \rangle^{1/2}}{M} \quad (8)$$

Equation 7 was found to agree with the experimental data of polyelectrolytes very well if the expansion is not very high. Therefore, our first trial is to examine the linearity of $[\eta]/M^{1/2}$ with respect to $M^{1/2}$. All data obtained in this work clearly show that a good linear relationship holds between $[\eta]/M^{1/2}$ vs. $M^{1/2}$ if the molecular weights are not too high and the concentration of added salt is not too low. Some examples at a low degree of dissociation are shown in Figure 4, while examples at the full neutralization were shown previously.¹⁰ However, if the expansion factor of polyion coil is very high because of high charge density or low ionic strength, a deviation from the linear relationship is observed. A similar deviation from the linearity was often reported for nonionic polymers.²⁴ Thus, it may be concluded that the "apparent" long-range interaction parameter B may be estimated from the slope in the $[\eta]/M^{1/2}$ vs. $M^{1/2}$ plot.

The values of B thus determined are plotted against the inverse square root of added salt concentration in Figure 5. It is clear that the linear relationship between B and $1/C_s^{1/2}$ holds not only at high charge density but also at low charge density. It is also observed that B increases with increasing charge density as shown in Figure 6. These results imply that B may be expressed as

$$\begin{aligned} B &= B_0 + B_e \\ &= B_0 + B'f(i)1/C_s^{1/2} \end{aligned} \quad (9)$$

where B_0 and B_e are the terms due to the nonelectrostatic and electrostatic interactions, respectively, B' is a numerical constant, and $f(i)$ is an increasing function of charge density i . The value of B_0 seems independent of the charge density as shown in Figure 5. The linear relationship between B and $1/C_s^{1/2}$ corresponds to the fact that $[\eta]$ is in linear relationship with $1/C_s^{1/2}$ for the present samples, too.

As is clear from eq 7, the values of K_0 , i.e., the unperturbed dimension of the polyion, $\langle h_0^2 \rangle^{1/2}$, can be obtained from the intercept of $[\eta]/M^{1/2}$ vs. $M^{1/2}$ plot at $M^{1/2} = 0$. Although there have been many discussions^{3,4} concerning the validity of the theory of Stockmayer and Fixman, it was confirmed experimentally⁵ that the values of K_0 thus determined agree with the values determined in θ solvents. Moreover, there is no appreciable difference between the values of K_0

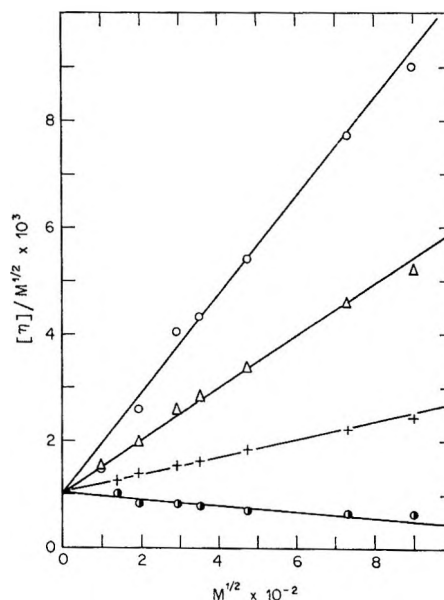


Figure 4. Examples of $[\eta]/\sqrt{M}$ vs. \sqrt{M} plot of PAA; degree of ionization i , 0.103; concn. 0.01 (O), 0.025 (Δ), 0.1 (+), 0.5 (\bullet).

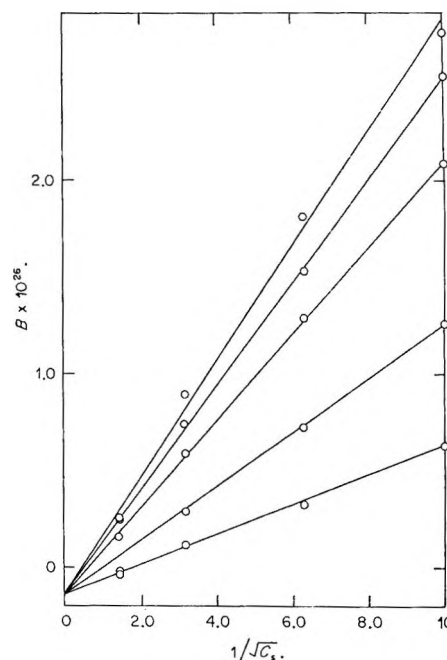


Figure 5. Ionic strength dependence of the "apparent" long-range interaction parameter B . Degree of ionization, 0.103, 0.200, 0.400, 0.600, and 1.0 from bottom to top.

determined from Stockmayer and Fixman's theory and those from the following Berry's equation³ if the expansion is not high.

$$\left(\frac{[\eta]}{M^{1/2}}\right)^{1/2} = K_0^{1/2} + 0.035 \frac{K_0^{3/2}}{\Phi_0} B \frac{M}{[\eta]} \quad (10)$$

The average values of K_0 determined in solutions of various ionic strengths using these equations are given

(24) I. Noda, S. Saito, T. Fujimoto, and M. Nagasawa, *J. Phys. Chem.*, **71**, 4048 (1967).

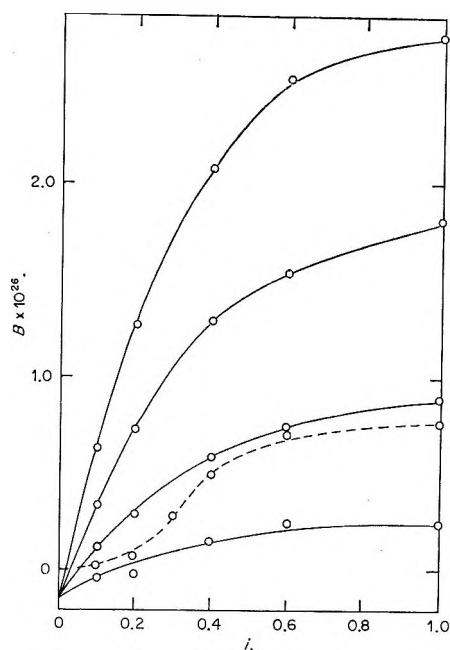


Figure 6. Variation of the "apparent" long-range interaction parameter B with degree of ionization. Solid lines, sodium polyacrylate; concn of NaBr, 0.5, 0.1, 0.25, and 0.01 N from bottom to top. Broken line, sodium polymethacrylate; concn of NaCl 0.1.

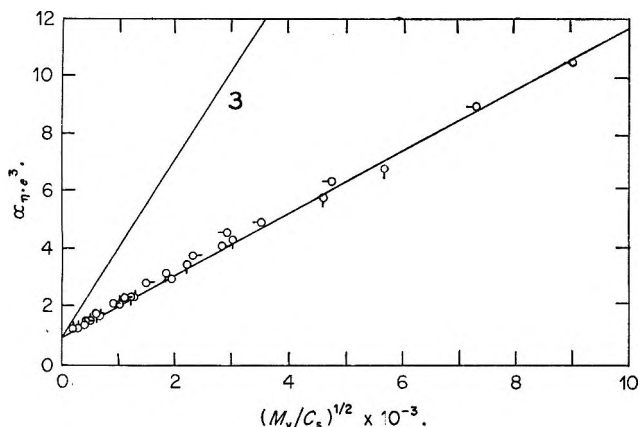


Figure 7. Plot of the electrostatic expansion factor vs. $(M/C_s)^{1/2}$; $i = 0.103$. Concn of NaBr, (○) 0.5; (○-) 0.1; (◐) 0.025; (◑) 0.01 N . Solid line 3 denotes the calculated values of eq 31.

as a function of charge density in Table III and the so-called σ value which is defined as the ratio of $\langle h_0^2 \rangle^{1/2}$ to that of the ideal chain with free rotation about each carbon-carbon bond are also given in Table III. The values of σ for PAA at all charge densities are in the intermediate between that of the fully charged PAA at 15° (2.38)¹⁰ and that of the acid form in dioxane at 30° (1.85).²⁵ For PMAA, both K_1 and B are almost constant at low charge density and begin to increase steeply at a charge density as shown in Figure 6 and in Table III.

Thus, the intrinsic viscosity of PAA in NaBr solu-

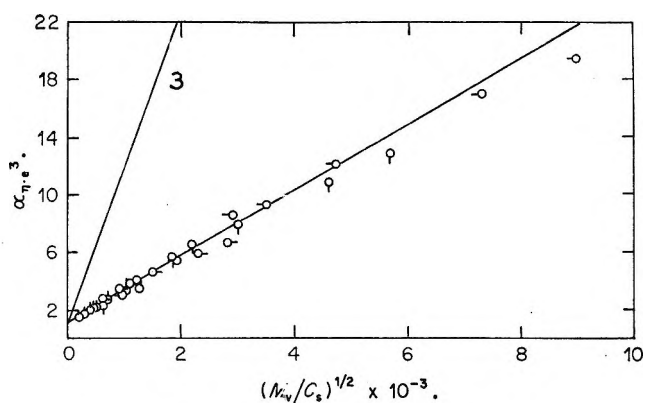


Figure 8. Plot of the electrostatic expansion factor vs. $(M/C_s)^{1/2}$; $i = 0.600$. Concn of NaBr the same as in Figure 7. Solid line 3 denotes the calculated values of eq 31.

Table III

i	PAA		PMAA	
	$K \times 10^3$	σ	$K \times 10^3$	σ
0.103	1.02	1.95		
0.200	1.20	2.06	0.7	1.9
0.300			0.9	2.1
0.400	1.40	2.17	1.2	2.2
0.500			2	2.7
0.600	1.60	2.27	2	2.7
1.00	1.85	2.38	2	2.7

tions is empirically expressed by the following equation if the molecular weight is not very high.

$$[\eta] = [\eta]_0 + [B_0 + B'f(i)1/C_s^{1/2}]M + \dots \quad (11)$$

where

$$[\eta]_0 = K_0(i)M^{1/2}$$

If we define the electrostatic part of the expansion factor $\alpha_{\eta_e}^3$ by

$$\alpha_{\eta_e}^3 = \alpha_{\eta}^3 - \lim_{C_s \rightarrow \infty} (\alpha_{\eta}^3 - 1)$$

eq 11 becomes

$$\alpha_{\eta_e}^3 = 1 + \frac{B'f(i)}{K_0(i)} \left(\frac{M}{C_s} \right)^{1/2} + \dots \quad (12)$$

The nonelectrostatic part of expansion factor $(\lim_{C_s \rightarrow \infty} \alpha_{\eta}^3 - 1)$ can be estimated by extrapolating $([\eta]/[\eta]_0 - 1)$ to $1/C_s^{1/2} = 0$. Typical examples of $\alpha_{\eta_e}^3$ vs. $(M/C_s)^{1/2}$ plots are shown in Figures 7 and 8. A good linear relationship is observed between $\alpha_{\eta_e}^3$ and $(M/C_s)^{1/2}$ but a slight deviation from the linearity appears at high values of $(M/C_s)^{1/2}$. The data at all other degrees of neutralization are similar to those in Figures 7 and 8.

(25) P. J. Flory and J. E. Osterheld, *J. Phys. Chem.*, **58**, 653 (1954).

Discussion

The mean square end-to-end distance of the polyion coil $\langle h^2 \rangle$ may be given by eq 13 if the excluded volume effect exists.

$$\langle h^2 \rangle = \frac{\int_0^\infty h^4 \exp(-3h^2/2\langle h_0^2 \rangle - F_c/kT - F_{el}/kT) dh}{\int_0^\infty h^2 \exp(-3h^2/2\langle h_0^2 \rangle - F_0/kT - F_{el}/kT) dh} \quad (13)$$

where F_0 and F_{el} represent the nonelectrostatic and electrostatic parts of free energy due to the long-range interaction between segments when the end-to-end distance is kept at h . It was pointed out that the additivity of the entropy term $-3h^2/2\langle h_0^2 \rangle$ and nonelectrostatic free energy F_0 may be assumed for nonionic polymers, but the additivity cannot be assumed for ionic polymers since it is inconceivable that all conformations of a polyion with a fixed end-to-end distance have the same electrostatic free energy.²⁶ The assumption that all conformations of polyion with the same radius of gyration have the same electrostatic free energy may be more reasonable, since the electrostatic free energy of a polyion depends on its radius of gyration. The conformational entropy of a polymer coil as a function of radius of gyration was calculated by Fixman.²⁷ Using the approximation of Flory and Fisk,²⁸ we have the following equation instead of eq 13

$$\langle s^2 \rangle = \frac{\int_0^\infty s^3 \exp(-7s^2/2\langle s_0^2 \rangle - F_0/kT - F_{el}/kT) ds}{\int_0^\infty s^5 \exp(-7s^2/2\langle s_0^2 \rangle - F_0/kT - F_{el}/kT) ds} \quad (14)$$

If the familiar Hermans and Overbeek method²⁹ is applied to eq 13 and 14, we have

$$\alpha^2 - 1 = -\frac{h}{3kT} \left(\frac{\partial F_0}{\partial h} + \frac{\partial F_{el}}{\partial h} \right) \quad (15)$$

or

$$\alpha^2 - 1 = -\frac{s}{7kT} \left(\frac{\partial F_0}{\partial s} + \frac{\partial F_{el}}{\partial s} \right) \quad (16)$$

Thus, there is no appreciable difference between the functional forms of two equations though the numerical values are different. For the later discussion, therefore, we use eq 15 for the convenience of calculation. As is clear from eq 15, the type of equation applicable to the expansion of polyion coil is determined by the relationship between F_{el} and molecular parameters such as molecular weight and charge density, since the change in F_0 is almost negligible compared with that in F_{el} .

Two different molecular models are in common use for calculating the electrostatic free energy F_{el} ; the smeared charge model in which all fixed charges are

assumed to be distributed uniformly inside a sphere or an ellipsoid and the chain model in which all fixed charges are arranged on a flexible chain. On the latter model which is no doubt more realistic than the former, the free energy of a polyion coil may be given by the following equation³⁰ if the potential is pairwise additive.

$$F_{el} = \int_0^1 \sum_{i=1}^{\nu} \sum_{j \neq i}^{\nu} \int_0^\infty \psi_j^i(r, \lambda) \bar{W}(r, |i-j|, \lambda, h) dr \epsilon d\lambda \quad (17)$$

where ν is the number of fixed charges on the polyion, *i.e.*, $\nu = n_i$, ψ_j^i is the electrostatic potential at the i th segment owing to the charge at the j th segment and W is the probability of finding a distance r between two charged segments i and j in the polyion of root-mean-square end-to-end distance $\langle h^2 \rangle^{1/2}$ when the charging parameter is λ . By substituting $x = |i-j|/\nu$ into eq 17 and also by assuming that all charged segments are equivalent, eq 17 may be recast into

$$F_{el} = 2\nu^2 \int_0^1 \int_0^1 (1-x) \int_0^\infty \psi_j^i(r, \lambda) \bar{W}(r, x, \lambda, h) dr dx \epsilon d\lambda \quad (18)$$

If the charge density is low enough, the electrostatic potential of the Debye-Hückel type may be safely assumed for ψ_j^i , that is

$$\psi_j^i(r, \lambda) = \frac{\lambda e e^{-\kappa r}}{Dr} \quad (19)$$

and

$$\kappa^2 = \frac{8\pi\epsilon^2 N_A C_s}{DkT \times 10^3}$$

where κ is the Debye-Hückel reciprocal length of ionic atmosphere in a uni-univalent electrolyte solution of concentration C_s . W was calculated by Kuhn, Künzle, and Katchalsky³¹ and others assuming that it is equal to the probability of finding a distance between two charged segments i and j in the conformation of end-to-end distance h when their mean-square end-to-end distance $\langle h^2 \rangle$ is equal to the unperturbed dimension $\langle h_0^2 \rangle$.

$$W(r, x, \lambda, h) = \left[\frac{2}{3} \pi \langle h_0^2 \rangle x(1-x) \right]^{-1/2} \times \frac{r}{h\kappa} \left[\exp\left(-\frac{3}{2} \frac{(r-xh)^2}{\langle h_0^2 \rangle x(1-x)} \right) - \exp\left(-\frac{3}{2} \frac{(r+xh)^2}{\langle h_0^2 \rangle x(1-x)} \right) \right] \quad (20)$$

(26) S. Lifson, *J. Polymer Sci.*, **23**, 431 (1957).

(27) M. Fixman, *J. Chem. Phys.*, **36**, 306 (1962).

(28) P. J. Flory and S. Fisk, *ibid.*, **44**, 2243 (1966).

(29) J. J. Hermans and J. T. G. Overbeek, *Rec. Trav. Chim.*, **67**, 761 (1948).

(30) T. L. Hill, "Introduction to Statistical Thermodynamics," Addison-Wesley Publishing Co., Inc., Reading, Mass., 1960.

(31) W. Kuhn, O. Künzle, and A. Katchalsky, *Helv. Chim. Acta*, **31**, 1994 (1948).

The insertion of eq 19 and 20 into eq 18 gives

$$F_{el} = \frac{\nu^2 \epsilon^3}{Dh} \ln \left(1 + \frac{6h}{\kappa \langle h_0^2 \rangle} \right) \quad (21)$$

which is the equation of Katchalsky and Lifson³² for the electrostatic free energy of polyion. Neglecting the F_0 term compared with the F_{el} term, the insertion of eq 19 into eq 15 gives³²

$$\alpha^2 - 1 = \frac{\nu^2 \epsilon^2}{3DkT \langle h_0^2 \rangle \alpha} \left[\ln \left(1 + \frac{6\alpha}{\kappa \langle h_0^2 \rangle^{1/2}} - \frac{6\alpha / \kappa \langle h_0^2 \rangle^{1/2}}{1 + 6\alpha / \kappa \langle h_0^2 \rangle^{1/2}} \right) \right] \quad (22)$$

If $6\alpha / \kappa \langle h_0^2 \rangle^{1/2}$ is smaller than unity, that is, if the molecular weight and/or the ionic strength are high, it follows that

$$\alpha - \frac{1}{\alpha} = \frac{6\nu^2 \epsilon^2}{DkT \langle h_0^2 \rangle^{3/2} \kappa^2} = 1.45 z_{el} \quad (23)$$

where z_{el} is defined by

$$z_{el} = \left(\frac{3}{2\pi} \right)^{3/2} \frac{1}{m_s^2} \left(\frac{M}{\langle h_0^2 \rangle} \right)^{3/2} \frac{10^8}{2N_A C_s} M^{1/2} \quad (24)$$

for uni-univalent salts. The z_{el} is the excluded volume parameter due to electrostatic interaction.

However, since the mean-square end-to-end distance of a polyion perturbed by electrostatic interaction is not given by $\langle h_0^2 \rangle$ as assumed in eq 20 but should be given by $\langle h^2 \rangle = \alpha^2 \langle h_0^2 \rangle$ if we may assume the uniform expansion during the charging-up process,³³ W may be better expressed by

$$W(r, x, \lambda, h) = \left[\frac{2}{3} \pi \langle h_0^2 \rangle \alpha^2 x (1-x) \right]^{-1/2} \frac{r}{hx} \times \left[\exp \left(-\frac{3}{2} \frac{(r-xh)^2}{\langle h_0^2 \rangle \alpha^2 x (1-x)} \right) - \exp \left(\frac{3}{2} \frac{(r+xh)^2}{\langle h_0^2 \rangle \alpha^2 x (1-x)} \right) \right] \quad (25)$$

By using this distribution function for W and eq 19 for ψ_i^1 in eq 17, we have

$$F_{el} = \frac{\nu^2 \epsilon^2}{Dh} \ln \left(1 + \frac{6h}{\alpha^2 \langle h_0^2 \rangle \kappa} \right) \quad (26)$$

The insertion of eq 26 into eq 15 gives

$$\alpha^2 - 1 = \frac{\nu^2 \epsilon^2}{3DkT \langle h_0^2 \rangle^{1/2} \alpha} \left[\ln \left(1 + \frac{6}{\kappa \alpha \langle h_0^2 \rangle^{1/2}} - \frac{6 / \kappa \alpha \langle h_0^2 \rangle^{1/2}}{1 + 6 / \kappa \alpha \langle h_0^2 \rangle^{1/2}} \right) \right] \quad (27)$$

If $6 / \kappa \alpha \langle h_0^2 \rangle^{1/2} \ll 1$, it follows that

$$\alpha^5 - \alpha^3 = \frac{6\nu^2 \epsilon^2}{DkT \langle h_0^2 \rangle^{3/2} \kappa^2} = 1.45 z_{el} \quad (28)$$

This is identical with the equation of Flory⁹ except for the numerical factor. Thus, we can have either an equation of the α type or of the α^5 type for the expansion factor of a polyion depending on the approximations used for distribution of segments.

Concerning the molecular weight dependence of the expansion factor of a polyion, an equation of the α type was presented by Katchalsky and Lifson,³² equations of the α^3 type were presented by Ptitsyn,³⁴ Fixman,¹² and Kurata,¹³ an equation of the α^4 type was presented by Alexandrowicz¹⁴ and equations of the α^5 type were presented by Hermans and Overbeek,²⁹ Flory,⁹ and others. Although all those theories are expressed in their own ways, here it is important to point out that all those theoretical equations, except for the equation of Fixman,¹² can be expressed by using the same parameter z_{el} if the molecular weight and/or the ionic strength are high and also if the interaction energy between two charged sites $u(r)$ is given by the theory of Debye and Hückel. The theory of Debye and Hückel

$$u(r) = \frac{\epsilon^2 e^{-\kappa r}}{Dr} \quad (29)$$

must be applicable at the limit of low charge density. In the theory of Alexandrowicz, the meaning of the excluded volume function is entirely different from that in most theories, but we assume that eq 29 or eq 24 may be used in his theory at the limit of low charge density. (The equations are given for a uni-univalent salt such as NaBr.)

A. Katchalsky and Lifson³²

$$\alpha - 1/\alpha = 1.45 z_{el} \quad (30)$$

B. Fixman¹²

$$\alpha^3 - 1 = 1.52 \times 10^{-8} \frac{1}{M_s} \left(\frac{M}{\langle h_0^2 \rangle} \right)^{1/2} \frac{i}{C_s^{1/2}} M^{1/2} \quad (31)$$

C. Kurata¹³

$$\alpha^3 - 1 = 2z_{el} \Gamma(f) \quad (32)$$

$$\Gamma(f) = 2f^{-2} [(1+f^2) - 1]$$

$$f = 3.38 \times 10^{-21} \frac{1}{m_s} \left(\frac{M}{\langle h_0^2 \rangle} \right)^{3/2} \frac{i}{M^{1/2}} \alpha^{-1} \left(1 + \frac{1}{3\alpha^2} \right)^{1/2}$$

D. Ptitsyn³³

$$\alpha^2 = \frac{1}{4.68} [3.38 + (1 + 9.68 z_{el})^{1/2}] \quad (33)$$

(32) A. Katchalsky and S. Lifson, *J. Polymer Sci.*, **11**, 409 (1953).

(33) H. Fujita, K. Okita, and T. Norisuye, *J. Chem. Phys.*, **47**, 2723 (1967).

(34) O. B. Ptitsyn, *Vysokomol. Soedin.*, **3**, 1084, 1251 (1961).

E. Alexandrowicz¹⁴

$$\alpha^2 = 1.7z_{el}^{1/2} + 0.35 \quad (\alpha^2 \text{ 2}) \quad (34)$$

F. Flory⁹

$$\alpha^5 - \alpha^3 = 2.60z_{el} \quad (35)$$

G. Hermans and Overbeek²⁹

$$\alpha^5 - \alpha^3 \doteq 7.0z_{el} \quad (35)$$

Here, it is to be noted that in the above theories the nonelectrostatic part of free energy F_0 is assumed to be negligible compared with the electrostatic part F_{el} , and hence, α^3 calculated corresponds to $\alpha_{\eta e^3}$.

Except for the equation of Fixman (31), all equations are expressed in terms of the reduced parameter z_{el} . That is, it is expected from their theories that the intrinsic viscosity is a function of $M^{1/2}/C_s$. Experimentally, however, the present data show that the intrinsic viscosity is a function of $(M/C_s)^{1/2}$. Thus, we may conclude that all the theories do not agree with the experimental results even qualitatively. Examples of the $\alpha_{\eta e^3}$ vs. $M^{1/2}/C_s$ plot are shown in Figures 9 and 10. It is clear that $\alpha_{\eta e^3}$ cannot be expressed by a unique function of $M^{1/2}/C_s$. The calculated values of eq 23 and 28 are shown in those figures for comparison.

Only eq 31 of Fixman predicts the linear relationship between α^3 and $(M/C_s)^{1/2}$ in accord with the experimental results. His conclusion stems from the assumption that inside a polyion coil the concentration of counter ions dissociated from the polyelectrolyte ρ_0 is much higher than that of added salt C_s (see eq 26 of ref 12) and, hence, the ionic strength inside the polyion domain is determined only by ρ_0 . This assumption, however, is not valid at low charge density even when C_s is as low as 0.01 mol/l. For example, $\rho_0/2C_s = 2.3 \times 10^{-1}$ for PAA5 and 3.4×10^{-2} for PAA1 when $i = 0.103$ and $C_s = 0.01$. If the ionic strength inside the polyion coil is not determined by ρ_0 but by C_s , the equation of Fixman becomes an equation of the α^5 -type similar to eq 35. Thus, we may conclude that to date there has been no theory which agrees with experimental results.

The calculated values of eq 31 are shown in Figure 7 for comparison with experimental data. In the original paper of Fixman, it is suggested that the dielectric constant inside the polymer domain D_0 may be adjusted to fit the calculated values to the experimental data in order to take into account the extra interaction between counterions and the segment cloud x_e . That is, $D_0 \neq D$. The use of effective dielectric constant in his theory is equivalent to the use of the effective charge density, that is, to the assumption of ion binding in other theories. Because of the reason discussed above, therefore, we may assume $D_0 = D$ in eq 31 and for the experimental data at $i = 0.103$ in Figure 7. In Figure 8, too, we show the line calculated on the same assumption for comparison with the experimental data at $i =$

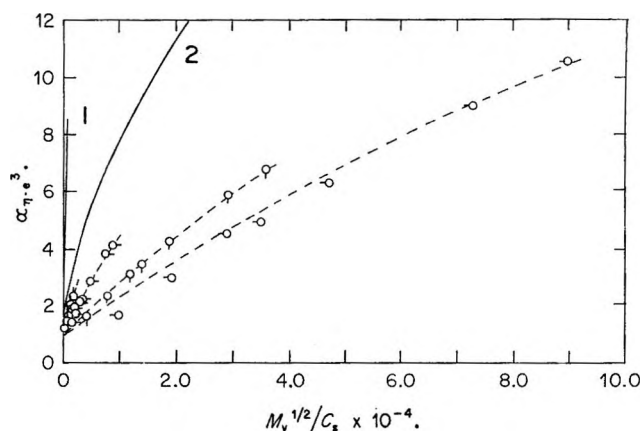


Figure 9. Plot of the electrostatic expansion factor vs. $M^{1/2}/C_s$; $i = 0.103$. Concn. of NaBr the same as in Figure 7. Solid lines 1 and 2 denote the calculated values of eq 10 and 35, respectively.

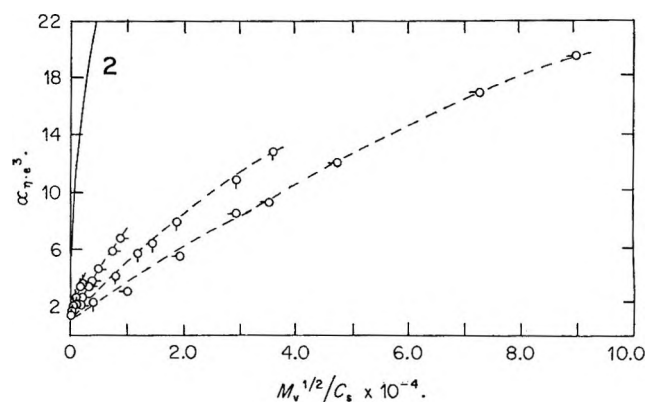


Figure 10. Plot of the electrostatic expansion factor vs. $M^{1/2}/C_s$; $i = 0.600$; concn of NaBr, the same as in Figure 7. Solid line 2 denotes the calculated values of eq 35.

0.6, but in this case it may be justified to assume $D_0/D = 0.22$ to give good agreement between the calculated values and the experimental ones. In the theory of Fixman, moreover, the hydrodynamic radius of polyion coil R_0 , i.e., b_0 defined by $R_0 = n^{1/2} b_0$, is treated as a parameter, n being the number of segments in a molecule. In Figures 7 and 8, we assumed

$$(M/m_s)b_0^2 = \langle h_0^2 \rangle$$

where $\langle h_0^2 \rangle$ can be determined experimentally. Because of these assumptions, too strict quantitative comparison between the theory of Fixman and experimental results is not meaningful.

In the use of the Debye-Hückel potential, it is assumed that the charge density of the polyion is so low that the ionic atmosphere around neighboring fixed charges do not extensively overlap each other. The Debye-Hückel radii of ionic atmosphere $1/\kappa$ are about 4, 10, 20, and 30 Å in 0.5, 0.1, 0.025, and 0.01 mol/l. of NaBr at 25°, respectively, while the average distances between neighboring fixed charges are about 18 Å at $i = 0.103$ and about 8 Å at $i = 0.6$, if we estimate them

from the characteristic ratio of PAA, $\langle h_0^2 \rangle / M$. Therefore, a part of the disagreement between the theoretical equations and experiments at high charge densities is undoubtedly caused by the failure of the assumption of pairwise addition of the Debye-Hückel potential and may be so even at a low charge density $i = 0.1$ if the ionic strength is as low as 0.01. Moreover, the disagreement cannot be explained by the assumption of ion binding if the degree of ion binding is assumed to be independent of ionic strength.

Beside the use of the Debye-Hückel potential, therefore, some other reasons must be responsible for the disagreement, considering the disagreement between the theories and the experiments at $i = 0.103$. One may be the assumption of eq 5 or the effect of partial drainage through polymer coils as was discussed in the introduction, and the other may be the assumption concerning the probability W of finding a distance r between two charged segments. Since the distribution of segments is affected by the electrostatic interaction in

polyion, the assumption of the uniform expansion would certainly have to be reexamined. The third reason may be in the assumption that the thickness of ionic atmosphere around a fixed charge is much smaller than the radius of gyration, *i.e.*, $6/\kappa\alpha\langle h_0^2 \rangle^{1/2} \ll 1$. Under the present experimental conditions, however, the values of $6/\kappa\alpha\langle h_0^2 \rangle^{1/2}$ are not smaller than unity, *e.g.*, 0.29 for PAA1 and 2.6 for PAA8 in 0.01 *N* solution. If eq 27 is used for comparison with experimental data, α^3 calculated for the same value of $M^{1/2}/C_s$ differs with concentration of added salt and molecular weight. The ionic strength and molecular weight dependences show almost similar behavior to the experimental results. Moreover, if we plot the calculated values of α^3 against $(M/C_s)^{1/2}$, the plot is close to the calculated values of Fixman, eq 3.

Acknowledgment. We wish to thank Mr. S. Narita and Mr. K. Furuta for their assistance in measuring viscosities.

Thermochemistry of Simple Alkylsilanes^{1a}

by P. Potzinger and F. W. Lampe

Whitmore Laboratory, The Pennsylvania State University, University Park, Pennsylvania 16802
(Received August 11, 1969)

The results of previous thermochemical studies of alkylsilanes are reviewed critically and shown to be internally inconsistent with what is expected on the basis of reliable data for analogous carbon and tin compounds. It is further shown that the constancy of $\Delta H_f^\circ(\text{SiH}_2^+)$, as derived from electron impact studies of SiH_4 , Si_2H_6 , and CH_3SiH_3 , and of the standard heats of formation of the major organosilicon ions from $(\text{CH}_3)_2\text{SiH}_2$, $(\text{CH}_3)_3\text{SiH}$, and $(\text{CH}_3)_4\text{Si}$ permit the determination of the standard heats of formation of the methylsilanes and of the parameters necessary to apply the bond interaction scheme developed by Allen. Formulas are given which can be used to calculate standard heats of formation of alkylsilanes which are believed accurate to ± 5 kcal/mol.

Principally because of the difficulties encountered in the application of conventional calorimetric techniques to organometallic compounds in general,^{1b} very little reliable thermochemical information is available for simple alkylsilane molecules. In this paper we review critically prior work on alkylsilane thermochemistry, present and compare the results of our electron impact studies on silane, disilane, and all the methylsilanes with this prior thermochemical work, and show that from this comparison bond-energy parameters may be derived which permit calculation of internally consistent heats of formation of alkylsilanes.

Experimental Section

All electron impact studies were carried out in a Nuclide Associates 12-90G mass spectrometer using a modulated retarding-potential-difference technique, that has been described previously, to obtain ionization from electrons effectively monoenergetic to ± 0.1 eV.²

The preparation and purification of silane, disilane,

- (1) (a) Atomic Energy Commission Document No. NYO-3570-14.
- (b) H. A. Skinner, *Advan. Organometal. Chem.*, **2**, 49 (1964).
- (2) P. Potzinger and F. W. Lampe, *J. Phys. Chem.*, **73**, 3912 (1969).

Table I

Compound	Ion	This work	Ref 12	Ref 20	Ref 9	Ref 19, 26	Ref 21
SiH ₄	SiH ₂ ⁺	11.90 ± 0.02 ^a			11.91		
CH ₃ SiH ₃	SiH ₂ ⁺	11.50 ± 0.05			11.62		
CH ₃ SiH ₂	CH ₃ Si ⁺	14.05 ± 0.05					
	CH ₃ SiH ⁺	11.45 ± 0.05					
	CH ₃ SiH ₂ ⁺	11.80 ± 0.05					
	CH ₃ Si ⁺	14.00 ± 0.15					
	CH ₃ SiH ⁺	13.85 ± 0.05					
(CH ₃) ₂ SiH ₂	CH ₃ SiH ₂ ⁺	11.51 ± 0.05					
	(CH ₃) ₂ Si ⁺	10.71 ± 0.05					
	(CH ₃) ₂ SiH ⁺	11.12 ± 0.05					
	CH ₃ Si ⁺	13.40 ± 0.10				12.4 ± 0.3	
	(CH ₃) ₂ Si ⁺	10.50 ± 0.05				10.3 ± 0.2	
(CH ₃) ₃ SiH	(CH ₃) ₂ SiH ⁺	10.91 ± 0.05	11.2 ± 0.1	11.70 ± 0.06		11.9 ± 0.3	
	(CH ₃)Si ⁺	10.52 ± 0.05	10.6 ± 0.1	10.78 ± 0.07		10.9 ± 0.2	10.7 ± 0.1
	(CH ₃) ₃ Si ⁺	10.25 ± 0.05	10.4 ± 0.1	10.63 ± 0.13		11.3 ± 0.15	10.5 ± 0.1
(CH ₃) ₄ Si	(CH ₃) ₃ Si ⁺	9.74 ± 0.05	9.9 ± 0.1	9.90 ± 0.03		9.8 ± 0.3	

^a Reference 2.

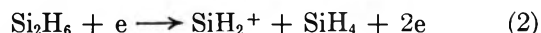
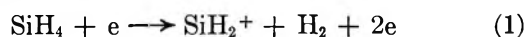
and methylsilane have been described previously.^{2,3} Dimethylsilane was obtained from Peninsular Chemical Research, Inc., and was purified by successive fractionation on a high-vacuum line immediately before use until satisfactory purity by mass spectrometric standards was obtained. Trimethylsilane was prepared by the reduction of trimethylchlorosilane (Peninsular Chemical Research Inc.) with lithium aluminum hydride; it was purified before use by vacuum-line distillation. Tetramethylsilane was obtained from Stauffer Chemical Company in 99.9% purity and was used after vacuum-line degassing.

Results and Discussion

The results of our electron impact measurements are shown in Table I where they are compared with other appearance potentials that have appeared in the literature. Some disagreement exists for fragment ions from (CH₃)₄Si and (CH₃)₃SiH, but we consider the agreement of our values for the pertinent ions (which are the lowest measured) with those shown in the 4th and 8th columns of Table I to be satisfactory, and on this basis we take our values to be correct.

Early measurements of the heat of formation of SiH₄ gave values ranging from -8.7 kcal/mol⁴ to -14.87 kcal/mol⁵, which were simply not consistent with other observed properties of SiH₄.⁶ More recently, Brimm and Humphreys⁷ determined $\Delta H_f^\circ(\text{SiH}_4)$ by decomposing SiH₄ at 680° in a calorimeter to Si_{solid} and 2H₂ and found the value 7.8 ± 3.5 kcal/mol. This value was later confirmed by Gunn and Green,⁸ who measured the heat of explosive decomposition of SiH₄ in a mixture with SbH₃ and reported a value for $\Delta H_f^\circ(\text{SiH}_4)$ of 7.3 ± 0.3 kcal/mol. The same experimental technique was applied by them to disilane and resulted in the value $\Delta H_f^\circ(\text{Si}_2\text{H}_6) = 17.1 \pm 0.3$ kcal/mol.⁸ We have found,² in agreement with Steele, Nichols, and

Stone,⁹ that values of $\Delta H_f^\circ(\text{SiH}_2^+)$ calculated from the appearance potentials of SiH₂⁺ from SiH₄ and Si₂H₆, assuming processes (1) and (2), agree within experimental error. This agreement attests to the internal consistency of the results of Gunn and Green⁸ and, as a postulate, in all our further considerations we take their values for $\Delta H_f^\circ(\text{SiH}_4)$ and $\Delta H_f^\circ(\text{Si}_2\text{H}_6)$ as correct.



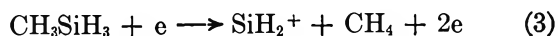
The only thermochemical data for alkylsilanes are due to Tannenbaum, *et al.*,¹⁰ who reported the heats of formation of the methylsilanes (with the exception of methylsilane itself), all four ethylsilanes, and four other alkylsilanes, as obtained by combustion calorimetry. The difficulties encountered in these experiments^{10,11} can be appreciated by the error reported for their results, namely up to ±30 kcal/mol. Tannenbaum's ΔH_f° values decrease with increasing methyl substitution in the methylsilanes as one would expect. However, Band, *et al.*,¹² have pointed out that there is a lack of internal consistency in the results of Tannenbaum,

- (3) P. Potzinger and F. W. Lampe, *J. Phys. Chem.*, **74**, 587 (1970).
- (4) H. von Wartenberg, *Z. Anorg. Allg. Chem.*, **79**, 71 (1913).
- (5) "Selected Values of Chemical Thermodynamic Properties," National Bureau of Standards Circular 500, U. S. Government Printing Office, Washington, D. C., 1950.
- (6) T. R. Hogness, T. L. Wilson, and W. C. Johnson, *J. Amer. Chem. Soc.*, **58**, 108 (1936).
- (7) E. O. Brimm and H. M. Humphreys, *J. Phys. Chem.*, **61**, 829 (1957).
- (8) S. R. Gunn and L. G. Green, *ibid.*, **65**, 779 (1961).
- (9) W. C. Steele, L. D. Nichols, and F. G. A. Stone, *J. Amer. Chem. Soc.*, **84**, 4441 (1962).
- (10) S. Tannenbaum, S. Kaye, and G. F. Lewenz, *ibid.*, **75**, 3753 (1953).
- (11) S. Tannenbaum, *ibid.*, **76**, 1027 (1954).
- (12) S. J. Band, I. M. T. Davidson, and C. A. Lambert, *J. Chem. Soc.*, A 2068 (1968).

et al., which is more pronounced in the ethylsilane series where the heats of formation go through a minimum with increasing ethyl content. It is further difficult to rationalize the result that $\Delta H_f^\circ[(C_2H_5)_n SiH_{4-n}] \leq \Delta H_f^\circ[(CH_3)_n SiH_{4-n}]$. One must conclude that the results reported by Tannenbaum, *et al.*, simply do not permit a rationalization by any of the usual bond-energy term schemes.¹³ Although one might at first consider this to result from some peculiar properties of organometallic compounds this possibility is at once ruled out by the observation of Davies, Pope, and Skinner¹⁴ and Coleman and Skinner¹⁵ that the bond interaction scheme of Allen¹⁶ can be applied with considerable success to alkylstannanes. Hence, there seems no doubt that the values of Tannenbaum, *et al.*,^{10,11} are quite unreliable.

In a very important paper, Steele, Nichols, and Stone⁹ reported the first use of electron impact data to obtain thermochemical information on silane compounds. They measured the appearance potentials of selected ions from a number of alkylsilanes, as well as from silane, disilane,¹⁷ and some chlorosilanes in a conventional mass spectrometer, evaluating their data from semilog plots of their ionization-efficiency curves using a vanishing current method.¹⁸ From their data they were able to derive the heats of formation of CH_3SiH_3 , $C_2H_5SiH_3$, *i*- $C_3H_7SiH_3$, and *t*- $C_4H_9SiH_3$. One should add that the heats of formation are derived from the respective appearance potentials by assuming a specific fragmentation; thus their $\Delta H_f^\circ(CH_3SiH_3) = -4$ kcal/mol value was derived from $AP(SiH_2^+)$ while with $AP(SiH_3^+)$ one calculates a value of -20 kcal/mol from their data. Similarly, for $\Delta H_f^\circ(C_2H_5SiH_3)$ one gets -15 kcal/mol from $AP(SiH_2^+)$, -25 kcal/mol from $AP(SiH_3^+)$ and -21.4 kcal/mol from $AP(C_2H_5^+)$, if the value $\Delta H_f^\circ(C_2H_5^+) = 219$ kcal/mol is chosen. The evaluations of $\Delta H_f^\circ(i-C_3H_7SiH_3)$ and $\Delta H_f^\circ(t-C_4H_9SiH_3)$ are even more ambiguous because the structures of the ions in the chosen cases ($C_3H_7^+$, $C_4H_9^+$) are not known. The discrepancies in the heats of formation from different fragment ions may be due to the chosen experimental method or may be inherent in the parent substances (different kind of excess energies), but, regardless of the reason(s), they do not inspire confidence.

Our value for $AP(SiH_2^+)$ from CH_3SiH_3 is in excellent agreement with that determined by Steele, Nichols, and Stone.⁹ Since this is the lowest appearance potential of any fragment ion formed, the corresponding neutral fragment must be molecular and hence the process must be (3), *viz.*



Since $\Delta H_f^\circ(SiH_2^+)$ and $\Delta H_f^\circ(CH_4)$ are known, we use our value $AP(SiH_2^+)$ to calculate $\Delta H_f^\circ(CH_3SiH_3) = 0 \pm 2$ kcal/mol.

Utilizing our data in Table I it is possible to apply the bond interaction scheme of Allen¹⁶ to calculate standard heats of formation of alkylsilane compounds. In our first attempt we used our derived value of $\Delta H_f^\circ(CH_3SiH_3)$ to calculate the thermochemical Si-C bond energy to be: $B(Si-C) = 61.3$ kcal/mol; the C-Si-C bond interaction energy, $\alpha(CSiC)$, must also be obtained and in principle this should be possible from the appearance potentials (and heats of formation) of any of the ions *m/e* 43, 44, and 45 from CH_3SiH_3 and $(CH_3)_2SiH_2$. However, these different fragment ions yield different values of $\alpha(CSiC)$ and there is no unambiguous way to decide which is correct. We decided, therefore, to derive a "best" value of $\alpha(CSiC)$ from a least-squares treatment of all our appearance potential data for alkylsilanes (with the exception of *m/e* 43, which involves considerable fragmentation) in Table I. Such a treatment yields a value $\alpha(CSiC) = 2.0$ kcal/mol and the following heats of formation for the methylsilanes

$$\begin{aligned} \Delta H_f^\circ(CH_3SiH_3) &= 0.0 \text{ kcal/mol} \\ \Delta H_f^\circ[(CH_3)_2SiH_2] &= -9.3 \text{ kcal/mol} \\ \Delta H_f^\circ[(CH_3)_3SiH] &= -20.6 \text{ kcal/mol} \\ \Delta H_f^\circ[(CH_3)_4Si] &= -33.9 \text{ kcal/mol} \end{aligned}$$

Table IIa gives the heats of formation of the fragment ions from the methylsilanes derived from these values. As indicated by inspection and by the standard deviation of 3.3 kcal/mol, the agreement is rather good. If now we also allow $\Delta H_f^\circ(CH_3SiH_3)$ to vary, then the amount of decrease in the standard deviation should give us a measure of how good our assumption was that $\Delta H_f^\circ(SiH_2^+)$ from SiH_4 and Si_2H_6 equals $\Delta H_f^\circ(Si_2H^+)$ from CH_3SiH_3 .

A minimum standard deviation of ± 3 kcal/mol in the ΔH_f° value of the fragment ions from the methylsilanes is obtained, with $\Delta H_f^\circ(CH_3SiH_3) = 1 \pm 3$ kcal/mol, $\alpha(CSiC) = 2.5$ kcal/mol, and $B(Si-C) = 60.3 \pm 3.2$ kcal/mol. The very small decrease in the standard deviation (see Table IIb) and the small increase in $\Delta H_f^\circ(CH_3SiH_3)$ (which is within our error limits) necessary to obtain the minimum standard deviation, indicate strongly that $AP(SiH_2^+)$ from SiH_4 and CH_3SiH_3 contain very little excess energy and that the bond interaction scheme of Allen¹⁶ can be applied to alkyl- or at least to methylsilanes. As a result of the

(13) H. A. Skinner and G. Pilcher, *Quart. Rev.*, **17**, 264 (1963).

(14) J. V. Davies, A. E. Pope, and H. A. Skinner, *Trans. Faraday Soc.*, **59**, 2233 (1963).

(15) D. J. Coleman and H. A. Skinner, *ibid.*, **62**, 1721 (1966).

(16) T. L. Allen, *J. Chem. Phys.*, **31**, 1039 (1959).

(17) W. C. Steele and F. G. A. Stone, *J. Amer. Chem. Soc.*, **84**, 3599 (1962).

(18) F. H. Field and J. L. Franklin, "Electron Impact Phenomena," Academic Press, New York, N. Y., 1957, pp 28-30.

Table II: A. Heat of Formation of Fragment Ions from Silane and Methylsilanes $\Delta H_f^\circ(\text{CH}_3\text{SiH}_3) = 0$ kcal/mol, $\alpha = 2.0$ kcal/mol, $B(\text{Si-C}) = 61.3$ kcal/mol

Ion	SiH ₄	CH ₃ SiH ₃	(CH ₃) ₂ SiH ₂	(CH ₃) ₃ SiH	(CH ₃) ₄ Si
SiH ₂ ⁺	283	283			
CH ₃ SiH ⁺		264	257.5		
CH ₃ SiH ₂ ⁺		220	221.8		
(CH ₃) ₂ Si ⁺			236.7	238.6	
(CH ₃) ₂ SiH ⁺			193.8	195.9	
(CH ₃) ₃ Si				168.7	169.6

B. Heat of Formation of Fragment Ions from Silane and Methylsilane $\Delta H_f^\circ(\text{CH}_3\text{SiH}_3) = 1.0$ kcal/mol, $\alpha = 2.5$ kcal/mol, $B(\text{Si-C}) = 60.3$ kcal/mol

Ion	SiH ₄	CH ₃ SiH ₃	(CH ₃) ₂ SiH ₂	(CH ₃) ₃ SiH	(CH ₃) ₄ Si
SiH ₃ ⁺	283	284			
CH ₃ SiH ⁺		265	259		
CH ₃ SiH ₂ ⁺		221	223.3		
(CH ₃) ₂ Si ⁺			238.8	240.8	
(CH ₃) ₂ SiH ⁺			196	198.2	
(CH ₃) ₃ Si				170.8	171.3

modification given by the data in Table IIb, the heats of formation derived for the methylsilanes are

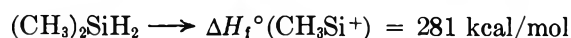
$$\Delta H_f^\circ(\text{CH}_3\text{SiH}_3) = 1.0 \text{ kcal/mol}$$

$$\Delta H_f^\circ[(\text{CH}_3)_2\text{SiH}_2] = -7.8 \text{ kcal/mol}$$

$$\Delta H_f^\circ[(\text{CH}_3)_3\text{SiH}] = -18.0 \text{ kcal/mol}$$

$$\Delta H_f^\circ[(\text{CH}_3)_4\text{Si}] = -33.0 \text{ kcal/mol}$$

The *AP*(*m/e* 43) values from CH₃SiH₃, (CH₃)₂SiH₂, and (CH₃)₃SiH, which were not used in our least-squares treatment, should provide a further test for the internal consistency of our data. Thus, from the appearance potentials of *m/e* 43 in Table I one finds the following



The agreement can be considered good if one takes into account the higher error limits of these data; also the $\Delta H_f^\circ(\text{CH}_3\text{Si}^+)$ value from (CH₃)₄Si obtained by Hobrock and Kiser¹⁹ agrees within the combined limits of our errors, when their value is recalculated with our new $\Delta H_f^\circ[(\text{CH}_3)_4\text{Si}]$ value. Very good also is the agreement with our values for $\Delta H_f^\circ(\text{CH}_3\text{SiH}^+)$ from (CH₃)₃SiH. The agreement of $\Delta H_f^\circ(\text{CH}_3\text{Si}^+)$ obtained from *AP*(CH₃Si⁺) from (CH₃)₃SiH and $\Delta H_f^\circ[(\text{CH}_3)_2\text{Si}^+]$ obtained from *AP*[(CH₃)₂Si⁺] from (CH₃)₄Si is poor and may be due to excess energy in the formation of these ions.

It is easy to derive the following equations from Allen's scheme¹⁶ and all calculated values in Table III

Table III: Standard Heats of Formation of Alkylsilanes

Compound	ΔH_f° , ref 11	ΔH_f° , ref 9	ΔH_f° (calcd) this work
CH ₃ SiH ₃		-4	1.0
(CH ₃) ₂ SiH ₂	-42		-7.8
(CH ₃) ₃ SiH	-60		-18.1
(CH ₃) ₄ Si	-69		-33.0
C ₂ H ₅ SiH ₃	-21	-15	-4.0
(C ₂ H ₅) ₂ SiH ₂	-36		-17.7
(C ₂ H ₅) ₃ SiH	-39		-33.0
(C ₂ H ₅) ₄ Si	-37		-52.8
<i>i</i> -C ₄ H ₉ SiH ₃		-14	-11.5
<i>n</i> -C ₄ H ₉ SiH ₃	-14		-13.9
<i>i</i> -C ₄ H ₉ SiH ₂	-24		-16.5
<i>t</i> -C ₄ H ₉ SiH ₂		-11	-21.7
(CH ₂) ₂ Si(CH ₂ CH ₂ CH ₃) ₂	-41		-52.8

have been obtained with these formulas

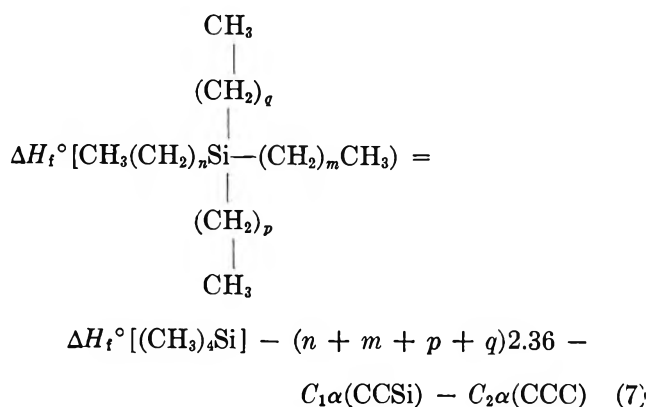
$$\Delta H_f^\circ[\text{CH}_3(\text{CH}_2)_n\text{SiH}_3] = \Delta H_f^\circ(\text{CH}_3\text{SiH}_3) - 2.36n - C_1\alpha(\text{CCSi}) - C_2\alpha(\text{CCC}) \quad (4)$$

$$\Delta H_f^\circ[\text{CH}_3(\text{CH}_2)_n\text{SiH}_2(\text{CH}_2)_m\text{CH}_3] = \Delta H_f^\circ[(\text{CH}_3)_2\text{SiH}_2] - (n+m)2.36 - C_1\alpha(\text{CCSi}) - C_2\alpha(\text{CCC}) \quad (5)$$

$$\Delta H_f^\circ[\text{CH}_3(\text{CH}_2)_n\text{SiH}(\text{CH}_2)_m\text{CH}_3] = \Delta H_f^\circ[(\text{CH}_3)_3\text{SiH}] - (n+m+p)2.36 - C_1\alpha(\text{CCSi}) - C_2\alpha(\text{CCC}) \quad (6)$$

$$\begin{array}{c} | \\ (\text{CH}_2)_p \\ | \\ \text{CH}_3 \end{array}$$

(19) B. G. Hobrock and R. W. Kiser, *J. Phys. Chem.*, **65**, 2186 (1961).



where C_1 and C_2 are the number of C-C-Si interactions and C-C-C interactions, respectively.¹⁶ The value $\alpha(\text{CCSi})$ is not known but as a first approximation we take the same value as for $\alpha(\text{CCC})$. The error limits involved are certainly not higher than those we would obtain if we derive $\alpha(\text{CCSi})$ from the reported ΔH_f° for $(\text{C}_2\text{H}_5)\text{SiH}_3$, $i\text{-C}_3\text{H}_7\text{SiH}_3$, and $t\text{-C}_4\text{H}_9\text{SiH}_3$; in this case the $\alpha(\text{CCSi})$ values vary from +13.6 kcal to -1 kcal which attests to the inconsistency of these measured heats of formation.

The agreement between calculated and measured heats of formation in Table III is so poor that it does not deserve further consideration but, as pointed out earlier in this paper and by others,¹² the measured values are quite unreliable. The parameters derived for the bond energy scheme are certainly reasonable when one compares them with other similar parameters.¹³ For example, our optimum $B(\text{Si}-\text{C})$ value is slightly less than the arithmetic mean of $B(\text{Si}-\text{Si})$ and $B(\text{C}-\text{C})$ and this is also true for the $B(\text{Sn}-\text{C})$ case.¹⁴ Indeed, in view of the consistency of measured ΔH_f° values for SiH_4 and Si_2H_6 ,^{7,8} the consistency of $AP\text{-}(\text{SiH}_2^+)$ from SiH_4 ,^{2,9} Si_2H_6 ,^{2,17} and CH_3SiH_3 ,^{2,9} and the observation of Skinner, *et al.*,¹³⁻¹⁵ that the bond interaction scheme of Allen¹⁶ can be applied with success to alkylstannanes, we are convinced that the calculated values are more reliable. We believe the calculated values to be precise to within 2 kcal/mol and accurate to within 5 kcal/mol.

There is one further example to test the correctness of our parameters. Hess, *et al.*,²⁰ have reported the $AP[(\text{CH}_3)_3\text{Si}^+]$ from hexamethyldisilane to be 10.69 eV. With the measured $AP[(\text{CH}_3)_3\text{Si}^+]$ from tri- and tetramethylsilane, Tannenbaum's ΔH_f° values for these compounds,¹¹ and an estimated ΔH_f° value for $(\text{CH}_3)_6\text{Si}_2$, they calculated the dissociation energy of the Si-Si bond in $(\text{CH}_3)_6\text{Si}_2$ to be $D(\text{Si}-\text{Si}) = 86$ kcal/mol. This value was criticized by Connor, *et al.*,²¹ since they had derived a value of 49-58 kcal/mol for the bond dissociation energy from studies of the thermal decomposition of hexamethyldisilane. The value of 49-58 kcal/mol, in turn, has been criticized by Davidson and Stephenson,²² who derive a value of 67 kcal/mol from their kinetic measurements. Both groups^{21,22} have

repeated the measurement of $AP[(\text{CH}_3)_3\text{Si}^+]$ from hexamethyldisilane and tri- and tetramethylsilane.^{21,22} The values found for $AP[(\text{CH}_3)_3\text{Si}^+]$ from tri- and tetramethylsilane^{21,22} are in very good agreement with our values (see Table I, so that we may with confidence adopt their $AP[(\text{CH}_3)_3\text{Si}^+] = 10.0$ eV from hexamethyldisilane. From $AP[(\text{CH}_3)_3\text{Si}^+] = 10.0$ ^{21,22} and $D(\text{Si}-\text{Si}) = 67$ kcal/mol,²² we can at once derive the heat of formation of $(\text{CH}_3)_6\text{Si}_2$, since

$$\Delta H_f^\circ [(\text{CH}_3)_6\text{Si}_2] + AF = \Delta H_f^\circ [(\text{CH}_3)_3\text{Si}^+] + \Delta H_f^\circ [(\text{CH}_3)_3\text{Si}]$$

and

$$\Delta H_f^\circ [(\text{CH}_3)_6\text{Si}_2] + D(\text{Si}-\text{Si}) = 2\Delta H_f^\circ [(\text{CH}_3)_3\text{Si}]$$

With $AP = 230$ kcal/mol,^{21,22} $D(\text{Si}-\text{Si}) = 67$ kcal/mol,²² and $\Delta H_f^\circ [(\text{CF}_3)_3\text{Si}^+] = 171$ kcal/mol (see Table IIb), we find

$$\Delta H_f^\circ [(\text{CH}_3)_6\text{Si}_2] = -50 \text{ kcal/mol}$$

From our bond energy term values we derive

$$\Delta H_f^\circ [(\text{CH}_3)_6\text{Si}_2] = -35 \text{ kcal} - 6\alpha(\text{CSiSi})$$

which leads to the very reasonable value of $\alpha(\text{CSiSi}) = 2.5$ kcal/mol.²⁶⁻²⁹

The value obtained for $\Delta H_f^\circ [(\text{CH}_3)_6\text{Si}_2]$ may be combined with $D[(\text{CH}_3)_3\text{Si}^+ - \text{Si}(\text{CH}_3)_3]$ ²² to yield the standard heat of formation of the trimethylsilyl radical as $\Delta H_f^\circ [(\text{CH}_3)_3\text{Si}] = 9$ kcal/mol, and this in turn may be combined with $\Delta H_f^\circ [(\text{CH}_3)_3\text{Si}^+]$ to give for the ionization potential of the radical the value, $I_z[(\text{CH}_3)_3\text{Si}] = 7.0$ eV. Comparison of this radical ionization potential with those reported for $(\text{CH}_3)_3\text{C}$ ^{23,24} and $(\text{CH}_3)_3\text{Sn}$ radicals^{24,25} attest to our $I_z[(\text{CH}_3)_3\text{Si}]$ being of the expected magnitude.²⁶⁻²⁹

If our value of $\Delta H_f^\circ [(\text{CH}_3)_3\text{Si}] = 9$ kcal/mol is combined with $\Delta H_f^\circ (\text{Cl}) = 28.9$ kcal/mol³⁰ and $\Delta H_f^\circ [(\text{CH}_3)_3\text{SiCl}] = -84.7$ kcal/mol,³¹ one obtains

(20) G. G. Hess, F. W. Lampe, and L. H. Sommer, *J. Amer. Chem. Soc.*, **85**, 5327 (1965).

(21) J. A. Connor, G. Finney, G. J. Leigh, R. N. Haszeldine, P. J. Robinson, R. D. Sedgwick, and R. F. Simmons, *Chem. Commun.*, 178 (1966).

(22) I. M. T. Davidson and I. L. Stephenson, *J. Chem. Soc.*, A, 282 (1968).

(23) F. P. Lossing and J. P. deSousa, *J. Amer. Chem. Soc.*, **81**, 281 (1959).

(24) F. W. Lampe and A. Nehaus, *J. Chem. Phys.*, **49**, 2949 (1968).

(25) A. L. Yergey and F. W. Lampe, *J. Organometal. Chem.*, **15**, 339 (1968).

(26) B. G. Hobrock and R. W. Kiser, *J. Phys. Chem.*, **66**, 155 (1962).

(27) "JANAF Interim Thermochemical Tables," The Dow Chemical Company, Midland, Mich., 1960.

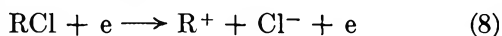
(28) National Bureau of Standards Technical Note 270-3, U. S. Government Printing Office, Washington, D. C., 1968.

(29) D. M. Golden, R. Wash, and S. W. Benson, *J. Amer. Chem. Soc.*, **87**, 4053 (1965).

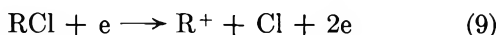
(30) C. T. Mortimer, "Reaction Heats and Bond Strengths," Pergamon Press, New York, N. Y., 1962 p 130.

(31) A. E. Beezer and C. T. Mortimer, *J. Chem. Soc. A*, 514 (1966).

the dissociation energy, $D[(\text{CH}_3)_3\text{Si} - \text{Cl}] = 123$ kcal/mol. This is in serious disagreement with the value of 88 kcal/mol deduced by Band, Davidson, Lambert, and Stephenson¹² for this dissociation energy from their measured appearance potential of $(\text{CH}_3)_3\text{Si}^+$ from $(\text{CH}_3)_3\text{SiCl}$. Band, *et al.*,¹² obtained a value of 10.9 eV, for the appearance potential of $(\text{CH}_3)_3\text{Si}^+$ from $(\text{CH}_3)_3\text{SiCl}$. Comparing this value with 11.5 eV²¹ and 12.40 eV,²⁰ that had been reported earlier, these authors¹² have assumed their value of 10.9 eV to be more nearly correct because it is the lowest reported. While it is often true that for the *minimum energy process* the lowest appearance potential is most likely to be correct, this "rule" is particularly difficult to apply in the case of halogen-containing compounds. For example, it is well known that the ionization-efficiency curves of alkyl ions from alkyl chlorides³²⁻³⁴ exhibit a low-intensity step function at low energies due to the ion-pair process



and that this low-intensity step function is later joined by the normal high-intensity direct ionization process, *viz.*



Furthermore, the ion-pair process itself (8) exhibits structure, as a result of different degrees of excitation in the R^+ ion, and the lowest-energy ion-pair process is not necessarily the most intense.³³ The pertinent conclusion of these considerations is that the use of a high-sensitivity electron-impact method, such as using the full energy spread of a normal electron beam,^{12,21} can lead one to extrapolate the low-intensity tail of the ionization efficiency curve of R^+ to values below the onset of (9) but above the onset of (8). On the other hand, the low-sensitivity RPD method employed by Hess, Lampe, and Sommer²⁰ would not detect the low-intensity ion-pair process and so would be expected to yield reliably the onset energy of (9). This expectation furthermore is consistent with all the alkylsilane thermochemical data reported in this paper. Thus if we take the value of 12.40 eV²⁰ to be the onset energy of (9), for $\text{R} = (\text{CH}_3)_3\text{Si}$, and combine it with $\Delta H_f^\circ(\text{Cl})$ and $\Delta H_f^\circ[(\text{CH}_3)_3\text{SiCl}]$, we obtain $\Delta H_f^\circ[(\text{CH}_3)_3\text{Si}^+] = 172.2$ kcal/mol, which is in excellent agreement with the

values for this ion in Table II, and substantiates our value of 9 kcal/mol for $\Delta H_f^\circ[(\text{CH}_3)_3\text{Si}]$. It is thus also indicated that the Si-Cl bond in trimethylchlorosilane has indeed a strength of 123 kcal/mol.

Acknowledgment. This research was supported by the United States Atomic Energy Commission under Contract No. At(30-1) - 3570. We also wish to thank the National Science Foundation for providing funds to assist in the original purchase of the mass spectrometer.

Appendix

The thermochemical values used in the calculations are tabulated below.

$$\Delta H_f^\circ(\text{SiH}_4) = 7.3 \pm 0.3 \text{ kcal/mol}^8$$

$$\Delta H_f^\circ(\text{Si}_2\text{H}_6) = 17.1 \pm 0.3 \text{ kcal/mol}^8$$

$$\Delta H_f^\circ(\text{Si}_2) = 106.0 \pm 4.0 \text{ kcal/mol}^{27}$$

$$\Delta H_f^\circ(\text{C}_2) = 170.89 \pm 0.45 \text{ kcal/mol}^{27}$$

$$\Delta H_f^\circ(\text{H}) = 52.102 \pm 0.06 \text{ kcal/mol}^{27}$$

$$\Delta H_f^\circ(\text{CH}_4) = -17.88 \text{ kcal/mol}^{28}$$

$$\Delta H_f^\circ(\text{C}_2\text{H}_6) = -20.24 \text{ kcal/mol}^{28}$$

$$\Delta H_f^\circ(\text{CH}_3) = 34 \text{ kcal/mol}^{29}$$

$$B(\text{Si-C}) = 60.3 \pm 3.3 \text{ kcal/mol}^{35}$$

$$B(\text{Si-H}) = 76.77 \text{ kcal/mol}^{35}$$

$$B(\text{C-C}) = 78.85 \text{ kcal/mol}^{16}$$

$$B(\text{C-H}) = 99.29 \text{ kcal/mol}^{16}$$

$$B(\text{Si-Si}) = 46.16 \text{ kcal/mol}^{35}$$

$$\alpha(\text{CCC}) = 2.6 \text{ kcal/mol}^{13}$$

$$\alpha(\text{CSiC}) = 2.5 \text{ kcal/mol}^{36}$$

$$\alpha(\text{CCSi}) = 2.6 \text{ kcal/mol}^{36}$$

$$\alpha(\text{CSiSi}) = 2.7 \text{ kcal/mol}^{35}$$

(32) V. H. Dibeler and R. M. Reese, *J. Res. Nat. Bur. Stand.*, **54**, 127 (1955).

(33) S. Tsuda, C. E. Melton, and W. H. Hamill, *J. Chem. Phys.*, **41**, 689 (1964).

(34) V. H. Dibeler and J. A. Walker, *ibid.*, **43**, 1842 (1965).

(35) Values estimated from data in this paper.

(36) Values assumed.

Thermal Conductivity of Binary Mixtures of Alkali Nitrates

by John McDonald and H. Ted Davis¹

Department of Chemical Engineering, University of Minnesota, Minneapolis, Minnesota (Received June 19, 1969)

Experimental data are reported for the thermal conductivity of binary mixtures of alkali nitrates in the molten state. The excess thermal conductivities are negative and increase as the square of the difference between cation radii. A simple solution model shows that the behavior of the excess viscosity and thermal conductivity can also be attributed to differences between ionic masses.

I. Introduction

The purpose of this paper is to report measurements of the thermal conductivities of several binary alkali nitrate mixtures as a function of composition and temperature. The excess thermal conductivities are negative for all systems studied. Murgulescu and Zuca² observed the same behavior for the excess viscosities of several binary alkali nitrate mixtures. Also reported in this paper are viscosities of potassium and sodium nitrate solutions.

The excess thermal conductivities are plotted *vs.* the difference between the radii of the cations in the mixtures. It is found that the excess thermal conductivities increase as the square of the difference between cation radii.

On the basis of a simple solution model it is shown that the behavior of the excess viscosity and thermal conductivity can be attributed to differences between the masses instead of to differences between radii of the cations composing the mixture. Whether either the mass effect or size effect dominate cannot be determined in this work since the cation mass differences vary very similarly to the cation radius differences for the alkali nitrate systems. Systems in which the mass difference is important and the size difference is not, such as silver nitrate-alkali nitrate mixtures, thallium nitrate-alkali nitrate mixtures, etc., must be studied to sort out the effects. Such studies are underway now.

II. Experimental Technique and Results

Several methods are available for the measurement of the thermal conductivity of alkali nitrates. Bloom, *et al.*,^{3a} made use of a concentric cylinder apparatus as did White and Davis^{3b} recently. Turnbull⁴ used a hot wire method, but White⁵ has claimed that this method gives erroneous results due to the electrical conductivity of the salt. This method does work successfully for electrically nonconducting fluids. A list of experiments performed using this method is given by Turnbull. Gustafsson, Halling, and Kjellander⁶ have used an optical method for the pure alkali nitrates.

In our experiments, we have made use of a concentric cylinder apparatus sketched in Figure 1. The inner

cylinder was made of silver and the outer cylinder of type 446 stainless steel. The gap holding the molten salt between the cylinders was 0.1 in. and the length of the inner cylinder 7 in. White⁵ has shown that convective and radiative heat flows in such a cell are small. The total thermal end losses were kept below 5% by making use of a Mycalex cap at the base of the cell and a thin-walled stainless steel tube supporting the inner cylinder and housing the heater leads at the top. Two tubes from the cylinder gap, one from the base and the other from the top, enabled the cell to be filled and emptied, using a remote reservoir of molten salt and a simple vacuum-argon pressure arrangement. This arrangement enabled the cell to be left undisturbed throughout the total period of experimentation—a useful attribute in high-temperature work where corrosion of electrical leads and other delicate parts is occurring.

Since the end losses were small, a first-order estimation of these losses was considered sufficiently accurate. Thus we can write

$$Q = Q_1 + Q_2 = (C + D\kappa)\Delta T \quad (1)$$

where Q is the total heat flow from the inner to the outer cylinder, Q_1 is the heat flow through the solid end connections, and Q_2 is the heat flow through the salt.

κ is the thermal conductivity of the molten salt and ΔT the temperature difference between the two cylinders. The constants C and D were found by standardizing the cell with ethylene glycol and Dowtherm A. The temperature difference across the gap was found by means of chromel-alumel thermocouples linked to a Leeds and Northrup microvolt amplifier. Care was taken to shield the preamplification parts of the circuit electrically and thermally where necessary. The power

(1) Alfred P. Sloan Fellow.

(2) I. G. Murgulescu and S. Zuca, *Electrochim. Acta*, 1383 (1966).

(3) (a) H. Bloom, A. Doroszowski, and S. B. Tricklebank, *Aust. J. Chem.*, 18, 1171 (1965); (b) L. R. White and H. T. Davis, *J. Chem. Phys.*, 47, 5433 (1967).

(4) A. G. Turnbull, *Aust. J. Appl. Sci.*, 12, 30, 324 (1961).

(5) L. R. White, Doctoral Dissertation, Univ. of Minn., 1967.

(6) S. E. Gustafsson, N. O. Halling, and R. A. E. Kjellander, *Z. Naturforsch.*, 23A, 44, 682 (1968).

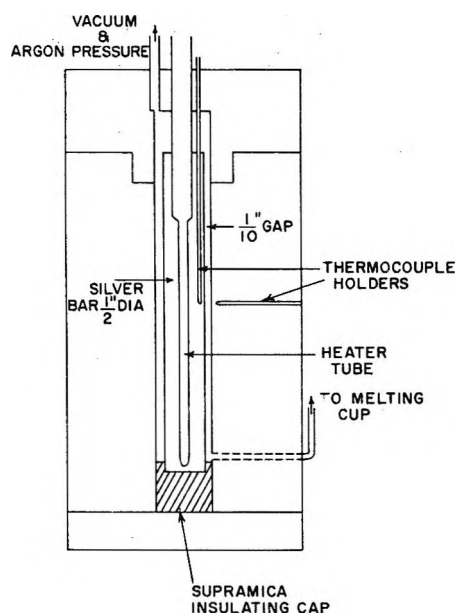


Figure 1. Concentric cylinder apparatus.

to the nichrome heater was calculated by measuring the voltage drop across the heater and a precision 1-ohm resistor in series with the heater. The cell was housed inside a furnace constructed from a design by Kleppa.⁷ The simple calculation of the thermal conductivities was made possible largely by the low thermal end losses which made an exact knowledge of the cell geometry in these regions unnecessary and made a standardization procedure quite sufficient.

We have obtained the thermal conductivity of binary mixtures of alkali nitrates for the cation pairs Na-K, Na-Cs, Li-Cs, K-Rb, and Rb-Cs. The experimental data have been fitted to a linear dependence of thermal conductivity on temperature by means of a least-mean-squares calculation. A small nonlinear dependence if present cannot be distinguished due to the inevitable small deviations of data from the best fitting line, caused by consistent and random experimental errors. The thermal conductivities of the pure and binary systems are given in Table I. We have approximated the data of Bloom^{3a} and of Gustafsson, *et al.*,⁶ by a linear curve fitting. Their data and the corresponding linear fits together with those of White and Davis^{3b} and of this paper are given in Figure 2 for pure KNO_3 . The equations for the linear fits are given in Table II along with the standard deviations σ of the least-mean-squares fits. As can be seen from Figure 2 and Table II, our data are intermediate between those of the other authors and the standard deviation of our results is small.

The thermal conductivities for the Li-Cs system at 450° are shown in Figure 3. For our purposes, the excess thermal conductivity of mixing (or deviation from "ideality") is defined by the equation

$$\Delta\kappa = \kappa_{\text{mix}} - x_1\kappa_1 - x_2\kappa_2 \quad (2)$$

Table I: Thermal Conductivities of Pure and Binary Alkali Nitrate Systems^a

Salt	%	Salt	%	κ
Li	100			$13.30 + 0.0050T$
Na	100			$11.36 + 0.0064T$
K	100			$8.04 + 0.0087T$
Rb	100			$6.28 + 0.0067T$
Cs	100			$6.57 + 0.0019T$
Li	25	Cs	75	$4.07 + 0.0081T$
Li	50	Cs	50	$6.77 + 0.0041T$
Li	75	Cs	25	$9.17 + 0.0041T$
Na	25	K	75	$9.01 + 0.0075T$
Na	50	K	50	$10.50 + 0.0048T$
Na	75	K	25	$11.61 + 0.0034T$
Na	25	Cs	75	$4.83 + 0.0068T$
Na	50	Cs	50	$6.46 + 0.0064T$
Na	75	Cs	25	$8.32 + 0.0055T$
K	25	Rb	75	$7.71 + 0.0045T$
K	50	Rb	50	$8.16 + 0.0042T$
K	75	Rb	25	$7.73 + 0.0072T$
Rb	50	Cs	50	$6.20 + 0.0045T$

^a Compositions are in molar percentages. Conductivity units are 10^{-4} cal/cm sec deg, and temperature T , degrees. $T < 460^\circ$.

Table II: Least-Mean-Squares Fit of Thermal Conductivity for KNO_3

Source	$\kappa(10^{-4}$ cal/cm sec deg)	σ^b
This work	$8.04 + 0.0087T^a$	0.14
Gustafsson, <i>et al.</i>	$10.76 + 0.0022T$	0.25
Bloom, <i>et al.</i>	$5.14 + 0.0194T$	0.28
White	$7.46 + 0.0088T$	0.23

^a T , °C. ^b Standard deviation.

where κ_{mix} is the thermal conductivity of the mixture and x_i is the mole fraction of the i th salt. As can be seen from Figure 3, which is typical for the systems studied, the values of $\Delta\kappa$ are negative. Palyvos, *et al.*,⁸ have predicted a negative value of $\Delta\kappa$ for binary mixtures of argon, methane, krypton, and xenon in the liquid state. Experimental results for the thermal conductivity of liquid mixtures (usually organic) have been obtained by Filippov and Novoselova.⁹ The excess thermal conductivities that they report are also negative.

In Figure 4, the values of the excess thermal conductivities of mixing are plotted *vs.* the mole fraction of the salt having the heavier cation. Smooth curves have been drawn through the experimental points by sight with the tacit assumption that the points lie on almost parabolic curves. All of the curves in Figure 4 are skewed toward the lighter cation-rich portion of the

(7) O. J. Kleppa, *J. Phys. Chem.*, **59**, 175 (1955).

(8) J. Palyvos, K. D. Luks, I. L. McLaughlin, and H. T. Davis, *J. Chem. Phys.*, **47**, 2082 (1967).

(9) L. P. Filippov and N. C. Novoselova, *Vestn. Mosk. Univ. No. 3*, 37 (1955).

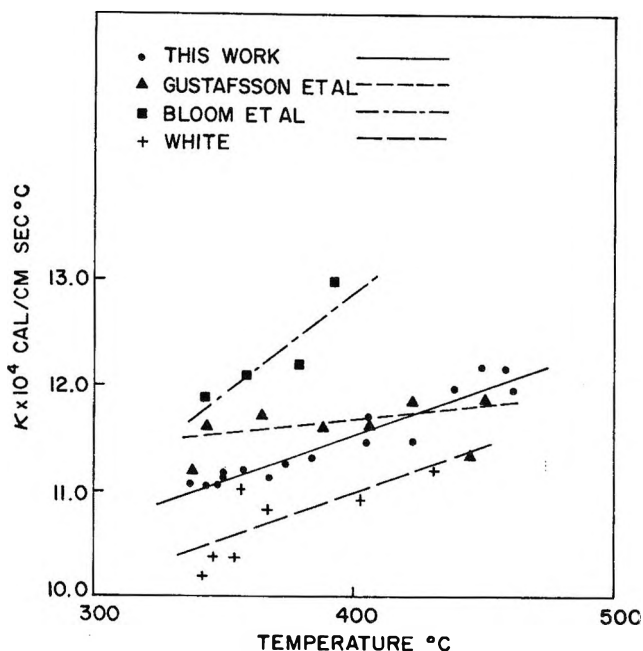


Figure 2. Comparison of thermal conductivity data of KNO_3 with earlier work.

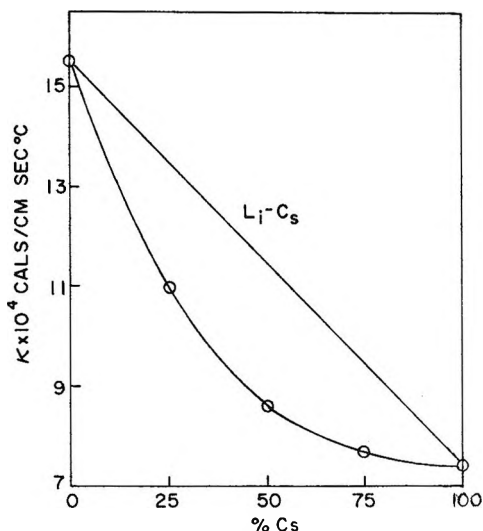


Figure 3. Thermal conductivity of the $(\text{Li-Cs})\text{NO}_3$ system at 450°C .

graph. The corresponding curves plotted by Murgulescu and Zuca² for excess viscosities are less skewed. It should be noted, however, that the curve for which the experimental error is least important due to relatively large $\Delta\kappa$, namely the Li-Cs curve, is fairly symmetric. Thus, if the excess thermal conductivities could be measured as accurately as the excess viscosities, the qualitative differences between the two quantities as a function of composition might be reduced.

III. Correlations of Excess Thermal Conductivities and Viscosities with Molecular Parameters

Kleppa and Hersh¹⁰ have found experimentally that the enthalpies of mixing of binary alkali nitrates obey the formula

$$\Delta H_m = x_1 x_2 \Omega \left(\frac{\lambda_2 - \lambda_1}{\lambda_1 \lambda_2} \right)^2 \quad (3)$$

where x_i is the mole fraction of the i th component of the mixture, Ω is a quantity (perhaps temperature dependent) having the same value for all the mixtures studied, and λ_i is the sum of the cation and anion radii of the i th component of the mixture. A correlation similar to eq 3 was also observed by Powers, Katz, and Kleppa¹¹ for the volumes of mixing of the alkali nitrates. The form of eq 3 has been predicted by Reiss, Katz, and Kleppa¹² by developing a conformal solution theory based on a simple potential model in which the short-range repulsive interactions between like ions are ignored and the potential energy is assumed to be pairwise additive with the pair potentials of the form

$$u(r)_{\alpha\beta} = \frac{1}{\lambda} f_{\alpha\beta} \left(\frac{r}{\lambda} \right) \quad (4)$$

where the form of $f_{\alpha\beta}$ depends only on whether $\alpha\beta$ is a like ion pair or an unlike ion pair. An example of the model defined by eq 3 is the Coulomb potential between like ions and the Coulomb potential plus a hard core cutoff at distance λ for unlike ions. The RKK theory has been shown¹³ to predict that all the excess thermodynamic quantities of mixing are of the form illustrated by eq 3.

Due to the fact that transport properties depend on the masses of the ions as well as the potential energy of interaction between the ions, there is no reason to expect that the excess transport properties can be correlated in

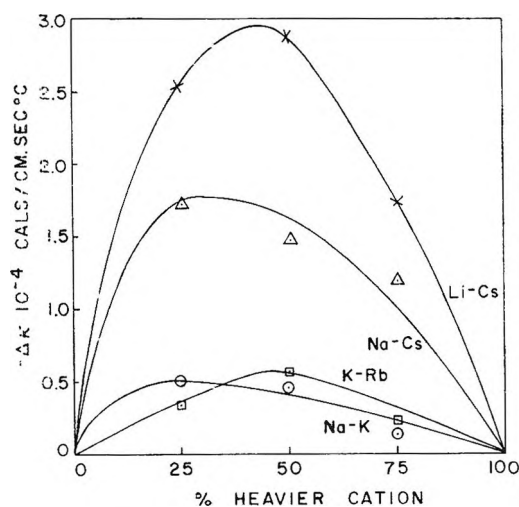


Figure 4. Excess thermal conductivity of binary mixtures of alkali nitrates at various compositions. $T = 450^\circ\text{C}$.

- (10) O. J. Kleppa and L. S. Hersh, *J. Chem. Phys.*, **34**, 351 (1961).
- (11) B. F. Powers, J. L. Katz, and O. J. Kleppa, *J. Phys. Chem.*, **66**, 103 (1962).
- (12) H. Reiss, J. Katz, and O. J. Kleppa, *J. Chem. Phys.*, **36**, 144 (1962).
- (13) H. T. Davis and J. McDonald, *ibid.*, **48**, 1644 (1968).

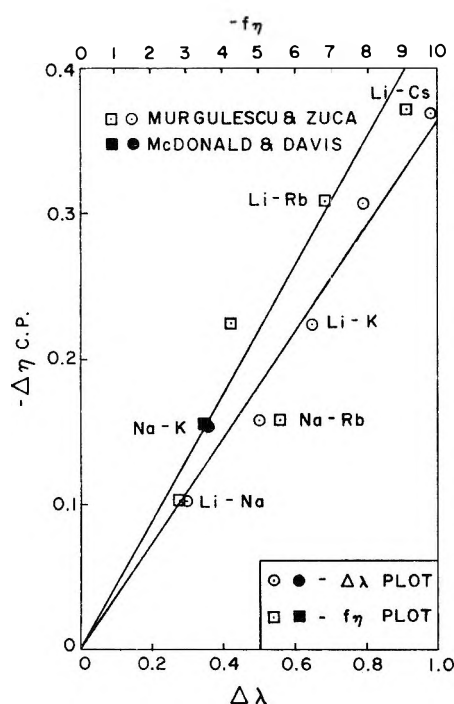


Figure 5. Excess viscosity *vs.* $\Delta\lambda$ and f_η for equimolar mixtures at 425°. Units of $\Delta\eta$ are centipoises.

terms of the length parameters alone. Nevertheless, Murgulescu and Zuca² have found that the excess viscosities of mixing of several binary mixtures of alkali nitrates obey the formula

$$\Delta\eta = -x_1x_2a(\lambda_2 - \lambda_1) \quad (5)$$

where a is a (temperature dependent) parameter having the same value for all the mixtures studied. Equation 5 is illustrated in Figure 5 in which we have plotted the excess viscosities of several equimolar binary alkali nitrate mixtures *vs.* the difference of the radii of the cation components of the mixtures. Except for the point for the $\text{NaNO}_3\text{-KNO}_3$ mixture the data plotted in Figure 5 are taken from Murgulescu and Zuca's work. The viscosity of the $\text{NaNO}_3\text{-KNO}_3$ mixture was studied in this laboratory and is presented in Table III. Our data compare favorably with that given by Janz.¹⁴

Table III: Viscosity of (Na-K)NO₃ Mixtures at $T = 425^\circ$

% Na	% K	η , cP	η (ref 14)
100	0	1.715	1.72
75	25	1.660	
50	50	1.641	
25	75	1.740	
0	100	1.876	1.87

In Figure 6, the excess thermal conductivities of the mixtures (at equimolar composition) studied in this work are plotted *vs.* the parameter $\lambda_2 - \lambda_1$. The correlation is not as good as that for viscosity. A plot of $\Delta\kappa$

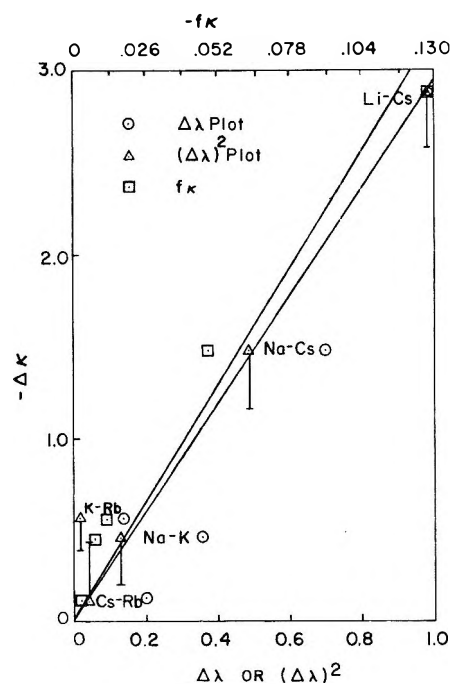


Figure 6. Excess thermal conductivities *vs.* $\Delta\lambda$, $(\Delta\lambda)^2$, and f_η for equimolar mixtures at 450°. Units of $\Delta\eta$ are 10^{-4} cal/cm sec deg.

vs. $(\lambda_2 - \lambda_1)^2$, also given in Figure 6, yields a better correlation, indicating that $\Delta\kappa$ is proportional to the square of $\lambda_2 - \lambda_1$ in contrast to $\Delta\eta$ which is linear in $\lambda_2 - \lambda_1$. This difference in behavior of $\Delta\eta$ and $\Delta\kappa$ is surprising in view of the strong similarities in the dependence of the viscosity and thermal conductivity on the potential energy. This similarity is most clearly evident in the autocorrelation function formulas¹⁵ for the transport coefficients.

In view of the fact that $\Delta\kappa$ and $\Delta\eta$ correlate differently with respect to the parameter $\lambda_2 - \lambda_1$ and an intuitive feeling that a mass effect should be observed in transport phenomena, we introduce here an alternative correlation scheme for the excess transport quantities. If the kinetic contribution to transport is ignored (an excellent approximation for the coefficients of viscosity and thermal conductivity of liquids as dense as the molten salts) the coefficient of thermal conductivity (and of viscosity) of the pure i th salt can be written in the form

$$\kappa^{(i)} = \kappa_{AA}^{(i)} + \kappa_{AC}^{(i)} + \kappa_{CC}^{(i)} \quad (6)$$

where $\kappa_{AA}^{(i)}$ represents the contribution to κ from anion-anion interactions, $\kappa_{CC}^{(i)}$ that from cation-cation interactions. A contribution $\kappa_{\alpha\beta}^{(i)}$, if it is assumed that energy is transported *via* a pairwise additive potential of interaction, will depend explicitly on the product $N_\alpha N_\beta$ (N_α and N_β being the number of molecules of types α and β , respectively) and will depend implicitly

(14) G. J. Janz, A. T. Ward, and R. D. Reeves, "Molten Salt Data," Rensselaer Polytechnic Institute, Troy, N. Y., 1964.

(15) R. Zwanzig, *Ann. Rev. Phys. Chem.*, **16**, 67 (1965).

on composition through the effect of composition on the structure of fluid around the interacting pair $\alpha\beta$. Next consider a mixture of charge symmetric salts 1 and 2 having a common anion A. The thermal conductivity of the mixture may be conveniently written in the form

$$\kappa^{(1,2)} = \kappa_{AA}^{(1,2)} + x_1\kappa_{AC}^{(1,2)} + x_2\kappa_{AC'}^{(1,2)} + x_1^2\kappa_{CC}^{(1,2)} + x_2^2\kappa_{C'C'}^{(1,2)} + 2x_1x_2\kappa_{CC'}^{(1,2)} \quad (7)$$

where x_i denotes the mole fraction of the i th salt and C and C' denote the cations of salts 1 and 2, respectively. In writing the mole fractions in eq 7, we have again noted the explicit dependence of a term $\kappa_{\alpha\beta}$ on the product $N_\alpha N_\beta$. In a pure charge symmetric salt of N molecules, there are N anions and N cations. In a binary mixture having a total of N molecules of charge symmetric salts having a common anion, there are N anions, $x_1 N$ cations of type C, and $x_2 N$ cations of type C'.

Equations 6 and 7 are general at this point. Indeed, they represent definitions of the quantities $\kappa_{\alpha\beta}$. We shall now introduce our model solution assumptions.

$$(I) \quad \kappa_{\alpha\beta}^{(1,2)} = \kappa_{\alpha\beta}^{(1)} = \kappa_{\alpha\beta}^{(2)} \text{ for all pairs } \alpha\beta \quad (8)$$

$$(II) \quad \kappa_{CC'} = \left(\frac{m_C m_{C'}}{(m_C + m_{C'})^3} \right)^{1/2} \kappa^*_{CC'} \quad (9)$$

$$\kappa_{CC} = \frac{1}{(2^3 m_C)^{1/2}} \kappa^*_{CC} \quad (10)$$

$$\kappa_{C'C'} = \frac{1}{(2^3 m_{C'})^{1/2}} \kappa^*_{C'C'} \quad (11)$$

where m_C and $m_{C'}$ denote the masses of cations C and C', respectively, and κ^*_{CC} is a reduced quantity common to all pure and mixed alkali nitrates. I is an "ideal solution" assumption implying that the environment around an interacting pair $\alpha\beta$ is not very different from the corresponding environment in the pure salt. Since we are considering a common anion mixture, assumption I is probably not bad as a first approximation. Assumption II, however, is more serious. It implies for one thing that the cations differ only in their masses, that is, that the differences in their cationic radii and dispersion interactions can be ignored. Moreover, we have assumed in II that the mass dependence of κ_{CC} , $\kappa_{CC'}$, and $\kappa_{C'C'}$ is the same as that predicted by the kinetic theory of collisional transport in fluids of molecules interacting *via* simple model potentials, such as the hard core or square-well model potentials.^{16,17}

On the basis of assumptions I and II, the excess thermal conductivity becomes

$$\Delta\kappa \equiv \kappa^{(1,2)} - x_1\kappa^{(1)} - x_2\kappa^{(2)} = x_1x_2\kappa^*_{CC'} f_\kappa \quad (12)$$

where

$$f_\kappa = 2 \left[\frac{m_C m_{C'}}{(m_C + m_{C'})^3} \right]^{1/2} - \frac{1}{(8m_C)^{1/2}} - \frac{1}{(8m_{C'})^{1/2}} \quad (13)$$

For viscosity, our model solution assumptions take the form

$$(I) \quad \eta_{\alpha\beta}^{(1,2)} = \eta_{\alpha\beta}^{(1)} = \eta_{\alpha\beta}^{(2)} \quad (14)$$

$$(II) \quad \eta_{CC'} = \left(\frac{m_C m_{C'}}{m_C + m_{C'}} \right)^{1/2} \eta^*_{CC'} \quad (15)$$

$$\eta_{CC} = \left(\frac{m_C}{2} \right)^{1/2} \eta^*_{CC} \quad (16)$$

$$\eta_{C'C'} = \left(\frac{m_{C'}}{2} \right)^{1/2} \eta^*_{C'C'} \quad (17)$$

Again the mass dependence of $\eta_{CC'}$, etc., has been assumed to be the same as that predicted by simple molecular models.^{16,17} Equations 14–17 lead to the following result for the excess viscosity

$$\Delta\eta \equiv \eta^{(1,2)} - x_1\eta^{(1)} - x_2\eta^{(2)} = x_1x_2\eta^*_{CC'} f_\eta \quad (18)$$

where

$$f_\eta = 2 \left(\frac{m_C m_{C'}}{m_C + m_{C'}} \right)^{1/2} - \left(\frac{m_C}{2} \right)^{1/2} - \left(\frac{m_{C'}}{2} \right)^{1/2} \quad (19)$$

The implications of our model are readily tested. First, since it can be readily shown that

$$f_\kappa \leq 0 \text{ and } f_\eta \leq 0 \quad (20)$$

eq 12 and 18 predict, respectively

$$\Delta\kappa \leq 0 \text{ and } \Delta\eta \leq 0 \quad (21)$$

This prediction is consistent with the excess thermal conductivities reported here and the excess viscosities reported by Murgulescu and Zuca. Secondly, at a fixed composition plots of $\Delta\kappa$ and $\Delta\eta$ *vs.* f_κ and f_η , respectively, for the various mixtures studied should yield straight lines. Such plots are shown in Figures 5 and 6. It is evident from these plots that the excess coefficients correlate about as well with respect to the mass parameters f_κ and f_η as they do with respect to the length parameter λ_2 and λ_1 . Finally, our model implies that $\Delta\eta$ and $\Delta\kappa$ should be directly proportional to the product x_1x_2 . This behavior is observed for $\Delta\eta$ for all the systems studied by Murgulescu and Zuca and for the potassium–sodium system reported here. However, the plots of $\Delta\kappa$ *vs.* composition shown in Figure 4 are skewed to the left of the predicted parabola, although for the system Li–Cs for which the experimental error is smallest compared to $\Delta\kappa$, the plot is almost of the form of the predicted parabola.

All in all, the agreement between the predictions of our model and experiment and the fact that $\Delta\kappa$ and $\Delta\eta$ cannot be correlated with the same power of $\lambda_2 - \lambda_1$

(16) S. Chapman and T. G. Cowling, *The "Mathematical Theory of Non-Uniform Gases,"* Cambridge, London, 1964.

(17) I. L. McLaughlin and H. T. Davis, *J. Chem. Phys.*, **45**, 2020 (1966).

suggests that the differences in cation masses is at least as important as, and maybe more important than, the differences in cation radii in determining the excess transport quantities.

Acknowledgments. We are grateful for financial support of this research furnished by the National Science Foundation, the U. S. Army Research Office, Durham, and the Alfred P. Sloan Foundation.

The Electrical Conductance of Molten Lead Chloride and Its Mixtures with Potassium Chloride

by A. J. Easteal^{1a} and I. M. Hodge^{1a}

Department of Chemistry, University of Auckland, Auckland, New Zealand (Received July 21, 1969)

The specific conductances of molten $\text{PbCl}_2 + \text{KCl}$ mixtures have been measured as functions of temperature and composition, for the ranges *ca.* 500–800° and *ca.* 20–100 mol % PbCl_2 , respectively. In the experimental temperature range the specific conductances of all melts follow (a) quadratic temperature dependences and (b) modified Arrhenius temperature dependences which can be expressed by equations due to Cohen and Turnbull and Adam and Gibbs. Bases for the interpretation of the composition dependence of conductance for these mixtures are examined, and the composition dependence is put on a rational basis in terms of the temperature T_0 , a parameter associated with the temperature of zero free volume, or zero configurational entropy.

Introduction

The composition and (to a lesser extent) temperature dependences of the transport properties of binary salt mixtures have been the subject of many papers in the molten salt field. Deviations from additivity relationships of, *inter alia*, conductance isotherms have been used diagnostically to infer the constitutions of many mixtures. Such deviations have led, for example, to the hypothesis that complex anionic species exist in molten lead halide-alkali metal halide and cadmium halide-alkali metal halide mixtures.^{1b} However, published interpretations of isotherms of conductance and other transport properties are open to doubt on several grounds. In particular, the absence of a suitable reference temperature for comparison of conductances makes deductions based on such comparison hazardous. It is not physically meaningful to ascribe differences in conductance of mixtures wholly to differences in the constitution of the mixtures, since the conductances may also differ because the comparison is made at nonequivalent temperatures.

It has been suggested that the freezing point be used as such a reference temperature,^{1b,2} and that conductances be compared at temperatures θ_f given by

$$\theta_f = \alpha T_f \quad (1)$$

where T_f is the liquidus temperature of a given mixture and α is a constant assigned arbitrary values (*e.g.*, 1.1,

1.2, . . .) However, the liquidus temperature of a given liquid mixture is determined at least as much by the structure of the solid phase formed on freezing as by the constitution to the liquid, so that T_f has no particular significance in respect to the transport properties of liquid mixtures. The critical temperatures would, perhaps, serve as reference temperatures, but again these are not governed wholly by the properties to the liquid phases and hence are still not entirely satisfactory.

The development of liquid free volume and other theories of transport processes in liquids now indirectly provides a sound basis for comparison of the transport properties of mixtures of different composition.³⁻¹⁰

(1) (a) Department of Chemistry, Purdue University, West Lafayette, Ind. 47907; (b) H. Bloom and E. Heymann, *Proc. Roy. Soc.*, **A188**, 392 (1947).

(2) I. S. Yaffe and E. R. Van Artsdalen, *J. Phys. Chem.*, **60**, 1125 (1956).

(3) C. A. Angell, *ibid.*, **68**, 218, 1917 (1964); **69**, 2137 (1965); **70**, 2793 (1966).

(4) R. Araujo, *J. Chem. Phys.*, **44**, 1299 (1966).

(5) M. H. Cohen and D. Turnbull, *ibid.*, **31**, 1164 (1959).

(6) M. H. Cohen and D. Turnbull, *ibid.*, **34**, 120 (1961).

(7) G. Adam and J. H. Gibbs, *ibid.*, **43**, 139 (1965).

(8) H. Bloom and A. J. Easteal, *Aust. J. Chem.*, **19**, 1577, 1779 (1966).

(9) M. F. Lantratov and O. F. Moiseeva, *Russ. J. Phys. Chem.*, **34**, 367 (1960).

(10) C. T. Moynihan, *J. Chem. Educ.*, **44**, 531 (1967); *J. Phys. Chem.*, **70**, 3399 (1966).

Equation 2 has been found by Angell,³ Araujo,⁴ and other workers to describe well the temperature dependence of transport properties of several molten salts.

$$D, \Lambda T, \phi T = AT^{1/2} \exp[-k/(T - T_0)] \quad (2)$$

θ = fluidity, D = diffusion coefficient, Λ = equivalent conductance, A , k , T_0 are constants. This equation is important because (a) it has a theoretical basis in the free volume theory of Cohen and Turnbull^{5,6} and (b) the parameter T_0 can be regarded as a "built in" reference temperature on which comparison of transport properties of mixtures and pure salts can be rationally based.

In this study we have investigated in some detail (with respect to both temperature and composition) the electrical conductance of lead chloride + potassium chloride mixtures. This system was chosen because the investigation forms part of a broader study of lead halide based binary systems, of which the results of some emf studies have been published,⁸ and because published data on the conductance of these mixtures^{1b,9} have shown areas of marked disagreement and some curious features worthy of reinvestigation. Furthermore, lead chloride + potassium chloride mixtures have been studied by a variety of equilibrium and non-equilibrium techniques, so that many independent experimental data are available for use in testing models of these mixtures.

To determine the temperature dependence of conductance we have used a well established technique (see Experimental Section) to measure the specific conductances of the melts at small temperature intervals (*ca.* 5°).

The data can be fitted with high precision to four analytical functions, eq 2-5

$$\kappa = A'T^{-1/2} \exp[-k'/(T - T_0')] \quad (3)$$

$$\kappa = A'' \exp[-k''/T \ln(T/T_0'')] \quad (4)$$

$$\kappa = a + bt + ct^2 \quad (5)$$

where

$$t = ^\circ\text{C}; T = ^\circ\text{K}; \kappa = \text{specific conductance}$$

Of these, eq 3 is a simplified form of eq 2, and eq 4 is similar to an equation derived by Adam and Gibbs;⁷ the parameter T_0 is the reference temperature referred to above. Equation 5 is a concise form in which to present the data and has implications to be discussed later; eq 2 has been used by Angell³ and Moynihan¹⁰ in analyses of the transport properties of other fused salts.

The composition dependence of specific conductance has been established from the measured conductances of pure PbCl_2 and of mixtures in the composition range 20-95 mol % PbCl_2 at intervals of *ca.* 5 mol %. This has been considered from both specific conductance isotherms and from graphs using θ_0 (eq 6) as a reference parameter

$$\theta_0 = \beta T_0 \quad (6)$$

Experimental Section

Lead chloride was prepared from May and Baker Ltd. AnalaR lead nitrate and hydrochloric acid and was purified by crystallization from very dilute aqueous hydrochloric acid followed by filtration in the molten state, under a nitrogen atmosphere, through a (nominal) porosity 2 silica frit. Potassium chloride was purified by precipitation from a cold saturated solution of the AnalaR salt with dried hydrogen chloride. Mixtures were prepared by fusion of the appropriate quantities of the two salts under a nitrogen atmosphere. Each experiment required approximately 12 g of mixture for conductance measurements and analysis. Each mixture was analyzed for lead before and after an experiment, by conversion of samples to the nitrates and titration with aqueous sodium molybdate using 0.2% aqueous Solochrome Red B as an adsorption indicator. The sodium molybdate solution was standardized against lead nitrate prepared from 99.999% zone refined lead metal.

Apparatus

A conventional vertical tube furnace was used, with 19 swg Kanthal Al resistance wire wound on a silica support tube. The heating element was differentially wound to give a uniform temperature zone at the center of the furnace. The silica support tube (3.8 cm inside diameter) was closed at the base. The furnace was supplied with power *via* a Variac autotransformer.

Temperatures were measured with a calibrated platinum vs. platinum + 13% rhodium thermocouple and a Leeds and Northrup millivolt potentiometer (Model 8686). The thermocouple was guarded with a quartz tube attached to the conductance cell, and the hot junction of the thermocouple was approximately 5 mm distant from the melt in the cell capillary.

Conductances were measured with a conventional ac Wheatstone bridge constructed in our laboratories. The bridge was fed by a 1000-Hz fixed-frequency oscillator, with variable capacitors in parallel with a calibrated (accuracy $\pm 0.01\%$) Tinsley Type 2641 H.F.I. noninductive resistance box. The bridge was also fitted with calibrated ratio arms, of Sullivan non-inductive resistors, to extend the resistance range by factor of 10 for cell constant determinations.

The sensitivity of the bridge for conductance measurements was 0.05%; for cell constant determinations an extra high gain amplifier could be switched into the detection circuit resulting in a sensitivity of 0.05% for a 20,000-ohm resistance. All leads connecting the conductance cell, resistance box, and ratio arms to the bridge were coaxial. A Wagner earth was not used.

The conductance cell, which was of all-quartz construction, was essentially a U-shaped capillary with an attached thermocouple sheath, similar to that described

by Yaffe and Van Artsdalen.¹¹ This design had the advantages that only small quantities of salt were required and that the cell constant was independent (within experimental precision) of the positions of the electrodes, provided they were completely immersed. The capillary was about 13 cm long with a bore of 0.7 ± 0.2 mm. Hollow cylindrical platinum electrodes were fabricated from 0.004-in. platinum sheet, and were welded to 26 swg platinum support wires. The electrodes were 2 cm long and 3 mm in diameter. To ensure a uniform temperature over the length of the capillary, the conductance cell was immersed in a bath of molten tin contained in a quartz tube which fitted closely into the furnace support tube. The surface of the tin was covered with charcoal to prevent excessive oxidation and subsequent attack (by oxides of tin) on the cell.

Experimental Procedure

Several cells were used in the course of the investigation; their cell constants were of the order 2500 cm^{-1} . The cell constant was determined with 1 demal solutions of potassium chloride in triple-distilled water at $25.00 \pm 0.01^\circ$, using the value of specific conductance $0.11134 \text{ ohm cm}^{-1}$ established by Jones and Bradshaw.¹² For each cell constant determination (made before and after each experiment) the electrodes were platinized according to the recommendations of Jones and Bollinger,¹³ and before each measurement of melt resistance the electrodes were washed and heated to red heat until no flame coloration was observed.

Melt resistances were measured at temperature intervals of $3\text{--}4^\circ$ while the melt cooled from approximately $760\text{--}800^\circ$, in most cases, to a lower limit determined by the liquidus temperatures of the mixtures (in the range $420\text{--}620^\circ$). In a typical experiment about 70 resistance measurements were made in the experimental temperature range. It was established that provided the cooling rate was not greater than about 3 deg min^{-1} , resistances determined during continuous cooling were within $\pm 0.1\%$ of the resistances measured at constant temperatures. After each experiment the cell and electrodes were cleaned with hot, concentrated aqueous solutions of ammonium acetate, washed with hot, distilled water, and soaked overnight in conductivity water. The cell was purged with nitrogen before each experiment.

Experimental Errors

A straightforward calculation shows that the cell constant at 1000° of a quartz cell of the type used in the present investigation is approximately 0.04% smaller than the value at 25° , and this temperature variation was neglected. The dimensional change in the platinum electrodes due to thermal expansion was also neglected, since the equivalent effect on cell resistance of variation in the position of the electrodes relative to the

capillary was shown experimentally to be negligible (less than 0.03%). The accuracy of the cell constant determinations was $\pm 0.1\%$, and on the average the cell constant changed by not more than 0.2% in the course of an experiment. The overall accuracy in specific conductances is considered to be within $\pm 0.4\%$.

The compositions of the mixtures were determined to $\pm 0.2 \text{ mol } \%$ PbCl_2 . The average change in composition in the course of an experiment was $0.5 \text{ mol } \%$ PbCl_2 , and the compositions quoted are considered to be accurate to $\pm 0.4\%$ PbCl_2 .

Results

In addition to pure PbCl_2 , mixtures of the following compositions were investigated (mol % PbCl_2): 93.6, 90.7, 83.7, 82.1, 79.6, 74.9, 70.3, 64.8, 59.3, 55.1, 49.0, 45.1, 41.4, 36.1, 29.8, 25.2, and 20.1.

The measured specific conductances of pure PbCl_2 obtained in this investigation are compared with published data in Table I. The close agreement indicates that the technique used for measuring conductance introduced negligible error into the data obtained.

Table I: Specific Conductance of PbCl_2

$T, ^\circ\text{C}$	Specific conductance		
	Present work ^a	Bloom and Heymann ^b	Lantratov and Moiseeva ^c
500	1.450 ^b	...	1.461
525	1.579 ^b	...	1.570
550	1.701	...	1.696
560	1.750	1.75	...
575	1.820	...	1.819
600	1.932	1.92	1.931
625	2.038	...	2.040
650	2.139	2.13	2.13
700	2.323	2.34	...
720	2.389	2.39	...

^a Frequency = 1000 Hz. ^b Extrapolated values from the analytical function for PbCl_2 (Table II).

The data for each mixture were fitted to a quadratic function of temperature, eq 5, using the IBM computer program POLRG, by the method of least-squares. This program allows a polynomial of degree seven or less to be fitted to the experimental data, and is formulated such that a calculation is terminated when the fit to the data is not improved by increasing the degree of the polynomial; in all cases the polynomial determined in this way was a quadratic. The parameters of these quadratics, together with the relative root-mean-square deviation of the experimental points from the computed curve, are given in Table II. It is important to note

(11) I. S. Yaffe and E. R. Van Artsdalen, *J. Phys. Chem.*, **59**, 118 (1955).

(12) G. Jones and B. C. Bradshaw, *J. Amer. Chem. Soc.*, **55**, 1780 (1933).

(13) G. Jones and G. M. Bollinger, *ibid.*, **57**, 280 (1935).

Table II: Parameters for the Quadratic Temperature Dependence of Specific Conductance at 1000 Hz

Composition, mol % PbCl_2	$\kappa = a + bt + ct^2$			rms deviation, %	Exptl temp range, °C
	a	$b \times 10^3$	$c \times 10^6$		
20.1	-2.192	7.660	-3.056	2.33	650-940
25.2	-1.018	4.499	-0.972	1.31	620-790
36.1	-1.542	6.290	-2.549	1.19	530-750
41.4	-1.334	5.758	-2.215	1.12	470-760
45.1	-1.327	5.837	-2.280	1.19	470-780
49.0	-1.356	6.142	-2.571	1.27	450-780
55.1	-1.366	6.252	-2.598	1.17	450-750
59.3	-1.373	6.382	-2.626	1.20	450-750
64.8	-1.490	6.906	-2.965	1.14	440-750
70.3	-1.631	7.457	-3.335	1.15	430-790
74.9	-1.691	7.635	-3.307	1.14	430-780
79.6	-1.815	8.098	-3.568	1.24	420-780
82.1	-1.844	8.124	-3.506	1.47	440-770
83.7	-1.958	8.537	-3.815	1.36	450-780
90.7	-2.060	8.920	-3.968	1.31	460-800
93.6	-2.220	9.419	-4.226	1.16	480-770
100.0	-2.377	9.994	-4.687	1.23	540-770

that the conductances given by the parameters in Table II are for 1000 Hz, but deviations from the infinite frequency values are expected to be small.

For pure PbCl_2 and all the mixtures, graphs of $\log \kappa$ and $\log \Lambda$ vs. $1/T$ showed marked curvature. Equations 2, 3, and 4 fit almost all of the data well. Equivalent conductances were calculated from the measured specific conductances and the density data of Boardmann, Dorman, and Heymann.¹⁴ The best-fit parameters of eq 2 are given in Table III. The fit of eq 2, 3, and 4 to the data for the 20.1 and 25.2 mol % PbCl_2 mixtures was poor, and the parameters for these mixtures have been omitted from Table III. Since the composition dependences of the parameters T_0' and

Table III: Equivalent Conductance Parameters;
 $\Lambda = AT^{-1/2} \exp[-k/(T - T_0)]$

Composition, mol % PbCl_2	$\ln A$	$k(\text{deg}^{-1})$	$T_0, ^\circ\text{K}$	rms deviation, %	Approximate uncertainty in $T_0, ^\circ\text{K}$
29.8	9.562	1507	196	0.16	± 35
36.1	9.506	1453	218	0.15	± 35
41.4	9.496	1518	192	0.13	± 15
45.1	9.517	1569	175	0.13	± 15
49.0	9.342	1368	209	0.16	± 30
55.1	9.404	1449	189	0.13	± 15
59.3	9.477	1513	172	0.16	± 15
64.8	9.369	1340	209	0.12	± 15
70.3	9.343	1289	222	0.11	± 15
74.9	9.407	1329	218	0.13	± 15
79.6	9.360	1248	238	0.18	± 15
82.1	9.375	1262	238	0.18	± 30
83.7	9.358	1237	244	0.14	± 30
90.7	9.379	1247	242	0.14	± 30
93.6	9.365	1194	260	0.11	± 15
100	9.321	1138	272	0.10	± 30

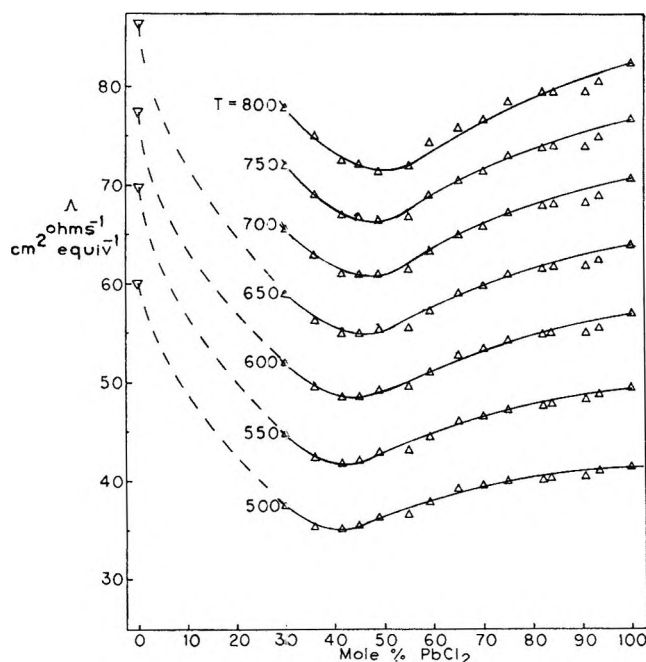


Figure 1. Equivalent conductance isotherms, T in $^\circ\text{C}$: Δ , our data; ∇ , from Yaffe and Vin Artsdalen (ref 2).

T_0'' in eq 3 and 4 closely follow that of T_0 in eq 2, only the best-fit parameters for the latter equation are given.

Discussion Section

The results of this investigation, with regard to the isothermal composition dependence of equivalent conductance for the $\text{PbCl}_2 + \text{KCl}$ system (Figure 1) agree

(14) N. K. Boardmann, F. E. Dorman, and E. Heymann, *J. Phys. Colloid Chem.*, **53**, 375 (1949).

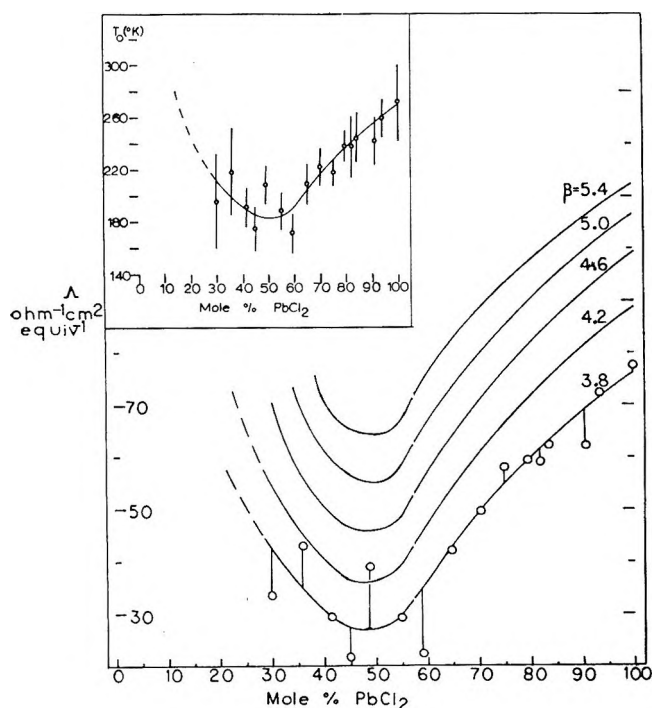


Figure 2. Equivalent conductance pseudo-isentropes, $\beta = T/T_0$. Inset, composition dependence of T_0 .

well with those of Lantratov and Moiseeva.⁹ The broad minimum at 40–50% PbCl_2 is common to both sets of data, and neither show the very small conductances at 20–25% PbCl_2 observed by Bloom and Heymann;^{1b} the latter appears to be an erroneous feature of Bloom and Heymann's work.

Equation 5 has been found to describe the temperature dependence of specific conductance of molten alkali metal halides,² and of their binary mixtures,¹¹ and appears to be a general description of the temperature dependence of specific conductance.¹⁵ A feature of this equation is that it predicts a maximum in conductance at a temperature given by

$$t = -b/2c \quad (7)$$

Maxima in conductance *vs.* temperature graphs have been observed by Grantham and Yosim for several salts,¹⁶ but our measurements did not extend to high enough temperatures to test this for the present system.

The magnitudes of the deviations from Arrhenius temperature dependence are illustrated by the large values of T_0 for eq 3. It follows that the transition state model of ionic migration is not valid for the $\text{PbCl}_2 + \text{KCl}$ system.

Equation 2 is based on the "free volume" model for transport properties due to Cohen and Turnbull,^{5,6} in which T_0 is the temperature below which the free volume of the system is zero.

Equation 4 is based on the "co-operative rearrangement" model of Adam and Gibbs,⁷ in which T_0'' represents the temperature below which the configurational

entropy of the system is zero. The composition dependence of T_0'' is strikingly similar to the composition dependences of T_0 and T_0' , suggesting that these parameters have a common origin. It can be shown mathematically that $T \ln(T/T_0'') = a + b(T - T_0'') = b(T - T_0')$, to within 1% over a 300° temperature range. Thus, apart from the preexponential function, equations 3 and 4 are functionally related.

The Cohen-Turnbull and Adam-Gibbs models are attempts to describe the glass transition phenomenon, and the parameters T_0 and T_0'' are the idealized temperatures at which the second-order transition responsible for the glass transition phenomenon occurs for infinitely slow cooling rates. The two models ascribe the glass transition to different causes, but it is evident that the parameters T_0 and T_0'' are both closely correlated with the experimental glass transition temperature T_g . This has been demonstrated experimentally for the system zinc chloride + pyridinium chloride,¹⁷ and for other glass-forming systems.

The temperature T_g is clearly a function only of the liquid structure and is unaffected by properties of the vapor or of the crystalline solid. Glasses may be considered to be solids in which the liquid structure has been "frozen in," the chief characteristic which differentiates between glass and liquid being the mobility of the constituent entities. The temperature T_0 thus appears to be an ideal reference temperature for the liquid state.

In terms of the Adam-Gibbs model, T_0'' is related to the macroscopic thermodynamic parameters of the liquid by the equation

$$S_C = \Delta c_p \ln(T/T_0'') \quad (8)$$

where S_C = configurational entropy and Δc_p is the difference in heat capacities of the liquid and glassy states. If Δc_p is invariant with composition, then T/T_0'' is directly proportional to the configurational entropy of the liquid at temperature T . Thus comparisons of conductance at equal values of T/T_0'' may be considered to be made under isentropic conditions, and graphs of the composition dependence of conductance at equal values of T_0/T_0'' may be termed "isentropes." Because of the assumption made about Δc_p , and because T_0'' is only approximately the temperature of zero configurational entropy (see later discussion), we propose to call these graphs "pseudo-isentropes." The equivalent conductance pseudo-isentropes for the $\text{KCl} + \text{PbCl}_2$ system are given in Figure 2. The curves of Figure 2 have been plotted from equivalent conductances calculated from the best-fit parameters of eq 2.

(15) G. J. Janz, "Molten Salt Handbook," Academic Press, New York, N. Y., 1967, pp 290–297.

(16) L. F. Grantham and S. J. Yosim, *J. Phys. Chem.*, **67**, 2506 (1963); *J. Chem. Phys.*, **43**, 1415 (1965); **44**, 1509 (1966); **45**, 1192 (1966).

(17) A. J. Easteal and C. A. Angell, to be published.

The open circles show one set of calculated conductances. The scatter of the points about the curve is due in part to uncertainty in the density data from which the conductances were calculated; densities were available for only a few of the mixtures so that densities for most mixtures were obtained by interpolation of density isotherms. The inset of Figure 2 shows the composition variation of T_0 , and it is the same (within the limits indicated) as the composition variations of T_0' and T_0'' . The limits of uncertainty shown are the ranges of T_0 which correspond to ± 1.5 times the minimum rms deviation of the experimental points from the curves calculated on the basis of eq 2. It can be seen that in the composition region rich in PbCl_2 the experimental scatter about the curve of best fit is quite small.

A comparison of the pseudo-isotherms with the isotherms of equivalent conductance indicates the usefulness of the concept of pseudo-isentropic comparison. Figure 2 shows a clearly defined minimum at 50 mol % PbCl_2 , which does not shift with temperature (*i.e.*, with configurational entropy), whereas in Figure 1 the minimum is much broader and shifts from 40 mol % PbCl_2 at lower temperatures to 50 mol % PbCl_2 at higher temperatures. It is difficult to account for this shift in the isotherm minimum. On the other hand, the pseudo-isotherms indicate that the structural characteristics responsible for the decrease in conductance do not change with temperature. Furthermore, the composition at which the pseudo-isentrope minimum occurs corresponds to the stoichiometry of the entity PbCl_3^- , which has been postulated to account for, *inter alia*, vapor pressure data.¹⁸ A tentative correlation of T_0'' (and T_0 , T_0') with ion association in $\text{PbCl}_2 + \text{KCl}$ mixtures is thus suggested, but a more detailed interpretation is not justified on the basis of the results reported here.

Because the absolute magnitudes of T_0 , T_0' , and T_0'' are not significant it cannot be said that they are precisely the temperatures of zero free volume (and configurational entropy) and similarly the other parameters

have no unambiguous interpretation. However, T_0 , T_0' , and T_0'' should be reasonably good approximations to these temperatures.

The closeness of fit of the functions defined by eq 3 and 4 to the experimental conductance data (rms deviation 0.1–0.2%) is suggestive that the mechanism of ionic transport in $\text{PbCl}_2 + \text{KCl}$ electrolytes is related to a cooperative rearrangement mechanism. However, the fact that quadratic functions of temperature (eq 5) fit the data almost equally well on the whole indicates that some caution must be exercised in applying a cooperative relaxation model to these liquids. Indeed there may be still further functional relationships between conductance and temperature which fit the data with precision of the same order as for the functions discussed here (the Arrhenius equation is a notable exception), and which are derivable from quite different transport mechanisms. A more decisive assessment of the applicability of cooperative relaxation and liquid free volume type models to these electrolytes must await detailed analyses of the temperature dependence of precise data for other transport properties of the mixtures and/or estimation of T_0 from heat capacity data.

Conclusions

The use of the temperatures of zero free volume or zero configurational entropy, as a reference temperature appears to be useful for $\text{PbCl}_2 + \text{KCl}$ fused mixtures. Similar analyses of transport data for other high-temperature molten electrolytes may well yield more detailed interpretations of such data than have been obtained previously.

Acknowledgment. We are indebted to C. A. Angell and C. T. Moynihan for helpful and stimulating discussions, and the New Zealand Universities Research Grants Committee for an equipment grant.

(18) K. Hagemark, D. Hengstenburg, and M. Blander, *J. Phys. Chem.*, **71**, 1819 (1967).

Mass Transport in Ionic Melts at Low Temperatures. Chronopotentiometric Diffusion Coefficients of Silver(I), Cadmium(II), and Thallium(I) in Calcium Nitrate Tetrahydrate

by C. T. Moynihan and C. A. Angell

Department of Chemistry, Purdue University, Lafayette, Indiana 47907 (Received July 21, 1969)

Chronopotentiometric diffusion coefficients have been measured for Ag^+ , Tl^+ , and Cd^{2+} ions in molten calcium nitrate tetrahydrate over the temperature interval 15–60°. The diffusion coefficients, which are in the range 10^{-8} to 10^{-6} cm^2/sec , all show non-Arrhenius temperature dependences. Despite the differences in charge and size, the Arrhenius coefficients of the diffusivities at equal temperatures are almost the same for all ions and are also very close to those previously observed for electrical conductance and shear and bulk fluidities of the pure solvent. The cooperative character of the basic mass-transporting event is thus further supported. At a given temperature, D_{Ag^+} and D_{Tl^+} are about twice as large as $D_{\text{Cd}^{2+}}$. Application to these data of an empirical, Stokes-Einstein type of correlation between diffusivity and fluidity for fused nitrates suggests that for $D_{\text{Cd}^{2+}}$ the mobile entity is the hydrated cation $\text{Cd}(\text{H}_2\text{O})_4^{2+}$.

In the past few years a number of investigations of the temperature dependence of transport properties have been reported for the ionic liquid calcium nitrate tetrahydrate (mp 42.7°). These include studies of conductance,¹⁻⁴ shear viscosity,^{1,4} bulk viscosity,⁵ and polarographic diffusion coefficient of Cd^{2+} at two temperatures.⁶ Much of the interest in this system has been generated because it is an easily studied example of an ionic liquid in which measurements can be extended well into the metastable supercooled region. It has been found for such liquids that the first few orders of magnitude of transport properties in the supercooled region generally exhibit a non-Arrhenius temperature dependence and are well described by the three-parameter Fulcher equation.⁷

$$w_j = A_j T^{-1/2} \exp\left(\frac{-k_j}{T - T_{0,j}}\right) \quad (1)$$

A_j , k_j , and $T_{0,j}$ are empirical parameters and w_j is a transport property, e.g., equivalent conductance (Λ), the reciprocal of the shear viscosity ($1/\eta_s$) or bulk viscosity ($1/\eta_v$), or the diffusivity/temperature quotient (D_i/T).⁸ Equation 1 can be derived from theories which take the free volume⁹ or the configurational entropy¹⁰ as the important quantities in setting the temperature dependence of the liquid transport properties. In these theories the T_0 parameter appears as an equilibrium property of the liquid, a theoretical glass transition temperature at which the free volume or configurational entropy of the liquid vanishes on cooling at an infinitely slow rate. Inherent in the configurational entropy derivation¹⁰ of eq 1 is also the notion that transport in the liquid at low temperatures occurs *via* a cooperative rearrangement of relatively large numbers

of liquid particles, a conclusion which has also been reached experimentally from a comparison of transport properties and structural relaxation times for a variety of liquids.^{11,12}

Although the applicability of eq 1 to low-temperature melts has been demonstrated many times for transport properties which reflect the combined mobilities of all ions present, it has not so far been upheld for the motion of a single species. Since the possibility that non-Arrhenius transport behavior might arise from some combination of individual ionic properties has not, to date, been eliminated, and because in any case the factors determining the preexponential term in eq 1 are

- (1) C. T. Moynihan, *J. Phys. Chem.*, **70**, 3399 (1966).
- (2) C. A. Angell, *J. Electrochem. Soc.*, **112**, 1224 (1965).
- (3) C. A. Angell, *J. Phys. Chem.*, **70**, 3988 (1966).
- (4) C. T. Moynihan, C. R. Smalley, C. A. Angell, and E. J. Sare, *ibid.*, **73**, 2287 (1969).
- (5) G. S. Darbari and S. Petrucci, *ibid.*, **73**, 921 (1969).
- (6) J. Braunstein, L. Orr, A. R. Alvarez-Funes, and H. Braunstein, *J. Electroanal. Chem.*, **15**, 337 (1968).
- (7) C. A. Angell and C. T. Moynihan in "Molten Salts: Characterization and Analysis," G. Mamantov, Ed., Marcel Dekker, Inc., New York, N. Y., 1969, p 315.
- (8) The preexponential $T^{-1/2}$ in eq 1 and the T^{-1} term in the w_j for diffusion coefficient arise from the application of the $T^{1/2}$ temperature dependence of ideal gas molecular velocities to diffusion coefficients in the liquid⁹ and from the Nernst-Einstein and Stokes-Einstein relationships among the various transport properties. These temperature factors are frequently omitted in applying eq 1, with little effect on the derived temperature dependence parameters k_j and $T_{0,j}$.
- (9) M. H. Cohen and D. Turnbull, *J. Chem. Phys.*, **31**, 1164 (1959).
- (10) G. Adam and J. H. Gibbs, *ibid.*, **43**, 139 (1965).
- (11) T. A. Litovitz and C. M. Davis in "Physical Acoustics," Vol. 2, Part A, W. P. Mason, Ed., Academic Press, New York, N. Y., 1965, p 281.
- (12) F. J. Bartoli, J. N. Birch, N.-H.-Toan, and G. E. McDuffie, *J. Chem. Phys.*, **49**, 1916 (1968).

poorly understood, the lack of self-diffusion coefficient measurements in the low-temperature region has been an obvious defect in the available data. Hence it was felt that an investigation of self-diffusion, again using calcium nitrate tetrahydrate as a trial system, should be undertaken.

Conventional self-diffusion coefficient measurements for the bulk ions of the melt by tracer methods suffer from two disadvantages: (a) because of the low values of the diffusion coefficients ($\sim 10^{-6}$ to 10^{-8} cm²/sec), inordinately long diffusion times, of the order of several days, are required, and (b) over this long a period there is a high likelihood that the run will be interrupted by crystallization of the metastable, supercooled melt. Consequently, it was decided to perform diffusion coefficient measurements for reducible cations (Ag⁺, Cd²⁺, and Tl⁺) present in low concentration in calcium nitrate tetrahydrate melts by the much more rapid method of chronopotentiometry.¹³

In this technique, an electrochemically active species in an unstirred, dilute solution with a large excess of inert electrolyte is electrolyzed at constant current, and the transition time, τ , required to exhaust the active species at the electrode surface is determined from the potential-time curve for the electrolysis. The diffusion coefficient of the active species i is given by the Sand equation

$$D_i = \frac{4I^2\tau}{\pi F^2 n^2 A^2 c_i^2} \quad (2)$$

where I is the current, F the Faraday constant, n the number of electrons required for electrolysis of an ion of i , A the electrode area, and c_i the concentration of i . Equation 2 is derived on the assumption that all of the current is consumed in the Faradaic electrolysis process, but in fact part of the current is always used in charging the electrode double-layer capacitances. A number of workers¹⁴⁻¹⁶ have considered this problem and shown, in effect, that eq 2 may be employed provided that the transition time, τ , is measured in a proper fashion to compensate for the effect of the double-layer charging. Laity and McIntyre¹⁴ have shown *via* irreversible thermodynamics that for fused salts the chronopotentiometric diffusion coefficient of an ion at low concentration can be equated to both its interdiffusion and self-diffusion coefficients.

Experimental Section

Calcium nitrate tetrahydrate, cadmium nitrate tetrahydrate, and silver nitrate were reagent grade chemicals and were used without further purification. The water content of the calcium nitrate tetrahydrate was determined by dehydrating the salt at 160° in a vacuum oven; the two lots used gave mole H₂O:mole Ca(NO₃)₂ ratios of 4.09 ± 0.01 . Thallium nitrate (British Drug Houses, Ltd.) was recrystallized once from water and dried at 110° before use. All solutions

were prepared by weighing the solid components directly into the chronopotentiometric cell. The calcium nitrate tetrahydrate was then melted in a hot water bath at about 50° and the reducible cation nitrates dissolved by agitating the melt with a magnetic stirrer.

The constant current source for the chronopotentiometry apparatus was a 225-V bank of dry cells connected in series with three potentiometers (10 M, 1 M, and 100 k) which were used as adjustable resistors to regulate the current. The magnitude of the current could be adjusted initially by passing it through a dummy 500-ohm resistor, after which the chronopotentiometric cell could be switched into the circuit by means of a DPDT switch. Current was measured during the electrolysis with a Keithley 610B electrometer which was found by calibration to be accurate to $\pm 0.5\%$. Potential-time curves were measured with an Esterline-Angus Speed Servo recorder, for which less than 0.1 sec was required for full scale recorder pen deflection. A chart speed of 0.75 in./sec was used in recording the chronopotentiograms.

The calcium nitrate tetrahydrate melts (about 90 g) were contained in tightly capped 35 or 38-mm od Pyrex tubes into which dipped two electrolysis electrodes. For experiments with Ag⁺ the tubes were painted black on the outside to lessen the chances of photodecomposition of silver ion. The anode and combined reference and counterelectrode was a 3-mm length of 0.5-mm diameter platinum wire emerging from a Pt-Pyrex seal in a piece of Pyrex tubing. For the melts containing Ag⁺ ion the cathode and indicator electrode was a platinum foil of approximate dimensions 10 × 12 mm. The foil was welded to a short length of platinum wire which emerged from a Pt-Pyrex seal in a piece of Pyrex tubing. The exact surface area of the Pt cathode (including foil edges and wire) was calculated from measurements of its dimensions and was found to be 2.54 ± 0.02 cm². Cd²⁺ and Tl⁺ cannot be reduced at a platinum electrode in calcium nitrate tetrahydrate melts due to the low hydrogen-or-platinum overvoltage. Hence for these two ions, a mercury pool cathode had to be employed. The mercury was contained in a J-shaped piece of 7-mm od Pyrex tubing, the short arm of which terminated in a cup formed from 14-mm od Pyrex and dipped below the surface of the melt. The long arm of the J-tube extended out through the cell cap, and contact to the mercury was made by a platinum wire in-

(13) Reviews of applications of chronopotentiometry to fused salts are given by C. H. Liu, K. E. Johnson, and H. A. Laitinen in "Molten Salt Chemistry," M. Blander, Ed., Interscience, New York, N. Y., 1964, p 681, and by H. A. Laitinen and R. A. Osteryoung in "Fused Salts," B. R. Sundheim, Ed., McGraw-Hill, New York, N. Y., 1964, p 255.

(14) R. W. Laity and J. D. E. McIntyre, *J. Amer. Chem. Soc.*, **87**, 3806 (1965).

(15) M. L. Olmstead and R. S. Nicholson, *J. Phys. Chem.*, **72**, 1650 (1968).

(16) R. S. Rodgers and L. Meites, *J. Electroanal. Chem.*, **16**, 1 (1968).

served down this arm. The area of the mercury pool electrode was determined by measuring the id of the cup (1.17 cm) and the height of the mercury meniscus when the cell was filled with melt (0.15 cm) and calculating the area on the assumption that the surface had the shape of an oblate hemispheroid. This gave an area of $1.15 \pm 0.02 \text{ cm}^2$ for the mercury surface.

The chronopotentiometry cells were thermostated in a Lauda K-2/R constant temperature circulator. Bath temperatures were measured to $\pm 0.05^\circ$ with a calibrated mercury-in-glass thermometer. The circulator was turned off briefly while recording a chronopotentiogram to avoid agitation of the melt.

Normally a third reference electrode is incorporated into a chronopotentiometric cell, and the potential of the indicator electrode is measured with respect to it. In our case, however, we were not concerned with the determination of the quarter-wave potentials of the reducible tracer cations, so we measured the potential of the indicator electrode with respect to the Pt wire anode. In calcium nitrate tetrahydrate melts oxygen is evolved at a platinum anode,¹⁷ so that the anode maintains a constant potential during electrolysis at constant current and, hence, is suitable as a reference electrode for measuring transition times. To check this point, however, in one of the runs with silver as the reducible cation a heavy silver wire was incorporated into the cell as a third reference electrode. No difference was found between transition times measured using the Ag wire as reference electrode and those measured using the Pt anode as reference.

Blank runs were performed with both platinum and mercury cathodes on samples of melt to which no reducible cation had been added in order to detect any possible contributions to transition times from reducible impurities or dissolved oxygen. At the current densities used in these experiments, no such transition times were found in the blank runs, even after bubbling pure O_2 through the melt. Hence no precautions were taken to exclude air from the melts, save for tightly capping the cells to avoid loss of water at the higher temperatures.

Runs were begun by measuring chronopotentiograms at 50° , then lowering the cell temperature and performing measurements at several temperatures down to 15° . Finally, the cell temperature was raised again to 50° , a series of chronopotentiograms run, and a final series of measurements taken at 60° . At least three potential-time scans were run at each temperature with agreement among transition times measured at the same temperature of 1–2%. In these viscous melts, it was necessary to wait 10–20 min, with intermittent stirring, between successive chronopotentiograms to allow the bulk tracer-ion concentration to be reestablished at the electrode surface. It was generally not possible to avoid freezing of the melt when measurements were attempted below 15° .

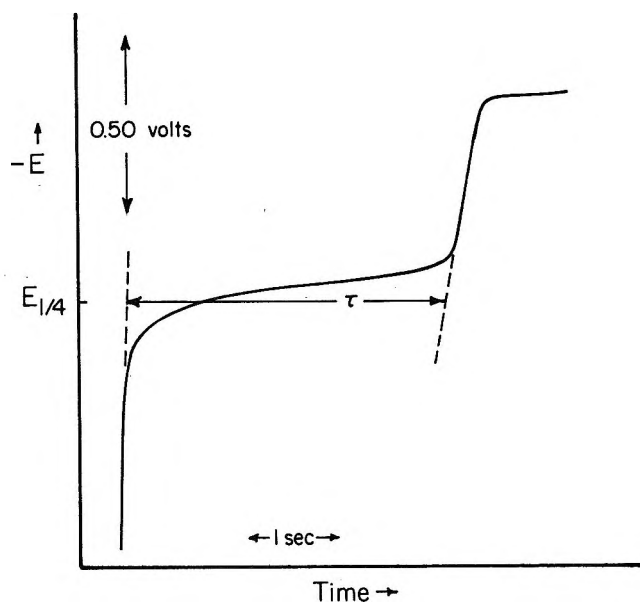


Figure 1. Chronopotentiogram of 0.00809 M Cd^{2+} solution in $\text{Ca}(\text{NO}_3)_2 \cdot 4.09 \text{ H}_2\text{O}$ at 49.6° . $I/A = 0.436 \text{ mA/cm}^2$, $\tau = 3.72 \text{ sec}$.

Measured transition times were kept in the range 2–5 sec, which required currents in the range 0.1–1 mA. The quantities of melt and concentrations of reducible tracer ion were such that at these currents upward of thirty chronopotentiograms could be run on a sample without changing the initial tracer ion concentration by more than 0.1%.

Results

A typical chronopotentiogram is shown in Figure 1. In analyzing the chronopotentiograms we have followed the method of Olmstead and Nicholson,¹⁵ who characterize the effect of double-layer charging on measured transition times in terms of a parameter ψ

$$\psi = \frac{RTC_{dl}}{nFI\tau_{Sand}}$$

where C_{dl} is the double-layer capacitance, and τ_{Sand} is the value of τ which satisfies the Sand equation. They show that if ψ is less than 0.005, experimental values of τ determined by the method of Delahay and Berzins¹⁸ deviate from τ_{Sand} by less than 1.7%. For our experiments ψ , evaluated using values of C_{dl} calculated from the slope of the initial steeply rising portion of the potential-time curves, was generally less than 0.001. Hence we have used the Delahay and Berzins method of determining τ , as is shown in Figure 1.

Diffusion coefficients for Ag^+ , Cd^{2+} , and Tl^+ were calculated from the experimental data via eq 2. Ionic concentrations were calculated from the masses of the

(17) R.-P. Courgnaud and B. Trémillon, *Bull. Soc. Chim. Fr.*, 758 (1965).

(18) P. Delahay and T. Berzins, *J. Amer. Chem. Soc.*, 75, 2486 (1953).

components used in making up the melts and the density-temperature-composition data for $\text{Ca}(\text{NO}_3)_2\text{-H}_2\text{O}$ solutions of Ewing and Mikovsky.¹⁹ Results are tabulated in Table I and shown in the form of Arrhenius plots in Figure 2.

Table I: Diffusion Coefficients of Ag^+ , Cd^{2+} , and Tl^+ in $\text{Ca}(\text{NO}_3)_2 \cdot 4.09\text{H}_2\text{O}$ Melts

Silver(I)			
Temp °C	Run 1	Run 2	
	$c_{50}^a = 5.42 \times 10^{-6}$	$c_{50}^a = 8.04 \times 10^{-6}$	
	$D_{\text{Ag}^+} \times 10^7, \text{cm}^2/\text{sec}$		
59.60	10.7	10.7	
49.60	7.4	7.4	
39.70	4.4	4.6	
29.75	2.54	2.60	
21.80	1.64	1.51	
14.85	0.96	0.93	

Cadmium(II)			
Temp °C	Run 1	Run 2	Run 3
	$c_{50}^a = 7.26 \times 10^{-6}$	$c_{50}^a = 8.09 \times 10^{-6}$	$c_{50}^a = 7.68 \times 10^{-6}$
	$D_{\text{Cd}^{2+}} \times 10^7, \text{cm}^2/\text{sec}$		
59.60	5.0	5.5	5.3
49.60	3.1	3.7	3.5
39.70	1.9	2.2	2.1
29.75	1.09	1.25	
21.80	0.57	0.66	
14.85	0.32	0.42	

Thallium(I)		
Temp °C	Run 1	Run 2
	$c_{50}^a = 11.55 \times 10^{-6}$	$c_{50}^a = 10.72 \times 10^{-6}$
	$D_{\text{Tl}^+} \times 10^7 \text{cm}^2/\text{sec}$	
59.60	10.4	10.9
49.60	7.0	7.3
39.70	4.2	4.4
29.75	2.30	2.47
21.80	1.26	1.42
14.85	0.71	0.75

^a Concn of ion at 50° in mol/cm³.

The internal precision of a set of diffusion coefficients measured during a single run, which affects the uncertainty in the calculated temperature dependences of D_i , is determined by the uncertainties in the measured currents, transition times, and temperatures and is estimated to be about 3%. The relative precision expected when diffusion coefficients measured during different runs are compared depends in addition on the uncertainties in the tracer-ion concentration and melt water content and is estimated to be around 5%. Finally, the absolute accuracy of the D_i measurements depends on the accuracy of the electrode area measurement as well as on the previously mentioned factors and is estimated to be 7% for D_{Ag^+} and 9% for $D_{\text{Cd}^{2+}}$ and D_{Tl^+} .

Agreement between values of D_i measured in different runs for Cd^{2+} and for Tl^+ at lower temperatures is somewhat outside the estimated relative precision of

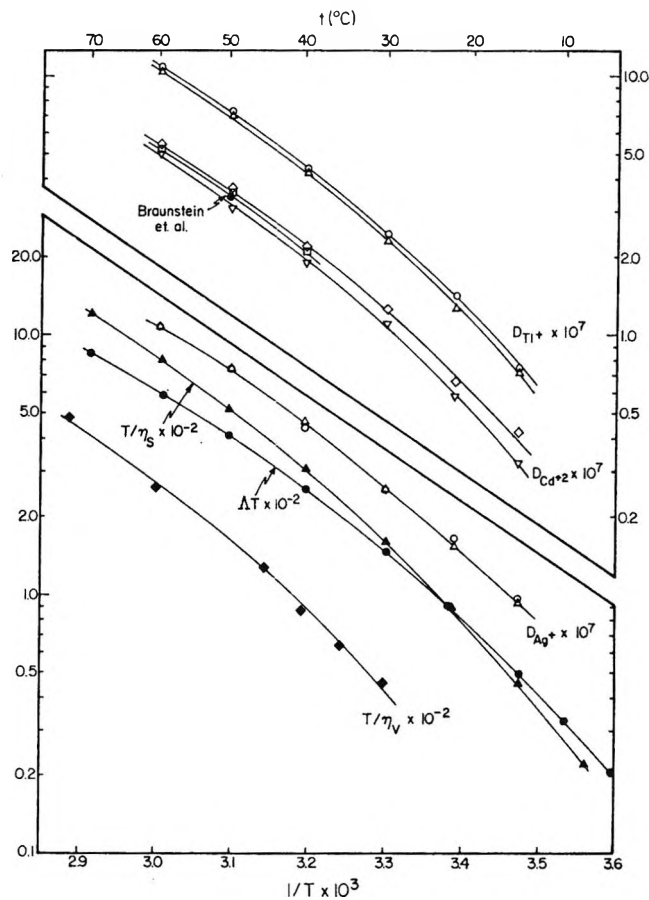


Figure 2. Arrhenius plots for diffusion coefficients, equivalent conductance, and shear and bulk viscosity for $\text{Ca}(\text{NO}_3)_2 \cdot 4.09\text{H}_2\text{O}$. Ordinates: D_i , cm^2/sec ; ΔT , $\text{cm}^2 \text{ deg}/\text{ohm equiv}$; T/η_s and T/η_v , deg/P .

5%. The most likely source of the discrepancies is a small amount of creepage of melt between the mercury and glass in the cathode, leading to some deviation from run to run in the actual area of the electrode. The agreement between values of D_{Ag^+} for different runs is well within the estimated relative precision, indicating that the poor relative precisions for $D_{\text{Cd}^{2+}}$ and D_{Tl^+} are indeed due to the cause suggested, since the problem of poorly defined electrode area is not encountered with the Pt-foil electrode.

Braunstein and coworkers⁶ have measured $D_{\text{Cd}^{2+}}$ by polarography in $\text{Ca}(\text{NO}_3)_2 \cdot 4.00\text{H}_2\text{O}$ at 50 and 100°; at 50° their result was $(3.12 \pm 0.010) \times 10^{-7} \text{cm}^2/\text{sec}$. We may correct this result to the melt composition studied here by an empirical method,^{3,4,20,21} by which all of the isothermal composition dependence of transport properties in $\text{Ca}(\text{NO}_3)_2\text{-H}_2\text{O}$ solutions is lumped into a variation in the T_0 parameter in eq 1. This gives for the result of Braunstein, *et al.*, $D_{\text{Cd}^{2+}} 3.38 \times$

(19) W. W. Ewing and R. J. Mikovsky, *J. Amer. Chem. Soc.*, **72**, 1390 (1950).

(20) C. A. Angell, *J. Chem. Phys.*, **46**, 4673 (1967).

(21) C. A. Angell, E. J. Sare, and R. D. Bressel, *J. Phys. Chem.*, **71**, 2759 (1967).

Table II: Fit of Equation 1 to Transport Data for $\text{Ca}(\text{NO}_3)_2 \cdot 4.09\text{H}_2\text{O}$ with Same $T_{0,j}$ for All Data

w_j^a	A_j	k_j	$T_{0,j}$	Stand dev in $\ln w_j$
D_{Ag^+}/T (Run 1)	5.06×10^{-6}	582.4	202.5	0.038
D_{Ag^+}/T (Run 2)	5.84×10^{-6}	598.2	202.5	0.023
$D_{\text{Cd}^{2+}}/T$ (Run 1)	4.42×10^{-6}	663.0	202.5	0.030
$D_{\text{Cd}^{2+}}/T$ (Run 2)	3.97×10^{-6}	635.0	202.5	0.044
$D_{\text{Cd}^{2+}}/T$ (Run 3)	4.31×10^{-6}	650.4	202.5	0.012
D_{Tl^+}/T (Run 1)	8.92×10^{-6}	655.2	202.5	0.017
D_{Tl^+}/T (Run 2)	8.60×10^{-6}	644.8	202.5	0.025
Λ	3.063×10^3	591.86	202.5	0.007
$1/\eta_s$	1.087×10^{-4}	694.51	202.5	0.004
$1/\eta_v$	2.47×10^{-4}	726.8	202.5	0.033

^a Units: (D_i/T), $\text{cm}^2/\text{sec deg}$; Λ , $\text{cm}^2/\text{ohm equiv}$; η_s and η_v , P.

$10^{-7} \text{ cm}^2/\text{sec}$ at 50° for $\text{Ca}(\text{NO}_3)_2 \cdot 4.09\text{H}_2\text{O}$. This datum is shown plotted in Figure 2 and is in excellent agreement with our results, suggesting that there are no undetected systematic errors in our method.

To facilitate comparison of temperature coefficients, our diffusion coefficient data have been computer fitted to eq 1 using the value $T_0 = 202.5$, which was found previously⁴ to give an adequate fit for conductance and shear viscosity at this melt composition. The calculated parameters are given in Table II. The standard deviations in $\ln(D_i/T)$ are consistent with our estimate of about 3% for the internal precision of a given run.

Discussion

In Figure 2 the temperature dependences of the tracer diffusion coefficients are compared with those for the conductance and shear viscosity determined previously⁴ for $\text{Ca}(\text{NO}_3)_2 \cdot 4.09\text{H}_2\text{O}$ and with the bulk viscosity data of Darbari and Petrucci⁵ for $\text{Ca}(\text{NO}_3)_2 \cdot 4.0 \text{H}_2\text{O}$. The bulk viscosity data shown considerable scatter when plotted as a function of concentration, so that no attempt has been made in Figure 2 to correct them to the melt composition used in this study. In Table II similar comparisons are made among the transport properties in terms of the parameters of eq 1 needed to describe the data. In this case, the bulk viscosity parameters determined for $\text{Ca}(\text{NO}_3)_2 \cdot 4.0 \text{H}_2\text{O}$ have been corrected to the composition $\text{Ca}(\text{NO}_3)_2 \cdot 4.09\text{H}_2\text{O}$ as before.^{3,4,20,21}

As expected from the behavior of the other transport properties, the Arrhenius plots of D_i are not linear, but are curved in a direction corresponding to an apparent increase in activation energy with decreasing temperature. Similarly, as expected from the theoretical interpretation of $T_{0,j}$ in eq 1 as an equilibrium rather than a transport property of the melt,^{1,4,7} an adequate fit to all the transport data for the melt can be obtained with the same value of $T_{0,j}$, as is shown in Table II.

The various transport properties show a remarkable similarity to one another in their temperature dependences when compared on a logarithmic scale. The

largest discrepancy between the k_j terms in Table II (582.4 for D_{Ag^+}/T vs. 726.8 for $1/\eta_v$) is about 22%. For comparison purposes, the agreement between the temperature dependences of the transport properties could probably be improved if one could dissect the shear and bulk viscosities into contributions from the appropriate relaxation times and moduli

$$\eta_s = G_\infty \tau_s$$

$$\eta_v = (K_\infty - K_0) \tau_v$$

G_∞ is the infinite frequency modulus of shear rigidity, K_∞ and K_0 the infinite and zero frequency moduli of compression, and τ_s and τ_v , respectively, the shear and structural relaxation times. Litovitz and McDuffie and their coworkers^{11,12,22} have shown experimentally that better correlations are achieved when one compares the temperature and pressure dependences of τ_s or τ_v with those of other transport properties than when the similar comparison is made using η_s and η_v . This result is a reasonable one, since G_∞ and $(K_\infty - K_0)$ measure elastic, solid-like properties, rather than fluid-like properties of the liquid. G_∞ and $(K_\infty - K_0)$ both increase with decreasing temperature, so that it seems likely that part of the discrepancy between the k_j values for $1/\eta_s$ and $1/\eta_v$ and the k_j values for the other transport properties would disappear if one were able to take these factors into account.

The close agreement between the temperature dependences on a logarithmic scale (or activation energies) of the diffusion coefficients of various ions in the same melt seems to be a fairly general phenomenon in anhydrous fused salts, having been observed both for cation and anion self-diffusion coefficients in high-temperature pure fused salts^{7,23,24} and mixed melts²⁵⁻²⁸ and for

(22) T. A. Litovitz and G. E. McDuffie, *J. Chem. Phys.*, **39**, 729 (1963).

(23) C. A. Angell and J. W. Tomlinson, *Trans. Faraday Soc.*, **61**, 2312 (1965).

(24) C. A. Sjöblom, *Z. Naturforsch.*, **23a**, 933 (1968).

(25) F. Lantelme and M. Chemla, *Bull. Soc. Chim. Fr.*, 969 (1963).

polarographic diffusion coefficients in lower temperature melts.^{7,29} On the other hand, in high-temperature melts discrepancies frequently occur between the activation energies of diffusion coefficients and shear viscosity²⁴ and even more frequently between the activation energies of shear viscosity and equivalent conductance,^{7,30} usually having the lower temperature coefficient. Hence, it would appear that for ionic liquids close similarity among the temperature dependences of all the different transport properties is a phenomenon associated primarily with low temperatures. We interpret this similarity in temperature coefficients observed in our study as a manifestation of the cooperative nature of the mass transport mechanism at low temperatures, such that the "activated jump" involved in the transport of any single particle occurs in concert with a simultaneous rearrangement of a large number of other particles in its vicinity.

At a given temperature, the actual magnitude of the diffusion coefficient of an ion in calcium nitrate tetrahydrate appears to depend more on its coulombic charge than on any other factor, as is seen from the relatively small difference in the diffusional mobilities of Ag^+ and Tl^+ in comparison to that of Cd^{2+} , which is only about half as mobile as either of the singly charged ions. A similar preponderance of charge effects in determining cationic mobilities has been observed in higher temperature anhydrous melts for tracer ion diffusion coefficients,^{29,31-34} as well as for electrical ion mobilities.³⁵⁻³⁷ Although the decrease in cationic mobility with increase in coulombic charge is in accord with the more or less intuitive feeling possessed by physical chemists that increased charge should lead to local electrostriction in the melt and a corresponding restriction in the "freedom of motion" of the ion, no one has yet put forth a satisfactory theory for the effect in anhydrous melts. The formation of "complex ions" by highly charged cations is clearly too simplistic an explanation. It does not account, among other things, for the fact that temperature coefficients of transport properties of multivalent ions are comparable to those of univalent ions and do not appear to reflect changing equilibrium constants and that electrical mobility behavior is quite similar in systems such as $\text{Ca}(\text{NO}_3)_2\text{-LiNO}_3$ and $\text{CdCl}_2\text{-KCl}$, where the "complex-forming" abilities of the ions are presumably quite different.³⁶

A note of caution needs to be injected here, of course, in comparing our results for a hydrate melt with anhydrous systems, namely, that the presence of water may invalidate the comparison. In this light it is interesting to interpret our diffusion results in terms of the Stokes-Einstein equation

$$D_i = \frac{kT}{a\eta_s r_i} \quad (3)$$

The original derivation of the equation was based on

the identification of the friction coefficient, ζ_i , of the Einstein equation

$$D_i = kT/\zeta_i$$

with the hydrodynamic force impeding the steady movement of a sphere of radius r_i in a continuous fluid medium of viscosity η_s . k is the Boltzmann constant, and the numerical factor a is equal to 6π if there is no slippage at the fluid-sphere interface and 4π if there is complete slippage.³⁸ Although this model has no obvious relevance to the case of ionic motion, many studies show that a relation of the form of eq 3 exists between diffusion coefficients of atomic size particles and the fluid viscosity. Forcheri and Wagner,²⁸ for instance, have shown that a plot of univalent ion diffusion coefficients in univalent nitrates *vs.* $T/\eta_s r_i$ gives, with considerable scatter, a straight line with a slope corresponding to $a = 4.6\pi$ in eq 3. Similar plots for molten nitrates and halides, with similar slopes, have been presented by Bockris and coworkers.³⁹

To test this correlation for the present results, we first note that proton magnetic resonance studies^{4,40} have shown that in calcium nitrate tetrahydrate large univalent ions such as K^+ or $(\text{CH}_3)_4\text{N}^+$ are unhydrated, while Cd^{2+} has a hydration number of 4. It seems a safe presumption that Ag^+ and Tl^+ , which are similar in size to K^+ , are likewise unhydrated. Hence for calculations with eq 3 we may use the "bare" ionic radii⁴¹ for Ag^+ and Tl^+ , but for Cd^{2+} we have a choice of using the "bare" ionic radius or the "hydrated" ionic radius ($= r_{\text{Cd}^{2+}} + 2r_{\text{H}_2\text{O}}$).

In Table III are shown ratios of the observed D_i in calcium nitrate tetrahydrate to the D_i calculated *via* eq 3 using $a = 4.6\pi$ at two temperatures. The results

- (26) F. Lantelme and M. Chemla, *C. R. Acad. Sci.*, **258**, 1484 (1964).
 (27) P. L. Spedding and R. Mills, *J. Electrochem. Soc.*, **113**, 599 (1966).
 (28) S. Forcheri and V. Wagner, *Z. Naturforsch.*, **22a**, 1171 (1967).
 (29) M. Francini and S. Martini, *ibid.*, **23a**, 795 (1968).
 (30) J. P. Frame, E. Rhodes, and A. R. Ubbelohde, *Trans. Faraday Soc.*, **55**, 2039 (1959).
 (31) H. A. Laitinen and W. S. Ferguson, *Anal. Chem.*, **29**, 4 (1957).
 (32) H. A. Laitinen and H. C. Gaur, *Anal. Chem. Acta*, **18**, 1 (1958).
 (33) C. E. Thalmayer, S. Brackenstein, and D. M. Gruen, *J. Inorg. Nucl. Chem.*, **26**, 347 (1964).
 (34) F. Caligara, L. Martinot and G. Duyckaerts, *J. Electroanal. Chem.*, **16**, 335 (1968).
 (35) W. K. Behl and J. J. Egan, *J. Phys. Chem.*, **71**, 1764 (1967).
 (36) J. C. T. Kwak, Ph.D. Thesis, University of Amsterdam, 1967.
 (37) A. Berlin, F. Menes, S. Forcheri, and C. Monfrini, *J. Phys. Chem.*, **67**, 2505 (1963).
 (38) H. Eyring, D. Henderson, B. J. Stover, and E. M. Eyring, "Statistical Mechanics and Dynamics," John Wiley & Sons, Inc., New York, N. Y., 1964, p 463.
 (39) (a) J. O'M. Bockris, S. Ycshikawa, and S. R. Richards, *J. Phys. Chem.*, **68**, 1838 (1964); (b) J. O'M. Bockris, S. R. Richards, and L. Nanis, *ibid.*, **69**, 1627 (1965).
 (40) C. T. Moynihan and A. Fratiello, *J. Amer. Chem. Soc.*, **89**, 5546 (1967).
 (41) C. S. G. Phillips and R. J. P. Williams, "Inorganic Chemistry," Oxford University Press, New York, N. Y., 1965, p 152.

Table III: Comparison of Observed Diffusion Coefficients in Calcium Nitrate Tetrahydrate to Those Calculated from the Stokes-Einstein Equation using $a = 4.6\pi$

Ion	$r_i, \text{\AA}$	$D_{i,\text{obsd}}/D_{i,\text{calcd}}$	
		14.85°	59.60°
Ag ⁺	1.26	2.63	1.72
Tl ⁺	1.40	2.24	1.89
Cd(H ₂ O) ₄ ²⁺	3.73	3.03	2.52
Cd ²⁺	0.97	0.79	0.65

show for the first three entries that the calculated D_i are too low, the discrepancies becoming worse the lower the temperature. Since the a value of 4.6π taken from Forcheri and Wagner is strictly empirical and applies to melts with viscosities lower by two orders of magnitude than those encountered here, the low values of $D_{i,\text{calcd}}$ simply reflect the fact already noted that the temperature coefficient of $1/\eta_s$ is somewhat greater than that for D_i/T . The fact remains, however, that for a given value of η_s there is some correlation between D_i and ionic radius, and at a given temperature the agreement among $(D_{i,\text{obsd}}/D_{i,\text{calcd}})$ for Ag⁺, Tl⁺, and Cd(H₂O)₄²⁺ is as good as that noted by Forcheri and Wagner²⁸ for the higher temperature melts. On the other hand, $(D_{i,\text{obsd}}/D_{i,\text{calcd}})$ for the unhydrated Cd²⁺ ion is clearly out of line with the other three values. The implication here is that possibly one can account for the magnitude of D_i of a multivalent ion in a hydrate melt in terms of ionic size, if one takes the kinetic entity to be the hydrated ion for the multivalent ions and the unhydrated ion for the monovalent ions, an option not available in anhydrous melts.

The mobile hydrated cation is not entirely unexpected, since it has previously been shown that Cd²⁺ and Ca²⁺ hydrate equally in their tetrahydrate melts⁴ and that T_0 values for the melts are consistent with the presence of cations with the charge:radius ratio of the tetrahydrate cation.³ On the other hand, it has not

previously been possible to provide even ambiguous evidence that this cation is also a kinetic entity.

We have noted before^{4,7} that factors determining the magnitude of the preexponential A_j in eq 1 are poorly understood. The above discussion accepts that there is a difference of T/r_i and a numerical factor between A_{D_i} and A_{1/η_s} , but does not consider what factors may be common. To avoid circularity we must restrict comparisons to the data on Ag⁺ and Tl⁺. This, however, is sufficient to point up (Table II) the absence of any $m^{-1/2}$ mass dependence of A_{D_i} , which most treatments of rate processes suggest should enter either as a particle velocity term⁹ or as a vibration frequency.⁴² Again, the problem seems resolved by the cooperative rearrangement mechanism, for which the appropriate frequency is presumably a property of the cooperative region involving a complex of frequencies, rather than a property of the particular particle whose motion is being followed.

In the future we hope to report chronopotentiometric diffusion coefficients for ions in an anhydrous melt capable of a large degree of supercooling, *e.g.*, a Ca(NO₃)₂-KNO₃ melt,⁴³ in which the diffusion coefficients may be studied over a temperature interval sufficient to encompass at least three orders of magnitude in D_i , including the "normal" high temperature values of around 10⁻⁵ cm²/sec. Such a study should resolve some of the questions we have raised here in regard to the dependence of cationic mobilities on coulombic charge, as well as provide some insight into the breakdown in cooperative transport behavior which is presumed to coincide roughly with the onset of an Arrhenius temperature dependence of transport properties.

Acknowledgment. This work was supported by a grant from the Department of the Interior, Office of Saline Water.

(42) C. Kittel, "Introduction to Solid State Physics," John Wiley & Sons, New York, N. Y., 1966, p 568.

(43) C. A. Angell, *J. Phys. Chem.*, **68**, 1917 (1964).

Proton Magnetic Resonance Study of Aluminum Chloride and Aluminum Perchlorate in Acetonitrile¹

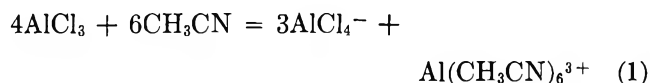
by James F. O'Brien and Mohammed Alei, Jr.

University of California, Los Alamos Scientific Laboratory, Los Alamos, New Mexico 87544 (Received August 25, 1969)

Solutions of AlCl_3 in acetonitrile were studied from -40 to 80° by proton magnetic resonance. The apparent solvation number of 1.5 was verified by integration of free and bound proton resonances. The value of the rate constant for exchange of solvent from the Al(III) coordination sphere was 8.1 sec^{-1} at 25° . The enthalpy and entropy of activation were $19.1 \pm 0.4 \text{ kcal mol}^{-1}$ and $9.7 \pm 1.3 \text{ cal deg}^{-1} \text{ mol}^{-1}$, respectively. Proton nmr was also used to show that the apparent solvation number of Al(III) in acetonitrile when perchlorate is the anion is 2.9 ± 0.3 . The result has been observed before and did not seem to vary significantly with temperature. Evidence was found for several different species in the aluminum perchlorate solutions, indicating that 2.9 is an average value for the solvation number.

Introduction

Al(III) has been shown by pmr to have solvation numbers of 6 in water,² dimethyl sulfoxide (DMSO),³ dimethylformamide (DMF),⁴ and a mixed solvent of water-DMSO.⁵ In all of these cases the anion, Cl^- or ClO_4^- , is completely displaced by solvent from the metal ion coordination sphere. In acetonitrile, however, the Al(III) species in solution appear to depend upon the anion. In solutions of $\text{Al}(\text{ClO}_4)_3$ in acetonitrile, the Al(III) has been reported⁶ to have an average solvation number of 2.8. The suggestion has been made, supported by evidence from infrared spectra,⁶ that the perchlorate ion competes with CH_3CN for coordination shell positions. A recent study⁷ of AlCl_3 in CH_3CN using ^{27}Al and ^1H magnetic resonance pointed out that two ^{27}Al resonances exist in a 3:1 area ratio, that there is only one Al containing species that also exhibits a proton resonance, and that the apparent solvation number, determined by integration of the proton peaks, is 1.5. The author proposed⁷



This is consistent with the observation of Raman lines due to AlCl_4^- .⁸

In addition to the apparent anion effect on the Al(III) solvation number in acetonitrile, it is also possible that both the solvent exchange rate and the chemical shift of bound protons are affected by the anion. Table I contains rate constants and chemical shifts for DMF solutions of aluminum salts. The rate constants are for exchange of one solvent molecule and have been adjusted to 25° for easy comparison. The solution containing Cl^- has a rate constant larger than the others by a factor of about 30. In all cases listed in Table I,^{9,10} the exchanging species is $\text{Al}(\text{DMF})_6^{3+}$. Movius and

Matwiyoff¹⁰ have concluded that anions in the second shell affect solvent molecules in the first sphere.

The purpose of the present work was to confirm the reported values of the solvation numbers and to investigate the possibility of an anion effect on the solvent exchange rate and chemical shift of bound acetonitrile molecules.

Table I: Nmr Data for Al(III)-DMF Solutions

Salt	k^a , sec^{-1}	δ^b , Hz	Reference
AlCl_3	11.0 sec^{-1}	49	9, 10
AlBr_3	0.36	41	9, 10
AlI_3	0.38	31	9, 10
$\text{Al}(\text{ClO}_4)_3$	0.20	17	4, 10

^a 25° . ^b δ is the shift of the bound formyl proton from the free formyl resonance.

Experimental Section

Acetonitrile was purified by successive distillations from P_2O_5 under argon, followed by a simple distillation.

The starting material for preparation of solutions of aluminum chloride in acetonitrile was AlCl_3 prepared by reaction of 99.998% Al metal with Cl_2 at 400° . Care

(1) Work done under the auspices of the United States Atomic Energy Commission.

(2) R. E. Schuster and A. Fratiello, *J. Chem. Phys.*, **47**, 1554 (1967).

(3) S. Thomas and W. L. Reynolds, *ibid.*, **44**, 3148 (1966).

(4) W. G. Movius and N. A. Matwiyoff, *Inorg. Chem.*, **6**, 847 (1967).

(5) A. Fratiello, R. E. Lee, V. M. Nishida, and R. E. Schuster, *J. Chem. Phys.*, **47**, 4951 (1967).

(6) L. Supran and N. Sheppard, *Chem. Commun.*, 832 (1967).

(7) J. F. Hon, *Mol. Phys.*, **15**, 57 (1968).

(8) C. D. Schmulbach, *J. Inorg. Nucl. Chem.*, **26**, 745 (1964).

(9) A. Fratiello and R. E. Schuster, *J. Phys. Chem.*, **71**, 1948 (1967).

(10) W. G. Movius and N. A. Matwiyoff, *ibid.*, **72**, 3063 (1968).

was taken to exclude water from the resulting solid, and acetonitrile was then distilled onto it *in vacuo*. The resulting solutions were then evaporated until $\text{AlCl}_3 \cdot 2\text{CH}_3\text{CN}$ crystallized. This solid was analyzed for Al by the 8-hydroxyquinoline gravimetric method, and for Cl by AgCl gravimetric. *Anal.* Calcd for $\text{AlCl}_3 \cdot 2\text{CH}_3\text{CN}$: Al, 12.52; Cl, 49.37. Found: Al, 12.59; Cl, 50.18. Nmr samples were prepared by dissolving this solid in acetonitrile *in vacuo* and sealing the nmr tubes.

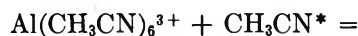
Aluminum perchlorate in acetonitrile was prepared by reaction of aluminum chloride and silver perchlorate in acetonitrile under anhydrous conditions. Silver perchlorate was dried at 80° *in vacuo* and dissolved in anhydrous acetonitrile. This solution was added to an anhydrous solution of AlCl_3 in CH_3CN . After heating to 70° under argon, AgCl , which has a solubility product of $10^{-12.4}$ in CH_3CN ,¹¹ was allowed to separate out. After 2 days 99.5% of the AgCl expected on the basis of AlCl_3 , the limiting reagent, had been collected. The remaining solution was then degassed, concentrated, and cooled. A white solid, soluble in both H_2O and CH_3CN , resulted. This solid was tested for Cl^- and Ag^+ and contained neither. An aluminum analysis showed that the solid contained 5.2% Al. Assuming acetonitrile to be the only other constituent of the solid, the molecular formula would be $\text{Al}(\text{CH}_3\text{CN})_{4.7}(\text{ClO}_4)_3$. This formula was confirmed by comparing the proton resonance areas of *p*-dioxane and acetonitrile in an aqueous solution containing known amounts of the aluminum solid and *p*-dioxane. The result was 4.8 acetonitrile molecules per aluminum atom.

Pmr line width and shift measurements were made in normal fashion on a Varian DA-60A instrument. Samples were contained in standard 50-mm od nmr tubes, which were sealed to prevent possible uptake of water from the atmosphere. The aluminum chloride samples contained TMS as an internal standard.

Results and Discussion

Exchange rate and solvation number studies were made on two solutions of AlCl_3 in CH_3CN , one of which was 2.01 *m* in Al(III) and the other 3.71 *m*. At appreciably lower Al(III) concentrations, insufficient line-broadening makes it difficult to obtain accurate kinetic data. Integration of bound and free acetonitrile peaks in these solutions were performed at 30, -29 , and -38° . The resulting apparent solvation numbers showed no trend with temperature and were 1.4 ± 0.1 and 1.5 ± 0.1 for the 3.7 and 2.0 *m* solutions, respectively. These values are in agreement with those previously reported by Hon.⁷

Figure 1 illustrates the effect of temperature on the principal resonance in the 3.7 *m* solution. The chemical exchange reaction affecting the proton line width is that shown in eq 2. A complete line shape analysis using the McConnell equations for the magnetization



was performed on an IBM 7094 computer. First-order rate constants were calculated for both solutions at ten temperatures from 30 to 81° . Figure 2 shows the results of a least-squares analysis of the rate constants performed on a CDC 6600. The enthalpy and entropy of activation were $\Delta H^\ddagger = 19.1 \pm 0.4$ kcal mol⁻¹ and $\Delta S^\ddagger = 9.7 \pm 1.3$ cal deg⁻¹ mol⁻¹. The rate constant for the exchange of one solvent molecule at 25° was 8.1 sec⁻¹. The above measurements were made on the free solvent and coalesced resonances. A study¹² of the bound acetonitrile resonance in a 0.70 *m* solution of AlCl_3 in CH_3CN found $\Delta H^\ddagger = 18.8 \pm 1.1$ kcal mol⁻¹ and $\Delta S^\ddagger = 8.4 \pm 3.5$ cal deg⁻¹ mol⁻¹. The value of 8.1 sec⁻¹ is similar to the AlCl_3 -DMF exchange rate shown in Table I. The fact that all Al(III) solvent exchange rate constants in H_2O , DMSO, and DMF are essentially the same when Cl^- is not present suggests that chloride ion catalyzes Al(III) solvent exchange when acetonitrile is the solvent.¹³

We prepared an aluminum perchlorate-acetonitrile solid as described in the Experimental Section. This solid was used to make an acetonitrile solution that was

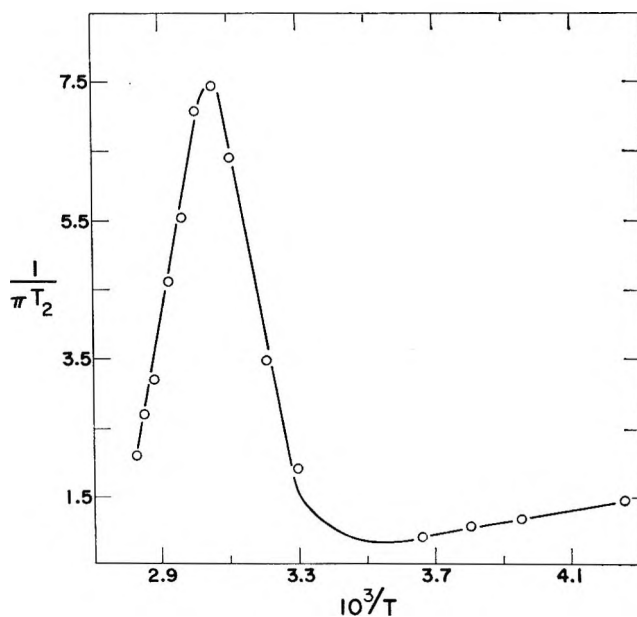


Figure 1. Temperature dependence of the full line width at half-height for the principal acetonitrile proton resonance in a 3.71 *m* solution of AlCl_3 in CH_3CN .

(11) D. C. Luehrs, R. J. Iwamoto, and J. Kleinberg, *Inorg. Chem.*, **5**, 201 (1966).

(12) J. F. O'Brien, Ph.D. Thesis, University of Minnesota, (1968).

(13) $\text{Al}(\text{ClO}_4)_3$ in DMSO has a rate constant for the exchange of one solvent molecule of 0.31 sec⁻¹ at 25° ; S. Thomas, M.S. Thesis, Univ. of Minnesota, 1966. $\text{Al}(\text{ClO}_4)_3$ in H_2O has a rate constant of 0.13 sec⁻¹ at 25° ; D. Fiat and R. E. Connick, *J. Amer. Chem. Soc.*, **90**, 608 (1968).

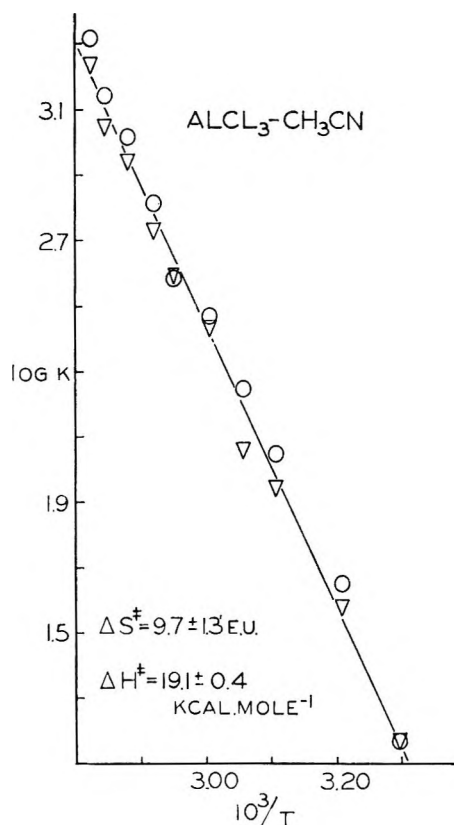


Figure 2. Least-squares plot of solvent exchange rate constant for AlCl_3 - CH_3CN system: ∇ , values for 3.71 *m* AlCl_3 ; \circ , values for 2.01 *m* AlCl_3 .

0.09 *m* in $\text{Al}(\text{III})$. In addition to comparing rate constants, we wanted to confirm the reported⁶ value of the apparent solvation number of $\text{Al}(\text{ClO}_4)_3$ in CH_3CN . The low solubility of $\text{Al}(\text{ClO}_4)_3$ in acetonitrile restricted measurements to solutions in which the area of the bound solvent resonance was very small compared to that for free solvent. Consequently, we found it more convenient and precise to compare the area of the bound proton resonance with that of the ^{13}C satellite of the free solvent peak. The integrations were made difficult by the low intensity of the signals and their position near the very intense free solvent peak. The ratio of the bound CH_3CN area to the ^{13}C satellite area, determined at 30° with the aid of a time averaging device (CAT), was 1.95 ± 0.18 . This corresponds to an apparent solvation number of 2.9 ± 0.3 . Attempts to measure the solvation number at temperatures down to -30° resulted in similar values. There does not seem to be a trend with temperature, although the accuracy of the integrations was such that this possibility cannot be ruled out. The value 2.8 has been reported previously by Supran and Sheppard,⁶ who attributed the low solvation number to competition by the perchlorate ion for first coordination sphere sites. Other evidence from infrared and magnetic measurements¹⁴⁻¹⁷ also indicates that the perchlorate group can indeed act as a ligand. The infrared evidence has been ques-

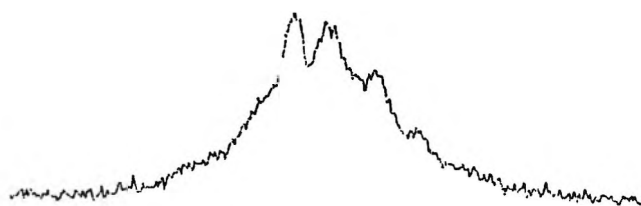


Figure 3. Bound CH_3CN resonance at $+10^\circ$ in 0.09 *m* $\text{Al}(\text{ClO}_4)_3$.

tioned.¹⁸ However, Hon has found that addition of LiClO_4 to solutions of AlCl_3 in CH_3CN reduces the number of acetonitrile molecules in the $\text{Al}(\text{III})$ coordination sphere.¹⁹ Our work and that of Supran and Sheppard⁶ indicates that in anhydrous solutions of $\text{Al}(\text{ClO}_4)_3$ in CH_3CN , the perchlorate ion does compete with acetonitrile for coordination sites.

The solvation number of 2.9 ± 0.3 can be explained by the presence of all aluminum in the form $\text{Al}(\text{CH}_3\text{CN})_3(\text{ClO}_4)_3$ or by a mixture of species containing various ratios of acetonitrile and perchlorate in the coordination sphere of the $\text{Al}(\text{III})$. In the latter case, one might expect different chemical shifts for the various species. Figure 3 is a trace of the bound CH_3CN resonance. There are clearly at least four different kinds of bound acetonitrile, with resonances separated by about 0.8 Hz. That the multiplet is not the result of ^{27}Al - ^1H coupling can be seen by the fact that such coupling would result²⁰ in six peaks of equal intensity and peak height ratios of 138:90:115:115:90:138. Obviously then, there is a mixture of species in the solution.

Evaluation of the rate constant for solvent exchange was not possible in the $\text{Al}(\text{ClO}_4)_3$ system. The solution was too dilute to cause appreciable broadening of the free solvent peak. Measurement of the bound solvent line width was complicated by the splitting shown in Figure 3. It is clear, however, that solvent exchange is slower than in the chloride case since the bound resonance persisted to 80° , a temperature at which, as shown in Figure 1, the Cl^- solution gives a narrow coalesced line. Since the exchanging species in the AlCl_3 solutions has only acetonitrile in the first sphere, while in the perchlorate case it is likely that a given $\text{Al}(\text{III})$ first coordination shell will contain both ClO_4^- and CH_3CN , it is probably not valid to consider the difference in solvent exchange rate to be due to an anion effect in the same sense as in the DMF case. In the

(14) B. J. Hathaway, D. J. Holah, and A. E. Underhill, *J. Chem. Soc.*, 2444 (1962).

(15) B. J. Hathaway and A. E. Underhill, *ibid.*, 3091 (1961).

(16) A. E. Wickenden and R. A. Krause, *Inorg. Chem.*, 4, 404 (1965).

(17) L. E. Moore, R. B. Gashart, and W. E. Bull, *J. Inorg. Nucl. Chem.*, 26, 896 (1964).

(18) N. A. Matwiyoff, P. E. Darley, and W. G. Movius, *Inorg. Chem.*, 7, 2173 (1968).

(19) J. F. Hon, private communication.

(20) J. A. Pople, *Mol. Phys.*, 1, 168 (1958).

DMF systems anions in the second shell affect the first shell solvent molecules.

There did not appear to be an anion effect on the chemical shift of bound CH_3CN protons. The bound resonance was 35 Hz downfield from free acetonitrile in AlCl_3 solutions and 33 to 37 Hz in the $\text{Al}(\text{ClO}_4)_3$ solutions. The position in the perchlorate solutions is a bit surprising in view of the mixed species in the coordination sphere. There also is a published spectrum⁶ of $\text{Al}(\text{ClO}_4)_3$ in $\text{H}_2\text{O}-\text{CH}_3\text{CN}$ which shows the bound CH_3-

CN at about 57 Hz downfield from free CH_3CN . It is interesting to note, however, that the bound proton peak for acetonitrile when $(\text{NH}_3)_2\text{Pt}(\text{ClO}_4)_2$ is the solute is also 35 Hz downfield from bulk CH_3CN .²¹

Acknowledgment. The authors wish to acknowledge the valuable assistance of A. E. Florin in obtaining spectra and discussing the results.

(21) J. F. O'Brien, G. E. Glass, and W. L. Reynolds, *Inorg. Chem.*, **7**, 1664 (1968).

The Importance of the Effect of the Solvent Dielectric Constant on Ion-Pair Formation in Water at High Temperatures and Pressures

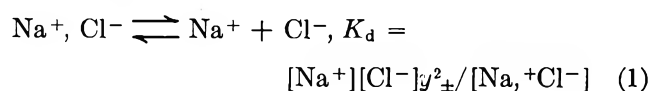
by W. R. Gilkerson¹

Department of Chemistry, University of South Carolina, Columbia, South Carolina 29208
(Received June 24, 1969)

The contention of Marshall, Quist, and coworkers that ion-pair formation of a number of electrolytes in water at high temperatures and pressures does not depend on changes in the solvent dielectric constant but only on changes in the solvent density and temperature is examined and rejected. Their data are analyzed in terms of the Gilkerson modification of the Fuoss equation for the ion-pair dissociation constant. The data reported by Marshall and coworkers is uniquely suited to experimental separation of the effects of specific ion-solvent and ion-pair-solvent interaction and the effects of changes in solvent dielectric constant. Distances of closest approach are obtained which are somewhat smaller than interionic distances in crystals.

Marshall and coworkers,² in reporting a series of studies of the electrical conductances of aqueous electrolytes up to 800° and 4000 bars, have proposed that changes in ion-pair formation in solution at constant temperature are independent of changes in the solvent dielectric constant and depend only on changes in the concentration of a specifically solvating solvent species.³ This view is quite contrary to that taken by most workers in the field of electrolyte solutions.⁴

The low densities of water (and consequent low values of its dielectric constant) at high temperatures under high pressure result in measurably low values of the ion-pair dissociation constant, K_d , for the process (for NaCl for instance)



where $[\text{Na}^+\text{Cl}^-]$ represents the molar concentration of the ion pair, Na^+Cl^- , and y_{\pm} is the mean ionic activity coefficient calculated using the Debye-Hückel equation. I shall be concerned in this report with the

correlation of the values of K_d obtained by Marshall and coworkers with the physical properties (dielectric constant, density, and temperature) of the solvents used. I shall not be concerned with the treatment of the conductance data (equivalent conductance, concentration) to yield limiting equivalent conductances and the ion-pair dissociation constant,⁵ K_d . The magnitudes of the changes in the values of K_d as the solvent system changes can be illustrated by one example;^{2b} for NaCl at 400°, $-\log K_d = 4.43$ at $d = 0.30$ g/ml, dielectric

(1) This work has been supported in part by a grant from the National Science Foundation, GP-6949.

(2) (a) A. S. Quist and W. L. Marshall, *J. Phys. Chem.*, **70**, 3714 (1966); (b) *ibid.*, **72**, 684 (1968); (c) *ibid.*, **72**, 2100 (1968); (d) *ibid.*, **72**, 1545 (1968); (e) L. A. Dunn and W. L. Marshall, *ibid.*, **73**, 723 (1969).

(3) A. S. Quist and W. L. Marshall, *ibid.*, **72**, 1536 (1968).

(4) (a) M. Szwarc, *Accounts Chem. Res.*, **2**, 87 (1969); (b) D. F. Evans and P. Gardam, *J. Phys. Chem.*, **73**, 158 (1969); (c) J. C. Poirier in "Chemical Physics of Ionic Solutions," B. E. Conway and R. G. Barrades, Ed., John Wiley & Sons, New York, N. Y., 1966, p 9; (d) J. E. Prue, ref 4c, p 163.

(5) Called the conventional ionization constant by Marshall, *et al.*

constant, $D = 4.9$, pressure, P , approximately 220 bars,⁶ while $-\log K_d = 0.97$ at $d = 0.70$ g/ml, and $P \approx 1000$ bars.⁶

Marshall and Quist found that, at constant temperature, plots of $\log K_d$ vs. $\log C_{H_2O}$ are linear. C_{H_2O} is the molar concentration of water. They concluded that water should be included explicitly in a "complete equilibrium"



with the equilibrium constant given by

$$K^\circ = a_{M^+} a_{X^-} / a_{MX} a_{H_2O}^k = K_d / a_{H_2O}^k \quad (3)$$

Marshall and Quist then set the activity of water in the infinitely dilute salt solution to be equal to the molar concentration of water. Their statement regarding the choice of standard state that leads to this is, in one instance,^{2e} "... a_{H_2O} is replaced by the molar concentration of water (C_{H_2O}) with a hypothetical standard state of unit molarity at the particular density (or pressure), ..." I submit that this is incorrect if one is concerned with the changes in the activity of the water solvent as the density (pressure) changes. The activity of a substance is defined by the relation

$$\mu_i = \mu_i^\circ + RT \ln a_i \quad (4)$$

where μ_i is the chemical potential (partial molar free energy) of component i and μ_i° is the chemical potential in some chosen standard state at the temperature T . If the effects of changes in activity (concentration) of water solvent at different densities on a chemical reaction are to be investigated, the standard state chosen should *not* change with solvent density or pressure. A suitable choice here would be any invariant state of water (constant T and P). Now

$$d\mu_i = \bar{V}_i dP - \bar{S}_i dT \quad (5)$$

where \bar{V}_i is the partial molar volume of i and \bar{S}_i is the partial molar entropy of i . At constant temperature, this becomes

$$d\mu_i = \bar{V}_i dP$$

and thus

$$d\mu_i^\circ + RT d \ln a_i = \bar{V}_i dP$$

at constant T . The only variable here is the pressure. I take as a suitable standard state, water at one particular density, say 0.300 g/ml, at the temperature T . Then $d\mu_i^\circ = 0$ and

$$d \ln a_i = \bar{V}_i dP / RT$$

or

$$\log a_{H_2O} = (1/2.303RT) \int_{P^\circ}^P \bar{V}_{H_2O} dP \quad (6)$$

where P° is the pressure corresponding to the density in the standard state at T , and P is the pressure corre-

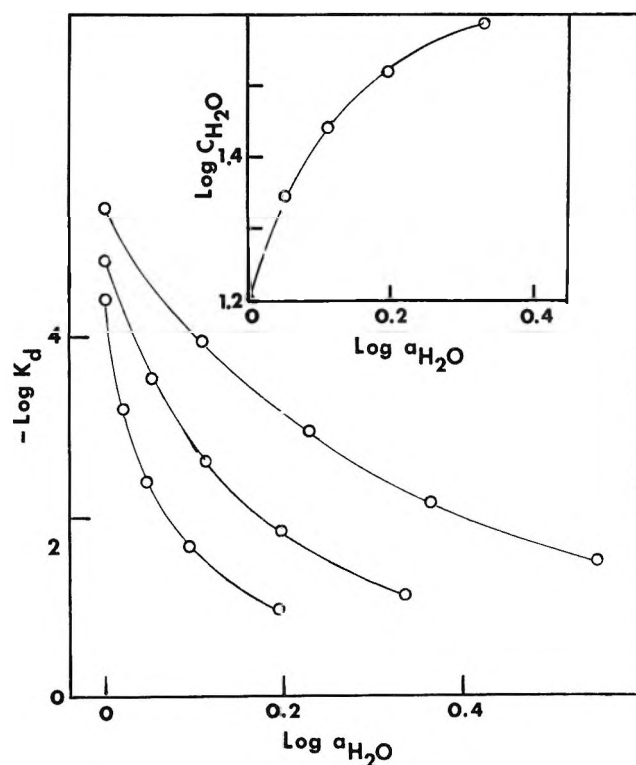


Figure 1. The water concentration, C_{H_2O} , in the insert, and the ion-pair dissociation constants for NaCl at 400, 500, and 700° as a function of the water activity, a_{H_2O} . The standard state for the water solvent at all temperatures was taken to be pure water at a pressure producing a density of 0.300 g/ml.

sponding to the density of water whose activity is a_{H_2O} . Values of $\log a_{H_2O}$ were calculated from eq 6 at 400, 500, and 700° using available specific volume (or density)-pressure data⁷ referenced by Quist and Marshall.^{2b} These values at 500° at densities of 0.4, 0.5, 0.6, and 0.7 g/ml are plotted vs. $\log C_{H_2O}$ in the insert, Figure 1. It can be seen that the activity of water increases at a greater rate with increasing pressure than does the concentration. It might be noted here that the pressure at a density of 0.30 g/ml is 550 bars, while at the highest density here, 0.70 g/ml, the pressure is 2000 bars, at 500°.

I have plotted values of $\log K_d$ for NaCl vs. these values of $\log a_{H_2O}$ at the corresponding densities at 400, 500, and 700°, Figure 1, to emphasize the fact that if equation 3 is correct, then the "complete" constant K° certainly is *not* constant as the density of solvent water changes. Marshall and Quist concluded on the basis of the linearity of isothermal $\log K_d$ vs. $\log C_{H_2O}$ plots that the complete equilibrium constant was independent of changes in the solvent dielectric constant. I conclude that the conclusions of Marshall and Quist are

(6) Interpolated from data compiled by A. W. Lawson and A. J. Hughes in "High Pressure Physics and Chemistry," Vol. I, R. S. Bradely, Ed., Academic Press, Inc., New York, N. Y., 1963, p 209.

(7) (a) W. T. Holser and G. C. Kennedy, *Am. J. Sci.*, 257, 71 (1959); (b) S. Maier and E. U. Franck, *Ber. Bunsenges. Phys. Chem.*, 70, 639 (1966).

invalid, being based on an incorrect assumption regarding the relationship of changes in water activity to changes in water concentration due to large pressure changes.

The results of the great amount of work by Marshall, *et al.*, are uniquely suited to a separation of specific ion-solvent interaction effects from the effects of changes in solvent dielectric constant; the latter I shall show is by no means unimportant. The effect of varying the dielectric constant of the solvent at constant temperature on ion-pair dissociation has been studied in most instances by either varying the composition of a polar-nonpolar solvent mixture⁸ over a wide range or by determining K_d in a series of similar solvents of varying dielectric constants.⁹ In either case, the ion-pair dissociation constants have been considered in terms of the equation¹⁰

$$K_d = (3000/4\pi Na^3) \exp(-E_s/RT) \times \exp(-e^2/akDT) \quad (7)$$

where N is Avogadro's number, a is the distance of closest approach of the anion and cation in the ion pair, E_s is the molar internal energy of specific solvation of the free ions less that of the ion pair, e is the electronic charge, and k is Boltzmann's constant. The transformation from the free-volume formulation^{10b} of the ion-pair dissociation process to the hard sphere in a continuum approach¹¹ to which is grafted^{10b,12} a specific solvation term was not rigorous. One correction that should be made in eq 2 is the replacement of E_s by the change in molar free energy of specific solvation, $\Delta G_s = \Delta H_s - T\Delta S_s$.

$$K_d = (3000/4\pi Na^3) \exp[-\Delta H_s/RT + \Delta S_s/R - e^2/akDT] \quad (8)$$

Clearly, if one varies the solvent composition as in either of the approaches outlined above, not only does the dielectric constant change, but also does the value of ΔG_s change. These changes in the difference in free energy of solvation, ΔG_s , will in general lead to curvature in the usual plots of $\log K_d$ vs. $1/D$, or to physically unreal values of the distance of closest approach, a .

Experimental separation of the three terms in the exponential of eq 8 is almost impossible without some simplifying assumptions. Two different approaches, and the assumptions necessary, are set out as follows: (a) study a set of systems in which it is known or assumed that ΔG_s (or $\Delta G_s/T$) and the distance of closest approach, a , are constant, but in which the product DT varies; or (b) study a set of systems in which a and ΔS_s are known or may be assumed to be constant and in which the product DT is held constant while T varies. I believe the data of Marshall and coworkers satisfy the criteria for approach (b). Examination of Marshall and Quist's compilation¹³ of the dielectric constants of water as a function of density shows that the DT

Table I: DT Product for Water

$T, ^\circ\text{C}$	Density, g/ml				
	0.3	0.4	0.5	0.6	0.7
400	3300	4780	6520	8560	10,800
500	3320	4710	6420	8360	10,400
600	3400	4710	6380	8200	10,200
700	3400	4770	6330	8080	10,100
800	3440	4840	6340	8050	10,000

product, at constant density, remains almost constant from 400 to 800°, Table I.

Examination of eq 8 shows that, if the parameters ΔH_s , ΔS_s , and a are independent of the temperature at constant density, then the only variables remaining that determine K_d are the temperature T in the first term of the exponential and the product DT in the third term of the exponential factor. Further, if this last, the DT product, is almost constant as the temperature changes from 400 to 800°, the only remaining variable is the temperature in the first exponential term. Under the conditions of constant density then

$$\log K_d = [\log (3000/4\pi Na^3) + \Delta S_s/2.30R - e^2/2.30akDT] - \Delta H_s/2.30RT \quad (9)$$

The term in brackets on the right-hand side is a constant. A plot of $\log K_d$ vs. $1/T$ should then yield values of ΔH_s from the slope. Using Marshall and Quist's data we can obtain values of ΔH_s for each electrolyte at each water density. The plots are in general linear, as Marshall has already pointed out.^{2b} The slopes of these plots do change with density, however. As an example, for the NaCl system, I obtained the values of the slopes (in units of deg K) of $\log K$ vs. $1/T$ at 0.3 g/ml, 2300; at 0.4 g/ml, 1660; at 0.5 g/ml, 1200; at 0.6 g/ml, 1120; and at 0.7 g/ml, 1180. The value of the solvation energy difference *does* depend on the solvent density in these systems.

If now at constant temperature, for each density of water solvent, we form the sum ($\log K_d + \Delta H_s/2.30RT$) this, according to eq 8, should be related to DT as follows,

$$(\log K_d + \Delta H_s/2.30RT) = [\log (3000/4\pi Na^3) + \Delta S_s/2.30RT] - (e^2/2.30ak)(1/DT) \quad (10)$$

Values of the left-hand side of eq 10 have been calculated for NaCl at 500° and were plotted vs. $1/DT$.

(8) The classical studies of this sort were those of C. A. Kraus and R. M. Fuoss, *J. Amer. Chem. Soc.*, **55**, 21 (1933).

(9) References 4b and 4d are examples of this approach.

(10) (a) H. Sadek and R. M. Fuoss, *J. Amer. Chem. Soc.*, **81**, 4511 (1959); (b) W. R. Gilkerson, *J. Chem. Phys.*, **25**, 1199 (1956).

(11) R. M. Fuoss, *J. Amer. Chem. Soc.*, **80**, 5059 (1958).

(12) W. R. Gilkerson and R. E. Stamm, *ibid.*, **82**, 5295 (1960).

(13) A. S. Quist and W. L. Marshall, *J. Phys. Chem.*, **69**, 3165 (1965).

The graph was quite linear and encouraged a more thorough investigation.

I have proceeded to treat the data for NaCl,^{2b} NaBr,^{2c} NaI,^{2e} and HBr,^{2d} using eq 8 in the following manner; for each salt, initial values of ΔH_s were obtained at each density for plots of $\log K_d$ vs. $1/T$ (eq 9). These values of ΔH_s were used to form, at constant temperature, the sums $(\log K_d + \Delta H_s/2.30RT)$, which were then plotted vs. $1/DT$ (eq 10). Recalling that the DT products showed some variation with temperature, Table I, the slopes from the plots vs. $1/DT$, being initial values of $(e^2/2.30ak)$, were used to correct for the variation of DT at constant density, eq 9. The sums $(\log K_d + e^2/2.30akDT)$ were formed at each density and plotted vs. $1/T$. This gave new and improved values of ΔH_s for each solvent density. These values of ΔH_s were used again to form the sums, at constant temperature, $(\log K_d + \Delta H_s/2.30RT)$, which were again plotted vs. $1/DT$, eq 10. These revised plots are shown in Figure 2. The linearity of these plots of $\log K_d$, corrected for specific (ion, ion-pair)-solvent interaction, in terms of the variable $1/DT$ furnish strong evidence that the data of Marshall, *et al.*, are in agreement with previous ideas concerning the influence of both solvent dielectric constant¹¹ and the influence of specific ion-solvent interaction,^{10b} rather than requiring complete revision of our notions concerning the relative importance of these two factors.

Repetition of the calculational procedure beyond the point described in the paragraph above was not attempted for the following reasons; Marshall and Quist^{2b} point out that the values of K_d (10^{-4} to 10^{-5}) at low densities are uncertain due to difficulties in extrapolating to infinite dilution, while I believe the values of K_d (10^{-1} to 10^{-2}) at high densities are uncertain since it is well known that the value calculated from a set of data when such a small fraction of the salt is ion paired depends on the particular form of the conductance equation used. The values of the dielectric constant of water at high temperatures and pressures¹² were obtained by extrapolation of experimental data at lower to higher temperatures. There is some uncertainty then in these resulting values of the dielectric constant of water. These are the same reasons I use here to argue that more sophisticated data-handling techniques such as least-squares procedures are of doubtful applicability in this case.

Comparison of the Two Approaches. The experimental limitations listed above should be kept in mind in the following discussion. Note that the plots of eq 10, Figure 2, for the several electrolytes, fall on the same straight lines at the two temperatures, 500 and 700°, with the exception of several sets of data at lowest densities. The approach to ion-pair dissociation outlined in this paper allows, at one temperature, for changes in differences in energies of solvation as the water density changes. The entropy differences had to be assumed

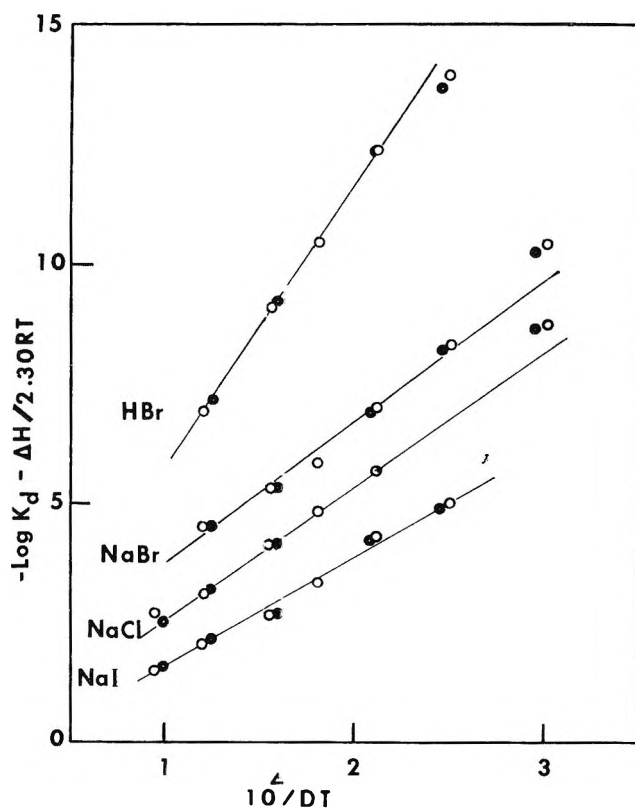


Figure 2. The logarithms of the ion-pair dissociation constants, corrected for specific ion-solvent and ion pair-solvent interaction, for HBr, NaBr, NaCl, and NaI at 500° (open circles) and at 700° (closed circles) vs. the reciprocal of the product of the dielectric constant and the temperature, $1/DT$.

to be constant. This approach also allows for the change in electrical free energy as the solvent dielectric changes. To be more specific, the free energy change, upon ion-pair dissociation, is assumed to contain three terms, an energy term (ΔH_s) which is independent of temperature and solvent dielectric constant, an energy term (W_{el}) which is inversely proportional to the solvent dielectric constant, and an entropy term ($T\Delta S$) which includes all other factors, is not dependent on the solvent dielectric constant, and of which the factor ΔS itself is temperature independent. These are all simplifications of an admittedly complex process. It is difficult to imagine the process broken into discrete steps, the free energy changes for which would correspond to those outlined above.

Marshall and Quist, in their treatment of these data, allowed only for changes in the free energy of solvation through changes in the water concentration as the density changed. This approach has been shown above to be incorrect in principle. One of the most interesting aspects, to this author, of these data of Marshall and Quist is that they provide a vivid illustration of an experimental technique by means of which the contribution to K_d of changes in dielectric constant may be separated from the contribution to K_d of changes due to specific solvation effects.

I cannot claim that the present treatment compared to that of Marshall and Quist reduces the number of parameters necessary to describe the data for a particular salt in water at high pressures and temperatures. Marshall and Quist need a value of K° (their complete dissociation constant), a value of n , and ΔE_v° (related to the change of K° with temperature). The present approach requires values of ΔH_s at each solvent density and a constant a , and one value of K_d at some temperature.

Ion-Pairing Parameters. Values of ΔH_s and distances of closest approach, a , appear in Table II, as well

Table II: Ion Pairing Parameters in Water at High P and T

density, g/ml	- ΔH_s , kcal/mol			
	NaCl	NaBr	NaI	HBr
0.3	13.9	17.7	8.5 ^a	29.8 ^a
0.4	7.6	9.5	7.9	26.6
0.5	5.6	7.0	5.2	19.8
0.6	4.6	6.5	6.0	16.3
0.7	4.4	7.1	6.2	...
a , 10^{-8} cm	2.57	2.47	3.16	1.15
$(r_+ + r_-)^b$	2.31	2.97	3.22	1.43 ^c

^a At a density of 0.35 g/ml. ^b Interionic distance in the crystals from N. K. Adam, "Physical Chemistry," Clarendon Press, Oxford, 1952, p 197. ^c HBr bond distance, gas phase.

as the sums of crystallographic ionic radii, $r_+ + r_-$. ΔH_s is exothermic for the ion-pair dissociation process, in accord with the view that this process is attended by a net increase in the numbers of water molecules specifically solvating the ions. Note that ΔH_s tends to become more negative as the solvent density decreases. The water molecules being specifically bound to the ions in this process are being removed from bulk water and transferred to the immediate neighborhood of the free ions. The removal of water molecules from bulk water must be attended by the rupture of hydrogen bonds. At lower water densities, it is expected that the fraction of water molecules in an H-bonded condition would be less than at higher densities.¹³ I believe then that the observed trend in ΔH_s with water density is a reflection

of the smaller energies required to remove water molecules from bulk water as the density decreases.

The distances of closest approach, a , are much smaller than values for the alkali metal halides usually obtained from slopes of isothermal $\log K$ vs. $1/D$ plots in water-dioxane mixtures;¹⁴ the a value for NaCl at high dioxane content is found to be 6.9 Å in this system. The a values found in the present treatment, Table II, are even slightly smaller than the sums of the crystallographic radii. I shall not argue that these small a -values are real; the electrostatic model is primitive, attractive forces other than simple charge-charge interaction are involved, in addition to repulsive forces of a form which can only be guessed. The macroscopic dielectric constant D factor is only a crude representation of the real reduction in charge-charge interaction due to polarization of the solvent molecules by the intense electric fields surrounding the ions. It must be admitted that until the contribution of specific ion-solvent interaction to the ion-pairing process can be separated experimentally and understood theoretically most distances of closest approach contain this variable (polarization of the solvent molecules by the ions) as a hidden parameter. The ion pairs formed at 25° in water-dioxane mixtures may well be solvent-separated while those formed at high temperatures and low densities in water fluid are contact ion pairs. Both species may be present to an appreciable extent in both systems. An effort to experimentally determine the separate influences of specific ion solvent interaction and charge-charge interaction in the water-dioxane system would be profitable in this connection. I understand¹⁵ that high-temperature-high-pressure conductance measurements are being carried out on alkali metal salts in water-dioxane mixtures. It is strongly urged that measurements of the dielectric constants of the solvent systems be carried out to as high a precision as possible. Analysis of the results of these experiments using the approach suggested here would then throw further light on the problem of the distance of closest approach.

(14) R. M. Fuoss and K. L. Hsia, *Proc. Natl. Acad. Sci. U. S.*, **57**, 1550 (1967); **58**, 1818 (1967).

(15) Private communication from W. L. Marshall.

Molecular Complexes of Iodine with Pyrone-(4) and 1-Thiopyrone-(4)

by N. Kulevsky and G. J. Liu

Department of Chemistry, University of North Dakota, Grand Forks, North Dakota 58201
(Received July 31, 1969)

Thermodynamic data for the formation of iodine complexes with pyrone-(4) (I) and 1-thiopyrone-4 (II) have been obtained from measurements of the blue-shifted iodine band. The thiocarbonyl analogs of I and II are found to undergo irreversible reactions with iodine. The values of ΔH° and ΔG°_{298} indicate that II is only slightly more basic toward iodine than is I. From a comparison of thermodynamic data for iodine complexes of ethers, thioethers, and ketones with that reported here for I and II with iodine, it is evident that the bonding site in I and II is the carbonyl oxygen. The differences between I and II may be explained mainly in terms of the electron density at the carbonyl oxygen.

Introduction

It is well established that in *n*-donor molecules the replacement of an oxygen atom by sulfur enhances the electron donor abilities of these molecules toward iodine. This has been shown by comparisons of such diverse types of molecules as the series of aliphatic acyclic and cyclic ethers with the corresponding thioethers^{1,2} and various amides with thioamides.³⁻⁶ In contrast to the above series, there are few data available on the effect caused by sulfur replacing an oxygen atom that is distant from the donor site. The series of γ -pyrone and its sulfur analogs appeared to be a good system for investigating such an effect, since studies on the infrared spectra of I₂ complex with 2,6-dimethylpyrone-(4) by Cook⁷ and Glusker, *et al.*,⁸ indicate that the carbonyl oxygen is the basic site. This report will discuss the reaction of I₂ with the carbonyl compounds, pyrone-(4) (I) and 1-thiopyrone-(4) (II) and the thiocarbonyl compounds, 4-thiopyrone (III) and 1,4-dithiopyrone (IV).

Experimental Section

Materials. Pyrone-(4) (I) was prepared by the pyrolysis under reduced pressure⁹ of chelidonic acid mixed with copper powder. The crude product was refluxed with dry benzene and distilled under vacuum. After two distillations the product obtained had a melting point of 31.5–32.5° (lit. 32–32.5°).⁹ 1-Thiopyrone-(4) (II) was prepared from the reaction of KES with I.¹⁰ After three recrystallizations from CCl₄, a compound was obtained which melted at 109–109.5° (lit. 109.5–110°).¹⁰ An infrared spectrum of the compound agreed with that reported for II.¹¹ 4-Thiopyrone (III) was prepared by the reaction of P₄S₁₀ with I.¹² After extracting the product with benzene, III was purified by a vacuum sublimation. Its melting point is 48.5–49.5° (lit. 49.0°).¹² 1,4-Dithiopyrone (IV) was prepared from II by the method of Traverso.¹³ After purifying by a vacuum sublimation, the compound melted at 48° (lit. 48°).¹³ All of these com-

pounds are hygroscopic and were stored in a desiccator over P₂O₅. Baker analyzed iodine was sublimed under vacuum three times and stored in a desiccator. Spectral grade CCl₄ was used without further treatment as the solvent.

Preparation of Solutions. Stock solutions of donor and iodine were prepared by weighing out both the solvent and solute. Since all the donors are hygroscopic, stock solutions of the donors were prepared in a drybox under nitrogen. The solutions to be used in the measurements were prepared by mixing weighed quantities of stock donor, stock iodine, and pure solvent. By using these weights and assuming that the final dilute solutions had the same density as the pure solvent, the initial molar concentrations could be calculated.

Apparatus. All of the spectra were recorded in the visible region using a Cary 14 spectrophotometer. The cell compartment was thermostated to $\pm 0.1^\circ$. Cells of 1 cm path length were used for recording all spectra.

Results and Discussion

On mixing the individual donors (I–IV) with iodine a noticeable color change could be immediately observed. The spectra of the iodine complexes of I and II have

- (1) J. D. McCullough and I. C. Zimmermann, *J. Phys. Chem.*, **65**, 888 (1961).
- (2) M. Tamres and S. Searles, *ibid.*, **66**, 1099 (1962).
- (3) R. J. Niedzielski, R. S. Drago, and R. L. Middaugh, *J. Amer. Chem. Soc.*, **86**, 1694 (1964).
- (4) K. S. Bhaskar, S. N. Bhat, A. S. Murthy, and C. N. R. Rao, *Trans. Faraday Soc.*, **62**, 788 (1966).
- (5) R. P. Lang, *J. Amer. Chem. Soc.*, **84**, 1185 (1962).
- (6) R. P. Lang, *J. Phys. Chem.*, **72**, 2129 (1968).
- (7) D. Cook, *Can. J. Chem.*, **39**, 1184 (1961).
- (8) D. L. Glusker and H. W. Thompson, *J. Chem. Soc.*, 471 (1955).
- (9) R. Cornubert, R. Delmas, S. Monteil, and J. Viriot, *Bull. Soc. Chem. Fr.*, **17**, 36 (1950).
- (10) R. Mayer, *Chem. Ber.*, **9C**, 2362 (1957).
- (11) D. S. Tarbell and P. Hoffman, *J. Amer. Chem. Soc.*, **76**, 2451 (1954).
- (12) F. Arndt, E. Scholz, and P. Nachtwey, *Chem. Ber.*, **57**, 1903 (1924).
- (13) G. Traverso, *ibid.*, **91**, 1224 (1958).

peaks at 444 $m\mu$ and 445 $m\mu$, respectively. These peaks have not been corrected for the absorption caused by uncomplexed iodine. Solutions of these complexes did not show any changes in the positions or heights of these peaks for about 3 hr after mixing. After this period some changes could be observed, and thus all measurements on these solutions were recorded in the first 3 hr after mixing. Compounds III and IV were found to have undergone secondary reactions almost immediately upon mixing the components, as evidenced by the appearance of peaks at 290 $m\mu$ and 370 $m\mu$ which can be attributed to the formation of I_3^- .¹⁴ Also, a few minutes after mixing, a black precipitate appeared. Therefore, measurement of the equilibrium constants for complex formation could be made on compounds I and II only.

Due to the limited solubility of I and II in the solvent, only rather dilute solutions of the donors can be prepared. In order to have reasonable values of the absorbance at the maximum of the blue shifted iodine peak, it was necessary that the concentration of iodine be fairly high. For the complex with I the range of donor concentrations was from 40×10^{-3} to 80×10^{-3} M while the iodine concentrations were 1×10^{-3} to 1.7×10^{-3} M . For compound II the range of donor concentrations was 10^{-2} to 10^{-3} M and iodine from 3×10^{-3} to 6×10^{-3} M . This narrow range of concentrations has two important consequences. The first one is that an isobestic point for the complex of II could not be observed because of the high absorbance of free iodine in the solution. Thus, for this complex, the existence of only one complex could not be proven. However, only one complex was assumed to be present, as the position of the blue-shifted I_2 peak did not vary when the concentrations and temperatures of the solutions were changed. For the complex of I, an isobestic point was observed at 490 $m\mu$, a good indication that over the concentration range used there is only one complex formed.

The second result of the limited range of concentrations used in these experiments is that the association constant (K_c) of the complexes could not be calculated by the Benesi-Hildebrand equation¹⁵ or any variation of it which requires $C_D > C_A$, where C_D and C_A are the concentrations of donor and acceptor, respectively. A treatment which appears to be valid in these circumstances is that given by Tamres,¹⁶ which is a variation of one given by Ross and Labes.¹⁷ Equation 1 was derived by Tamres and is valid for the association of 1:1 complexes if the complexes are weak and/or if the solutions are both dilute. In eq 1 a_c is the absorption

$$C_A C_D / (A) = (C_A + C_D) / (a_c - a_i) + 1 / K_c (a_c - a_i) \quad (1)$$

coefficient of the complex, a_i is the absorption coefficient of free iodine, and A is the absorbance of the

solution measured with a reference solution containing the same concentration of iodine used in the solution of the complex. A plot of $(C_A C_D) / A$ vs. $C_A + C_D$ for several solutions gives a straight line whose slope is $1 / (a_c - a_i)$ and intercept is $1 / K_c (a_c - a_i)$.

The values of K_c and $(a_c - a_i)$ shown in Table I for compounds I and II were obtained using eq 1.

Table I: Equilibrium Constants and $a_c - a_i$ as a Function of Temperature for Pyrone-(4) and 1-Thiopyrone-(4) Complexes with I_2 in CCl_4

	$T, ^\circ C$	$K_c, l./mol$	$a_c - a_i$
Pyrone-(4)	11.0	4.5 ± 0.2	1470 ± 60
	19.7	3.8 ± 0.4	1400 ± 100
	25.4	3.3 ± 0.3	1300 ± 100
1-Thiopyrone-(4)	11.0	6.0 ± 0.2	1570 ± 200
	19.7	5.0 ± 0.3	1540 ± 80
	28.9	4.2 ± 0.5	1400 ± 180

The slopes and intercepts were calculated using the method of least squares. The values of ΔH° presented in Table II were calculated from a plot of $\ln K_c$ vs. $1/T$. The value of K_{c298} given in Table II was calculated from the line obtained in the least-squares calculation of the data given in Table I. All of the error limits presented in the tables are the standard deviations obtained from the least-squares treatment.

From the data given in Table II it can be seen that the complex of the thio compound (II) is only slightly more stable than the complex of its oxygen analog (I). In contrast to this, the difference in stability of the iodine complexes of ethers and thioethers is large (thioethers, ΔH° range from 6.0 to 8.7 kcal/mol and K_{298} range from 23 to 186 M^{-1} ; analogous ethers, ΔH° range from 4.3 to 6.4 kcal/mol and K_{298} range from 6.4 to 26.1 M^{-1}).^{1,2} The reason for this contrasting behavior must lie in the fact that in compounds I and II the carbonyl oxygen atom is the donor site, and this atom is affected only to a small extent by the substitution of sulfur for oxygen within the ring. Further evidence for the donor site being assigned to the carbonyl group is apparent if one compares the data for compounds I and II with those reported by Wobschall and Norton for some iodine complexes with ketones.¹⁸ The values of ΔH° and K_{298} determined by them for cyclohexanone, $\Delta H^\circ = 5.4$ kcal/mol and $K_{298} = 3 M^{-1}$, are similar to those reported here for pyrones. Previously, Cook⁷ had assumed that the carbonyl in 2,6-

(14) R. E. Buckles, J. P. Yuk, and A. I. Popov, *J. Amer. Chem. Soc.*, **74**, 4379 (1952).

(15) H. A. Benesi and J. H. Hildebrand, *ibid.*, **70**, 2832 (1949).

(16) M. Tamres, *J. Phys. Chem.*, **65**, 654 (1961).

(17) S. D. Ross and M. M. Labes, *J. Amer. Chem. Soc.*, **79**, 76 (1957).

(18) D. Wobschall and D. A. Norton, *ibid.*, **87**, 3559 (1965).

Table II: Thermodynamic Data and Spectral Maxima of Iodine-Pyrone Complexes in CCl_4

Donor	λ_{max} , m μ	K_{298} , l./mol	$-\Delta G^\circ_{298}$, kcal/mol	$-\Delta H^\circ$, kcal/mol	$-\Delta S^\circ_{298}$, eu
Pyrone-(4)	444	3.5 ± 0.2	0.74 ± 0.03	3.2 ± 0.2	8.3
1-Thiopyrone-(4)	445	4.6 ± 0.1	0.90 ± 0.01	3.7 ± 0.1	9.4

dimethyl pyrone-(4) was the donor atom toward iodine and other Lewis acids.

The higher donor ability of II compared to I is easily explained by an examination of the resonance forms A and B that can be written for the γ -pyrones



where $X = \text{O}$ for I and $X = \text{S}$ for II. High contributions of B would increase the electron donor ability of the carbonyl oxygen. Because of the greater electronegativity of oxygen, compound I would have a lower contribution of B and thus be lower in donor ability than II. The results of molecular orbital calculations

are also pertinent to this argument. Mayer, *et al.*, in a recent review, gave a collection of the results of molecular orbital calculations for these molecules obtained with a variety of parameters.¹⁹ The results of these calculations show that I has a lower π -electron density at the carbonyl oxygen than does II. The measured dipole moments of I and II²⁰ also are in agreement with these calculations. Thus, it would seem that the differences between the donor abilities of I and II can be attributed mainly to the higher electron density at the carbonyl oxygen in II.

(19) R. Mayer, W. Broy, and R. Zahradnik in "Advances in Heterocyclic Chemistry," Vol. 8, A. R. Katritzky and A. J. Boulton, Ed., Academic Press, New York, N. Y., 1967, p 219.

(20) M. Rolla, M. Sanesi, and G. Traverso, *Ann. Chim. (Rome)*, **44**, 430 (1954).

A Bromine-79 Nuclear Magnetic Resonance Study of the Structure of Aqueous Solutions of Mono-, Di-, and Trialkylammonium Bromides

by Björn Lindman, Håkan Wennerström, and Sture Forsén

*Division of Physical Chemistry, The Lund Institute of Technology, 220 07 Lund 7, Sweden
(Received May 27, 1969)*

The nuclear quadrupole relaxation of ^{79}Br in aqueous solutions of mono-, di-, and trialkylammonium bromides has been studied. The relaxation rate of the ^{79}Br nuclei increases rapidly with increasing number of alkyl groups on the nitrogen, with increasing length of the alkyl groups and with the concentration of the salts. In all cases the ^{79}Br line widths are significantly greater than those observed in aqueous solutions of alkali bromides. The observed effects are found to be due to increased anion-water binding in the vicinity of the cations. The apparent energies of activation for the relaxation process have been determined in some cases. The activation energies indicate that the bromide ion-water interaction is stronger in these solutions than in aqueous solutions of some alkali bromides. Measurements on solutions containing long-chain alkyl amine hydrobromides show that there is an abrupt change in counterion binding in the region of the critical micelle concentration. An estimate is made of the bonding properties for the counterions adsorbed on the surface of the micelles.

Introduction

Aqueous solutions of substances containing hydrocarbon groups are of interest since the properties of these solutions are in many respects markedly different from those of aqueous solutions of inorganic electrolytes. In the last few years aqueous solutions of symmetrical quaternary alkylammonium salts have been studied extensively (see *e.g.*, ref 1-11). In spite of this, no detailed structural description of these solutions is yet available. Most workers in the field, however, agree in one respect, *viz.*, that the alkyl groups in the cations have a structure-forming effect on the water lattice (see *e.g.*, Hertz¹² and Frank¹³). The nuclear magnetic relaxation studies by Hertz and coworkers^{1,14} are especially informative (*cf.* also ref 15). Thus relaxation time measurements on protons, deuterons, and ^{17}O nuclei in water show that there is on the average a slowing down of the rotational motion of the water molecules when the tetraalkylammonium salts are dissolved. From measurements of self-diffusion coefficients of the water molecules, Hertz, Lindman, and Siepe¹⁶ found that also the translational motion of the water molecules in these solutions is much slower than in pure water.

The study by Lindman, Forsén, and Forslind¹⁷ of the ^{79}Br nuclear magnetic relaxation rates showed that the coupling between bromide ions and water in solutions of quaternary ammonium bromides is markedly different from that in aqueous solutions of alkali halides. (Later measurements have demonstrated that this also holds true for chloride ions and iodide ions.¹⁸) This work initiated the study by Hertz, *et al.*,¹⁶ which was concerned with the determination of self-diffusion coefficients for the cations and the water molecules, the relaxation times (for protons and deuterons) of the cat-

ions as well as the relaxation rate of ^{85}Rb (in added RbCl) in aqueous solutions of tetraalkylammonium chlorides. This work showed that the slowing down in the motion of the solvent molecules is not restricted to the first hydration layer of the cation, but that there is a considerable spreading out of the structure-stabilizing effect, at least at reasonably high concentrations.

Whereas a large number of papers have been devoted to the study of aqueous solutions of tetraalkylammonium salts, comparatively few articles treat aqueous solutions of other alkylammonium salts (with the ex-

- (1) H. G. Hertz and M. D. Zeidler, *Ber. Bunsenges. Phys. Chem.*, **68**, 821 (1964).
- (2) B. E. Conway and R. E. Verrall, *J. Phys. Chem.*, **70**, 3952 (1966).
- (3) R. L. Kay, T. Vituccio, C. Zawoyski, and D. F. Evans, *ibid.*, **70**, 2336 (1966).
- (4) F. Franks, "Hydrogen-Bonded Solvent Systems," A. K. Covington and P. Jones, Ed., Taylor and Francis, Ltd., London, 1968.
- (5) B. E. Conway, R. E. Verrall, and J. E. Desnoyers, *Trans. Faraday Soc.*, **62**, 2738 (1966).
- (6) F. Franks and H. T. Smith, *ibid.*, **63**, 2586 (1967).
- (7) R. Zana and E. Yeager, *J. Phys. Chem.*, **71**, 4241 (1967).
- (8) H. E. Wirth, *ibid.*, **71**, 2922 (1967).
- (9) H. E. Wirth and A. LoSurdo, *ibid.*, **72**, 751 (1968).
- (10) R. Gopal and M. A. Siddiqi, *ibid.*, **72**, 1814 (1968).
- (11) W-Y. Wen and K. Nara, *ibid.*, **71**, 3907 (1967).
- (12) H. G. Hertz, *Ber. Bunsenges. Phys. Chem.*, **68**, 907 (1964).
- (13) H. S. Frank, *Proc. Roy. Soc.*, **A247**, 481 (1958).
- (14) F. Fister and H. G. Hertz, *Ber. Bunsenges. Phys. Chem.*, **71**, 1032 (1967).
- (15) S. S. Danyluk and E. S. Gore, *Nature*, **203**, 748 (1964).
- (16) H. G. Hertz, B. Lindman, and V. Siepe, *Ber. Bunsenges. Phys. Chem.*, **73**, 542 (1969).
- (17) B. Lindman, S. Forsén, and E. Forslind, *J. Phys. Chem.*, **72**, 2805 (1968).
- (18) H. Wennerström and B. Lindman, to be published.

ception of work concerning micelle formation and related properties of solutions of long-chain monoalkylammonium salts). One possible step toward a better understanding of the influence of alkyl groups on the water structure is to study also aqueous solutions of mono-, di-, and trialkylammonium salts. Previous studies of aqueous solutions of these alkylammonium salts have been concerned with, *e.g.*, dielectric relaxation times,¹⁹ partial molal heat capacities,²⁰ densities,²¹ viscosities,²² and conductivities,²² and demonstrate the structure-stabilizing effect of the cations on the water lattice.

In the present paper, measurements of ⁷⁹Br nuclear magnetic resonance line widths of aqueous solutions of mono-, di-, and trialkylammonium bromides will be reported. The aim of the work is to investigate the degree to which the change in bromide ion bonding as reflected in the ⁷⁹Br line widths (see ref 17) depends on the special symmetry of the alkylammonium ions and the degree to which it depends merely on the presence of alkyl groups in the solution. To this end we have studied the dependence of the ⁷⁹Br nuclear magnetic relaxation rate on the number of carbon chains on the nitrogen, on the carbon chain length, and on the concentration of the electrolyte. In order to obtain some information on the energetics of the processes in the solutions influencing the relaxation, the temperature dependence of the ⁷⁹Br line width has also been studied. The measurements on monoalkylammonium bromides were extended up to a carbon chain length of eleven in order to study micelle formation.

Experimental Section

Preparation and Purification of the Salts. The mono-, di-, and trialkylammonium bromides were prepared by either or both of the following two methods. In the first procedure (which could be used only when the amines were very pure and sufficiently water-soluble) the solutions were obtained directly from an aqueous solution of the corresponding amine which was neutralized with hydrobromic acid. In most cases, however, the amine hydrobromides were obtained from the amine (or in the case of methylamine, dimethylamine, trimethylamine, and ethylamine from an aqueous solution of the amine) and a concentrated aqueous solution of hydrobromic acid after evaporation *in vacuo*. In a few cases, both methods were used, and no difference could be detected between the alkylammonium bromide products. The amines were obtained from BDH and from Fluka AG. The hydrobromic acid used was the Analar quality from BDH. Triethylamine hydrobromide was also obtained from Eastman Organic Chemicals, Rochester, N. Y.

The hydrobromides were recrystallized (once or twice depending on the initial purity) from the following solvents: ethanol: CH₃NH₃Br, (CH₃)₂NH₂Br, (CH₃)₃NHBr, C₂H₅NH₃Br, (C₂H₅)₂NH₂Br, and

(C₂H₅)₃NHBr; ethanol–diethyl ether: C₃H₇NH₃Br, (C₃H₇)₂NH₂Br, (C₃H₇)₃NHBr, C₄H₉NH₃Br, C₅H₁₁NH₃Br, (C₆H₁₁)₂NH₂Br, C₆H₁₃NH₃Br, C₇H₁₅NH₃Br, C₈H₁₇NH₃Br, C₉H₁₉NH₃Br, and C₁₀H₂₁NH₃Br; chloroform–diethyl ether: C₁₁H₂₃NH₃Br. Tetrabutylammonium bromide was obtained from Fluka AG and was recrystallized from chloroform–diethyl ether or from acetone–diethyl ether.

Nmr Measurements. A Varian V-4200 nmr spectrometer equipped with a 12-in. V-3603 magnet was used for the measurements. The magnetic field was controlled by a Varian Mark II Fieldial. The modulation frequency and the amplitude of the modulation field were kept low compared with the line width and the derivative of the absorption curve was recorded. The line width was measured directly from the recorded curve as the distance between the maximum and minimum slopes of the absorption curve. The field modulation frequency was 40 Hz except in the case of some of the broadest signals where 80 or 400 Hz was used. The peak-to-peak field modulation amplitude was about 1/4 (and never greater than 1/3) of the line width. Our data have been corrected for modulation broadening (assuming Lorentzian lines) according to the Wahlquist^{23a} theory with data taken from Smith.^{23b} This correction is in the range 0.5–2%. The amplitude of the radio frequency field was chosen low enough not to give a saturation broadening greater than 1% (*cf.* Pake^{23c}). The resonance frequency was stabilized within 1 Hz at 14.98 MHz by means of a crystal oscillator circuit. An estimate of the inhomogeneity of the magnetic field was obtained by recording the ²³Na nmr signal at the same magnetic field strength as used for the ⁷⁹Br measurements. The field inhomogeneity as obtained from the line width of the ²³Na signal was found to be 20–30 mG, thus, less than 0.1 of the most narrow lines reported in this paper. No correction for inhomogeneity broadening has been applied. The sample temperature was 30 ± 2° except in the temperature dependence investigations. In the latter measurements the Varian V 4540 temperature controller was used to control the temperature. The temperature was measured (before and after the recording of the spectrum) with a thermocouple located in the sample and is accurate within ±0.3°. The samples were contained in test tubes with an inner diameter of 15 mm (9 mm for the investigation of temperature dependence). The reported line widths are the arithmetic

(19) G. H. Haggis, J. B. Hasted, and T. J. Buchanan, *J. Chem. Phys.*, **20**, 1452 (1952).

(20) T. Ackermann and H. Rüterjans, *J. Chim. Phys.*, Numéro special, Oct 1969, p 124.

(21) J. E. Desnoyers and M. Arel, *Can. J. Chem.*, **45**, 359 (1967).

(22) J. E. Desnoyers, M. Arel and P.-A. Leduc, *ibid.*, **47**, 547 (1969).

(23) (a) H. Wahlquist, *J. Chem. Phys.*, **35**, 1708 (1961); (b) G. W. Smith, *J. Appl. Phys.*, **35**, 1217 (1964); (c) G. E. Pake, *Am. J. Phys.*, **18**, 437 (1950).

means of 3-6 spectra (for the temperature variation study only 2-3 spectra at each temperature were recorded). The individual measurements were within 5% from the average except for the investigation of the temperature dependence where this figure increased somewhat owing to smaller sample volumes. The measurements at the lowest concentrations in the concentration dependence study for the mono-, di-, and triethylamine hydrobromides are also somewhat uncertain.

Experimental Results and Basic Principles

In Figure 1 are given the measured ^{79}Br nmr line widths for 0.100 M aqueous solutions of mono-, di-, tri-, and tetra- n -alkylammonium bromides. The data (with the exception of values concerning the temperature dependence of the line width) for the quaternary alkylammonium bromides are taken from ref 17. Figure 2 shows a plot equivalent to that in Figure 1 for 0.500 M solutions. As seen from these figures the ^{79}Br line width increases strongly with increasing carbon chain length as well as with increasing number of alkyl groups in the cation. The line width also increases with increasing electrolyte concentration. For di-, tri-, and tetraalkylammonium bromides, limited solubility prevents measurements when the carbon chain contains more than five carbon atoms. Monoalkylammonium bromides could be studied up to undecylamine hydrobromide. For still longer N -alkyl substituents the signal-to-noise ratio did not allow precise line width measurements. The data for mono- n -alkylammonium bromides are presented in Figure 3 for two concentrations (0.100 and 0.500 M). As may be inferred from this graph, the line width increases with increasing length of the alkyl group in the whole range investigated. The increase in line width is initially comparatively slow, but when one reaches the region where the cations are known to aggregate to micelles the slope increases drastically. For the ethylammonium salts the concentration dependence was investigated in more detail. The results are given in Figure 4, and as can be seen the concentration dependence is approximately linear at low concentrations.

For the butylammonium bromides the temperature dependence of the line widths was studied. The temperature range was 6-94°. In Figure 5 the logarithm of the observed line widths is plotted against the inverse absolute temperature. The plots are slightly curved, the slope being smaller at higher temperatures. Through a least-squares treatment we have calculated the average energies of activation for the relaxation process in the temperature range investigated (see Table I).

For three samples (0.500 M octylamine hydrobromide, 4.00 M triethylammonium bromide, and 0.500 M tetrabutylammonium bromide) the dependence of the line width on the resonance frequency (in the range

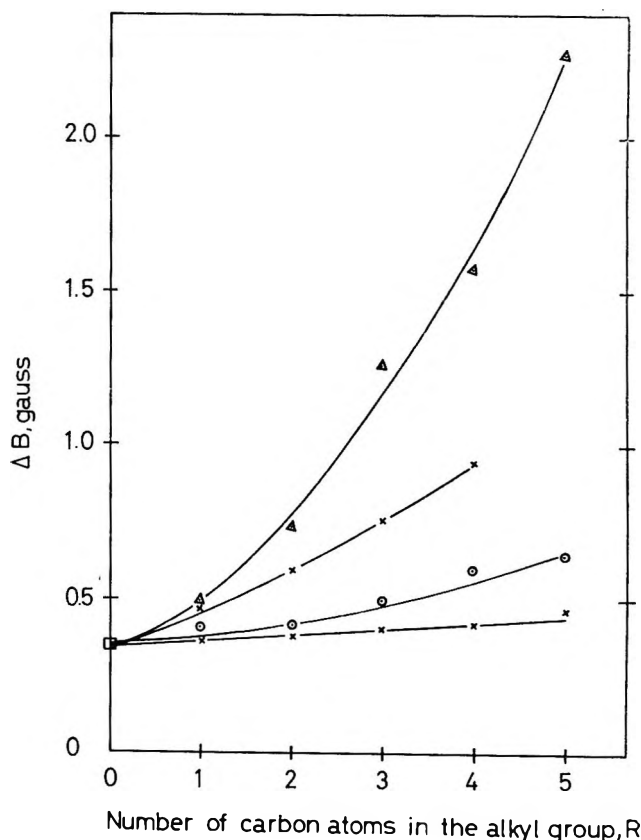


Figure 1. The line width, ΔB , for ^{79}Br in aqueous solutions of alkylammonium bromides as a function of the number of carbon atoms in the alkyl group, R . T , 30° (for $R_4\text{NBr}$ 25°); concn, 0.100 M ; \times (lower points), $R_1\text{NH}_3\text{Br}$; \circ , $R_2\text{NH}_2\text{Br}$; Δ (upper points), $R_3\text{NHBr}$; \square , $R_4\text{NBr}$; \square , NH_4Br . Data for $R_4\text{NBr}$ from ref 17; the lines in this and following figures are drawn just as an aid to the eye.

Table I: Average Energies of Activation (E_a) for the Relaxation Process in the Temperature Range 6-94° Obtained by a Least-Squares Treatment^a

Sample	E_a , kcal/mol
0.500 M BuNH ₃ Br	3.4 ± 0.2
0.500 M Bu ₂ NH ₂ Br	3.9 ± 0.2
0.500 M Bu ₃ NHBr	4.5 ± 0.2
0.500 M Bu ₄ NBr	5.7 ± 0.2
0.500 M Et ₄ NBr	4.4 ± 0.2
LiBr ^b	2.9 (from ref 26)
NaBr ^b	2.9 (from ref 26)
CsBr ^b	2.3 (from ref 26)
KBr ^c (0.1-4.0 M)	2.1 ± 0.4 (from ref. 31)

^a For comparison, some data are included from the work by Hertz²⁶ and by O'Reilly, *et al.*³¹ Except for KBr all investigations are performed with ^{79}Br resonance. ^b For the concentration dependence see ref 30. ^c From ^{81}Br relaxation.

8-16 MHz) was studied. Within the experimental error no change of the line widths with frequency was detected, thus proving that the "case of extreme narrowing" is applicable. This implies that the correlation time, τ_c , which gives the time scale for molecular mo-

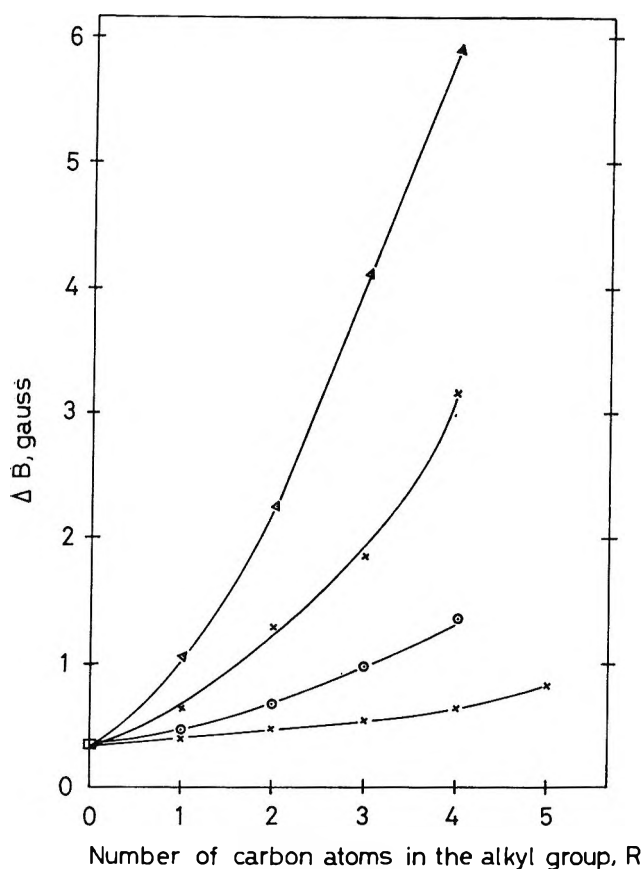


Figure 2. The line width of the ^{79}Br resonance for 0.500 M aqueous solutions of alkylammonium bromides. For further information, see the text to Figure 1.

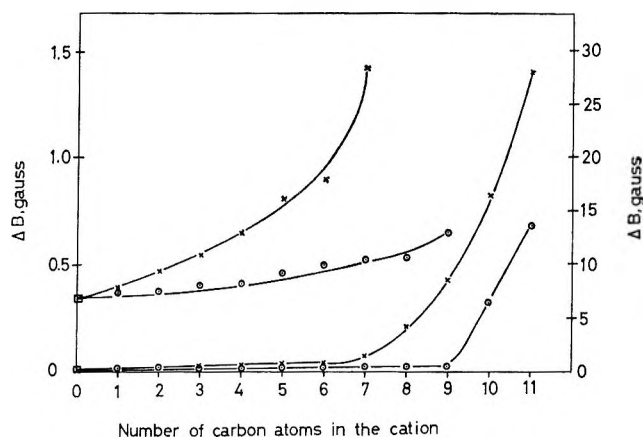


Figure 3. ^{79}Br nuclear magnetic resonance line widths for aqueous solutions of monoalkylammonium bromides: ○, 0.100 M solutions; ×, 0.500 M solutions; ◻, denotes the value for NH_4Br . The two upper curves are given in the scale of the left vertical axis whereas the lower curves are referred to the right vertical scale. T , 30°.

tion, is much smaller than the inverse Larmor precession frequency. Under conditions of extreme narrowing the spin-lattice relaxation time, T_1 , equals the spin-spin relaxation time, T_2 , and the quadrupole relaxation rates are given by the formula²⁴

$$\frac{1}{T_1} = \frac{1}{T_2} = \frac{3}{40} \frac{2I - 3}{I^2(2I - 1)} \left(1 + \frac{\eta^2}{3}\right) \left(\frac{eQ}{\hbar} \frac{\partial^2 V}{\partial z^2}\right)^2 \tau_c \quad (1)$$

I is the spin quantum number of the nucleus observed, $\hbar = h/2\pi$ (h is Planck's constant), eQ is the electric quadrupole moment, $\partial^2 V/\partial z^2$ is the largest of the components of the field gradient tensor along the principal axes, and η is the asymmetry parameter.²⁴ Other relaxation mechanisms than quadrupole interactions are certainly unimportant and consequently eq 1 will also with good accuracy give the total nuclear magnetic relaxation rate. As has recently been emphasized by Hertz, *et al.*,²⁵ eq 1 is strictly applicable only for a specific form of the correlation functions describing the molecular motion of the ion and its surroundings.

Since the nuclear magnetic resonance line width, ΔB , is proportional to the inverse transversal relaxation time (the proportionality factor contains one term

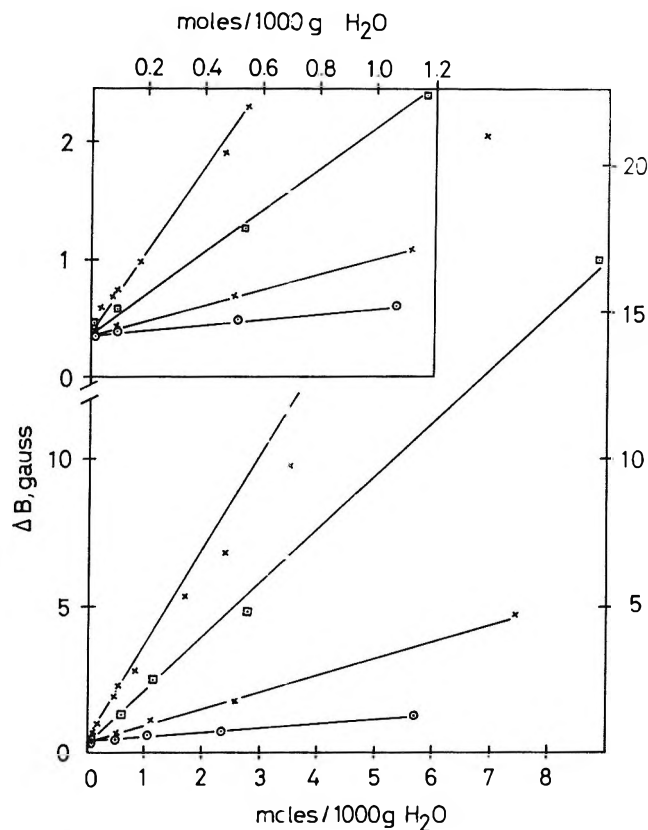


Figure 4. Concentration dependence of the ^{79}Br nmr line width in aqueous solutions of ethylammonium bromides. T , 30°: ○, $\text{C}_2\text{H}_5\text{NH}_3\text{Br}$; × (lower points), $(\text{C}_2\text{H}_5)_2\text{NH}_2\text{Br}$; ◻, $(\text{C}_2\text{H}_5)_3\text{NHBr}$; × (upper points), $(\text{C}_2\text{H}_5)_4\text{NBr}$ (from ref 17, 25°). The low concentration range is shown expanded in the upper left corner. For comparison straight lines are drawn through the points at low concentrations.

(24) A. Abragam, "The Principles of Nuclear Magnetism," Clarendon Press, London, 1961.

(25) H. G. Hertz, G. Stalidis, and H. Versmold, *J. Chim. Phys.*, Numéro special, Oct 1969, p 177.

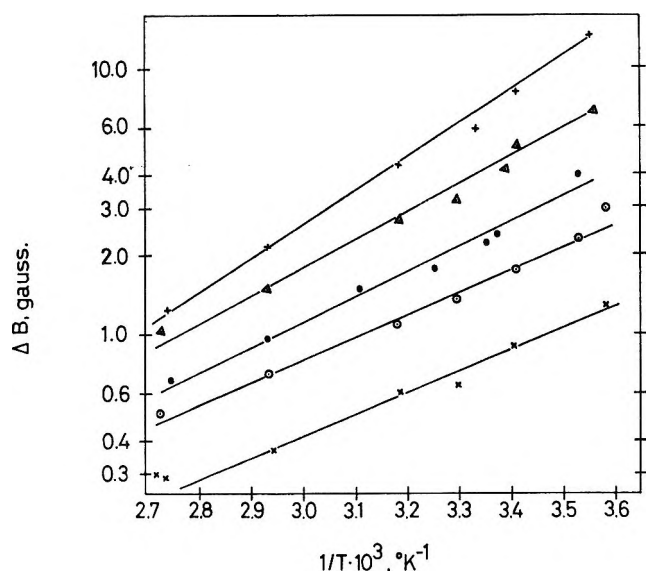


Figure 5. The temperature dependence of the ^{79}Br line width. The logarithm of the line width is given as a function of the inverse absolute temperature: \times , 0.500 M BuNH_3Br ; \circ , 0.500 M $\text{Bu}_2\text{NH}_2\text{Br}$; \triangle , 0.500 M Bu_3NHBr ; $+$, 0.500 M Bu_4NBr ; \bullet , 0.500 M Et_4NBr .

which depends on the curve shape and one term which equals the inverse magnetogyric ratio), we have

$$\Delta B = K \left(\frac{\partial^2 V}{\partial z^2} \right)^2 \tau_c \quad (2)$$

where K is a constant for a given nucleus. The asymmetry parameter has been neglected, which most likely is a good approximation in the interpretation of the large effects observed in the present work.

Equation 2 should give the line width in case of only one possible site of binding for the bromide ions. If the bromide ions are exchanging so rapidly between several sites with different bonding properties that the residence times in the different sites are much smaller than the relaxation times, the line width should be given by²⁶

$$\Delta B_{\text{obsd}} = \sum_i p_i \Delta B_i \quad (3)$$

Here ΔB_{obsd} is the observed line width, ΔB_i is the line width characterizing the bromide ion bonding in site i , and p_i is the mole fraction of bromide ions in site i . The sum in eq 3 should be taken over all possible sites in the solution.

To investigate whether eq 3 is applicable or not we have recorded the ^{31}Br nuclear magnetic resonance signals for some samples. The ^{31}Br data are given in Table II. As may be seen, the ratio between the line widths obtained for the two bromine isotopes is close to the theoretical value 1.545 (see ref 27) which will guarantee the validity of eq 3 (cf ref 17). The other arguments used to exclude the slow exchange case in ref 17 are also applicable in the present case.

Table II: Comparison of ^{31}Br Line Widths with ^{79}Br Line Widths. Temperature $30 \pm 2^\circ$

Sample	$\Delta B(^{79}\text{Br})$, G	$\Delta B(^{31}\text{Br})$, G	$\frac{\Delta B(^{79}\text{Br})}{\Delta B(^{31}\text{Br})}$
4.00 M Et_4NHBr	17.0	10.7	1.59
0.50 M $\text{C}_{11}\text{H}_{23}\text{NH}_3\text{Br}$	28.4	18.3	1.55
0.50 M $\text{C}_8\text{H}_{17}\text{NH}_3\text{Br}$	4.5	3.1	1.48

Discussion

In the present work we encounter many problems which were discussed in ref 17 and for the detailed arguments the reader is referred to this paper. The present discussion will be started with a consideration of those solutions which according to generally accepted views contain no micelles (*i.e.*, solutions of alkylammonium bromides where the carbon chains contain less than six carbon atoms) and we will continue with a discussion of the structural implications of the activation energies. We will conclude with a brief discussion of the structure of the micellar solutions from the point of view of the counterion relaxation rates.

On the Structure of the Solutions Which Contain No Micelles. Since the line widths of the ^{79}Br signals in aqueous solutions of mono-, di-, and trialkylammonium bromides show an analogous dependence on carbon chain length and electrolyte concentration to that observed for tetraalkylammonium bromides¹⁷ the causes are most likely very similar in all cases. That the marked changes in ^{79}Br line width primarily depend on anion-water coupling and not on anion-cation interaction is supported by the fact that the line width of the ^{79}Br signals is successively decreased when the number of carbon chains is decreased and thus the distance of closest approach between nitrogen and anion is diminished. If anion-cation coupling were dominant we should expect a change in line width in the opposite direction. Furthermore, Evans and Gardam²⁸ have recently shown that in ethanol and propanol the tendency for ion pairing of tetraalkylammonium bromides is greatest for tetramethylammonium bromide and then decreases steadily as the size of the cation increases.

Let us consider a simplified model in which the cations are surrounded by successive hydration layers and the bromide ions are distributed between the hydration layers and exchanging rapidly between them. The coupling between anion and water changes gradually as the distance between cation and anion changes and may be characterized by the ^{79}Br nmr line width, ΔB_i . From eq 3 we then obtain

(26) See *e.g.*, H. G. Hertz, "Progress in NMR Spectroscopy," Vol. III, Pergamon Press, Oxford, 1967, p 159.

(27) H. G. Hertz, *Z. Elektrochem.*, **65**, 20 (1961).

(28) D. F. Evans and P. Gardam, *J. Phys. Chem.*, **72**, 3281 (1968).

$$\Delta B_{\text{obsd}} = \sum_{i=1}^n p_i \Delta B_i + p_0 \Delta B_0 \quad (4)$$

where p_i is the mole fraction of bromides belonging to hydration layers denoted i and ΔB_i is the corresponding ^{79}Br line width. We assume that ΔB_i varies only slightly with the concentration of the salt, which is certainly correct at least at low concentrations. ΔB_0 and p_0 are the corresponding numbers for the part of the solution where the bromide ions are unaffected. It is easily shown that this equation will give a linear relation between ΔB_{obsd} and the salt concentration as long as the total number of water molecules belonging to hydration layers, in which ΔB_i is significantly different from ΔB_0 , is much smaller than the total number of water molecules in the solutions. Since according to our experimental data the linear relationship is valid up to comparatively high concentrations this means that ΔB_i is significantly different from ΔB_0 only in the very near vicinity of the cation. We thus see that most probably only the anions in the first hydration layer are involved in strengthened anion-water coupling.

We will next discuss possible reasons for ΔB_i being very great in the first hydration layer. As seen from eq 2, two factors have to be considered, *i.e.*, the correlation time and the field gradient. From the work by Hertz and coworkers (see *e.g.*, ref 26; *cf.* also ref 29) it may be inferred that the reorientation times for the water molecules close to the cations are not large enough to account for more than a minor part of the observed effects. Thus we may conclude that the field gradients experienced by the bromide ions near the cations are much larger than those in ordinary aqueous solutions. This indicates that the interaction between bromide ions and the water lattice is much stronger in the near vicinity of the cations than in regions far apart from the cations. Though this explanation seems to be the most probable one (since the field gradients are very great) we cannot at present exclude the possibility that the change in field gradient arises merely from a change in symmetry in the water lattice to which bromide ions are coupled.

We have not yet considered the possibility that the reorientation times for the water molecules (and ΔB_i) are essentially constant throughout the solution even at fairly low concentrations. This would give a correct description of the experimental findings if the correlation time increases linearly with the concentration. However, this explanation is ruled out by the fact that the ^{79}Br (and ^{81}Br) relaxation rates increase much faster with alkylammonium bromide concentration than do proton, deuteron, ^{17}O and ^{85}Rb relaxation rates in the same solutions.^{1,14,16} The case with uniform microdynamic properties throughout the solution can thus only explain our data if the field gradient term in eq 1 increases linearly with the concentration. Though we

have no possibility at present to exclude such an explanation, it seems to be very unlikely.

The model by Ackermann and Rüterjans²⁰ of a structure-broken zone outside the first hydration layer seems to lead to the same concentration dependence of the line widths as that found experimentally in the present work, since the difference between ΔB_i in the structure broken zone and ΔB_0 is probably negligible.

We may thus conclude that from anionic relaxation rates alone no certain model for the hydration structure can be obtained. It is, however, very likely that the observed line broadenings can be ascribed to a relaxation rate for the bromines in the near vicinity of the cations which is very different from the relaxation rates for bromines far away from the cations. The exchange of bromines between different hydration layers is fast compared to the relaxation rates.

Activation Energies. The energies of activation for the ^{79}Br relaxation rate in 0.500 *M* solutions of the four butylammonium bromides are summarized in Table I. The qualitative investigation of the temperature dependence of a 0.500 *M* solution of tetraethylammonium bromide presented in ref 17 has been repeated with improved temperature stabilization and gave a somewhat higher value of the activation energy than that previously reported. Previous determinations of activation energies for bromine (^{79}Br and ^{81}Br) relaxation rates are reported by Endom, *et al.*,³⁰ and by O'Reilly, *et al.*³¹ These data are included in Table I.

The activation energy, E_a , is formally defined by the equation

$$\Delta B = \Delta B^0 e^{E_a/RT}$$

where ΔB^0 is a constant, R the gas constant, and T the absolute temperature. E_a is a measure of the temperature dependence of the parameters in eq 2 and 3. In the present case only τ_c and the p_i 's have to be considered.

As may be seen from Table I the energies of activation of the alkylammonium bromides investigated are considerably higher than those observed for aqueous solutions of *e.g.*, KBr, LiBr, NaBr, and CsBr. We have not been able to separate the factors contributing to the activation energies, but it may be informative to discuss the two extreme cases. First we may attribute the whole observed effect to temperature variation of τ_c . According to Endom, *et al.*,³⁰ we may then say that the change in potential energy, for the species in the solution responsible for relaxation, occurring during the dynamic processes is greater in the present case than in an aqueous solution of, *e.g.*, NaBr. This strongly suggests that

(29) R. Pottel and O. Lossen, *Ber. Bunsenges. Phys. Chem.*, **71**, 135 (1967).

(30) L. Endom, H. G. Hertz, B. Thül, and M. D. Zeidler, *ibid.*, **71**, 1008 (1967).

(31) D. E. O'Reilly, G. E. Schacher, and K. Schug, *J. Chem. Phys.*, **39**, 1756 (1963).

the bromide ions are more firmly bound in the present case than in ordinary aqueous solutions. Secondly, the observed great difference in activation energy between aqueous solutions of, *e.g.*, Bu₄NBr and aqueous solutions of an ordinary salt may have its origin in a temperature dependence in p_i ; this amounts to saying that it is a measure of ΔH for an equilibrium. In this case there must be different binding sites for the bromide ions, *i.e.*, at least part of the bromines should be coupled to surrounding species differently than in ordinary aqueous solutions. In both cases the ideas presented above for the interpretation of the line-width data are supported.

As may be seen from Table I the energy of activation increases with increasing number of alkyl groups on the nitrogen as well as with increasing chain length, *i.e.*, the same trend is observed in the activation energies as in the relaxation rates themselves.

On the Structure of the Micellar Solutions. The first study of counterion binding in micellar solutions by nuclear magnetic quadrupole relaxation was that of Eriksson, Johansson, and Andersson.³² They found a rapid increase in the relaxation rate of ⁸¹Br in the region of the critical micelle concentration (cmc) for aqueous solutions of octylammonium bromide. This was attributed to an adsorption of part of the counterions in a Stern layer next to the ionic groups of the surfactant molecules.

In the present work we have studied solutions of alkylamine hydrobromides, CH₃(CH₂)_nNHBr, with $n = 0-10$. As may be seen in Figure 3 the appearance of micelles is very clearly reflected in the line-width data. For solutions of the micelle-forming substances below the cmc it is obvious that even at low concentrations the binding of the bromide ions is distinctly different from the binding of bromide ions in aqueous solutions of, *e.g.*, sodium bromide or ammonium bromide. Thus, for instance, the relaxation rate of ⁷⁹Br in a 0.100 *M* solution of octylammonium bromide is about 50% greater than in a 0.100 *M* solution of an "ordinary" 1-1 electrolyte. This may be understood from the above discussion: the alkyl groups in the cations tend to stabilize the water lattice and close to the cations there is a strengthened coupling between the anions and the water molecules. This increased anion-water binding in the pre-micellar solutions must be taken into account when the dependence of cmc on the nature of the anion and the effect of added electrolytes on the cmc are interpreted (see *e.g.*, ref 33). Apart from this changed counterion-water coupling common to all types of alkylammonium bromides, the counterion binding is not altered before the cmc. Thus there is no evidence of any formation of pre-micellar aggregates in the solution, or at least there is no significant amount of bromide ions participating

in such an aggregation. This conclusion is in accordance with the results obtained by Desnoyers and Arel²¹ from density data (*cf.* also ref 22). The concentration dependence of the line widths is presently being studied in more detail in our laboratories. From these studies we hope to reach more definite conclusions about pre-micellar phenomena (in this work we will also investigate the effect of solubilization and of changing the end group of the cations on the counterion binding).

The fact that the line widths are independent of the applied magnetic field strength indicates that eq 2 is valid. Moreover the ⁸¹Br data show that there is a "fast exchange" of bromide ions between the surface of the micelles and the bulk of the solution and that eq 3 is valid. If we make a simplification and assume that there are only two binding states for the bromines, *i.e.*, one in the close vicinity of the micellar surface and one in the bulk of the solution, we may from a knowledge of the fraction of bromide ions on the micellar surface estimate the line width characteristic for the adsorbed counterions. We have performed a calculation of this type for 0.100 *M* decylammonium bromide and 0.500 *M* undecylammonium bromide. The amount of adsorbed counterions was estimated from the work by Shirai and Tamamushi.^{34,35} The line width for the bromide ions not bound to the micelles was taken as 0.7 G (this value is the line width observed at concentrations just below the cmc). Under these assumptions we obtain a line width of about 16 G for the bound counterions in the 0.100 *M* decylammonium bromide solution and about 35 G for the 0.500 *M* undecylammonium bromide solution. These figures indicate that the strength of the counterion binding lies somewhere between that of "free" ions (ΔB about 0.35 G in aqueous solutions) and that of covalently bonded bromine (ΔB in the range 300-400 G as calculated from the data of O'Reilly, Schacher, and Schug³¹). The binding at the micellar surface is probably best characterized as a type of ion pairing. Since the study of the micellar solutions is being continued, we will postpone a more elaborate treatment to a later date.

Acknowledgments. Professor H. G. Hertz is heartily thanked for valuable discussions, and Mr. Hans Lilja for helpful technical assistance, especially for constructing the frequency stabilizing circuit. We are indebted to Dr. Robert Carter for revising the manuscript.

(32) J. C. Eriksson, Å. Johansson, and L.-O. Andersson, *Acta Chem. Scand.*, **20**, 2301 (1966).

(33) M. N. Jones and R. A. Reed, Vth International Congress on Surface Active Substances, Barcelona, 1968. Preprint No. B IV/46.

(34) M. Shirai and B. Tamamushi, *Bull. Chem. Soc. Jap.*, **29**, 733 (1956).

(35) M. Shirai and B. Tamamushi, *ibid.*, **30**, 411 (1957).

Variation of Osmotic Coefficients of Aqueous Solutions of Tetraalkylammonium Halides with Temperature. Thermal and Solute Effects on Solvent Hydrogen Bonding¹

by S. Lindenbaum, L. Leifer, G. E. Boyd, and J. W. Chase

Chemistry Division, Oak Ridge National Laboratory, Oak Ridge, Tennessee 37830 (Received September 9, 1969)

Osmotic coefficients have been measured at 65° for aqueous solutions of tetra-*n*-butylammonium fluoride, tetramethyl-, tetra-*n*-propyl-, and tetra-*n*-butylammonium chloride, and tetramethyl- and tetra-*n*-propylammonium iodide. These data were combined with the available thermodynamic data at 25° to estimate relative partial molal entropies of the solvent. The thermodynamic properties of symmetric tetra-*n*-alkylammonium halide solutions have been interpreted in terms of the effect of increasing anion size and increasing temperature on the local structure of water. This interpretation is justified in terms of the recently published X-ray diffraction results on water and on aqueous ammonium halide and tetra-*n*-butylammonium fluoride solutions. The concept of "water-structure-enforced ion pairing" has been used to explain the reversal in the sequence of the magnitude of the osmotic coefficients on substituting iodide for chloride ions. It is suggested that this concept is not valid in cases involving either cations or anions which *reduce* the amount of local order in the solvent. However, osmotic coefficient reversals may be accounted for on the basis of the competition between *increased* hydrogen bonding of water as the size of the R₄N⁺ cation increases and *decreased* hydrogen bonding as the size of the halide ion increases.

Introduction

Thermodynamic property measurements at 25° on aqueous solutions of the symmetric tetraalkylammonium halides have been presented in previous communications from this laboratory^{2,3} and by others.⁴⁻⁶ The results have been interpreted in terms of the hypothesis of Frank and coworkers⁷ that large organic cations (or anions) promote local order in the aqueous solvent. The sequence of the magnitudes of the osmotic coefficients has been the subject of considerable interest. In dilute solutions of symmetric tetraalkylammonium fluorides and chlorides at 25°, the osmotic coefficients increase with increasing cation size. This order is reversed for the bromides and iodides at 0 and 25°. It has been suggested^{2,3} that the reversal is due to the formation of "water-structure-enforced ion pairs" between large tetraalkylammonium ions and large (*i.e.*, bromide or iodide) anions. These interpretations were *ad hoc*, but nevertheless they have provided a useful basis for making predictions which could be tested by experiment.

Recent X-ray diffraction studies on water and aqueous solutions⁹⁻¹¹ have been interpreted in terms of the slightly expanded ice-I model¹² for local structure in liquid water. Parameters calculated from the radial distribution function for tetra-*n*-butylammonium fluoride solutions¹⁰ for the model show that the short-range order in the solution differs from that in pure water: I, the number of interstitial (non-network) water molecules decreases; II, the nearest neighbor distances

in the network are shortened; and III, the root-mean-square displacements associated with near-neighbor network distances are significantly smaller than in pure water (*i.e.*, the interaction becomes sharper).

These effects would tend in the direction of increasing the heat capacity and decreasing the entropy of the solvent. The expanded ice-I model therefore provides an interpretation of the radial distribution function which is consistent with suggestions made on the basis of less direct thermodynamic evidence. It has been pointed out that the model is an oversimplification of the real structure of liquid water or solutions,¹⁰ and further work may indeed provide models which will extend and improve upon this one in its ability to account for physical properties of solutions.

(1) Research sponsored by the U. S. Atomic Energy Commission under contract with the Union Carbide Corporation.

(2) S. Lindenbaum and G. E. Boyd, *J. Phys. Chem.*, **68**, 911 (1964).

(3) S. Lindenbaum, *ibid.*, **70**, 814 (1966).

(4) W.-Y. Wen, S. Saito, and C. Lee, *ibid.*, **70**, 1244 (1966).

(5) R. H. Wood, H. L. Anderson, J. D. Becker, J. R. France, W. E. DeVry, and L. J. Soltzberg, *ibid.*, **71**, 2149 (1967).

(6) J. Lange, *Z. Phys. Chem.*, **A168**, 147 (1934).

(7) See, for example, H. S. Frank, *Z. Phys. Chem.*, (Leipzig), **228**, 367 (1965).

(8) R. M. Diamond, *J. Phys. Chem.*, **67**, 2513 (1963).

(9) A. H. Narten, M. D. Danford, and H. A. Levy, *Discussions Faraday Soc.*, **43**, 97 (1967).

(10) A. H. Narten and S. Lindenbaum, *J. Chem. Phys.*, **51**, 1108 (1969).

(11) A. H. Narten, *J. Phys. Chem.*, **74**, 765 (1969).

(12) O. Y. Samoilov, *Zh. Fiz. Chim.*, **20**, 1411 (1946).

It was the purpose of this work to determine what changes in the osmotic coefficients of the symmetric tetra-*n*-alkylammonium halides would be observed by increasing the temperature from 25 to 65° and if these changes may be understood in terms of relations between the local order in the solvent and the thermodynamic properties of the aqueous solutions.

Experimental Section

Solutions of tetra-*n*-butylammonium fluoride, tetramethyl-, tetra-*n*-propyl-, and tetra-*n*-butylammonium chloride, and tetramethyl- and tetra-*n*-propylammonium iodide were prepared and analyzed as previously described.² Molal osmotic coefficients were determined with a Mechrolab Model-301 vapor-pressure osmometer. The experimental procedure and equations for the calculation of the results have been published.¹³ Solutions of sodium chloride were used for the calibration of the osmometer and values of the osmotic coefficients of sodium chloride at 25 and 65° were interpolated from the tables of Robinson and Stokes.¹⁴ The precision and accuracy of the osmotic coefficient measurements is approximately 1%.

Results and Discussion

The osmotic coefficients are given in Figures 1, 2, and 3 together with previously reported values^{2,4} at 25° obtained with the gravimetric isopiestic comparison method. Agreement between the two methods is demonstrated where the data overlap. The data for the chloride and fluoride salts at 25° are from earlier publications.^{2,4} Osmotic coefficients interpolated from the smooth curves of Figures 1, 2, and 3 are given in Table I. The relative order of the values for the chloride and fluoride salts at 25° (*i.e.*, increasing osmotic coefficients with increasing cation size) is reversed at 65°. This inversion can be predicted from heat-of-dilution data at 25° as follows. The temperature coefficient of the osmotic coefficient may be obtained from heat-of-dilution data³ according to the following equation

$$d\phi/dT = 1000\bar{L}_1/M_wRT^2\nu m \quad (1)$$

where ϕ is the molal osmotic coefficient, M_w the molecular weight of water, T the temperature in °K, ν the number of ions per molecule of salt, m the molality, and \bar{L}_1 the relative apparent partial molal heat content of the solvent. \bar{L}_1 is derived from the apparent molal heat content, ϕ_L , using eq 2

$$\bar{L}_1 = -(1/2 m^{1/2}/55.51)(d\phi_L/dm^{1/2}) \quad (2)$$

Thus, by assuming that \bar{L}_1 does not vary with temperature, ϕ values at 65° may be calculated from those measured at 25°. This assumption is not strictly valid (see Table I), but it does permit a prediction of whether the osmotic coefficient increases or decreases as the temperature is altered. Because \bar{L}_1 is negative for

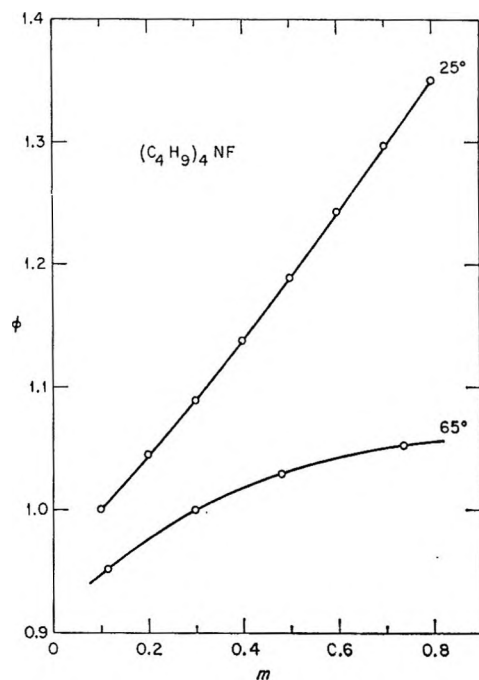


Figure 1. Osmotic coefficients of tetra-*n*-butylammonium fluoride at 25 and 65°. Data at 25° taken from ref 4.

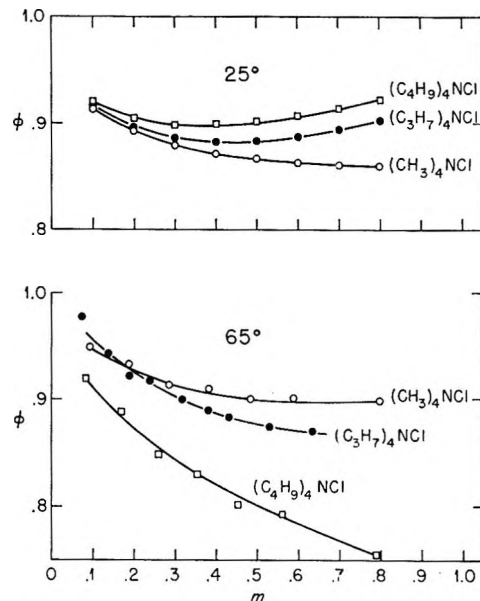


Figure 2. Osmotic coefficients of tetramethyl-, tetra-*n*-propyl-, and tetra-*n*-butylammonium chlorides at 25 and 65°. Data at 25° taken from ref 2.

(C_4H_9)₄NCl and positive for (CH_3)₄NCl, eq 1 predicts that ϕ for (C_4H_9)₄NCl will decrease while ϕ for (CH_3)₄NCl will increase with increasing temperature. Therefore, at least qualitatively, the reversal in the order (Figure 2) is accounted for; in fact, the differences in the

(13) G. E. Boyd, A. Schwarz, and S. Lindenbaum, *J. Phys. Chem.*, **70**, 821 (1966).

(14) R. A. Robinson and R. H. Stokes, "Electrolyte Solutions," 2nd ed, Revised, Butterworth and Co., Ltd., London, 1959.

Table I: Thermodynamic Properties of Aqueous Solutions of Tetra-*n*-alkylammonium Halides at 25 and 65°

	<i>m</i>	25°				65°			
		ϕ	\bar{F}_1	\bar{L}_1	$T(\bar{S}_1 - S_1^\circ)$	ϕ	\bar{F}_1	\bar{L}_1^a	$T(\bar{S}_1 - S_1^\circ)^a$
Bu ₄ NF ^b	0.2	1.045 ^c	-0.2	-2.1	-2	0.973	0.2	-3.2	-3.4
	0.4	1.138	-1.2	-9.1	-8	1.018	-0.2	-8.3	-8.1
	0.6	1.243	-3.2	-22	-19	1.042	-0.7	-23	-22
	0.8	1.350	-6.2	-41	-35	1.056	-1.1	-44	-43
Me ₄ NCl	0.2	0.892	0.5	0.3	-0.2	0.926	0.4	2.1	1.8
	0.4	0.872	1.0	1.2	0.2	0.904	0.9	3.5	2.6
	0.6	0.863	1.7	2.5	0.8	0.898	1.4	5.1	3.7
	0.8	0.860	2.1	4.0	1.9	0.898	1.7	7.0	5.3
Pr ₄ NCl	0.2	0.896	0.5	-0.1	-0.6	0.925	0.4	2.2	1.8
	0.4	0.882	1.0	-2.4	-3.4	0.887	1.0	3.1	2.1
	0.6	0.887	1.3	-4.2	-5.5	0.870	1.8	0.5	-1.3
	0.8	0.902	1.4	-8.8	-10.2	0.867	2.3	-1.4	-3.7
Bu ₄ NCl	0.2	0.904	0.4	-1.4	-2	0.873	0.6	-0.9	-1.5
	0.4	0.899	0.8	-6.1	-7	0.821	1.7	-5.2	-6.9
	0.6	0.907	1.1	-18	-19	0.784	3.0	-9	-12
	0.8	0.922	1.1	-32	-33	0.773	4.1	-11	-15
Me ₄ NI	0.2	0.846	0.7	0.6	-0.1	0.844	0.8	-0.7	-1.5
Pr ₄ NI	0.2	0.759	1.0	0.3	-0.7	0.729	1.3	-2.5	-3.8
	0.3	0.696	1.9	0.2	-1.7	0.679	2.3	-2.1	-4.4
	0.4	0.644	3.0	0.1	-2.9	0.634	3.5	-1.6	-5.1

^a Estimated as described in text. ^b \bar{L}_1 for Bu₄NF calcd from ϕ_L data for Bu₄NF at 25°; Lindenbaum, *J. Phys. Chem.*, **73**, 4334 (1969). ^c The ϕ values are reported to 3 significant figures beyond the decimal only for convenience in checking the calculations.

ϕ values between (C₄H₉)₄NCl and (CH₃)₄NCl at 65° are overestimated by this procedure. Alternatively, from the measured values of ϕ at 25 and 65°, an average temperature coefficient $d\phi/dT$ at 45° and hence a value of \bar{L}_1 may be calculated at this temperature. Consequently, the value of \bar{L}_1 at 65° may be derived by a linear extrapolation of the values at 25 and 45°, respectively.¹⁵ Relative apparent molal entropies of the solvent, ($\bar{S}_1 - S_1^\circ$), at 25 and 65° may be estimated

$$\begin{aligned} T(\bar{S}_1 - S_1^\circ) &= \bar{L}_1 - \bar{F}_1 \\ \bar{F}_1 &= RT \ln (a_1/N_1) \end{aligned} \quad (3)$$

where $-\ln a_1 = \nu m\phi/55.51$ and $N_1 = 55.51/(55.51 + 2m)$. Values of \bar{F}_1 , \bar{L}_1 , and $T(\bar{S}_1 - S_1^\circ)$ are listed in Table I.

The order of the osmotic coefficients of the chloride salts at 25° ($\phi_{\text{Bu}_4\text{NCl}} > \phi_{\text{Pr}_4\text{NCl}} > \phi_{\text{Me}_4\text{NCl}}$) is seen (Figure 3) to be reversed for the iodides at 25 and 65°. The reversed order for the iodides also has been observed at 0°.⁶ This reversal may thus be achieved either by substituting a larger anion for Cl⁻ (e.g., I⁻) or by increasing the temperature. An increase in temperature has been shown to reduce the local order in pure water⁹ by increasing two of the three near-neighbor distances in the expanded ice-I model, by increasing the mean-square displacements associated with all near-neighbor network distances, and by slightly increasing the fraction of water molecules in interstitial positions. It may be assumed that a decrease in interstitial molecules, in the mean-square displacements, and in the near-neighbor

distances would lead to reduced water activity and increased values of ϕ . If, therefore, the osmotic coefficient sequence of the chlorides at 25° is largely determined by the ability of the larger tetraalkylammonium ions to promote local order, then a sufficient increase in temperature would be expected to reverse the sequence.

X-Ray diffraction measurements with aqueous ammonium halide solutions¹¹ have been interpreted in terms of decreasing hydrogen bonding of the solvent with increasing size of the anion. The ability of an electrolyte in solution to increase hydrogen bonding (increase the number of network water molecules) may be thought of as resulting from the separate effects of the cations and anions.⁶ The substitution of iodide for chloride ions may therefore cause sufficient disruption of the short-range order in the water to offset the order-promoting ability of the large tetraalkylammonium ions. The net thermodynamic consequence of substituting iodide ions for chloride would be in the same direction as an increase in temperature. These effects should be reflected in the quantity ($\bar{S}_1 - S_1^\circ$), since the relative apparent molal entropy is a statistical

(15) This approximation assumes that \bar{C}_{p1} is independent of the temperature in the range 25 to 65°. Recent measurements (H. Rüttersjans, F. Schreiner, U. Sage, and Th. Ackermann, *J. Phys. Chem.*, **73**, 986 (1969)) with 0.3 to 0.7 *m* (*n*-C₄H₉)₄NBr solutions show that the value of \bar{C}_{p1} however, is quite small and changes sign between 50 and 70°.

(16) In fact, in studies of viscosity (a) R. W. Gurney, "Ionic Processes in Solution," Dover Publications, New York, N. Y., 1962, p 174; and nuclear magnetic resonance (b) G. Engel and H. G. Hertz, *Ber. Bunsenges. Phys. Chem.*, **72**, 303 (1968), the effects have been divided into cationic and anionic contributions.

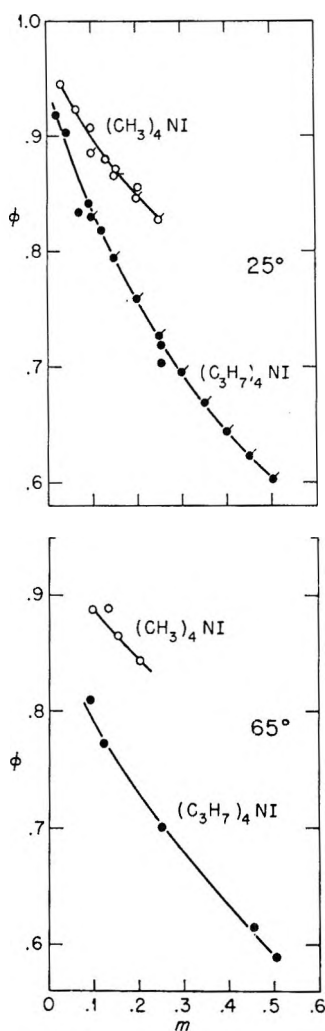


Figure 3. Osmotic coefficients of tetramethyl- and tetra-*n*-propyl ammonium iodides at 25 and 65°. ●, ○, isopiestic data taken from ref 2, ●, ○, vp osmometry data.

measure of order (or structure) in the solvent.¹⁷ This quantity increases with temperature for the chloride salts and decreases with temperature for the iodides.

An increase in entropy corresponds to the increased disorder in the solvent as the temperature is increased. This suggests that as the temperature is increased, the chloride salt solutions become more disordered; and, *relative to infinite dilution*, the iodide solutions become more ordered at the higher temperatures. In the case of Bu_4NF solutions, which have the most negative values of $(\bar{S}_1 - S_1^\circ)$ and therefore the greatest amount of short-range order, only a small relative change occurs with increasing temperature, and this change is in the direction of decreasing $(\bar{S}_1 - S_1^\circ)$. Apparently Bu_4NF is so effective at enhancing the structure of water (by all of the aforementioned mechanisms) that this structure is not altered appreciably by elevating the temperature to 65°. Studies with fluoride salts at yet higher temperatures would be of interest.

It has been shown that the reversal in the sequence of the magnitudes of the osmotic coefficients on changing the size of the anion may be accounted for qualitatively on the basis of the relative effect of the cation and anion on the degree of hydrogen bonding of the solvent. It therefore seems unnecessary to invoke a special, non-coulombic ion pairing mechanism to explain this reversal. The concept of "water-structure-enforced ion pairing" may have merit in cases where both the cation and anion have "water-structure" promoting properties; however, it probably does not apply when either cation or anion decreases the local order in the solvent. It will be of interest to study systems involving structure promoting anions as well as cations to provide further tests of these ideas. It should be noted that the ϕ vs. \sqrt{m} curves for the iodides at the freezing point,⁶ 25, and 65° approach zero concentration from below the limiting law curve. This does not necessarily imply ion pairing but may be due to the smaller hydration of the iodide ion.¹⁸

(17) H. S. Frank and A. L. Robinson, *J. Chem. Phys.*, **8**, 933 (1940).

(18) O. D. Bonner, *J. Phys. Chem.*, **72**, 2512 (1968).

Diffraction Pattern and Structure of Aqueous Ammonium Halide Solutions¹

by A. H. Narten

Chemistry Division, Oak Ridge National Laboratory, Oak Ridge, Tennessee 37830 (Received August 7, 1969)

The scattering of X-rays from aqueous ammonium chloride, bromide, and iodide solutions ($\text{NH}_4\text{X} \cdot \sim 8\text{H}_2\text{O}$) has been measured and analyzed at 25°. Radial distribution functions for the three solutions are compared with previously obtained results for ammonium fluoride solutions and for pure water at the same temperature. Intensity and radial distribution functions calculated for the proposed ice-I model for water (Samoilov; Danford and Levy) are in excellent agreement with those derived from the diffraction data. This model describes the influence of Cl^- , Br^- , and I^- ions on water structure as deformation and expansion of the hydrogen-bonded network of water molecules, accompanied by an increase in the fraction of molecules in cavity positions.

Introduction

For heteratomic liquids such as water the analysis of X-ray scattering data yields intensity and radial distribution functions which contain information about average atomic and molecular configurations. This information cannot be deduced uniquely from the diffraction data. However, assumptions about the average arrangement of molecules with respect to each other may be made, and such a model of liquid structure can be tested against the observations.

A considerable amount of evidence^{2,3} supports the idea that the hydrogen bonds in liquid water form an extensive three-dimensional network, the detailed features of which are short-lived. Such a structure may arise in a variety of ways from units of nearly tetrahedral symmetry. Most of the proposed models for water are either incompatible with observed X-ray scattering or insufficiently defined for adequate testing.⁴ Only the ice-I model proposed by Samoilov⁵ and specified in detail by Danford and Levy⁶ has been shown^{6,7} to give agreement with both large and small angle X-ray scattering data. This model assumes that the hydrogen-bonded network of water molecules is (on the average, and over short distances from any origin molecule) closely related to a slightly expanded ice-I lattice.⁸ The average structure of this network is very open, with spaces between the groups of molecules in tetrahedral coordination sufficiently large to accommodate additional water molecules.

The ice-I model also describes quantitatively the radial distribution in aqueous solutions of nearly tetrahedral molecules^{9,10} and ions.^{11,12} In particular, the idea that ammonium ions can replace water molecules without much change in the average molecular arrangement¹³ is strongly supported by X-ray diffraction studies.¹¹ Thus, aqueous ammonium halide solutions may be considered, to a good approximation, as solutions of halide ions in water, and the effect of the ammonium salts on water structure may be regarded as arising primarily from the anions alone. Also, the distribution of electron density in H_2O and NH_4^+ is not

sufficiently different for the X-ray method to distinguish between the two species, and this leads to a significant simplification in the interpretation of the diffraction data.

Experimental Section

The scattering of monochromatic $\text{Mo K}\alpha$ X-rays from aqueous ammonium chloride, bromide, and iodide solutions ($\text{NH}_4\text{X} \cdot \sim 8\text{H}_2\text{O}$) has been measured at 25°. Preparation of the solutions, the diffractometer, the procedure for data collection, the various corrections applied to the raw data, and the final reduction of the data have been discussed in detail elsewhere.^{14,15} Both the raw data and the reduced intensity and radial distribution functions derived from them are available in tabulated form.¹⁵ Only a short definition of terms will be given here.

Let $4\pi r^2 \rho_{\alpha\beta}(\tau)$ be a distribution function giving the probability that distinct pairs of atoms of type α , β

- (1) Research sponsored by the U. S. Atomic Energy Commission under contract with the Union Carbide Corporation.
- (2) J. L. Kavanau, "Water and Solute-Water Interactions," Holden-Day, Inc., San Francisco, Calif., 1964.
- (3) D. Eisenberg and W. Kauzmann, "The Structure and Properties of Water," Oxford University Press, New York, N. Y., 1969.
- (4) A. H. Narten and H. A. Levy, *Science*, **165**, 447 (1969).
- (5) O. Y. Samoilov, *Zh. Fiz. Chim.*, **20**, 1411 (1946).
- (6) M. D. Danford and H. A. Levy, *J. Amer. Chem. Soc.*, **84**, 3965 (1962).
- (7) A. H. Narten, M. D. Danford, and H. A. Levy, *Discussions Faraday Soc.*, **43**, 97 (1967).
- (8) S. W. Peterson and H. A. Levy, *Acta Cryst.*, **10**, 70 (1957).
- (9) A. H. Narten, *J. Chem. Phys.*, **49**, 1692 (1968).
- (10) C. Folzer and A. H. Narten, presented at the Eighth International Congress of Crystallography, Stony Brook, N. Y., Aug 7-24, 1969, and published in the Proceedings.
- (11) M. D. Danford, "Diffraction Pattern and Structure of Aqueous Ammonium Fluoride Solutions," ORNL-4244 (1968).
- (12) A. H. Narten and S. Lindenbaum, *J. Chem. Phys.*, **51**, 1108 (1969).
- (13) K. Fajans and O. Johnson, *J. Amer. Chem. Soc.*, **64**, 668 (1942).
- (14) H. A. Levy, M. D. Danford, and A. H. Narten, "Data Collection and Evaluation with an X-Ray Diffractometer Designed for the Study of Liquid Structure," ORNL-3960 (1966).
- (15) A. H. Narten, "X-Ray Diffraction Data on Aqueous Ammonium Halide Solutions at 25°," ORNL-4367 (1969).

are to be found separated by a distance r . The functions $\rho_{\alpha\beta}(r)$ represent the average distribution of pairs both over time and over the volume of the sample. In these terms, the scattered intensity becomes⁴

$$i(s) \equiv I(s)/n - \sum_{i=1}^m f_i^2(s) = \sum_{\alpha=1}^m \sum_{\beta=1}^m f_{\alpha}(s)f_{\beta}(s) \int_0^{\infty} 4\pi r^2 [\rho_{\alpha\beta}(r) - \rho_0] \times \sin(sr)/sr dr \quad (1)$$

in which a stoichiometric unit containing m atoms is visualized as representative of the whole sample, which contains n such units. The angular variable s is defined as $(4\pi/\lambda) \sin \theta$, with λ the X-ray wavelength and 2θ the scattering angle. The term $\sum_{i=1}^m f_i^2(s)$ is the independent atomic scattering, and the reduced intensity $i(s)$ is the structurally sensitive part of $I(s)/n$, the measured intensity normalized to one stoichiometric unit. The bulk number density of stoichiometric units $(\text{H}_2\text{O})_x(\text{NH}_4^+)_y\text{X}_y^-$ is denoted by ρ_0 , x and y being mole fractions ($x + 2y = 1$).

The atom pair distribution functions $\rho_{\alpha\beta}(r)$ are not obtainable individually from a single diffraction experiment. It is nevertheless useful to construct a modified radial distribution function (RDF) by Fourier transformation, namely

$$D(r) \equiv \sum_{\alpha=1}^m \sum_{\beta=1}^m D_{\alpha\beta}(r) = 4\pi r^2 \rho_0 + (2r/\pi) \int_0^{\infty} si(s)M(s)\sin(sr) ds \quad (2)$$

with $M(s) = \left[\sum_{\alpha=1}^m f_{\alpha}(s) \right]^{-2}$ for $s \leq s_{\text{max}}$, the maximum values of s accessible in scattering experiments, and $M(s) = 0$ otherwise. Introduction of this modification function into (2) makes the product $f_{\alpha}(s)f_{\beta}(s)M(s)$ nearly independent of s and, thus, removes from the resulting RDF the average breadth of the distribution of electron density in the atoms. The relationship between component X-ray pair distribution functions $D_{\alpha\beta}(r)$ and $4\pi r^2 \rho_{\alpha\beta}(r)$ is one of convolution.¹⁶

A convenient way to present radial distribution functions for liquids of different density ρ_0 is to introduce a normalized RDF

$$G(r) \equiv D(r)/4\pi r^2 \rho_0 \quad (3)$$

which approaches unity for large values of r . The function $G(r)$ should not be confused with the atom pair correlation function $g(r)$ to which it would be equal only if $f_{\alpha}(s)f_{\beta}(s)M(s) = 1$, for all α, β .

Results

Observed Diffraction Pattern. Radial distribution functions for the three ammonium halide solutions studied here are shown in Figure 1, together with the

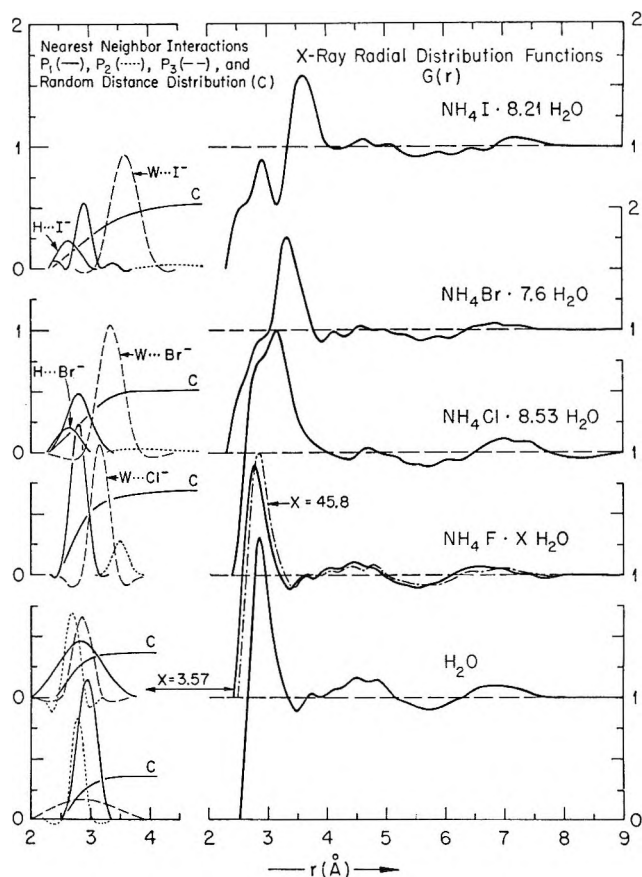


Figure 1. X-Ray distribution functions for aqueous ammonium halide solutions. Resolution of near-neighbor interactions between halide and water (W) based on ice I model of Figure 3.

curves for pure water¹⁷ and for two ammonium fluoride solutions¹¹ studied previously. The curves for the ammonium fluoride solutions are very similar to the RDF of pure water, and the significance of small differences has been discussed elsewhere.¹¹ Throughout the following discussion, the term water (W) will be used to describe interactions involving the oxygen atoms of water molecules and/or the nitrogen atoms of ammonium ions (indistinguishable in this treatment).

The maximum at 2.85 Å in the RDF of pure water (Figure 1) corresponds to ~ 4.4 interactions between oxygen atoms.⁷ A corresponding water-water interaction is visible as a shoulder in the chloride and bromide solutions, and as a partially resolved maximum at 2.91 Å in the ammonium iodide solution. The halide-water interaction occurs at 3.2 Å for the chloride, 3.3 Å for the bromide, and 3.6 Å for the iodide solution. A distinct shoulder on the short-distance side of the water-water peak in the NH_4I solution (less pronounced in the NH_4Br solution, and not resolved in NH_4Cl) must be ascribed to interactions between hydrogen atoms and

(16) J. Waser and V. Schomaker, *Rev. Mod. Phys.*, **25**, 671 (1953).

(17) A. H. Narten, M. D. Danford, and H. A. Levy, "X-Ray Diffraction Data on Liquid Water in the Temperature Range 4-200°C," ORNL-3997 (1966).

halide ions. Since these interactions contribute to the RDF in proportion to the product $f_H f_X$ of the X-ray form factors of hydrogen and halide, that is proportional to 54:36:18:10 from iodide to fluoride, one would not expect their resolution for the chloride and fluoride solutions. In the iodide solution, this shoulder is most pronounced and occurs around 2.6 Å; since this distance is very nearly equal to the difference between $W \cdots I^-$ (3.6 Å) and the intramolecular $W-H$ (~1 Å) distance, the conclusion is that some water molecules (ammonium ions) have average orientations such that one $W-H \cdots I^-$ angle is close to 180° . Although there is no reasonable doubt about the preceding interpretation of the RDF features below ~4 Å, quantitative resolution of these peaks and shoulders is quite uncertain without additional assumptions.

Proposed Model. In water and in the ammonium fluoride solutions, each water molecule (or ion) has an average of ~4.4 first neighbors, indicating predominantly tetrahedral coordination. Further evidence for tetrahedral coordination comes from the sequence of positions of maxima and minima in the RDF (Figure 1): there is a high concentration of neighbors centered around an average distance $r_1 = r_0(8/3)^{1/2}$, with r_0 the first neighbor water-water peak, for all curves in Figure 1. Furthermore, the broad minima and maxima around 5.5 Å and 7 Å roughly coincide with distances of low and high atom pair concentrations expected for a slightly expanded ice-I lattice. It has already been mentioned that the proposed ice-I model^{5,6} describes the radial distribution in water⁷ and the ammonium fluoride solutions¹¹ quantitatively. Intensity and radial distribution functions calculated for this model are also in excellent agreement with the X-ray data for

the ammonium chloride, bromide, and iodide solutions (Figures 1 and 2).

This model describes the average short-range order in liquid water in terms of a slightly expanded ice-I-like network of hydrogen-bonded water molecules, each network molecule being tetrahedrally surrounded by four others. Three of these network neighbors occur at an average distance P_1 , and the fourth at an average distance P_2 (in the solid $P_1 \simeq P_2$). The structure of this network is very open, with spaces between the groups of molecules in tetrahedral coordination sufficiently large to accommodate additional water molecules at a distance P_3 from the nearest network molecule (these cavities are not occupied in solid ice-I). In pure water,⁷ about half the cavities are occupied by "interstitial" molecules which interact with the network by less directional but by no means negligible forces. The complexity of the first coordination shell is explained by the model in terms of the distinctly different average environments of network and cavity molecules. However, both of these "species" exist in environments which are distorted from the average, and these distortions are implied by sizeable root-mean-square (rms) variations in interatomic distance.

The parameters of the ice-I model for the ammonium fluoride solutions¹¹ are very similar to those of pure water at the same temperature, and Danford¹¹ concluded that the nearly tetrahedral NH_4^+ and F^- ions

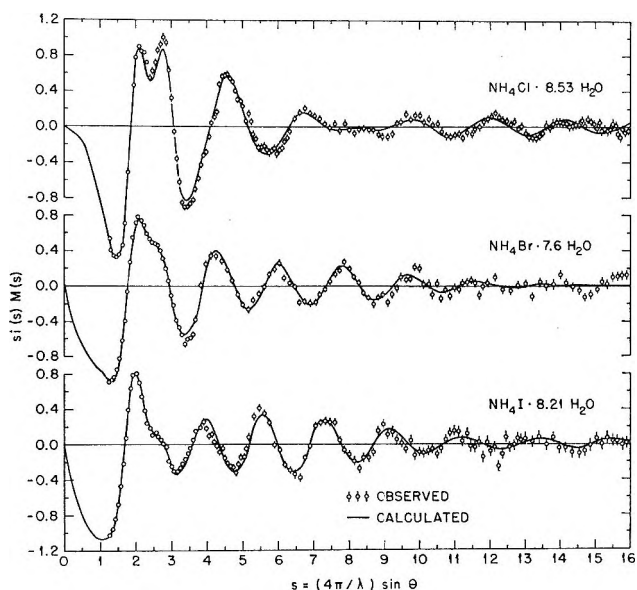


Figure 2. Reduced intensity functions for aqueous ammonium halide solutions. Calculated curves for ice-I model of Figure 3.

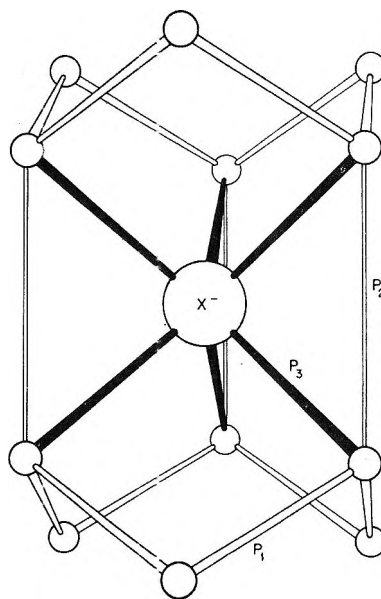


Figure 3. Average arrangement of water molecules and ammonium ions around a halide ion (ice-I model). Each halide ion has six neighbors at a distance P_3 , point symmetry D_{3h} . Each water molecule (ammonium ion) has three water (ammonium) neighbors at a distance P_1 , of which only two are shown, and one neighbor at a distance P_2 (Table I). The six water molecules (ammonium ions) are oriented such that one hydrogen atom points toward the halide ion. Large instantaneous distortions from this average configuration occur in the solutions.

Table I: Some Relevant Parameters for the Ice-I Model of Water and Aqueous Ammonium Halide Solutions

	H_2O	$\text{NH}_4\text{F} \cdot 3.57\text{H}_2\text{O}$	$\text{NH}_4\text{Cl} \cdot 8.53\text{H}_2\text{O}$	$\text{NH}_4\text{Br} \cdot 7.6\text{H}_2\text{O}$	$\text{NH}_4\text{I} \cdot 8.2\text{H}_2\text{O}$
	r	r	r	r	r
	$(\Delta r^2)^{1/2}$	$(\Delta r^2)^{1/2}$	$(\Delta r^2)^{1/2}$	$(\Delta r^2)^{1/2}$	$(\Delta r^2)^{1/2}$
P_1^a	2.94 ± 0.01	2.88 ± 0.01	2.80 ± 0.01	2.82 ± 0.02	2.91 ± 0.01
P_2	2.78 ± 0.01	2.69 ± 0.01	3.50 ± 0.02	4.11 ± 0.04	4.70 ± 0.04
P_3	2.96 ± 0.01	2.87 ± 0.01	3.17 ± 0.02	3.36 ± 0.04	3.61 ± 0.04
Fraction of water molecules in network positions	0.80 ± 0.01	0.78 ± 0.01	0.85 ± 0.02	0.77 ± 0.02	0.66 ± 0.02
Fraction of empty cavities	0.50 ± 0.02	0.45 ± 0.02	0.39 ± 0.03	0.07 ± 0.04	0

^a P_1 , P_2 , and P_3 are independently variable near-neighbor distances (see Figure 3), characterized by an average distance r (Å) and an associated rms displacement $(\Delta r^2)^{1/2}$ (Å).

can replace a water molecule in either a network or cavity position. The same assumption was therefore made for the ammonium ions in the chloride, bromide, and iodide solutions. In contrast, the large and spherically symmetric chloride, bromide, and iodide ions were assumed to occupy cavity position only. Some relevant parameters of the model for water and the ammonium halide solutions are summarized in Table I. While the P_1 distance between network molecules (Figure 3) remains nearly constant, the P_2 distance increases drastically from water and the ammonium fluoride solutions to the chloride, bromide, and iodide solutions. The rms variation in the P_2 interaction shows a corresponding increase, indicating that there is a wide distribution of instantaneous P_2 distances about the mean value. This may be taken as an indication that the hydrogen-bonded network is severely distorted from the average, so that the cavities occupied by chloride, bromide, and iodide ions are much larger than those containing a water molecule.

While in water and in the ammonium fluoride solutions only about half of the cavities are occupied, this fraction increases with the size of the halide ion until all cavities are occupied by water molecules or ions in the case of the iodide solution (Table I). At the same time, the interactions between cavity water molecules and the network, as well as between cavity water molecules and the chloride, bromide, or iodide ions, become so diffuse that they give rise to uniform distributions of average distances.

Conclusions

The effect of chloride, bromide, and iodide ions on the structure of liquid water at 25°, insofar as it can be deduced from the RDF directly, thus seems to be two-fold: the average distance between near-neighbor water molecules increases from 2.85 Å in pure water to 2.91 Å in NH_4I , indicating weaker hydrogen bonding in the solutions. At the same time, the average number of nearest (water-water) neighbors decreases significantly, and this may be taken as an indication that not only the average strength but also the average number of hydrogen bonds per water molecule is smaller in the chloride, bromide, and iodide solutions than in pure water and in the ammonium fluoride solutions.

In terms of the ice-I model, the influence of halide ions on water structure can be summarized as follows. In order to accommodate the relatively large chloride, bromide, and iodide ions, the hydrogen-bonded network of water molecules expands anisotropically; in this way, each water molecule in the network retains three nearest water neighbors within hydrogen-bond distance, while the bond corresponding to the P_2 distance is broken (Figure 3). At the same time, the fraction of water molecules in cavity positions increases significantly from chloride to iodide; *i.e.*, the degree to randomness of the system increases.

The Crystal Structure of 1-Phenyl-3-(2-thiazolin-2-yl)-2-thiourea

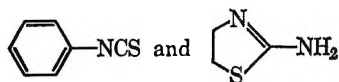
by J. L. Flippen and I. L. Karle

Laboratory for the Structure of Matter, U.S. Naval Research Laboratory, Washington, D. C. 20390
(Received September 18, 1969)

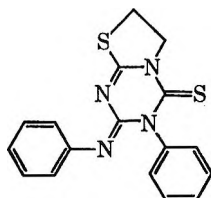
1-Phenyl-3-(2-thiazolin-2-yl)-2-thiourea is one of several new N-substituted thioureas being investigated for potential antiradiation drug properties. The thiazolinyl ring is nearly coplanar with the thiourea group and results in an intramolecular S...S distance of only ~ 3.0 Å. The phenyl group is rotated about 45° out of the plane of the thiourea group. The eight molecules in the unit cell are linked into infinite sheets by S...HN and N...HN hydrogen bonds, although the hydrogen bonding scheme is quite different for the two independent molecules in the asymmetric unit. The molecules crystallize in space group $P2_1/c$ with $a = 8.48$ Å, $b = 17.24$ Å, $c = 17.60$ Å, and $\beta = 120.5^\circ$. The structure was solved by using the symbolic addition procedure for phase determination.

Introduction

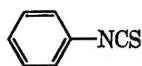
Potentially useful antiradiation drugs have been synthesized¹ from the reactions between



The elucidation of the structural formula as well as the crystal structure of one of these materials

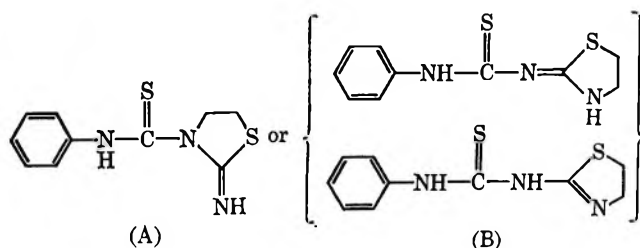


obtained by using an excess of



has been reported.²

The present investigation concerns a different product whose structural formula was presumed to be either



The crystal structure analysis proved formula B to be correct and established the geometry of the molecule. A paper describing the preparation and chemistry of this material has been published.³

Two independent molecules crystallize in an asymmetric unit of the unit cell. The packing arrangement, hydrogen bonding between C=S and HN—, and the

intramolecular attraction between S atoms will be discussed.

Experimental Section

The crystals were supplied by Dr. D. L. Klayman of the Walter Reed Army Medical Center, Washington, D. C. Pertinent physical constants are listed in Table I. Intensity data were collected along the (001) axis using multiple-film equiinclination Weissenberg photographs. The intensities were estimated visually by comparison with a calibrated film strip and were corrected for spot size and Lorentz and polarization factors. For reflections with $l \leq 5$, the data were corrected approximately for the crystal shape using the empirical expression $1 + w(2\phi - 10^\circ)$ where $w = -0.10$ and ϕ is the angular coordinate of the reciprocal lattice points as expressed in conventional polar coordinates.

Table I: Physical Constants

Molecular formula	$C_{10}H_{11}N_3S_2$
Molecular weight	227.4
Melting point	130°
Color	yellow
Habit	irregular prisms
Crystal size	$\sim 0.70 \times 0.61 \times 0.36$ mm
Space group	$P2_1/c$
a	8.48 ± 0.02 Å
b	17.24 ± 0.03 Å
c	17.60 ± 0.03 Å
β	$120.5 \pm 0.5^\circ$
Volume	2217.1 Å ³
Z	8 molecules
ρ X-ray	1.480 g/cm ³
Radiation	Cu $K\alpha$ (1.5418 Å)
No. independent reflections	2508

(1) D. L. Klayman and G. W. A. Milne, *Tetrahedron*, **25**, 191 (1969).

(2) J. Karle, J. Flippen, and I. L. Karle, *Z. Kristallogr.*, **73**, 52 (1967).

(3) D. L. Klayman, J. J. Maul, and G. W. A. Milne, *J. Heterocycl. Chem.*, **5**, 517 (1968).

Structure factor magnitudes $|F_{\bar{h}}|$ which had been corrected for vibrational motion and placed on an absolute scale by means of a K curve⁴ were used to obtain normalized structure factor magnitudes $|E_{\bar{h}}|$.

Phases for 1-phenyl-3-(2-thiazolin-2-yl)-2-thiourea were determined by means of the symbolic addition procedure.^{5,6} The Σ_2 relationship

$$sE_{\bar{h}} \sim s \sum_{\bar{k}} E_{\bar{k}} E_{\bar{h}-\bar{k}} \quad (1)$$

(where s means "sign of"), which is contained in inequality (34) in the complete set of inequalities derived from the nonnegativity principle,⁷ and the associated probability expression

$$P_+(E_{\bar{h}}) = 1/2 + 1/2 \tanh \frac{\sigma_3 E_{\bar{h}} \sum_{\bar{k}} E_{\bar{k}} E_{\bar{h}-\bar{k}}}{\sigma_2^{3/2}} \quad (2)$$

where $\sigma_n = \sum_{j=1}^n Z_j^n$,^{8,9} were used to obtain the phases.

The origin was specified by assigning positive signs to three linearly independent reflections having large $|E|$ magnitudes. The Σ_2 relationship was implemented by the use of the origin determining reflections and five other structure factors of large $|E|$ magnitude whose signs were specified by the symbols a, b, c, d, and e. This set is shown in Table II. Approximately 65 phases with $|E| > 1.5$ were determined in terms of the starting signs and symbols with $P_+(E_{\bar{h}}) > 0.96$. Among the Σ_2 combinations there were several relations among the symbols indicating that b should be negative and that c and d should be positive. These indications along with relationships such as $bd = e$, $ab = -$ and $abc = e$ led to the assignment $a = c = d = +$ and $b = e = -$. On the basis of this set of phases, phases for 610 additional reflections with $|E| > 1.0$ were obtained with the use of a computer program which continues the application of the Σ_2 relationship. The E map computed with these 674 terms revealed the positions of the 30 atoms in the two independent molecules as shown in Figure 1. There were no extraneous peaks with weights equal to or greater than those for the 30 atoms.

The coordinates and thermal factors were refined using a full matrix three-dimensional least-squares

Table II: Set of Reflections Used to Implement the Σ_2 Relation

Phase	h	k	l	$ E $
+	5	4	3	3.01
+	4	2	7	2.83
+	9	5	5	2.93
a	5	6	3	2.77
b	6	0	6	2.65
c	8	3	5	2.54
d	5	3	3	2.48
e	6	11	0	2.88

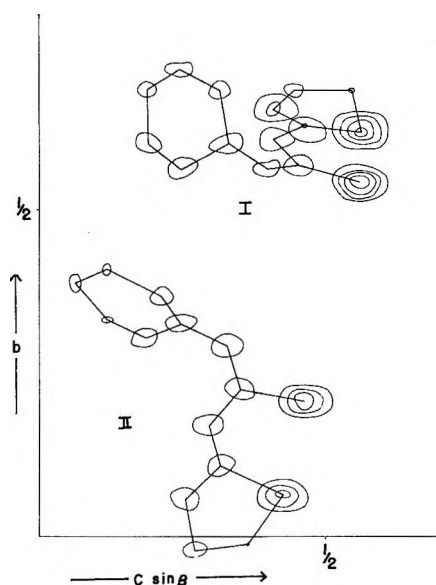


Figure 1. Initial E map obtained from 674 reflections with $|E| \geq 1.0$. Contours are equally spaced on an arbitrary scale. Every other contour has been omitted for the S atoms.

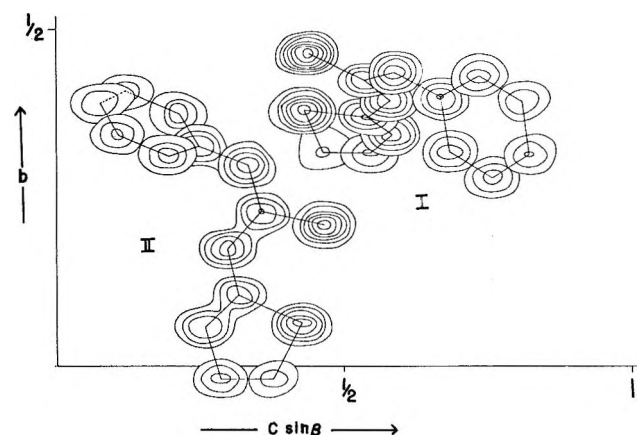


Figure 2. An electron-density map computed from the final parameters. Contours for the sulfur atoms are at intervals of $4e \cdot \text{\AA}^{-3}$, starting with the $4e \cdot \text{\AA}^{-3}$ contour. For the other atoms the contours are at intervals of $2e \cdot \text{\AA}^{-3}$, starting with the $2e \cdot \text{\AA}^{-3}$ level.

program¹⁰ using all 2508 independent data. Not all parameters could be varied simultaneously owing to a limitation in the capacity of the computer; hence different parameters were kept constant in each cycle of refinement. Unobserved reflections were weighted by

(4) J. Karle and H. Hauptman, *Acta Crystallogr.*, **6**, 473 (1953).

(5) I. L. Karle and J. Karle, *ibid.*, **16**, 969 (1963).

(6) J. Karle and I. L. Karle, *ibid.*, **21**, 849 (1966).

(7) J. Karle and H. Hauptman, *ibid.*, **3**, 181 (1950).

(8) M. M. Woolfson, *ibid.*, **7**, 61 (1954).

(9) H. Hauptman and J. Karle, "Solution of the Phase Problem. I. The Centrosymmetric Crystal," A.C.A. Monograph No. 3, Polycrystal Book Service, Pittsburgh, Pa., 1953.

(10) W. R. Busing, K. O. Martin, and H. A. Levy, "ORFLS, A FORTRAN Crystallographic Least-Squares Program," U. S. Atomic Energy Commission Report ORNL-TM-306, 1962.

$\frac{1}{2}$; unit weights were used for F_o 's up to 15.0 and all F_o 's greater than 15.0 were weighted $15.0/|F_o|$. After anisotropic refinement, the R factor was 9.8%.

Even though the value of the agreement factor R was quite reasonable for visually estimated data, the difference map did not reveal the H atom positions. Since the H atoms were not included in the refinement

Table III: Fractional Coordinates and Isotropic Thermal Parameters

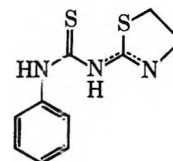
Atom	x	y	z	$B, \text{\AA}^2$
Molecule I				
S(1)	0.2058	0.4617	0.4375	2.2
S(2)	-0.1168	0.3786	0.4291	3.2
N(1)	-0.0138	0.3391	0.5877	2.5
N(2)	0.2249	0.3912	0.5803	1.8
N(3)	0.4906	0.4338	0.5913	2.4
C(1)	0.3023	0.4265	0.5384	1.8
C(2)	0.0473	0.3704	0.5394	1.7
C(3)	-0.2816	0.3284	0.4486	6.4
C(4)	-0.2060	0.3150	0.5426	3.5
C(5)	0.6044	0.3946	0.6713	2.2
C(6)	0.5811	0.3161	0.6805	2.6
C(7)	0.7047	0.2782	0.7591	3.3
C(8)	0.8617	0.3162	0.8260	4.3
C(9)	0.8852	0.3945	0.8134	4.0
C(10)	0.7591	0.4338	0.7355	2.9
Molecule II				
S(3)	0.3636	0.2100	0.4636	3.5
S(4)	0.4771	0.0634	0.4231	4.2
N(4)	0.3506	0.0600	0.2563	2.9
N(5)	0.2832	0.1746	0.2959	2.3
N(6)	0.2198	0.2981	0.3280	2.5
C(11)	0.2882	0.2238	0.3585	1.9
C(12)	0.3599	0.1050	0.3200	2.0
C(13)	0.5528	-0.0171	0.3810	5.4
C(14)	0.4265	-0.0185	0.2808	3.7
C(15)	0.1495	0.2250	0.2410	2.0
C(16)	0.2245	0.3129	0.1887	3.2
C(17)	0.1496	0.3426	0.1046	4.1
C(18)	-0.0136	0.3907	0.0708	4.6
C(19)	-0.0788	0.4055	0.1267	4.4
C(20)	-0.0074	0.3737	0.2102	3.5
Standard deviations ^a				
S	3	2	3	
N	10	4	7	
C	14	6	11	

^a The standard deviations are multiplied by 10^4 .

and because the intensity data were collected on one axis only and since the shape of the crystal used for obtaining the diffraction data was quite irregular, the anisotropic thermal parameters are probably not particularly meaningful. Only isotropic thermal parameters are listed with the atomic coordinates in Table III. An electron density map computed from the final parameters is illustrated in Figure 2.

Discussion

The primary objective of this investigation was to establish the structural formula which has been shown to be the disubstituted thiourea



The configurations of the two independent molecules, I and II, in the asymmetric unit are shown in the stereo diagram in Figure 3. Both stereo drawings in this paper were drawn by a computer-driven Calcomp plotter using the ORTEP program.¹¹ The thiazolinyl ring is *syn* to the C=S bond with the two S atoms near each other while the phenyl group is *anti* to the C=S bond. The thiourea groups are planar to within $\pm 0.006 \text{ \AA}$ and the phenyl groups are planar to within $\pm 0.028 \text{ \AA}$. In the five-membered rings in both molecules, four atoms are coplanar to within 0.02 \AA while C(3) in molecule I and C(13) in molecule II are 0.11 \AA and 0.37 \AA , respectively, out of the plane formed by the other four atoms in each ring. The N atoms connected to these rings are within 0.05 \AA of the planes of the rings. The dihedral angle between the plane of the thiourea group and the four coplanar atoms in the thiazolinyl ring is 10° in molecule I and 5.5° in molecule II. On the other hand, the dihedral angle between the thiourea group and the phenyl ring is 49° in molecule I and 41° in molecule II. In other words, in each molecule, the five-membered ring is nearly coplanar with the thiourea group while the phenyl ring is twisted considerably about the N(3)-C(5) or N(6)-C(15) bond. The values of the bond lengths reflect this difference of configuration between the thiourea group and the two rings to which it is bonded. The C-N bond lengths to the phenyl rings are 1.41 \AA while the C-N bonds to the five-membered rings are only $\sim 1.34 \text{ \AA}$, Figure 4, indicating a strong interaction between the external

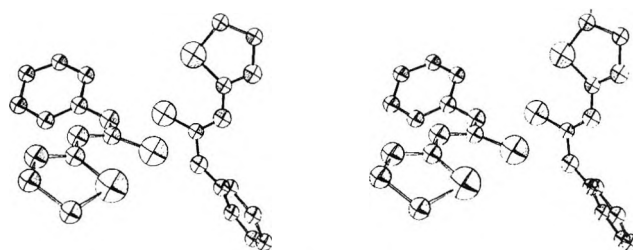


Figure 3. Stereodiagram of the two molecules in an asymmetric unit of 1-phenyl-3-(2-thiazolin-2-yl)-2-thiourea. The atoms are represented by spheres of arbitrary size which are unrelated to the actual thermal parameters.

(11) C. K. Johnson, "ORTEP, A FORTRAN Thermal-ellipsoid Plot Program for Crystal Structure Illustrations," U. S. Atomic Energy Commission Report ORNL-3794, 1965.

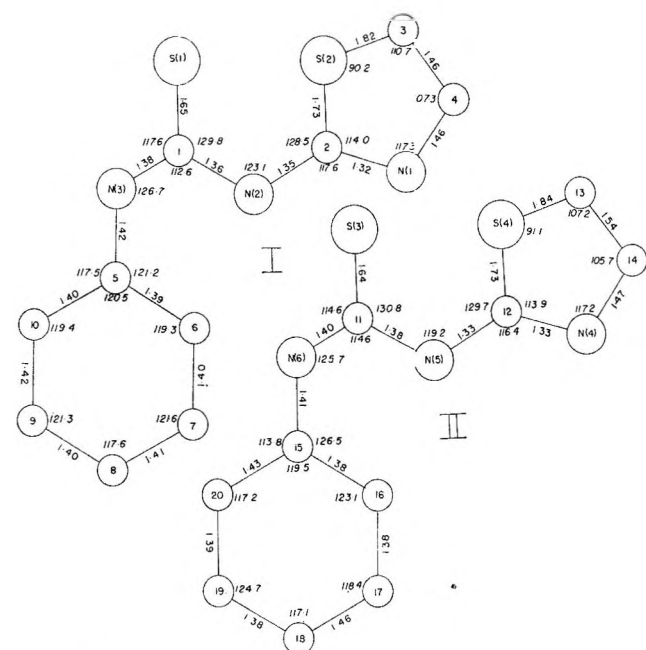
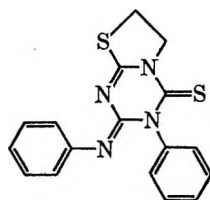


Figure 4. Bond distances and angles.

C \cdots N bonds and internal C \cdots N bonds in the thiazoliny ring. It is not possible to distinguish between the two forms illustrated in formula B due to the similar values for the C-N bond lengths involved.

Bond lengths and angles are listed in Table IV and shown in Figure 4. Standard deviations based only on the least-squares agreement range from 0.016 Å for the C=S bonds to 0.03 Å for C-C bonds. Standard deviations for the angles are less than 1°. The values are quite similar for the two molecules except for C(3)-C(4) where the bond length is quite short for a single bond. Atom C(3) had a large thermal parameter, $B = 6.4 \text{ \AA}^2$, compared to the remainder of the atoms. Most likely there is some disorder in this ring. Since it is atom C(3) which is displaced from the plane of the other four atoms in the thiazoliny ring, it may possibly occur on either side of the plane and its average displacement (only 0.1 Å from the plane as compared to 0.4-0.5 Å usually found in other kinds of five-membered rings) may account for the short C-C value. The difference map was not sufficiently clear to show this point.

The two C-S distances in the thiazoliny ring are unequal, 1.73 Å and 1.82-4 Å, in good agreement with those found in other molecules with similar groups, as for example²



In the thiourea moiety, the C=S distance is 1.65 Å, the

Table IV: Bond Lengths and Angles

Length, Å		Angle, deg	
Molecule I			
S(1)-C(1)	1.65	C(2)-S(2)-C(3)	90.2
S(2)-C(2)	1.73	C(2)-N(1)-C(4)	117.3
S(2)-C(3)	1.82	C(1)-N(2)-C(2)	123.1
N(1)-C(2)	1.32	C(1)-N(3)-C(5)	126.7
N(1)-C(4)	1.46	S(1)-C(1)-N(2)	129.8
N(2)-C(1)	1.36	S(1)-C(1)-N(3)	117.6
N(2)-C(2)	1.35	N(2)-C(1)-N(3)	112.6
N(3)-C(1)	1.38	S(2)-C(2)-N(1)	114.0
N(3)-C(5)	1.42	S(2)-C(2)-N(2)	128.5
C(3)-C(4)	1.46	N(1)-C(2)-N(2)	117.6
C(5)-C(6)	1.39	S(2)-C(3)-C(4)	110.7
C(5)-C(10)	1.40	N(1)-C(4)-C(3)	107.3
C(6)-C(7)	1.40	N(3)-C(5)-C(6)	121.2
C(7)-C(8)	1.41	N(3)-C(5)-C(10)	117.5
C(8)-C(9)	1.40	C(6)-C(5)-C(10)	120.5
C(9)-C(10)	1.42	C(5)-C(6)-C(7)	119.3
		C(6)-C(7)-C(8)	121.6
		C(7)-C(8)-C(9)	117.6
		C(8)-C(9)-C(10)	121.3
		C(5)-C(10)-C(9)	119.4
Molecule II			
S(3)-C(11)	1.64	C(12)-S(4)-C(13)	91.1
S(4)-C(12)	1.73	C(12)-N(4)-C(14)	117.2
S(4)-C(13)	1.84	C(11)-N(5)-C(12)	119.2
N(4)-C(12)	1.33	C(11)-N(6)-C(15)	125.7
N(4)-C(14)	1.47	S(3)-C(11)-N(5)	130.8
N(5)-C(11)	1.38	S(3)-C(11)-N(6)	114.6
N(5)-C(12)	1.33	N(5)-C(11)-N(6)	114.6
N(6)-C(11)	1.40	S(4)-C(12)-N(4)	113.9
N(6)-C(15)	1.41	S(4)-C(12)-N(5)	129.7
C(13)-C(14)	1.54	N(4)-C(12)-N(5)	116.4
C(15)-C(16)	1.38	S(4)-C(13)-C(14)	107.2
C(15)-C(20)	1.43	N(4)-C(14)-C(13)	105.7
C(16)-C(17)	1.38	N(6)-C(15)-C(16)	126.5
C(17)-C(18)	1.46	N(6)-C(15)-C(20)	113.8
C(18)-C(19)	1.38	C(16)-C(15)-C(20)	119.5
C(19)-C(20)	1.39	C(15)-C(16)-C(17)	123.1
		C(16)-C(17)-C(18)	118.4
		C(17)-C(18)-C(19)	117.1
		C(18)-C(19)-C(20)	124.7
		C(15)-C(20)-C(19)	117.2

same value as in the aforementioned molecule, but considerably shorter than in unsubstituted thiourea where it is 1.72 Å.¹²

One of the striking features of the phenyl-thiazoliny thiourea molecule is the *intramolecular* distance S(1) \cdots S(2) or S(3) \cdots S(4), which is only 3.0 and 2.9 Å, respectively. Using the currently accepted van der Waals radius for S of 1.85 Å,¹³ a S \cdots S separation would be expected to be of the order of 3.7 Å. Even though the SCN angles are quite large, the near coplanarity of the thiourea and thiazoliny groups brings the two S atoms

(12) M. R. Truter, *Acta Crystallogr.*, **22**, 556 (1967).

(13) L. Pauling, "The Nature of the Chemical Bond," Cornell University Press, Ithaca, N. Y., 1960, p 260.

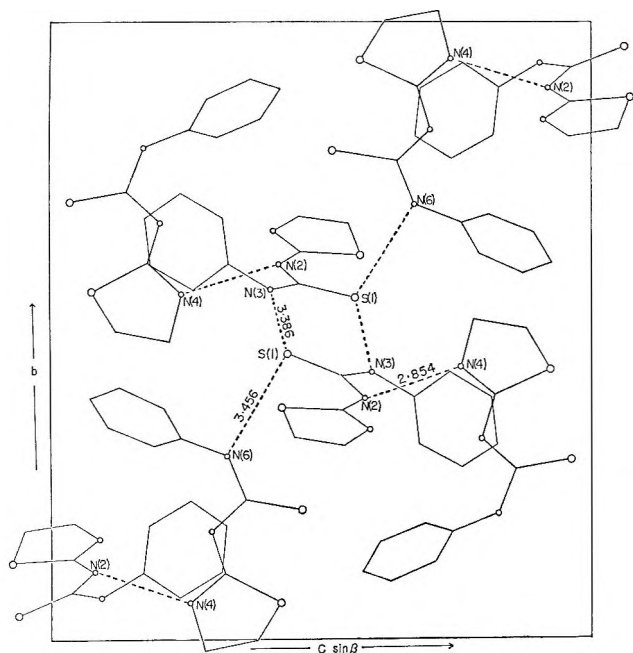
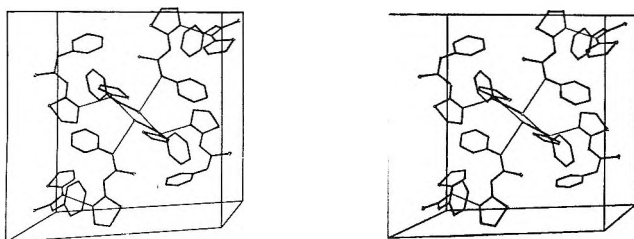


Figure 5. Contents of the unit cell.

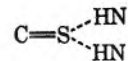
Figure 6. Stereodiagram of the packing and hydrogen bonding drawn looking down the *a* axis with the *c* axis horizontal and the *b* axis vertical.

in proximity to each other. A somewhat similar situation occurs in *N*-phenyl-*N'*-benzoylselenourea,¹⁴ a molecule which has a general conformation very similar to that in the present study, where an intramolecular $\text{Se} \cdots \text{C}$ distance of 3.3 Å occurs, analogous to the short $\text{S} \cdots \text{S}$ separation found in this investigation.

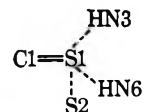
An extensive system of hydrogen bonds links together all eight molecules in the unit cell and forms continuous sheets perpendicular to the *a* direction, Figures 5 and 6. There are three independent hydrogen bonds. In molecule I there are two $\text{C}=\text{S}(1) \cdots \text{HN}(3)$ bonds across a center of symmetry to form dimeric units. Molecule I is linked to molecule II by a hydrogen bond between $\text{S}(1)$ and $\text{N}(6)$ and, in turn, molecule II is linked to a symmetry related molecule I by the $\text{N}(4) \cdots \text{HN}(2)$ bond (or alternatively an $\text{N}(4) \cdots \text{H} \cdots \text{N}(2)$ bond). The $\text{NH} \cdots \text{N}$ bond length is 2.85 Å, a value similar to

that found in other molecules. The $\text{S} \cdots \text{HN}$ bond lengths are 3.39 Å and 3.45 Å. Values in the literature for $\text{S} \cdots \text{HN}$ bonds vary from 3.24 Å to 3.50 Å.¹⁵

The configuration about $\text{C}=\text{S}$ with respect to the directions of the hydrogen bonds has been found to vary in different crystals. For example, the moiety is planar



in allylthiourea¹⁶ while it is pyramidal in trimethylene thiourea.¹⁷ In phenyl thiazolinyl thiourea, the $\text{S}(1)$ atom is surrounded by the bond to $\text{C}(1)$, the hydrogen bonds to $\text{N}(3)$, and $\text{N}(6)$, and the near approach to $\text{S}(2)$, making a roughly tetrahedral array.



The angles about $\text{S}(1)$ are $\text{C}(1) \cdots \text{S}(1) \cdots \text{N}(3)$ 111.0°; and $\text{N}(3) \cdots \text{S}(1) \cdots \text{N}(6)$, 96.0°; $\text{C}(1) \cdots \text{S}(1) \cdots \text{N}(6)$ 99.5°; and $\text{N}(3) \cdots \text{S}(1) \cdots \text{S}(2)$, 169.3°; $\text{C}(1) \cdots \text{S}(1) \cdots \text{S}(2)$ 79.6°; and $\text{N}(6) \cdots \text{S}(1) \cdots \text{S}(2)$, 82.7°

The analogous $\text{C}(11) = \text{S}(3)$ group in molecule II does not participate in hydrogen bonding. It is also interesting to note that $\text{N}(5)\text{-H}$ (or alternatively $\text{N}(3)\text{-H}$) does not participate in any hydrogen bonding.

The nearest approaches between atoms in different molecules, other than those atoms involved in hydrogen bonding, are listed in Table V. It is noteworthy that the $\text{S}(4) \cdots \text{S}(4)$ distance across a center of symmetry, is only 3.35 Å.

Table V: Intermolecular Distances < 3.5 Å

Atom (1)	Atom (2)	Symmetry (2)	Distance
N(1)	N(4)	$x \frac{1}{2} - y \frac{1}{2} + z$	3.48
N(1)	N(5)	$x \frac{1}{2} - y \frac{1}{2} + z$	3.24
N(1)	C(17)	$x \frac{1}{2} - y \frac{1}{2} + z$	3.38
N(1)	C(16)	$x \frac{1}{2} - y \frac{1}{2} + z$	3.24
C(5)	N(4)	$x \frac{1}{2} - y \frac{1}{2} + z$	3.28
C(11)	C(8)	$x \frac{1}{2} - y \frac{1}{2} + z$	3.43
C(13)	C(17)	$x \frac{1}{2} + \bar{y} \frac{1}{2} - \bar{z}$	3.41
S(4)	S(4)	$x \bar{y} \bar{z}$	3.35

(14) H. Hope, *Acta Crystallogr.*, **18**, 259 (1965).

(15) W. C. Hamilton and J. A. Ibers, "Hydrogen Bonding in Solids," W. A. Benjamin, New York, N. Y., 1968, p 168.

(16) K. S. Dragonette and I. L. Karle, *Acta Crystallogr.*, **19**, 978 (1966).(17) H. W. Dias and M. R. Truter, *ibid.*, **17**, 937 (1964).

Charge Transfer to Molecules on the Surface of Irradiated Porous Glass¹

by P. K. Wong and A. O. Allen

Chemistry Department, Brookhaven National Laboratory, Upton, New York 11973 (Received August 14, 1969)

Tetracyanoethylene (TCNE) adsorbed on porous Vycor glass forms under γ rays at room temperature its radical anion TCNE^- with a yield $G = 6.5$ ions per 100 eV absorbed in the glass, independent of the surface concentration of TCNE. When the glass is first irradiated alone and the TCNE then added, the anion still forms with a yield $G = 4.2$. Presence of TCNE during irradiation prevents formation of the sharp trapped-electron spin resonance (esr) signal characteristic of irradiated glass, but when TCNE is added to irradiated glass, the trapped-electron signal is not affected, although the signal characteristic of TCNE^- appears with an intensity around 5 times that of the trapped electron signal. Thus the electron-donating centers formed on the glass surface are not the trapped electrons seen by esr. Tetra-*N*-methyl-phenylenediamine (TMPD), triphenylamine, and perylene adsorbed on the glass form under γ rays radical cations stable at room temperature. Methylaniline, diethylaniline, and triphenylphosphine yield cations, and acetone, butanone, and acetophenone yield anions when irradiated on the glass at 77°K, but these ions disappear when warmed to room temperature.

The radiation chemistry of surfaces has now been the subject of many publications. The studies involve irradiation of a molecular substance, usually organic, adsorbed on a mineral oxide or halide. The results appear to fall into two classes, depending on whether (a) energy transfer or (b) charge transfer from the mineral to the adsorbed molecules is involved. In the first case, the molecules acquire activation energy from the solid during irradiation which causes their decomposition; the yield of the reaction increases gradually with concentration of molecules on the surface, leveling off only after a complete monolayer is formed, and very little reaction occurs if the solid is irradiated first and the substrate added subsequently. Examples include the radiolysis in the adsorbed state of aliphatic hydrocarbons,² azoethane,³ and ethanol.⁴ In the second case, molecules are chosen which are good electron acceptors or donors, and the reaction products result from a one-electron reduction or oxidation. Here it is generally found that the radiolytic yield remains constant down to very low surface concentrations of the substrate, and considerable yield is in some cases obtained if the solid is irradiated first and the substrate then added. Among the examples are the production of radical anions or cations from benzene, naphthalene, biphenyl, galvinoxyl,⁵ and oxygen,⁶ and dealkylation of isopropylbenzene.⁷ Sometimes the reaction follows different courses if the substrate is present during irradiation or is added later; thus CO_2 gives the radical CO_2^- if present during irradiation but yields the radical O_2^- if added after the irradiation.⁸ It thus appears that the surface of silica or similar solids is activated by radiation to a state which can transfer electric charge to a passing molecule if the molecule happens to be readily liable to one-electron oxidation or reduction, but cannot generally activate other molecules. During irradiation,

however, these active charge-donating centers must frequently be neutralized by further migrating charges continually forming in the material, and the energy of neutralization thus released can activate an adsorbed hydrocarbon or other molecule in the immediate neighborhood and bring about its decomposition.

The present work is a study of transfer of both positive and negative charge from irradiated porous Vycor glass. This material was chosen in part because it is known to yield, under irradiation, centers which react with added hydrogen and other substances,⁹ but mainly because its transparency allows accurate quantitative determination of reaction products by optical absorption spectrophotometry.

Experimental Section

Materials. *N,N,N',N'*-Tetramethyl-*p*-phenylenediamine (TMPD) was purified as described previously.¹⁰ Triphenylamine (TPA) from Baker Chemical was purified by crystallization in methanol and sublimation.

- (1) Research performed under the auspices of the U. S. Atomic Energy Commission.
- (2) (a) J. M. Caffrey and A. O. Allen, *J. Phys. Chem.*, **62**, 33 (1958); (b) J. W. Sutherland and A. O. Allen, *J. Amer. Chem. Soc.*, **83**, 1040 (1961); (c) N. H. Sagert and D. J. Dyne, *Can. J. Chem.*, **45**, 615 (1967).
- (3) J. G. Rabe, B. Rabe, and A. O. Allen, *J. Phys. Chem.*, **70**, 1098 (1966).
- (4) L. Abrams and A. O. Allen, *ibid.*, **73**, 2741 (1969).
- (5) (a) P. K. Wong and J. E. Willard, *ibid.*, **72**, 2623 (1968); (b) O. Edlund, P.-O. Kinell, A. Lund, and A. Shimizu, *J. Chem. Phys.*, **46**, 3679 (1967).
- (6) P. H. Kasai, *ibid.*, **43**, 3322 (1965).
- (7) (a) E. A. Rojo and R. R. Hentz, *J. Phys. Chem.*, **70**, 2919 (1966); (b) R. R. Hentz and D. K. Wickenden, *ibid.*, **73**, 817 (1969).
- (8) P. K. Wong and J. E. Willard, *ibid.*, **73**, 2226 (1969).
- (9) G. M. Muha and D. J. C. Yates, *ibid.*, **70**, 1399 (1966).
- (10) C. Capellos and A. O. Allen, *ibid.*, **72**, 4265 (1968).

Perylene from K and K Laboratories was sublimed twice. N-Methylaniline and N,N'-diethylaniline from Eastman Chemicals were vacuum distilled. Triphenylphosphine (TPP) from Mallinckrodt, acetone, and 2,3-butanedione from Baker Chemicals were used without purification. Tetracyanoethylene (TCNE) from Aldrich Chemical was crystallized from chlorobenzene and twice sublimed according to Merrifield and Phillips.¹¹ The surface area of the porous Vycor glass (No. 7930) from Corning was determined as 140 m²/g by the BET method using nitrogen.¹² The glass plates, 1 × 6 × 35 mm, were thermostated at 600° in a muffle oven before being evacuated from 12–16 hr to 3–5 × 10⁻⁶ Torr at the same temperature.

Adsorption. Liquids were adsorbed on the glass plates by bulb-to-bulb distillation. Solids were sublimed at 80° and the vapor was brought in contact with the glass. The sample preparations were carried out in a grease-free system using Hoke valves with Teflon seats. The Vycor plates were irradiated in Pyrex ampoules to which either Suprasil windows or 4-mm od tubes were attached for optical or esr observation, respectively. The ampoules were positioned so that the Suprasil section was 8–9 in. away from the γ source and received very little irradiation.

Irradiation. Samples were irradiated at about 23°C or 77°K with a cobalt-60 γ source operating at a dose rate of 0.858 Mrad/hr.

Spectra. Optical spectra were obtained on a Cary 14 automatic recording spectrophotometer. For low-temperature measurements, the samples were cooled in a copper cell-holder attached to a brass Dewar filled with liquid nitrogen. For electron spin resonance (esr) observations, we used a Varian Associates 4500 spectrometer equipped with 100-kHz field modulation and a V-4531 multiple purpose cavity. A standard Varian Associates quartz Dewar was used for measurements at 77°K.

Results

Addition of Charge Scavengers to Preirradiated Vycor. The irradiated Vycor glass formed a brownish purple color, which has a rising absorption starting at 360 nm into the uv region. Addition of charge scavengers produced optical bands in the region 400–700 nm; TMPD and TPA produced spectra similar to Figure 1. TCNE on preirradiated Vycor yielded a band closely resembling that of TCNE⁻ generated by reducing the compound with 1,2-diazabicyclo(2,2,2)octane (Figure 2). TMPD and TPA on preirradiated Vycor gave broad and unresolved esr spectra, superimposed on which was a sharp asymmetric line characteristic of trapped electrons in irradiated silica.¹³ When an irradiated sample of Vycor (Figure 3) was exposed to the vapor of TCNE, an extra esr signal appeared on the low-field side of the sharp asymmetric signal (Figure 4). The appearance of the new signal did

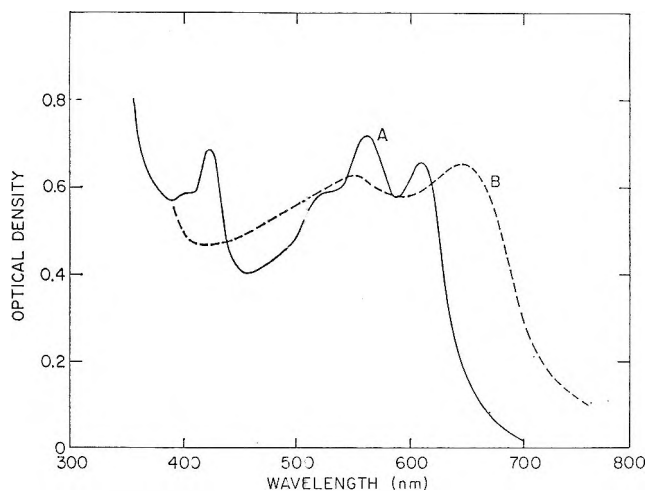


Figure 1. Optical spectra of cation radicals on Vycor surface at room temperature: A, TMFD, 0.75 Mrad; B, TPA, 2.38 Mrad.

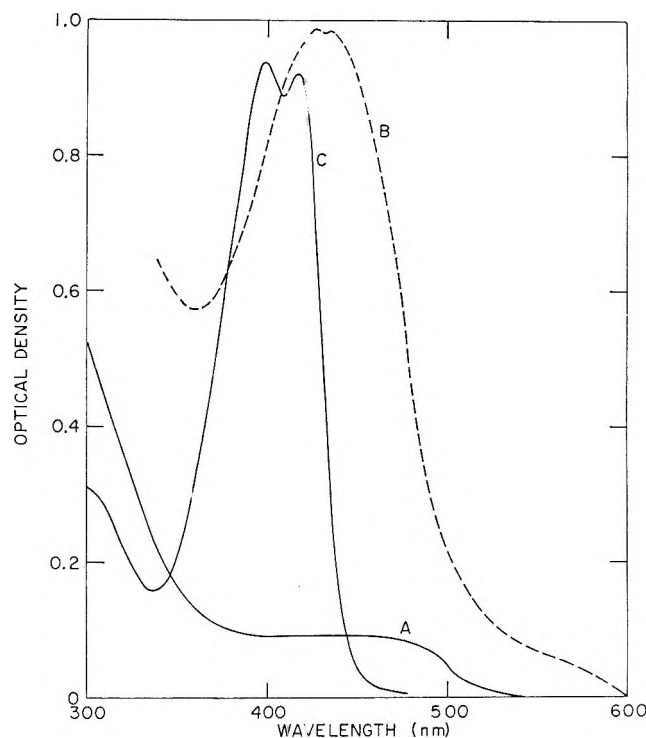


Figure 2. Optical spectra of (TCNE)⁻ at room temperature: A, before irradiation on Vycor; B, after irradiation on Vycor at 0.43 Mrad; C, by reduction with 1,2 diazabicyclo [2,2,2]octane in dioxane.

not affect the original esr line due to trapped electrons. The new signal is attributed to TCNE⁻ and the yield of this species is about five times larger than that of trapped electrons.

(11) R. E. Merrifield and W. D. Phillips, *J. Amer. Chem. Soc.*, **80**, 2778 (1958).

(12) D. M. Young and A. D. Crowell, "Physical Adsorption of Gases", Butterworth and Co., Ltd., London, 1962, p 150.

(13) C. M. Nelson and R. A. Weeks, *J. Amer. Ceram. Soc.*, **43**, 399 (1960).

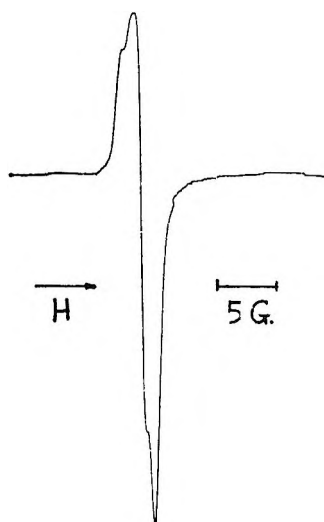


Figure 3. ESR spectrum of irradiated Vycor; dose, 0.57 Mrad.

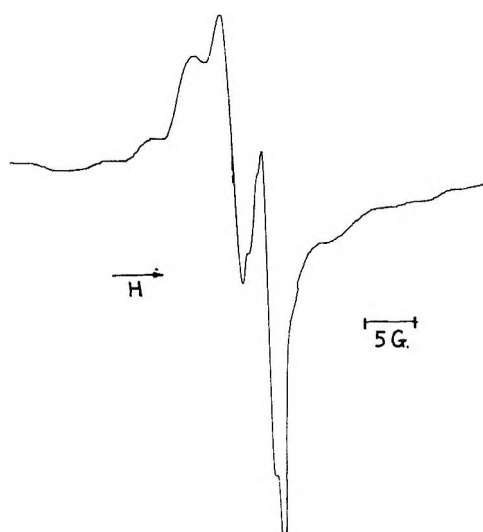


Figure 4. ESR spectrum of irradiated Vycor on which TCNE has been adsorbed; dose, 0.57 Mrad.

The yields of the ion radicals (TMPD^+ , TPA^+ , and TCNE^-) were estimated by their optical absorption. Beer's law gives $\text{OD} = kc$, where c is the concentration of the absorbing material in mol/g and OD is the optical density. The constant k is found for each species by adsorbing a known concentration of the material on Vycor and measuring its optical density. This was accomplished by oxidizing the TMPD and TPA by oxygen or iodine on the surface. A weighed quantity of TMPD or TPA was distilled onto the glass under vacuum; exposure at room temperature to either oxygen or iodine vapor immediately oxidized the material completely. TCNE^- was prepared in CCl_4 according to Turkevich.¹⁴ When a Vycor plate was immersed in the solution (in air at room temperature) the TCNE^- was spontaneously absorbed into the Vycor. The solvent was then evaporated away and the optical density of the plate was measured. The radiolytic yields of

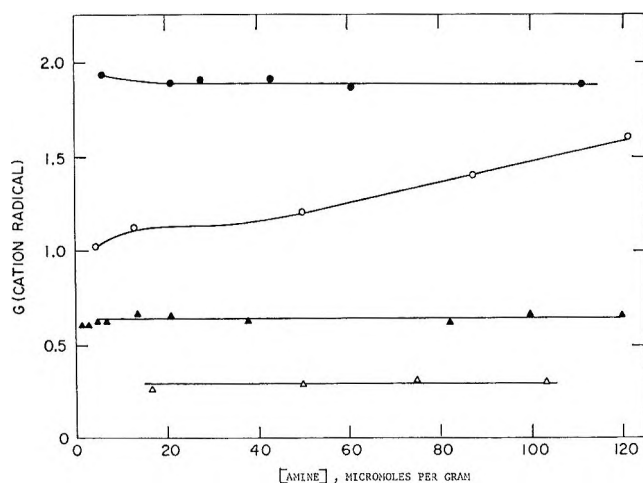


Figure 5. G values for cation radicals on Vycor as a function of substrate concentration. Dose, 0.75 Mrad: ●, TMPD irradiated on Vycor; ○, TMPD added to preirradiated Vycor; ▲, TPA, irradiated on Vycor; △, TPA added to preirradiated Vycor.

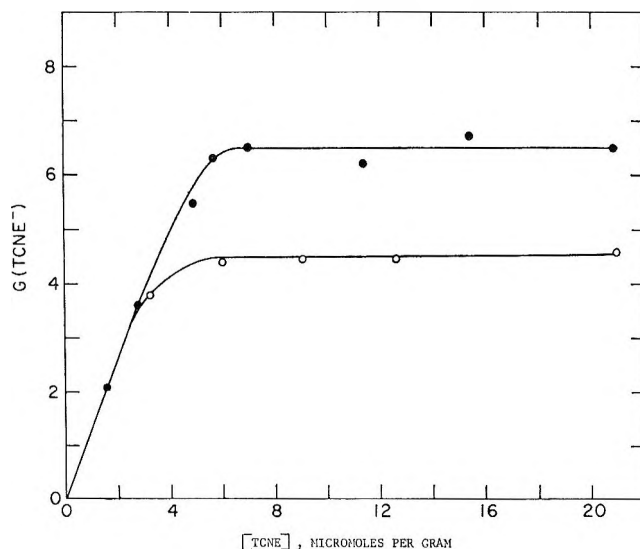


Figure 6. G values for $(\text{TCNE})^-$ on Vycor as a function of TCNE concentration. Dose, 0.75 Mrad: ●, TCNE irradiated on Vycor; ○, TCNE added to preirradiated Vycor.

TMPD^+ , TPA^+ , and TCNE^- are given in Figures 5 and 6. $G(\text{TMPD}^+)$ (molecules formed per 100 eV adsorbed by the whole system) varies from 1 to 1.6, depending on the concentration of TMPD. $G(\text{TPA}^+)$ has a constant value of 0.31, independent of TPA concentration from 20 to 100 $\mu\text{mol/g}$. $G(\text{TCNE}^-) = 4.5$ from 6 to 21 $\mu\text{mol/g}$ of adsorbate. Figure 7 is a plot of TPA^+ concentration against γ dose. At a total dose of 7 Mrads, the concentration of TPA^+ attains $4.4 \times 10^{17}/\text{g}$. The accumulation of ion radicals is independent of initial TPA concentration from 13 to 70 $\mu\text{mol/g}$.

Irradiation of Vycor Containing Adsorbed Material.

(14) D. N. Stamires and J. Turkevich, *J. Amer. Chem. Soc.*, **85**, 2557 (1963).

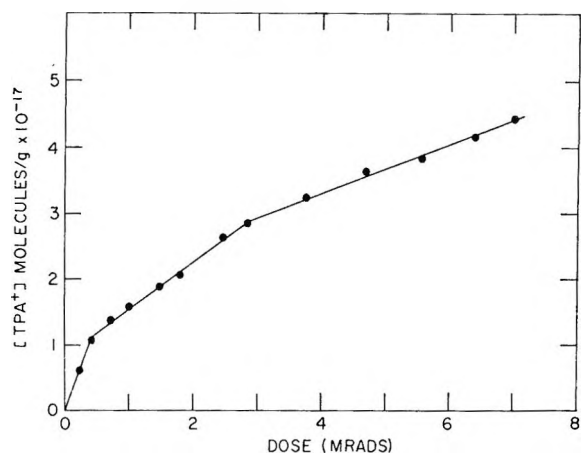


Figure 7. Concentration of $(\text{TPA})^+$ as a function of dose at 0.89 Mrad/hr (room temperature).

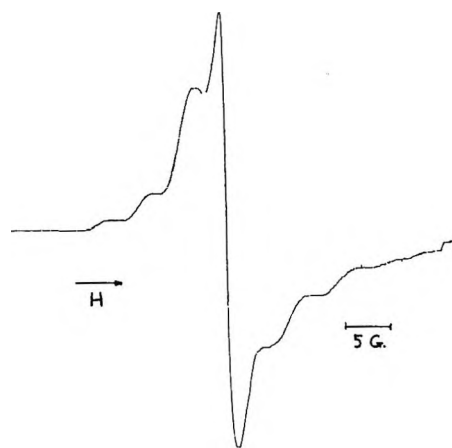


Figure 8. ESR spectra of $(\text{TCNE})^-$ on Vycor; dose, 0.57 Mrad.

When a substrate was present on the Vycor surface and the combination γ -irradiated, colored species were generated which could be detected by the optical or the esr method. TMPD and TPA when irradiated in this manner produced spectra shown in Figure 1. Other oxidizable substrates produced optical bands and esr spectra similar to those of their cation radicals. Table I summarizes the optical results.

The esr signals of cation radicals appear as poorly resolved broad spectra plus a sharp asymmetric line due to trapped electrons in the irradiated Vycor. The species attributable to TMPD^+ , TPA^+ and perylene $^+$ were stable at room temperature on Vycor; the rest in Table I were stable at 77°K, but disappeared when brought to room temperature.

When electron scavengers were present on Vycor, the irradiated samples produced species that have optical bands and esr signals. Acetone, butanone, biacetyl, and acetophenone irradiated and measured at liquid nitrogen temperature, showed absorption peaks in the visible region. TCNE formed at room temperature a band shown in Figure 2 and an esr

Table I: Absorption Bands of Cation Radicals

Species	λ_{max} (nm)		Preparation
	Vycor	Other matrices	
$\left(\begin{array}{c} \text{CH}_3 \\ \\ \text{N} - \text{C}_6\text{H}_4 - \text{N} \\ \quad \\ \text{CH}_3 \quad \text{CH}_3 \end{array} \right)^+$	522	538 ^a	Photolysis in 3-methylpentane glass at 77°K
	561	575	
	608	632	
$\left(\begin{array}{c} \text{C}_6\text{H}_5 \\ \\ \text{N} \\ \\ \text{C}_6\text{H}_5 \end{array} \right)^+$	550	560 ^b	γ Radiolysis in methyltetrahydrofuran at 77°K
	640	640	
$\left(\begin{array}{c} \text{CH}_3 \\ \\ \text{NH} \\ \\ \text{C}_6\text{H}_5 \end{array} \right)^+$	425	$\sim 445^c$	Flash photolysis in H_2SO_4
	453	455	
$\left(\begin{array}{c} \text{C}_2\text{H}_5 \\ \\ \text{N} \\ \\ \text{C}_2\text{H}_5 \end{array} \right)^+$	450	$\sim 450^b$	γ Radiolysis in CCl_4 at 77°K
	468	~ 475	
$\left(\begin{array}{c} \text{C}_6\text{H}_5 \\ \\ \text{P} \\ \\ \text{C}_6\text{H}_5 \end{array} \right)^+$	330	320 ^d	Flash photolysis in aqueous alcohol
	345	330	
	438		
$\left(\begin{array}{c} \text{C}_6\text{H}_5 \\ \\ \text{C} \\ \\ \text{C}_6\text{H}_5 \end{array} \right)^+$	535	545 ^e	Chemisorption on silica alumina

^a A. C. Albrecht and W. T. Simpson, *J. Amer. Chem. Soc.*, **77**, 4454 (1955). ^b M. Kondo, M. R. Ronayne, J. P. Guarino, and W. H. Hamill, *ibid.*, **86**, 1297 (1964). ^c E. J. Land and G. Porter, *Trans. Faraday Soc.*, **59**, 2027 (1963). ^d H. I. Joschek and L. I. Grossweiner, *J. Amer. Chem. Soc.*, **88**, 3261 (1966). ^e W. K. Hall, *J. Catal.*, **1**, 53 (1962).

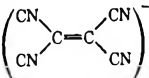
Table II: Absorption Bands of Anion Radicals

Species	λ_{max} , nm		Preparation
	On Vycor	In other matrices	
$[(\text{CH}_3)_2\text{CO}]^-$	73)	740 ^a	γ Radiolysis in sec-butyl chloride
$[\text{C}_4\text{H}_7\text{COCH}_3]^-$	775	808 ^a	γ Radiolysis in sec-butyl chloride
$[\text{C}_4\text{H}_9\text{COCH}_3]^-$	42)	440 ^a	γ Radiolysis in ethanol
$\left[\begin{array}{c} \text{CN} \quad \text{CN} \\ \diagdown \quad / \\ \text{C}=\text{C} \\ / \quad \diagdown \\ \text{CN} \quad \text{CN} \end{array} \right]^-$	≤ 25	410	Reduction by amine in dioxane
		432 ^b	NaI reduction in tetrahydrofuran

^a T. Shida and W. H. Hamill, *J. Amer. Chem. Soc.*, **88**, 3683 (1966). ^b W. D. Phillips, J. C. Rowell, and S. I. Weissman, *J. Chem. Phys.*, **33**, 626 (1960).

spectrum shown in Figure 8. The results are given in Table II. The details of their esr data are given in Table III. All the ketyl anion radicals are stable

Table III: ESR Spectra of Anion Radicals

	—On Vycor ^a —		—In other matrices—	
	No. of lines	Coupling const., G	No. of lines	Coupling const., G
$[(\text{CH}_3)_2\text{CO}]^-$	7	17.6	7	16.4 ^b
$[(\text{C}_2\text{H}_5)_2\text{COCH}_2]^-$	5	19.7	1	30 ^b
$[\text{CH}_2\text{COCOCCH}_2]^-$	7	8.6	7	7.3 ^b
$(\text{CH}_2\text{COC}_2\text{H}_5)^-$	1	~24
	9	2.2	9	1.61 ^c 4.9 ^d

^a This work. ^b J. E. Bennett, B. Mile, and A. Thomas, *J. Chem. Soc., A*, 298 (1968). ^c J. Gendell, J. H. Freed, and G. K. Fraenkel, *J. Chem. Phys.*, **41**, 949 (1964). ^d B. D. Flockhart, I. R. Leith, and R. C. Pink, *Trans. Faraday Soc.*, **65**, 542 (1969).

only at low temperatures, while TCNE^- is stable at 23°.

The dependence of scavenging efficiency on the concentration of scavengers is shown in Figures 5 and 6. $G(\text{TMPD}^+)$ and $G(\text{TPA}^+)$ are constant with respect to amine concentrations from 1 to 120 $\mu\text{mol/g}$. $G(\text{TCNE}^-)$ is approximately proportional to $[\text{TCNE}]$ up to 6 $\mu\text{mol/g}$, above which it plateaus off at a mean value of 6.5. Estimated on the basis of $G(\text{TCNE}^-) = 6.5$ and a total dose of 0.75 Mrad, the concentration of TCNE^- on the Vycor surface would be about 5 $\mu\text{mol/g}$. Thus the low value of $G(\text{TCNE}^-)$ at $[\text{TCNE}] < 6 \mu\text{mol/g}$ is probably due to a depletion of the substrate.

When TPA was irradiated at 77°K, the G value for TPA^+ was 0.76. When the sample was warmed to room temperature, the optical density decreased to a value corresponding to $G = 0.65$.

Discussion

The use of esr to study irradiated solids is very popular, since by its aid detailed information can be obtained with relatively little effort. The present results show that esr is far from telling the whole story. The electron-donating centers available to the scavenger TCNE when this is added to irradiated porous Vycor are entirely independent of, and are about five times more numerous than, the trapped electrons seen by esr, which are presumably located in the bulk solid away from the surface of the pores. The irradiated surface both donates and accepts electrons; it is not clear whether there are two types of centers, which could be regarded as trapped holes and trapped electrons, or whether active centers exist that can either donate or accept electrons, and which could be regarded as trapped excitons. In the latter case, the centers might not be paramagnetic; if they are, their spin resonance absorption must be so broad that it cannot be seen.

Ionization produces electrons and holes throughout the solid, yet when TCNE is present on the surface during irradiation no electrons are trapped in the bulk; all reach the surface. The charges or precursors of the trapped electrons must therefore all diffuse to a distance at least of the order of 30 Å, the characteristic thickness for a solid of area 140 m^2/g and density around 2.5.

The value of $G(\text{TCNE}^-) = 6.5$ gives a lower limit to the electron yield. As the irradiation continues, the rate of formation of active centers decreases (Figure 7), probably because some of the arriving centers neutralize some of those already present. Eventually the number of centers should attain a maximum value, as reported by Rojo and Hentz.^{7a} We did not reach this plateau, but the data of Figure 7 suggest that it might occur at about 10^{18} TPA-active centers per gram. Since the initial yield of TPA^+ is only 10% of that of TCNE^- , this would correspond to a maximum of 10^{19} electron-donating centers per gram, or about 7×10^{12} per cm^2 of surface, or about 40 Å apart, which seems reasonable.

The existence of such centers at the surface undoubtedly causes a great range of distortions in the normal arrangements of the surface atoms. In particular, the published results that irradiated silica surfaces react with CO to yield CO_2^- ^{7b} and with CO_2 to yield O_2^- ⁸ suggest that in a small proportion of the centers an O^- radical ion may be held sufficiently loosely to undergo the reactions $\text{O}^- + \text{CO} = \text{CO}_2^-$ and $\text{O}^- + \text{CO}_2 = \text{CO} + \text{O}_2^-$.

Variations in G value and temperature stability among the various radical ions may be due in part to energetic factors. The ionization potential of TMPD is only 6.6 eV,¹⁵ while that of TPA, though apparently not known exactly, is no doubt higher. The electron-donating centers possess a range of trap depths; many hold their electrons too firmly to react with TMPD^+ , but a larger proportion will give up their electrons to the more strongly attractive TPA^+ , even at 77°K, while the greater thermal activation of room temperature induces a further proportion to undergo neutralization. However, it is reported¹⁴ that perylene and diethylaniline (DEA) have the same ionization potential, 7.1 eV, yet perylene cations remain on the irradiated surface at room temperature, while DEA^+ formed at 77°K is entirely neutralized well below room temperature. This fact probably shows that the electron-donating centers do not move along the surface; if they did, both ions would be neutralized equally readily. Probably the DEA^+ is mobile on the surface and can reach the electron-donating centers, while some of the larger perylene ions are either fixed to points on the surface, or are too large to enter the smaller pores where many of the active centers must be located.

(15) G. Briegleb and T. Czekalla, *Z. Elektrochem.*, **63**, 6 (1959).

Effect of Hydrogen Chemisorption on the Electrical Conductivity of Zinc Oxide Powder

by D. Narayana, V. S. Subrahmanyam, Jagdish Lal, M. Mahmood Ali, and V. Kesavulu

Regional Research Laboratory, Hyderabad-9, India (Received May 20, 1969)

A cell for the simultaneous measurement of chemisorption of gases and the accompanying conductivity changes in solid powders is described. Hydrogen chemisorption and its effect on the conductivity of zinc oxide in the temperature range 30–300° has been studied. Activation of zinc oxide by treatment with hydrogen above 300° is accompanied by an increase in the conductivity of the oxide, which is attributed to excess Zn atoms at the surface. Chemisorption of hydrogen on activated zinc oxide leads to an increase in the conductivity of the oxide throughout the temperature range studied. The donors responsible for the conductivity increase are shown to be H atoms. This form of chemisorption has its maximum around 180°. Below about 100° it occurs as a slow, irreversible process along with another form which occurs rapidly and reversibly without causing any marked change in the conductivity of the oxide. The latter has its maximum at about 50° and appears to be covalently bound to the surface sites which are probably excess Zn atoms formed at the surface by activation. Above 180° a third, un-ionized form of hydrogen chemisorption is superposed on the ionic form. This form reaches its maximum around 230°.

Introduction

Earlier attempts^{1–3} at correlation of chemisorption of hydrogen on zinc oxide with the conductivity changes in the solid involved conductivity measurements on sintered pellets and chemisorption studies on powders. The two sets of results obtained on different samples are not strictly comparable. Since the chemisorptive property of zinc oxide varies very sensitively with the type of pretreatment,⁴ it is necessary to measure both the properties with the same sample under identical conditions. In the present study the two properties were measured simultaneously on a sample of zinc oxide powder, in which form its catalytic activity is maximum.

Since the hydrogenating activity of zinc oxide has been shown to be connected with the capacity of the oxide for hydrogen chemisorption in the low-temperature region (around 50°)⁴ and since it is known that zinc oxide chemisorbs hydrogen in more than one form, it is necessary to distinguish the different forms of hydrogen chemisorption and to determine which of the forms is catalytically active. In this, a simultaneous measurement of chemisorption and conductivity changes can be of much help.

Experimental Section

Apparatus and Procedure. Figure 1 gives a sketch of the conductivity cell used to study chemisorption and conductivity simultaneously. Zinc oxide powder, 0.550 g, was placed between two gold plates (10 mm diam). The weight (55.5 g) enclosed in glass keeps the upper plate pressed against the powder. This arrangement was found to be quite satisfactory as reproducible con-

ductivity measurements could be made and there was no disturbance in the position of the plates during several heating and evacuating procedures. Thin gold wires were spot welded to the plates and to glass-clad tungsten wires sealed to the outer tube. In the annular space between the inner and the outer tubes were placed 5.223 g of zinc oxide so that chemisorption could be studied by conventional methods while measuring conductivity changes. A dibutyl phthalate manometer was used to follow the pressure changes in the system during chemisorption. A Pt—13% Rh—Pt thermocouple placed just below the lower electrode was used to measure the temperature. An electric furnace (noninductive) was used to raise the temperature of the powder. During experiments the temperature was held constant within $\pm 1^\circ$. A conventional high-vacuum system was employed. The resistance values were obtained using an ac bridge with a precision of 1% in the range 1 ohm to 1 megohm at 10 kHz.

Materials. Zinc oxide was prepared by decomposing zinc oxalate in a current of dry oxygen at 420°. X-Ray powder patterns showed the sample to be crystalline. Electrolytic hydrogen was purified by passing over heated platinized asbestos, through silica gel traps, and finally through traps cooled in liquid nitrogen. Helium used for calibration was passed through traps containing activated charcoal cooled in liquid nitrogen.

- (1) Y. Kubokawa and O. Toyama, *J. Phys. Chem.*, **60**, 833 (1956).
- (2) T. S. Nagarjunan, M. V. C. Sastri, and J. C. Kuriacose, *Proc. Natl. Inst. Sci. (India)*, **27A**, 496 (1961).
- (3) A. Cimino, E. Molinari, F. Cramarossa, and G. Ghersini, *J. Catal.*, **1**, 275 (1962).
- (4) V. Kesavulu and H. A. Taylor, *J. Phys. Chem.*, **64**, 1124 (1960).

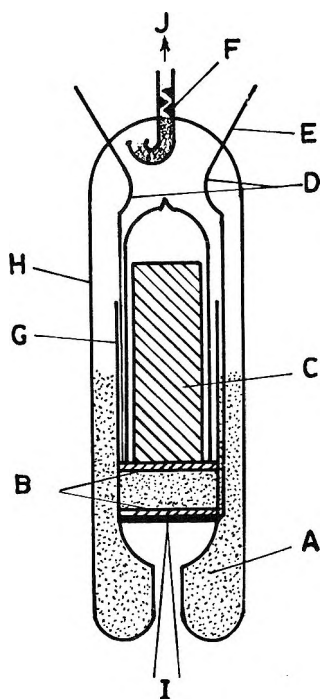


Figure 1. Conductivity cell for measuring simultaneously conductivity and chemisorption on solid powders: A, ZnO powder; B, gold plates (electrodes); C, metal weight enclosed in glass; D, gold wires from the electrodes spot welded to tungsten seals; E, glass-clad tungsten wires; F, glass wool; G, inner tube; H, outer tube; I, Pt-13% Rh-Pt thermocouple; J, connection to vacuum system.

Results and Discussion

It has been shown⁴ that zinc oxide surface undergoes irreversible changes as a result of treatment with hydrogen at elevated temperatures. The capacity of the oxide for hydrogen chemisorption around 50° increases markedly when the oxide is subjected to an activating pretreatment of heating in hydrogen and evacuating above 300°. This enhanced activity for hydrogen chemisorption has been attributed to the formation of excess zinc atoms at the surface by chemical reduction. In the present study, it has been found that at room temperature the fresh, unactivated oxide has a resistance much higher than 10⁶ ohms while the activated sample has a resistance of a few thousand ohms. This shows that the excess zinc atoms formed by activation also act as surface donors causing enhanced conductivity. It may be noted that zinc atoms adsorbed on zinc oxide also behave similarly.⁵

The chemisorption and conductivity measurements reported here have been carried out on activated sample of zinc oxide. Between experiments the oxide was evacuated for 4 hr at 340°.

Figure 2A gives a typical q - T curve (quantity adsorbed vs. temperature) for hydrogen chemisorption on activated zinc oxide. A known volume of hydrogen ($P_0 = 60.15$ mm) was introduced into the cell at 30° and after 0.5 hr the temperature was raised gradually and the

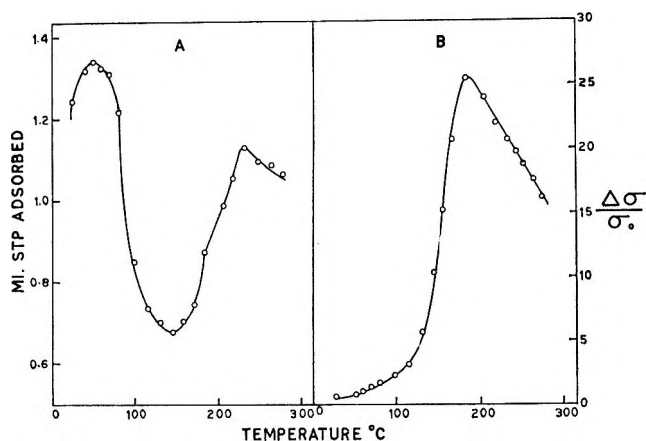


Figure 2. A, q - T curve for hydrogen chemisorption ($P_0 = 60.15$ mm) and B, the accompanying conductivity changes in the oxide.

volume of hydrogen adsorbed was determined as a function of temperature. The conductivity changes observed during chemisorption are plotted in Figure 2B. The two maxima in the chemisorption curve have been attributed to the occurrence of two types of hydrogen chemisorption (types A and B). The first maximum around 50° corresponds to adsorption and desorption on type A sites while the second maximum around 230° refers to a similar process at type B sites. The conductivity curve, on the other hand, does not show the occurrence of two processes. There is a steady increase in conductivity, which appears to parallel a similar increase in the type B chemisorption. In previous studies,¹⁻³ since no conductivity change due to hydrogen was observed below 100°, it was concluded that only type B chemisorption occurring above 100° is responsible for the conductivity increase. However, a comparison of the two curves in Figure 2 shows that this conclusion is not correct. First, there is increase in conductivity throughout the temperature range studied. The failure of the earlier workers to observe any conductivity change below 100° appears to be due to the fact that they used sintered samples having poor chemisorption properties. Secondly, the maximum of the conductivity curve is about 50° below the second maximum of the chemisorption curve, showing that the two maxima do not represent the same process. That this is not due to any variation in the temperature of the sample has been verified. It is seen that the maximum in the conductivity curve at 180° corresponds to the shoulder at the same temperature in the chemisorption curve. Above 180° the conductivity decreases steadily though chemisorption continues to increase (+0.26 ml) up to 230°. It may therefore be inferred that the ionic form of hydrogen chemisorption responsible for the conductivity increase has its maximum at 180° and

(5) D. G. Thomas and J. J. Lander, *J. Phys. Chem. Solids*, 2, 318 (1957).

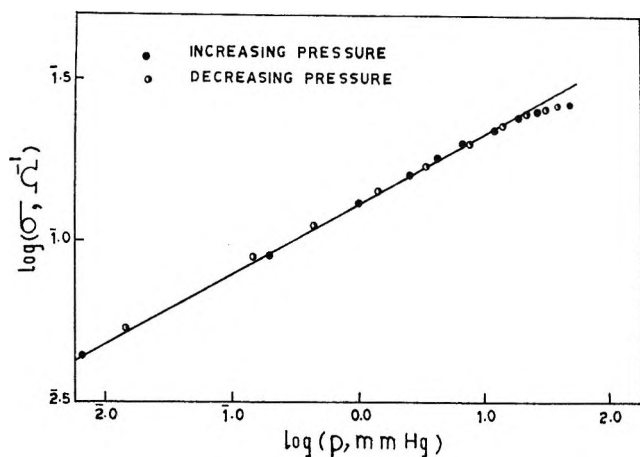


Figure 3. Pressure dependence of conductivity for hydrogen chemisorption at 275°.

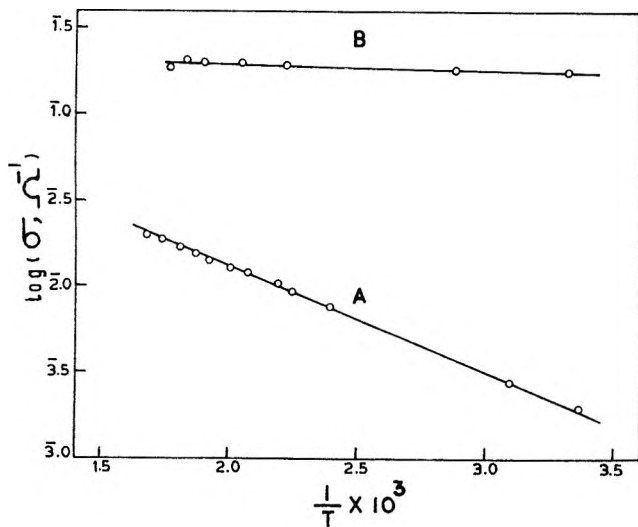


Figure 4. Temperature dependence of conductivity. Measurements were made while cooling the sample. A, activated zinc oxide with bare surface; B, oxide having chemisorbed hydrogen on the surface.

above this temperature a third form of hydrogen chemisorption is superimposed on the ionic form. These two forms appear to be the same as the types A-III and A-IV revealed in the desorption experiments of Narvaez and Taylor.⁶

There has been some difference of opinion as to the nature of the donors responsible for the enhanced conductivity. The donors could be either adsorbed H atoms⁷⁻⁹ or Zn atoms^{5,10} formed as a result of chemical reduction by hydrogen.

Figure 3 gives the pressure dependence of conductivity for hydrogen chemisorption at 275°. The points for both increasing and decreasing pressures fall on the same curve showing rapid establishment of equilibrium. If the donors were zinc atoms formed during adsorption by chemical reduction, then during desorption the conductivity would remain constant at the maximum value and not fall with pressure. The rever-

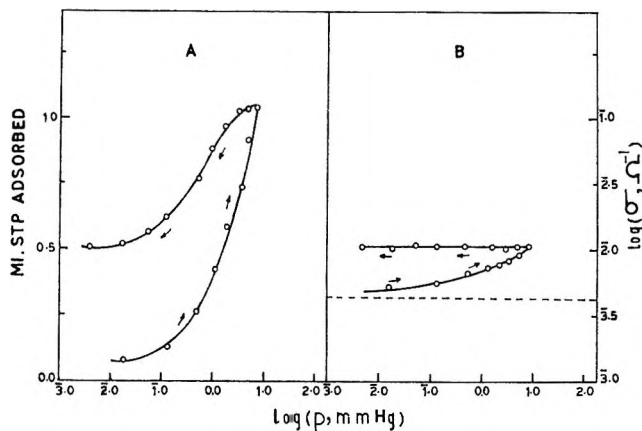


Figure 5. Pressure dependence of chemisorption (A) and conductivity (B) at 50°. The dotted line in B represents the conductivity of the oxide before chemisorption.

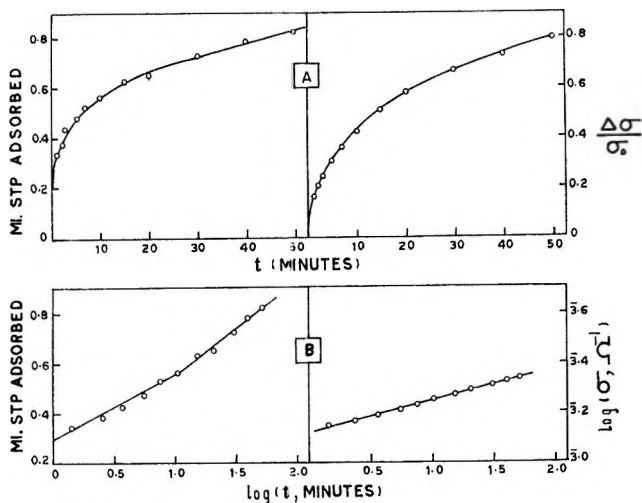
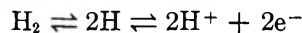


Figure 6. Kinetics of hydrogen chemisorption and conductivity changes at 30°. A, plots of quantity adsorbed vs. time, and relative change in conductivity vs. time. B, plots of $q - \log(t + t_0)$, and $\log \sigma - \log(t + t_0)$ for the same data; $t_0 = 0.5$ min.

sibility noted shows that the donors must be H atoms. The slope of the straight line is close to 1/4, which can be explained by assuming the following equilibrium at the surface



Assuming σ to be proportional to $n = [H^+] = [e^-]$ and applying the law of mass action, it can be shown that

$$\sigma = k[p_{H_2}]^{1/4}$$

At pressures higher than about 10 mm, the points do not fall on the straight line indicating the deviation of

- (6) R. Narvaez and H. A. Taylor, *J. Phys. Chem.*, **69**, 2500 (1965).
- (7) G. Heiland, *Z. Phys.*, **148**, 15 (1957).
- (8) I. A. Myashnikov, *Zh. Fiz. Khim.*, **32**, 841 (1958).
- (9) V. Kesavulu and H. A. Taylor, *J. Phys. Chem.*, **66**, 54 (1962).
- (10) Y. Kubokawa, *Bull. Chem. Soc. Jap.*, **33**, 739 (1960).

the equilibrium from the simple law of mass action. This may be due to the superposition of the third form of chemisorption at these pressures.

The temperature dependence of the conductivity of the oxide before and after hydrogen chemisorption is shown in Figure 4. Curve A refers to the oxide with bare surface and curve B refers to the oxide saturated with hydrogen. The resistance values were obtained while cooling. The energies of activation for the two cases are 0.112 eV and 0.007 eV, which indicate the difference in the nature of the donors responsible for the two conductivities.

Figure 5 shows the pressure dependence of chemisorption and conductivity at 50° at which temperature the type A chemisorption has a maximum. The chemisorption of hydrogen increases with increasing pressure (curve A) and this is accompanied by a slight increase in conductivity (curve B). When the pressure is decreased, only part of the gas is desorbed. During desorption there is no corresponding decrease in the conductivity. Even after evacuation for several minutes at this temperature, the conductivity of the oxide does not change. This shows that at 50° two forms of hydrogen chemisorption take place—one occurring rapidly and reversibly without having any marked effect on the conductivity and the other occurring slowly and irreversibly causing an increase in the conductivity.

Figure 6A gives the time dependence of chemisorption of hydrogen and the accompanying conductivity changes at 30°. These plots appear to indicate a simple connection between chemisorption and conductivity. However, Elovich plots of the same data (Figure 6B) show clearly the difference in the kinetics of chemisorption and conductivity changes. The chemisorption

curve shows the occurrence of two processes while the conductivity curve indicates only one process.

The results given above show that hydrogen chemisorption on zinc oxide is a complex process and involves simultaneous formation of more than one chemisorbed species on the surface. One form with its maximum around 50° does not have any marked effect on the conductivity of the oxide. This occurs rapidly and reversibly below 100° and appears to be covalently bound to the surface sites which are probably excess zinc atoms formed at the surface by "activation." This is accompanied by another form which causes an increase in the conductivity of the oxide. The second form is ionic and involves the dissociation of molecular hydrogen to H atoms which act as surface donors responsible for the enhanced conductivity. The ionic form increases with increase in temperature and reaches its maximum value at about 180°. At this temperature the amount of hydrogen chemisorbed (0.85 ml on 182 m²) corresponds to 2.5×10^{13} atoms per cm². The appearance of the conductivity maximum at this point is understandable since the maximum density of H⁺ ions to be expected^{7,11} at the surface is about 10^{13} cm⁻². Above 180° another form of hydrogen chemisorption is superposed on the ionic form. This third form which reaches its maximum around 230° may be un-ionized H-donors associated with O²⁻ ions.

Acknowledgment. D. N. and J. L. are thankful to the C. S. I. R., New Delhi, for awarding junior and senior research fellowships.

(11) G. Heiland, E. Mollwo, and F. Stockmann, *Solid State Phys.*, **8**, 310 (1959).

Infrared Spectroscopic Study of Carbon Monoxide Adsorption on Hydrogen and Oxygen Treated Silver Surfaces

by George W. Keulks and A. Ravi

The Department of Chemistry and Laboratory for Surface Studies, University of Wisconsin at Milwaukee, Milwaukee, Wisconsin 53201 (Received June 6, 1969)

The adsorption of carbon monoxide on silica and alumina-supported silver samples was studied by employing infrared spectroscopy. At room temperature, a single sharp band was observed at 2180 cm^{-1} with samples which had been pretreated with oxygen at $150\text{--}175^\circ$. Similar pretreatment with hydrogen rendered the samples inactive for the room temperature adsorption of carbon monoxide, as evidenced by the absence of the 2180-cm^{-1} band. The 2180-cm^{-1} band is attributed to the weak, reversible chemisorption of carbon monoxide on surface oxygen ions. No evidence was found for the room temperature chemisorption of carbon monoxide on bare silver metal.

Introduction

In recent years the infrared spectroscopic technique has been employed extensively to obtain information concerning the adsorption of carbon monoxide on a variety of metals as well as metal oxides.^{1,2} However, there have been relatively few studies by this technique of carbon monoxide adsorption on silver.

Kavtaradze and Sokolova³ observed a band at 2180 cm^{-1} for carbon monoxide adsorbed on alumina-supported silver samples that had been reduced with hydrogen. Gardner and Petrucci⁴ observed a band at 2165 cm^{-1} upon admitting carbon monoxide to a silica-supported silver nitrate sample in which the silver nitrate had been partially decomposed *in vacuo* at 250° for 15 min. Admitting hydrogen to this system produced another band at 2099 cm^{-1} .

The goal of this study was to examine in more detail the room temperature adsorption of carbon monoxide on silver samples pretreated with hydrogen and oxygen.

Experimental Section

The cell used in this study was a combination of those designed by Peri⁵ and Little.⁶ Sodium chloride windows were used in all of the experiments and were attached to the cell by an epoxy resin (Torr Seal, Varian Associates).

Samples containing 10% by weight of silver were prepared by impregnating Cab-O-Sil (Cabot Corp., Boston, Mass.) or alumina (γ -alumina, British Drug House) with aqueous silver nitrate using the incipient wetness method. Pressed disks were subsequently prepared from the finely ground powder. The thickness of the samples ranged from 12 to 25 mg/cm^2 .

Heating of the samples in the cell was achieved by means of an electrical heating element attached to the outside of the cell. All of the temperatures reported in this study were measured with a thermometer im-

bedded in the heating element and do not indicate the exact temperature of the samples themselves.

A portable vacuum system incorporating a mercury diffusion pump was used to evacuate the cell. The cold trap attached to the mercury diffusion pump was normally maintained at -78° . The ultimate pressure which could be attained in the cell was 10^{-5} Torr.

Purified gases were stored in 3-l. storage bulbs or small break-seal flasks and were introduced into the cell by means of a conventional gas inlet manifold. Gas pressures were measured by a mercury U-tube manometer attached to the gas inlet manifold.

All of the samples were given a standard initial pretreatment. After a sample was placed in the cell, the cell was evacuated for 30 min. Hydrogen (50–100 Torr) was then introduced into the cell and the temperature slowly increased to $150\text{--}175^\circ$. This temperature was maintained for 2 hr. During this period, the hydrogen was periodically evacuated and replaced. The sample was then cooled to room temperature *in vacuo*. The initial transmission of the hydrogen-treated samples was normally 20–50%.

All of the spectra were obtained at room temperature with a Beckman IR-9 grating spectrometer. The instrument was operated in the double beam mode without any reference cell and had a resolution of 2 cm^{-1} at 2200 cm^{-1} . In order to minimize background water

(1) L. H. Little, "Infrared Spectra of Adsorbed Species," Academic Press, New York, N. Y., 1966.

(2) M. L. Hair, "Infrared Spectroscopy in Surface Chemistry," Marcel Dekker, Inc., New York, N. Y., 1967.

(3) N. N. Kavtaradze and N. P. Sokolova, *Zh. Fiz. Khim.*, **36**, 2804 (1962); *Russ. J. Phys. Chem.*, 1529 (1962).

(4) R. A. Gardner and R. H. Petrucci, *J. Phys. Chem.*, **67**, 1376 (1963).

(5) J. B. Peri, *Discussions Faraday Soc.*, **41**, 121 (1966).

(6) L. H. Little, H. E. Klausner, and C. H. Amberg, *Can. J. Chem.*, **39**, 42 (1961).

vapor and carbon dioxide, the spectrometer was continually purged with a high flow rate of dry air.

Results

Hydrogen Pretreated Samples. The adsorption of carbon monoxide (50–100 Torr) was studied on silica and alumina-supported silver samples which had been pretreated with hydrogen at 150–175° (see Experimental Section). With the silica-supported samples, no new bands were observed in the spectra. With the alumina-supported samples, however, new absorption bands appeared at 1230, 1430, and approximately 1650 cm^{-1} (the 1650- cm^{-1} band fluctuated $\pm 25 \text{ cm}^{-1}$ from sample to sample). These bands remained after evacuating the cell but could not be assigned to the adsorption of carbon monoxide on silver metal. Following the interpretation of Parkyns,⁷ these bands were assigned to carbon dioxide adsorption on the alumina support. Possibly the carbon dioxide is a result of the slow oxidation of carbon monoxide over these samples, or more likely, a result of the adsorption of residual carbon dioxide remaining in the vacuum system, since Dry Ice was used as a coolant on the diffusion pump trap.

Introducing carbon monoxide or carbon dioxide to samples prepared from silica and alumina supports alone produced results similar to those obtained with the supported silver samples. Addition of carbon monoxide to silica produced no new bands, but addition to alumina produced bands at 1230, 1430, and approximately 1650 cm^{-1} . These three bands were also produced when carbon dioxide was added to the alumina, which is consistent with the interpretation given above.

Oxygen Pretreated Samples. Because no room temperature adsorption of carbon monoxide was detected on the samples which had been pretreated at 150° with hydrogen, it was decided to study the adsorption of carbon monoxide on samples pretreated with oxygen. Oxygen pretreatment consisted of heating the hydrogen-treated samples in 50–100 Torr of oxygen at 150° for 2 hr and then degassing them for 30 min. The transmission of the samples was essentially unaffected by the oxygen treatment. Upon admitting 20 Torr of carbon monoxide to an oxygen-pretreated sample, a sharp band of medium intensity appeared immediately at 2180 cm^{-1} (Figure 1). No change in the intensity or the frequency of the band was observed on prolonged contact of the gas with the sample. The intensity of the band increased slightly with an increase in pressure of the carbon monoxide. During evacuation of the cell, the intensity of the band was found to diminish to zero near 1 Torr, thus reflecting the weakness of the adsorption. Upon readmitting 20 Torr of carbon monoxide, however, its intensity returned to its initial value.

With the silica-supported samples which had been pretreated with oxygen, the 2180- cm^{-1} band was the only new band observed when carbon monoxide was in-

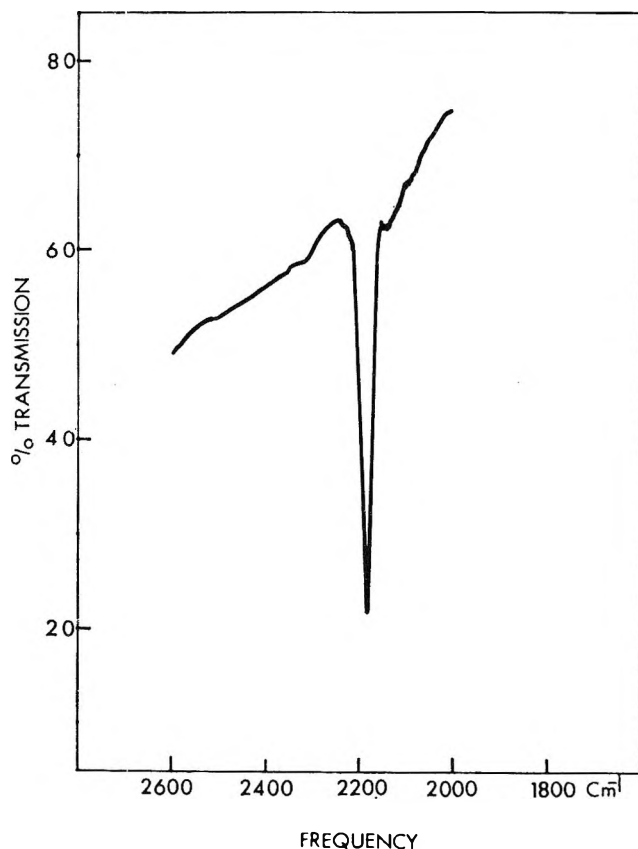


Figure 1. Infrared spectrum of 20 Torr of carbon monoxide adsorbed on alumina-supported silver at room temperature. The sample had been treated with hydrogen at 150° and then exposed to oxygen at 100° before the introduction of the carbon monoxide.

troduced. With the alumina-supported samples, the 2180- cm^{-1} band was observed, but the bands observed earlier with the hydrogen-pretreated samples (1230, 1430, 1650 cm^{-1}) were also observed. As indicated earlier, the latter bands are assigned to adsorbed carbon dioxide on the alumina support.

After exposing the oxygen pretreated samples to 50–100 Torr of hydrogen at 150°, carbon monoxide could not be adsorbed, as evidenced by the absence of the 2180- cm^{-1} band. Subsequent treatment with 50–100 Torr of oxygen at 150° again rendered the samples active for the adsorption of carbon monoxide. This sequence could be carried out many times. In every case, when the samples had been exposed to oxygen at 150°, the 2180- cm^{-1} band was observed when carbon monoxide was introduced into the cell. In every case, when the samples had been exposed to hydrogen at 150°, the 2180- cm^{-1} band was not observed.

The 2180- cm^{-1} band observed with the oxygen pretreated samples is not affected by subsequent addition of hydrogen or oxygen at room temperature. Large pressures (up to 100 Torr) of hydrogen or oxygen neither reduced nor enhanced the intensity of the 2180- cm^{-1}

(7) N. D. Parkyns, *J. Chem. Soc., A*, 1910 (1967).

band nor shifted its frequency. The addition of carbon dioxide prior to the introduction of carbon monoxide did not affect the appearance of the 2180-cm⁻¹ band. It was also observed that the samples had to be heated in oxygen in order to produce the 2180-cm⁻¹ band. Pretreatment of the hydrogen-treated samples with 50 Torr of oxygen at room temperature did not render the samples active to carbon monoxide adsorption. However, if the samples were heated above 100° in oxygen, the 2180-cm⁻¹ band was observed when 20 Torr of carbon monoxide was introduced into the cell.

When a mixture of 50 Torr of carbon monoxide and 50 Torr of oxygen was introduced into the cell containing a hydrogen-pretreated silica-supported silver sample, no new bands were observed that could be assigned to carbon monoxide adsorption. After heating the mixture at 100° for 30 min, a very weak band at 2162 cm⁻¹ appeared, but no detectable amount (by ir) of gas-phase carbon dioxide was observed. Further heating to 150° caused both the 2162-cm⁻¹ band and the gas-phase carbon dioxide bands to increase considerably. Even though the oxidation of the carbon monoxide to carbon dioxide predominated, the band at 2162 cm⁻¹ may be due to the adsorption of the carbon monoxide on oxygen-covered silver. At the present time, there is no explanation why the band appeared at 2162 cm⁻¹ instead of at 2180 cm⁻¹. It should be noted, though, that a similar observation was recently reported by Yates⁸ for the oxidation of carbon monoxide on gold surfaces.

The dissociation pressure of oxygen from Ag₂O is approximately 200 Torr at 150°. Since the silver samples were never exposed to a partial pressure of oxygen greater than 100 Torr, it is reasonable to assume that the silver in the samples was not converted to bulk silver oxide. However, in order to further minimize the possibility of bulk silver oxide formation, several samples were exposed to oxygen partial pressures of less than 100 Torr. After the initial hydrogen pretreatment, the samples were exposed to 2–5 Torr of oxygen at 150° for 2 hr, and the cell was then evacuated. Upon admitting 20 Torr of carbon monoxide to the cell, the 2180-cm⁻¹ band was immediately observed. Its intensity and behavior were similar to those observed with the higher pressures of oxygen.

Because the 2180-cm⁻¹ band was only observed when carbon monoxide was adsorbed on samples which had been treated with oxygen, several experiments utilizing isotopes were conducted with the aim of elucidating the structure of the surface species. In order to eliminate any outside possibility that the 2180-cm⁻¹ band did not involve the CO molecule, a mixture (10 Torr) of 60% ¹³CO and 40% ¹²CO was introduced into the cell. Using a hydrogen-pretreated sample, no new bands were observed. After a subsequent oxygen pretreatment, two bands at 2180 and 2130 cm⁻¹ were observed. The 2130-cm⁻¹ band occurs at the frequency expected for the shift due to the carbon-13 isotope.

It seemed reasonable that the 2180-cm⁻¹ band was due to the C–O stretching frequency of the carbon monoxide molecule and not due to a stretching frequency involving oxygen attached to silver. In order to confirm this assignment, a hydrogen-pretreated sample was exposed to 15 Torr of oxygen-18 (99.3 atom % ¹⁸O, 0.3 atom % ¹⁷O) at 150° for 2 hr. After evacuation, 20 Torr of carbon monoxide was added. Immediately, a single band at 2180 cm⁻¹ was observed. No change in the intensity or the frequency of this band was observed on prolonged contact of the gas with the sample, nor did any additional bands develop.

Discussion

The results of this work indicate that carbon monoxide does not adsorb at room temperature on bare silver metal. In each case, when the samples had been pretreated with hydrogen, no new bands were observed which could be assigned to carbon monoxide adsorption. The observation of the 2180-cm⁻¹ band by Kavtaradze and Sokolova³ with hydrogen-pretreated samples is still confusing. Several samples were prepared according to their reported procedure, but with none of them was the 2180-cm⁻¹ band observed. The studies by Guerra⁹ and Yates⁸ on copper and gold, however, suggest that their samples may not have been completely reduced. Possibly their silver samples, too, were contaminated with oxygen.

The 2165-cm⁻¹ band observed by Gardner and Petrucci⁴ with a silica-silver nitrate sample partially decomposed at 250° is also probably due to carbon monoxide adsorption on a sample contaminated with oxygen. In fact, Gardner¹⁰ recently has indicated that the partially decomposed samples produce a mixture of silver nitrate and silver oxide, and not silver metal.

The experiments with isotopes on the oxygen-pretreated samples indicate that the 2180-cm⁻¹ band is definitely due to a vibration involving the carbon and oxygen atoms of the carbon monoxide molecule. It cannot be due to a C–O vibration involving the oxygen attached to silver. If this had been the case, there should have been a shift in the 2180-cm⁻¹ band when the silver sample was pretreated with oxygen-18. As indicated earlier, on the sample pretreated with 15 Torr of 99.3 atom % oxygen-18, the band still was observed at 2180 cm⁻¹ when the sample was exposed to carbon monoxide.

Because the oxygen pressure in the cell was always below the oxygen dissociation pressure of Ag₂O, it does not seem reasonable that the 2180-cm⁻¹ band is due to carbon monoxide adsorption on bulk oxide ions. The experiments at oxygen pressures of less than 10 Torr are especially important. The work of Mallmann¹¹ on

(8) D. J. C. Yates, *J. Colloid Interfac. Sci.*, **29**, 194 (1969).

(9) C. R. Guerra, *ibid.*, **29**, 229 (1969).

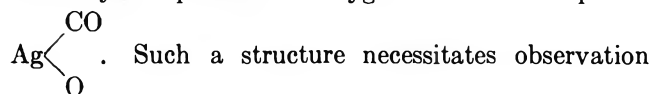
(10) R. A. Gardner, Preprints, Fourth International Congress of Catalysis, Moscow, 1968.

evaporated silver films tends to confirm this belief. He used evaporated silver films which had been exposed to high pressures of oxygen (up to 1 atm) and was specifically trying to detect the Ag-O stretching frequency (near 550 cm^{-1}) of silver oxide. None of his samples which had been treated with oxygen produced this band.

If it can be assumed that bulk oxide ions are not present or, at least, that their concentration is very small, the results of other workers¹²⁻¹⁶ indicate that in the temperature range $150\text{--}175^\circ$ oxygen chemisorption most likely produces several forms of adsorbed oxygen. Czanderna¹⁶ indicates that the most predominant form is likely to be O_2^- ions with some fraction of O^- ions a definite possibility. It is important to note that treatment of the reduced samples with oxygen at room temperature did not give rise to the 2180-cm^{-1} band when carbon monoxide was introduced. It was necessary to heat the samples in oxygen at higher temperatures before the 2180-cm^{-1} band was observed. The ionic forms of chemisorbed oxygen are only formed at elevated temperatures.¹⁶

Because of the weak nature of the carbon monoxide adsorption and because the oxygen is likely to be chemisorbed as ions, we prefer to assign the 2180-cm^{-1} band to the C-O stretching frequency of a surface species resulting from the weak chemisorption (ion-dipole

interaction) of carbon monoxide on oxygen ions adsorbed on the silver surface. It cannot be explained by a high-frequency shift of carbon monoxide attached to silver by the presence of oxygen to form the species



of a band corresponding to carbon monoxide adsorbed on silver metal at lower frequencies. On the hydrogen-pretreated samples, which should contain bare silver metal, no such band was observed in our experiments.

Acknowledgment. We gratefully acknowledge the benefit derived from stimulating discussions with Professors Paul H. Emmett and Robert G. Greenler. We also acknowledge the financial support in the form of a postdoctoral fellowship for A. Ravi from the National Science Foundation.

- (11) A. J. Mallmann, M.S. Thesis, University of Wisconsin at Milwaukee, Milwaukee, Wisconsin, 1968.
- (12) A. F. Benton and L. C. Drake, *J. Amer. Chem. Soc.*, **56**, 255 (1934).
- (13) W. W. Smeltzer, *Can. J. Chem.*, **34**, 1046 (1956).
- (14) G. H. Twigg, *Trans. Faraday Soc.*, **42**, 284 (1946).
- (15) L. Ya. Margolis, *Advan. Catalysis*, **14**, 451 (1963).
- (16) A. W. Czanderna, *J. Phys. Chem.*, **68**, 2765 (1964).

Magnetic Resonance Studies of Aromatic Hydrocarbons Adsorbed on Silica-Alumina. III. Chemical Exchange Effects

by G. M. Muha

University College, Rutgers—The State University of New Jersey, New Brunswick, New Jersey 08903
(Received August 7, 1969)

A combination of electron spin resonance (esr) and nuclear magnetic resonance (nmr) spectroscopy is used to follow the chemical exchange processes involved in the transfer of a surface hydrogen to adsorbed anthracene radical cations. The method used involves the "labeling" of the aromatic molecule at the acid surface site with deuterium and then comparing the time of appearance of deuterium effects in the nmr and esr spectra. Isotopic exchange effects are first observed in the nmr spectrum, then after a time delay dependent on the aromatic concentration, esr effects are also observed. This result demonstrates the difference in the rates of isotopic exchange for the weakly adsorbed neutral molecules and the more strongly adsorbed radical cations and hence is consistent with the hypothesis offered in a previous paper in this series concerning the pathway for the transfer of hydrogen atoms from the surface to the adsorbed molecule. The success of the experimental method reported here is thought to arise because of the hindered diffusion of the adsorbed aromatic ions due to the relative immobility of the surface counterion. Hence the method may be generally applicable to the study of problems in heterogeneous catalysis.

In the two previous papers in this series,^{1,2} hereafter referred to as I and II, an analysis was presented of the electron spin resonance (esr) spectrum of perylene and anthracene adsorbed on silica-alumina. With both systems it was found that the larger proton hyperfine coupling constants differed from the values observed when the radical cations are generated with sulfuric acid. This result, coupled with an analysis of the line width variations, suggested the presence of an ion pair. In the case of anthracene, an analysis of the exchange effects as a function of aromatic concentration showed that the radical cation is formed first, then after a relatively long interval of time, isotopic exchange with surface protons occurs.

To explain the exchange results, a hypothesis was developed² that involved the transfer of a proton from the surface to a neutral molecule, presumably through a carbonium ion intermediate, with the subsequent conversion of this neutral molecule to a radical cation by an electron exchange process. With the esr technique used, only paramagnetic species could be directly observed. Hence confirmation of the hypothesis was not possible.

In the present work, a combination of the nuclear magnetic resonance (nmr) and esr techniques are used to follow the isotopic exchange processes as functions of time and aromatic concentration. As will be seen, this approach demonstrates clearly the difference in the rates of isotopic exchange between the weakly adsorbed neutral molecules and the more strongly adsorbed radical cation. This latter point is of particular interest in the theory of the surface action of this catalyst.³

The success of the technique used here is thought to arise because of the difference in the diffusion rates of

the various molecular species involved. These differences are expected to be accentuated on a catalyst surface when charged species are involved in ion-pair formation with a relatively *immobile* surface site acting as the counterion. In essence, the method used involves the "labeling" of the molecule with deuterium at the carbonium ion site and then comparing the time of appearance of deuterium effects in the nmr and esr spectra. Since isotopic exchange processes are usually diffusion controlled,⁴ and since diffusion on a surface may be quite slow under some conditions,⁵ one might expect that this magnetic resonance approach may be of general applicability in the study of heterogeneous systems, and hence deserves further consideration in this respect. A limited number of studies⁶ on other types of catalyst has thus far shown this expectation to be true.

Results

The esr and nmr spectra obtained from samples with varying concentrations of anthracene in contact with a silica-alumina catalyst are shown in Figure 1. These spectra were recorded with standard Varian esr and nmr spectrometers. The nmr spectra were calibrated by using a coaxial cell, the inner tube of which contained

(1) G. M. Muha, *J. Phys. Chem.*, **71**, 633 (1967).

(2) G. M. Muha, *ibid.*, **71**, 640 (1967).

(3) For example, see the summary of arguments pertaining to the various aspects of this question given by A. E. Hirschler, *J. Catal.*, **5**, 390 (1966), and W. K. Hall and R. P. Porter, *ibid.*, **5**, 544 (1966).

(4) V. Gold in "Friedel-Crafts and Related Reactions," Vol. II, Part II, G. A. Olah, Ed., Interscience Publishers, Inc., New York, N. Y., 1964, p 1253.

(5) J. H. DeBoer, "The Dynamical Character of Adsorption," Oxford University Press, London, 1953, Chapter VI.

(6) G. M. Muha, unpublished results.

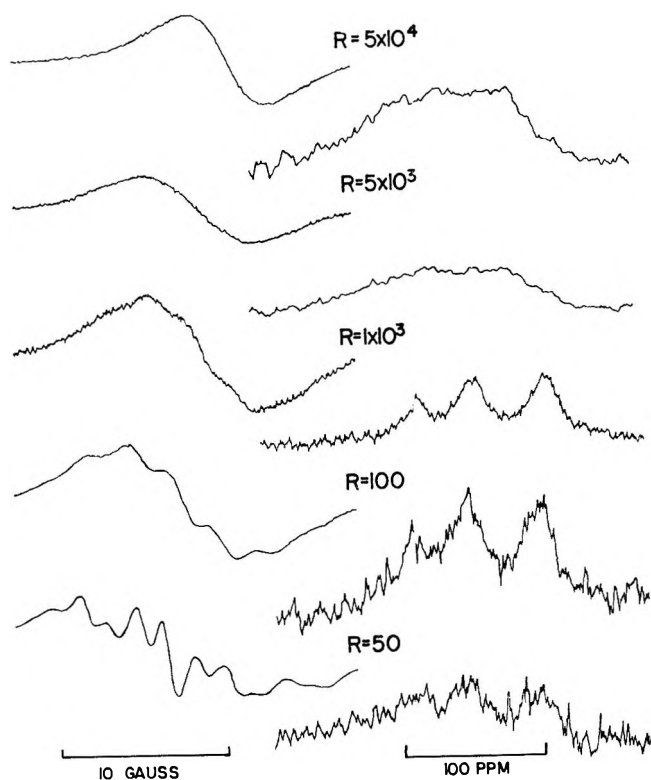


Figure 1. Typical resolution obtained in the X-band esr spectra (left column) and the corresponding 100 MHz nmr spectra (right column) as a function of the concentration ratio R . The spectrometer power level and amplifier gain vary among the different spectra, hence sensitivities are not directly comparable.

tetramethylsilane (TMS). The catalyst and aromatic solutions were prepared as described previously.¹ Carbon disulfide was used as a solvent for all work reported here.

The aromatic hydrocarbon concentration is reported in terms of the ratio (R) of the number of diamagnetic species (D) to numbers of paramagnetic radical cations (P) normalized to a unit weight of catalyst. This variable was chosen because in the concentration range used, the catalyst is saturated in its radical generating capacity² and hence $P = 1.8 \times 10^{17}$ spins/g. This value of P was determined in an independent experiment using standard techniques.^{1,7}

At the two highest values of R that are shown in Figure 1, both electron-exchange narrowing in the esr spectrum and line broadening in the nmr spectrum are evident. These line-width effects are diminished at the lower three concentrations; indeed as discussed below, the nmr line widths are essentially constant provided that electron-exchange narrowing is absent in the esr spectrum.

It is easily demonstrated that the nmr spectra shown in Figure 1 arise from molecules at the surface rather than in the bulk of solution by adjusting the insertion depth of the sample tube into the receiver coil. Thus the spectrum from either the catalyst slurry (which set-

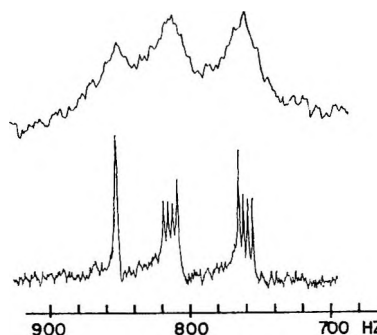


Figure 2. 100-MHz spectrum of anthracene adsorbed on the catalyst (top) and in the supernatant liquid (bottom). The two spectra are obtained on the same sample by adjusting the depth of insertion of the sample tube into the receiver coil. Relative sensitivities cannot be judged directly from these spectra, for the rf power and amplifier gain vary for the two cases.

tles to the bottom portion of the tube) or the supernatant liquid can be recorded. The results (Figure 2) are so markedly different that there can be little doubt that the contribution from aromatic molecules in the bulk solution phase makes a negligible contribution to the nmr spectra shown in Figure 1.

This same technique of manipulating the insertion depth of the sample tube allows a measurement of the relative integrated nmr intensities of the adsorbed and solution phases by comparison with a signal from a cyclohexane reference included in the TMS capillary. Thus it is found that if electron-exchange effects are absent in the esr spectrum, the intensity of the signal from the adsorbed phase is roughly proportional to that from the solution phase, the proportionality constant being of the order of 0.1.^{8,9}

The loss of resolution in the nmr spectrum (Figure 1) is a reversible phenomenon in the sense that varying the value of R for a given sample (*e.g.*, by adding solid aromatic or decanting the supernatant liquid and replacing it with a solution of lower aromatic concentration) causes the spectrum to change in the expected fashion. Thus in this respect, these nmr results parallel a similar reversible behavior observed in the esr spectrum.²

Before discussing the spectra obtained when deuterated samples are used, it is useful to summarize certain

(7) The actual weight of the catalyst used is chosen between 0.1 g and 0.3 g depending on the desired radical concentration. The concentration of the diamagnetic species is then adjusted by varying the volume (usually 1.00 ml) and the molarity of the aromatic solution ($5 \times 10^{-3} M$ to 1 M). The choice of weight and volume are not entirely independent for the resulting mass must fit into a coaxial nmr sample tube.

(8) The nature of the present work does not require high accuracy in the measurement of this constant and only an approximate value is quoted. However, by using precision-bore coaxial cells and taking sufficient care in experimental technique (particularly with regard to saturation), the nmr method could be conveniently expanded to measure adsorption isotherms of single or multicomponent solution-solid systems. In this connection, see further remarks in the next footnote reference.

(9) G. M. Muha and D. J. C. Yates, *J. Chem. Phys.*, 49, 5073 (1968).

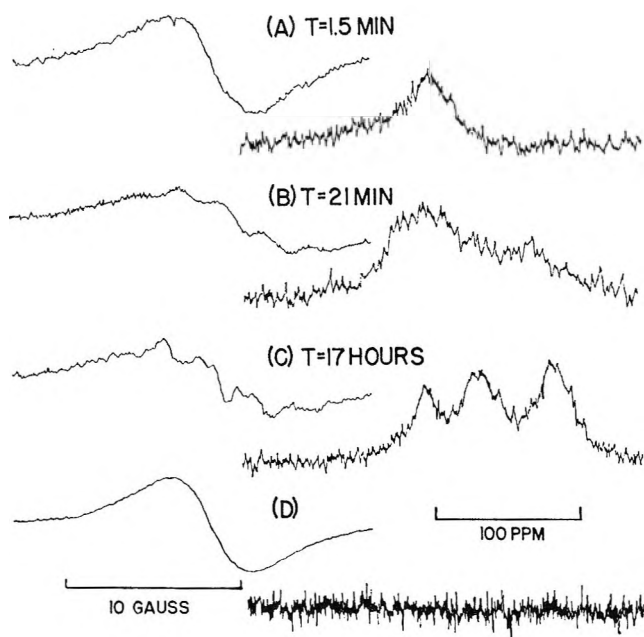


Figure 3. Time development of the X-band esr spectrum (left column) and corresponding 100-MHz nmr spectrum (right column) for perdeuterioanthracene adsorbed on silica-alumina with $R = 260$. The first proton effects are observed within 1.5 min in the nmr spectrum (A) but not for 3.5 min in the esr spectrum (see text). The bottom spectrum (D) is the typical result obtained in a control experiment using a deuterated surface as well as perdeuterioanthracene in the sample preparation.

of the results reported in II. Specifically, it was shown that (a) isotopic exchange effects are not a part of radical cation formation, (b) the source of hydrogen involved in the chemical exchange is the silica-alumina surface, and (c) there is no direct exchange interaction between the carbonium ion and the radical cation. These three results suggest the form of the experiment to be undertaken and are necessary in developing an understanding of the results obtained.

If perdeuterioanthracene is used as a starting material, it is possible to follow the appearance of hydrogen in the nmr spectrum and compare this result with the length of time required for the appearance of proton hyperfine structure in the esr spectrum of the radical cation. A typical spectrum obtained using this approach is shown in Figure 3A. Note that the fact that a proton nmr spectrum is observed necessarily implies that by some mechanism, a hydrogen has been exchanged between the surface and a neutral molecule; the absence of any corresponding hyperfine structure in the esr spectrum implies that the exchange reaction involving the radical cation has not yet occurred and hence must proceed at a slower rate than that involving the neutral molecules.¹⁰

To eliminate the possibility that the proton spectrum may arise directly from the surface proton or from an impurity, a control experiment using a deuterated surface as well as perdeuterioanthracene was run. The

absence of any nmr spectrum in this case (Figure 3D) demonstrates the correctness of the assertions in the preceding paragraph as well as furnishing a second independent proof that the source of hydrogen for isotopic exchange is the silica-alumina surface.

It is possible to verify these results by starting with a deuterated surface,² adding anthracene, $C_{14}H_{10}$, and observing the disappearance of proton effects in the esr and nmr spectra. Such experiments were carried out and the expected results were obtained. However, the spectra obtained in this case are quite complicated and hence more troublesome to assign.¹¹

By waiting a sufficient length of time, the proton hyperfine effects are, of course, observed in the esr spectrum provided that R is low enough so that electron exchange effects do not interfere with the spectral resolution. If electron exchange effects dominate, no definite statement can be made concerning the relative chemical exchange rates.

The time development of the isotopic exchange is shown in Figure 3C which corresponds to a rerun, 17 hr later, of the sample used to obtain Figure 3A. The general appearance of both the esr and nmr spectra suggest that complete protodeuteration has occurred. However, the integrated area in the nmr spectrum indicates an average composition of approximately $C_{14}H_8D_2$; hence, the exchange is not complete. Since the deuterium is expected to be statistically distributed among the various ring positions, the overall effect on the nmr and esr spectra is small and hence easily overlooked upon cursory examination.¹²

The failure to obtain isotopic exchange in the nmr spectrum is understandable in terms of the stoichiometry of the system.¹² For the sample size used, the total available surface hydrogen is $\sim 10^{20}$ atoms. A total of 5×10^{18} aromatic species are present; hence 5×10^{19} hydrogen atoms are required for complete chemical exchange. Since a distribution in deuterium among the various species and surface sites is expected, complete chemical exchange is not possible.

It has not been possible to make quantitative measurements of the chemical exchange rates in the experiments described, for even in the most favorable cases,

(10) At the value of R for this particular experiment, the esr spectrum is expected to show a hyperfine triplet if nmr and esr exchange effects were observed simultaneously. For the expected spectrum and further discussion see II, especially Figure 5.

(11) For an example of a typical esr spectrum obtained, see Figure 2e in II.

(12) W. K. Hall in a private communication to the author (1967) noted that, based on stoichiometric considerations, some of the conclusions in II concerning the complete isotopic exchange of the radical cation must necessarily be incorrect. The experimental technique used by the author to establish the conclusion was difficult (see footnote 24 in II) and certainly contributed to the error; also failure to pay sufficient attention to small observable difference in the esr spectra was a contributing factor. The present result bears out the contention by Hall. Hence the conclusion in II concerning the completeness of isotopic exchange requires revision. This partial invalidation does not affect any of the other conclusions in the paper.

the first steps in the isotopic exchange are completed within 2 or 3 min after the sample is prepared. An appreciable fraction of this time is required to lock the spectrometer mode of operation and to sweep through the spectrum.

Discussion

The most important result obtained from the present work arises from the demonstration that the neutral molecules undergo isotopic exchange more rapidly than radical cations. This result is consistent with the hypotheses offered in II concerning a carbonium ion as a kinetic intermediate in the isotopic exchange process, but clearly does not constitute a proof. Questions concerning the sensitivity of the detection scheme used and the complications introduced by surface diffusion effects render definite conclusions concerning precise details of the kinetic mechanism involved too hazardous.¹³ Also a mechanism based on electron-accepting acidic sites¹⁴ could be suggested.¹³ Hence, further consideration of the difference between one-electron and two-electron transfer reaction on the silica-alumina surface¹⁵ is not warranted at this time.¹³ Nevertheless, the *net effect* of the various exchanges processes involved is clear.

The overall process involved is depicted in Figure 4. In this diagram, dotted lines indicate interaction specifically ruled out by experimental evidence; solid lines indicate the overall pathway for hydrogen transfer from the surface to the radical cation. The diagram is not meant to imply a mechanism in the kinetic sense, for the magnetic resonance technique, as practiced here, only permits observation of the relative long-lived species present.

In this figure, the step involving the carbonium ion has not been directly observed by a magnetic resonance method. The evidence for the inclusion of this step² rests upon a wide range of chemical studies of acidic systems,^{4,16} including silica-alumina.¹⁷ The presence of the carbonium ion on silica-alumina has, of course, been directly verified by optical spectroscopy;¹⁸ the inability to observe the species in the present nmr work¹⁹ presumably arises because the line is too broad (*e.g.*, due to a short lifetime) or may be obscured by other more intense lines due to the adsorbed neutral molecules.

The possibility of observing different exchange rates with radical cations and neutral molecules may arise because the isotopic exchange phenomena is a diffusion-controlled process.⁴ In a homogeneous system, the exchange rates are expected to be much faster since mutual diffusion of the two species involved is possible. On a catalyst surface a slower rate is expected since the charged species are restricted to the vicinity of the surface where the immobile counterion is located. Hence isotopic exchange in this case necessarily involves diffusion to and from the surface or across the surface by the neutral molecules.

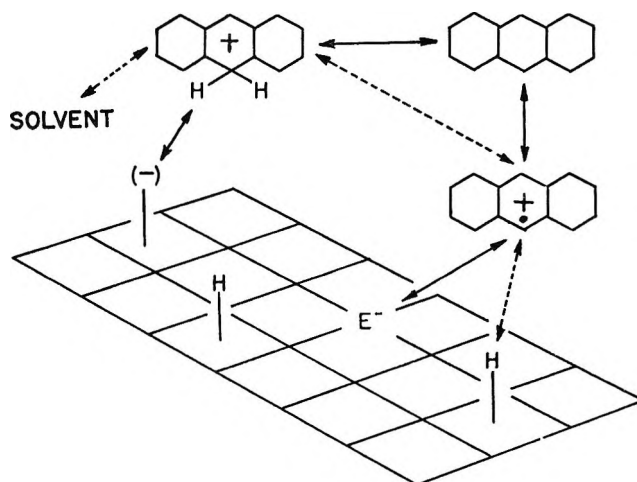


Figure 4. Diagram illustrating the pathway for transfer of surface hydrogen to the anthracene radical cation. The symbol (-) represents the conjugate base of the acid surface site; the symbol E^- represents the electrophilic surface site. Dotted lines indicate interactions specifically ruled out by experimental evidence. For clarity, dotted lines between the solvent and the neutral and paramagnetic species are omitted.

In this connection, simple calculations are quite instructive concerning the state of affairs on the surface. The silica-alumina catalyst used has a surface area of $\sim 300 \text{ m}^2/\text{g}$. If the radical cations are uniformly distributed over the surface, the interradsical distance is $\sim 400 \text{ \AA}$. There is no evidence of spin exchange,² hence these sites are independent. From the concentration data included in Figure 1, and assuming the specific area²⁰ of an anthracene molecule is 54 \AA^2 , the intermolecular distance corresponding to the onset of electron exchange is $\sim 8 \text{ \AA}$, if it is assumed that all the diamagnetic molecules are adsorbed on the surface. However, as noted in connection with Figure 2, only approximately 10% are adsorbed; hence the corresponding intermolecular distance is $\sim 26 \text{ \AA}$. For comparison, consider a homogeneous system involving free radicals in solution. In this case, to avoid electron exchange effects, solution concentrations of the order of $10^{-3} M$ or less are usually used, a concentration which corresponds

(13) The writer is indebted to the reviewers of the original version of the manuscript for helpful criticisms and suggestions in this regard.

(14) A. E. Hirschler, *J. Catal.*, **5**, 196 (1966).

(15) B. D. Flockhart and R. C. Pink, *ibid.*, **8**, 293 (1967).

(16) A. I. Shatenshtein, "Isotopic Exchange and the Replacement of Hydrogen in Organic Compounds," Consultants Bureau, New York, N. Y., 1962, Chapter 2.

(17) Cf. H. H. Voge in "Catalysis," Vol. 6. P. P. Emmett, Ed., Reinhold Publishing Corp., New York, N. Y., 1958, p 407.

(18) W. K. Hall, *J. Catal.*, **1**, 53 (1962); D. M. Brouwer, *ibid.*, **1**, 372 (1962).

(19) For example of typical nmr spectra of carbonium ions see: C. Mac Lean, J. H. van der Waals, and E. L. Mackor, *Mol. Phys.*, **1**, 247 (1958); H. H. Perhampus and E. Baumgarten, *Angew. Chem.*, **3**, 776 (1964).

(20) Value estimated from bond angles and bond distances; see A. I. Kitagorodskii, "Organic Chemical Crystallography," Consultants Bureau, New York, N. Y., 1961, p 420.

to an interradical distance of 22 Å. By analogy with the solution case then, a diffusion-controlled situation in the case of silica-alumina is consistent with the concentrations involved.

The observed nmr line width dependence also supports this explanation. As seen in Figure 1, the line widths are essentially constant when electron exchange effects are absent. T_2 is of the order of 20 msec, a value comparable to that found for olefins⁹ and aromatic hydrocarbons²¹ adsorbed on other types of surfaces on which paramagnetic species are not present. Hence it can be argued that at low values of R , the adsorbed species are sufficiently far apart so that any contribution to T_2 in the nmr spectrum due to the presence of paramagnetic cations is negligible compared to that due to the interaction between the molecule and the surface. When electron exchange effects dominate, the situation becomes more complicated, for then an additional contribution to T_2 dependent on surface coverage is also observed.^{6, 21, 22}

The argument offered in the preceding paragraph would only be valid if the line-width effects that are observed are reversible with changes in the aromatic concentration. This reversible behavior has been noted in the preceding section.

The observed difference in the isotopic exchange rate for the radical cations and the neutral molecules also explains an observation in II that was not previously understood. Namely, in the protodeuteration of the radical cation, it is found that the first hyperfine effects observed in the esr spectrum always corresponds to the exchange of two hydrogens into the ring.¹⁰ Based on the evidence presented above, the explanation simply requires that, at the concentrations used in the experiment, the differences in the isotopic exchange rates are such that both *meso* positions in the neutral molecules are exchanged before the first interaction (*i.e.*, electron exchange) between the radical cation and the neutral molecule.

We have at present no explanation as to why the diffusion processes involving radical cations are slower than those involving carbonium ions. Since isotopic exchange involves the net transfer of an electron in one

case and a proton in the other, no serious kinetic barriers are expected. The observed difference in behavior may reflect some peculiarity of the surface site involved, *e.g.*, the redox site may be less accessible than the acid site. Clearly, further information on the nature of the counterion involved and a direct means of observing the carbonium ion reactions are necessary before further comment on this question is possible.

In this connection, we have expended considerable effort in this laboratory in the study of the adsorption of 9,10-dihydroanthracene on silica-alumina. The particular interest in this compound arises because in the neutral molecule both sites for the formation of a stable carbonium ion are initially blocked, while to form the oxidized product (which is the anthracene radical cation²) two hydrogen atoms must be rejected to the surface or to other chemical species present. Thus the formation of either the carbonium ion or the radical involves the net transfer of at least one hydrogen.

Unfortunately, in the work to date, neither the esr² nor the nmr spectrum⁶ has proved illuminating. Since the system turns an orange color upon addition of the hydrocarbon to the catalyst, while under similar circumstances the addition of anthracene results in a green color, a study using optical spectroscopy may be useful. This experimental approach has not been undertaken.

Finally, we note that the magnetic resonance technique offers a method for measuring the rate constants for the exchange reactions involved as well as a means (in favorable cases) of identifying the reaction intermediates.²³ To accomplish this however, will require improvements in sample handling techniques and instrumentation. We are attempting to pursue this approach at present.

Acknowledgment. This work was supported in part by a grant from the Rutgers Research Council.

(21) J. H. Pickett and L. B. Rogers, *Anal. Chem.*, **39**, 1872 (1967); D. E. Woessner, *J. Chem. Phys.*, **39**, 2783 (1963).

(22) G. Karagounis, *Nature*, **201**, 604 (1964).

(23) Cf. E. De Boer and H. Van Willigen in "Progress in NMR Spectroscopy," Vol. 2, J. W. Embley, J. Feeney, and L. H. Sutcliffe, Ed., Pergamon Press, Long Island City, N. Y., 1967, p 111.

Interactions between Surface Hydroxyl Groups and Adsorbed Molecules. I. The Thermodynamics of Benzene Adsorption

by J. A. Cusumano and M. J. D. Low

Department of Chemistry, New York University, New York, New York 10458 (Received January 20, 1969)

Isotherms of benzene adsorption on porous glass were measured with a recording vacuum microbalance. Heats of adsorption and entropies derived from the data were compared with theoretical values computed for mobile and immobile adsorption. The thermodynamic considerations suggest a model for which benzene molecules are localized and quite strongly bound at low degrees of coverage. The benzene molecules become mobile as the coverage is increased, the adsorbed benzene molecule lying flat with the plane of the ring parallel to the surface and rotating freely in the ring plane. Filling of the micropore structure begins at $\theta \approx 0.6$, increasing interaction between adsorbate molecules hindering some of the motion of adsorbed benzene.

Introduction

It is widely recognized that hydroxyl groups play an important role in determining the properties of silica surfaces, and consequently much work has been done to characterize the nature, number, and distribution of the hydroxyl groups themselves.¹⁻³ Gas adsorption studies have had a prominent role in such work, partly because in recent years it has been possible to obtain direct information not only about the amount and rate of gas take-up *per se*, but also about the influence of adsorbate and adsorbent upon each other. The adsorption of cyclic aromatics would appear to be of special interest for this purpose because the π -electron density, and hence the reactivity, of the adsorbate can be varied over an extended range. Using suitable techniques to measure the adsorbate-adsorbent interaction, the aromatic adsorbate could be taken as a variable probe of molecular dimensions.

There have been a number of studies concerned with the adsorption of aromatics on pure silicas.⁴⁻¹² Infrared spectroscopic^{9,11} or gravimetric^{6-8,12} methods were employed, but these two complementary techniques were rarely^{4,5} used together. The adsorptions of various aromatics on porous glasses have also been examined¹³⁻²¹ (much of the work was reviewed by Little¹), but these studies were not at all extensive. Much of the infrared work was carried out in the overtone region and, as pointed out by Kiselev and Lygin,²² consequently is of limited utility. Also, the modifying effects of borica and other contaminants on the properties²³ of the porous glass were not then known, and much of the work can be considered inadequate with respect to sample preparation and spectrometric techniques.

Although the number of studies dealing with the adsorption of aromatics on siliceous surfaces is relatively large, additional information is desirable. We have therefore carried out detailed studies, using both

gravimetric and infrared techniques, of the interactions of cyclic aromatics with highly degassed porous glass surfaces with the intent of providing qualitative and

- (1) L. H. Little, "Infrared Spectra of Adsorbed Species," Academic Press, New York, N. Y., 1966.
- (2) E. A. Hauser, "Silica Science," D. Van Nostrand and Co., Inc., Princeton, N. J., 1953.
- (3) W. Eitel, "The Physical Chemistry of Silicates," University of Chicago Press, Chicago, Ill., 1954.
- (4) G. A. Galkin, A. V. Kiselev, and V. I. Lygin, *Zh. Fiz. Khim.*, **41**, 40 (1967).
- (5) V. Ya. Davydov, A. V. Kiselev, and B. V. Kuznetsov, *Russ. J. Phys. Chem.*, **39**, 1096 (1965).
- (6) J. A. Hockey and B. A. Pethica, *Trans. Faraday Soc.*, **59**, 2017 (1962).
- (7) L. H. Boulton, B. R. Clark, M. F. Coleman, and J. M. Thorp, *ibid.*, **62**, 2928 (1966).
- (8) M. L. Hair and I. D. Chapman, *J. Amer. Ceram. Soc.*, **49**, 651 (1966).
- (9) A. Zecchina, C. Versino, A. Appiano, and G. Occhiena, *J. Phys. Chem.*, **72**, 1471 (1968).
- (10) A. V. Kiselev and V. I. Lygin, *Kolloid Zh.*, **23**, 574 (1961).
- (11) G. A. Galkin, A. V. Kiselev, and V. I. Lygin, *Russ. J. Phys. Chem.*, **36**, 951 (1962).
- (12) J. W. Whalen, *J. Phys. Chem.*, **71**, 1557 (1967).
- (13) N. G. Yaroslavsky, *Zh. Fiz. Khim.*, **24**, 68 (1950).
- (14) N. G. Yaroslavsky, "Methods of Investigating the Structure of Highly Dispersed and Porous Bodies," USSR Academy of Science Press, 1953, (in Russian).
- (15) A. V. Kiselev and V. I. Lygin, *Russ. Chem. Rev.*, **31**, 175 (1962).
- (16) A. Ron, M. Folman, and O. Schnepf, *J. Chem. Phys.*, **36**, 2449 (1962).
- (17) V. N. Abramov, A. V. Kiselev, and V. I. Lygin, *Zh. Fiz. Khim.*, **38**, 1045 (1964).
- (18) V. N. Filimonov, *Opt. Spectrosk.*, **1**, 490 (1956).
- (19) V. N. Filimonov and A. N. Terenin, *Dokl. Akad. Nauk SSSR*, **109**, 982 (1956).
- (20) A. N. Sidorov, *Zh. Fiz. Khim.*, **30**, 995 (1956).
- (21) A. N. Sidorov, *Dokl. Akad. Nauk SSSR*, **95**, 1235 (1954).
- (22) A. V. Kiselev and V. I. Lygin, Supplementary Chapter in ref 1, p 226.
- (23) M. J. D. Low and N. Ramasubramanian, *J. Phys. Chem.*, **70**, 2740 (1966); Preprints, Division of Petroleum Chemistry, 152nd Meeting of the American Chemical Society, New York, N. Y., Sept 1966, p 133.

quantitative information about the π -OH interaction. Specifically, part I of the present series of three papers is concerned with a detailed analysis of the thermodynamics of the adsorption of benzene on porous glass. Part II considers the same adsorbate-adsorbent system from the point of view of detailed infrared spectroscopic measurements. The results of additional, extensive gravimetric and spectroscopic measurements for the adsorption of a variety of suitably substituted benzenes, as well as the mechanism of the π -OH interaction, are taken up in part III.

Experimental Section

Spectral grade benzene (Matheson Coleman and Bell) was triply distilled *in vacuo* over P_2O_5 . Water used for hydroxylation was doubly distilled *in vacuo*. Both benzene and water were freed from gas by freeze-pump-thaw cycles. Oxygen was prepared by the thermal decomposition of $KMnO_4$ *in vacuo*. The adsorbent specimens were 1×2 -cm pieces of a 1-mm thick sheet of Corning Code 7930 porous glass. Prior to adsorption experiments, a sample was alternately degassed and hydroxylated at 700° seven or eight times in order to obtain a reproducible surface. The sample was then subjected to the following "standard" treatment: (a) heating in 100 Torr of oxygen at 600° for 4 hr; (b) degassing at 700° for 1 hr; (c) exposure to 4 Torr of water vapor at 25° for 0.75 hr; (d) degassing for 12 hr at 500 or 750° ; (e) cooling *in vacuo* to the temperature at which the adsorption isotherm was to be measured.

A Cahn RG recording vacuum microbalance (1 μ g sensitivity, modified by the manufacturer for use with acetone and other condensable vapors) was used in conjunction with a conventional vacuum system capable of producing a dynamic vacuum of better than 10^{-6} Torr. Sections of the system exposed to the adsorbates were fitted with Teflon high-vacuum stopcocks. The sample was suspended from the balance beam by quartz fibers. During an adsorption experiment the sample temperature was controlled to $\pm 0.5^\circ$ by immersing the sample "leg" in a thermostat. A calibrated iron-core, Nichrome-wound furnace held the temperature to $\pm 5^\circ$ during the degassing steps.

The gravimetric work showed (a) that benzene adsorption on a sample which had been subjected to the standard treatment was reversible and reproducible; (b) reproducible results were obtained after a sample had been subjected to several adsorption-desorption-standard treatment cycles; and (c) identical isotherms were obtained with different samples which had been subjected to the same standard treatment. The infrared work, which will be described in part II, showed that the optical density and integrated area data for the bands of the surface hydroxyl groups were reproducible, *i.e.*, samples having the same surface hydroxyl group concentrations could be prepared by means of the standard treatment. Also, a series of

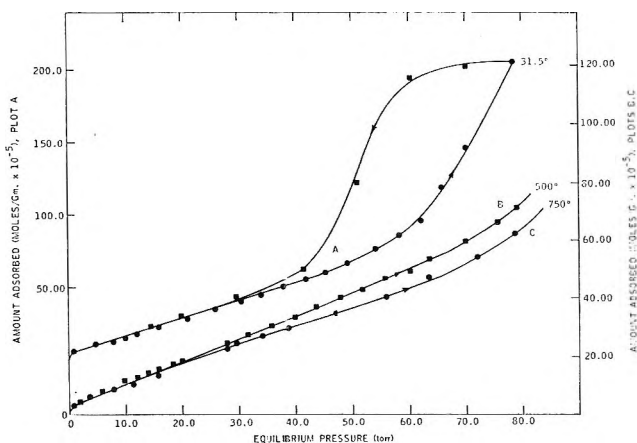


Figure 1. Adsorption isotherms. A, adsorption-desorption isotherm at 31.5° , sample degassed at 750° ; B and C, isotherms at 42° , samples degassed at 500° (B) or 750° (C).

experiments was carried out with the pure silica, Cab-O-Sil (G. Cabot Co., Boston, Mass.), using the above standard treatment. As with porous glass, the results obtained with Cab-O-Sil were reproducible, suggesting that the standard treatment was effective in permitting the preparation of reproducible surfaces.

Experiments and Results

Isotherms. Porous glass samples which had been subjected to a final degassing of 500 or 750° were prepared. Benzene adsorption-desorption isotherms were measured at each of three temperatures with each type of sample. The plots of Figure 1 are characteristic of the type of data obtained. The adsorption was entirely reversible, the amounts of benzene adsorbing at any particular relative pressure, P/P_0 , decreasing with increasing adsorption temperature, as expected. Individual isotherms exhibited Brunauer Type IV behavior;²⁴ *e.g.*, plot A Figure 1. The samples degassed at 500° adsorbed somewhat more benzene than those subjected to more severe dehydroxylation by the 750° degassing; *e.g.*, plots B, C, Figure 1. As the results obtained with the two types of samples were similar, only the data obtained with the 750° sample will be considered.

The area of the adsorbed benzene molecule has previously been taken to be 32.3 \AA^2 ,^{25a} 40 \AA^2 ,^{25b} 41 \AA^2 ,^{25c} but more generally as $\approx 2 \text{ \AA}^2$,^{7,16,25d-f} so that it seems difficult to choose the best value. However, if the BET²⁶ method is applied to our adsorption data,

(24) S. Brunauer, "The Adsorption of Gases and Vapours," Clarendon Press, Oxford, 1945.

(25) (a) H. K. Livingston, *J. Colloid Sci.*, **4**, 447 (1949); (b) A. V. Kiselev and V. I. Lygin, *Kolloid J. USSR*, **23**, 478 (1961); (c) P. G. Menon and P. Ramamurthy, *Kolloid-Z. Z. Polym.*, **206**, 159 (1965); (d) J. Smith, R. Pierce, and B. Cordes, *J. Amer. Chem. Soc.*, **72**, 5595 (1950); (e) J. M. Thorp and J. B. Woulf, *Trans. Faraday Soc.*, **63**, 2068 (1967); (f) ref 29, p 255.

(26) S. Brunauer, P. H. Emmett, and E. Teller, *J. Amer. Chem. Soc.*, **60**, 309 (1938).

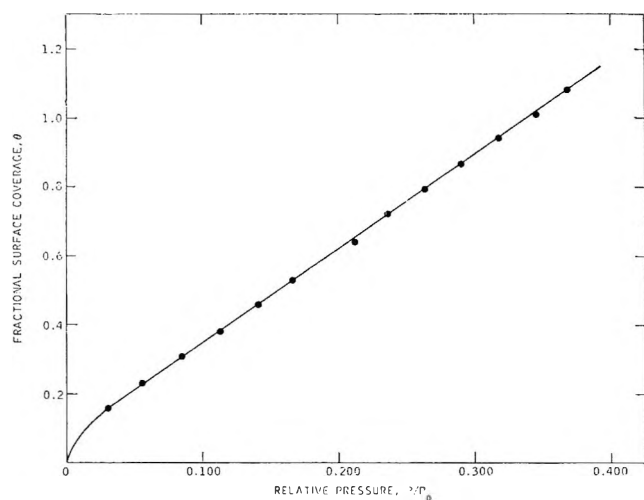


Figure 2. Surface coverage vs. relative pressure. The apparent surface coverage θ for adsorption at 32° as function of the relative pressure; the sample was degassed at 750° .

monolayer coverage occurred at 5.13×10^{-4} mol of benzene/g of sample. The nitrogen BET surface area of the samples was $135 \text{ m}^2/\text{g}$. Then, assuming a cross-sectional area of the benzene molecule of 42 \AA^2 for benzene lying "flat" on the surface (other data including the spectra of part II show this configuration to be the most probable one), the theoretical monolayer ($\theta = 1$) is estimated to occur at a surface concentration of 5.33×10^{-4} mol of benzene/g of sample (θ is the conventional fractional surface coverage). The choice of 42 \AA^2 would thus seem reasonable. It should be noted that, as shown in Figure 2, the amount of benzene adsorbed was almost a linear function of P/P_0 up to the monolayer point.

Experimental Thermodynamic Functions. The methods of de Boer²⁷ were used to estimate the thermodynamic functions from the adsorption data. For these calculations, the adsorbate gas phase at a pressure of 760 Torr was chosen as the initial standard state. Corresponding values for the equilibrium pressures P_1 and P_2 relative to the same degree of surface coverage were then selected from isotherms obtained at temperatures T_1 and T_2 . The isothermal change in the Gibbs free energy, ΔG_1 , in going from the three-dimensional gas standard state at a pressure P^0 of 760 Torr to the adsorbed state with equilibrium pressure P_1 at temperature T_1 , is given by $\Delta G_1 = -RT_1 \ln (P^0/P_1)$. The value of ΔG_2 was calculated in a similar manner. Values of the differential heat of adsorption, ΔH_a , were obtained from the temperature variation of the adsorbate vapor pressure at constant coverage, and those of the molar differential entropy of adsorption, ΔS_a , were then obtained from the relation $\Delta G_1 = \Delta H_a - T_1 \Delta S_a$. The values of these functions and their relations are shown in Figure 3.

Experimental ΔS_a Values for Two Limiting Models. In considering the thermodynamic aspects of a gas-

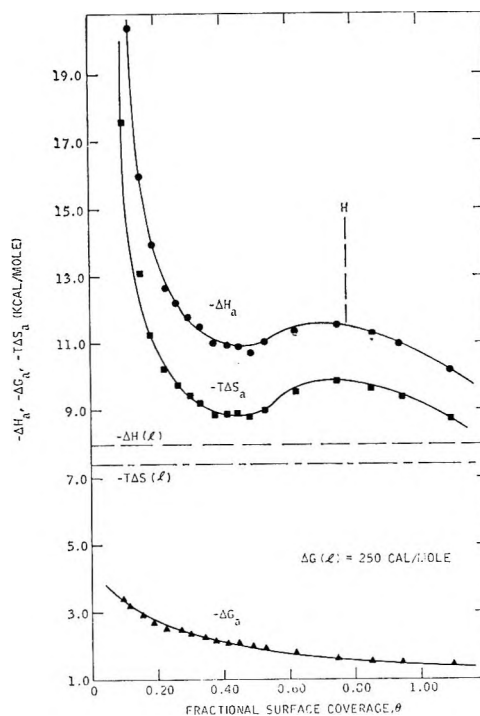


Figure 3. Thermodynamic functions. H indicates the surface coverage at which adsorption hysteresis begins; 750° -degassed sample. The values for liquid benzene are also shown.

solid interaction, it is frequently beneficial to compare the experimentally derived values of the adsorption entropy with theoretical values for both mobile and immobile adsorption. To permit the comparison with the two limiting models to be made, it is necessary that identical initial and final standard states be used in both sets of data. In the present work, the adsorbed state at half-monolayer coverage was arbitrarily but conveniently chosen as the adsorbed standard state for the immobile model, and that state which corresponds to a distribution of the adsorbate on the surface with an intermolecular distance equal to that of the three-dimensional gas phase at 0° and 760 Torr was chosen as the adsorbed standard state for the mobile model. The experimental entropy changes in going from the initial standard state (gas phase, 760 Torr) to the adsorbed standard state are,²⁷ then

$$-\Delta S_{ie}^\circ = -\Delta S - R \ln [\theta/(1 - \theta)] \quad (\text{immobile model}) \quad (1)$$

$$-\Delta S_{me}^\circ = -\Delta S - R \ln [A^\circ/A] \quad (\text{mobile model}) \quad (2)$$

where ΔS is the entropy of adsorption derived from the isotherm data. Values of A , the area available to each molecule at a given surface coverage θ , could readily be obtained from the surface area, cross section, and θ . The value of A° , the area available to each molecule in

(27) J. H. de Boer and S. Kruyer, *Proc. Koninkl. Ned. Akad. Wetenschap*, **55**, 451 (1952); *ibid.*, **56**, 67 (1953); *ibid.*, **56**, 238 (1953); *ibid.*, **57**, 92 (1954); *ibid.*, **58**, 61 (1955); *ibid.*, **65**, 17 (1961).

the adsorbed standard state for the mobile model, was obtained by applying the two-dimensional equation of state, $FA = kT$, to the standard-state conditions. The average distance between gaseous benzene molecules at 0° and 760 Torr is 3.339×10^{-7} cm, so that

$$F^\circ = kT/A^\circ = 0.338 \text{ dyn/cm}$$

and the standard molecular area is $4.08T \times 10^{-16}$ cm², T being taken as the average of the two isotherm temperatures. In the present study, $A^\circ = 1.265 \times 10^{-13}$ cm². Figure 4 shows the values of the experimental entropy changes, obtained by means of eq 1 and 2, as functions of coverage.

Theoretical ΔS_a Values for Two Limiting Models. The theoretical value of the entropy of adsorption for the immobile model is given by

$$-\Delta S^\circ_{it} = {}_gS^\circ_{tr} + {}_gS^\circ_{rot} + {}_gS^\circ_{vib} + {}_gS^{01}_{vib} - {}_aS^\circ_{config} - {}_aS^\circ_{rot} - {}_aS^{01}_{vib} - {}_aS^\circ_{vib} \quad (3)$$

and for the mobile model, by

$$-\Delta S^\circ_{mt} = {}_gS^\circ_{tr} + {}_gS^\circ_{rot} + {}_gS^\circ_{vib} + {}_gS^{01}_{vib} - {}_aS^\circ_{tr} - {}_aS^\circ_{rot} - {}_aS^\circ_{vib} - {}_aS^{01}_{vib} \quad (4)$$

where the subscripts g and a signify gas and adsorbed state, respectively, and the superscript $^\circ$ signifies the standard state. Also, tr stands for translation, rot for rotation, $config$ for configuration, and vib for vibration. Concerning the vibrational contributions, the superscript (01) refers to the internal modes, whereas $(^\circ)$ refers to the symmetrical vibrations of the entire adsorbed molecule with respect to the surface plane. The assumption is made that ${}_gS^{01}_{vib} = {}_aS^{01}_{vib}$, *i.e.*, that adsorption does not affect the internal vibrations of the benzene molecule. That assumption is not unreasonable, because infrared spectra showed (part II) that the perturbation of the C-C and C-H stretching modes caused by adsorption was very small. All entropies were calculated for the mean of two isotherm temperatures.

Each of the contributions to the total entropy change was calculated using the ensemble approach of statistical mechanics where the general expression relating the partition function Q of a system to its entropy can be shown to be²⁸

$$S = kT(\partial \ln Q / \partial T)_{vm} + k \ln Q \quad (5)$$

The partition functions were calculated by conventional techniques,²⁸ and found to be

$${}_gQ_{tr} = [\partial \pi (\sum_i m_i) kT / h^2]^{1/2} V^\circ \quad (6)$$

$${}_aQ_{tr} = [2\pi (\sum_i m_i) kT / h^2] L_A A^\circ \quad (7)$$

$${}_gQ_{rot} = \frac{1}{\pi \sigma} [8\pi^3 (I_A / I_B) kT / h^2]^{3/2} \quad (8)$$

$${}_aQ_{rot} = \frac{1}{\pi \sigma} [8\pi^3 (I_A) kT / h^2]^{1/2} \quad (9)$$

(for one axis of rotation)

$${}_aQ_{rot} = \frac{1}{\pi \sigma} [8\pi^3 (I_A I_B)^{1/2} kT / h^2] \quad (10)$$

(for two axes of rotation)

$${}_aQ_{vib} = \exp[-h\nu / 2kT] / [1 - \exp(-h\nu / kT)] \quad (11)$$

In these equations V° is the volume of a mole of gaseous benzene, L_A is Avogadro's number, I_A and I_B are molecular moments of inertia, σ is the symmetry number, and the rest of the symbols have their usual meaning. ν in eq 11 was taken to be 135 cm^{-1} as suggested by Ron, *et al.*¹⁶ The application of eq 5 to eq 6-11 gives the final expressions

$${}_gS^\circ_{tr} = R \ln [M^{1/2} T^{5/2}] - 2.30 \quad (12)$$

$${}_aS^\circ_{tr} = 2/3 {}_gS^\circ_{tr} + 1.52 \log T - 2.38 \quad (13)$$

$${}_gS^\circ_{rot} = R \{ \ln (1/\pi \sigma) [8\pi^3 (I_A I_B)^{1/2} kT / h^2]^{3/2} + 3/2 \} \quad (14)$$

$${}_aS^\circ_{rot} = R \{ \ln (1/\pi \sigma) [8\pi^3 (I_A) kT / h^2]^{1/2} + 1/2 \} \quad (15)$$

$${}_aS^\circ_{rot} = R \{ \ln (1/\sigma) [8^3 (L_A I_B)^{1/2} kT / h^2] + 1 \} \quad (16)$$

$${}_aS^\circ_{vib} = R \{ (h\nu / kT) [\exp(h\nu / kT) - 1]^{-1} - \ln [1 - \exp(-h\nu / kT)] \} \quad (17)$$

${}_aS^\circ_{config}$ was calculated from Boltzmann's equation, $S = k \ln W$, where $W = M! / N!(M - N)!$ for M sites and N molecules. By the usual statistical techniques this leads to

$${}_aS^\circ_{config} = -R \ln [\theta / (1 - \theta)] \quad (18)$$

The theoretical entropy changes for the two limiting physical models in their standard states were calculated using eq 12-17; the values are given in Table I.

Table I: Theoretical Contributions to the Entropy of Adsorption by Various Degrees of Freedom

Entropy mode	Immobile model (eu)	Mobile model (eu)
${}_gS^\circ_{tr}$	39.2	39.3
${}_gS^\circ_{rot}$	20.3	20.9
$-{}_aS^\circ_{config}$	0.0	...
$-{}_aS^\circ_{tr}$...	-29.6 ^a
$-{}_aS^\circ_{vib}$	-3.0	-3.0
$-{}_aS^\circ_{rot}$	-4.0 (-11.1) ^a	-4.0 (-11.1) ^b
$-\Delta S^\circ_t$	53.2 (42.1) ^a	23.6 (12.5) ^b

^a The theoretical integral and differential entropy terms are of equal value for the immobile model, but $-{}_aS^\circ_{tr}$ differs by R for the mobile model. To permit comparison with experimental values, which are differential ones, $-{}_aS^\circ_{tr}$ has been corrected and all terms in the table can be taken as differential entropies. ^b Values in parentheses refer to two modes of surface rotation as described by eq 16.

(28) T. L. Hill, "Introduction to Statistical Thermodynamics," Addison-Wesley, New York, N. Y., 1962, p 19.

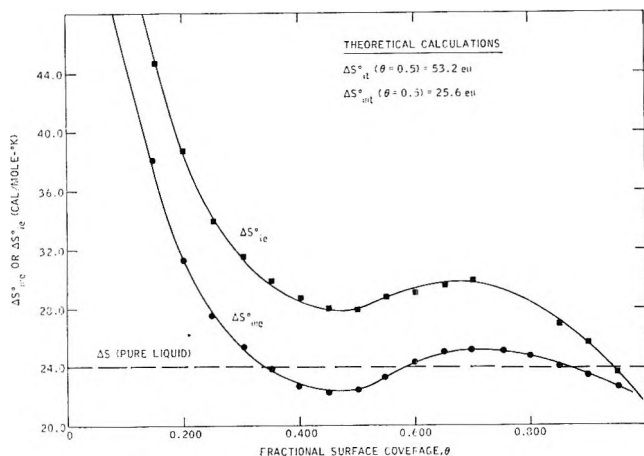


Figure 4. Entropy changes. Experimental entropy changes estimated for immobile (ΔS°_{ie}) and mobile (ΔS°_{me}) surface species; 750°-degassed sample.

Discussion

The hysteresis loops observed are of the general type E of de Boer's classification²⁹ and could be caused by the presence of tubular capillaries with short necks and wide, sloping bodies or by chains of similar pores which would form longer tubular capillaries having wide parts of various radii. However, as pointed out by de Boer,²⁹ type E loops could be caused by other pore assemblies, and the sloping part of the desorption branch in the low-pressure region (*e.g.*, ~40–20 Torr of trace A, Figure 1) suggests that a group of pores of widely varying neck dimensions makes a minor contribution to loops such as that shown in Figure 1. In view of the nature of the adsorbent and its method of manufacture, however, it is not unlikely that the majority of the pores active in benzene adsorption are of shape-group XV, *i.e.*, tubular capillaries with widened parts, shaped much like a string of uneven-sized beads. Such an interpretation is compatible with a model of porous glass as a random packing of approximately uniform spheres recently proposed by Cadenhead and Everett on the basis of benzene adsorption on heat-treated porous glass.³⁰

The weak, reversible adsorption process itself is taken as a physical adsorption, in part caused by an interaction of the benzene with surface hydroxyls. The occurrence of this interaction is merely suggested by the decreased adsorption of the more dehydroxylated 750°-degassed samples—*e.g.*, traces B, C, Figure 1—but is definitely established by the infrared data (part II). Multilayer formation and condensation occurred at the higher pressures, as indicated by the isotherms.

With increasing adsorption it is apparent that ΔH_a and ΔS_a values decreased rapidly and, after passing through a small maximum near $\theta = 0.75$, approached the values for pure liquid benzene (Figure 3). In judging the validity of these changes it should be noted that an error of $\pm 1\%$ in the pressure measurements,

larger than the error normally experienced, would lead to a corresponding error of ± 0.30 kcal/mol for ΔH_a and ± 1 cal/mol deg for ΔS_a . Such maxima in heats of adsorption have been observed previously, as with benzene adsorption on porous Aerosil.⁶ For example, Boulton, *et al.*,⁷ attributed a maximum in ΔH_a for benzene adsorption on porous silica gel to a compression of the liquid within the filled pores resulting from a decrease in curvature of the menisci near saturation. In the present case, the ΔH_a maximum near $\theta = 0.75$ occurred near the onset of adsorption hysteresis (the broken line marked H in Figure 3), so that it seems probable that it was brought about by enhanced cooperative interactions of adsorbed benzene within the micropore system of the glass.

The behavior of ΔS_a paralleled that of ΔH_a . As might be expected, the entropy loss was very high at low degrees of coverage, indicating a high degree of localization of the adsorbate. ΔS_a values decreased rapidly with increasing coverage, however, suggesting an increase in the mobility of the adsorbed benzene molecules. The ΔS_a maximum near the onset of hysteresis can be explained by a change in molecular mobility caused by a variation in the degree of surface-adsorbate interaction in the pore system. Conversely, the Gibbs free energy ΔG_a decreased continuously with increasing coverage, no maximum arising because of compensation between the ΔH_a and ΔS_a terms of the free energy expression. Such compensation of enthalpy gain by entropy loss is well known for hydrogen-bonded systems.³¹

Complementary to these interpretations is the fact that the maxima of the thermodynamic functions occurred at surface coverages at which there were distinct changes in the values of the various spectroscopic parameters, *e.g.*, frequencies and optical densities of the hydroxyl bands, and C–H band extinction coefficients. Those changes, which have not been found with adsorption on nonporous silicas, will be considered in part II. In contrast to the behavior found with the present porous adsorbent, ΔH_a and ΔS_a values have been found to decrease monotonically with increasing coverage for adsorption on nonporous systems as, for example, with Kiselev's³² data on the adsorption of benzene on nonporous Aerosil silica.

Comparison of the experimental and theoretical entropy values estimated for the mobile and immobile models provides further information about the adsorbed benzene, although, as pointed out by Everett,³³ the

(29) J. H. de Boer, in "The Structure and Properties of Porous Materials," Vol. X, Colston Papers, D. H. Everett and F. S. Stone, Ed., Butterworth and Co., Ltd., London, 1958, p 68 ff.

(30) D. A. Cadenhead and D. H. Everett, *J. Phys. Chem.*, **72**, 3201 (1968).

(31) G. C. Pimentel and A. L. McClellan, "The Hydrogen Bond," W. H. Freeman and Co., San Francisco, Calif., 1960, p 220.

(32) A. V. Kiselev and D. P. Poshkus, *Dokl. Akad. Nauk SSSR*, **120**, 834 (1958).

difficulties in differentiating between mobile and immobile adsorption are severe when complex molecules are adsorbed on very heterogeneous surfaces. However, the good agreement between the gravimetric and infrared effects, *i.e.*, the occurrence of maxima in the thermodynamic functions at the surface coverages at which distinct changes were observed in infrared spectra, suggests that some use can be made of the thermodynamic treatment. The theoretical values of 53.2 and 42.1 eu are much too high in comparison to the experimental value of 28.0 eu for an immobile species, and the theoretical value of 12.5 eu (for two modes of surface rotation) is too low for the mobile model (Figure 4 and Table I). For the mobile model, however, the theoretical value of 23.6 eu, estimated on the basis of one degree of rotational freedom about an axis perpendicular to the surface and to the plane of the benzene molecule, is close to an experimental value of 22.6 eu (taken from Figure 4). The 1 eu difference can easily be accounted for by a small amount of additional librational freedom and/or a small degree of vibration of the adsorbed molecule perpendicular to the surface, or by the 1 eu experimental error.

The mobile model is less suitable at coverages lower than $\theta = 0.5$. At $\theta = 0.1$, for example, $-\Delta S_{it}^{\circ} = 51.2$ eu, $-\Delta S_{ie}^{\circ} = 52$ eu, and $-\Delta S_{me}^{\circ} = 43.4$ eu, whereas $-\Delta S_{mt}^{\circ} = 23.6$ or 12.5 eu, depending on the number of degrees of rotational freedom, so that the immobile model appears to provide a better description at low coverages.

The thermodynamic considerations therefore lead to the following model for the state of benzene adsorbed on hydroxylated porous glass. At low degrees of coverage the benzene molecules are localized and quite strongly bound, as suggested by the high enthalpy and entropy values. As the coverage is increased, the

benzene molecules become mobile, the adsorbed benzene molecule lying flat with the plane of the ring parallel to the surface and rotating freely in the ring plane. In diffusing over the surface, the spinning adsorbed molecule may move slightly toward and away from the surface and may occasionally have an additional 180° rotation, much like a flat stone skipping over water and occasionally flipping over onto its back. Filling of the micropore structure begins at $\theta \approx 0.6$, increasing interaction between adsorbate molecules and hindering some of the motion of the adsorbed benzene.

The Frenkel equation³⁴

$$\tau = \tau_0 \exp(-\Delta H_a/RT)$$

where τ_0 is of the order of 10^{-13} sec and τ is the residence time of the adsorbed molecule, is also useful in considering the present system. For benzene at low coverages, $\Delta H_a \approx 20$ kcal/mol so that $\tau \approx 100$ sec, the benzene adsorption approaching the behavior expected in a chemisorption. However, at increasing coverages, ΔH_a falls rapidly to about 8 kcal/mol, at which point $\tau \approx 10^{-8}$ sec. This change in residence times of over 10 orders of magnitude implies a change in adsorbate from a tightly bound to a quite loosely bound state. This is expected for a physical adsorption and is thus congruent with the model of adsorbed benzene based on the thermodynamic parameters.

Acknowledgment. Support by means of grants from the Communicable Disease Center and the National Center for Air Pollution Control is gratefully acknowledged.

(33) D. H. Everett, *Proc. Chem. Soc.*, 38 (1957).

(34) J. H. de Boer, "The Dynamical Character of Adsorption," Clarendon Press, Oxford, 1945

Rotational Isomerism in Dichloroacetyl Halides

by A. J. Woodward and Neville Jonathan

Chemistry Department, The University, Southampton SO9 5NH, England (Received September 10, 1969)

Infrared and Raman spectra are reported for the acid fluoride, chloride, and bromide derivatives of dichloroacetic acid. Data are given for vapor, liquid, and solid state spectra. It is concluded that two molecular forms exist in the vapor and liquid phases of the acid halides of which the more polar form is present in excess in the solid state. The enthalpy difference between these isomers has been measured for CHCl_2COCl and CHCl_2COBr in the vapor phase and is less than 500 cal/mol in each case. The nature of the stable conformations is discussed with the help of (a) a vibrational analysis based on a Urey-Bradley potential function and (b) calculations of the conformational potential energy as a function of the internal rotation angle.

Introduction

Previous studies in this laboratory^{1,2} have shown that the monohaloacetyl halides exist as a mixture of two rotational isomers in the liquid and vapor states and that the more polar form is the only conformer present in the solid state. The present study has used the same techniques to investigate the dichloroacetyl halide series of compounds of which only the acid chloride has been studied previously.³

The object of the work was to establish the conformations of the rotational isomers of each member of the series. In the previous study³ the enthalpy difference between the isomers of dichloroacetyl chloride was found to be about 200 cal/mol in the vapor phase, the less polar form being the more stable. We have attempted to make such measurements for the acid chloride and the acid bromide in the vapor phase. Similar measurements were not attempted for the liquid phase since we believe such data have a limited value because the factors which influence stability in the liquid phase are not solely of an intramolecular nature. The data obtained for dichloroacetyl chloride are largely similar to those previously published, but are reproduced here for the sake of completeness.

Experimental Section

The three compounds were prepared as follows, all samples being fractionally distilled two or three times before use: (a) CHCl_2COF (bp 70–72°; lit. bp 71–72°⁴) by refluxing dichloroacetyl chloride with antimony trifluoride; (b) CHCl_2COCl (bp 108°; lit. bp 107–107.5°³) by reaction of the parent acid and excess thionyl chloride in the presence of a trace of dimethylformamide; (c) CHCl_2COBr (bp 125–128°; lit. bp. 125–129°⁵) by reaction of the acid with phosphorus tribromide.

Infrared spectra were recorded in the range 450–4000 cm^{-1} using a Grubb-Parsons GS2A grating spectrometer and a Perkin-Elmer Model 225 spectrometer was used from 200 to 450 cm^{-1} . Liquid Raman spectra were

measured with a Spex Raman spectrometer (Model 1401) equipped with an argon ion laser.

Vapor phase spectra were recorded using a 10-cm gas cell equipped with potassium bromide windows. In order to determine enthalpy differences, an infrared band unique to each isomer was recorded three or four times at each of a number of different temperatures. The mean of the areas under the optical density curves was taken as the correct value of the absorbance for each band. The cell was heated by means of an external heating jacket, the temperature being controlled to $\pm 1^\circ$ using an Ether 12-91 anticipatory controller and iron-constantan thermocouple.

Several techniques have been used to obtain solid spectra, *viz.*, (a) formation of the solid either by cooling a liquid film or by condensing the appropriate vapor onto a cooled KBr or CsI plate, (b) variation of the rate of cooling of the liquid or vapor, and (c) "annealing"⁶ the solid after its formation. It has, however, only been possible to reduce the spectrum of solid CHCl_2COF to that due to a single conformation of the molecule. Spectra of the solid acid chloride and acid bromide show only a partial reduction in the bands due to the less stable isomer.

Results

The spectral data for the three compounds are given in Table I together with suggested vibrational frequency assignments.

Discussion

The expected number of fundamental vibrations for each molecule is fifteen, including one carbonyl and two

(1) A. Y. Khan and N. B. H. Jonathan, *J. Chem. Phys.*, **50**, 1801 (1969).

(2) A. Y. Khan and N. B. H. Jonathan, *ibid.*, in press.

(3) S. Mizushima, *et al.*, *Spectrochim. Acta*, **13**, 161 (1958).

(4) W. Miller and A. Dittman, *J. Amer. Chem. Soc.*, **78**, 2797 (1956).

(5) F. King and P. Spensley, *J. Chem. Soc.*, 2144 (1952).

(6) J. K. Brown and N. Sheppard, *Discussions Faraday Soc.*, **9**, 144 (1950).

Table I: Spectral Data for the Dichloroacetyl Halides (cm⁻¹)

Vapor	CHCl ₂ COF		CHCl ₂ COCl		CHCl ₂ COBr		Raman Liquid	Assignment ^a
	Liquid	Infrared	Liquid	Infrared	Liquid	Infrared		
2985 m								
1876 } s	1859 } s	1856 (8)	3003 w	3003 w	3000 w	1923 w		M, L _p (C-H)
1859 } s	1859 } s		1961 w	1980 w	1905 w	1792 vs	1807 (4)	M
1282 m	1282 m	1279 (2)	1818 } vs	1795 vs	1798 } vs	1786 } vs	1784 (4)	M
1250 w	1282 m		1779 } vs	1773 msh	1776 (4)	1244 w		L
1250 (?)	1248 vw		1253 m	1266 m	1250 (1)	1227 vw		M
1214 (?)	1248 (?)		1230 m	1223 mw	1230 (1)	1212 w		L
873 m	1205 (?)	1207 (?)	1214 m	1192 mw	1214 (?)	1195 w		L
901 m	868 mw		1202 m	1070 mw	1202 (2)	1042 m		M
826 } s	898 s		1075 vs	995 s	987 (1)	968 s		L
826 } s	821 } s	819 (2)	986 s	806 s	804 (4)	796 s		M
	822 } s		838 m	806 s	781 w	796 s		M
	822 } s		800 vs	785 s	780 (3)	775 msh		M
	778 } mw		760 msh	752 ssh	753 (9)	737 m		M
762 m	763 } mw		739 vs	734 vs	740 m	699 vs		L
1214 s	1205 s	1207 (1)	640 m	631 m	704 vs	605 w		L
1111 s	1112 s		585 s	575 ms	604 m	571 w		L
478 s	477 m			491 m	571 w	569 (1/2)		M
	456 m			450 m	518 s	517 m		M
650 m	639 mw	639 (1)	503 m	505 w	514 m	517 m		L
643	671 ms	672 (7)	463 m	466 m	356 m	358 w		M
					356 m	358 w		L
					368 m	375 w		M
	424 s	422 (10)	414 vw	337 m	368 m	317 m		M
	401 s	398 (10)	338 m	264 } w	319 (10)	262 (2)		M
	275 s	268 (3)	262 } m	264 } w	262 (2)	241 (1/2)		L
	293 s	284 (4)	262 } m	240 m	238 m	217 (4)		M
	243 ms	238 (3)	240 m	242 w	237 (4)	151 (1)		M
	220 m	221 (1)	[(424)-(195)?]		176 (5)			L
	195 s	187 (3)	177 m					L

^a M denotes the more polar form and L the less polar form. ^b See text for the acid fluoride assignments. ^c See text.

carbon-chlorine stretching vibrations. However, two bands were observed in the region around 1800 cm^{-1} , and three to four bands in the $700\text{--}850\text{ cm}^{-1}$ region, in all liquid and vapor spectra. These results indicate that, as in the case of the chloroacetyl halide series, each of the acid halides exists as an equilibrium mixture of at least two isomers, at normal temperatures. However, there is no evidence to suggest the presence of more than two isomers.

A study has been made of changes in the relative intensities of the spectral bands with changing solvent polarity and on passing from the liquid to the solid state. From this an assignment of bands either to the more polar or to the less polar conformation of the molecule has been possible for all except the low-frequency bands of CHCl_2COBr (assignments for which are discussed below). All assignments are listed with the spectral data.

The assignment of bands to vibrational modes of the acid fluoride are considered only approximate since the calculation of the normal vibrations indicated that significant mixing occurred in certain cases. Unless otherwise stated the values given in the following text will be taken from the infrared liquid-state data.

Carbonyl Stretching Frequencies Two bands were observed for each compound in the 1800-cm^{-1} region. In each case the high-frequency band increased in intensity at the expense of the low-frequency band with increasing solvent polarity and it was therefore attributed to the more polar conformation of the molecule.

It is interesting to note the displacement of the carbonyl frequency of each isomer from that of the corresponding acetyl halide (see Table II). Bellamy and Williams⁷ have studied many α -halogenated ketones in which rotational isomerism occurs and associated the higher carbonyl stretching frequency with the conformation in which oxygen and halogen are close together. The interaction of the carbon-halogen and carbon-oxygen dipoles causes a decrease in polarization of the carbon-oxygen bond and increases the vibrational frequency. This is in agreement with the conformations considered later in the text. The carbonyl frequency may, however, be lowered by interaction of the α -chlorine atoms with the carbonyl halogen,⁸ so that no quantitative significance may be attached to these relatively small frequency shift values. One might, however, conclude that for the acid chloride and bromide at least, the rotational isomers have similar conformations.

Carbon-Chlorine Stretching Frequencies. The two bands occurring in the region $700\text{--}850\text{ cm}^{-1}$ for each isomer studied are readily attributed to the asymmetric and symmetric stretching modes of the $-\text{CHCl}_2$ group. They show the expected decrease in frequency with decreasing electronegativity of the carbonyl halogen and for each vibration the band due to the more polar isomer has the higher frequency.

Table II: Values for $\nu(\text{C}=\text{O})$ in the Vapor Phase (cm^{-1})

Molecule	$\nu(\text{C}=\text{O})$	$\Delta\nu$
CH_3COF^a	1879	...
	1851	...
$\text{CHCl}_2\text{COF M}$	1876	+11
$\text{CHCl}_2\text{COF L}$	1859	-6
CH_3COCl^b	1822	...
$\text{CHCl}_2\text{COCl M}$	1818	-4
$\text{CHCl}_2\text{COCl L}$	1786	-36
CH_3COBr^c	1821	...
$\text{CHCl}_2\text{COBr M}$	1815	-6
$\text{CHCl}_2\text{COBr L}$	1786	-35

^a B. P. Susz and J. J. Wuhrmann, *Helv. Chim. Acta*, **40**, 722 (1957). ^b J. Overend, R. A. Nyquist, J. C. Evans, and W. J. Potts, *Spectrochim. Acta*, **17**, 1205 (1961). ^c L. C. Hall and J. Overend, *ibid.*, **23**, 2535 (1967).

Carbonyl-Halogen Stretching Frequencies. The infrared spectrum of the acid fluoride shows intense absorptions at 1205 and 1112 cm^{-1} suggesting that the modes responsible have considerable $\text{C}(\text{O})\text{-F}$ stretching character. The results of the vibrational analysis, however, indicate a degree of mixing of the mode with the carbon-hydrogen and carbon-carbon stretching vibrations. The corresponding $\text{C}(\text{O})\text{-Cl}$ and $\text{C}(\text{O})\text{-Br}$ stretching vibrations of the acid chloride and acid bromide occur at $631, 575\text{ cm}^{-1}$ and $605, 571\text{ cm}^{-1}$, respectively. In all cases the higher frequency is attributed to the less polar conformation of the molecule.

Carbon-Hydrogen Vibrations. The assignment of the carbon-hydrogen bending modes for each isomer of dichloroacetyl fluoride is only tentative since the region is overlapped by the $\text{C}(\text{O})\text{-F}$ stretching mode of the less polar conformation. The assignment of the other carbon-hydrogen modes is straightforward.

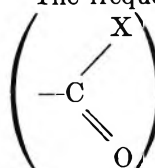
Skeletal Vibrations. The assignment of these bands has been made according to the solvent effect of the Raman spectra. For the acid fluoride and chloride this is relatively straightforward but for the bromide the change in the relative intensities of Raman bands from solution in a nonpolar solvent to those in a polar solvent was negligible. The assignment of the low-frequency bands for dichloroacetyl bromide is therefore tentative since it is based on a comparison with the acid chloride. However, there is sufficient evidence to justify such a comparison. For example, the shifts of the carbonyl frequency from that of the corresponding acetyl halide suggest that the stable conformations of these two compounds are approximately the same. This is supported by the calculation of the conformational potential energy. If this is the case the calculated frequencies for each molecule indicate that

(7) L. J. Bellamy and R. L. Williams, *J. Chem. Soc.*, 4295 (1957).

(8) L. J. Bellamy and R. L. Williams, *ibid.*, 3465 (1958).

their spectra should be very similar. Such similarity is observed in the low-frequency band shapes and frequency displacements, and in the high-frequency conformational assignments.

Certain low frequencies were not observed, namely, the torsional bands for each molecule and, for the acid fluoride and chloride, bands apparently due to a deformation of the (CH-Cl₂) group.

The frequencies for out-of-plane deformation of the  group (π bands) in dichloroacetyl fluoride

and chloride are tentatively assigned at 477 and 456 cm^{-1} , and 490 and 450 cm^{-1} , respectively, but were not observed for the acid bromide.

Our final assignment for dichloroacetyl chloride is in agreement with that of Mizushima, *et al.*, except that we find no evidence for a doublet at 407 cm^{-1} . The validity of the frequency assignments was tested by application of the Mizushima sum rule⁹ to the observed frequencies of Table VI. The results are summarized in Table III and it may be seen that the agreement is good.

Table III: Mizushima Sum Rule Agreement for the Dichloroacetyl Halides

Molecule	More polar $\Sigma \nu_i^2 \times 10^{-7}$	More polar $\Sigma \nu_i^2 \times 10^{-7}$	% Difference
CHCl ₂ COF	1.964	1.970	0.00
CHCl ₂ COCl	1.840	1.851	0.06
CHCl ₂ COBr	1.824	1.835	0.06

Enthalpy Differences. The vapor phase enthalpy difference for the equilibrium "less polar" \rightleftharpoons "more polar" has been calculated for CHCl₂COCl and CHCl₂COBr from the usual relation

$$\frac{A_{LP}}{A_{MP}} = \text{constant} \times \exp(-\Delta H^\circ/RT)$$

where A_{LP} and A_{MP} are the areas under the optical density plots of a band unique to the less polar and more polar conformations, respectively. The bands which have been assigned as being approximately due to the carbon-carbon stretching mode were studied for both compounds. No enthalpy difference measurements have been made for the acid fluoride for each infrared band overlaps a neighboring band to some extent. This adds an additional uncertainty to an already large experimental error. Hence from the data obtained it is only possible to say that for CHCl₂COCl the enthalpy difference between the two stable forms is in the range 100-500 cal/mol (Mizushima, *et al.*,³ give a value of "about 200 cal/mol"). For CHCl₂COBr the dif-

ference is calculated to be less than 100 cal/mol. In both cases the less polar form is the more stable in the vapor phase.

Although no determinations of the enthalpy difference in the liquid state have been made in this work, the previous workers state that the relative intensities of their two bands for CHCl₂COCl remain almost constant between room temperature and -150° indicating that in the liquid the enthalpy difference is negligibly small. This would explain why it has not been possible to isolate a one-isomer spectrum for the compound (although such a spectrum is claimed by Mizushima, *et al.*). The partial reduction in intensity of bands due to the less polar isomer on passing from the liquid to solid state suggests, however, that, although very small, the enthalpy difference is finite. The situation for dichloroacetyl bromide would appear similar to the above, whereas the one-isomer solid spectrum of the acid fluoride indicates a significant enthalpy difference in the liquid state of this compound.

Another possible explanation of the two-isomer spectra has been put forward by Crowder and Northam¹⁰ when discussing a similar problem in 2-bromo-2-methylpropionyl bromide. They attribute the spectrum to a lack of crystallinity in the solid sample studied. We consider the initial explanation more satisfactory in this case.

The Stable Conformation

The subsequent discussion will assume the definition of the azimuthal angle θ indicated in Figure 1, *i.e.*, the angle θ is taken to be zero when the carbon-oxygen bond and the carbon-hydrogen bond are eclipsed.

Mizushima, *et al.*, have calculated the dipole moment of CHCl₂COCl for various azimuthal angles. Their data are plotted in Figure 2. Since the bond dipoles for C-F, C-Cl, and C-Br are very similar (C-F, 1.4 D; C-Cl, 1.5 D; and C-Br, 1.4 D, respectively (C-H 0.4 D)¹¹), a similar curve will apply to each molecule. Our previous explanation of the carbonyl frequencies is in agreement with these data since the nonbonded distance between the oxygen and a chlorine of the -CHCl₂ group decreases as the polarity of the molecule increases.

The Conformational Potential Energy

We have calculated the potential energy as a function of the internal rotation angle for each molecule, using the method of Scott and Scheraga.¹² This technique has proved reasonably successful in predicting the internal rotation barriers in the acetyl halides and in

(9) S. Mizushima, *et al.*, *J. Chem. Phys.*, **21**, 215 (1953).

(10) G. A. Crowder and F. Northam, *J. Mol. Spectrosc.*, **26**, 98 (1968).

(11) J. W. Smith, "Electric Dipole Moments," Butterworth and Co., Ltd., London, 1955.

(12) R. A. Scott and H. A. Scheraga, *J. Chem. Phys.*, **42**, 2209 (1965).

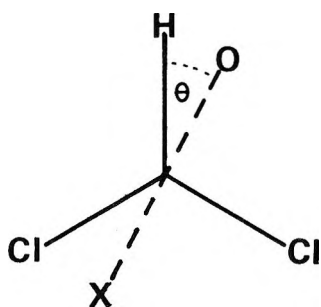


Figure 1. Definition of the azimuthal angle θ .

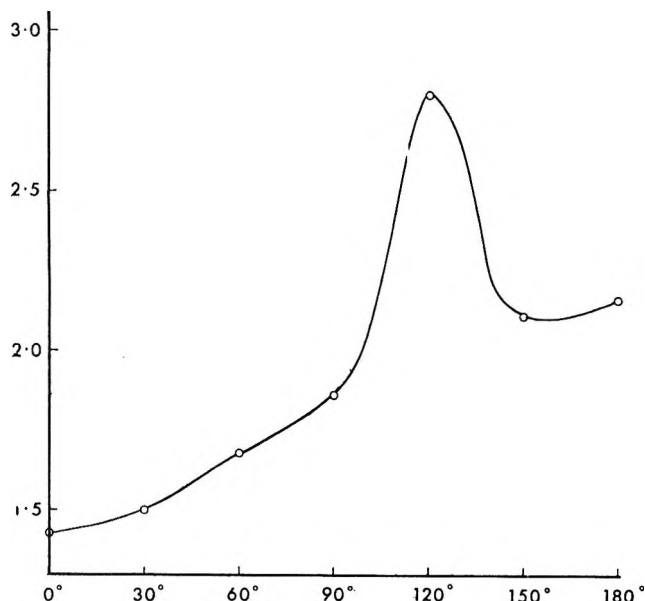


Figure 2. Calculated dipole moment of CHCl_2COCl . Data taken from Mizushima, *et al.*,³ ordinate, μ (10^{18} esu); abscissa, θ .

substituted ethanes. The potential function used is based on two effects, namely nonbonded interactions and exchange interactions of the electrons in the bonds adjacent to the bond about which internal rotation occurs. It takes the form

$$U(\omega) = \frac{1}{2}U_0(1 + \cos 3\omega) + \sum_{k=1}^m \{a_k \exp(-b_k r_k) - c_k/r_k^6 + d_k/r_k\} \quad (1)$$

where the first term on the right-hand side takes into account the electron exchange interactions and the second is a modified Buckingham potential for the nonbonded interactions. The parameters used for the nonbonded potential are listed in Table IV and were calculated according to the method of Scott and Scheraga¹² (some slight errors were found in the data in this reference and they have consequently been recalculated). The average value of $U_0 = 1.11$ kcal/mol used in the calculations is that given by Scott and Scheraga for this type of molecule. Figure 3 shows the resulting potential functions calculated assuming the molecular

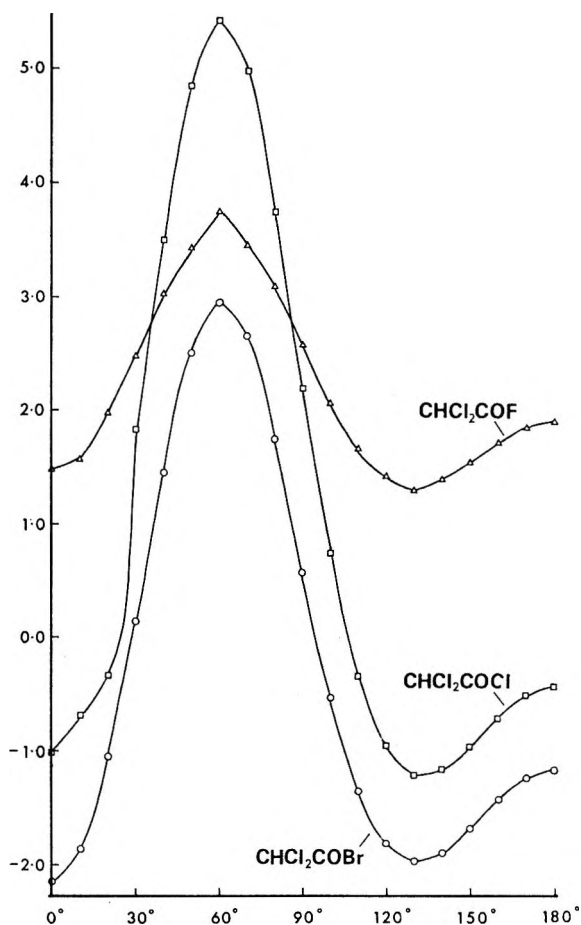


Figure 3. Calculated conformational potential energies for the dichloroacetyl halides. Ordinate, $U(\theta)$ kcal mol⁻¹; abscissa, θ .

Table IV: Parameters for the Nonbonded, 6-exp Potential Function

Interaction	a , kcal mol ⁻¹	b , Å ⁻¹	c , kcal mol ⁻¹ Å ⁶	d , kcal mol ⁻¹ Å
O...H	3.46×10^4	4.57	121	0
O...Cl	2.59×10^6	4.15	956	0
F...H	1.69×10^4	4.57	62.6	0
F...Cl	1.35×10^6	4.15	526	4.09
Cl...H	4.68×10^4	4.13	322	0
Cl...Cl	3.12×10^6	3.75	2513	1.16
Br...H	1.61×10^4	3.55	465	0
Br...Cl	9.55×10^4	3.23	3603	0

geometries used for the normal coordinate analyses. Although the calculated barrier heights and energy differences between the rotational isomers are of the right order, the application of the potential function to these molecules has some disadvantages. The assumption of a rigid geometry allows no relaxation of interactions when atoms of the two rotating groups are in or approaching an eclipsed position and the shape of the curves in the region $\theta = 80$ – 180° is particularly dependent on the geometry assumed for the molecule.

Table V: Force Constants and Molecular Parameters Used in Calculations

Force constants (mdyn/Å) ^{a-d}		
K(C-C) = 2.8	H(H-C-Cl) = 0.05	F(Cl...H) = 0.8
K(C-H) = 3.9	H(Cl-C-Cl) = 0.1	F(Cl...Cl) = 0.65
K(C-O) = 11.0	H(C-C-Cl) = 0.2	F(C...Cl) = 0.6
K(C-F) = 4.0	H(C-C-H) = 0.15	F(C...H) = 0.4
K(C-Cl) = 1.75	H(C-C=O) = 0.4	
	C-C=O	
K(C-Br) = 1.5	H(Cl-C=O) = 0.3	F(O...C) = 0.4
	H(C-CO-Cl) = 0.1	F(Cl...O) = 1.0
	H(Br-C=O) = 0.3	F(Br...C) = 0.7
	Br-C=O	
	H(C-CO-Br) = 0.1	F(Br...O) = 0.65
	H(F-C=O) = 0.3	F(F...C) = 1.3
	F-C=O	
	H(C-CO-F) = 0.1	F(F...O) = 1.6
	C-CO-F	
		F' = -(1/10)F
		K = 0.1
Structural parameters ^{a,e}		
Bond lengths, Å	Bond angles, deg	
C-H = 1.09	<O-C-C = 125	
C-C = 1.54	<F-C-O = 125	
C-Cl = 1.76	<F-C(O)-C = 110	
C=O = 1.22	<Cl-C-O = 125	
C-F = 1.37	<Cl-C(O)-C = 110	
C-Br = 2.00	<Br-C-O = 125	
	<Br-C(O)-C = 110	
	other angles = 109° 28'	

^a S. Mizushima, *et al.*, *Spectrochimica Acta*, **13**, 161 (1968). ^b Nakagawa, *et al.*, *J. Chem. Phys.*, **20**, 1723 (1952); ^c T. Simanouti, *ibid.*, **17**, 848 (1949); ^d J. Overend and J. R. Scherer, *ibid.*, **32**, 1296 (1960); ^e Tables of interatomic distance and configuration in molecules and ions (The Chemical Society, London).

However, although these calculations are not sufficiently precise to determine the conformation of the more polar isomer, they serve a useful purpose in that they give strong evidence that one rotational isomer of each molecule has a conformation with $\theta \approx 0^\circ$ which from consideration of Figure 2 may be seen to be the less polar form. Evidence for the conformation of the more polar isomer must be sought from the calculation of normal vibrations.

Calculations of Normal Vibrations

Thirteen of the fifteen normal vibrations have been calculated for each compound studied, using a Urey-Bradley type potential function similar to that employed by Mizushima, *et al.*,³ *i.e.*

$$V = \sum_i [K_i' r_{i0} (\Delta r_i) + \frac{1}{2} K_i (\Delta r_i)^2] + \sum_{ij} [H_{ij}' r_{i0} r_{j0} (\Delta \alpha_{ij}) + \frac{1}{2} H_{ij} r_{i0} r_{j0} (\Delta \alpha_{ij})^2] + \sum_{ij} [F_{ij}' q_{ij0} (\Delta q_{ij}) + F_{ij} (\Delta q_{ij})^2] \quad (2)$$

where the r_i 's and α_{ij} 's and q_{ij} 's represent bond lengths, bond angles, and distances between nonbonded atoms, respectively, and the subscript o signifies an equilibrium distance.

The calculations have been made neglecting interactions between atoms in different rotating groups. This obviously does not give an ideal representation of the acid halides and any conclusion based on the results must be regarded as tentative. Table V gives the force constants and molecular parameters used in the analyses and the resulting frequencies are presented in Table VI for various values of the azimuthal angle. The agreement between observed and calculated frequencies is only fair and does not warrant an attempt to assign each isomer to a particular conformation of the molecule. The so-called product rule⁹ does, however, enable a determination of the conformation of rotational isomers from the product of the normal frequencies, according to the equation

$$\frac{\pi \nu_M^2 \text{ (more polar isomer)}}{\pi \nu_L^2 \text{ (less polar isomer)}} = \frac{|G(\theta_M)|}{|G(0^\circ)|} \quad (3)$$

where G is the G matrix which is dependent only on the azimuthal angle θ .

It is assumed that our assignment of the less polar isomer to a conformation $\theta = 0^\circ$ is correct and attempts are then made to determine the conformation θ_M of the more polar isomer. Calculated values of the right-

Table VI: Frequencies Calculated for Various Values of the Azimuthal Angle

Calculated frequencies					Observed frequencies	
0°	45°	90°	135°	180°	More polar form	Less polar form
CHCl ₂ COF						
2938	2937	2936	2937	2937	2985	2985
1784	1786	1788	1785	1783	1876	1859
1255	1260	1267	1266	1258	1282	1250
1210	1202	1191	1205	1215	1214(?)	1250(?)
1165	1171	1177	1153	1141	1111	1214
917	924	935	943	946	901	873
775	816	841	825	782	826	826
758	722	703	714	760	784	769
664	655	637	644	650	671	647
418	416	405	405	409
383	367	369	376	383	398	422
277	274	267	267	274	284	268
227	213	192	226	240	238	187
CHCl ₂ COCl						
2937	2937	2936	2937	2937	3003	3003
1747	1748	1750	1747	1745	1818	1786
1254	1256	1260	1259	1255	1252	1242
1172	1173	1175	1179	1181	1212	1224
1086	1086	1080	1064	1054	986	1075
801	820	833	813	766	838	800
760	743	730	734	762	760	739
597	619	652	695	727	585	640
528	524	515	502	491	458	500
397	392	377	372	383
383	338	309	330	344	334	407
268	271	259	237	239	260	260
161	155	154	201	214	237	176
CHCl ₂ COBr						
2937	2937	2936	2937	2937	3000	3000
1745	1747	1748	1746	1744	1815	1786
1254	1257	1261	1260	1256	1242	1227
1173	1173	1175	1181	1185	1198	1218
1106	1107	1101	1083	1073	962	1042
804	823	835	815	765	794	774
760	745	736	740	762	744	704
604	621	649	694	736	571	604
467	465	453	431	405	451	517
383	380	370	368	383	338	358
364	314	285	313	339	319	371
264	268	246	225	238	246	262
128	128	135	180	182	217	151

hand side of eq 3 for various values of θ_M are given in Table VII together with the experimental values $\pi\nu_M^2/\pi\nu_L^2$ calculated from the observed frequencies of Table VI. Although only 12 of the necessary 13 frequencies are known for each isomer of the acid fluoride and acid chloride, the calculated frequencies of these unobserved bands show little variation with azimuthal angle and their neglect will have only a small effect on the value of $\pi\nu_M^2/\pi\nu_L^2$.

The best fit between experimental and calculated values for dichloroacetyl chloride and dichloroacetyl

Table VII: Values of $||G(\theta_M)|/|G(0^\circ)|$

θ_M , deg	CHCl ₂ COF	CHCl ₂ COCl	CHCl ₂ COBr
0	1.00	1.00	1.00
45	0.78	0.77	0.76
90	0.57	0.57	0.58
135	0.82	0.91	1.00
180	1.06	1.20	1.33
Experimental $\pi\nu_M^2/\pi\nu_L^2$	1.63	0.86	0.86

bromide will be for an azimuthal angle θ_M between 90° and 135° , and within the limitations of experiment and calculations one should not attempt to define the angle more precisely than this.

The previous workers decided on an angle of approximately 90° for dichloroacetyl chloride and state that an electron diffraction investigation on gaseous dichloroacetyl chloride³ may also be accounted for by the coexistence of two forms with azimuthal angles of 0 and 90° .

The experimental values of $\pi\nu^2_M/\pi\nu^2_L$ for dichloroacetyl fluoride shows no agreement with the calculated values of Table VII and can only be explained in terms of a less polar conformation with $\theta \sim 90^\circ$ and more polar

conformation with $\theta \sim 180^\circ$. This seems a surprising result in view of the conformational potential energy calculations. However, there is no way in which we can with any confidence or justification perform a major adjustment of the vibrational assignments to make the results conform with the acid chloride and bromide derivatives. This is particularly true in the present case because of the additional information which is obtained from studying a series of closely related molecules. Nevertheless, the result is unexpected and clearly the need for a further study using a different technique, perhaps that of electron diffraction, must be emphasized.

An Electron Spin Resonance Study of Several Purine and Pyrimidine Radical Anions¹

by Michael D. Sevilla

Atomic International Division of North American Rockwell Corp., Canoga Park, California 91304
(Received August 14, 1969)

Electron spin resonance spectra of purine, 6-cyanopurine, pyrimidine, and 5-methylpyrimidine anions were obtained during electrolysis in dimethylformamide solution at low temperature. These spectra were analyzed and reduced to hyperfine splitting constants. Analysis of the spectrum of the 5-methylpyrimidine anion aided in the complete assignment of splittings to positions on the pyrimidine structure. Interpretation of the spectrum of 6-cyanopurine enabled the assignment of the largest splitting to the 6 position on the purine structure. McLachlan SCF-MO calculations were performed for comparison to experiment and as an aid in the assignment of the remaining hyperfine splittings to molecular positions on the purines. For the purines the splittings and assignments are: purine $A_3^N = 4.4 \pm 0.3$ G, $A_6^H = 10.4 \pm 0.2$, $A_8^H = 4.4 \pm 0.3$, $A_2^H = 1.8$, $A_{1(9)}^N = 1.2$; 6-cyanopurine $A_1^N = 2.43 \pm 0.03$ G, $A_{2(9)}^H = 0.18 \pm 0.02$, $A_3^N = 3.81 \pm 0.05$, $A_{7(9)}^N = 0.74 \pm 0.02$, $A_8^H = 4.14 \pm 0.05$, $A_{9(7)}^N = 0.99 \pm 0.02$, $A_{11}^N = 1.55 \pm 0.02$. Good agreement between the magnitudes of the calculated and experimental hyperfine splittings is found for each anion. An aromatized dimer anion, 5,5'-dimethyl-2,2'-bipyrimidine⁻, is identified as a product of prolonged electrolysis of 5-methylpyrimidine.

The radical anions of nitrogen heterocycles have been the subject of numerous investigations by electron spin resonance (esr) spectroscopy.^{2a,b,c,d} These investigations have provided improved relations between spin density and the nitrogen hyperfine splittings as well as refined nitrogen coulomb and resonance parameters for use in molecular orbital calculations of the spin density. Past work has also shown that certain anions of nitrogen heterocycles dimerize when prepared by alkali metal reduction.³⁻⁵ The dimerization is often followed by aromatization (loss of hydrogen to form an aromatic system). Dimerization has also been suggested to occur during electrolysis of both pyridine and pyrimidine.^{2a} However, with this technique aromatization of the dimer has not been reported.

In this work the anions of pyrimidine, 5-methylpyrimidine, purine, and 6-cyanopurine (Figure 1) produced by low-temperature electrolysis in dimethylformamide have been investigated by esr spectroscopy. The anion of pyrimidine has been previously investigated in liquid

(1) This research was supported by the United States Atomic Energy Commission under Contract No. AT(04-3)-701.

(2) See the following and references therein: (a) J. C. M. Henning *J. Chem. Phys.*, **44**, 2139 (1966); (b) C. L. Talcott and R. J. Myers, *Mol. Phys.*, **12**, 549 (1967); (c) D. H. Geske and G. R. Padmanabhan, *J. Amer. Chem. Soc.*, **87**, 1651 (1965); (d) T. Kubota, K. Nishikida, H. Miyazaki, K. Iwatani, and Y. Oishi, *ibid.*, **90**, 5080 (1968).

(3) J. Chaudhuri, S. Kume, J. Jagur-Grodzinski, and M. Szwarc, *ibid.*, **90**, 6421 (1968).

(4) R. L. Ward, *ibid.*, **83**, 3628 (1961).

(5) A. Carrington and J. dos Santos Veiga, *Mol. Phys.*, **5**, 21 (1962).

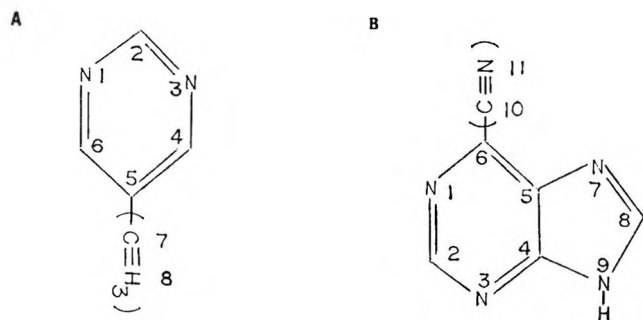


Figure 1. The structure and numbering scheme for the molecules in this study. A. Pyrimidine (5-methylpyrimidine). B. Purine (6-cyanopurine) shown as the 9 H tautomer. The numbering scheme for 5,5'-dimethyl-2,2'-bipyrimidine is based on that of 5-methylpyrimidine.

ammonia; however, this paper reports results which provide for a more complete assignment of splittings. An esr study of the purine anion has not been reported previously. The results found here should aid in the description of the electronic structure of this biologically significant molecule. Finally, strong evidence is found for dimerization and aromatization of the 5-methylpyrimidine anion.

Experimental Section

Materials. Reagent grade dimethylformamide was dried and purified by shaking with potassium hydroxide, then with calcium hydride, and finally by vacuum distilling.

Compounds used for anion generation and their sources were: purine, Waldhof and Aldrich; 6-cyanopurine, Waldhof and Cyclo Chem. Co.; pyrimidine, Aldrich Chem. and Cyclo Chem. Co.; 5-methylpyrimidine, Schwarz Bioreserch. Pyrimidine was purified by gas chromatography. The other compounds were used without further purification.

Electrolytic Generation of Anions. Anions studied in this work were produced by electrolysis. The electrochemical cell used was similar to that used by previous workers.^{2a,6} A tungsten electrode sealed in a 3-mm capillary acted as the cathode. A thin platinum plate acted as the anode. A fritted glass disk separated the cathode and anode. The cell was filled with a 0.1 M solution of the supporting electrolyte, *n*-tetrabutylammonium iodide, in dimethylformamide. Typically the concentration of the substance to be reduced was from 1 to 5 mM. To purge oxygen from the cell the solution was "bubbled" with argon, evacuated, and filled with nitrogen.

The voltage used in electrogeneration of anions was varied for adequate signal with the lowest possible voltage. Voltages used varied from 3.5 to 10 V. The temperature at which electrolysis took place was varied between -55 and 25° . At lower temperatures a drop in ion current took place. This was often more than compensated for by increased radical lifetime. Also at

lower temperatures the concentration of solute can often be increased while maintaining resolution.

A Varian V4510 esr spectrometer equipped with a Fieldial magnetic field regulator, 100-kc modulation, 6-in. ring shim magnet, and a dual cavity was utilized in this work. Measurements of hyperfine splittings were made *vs.* Fremy's salt whose spacings were taken as 12.97 and 13.03 G. ESR spectra were reconstructed for comparison to experiment by use of the GOLD program.⁷

The experimental hyperfine splitting (A_{exp}) in G is related to the radical g value (g_{mol}) by the relation $A_{\text{exp}} = g_e/g_{\text{mol}}A_{\text{true}}$. No attempt was made in this work to obtain accurate g values. However, g values for the molecules reported herein are within the range 2.002 to 2.005; thus the deviation of the experimental hyperfine splitting from the true value is negligible.

Results and Discussion

Pyrimidine Anion. Electrolysis of a 3×10^{-3} M solution of pyrimidine in dimethylformamide at -55° yielded a well-resolved spectrum of the pyrimidine anion (Figure 2). This spectrum differs slightly from that previously reported by Talcott and Myers.^{2b} They obtained the anion by electrolysis in liquid ammonia and found that the largest hydrogen splitting was a multiple of the nitrogen splitting. In dimethylformamide this condition was not found. We therefore have been able to make an unequivocal determination of these splittings which verifies the conclusions of Talcott and Myers. The results of the spectral analysis are reported in Table I along with those previously reported. The differences between the two results are small but beyond the limits of error and must therefore be attributable to a solvent effect.

Since the 9.54-G splitting arises from two equivalent protons and the 3.34-G splitting arises from two equivalent nitrogens they may be unequivocally assigned to the 4,6 and 1,3 positions, respectively. The smaller splittings have been assigned by analysis of the spectrum of 5-methylpyrimidine.

Continued electrolysis of 10^{-2} M solutions of pyrimidine in DMF at -30° resulted in a secondary spectrum. The spectrum consisted of 15 broad lines each separated by approximately 1.5 G. The same esr spectrum was found by reaction of a tetrahydrofuran solution of pyrimidine with a potassium mirror at room temperature.⁸ Due to the reported occurrence of aromatized dimer anions for similar molecules and the results found for 5-methylpyrimidine (see below), it is possible that this spectrum is due to a "dimer" anion or

(6) C. P. Poole Jr., "Electron Spin Resonance," Interscience Publishers, New York, N. Y., 1967, p 620.

(7) W. A. Young, *J. Appl. Phys.*, **35**, 460 (1964).

(8) However, a more complex spectrum has been previously reported as the product of alkali metal reduction. See R. L. Ward, *J. Amer. Chem. Soc.*, **84**, 332 (1962).

Table I: Experimental Hyperfine Splittings for the Pyrimidine and Purine Anions

Anion	Position ^a	Splitting, G	T, °C
Pyrimidine	1 (N)	3.34 ± 0.01 (3.26) ^b	-55
	2 (H)	0.72 ± 0.01 (0.72) ^b	
	4 (H)	9.54 ± 0.03 (9.78) ^b	
	5 (H)	1.24 ± 0.01 (1.31) ^b	
	5-Methylpyrimidine	1 (N)	
2 (H)	0.67 ± 0.02		
4 (H)	9.26 ± 0.03		
5 (CH ₃)	1.56 ± 0.02		
5,5'-Dimethyl-2,2'-bipyrimidine	1 (N)	1.92 ± 0.01	-24
4 (H)	<0.14		
	5 (CH ₃)	3.19 ± 0.01	-55
Purine	3 (N)	4.4 ± 0.3	
	6 (H)	10.4 ± 0.2	
	8 (H)	4.4 ± 0.3	
	2 (H)	(1.85) ^c	
	1 (9) (N) ^d	(1.25) ^c	25
6-Cyanopurine	1 (N)	2.43 ± 0.03	
	2 (9) (H) ^d	0.18 ± 0.02	
	3 (N)	3.81 ± 0.05	
	7 (9) (N) ^d	0.74 ± 0.02	
	8 (H)	4.14 ± 0.05	
	9 (7) (N) ^d	0.99 ± 0.02	
	11 (N)	1.55 ± 0.02	

^a For equivalent positions see Figure 1. ^b Liquid ammonia solvent (ref 2b). ^c Line components from these splittings are not completely resolved. The splittings were inferred from spectrum simulation. ^d Numbers in parenthesis refer to possible sites for this splitting.

a mixture of "dimer" anions. A possible "dimer," 2,2' bipyrimidine anion, has been previously reported;^{2c} however, this spectrum does not correspond to that found here.

5-Methylpyrimidine Anion. The anion of 5-methylpyrimidine was investigated to aid in the assignment of splittings to positions in the pyrimidine anion. The spectrum of 5-methylpyrimidine anion prepared by electrolysis of a $2 \times 10^{-3} M$ solution at -55° is depicted in Figure 3. A straightforward analysis of the spectrum gave the hyperfine splittings reported in Table I.

From the results for the 5-methylpyrimidine anion it can be seen that the methyl group has replaced the proton of 1.24-G splitting in pyrimidine. The possibility that the proton of 0.7-G splitting has been replaced and that the 1.24-G splitting has been reduced to 0.67 G is considered unlikely owing to the small effect of the methyl group on the larger splittings and the correspondence of the magnitude of the smaller splittings in 5-methylpyrimidine and pyrimidine. The smaller splittings in pyrimidine have therefore been assigned accordingly. The assignment of splittings to positions for 5-methylpyrimidine is, of course, unequivocal.

Upon *prolonged* electrolysis of $10^{-2} M$ solutions of 5-methylpyrimidine at temperatures greater than -30°

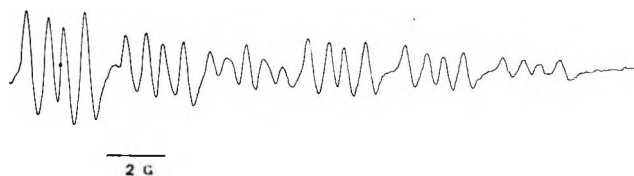


Figure 2. Approximately one-half the first derivative esr spectrum of pyrimidine anion in dimethylformamide at -55° . (Dot marks center.)

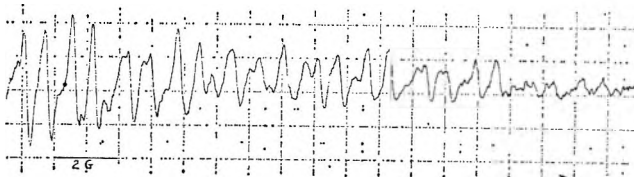


Figure 3. Approximately one-half the first derivative esr spectrum of 5-methylpyrimidine anion in dimethylformamide at -58° .

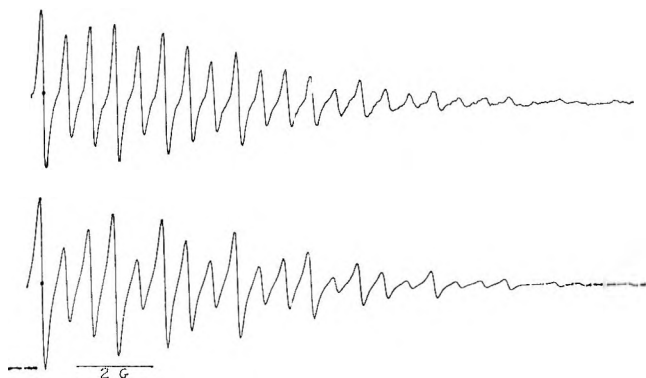


Figure 4. Upper curve, approximately one-half the first derivative esr spectrum of 5,5'-dimethyl-2,2'-bipyrimidine at -24° ; lower curve, calculated spectrum using a 3.19-G splitting arising from 6 hydrogens and a 1.92-G splitting arising from 4 nitrogens. The line width for the computed spectrum is slightly larger than the experimental.

a secondary spectrum appeared (Figure 4). The spectrum extends over 30 G and the intensity is sufficient to resolve all line components except for the end component (as interpreted). This always leads to some uncertainty in the interpretation, but several factors indicate that the spectrum is due to an aromatized anion. First, the spacing, regularity, and intensity ratios indicate a large number of equivalent protons such as would be found for two equivalent methyl groups. Second, the fact that this spectrum appeared at higher concentrations of 5-methylpyrimidine and only after prolonged electrolysis is consistent with "dimer" formation. Of the several possible aromatized dimers of 5-methylpyrimidine the only one that could yield such a regular spectrum is 5,5'-dimethyl 2,2'-bipyrimidine. Analysis of the spectrum on the basis of this structure yielded the splittings reported in Table I. The splitting due to the four *meta* protons is not resolved

and is therefore less than the line width (ca. 0.14 G). A spectrum computed on the basis of this analysis is shown in Figure 4. The good fit between theory and experiment is considered strong evidence for a 2,2' dimer.

The preferential observance of the 2,2' aromatized dimer is most likely explained by the fact that dimerization at the 4 position to produce 2,4' or 4,4' dimers is less likely due to steric interactions. Also, even if such species are formed and subsequently aromatized they would have many more hyperfine components than the 2,2' anion and therefore would be more difficult to observe.

Purine. Purine anion was formed by electrolysis of 0.001 *M* solutions of purine at temperatures between -34 and -55° . The esr spectrum observed for this radical is only moderately resolved, $\Delta H_{ms} \cong 0.9$ G (Figure 5). The large line width is most likely a result of unresolved hyperfine splittings. There is also evidence for a second radical species, present in lower concentrations, in the spectrum. It is possible that the second radical is associated with one of the two possible tautomeric forms of purine, *i.e.*, the hydrogen can be at the 7 or 9 position. Analysis of the spectrum in Figure 5 yields 10.4 and 4.4-G splittings due to one proton each and a 4.4-G nitrogen splitting. Owing to the poor resolution the two 4.4-G splittings could differ by as much as 0.6 G and still not be resolved. Two smaller splittings of approximately 1.8 G (proton) and 1.2 G (nitrogen) are inferred from analysis of the end portion of the spectrum. These splittings account for only 5 of the 8 possible. The remaining three splittings must be less in magnitude than the line width, 0.9 G. A computer reconstruction using the above splittings is shown in Figure 5. The excellent agreement between the experimental and theoretical spectra suggests that the analysis is correct. Assignment of the splittings to positions on the purine molecule is not possible from the experimental results, since all positions on the purine molecule are unequivalent. The splittings have therefore been assigned where possible by recourse to McLachlan SCF-MO theory (discussed below) as shown in Table I.

6-Cyanopurine. The anion of 6-cyanopurine was prepared to aid in the analysis of the purine anion spectrum and to confirm the assignment by theory of the 10.4-G splitting to the 6 position. This compound was chosen since the cyano group has been shown to have a relatively small electron withdrawing effect,⁹ *i.e.*, in electron withdrawing power $CN < COOCH_3 < COCH_3 < CHO < NO_2$. It is therefore reasonable to assume for the case of 6-cyanopurine anion that the cyano group will have only a modest effect on the spin density distribution.

The spectrum of 6-cyanopurine was observed from -50 to $+25^\circ$. Best resolution occurred at 25° (Figure 6). Analysis of this spectrum is complicated due to

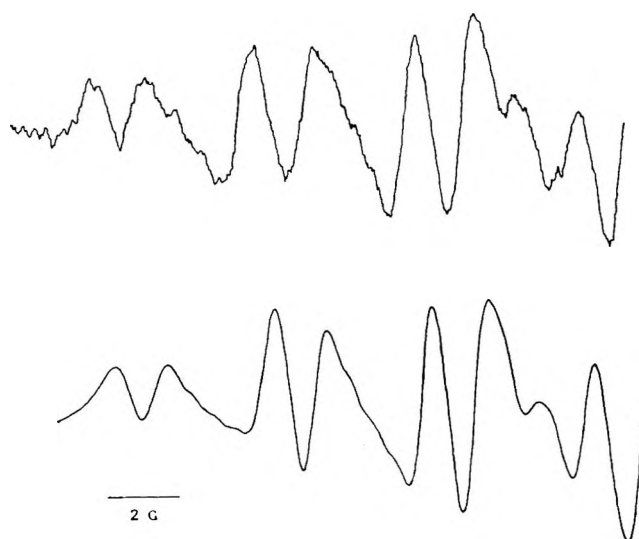


Figure 5. Upper curve, one-half the first derivative esr spectrum of purine anion at -55° ; lower curve, calculated spectrum using 10.4, 4.4, and 1.85-G splittings arising from one hydrogen each as well as 4.4 and 1.25-G splittings arising from one nitrogen each ($\Delta H_{ms} = 0.9$ G).

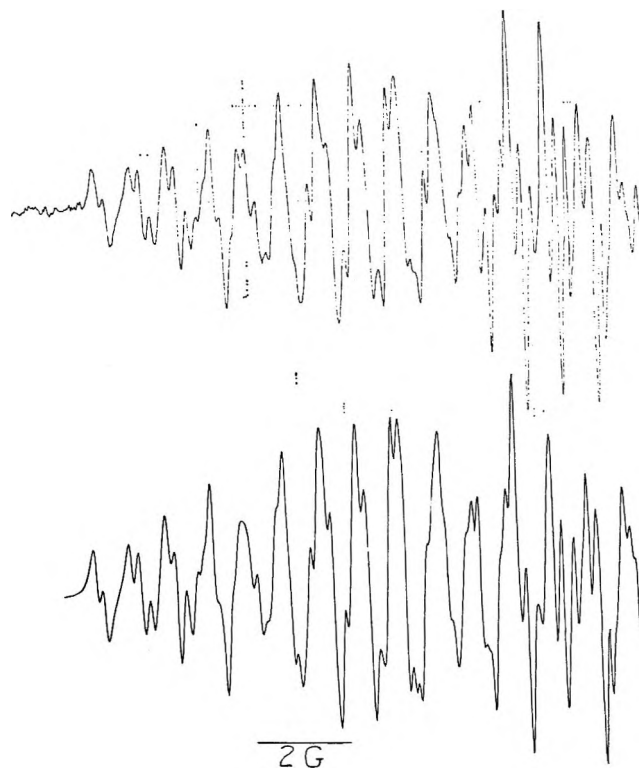


Figure 6. Upper curve; one-half of the experimental esr spectrum of 6-cyanopurine anion at 25° ; lower curve, computer simulated spectrum using hyperfine parameters discussed in text.

the fact that all positions on the molecule are unequivalent. In addition there are both nitrogen and hydrogen splittings, and there are a large number of theoretical

(9) M. Hirayama and T. Isobe, *Bull. Chem. Soc. Jap.*, **41**, 1502 (1968).

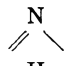
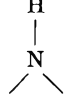
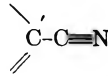
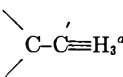
hyperfine lines. Interpretation of the spectrum proceeded by examination of the end portion of the spectrum. This yielded the splittings 0.18, 0.74, 0.99, 1.55, and 2.43 G. The spectrum shows that the 0.8-G splitting is obviously a proton splitting. The other splittings were all shown to be due to nitrogens by spectrum simulation. The remaining larger splittings were determined to be 4.14 G (proton) and 3.81 G (nitrogen) by an inspection of the central portion of the spectrum and many computer simulations. The reconstruction of the 6-cyanopurine spectrum with the above splittings is shown in Figure 6 and is in excellent agreement with experiment. The hyperfine splittings clearly show that the proton of 10.4-G splitting in purine has been replaced by the cyano group in 6-cyanopurine. The remaining proton splitting unaccounted for in the analysis must be less in magnitude than the line width of 0.13 G.

As in the case of purine, 6-cyanopurine also has two possible tautomeric forms, 9 H or 7 H. The clearly resolved spectrum for the anion shows that the concentration of one form is much greater than the other. Molecular orbital calculations performed for both of these possible species (see below) are used to assign the hyperfine splittings to positions on the 6-cyanopurine structure where possible (see Table I).

Spin Density Calculations

McLachlan SCF-MO calculations¹⁰ have been performed for the radical anions in this study to aid in the assignment of experimental splittings to molecular positions, to compare experimental and theoretically calculated splittings, and possibly to indicate which of the tautomeric forms of the purine anions predominate. The heteroatom coulomb and resonance parameters and hyperconjugation parameters used in these calculations are given in Table II. The parameters for the aromatic nitrogen are considered to be the most critical to the calculation. The value of h_N was therefore varied between 0.4 and 1.0. The results are found to be relatively insensitive to the different values of h_N and no improvement in the overall agreement with experiment over that for $h_N = 0.8$ is found. The spin density calculations are reported in Table III. The comparison of theory with experiment is best accomplished by calculation of theoretical values of the hyperfine splittings. This requires relationships which relate spin density and isotopic hyperfine splitting. The relations $A_H = Q_{C-H} \rho_C^\pi$ ($Q_{HC^H} = -24.5$) for >C-H ,^{2b} $A_N = Q_N^N \rho_N^\pi + Q_{CN}^N$ ($\rho_C^\pi + \rho_{C'}^\pi$) ($Q_N^N = 27.3$, $Q_{CN}^N = -1.7$) for >C-N ,^{2b} $A_N = Q_N^N \rho_N^\pi + Q_{CN}^N \rho_C^\pi$ ($Q_N^N = 23.1$, $Q_{CN}^N = -6.8$) for $\text{>C-C}\equiv\text{N}$,¹¹ and $A_{CH_3} = 217 \rho_{H_3}^\pi$ for >C-CH_3 ,^{12a,b} have been employed with good results in similar mole-

Table II: MO Parameters Used in Calculations

Group	Parameters	Ref
	$h_N = 0.8$ $k_{CN} = 1.08$	2b
	$h_N = 1.5$ $k_{CN} = 1.0$	18
	$h_N = 1.0$ $k_{C=N} = 2.0$ $k_{C-C} = 0.9$	11
	$h_{H_3} = 0.5$ $h_{C'} = -0.1$ $h_{C=H_3} = 2.5$ $h_{C-C'} = 0.93$	

^a R. Bershon, *J. Chem. Phys.*, **28**, 1188 (1958).

cules and are used in the calculation of hyperfine splittings. These results are listed in Table III.

The results found for pyrimidine anion are in reasonable agreement with experiment and have been discussed elsewhere.^{2b,13} The calculated splittings for 5-methylpyrimidine are nearly identical with those calculated for pyrimidine discounting the methyl proton splitting. In agreement with theory the experimental results for these two anions show only a small effect of the methyl group. Methyl groups do not usually result in large shifts in spin density but such a small change is unusual.¹⁴ This can be understood from the form of the Hückel molecular orbital (HMO) occupied by the unpaired electron in pyrimidine. This MO has a node at position 5 where the methyl group is substituted and consequently the methyl group has no effect on the coefficients of this MO, but several of the MO's associated with other energy levels do not have a node at position 5 and thus are affected by the methyl group. Although the HMO spin densities are unaffected by the methyl group, the McLachlan spin densities are altered slightly since they

(10) D. A. McLachlan, *Mol. Phys.*, **3**, 233 (1960).

(11) P. H. Rieger and G. K. Fraenkel, *J. Chem. Phys.*, **37**, 2795 (1962).

(12) (a) D. Lazdins and M. Karplus, *ibid.*, **44**, 1600 (1966); (b) D. H. Levy, *Mol. Phys.*, **10**, 233 (1966).

(13) The calculated spin densities for pyrimidine reported here differ from those reported by Talcott and Myers (ref 2b). The same parameters are employed in each calculation. The difference arises in the computation of the atom-atom polarizabilities. Important to the computation of the polarizabilities is a sum which is taken over the filled and vacant orbitals. The problem arises that for a radical one orbital is half-filled. In this work this orbital is included as part of the filled set as recommended by McLachlan (ref 10). Talcott and Myers include the half-filled orbital with the vacant set and achieve better agreement with experiment; however, the improvement in results is not found to extend to computations for purine and 6-cyanopurine where these methods give similar results.

(14) J. A. Valenzuela and A. J. Bard, *J. Phys. Chem.*, **73**, 779 (1969).

Table III: Theoretical Spin Densities and Hyperfine Splittings

Anion	Position	McLachlan spin density		Theoretical hyperfine splittings, G		Experimental hyperfine splittings G
Pyrimidine	1		0.177		4.23	3.34
	2		-0.028		0.69	0.72
	4		0.375		9.20	9.54
	5		-0.078		1.91	1.24
5-Methylpyrimidine	1		0.177		4.23	3.34
	2		-0.027		0.66	0.67
	4		0.377		9.24	9.26
	5		-0.073	
	7		-0.000	
5,5'-Dimethyl-2,2'-bipyrimidine	8		-0.0082		1.78	1.56
	1		0.082		1.91	1.92
	2		0.210	
	4		-0.013		0.32	<0.10
	5		0.137	
Purine	7		-0.003	
	8		0.0180		3.90	3.19
		9 H	7 H	9 H	7 H	
	1	0.048	0.082	0.49	1.63	1.2
	2	0.048	0.013	1.18	0.32	1.8
	3	0.162	0.156	4.22	4.06	4.4
	4	0.070	0.112
	5	0.007	-0.034
	6	0.436	0.391	10.68	9.59	10.4
	7	0.017	0.022	0.07	0.19 (N) 0.55 (H)	...
	8	0.220	0.274	5.38	6.72	4.4
9	-0.009	-0.016	0.64 (N) 0.22 (H)	1.09 7 H	(1.2)	
6-Cyanopurine		9 H	7 H	9 H	7 H	
	1	0.090	p.107	1.84	2.36	2.43
	2	0.011	-0.003	0.27	0.07	0.18 (<0.13)
	3	0.152	0.153	3.99	4.00	3.81
	4	0.081	0.112
	5	0.030	-0.005
	6	0.353	0.329
	7	0.002	0.007	0.28	0.17 (N) 0.18 (H)	0.74 (0.99) (N) ^a
	8	0.172	0.217	4.22	5.31	4.14
	9	-0.010	-0.018	0.72 (N) 0.25 (H)	1.05	0.99 (0.74) (N) <0.13 (0.18)
	10	0.032	0.027	...		
11	0.0872	0.0794	1.79	1.65	1.55	

^a The 0.18-G splitting could also arise from this position.

are calculated using atom-atom polarizabilities which depend on the coefficients of all the molecular orbitals.

The steric interaction of the pyrimidine groups of 5,5'-dimethyl-2,2'-bipyrimidine is such that a non-planar structure would be expected. For biphenyl, a molecule with a similar molecular structure but perhaps more steric interaction from its ortho hydrogens, the dihedral angle between the phenyl groups has been estimated to be approximately 40°. For this reason theoretical splittings for this 5-methylpyrimidine "dimer" have been calculated as a function of the angle between the two aromatic planes. The angle of twist has been simulated in the calculation by a reduction in the resonance integral between the carbon

atoms joining the two rings. The relation $k^* = k \cos \theta$ describes the reduction in the resonance parameter k with the angle of twist θ and has been both experimentally and theoretically justified.¹⁶ Results of the calculations showed that the methyl proton splitting is nearly invariant with angle while the nitrogen splitting is more sensitive. Best results are found at $k = 0.8$, $\theta = 37^\circ$. The results of this calculation are given in Table III. The uncertainty in the value of θ must be considered large due to the only moderate change in splitting with angle and the uncertainty in the calculation of the

(15) K. Mobius, *Z. Naturforsch.*, **20a**, 1117 (1965).

(16) M. D. Sevilla and G. Vincow, *J. Phys. Chem.*, **72**, 3647 (1968).

nitrogen hyperfine splitting constant; however, the results clearly suggest that the anion is nonplanar. It should be noted that the good agreement between the calculated and experimental splittings is further evidence for the structure of this molecule and consequently the dimerization reaction.

The molecular orbital calculations for purine and 6-cyanopurine listed in Table III are especially important since they must be used to assign hyperfine splittings to molecular positions. Further, they may aid in the assignment of the correct tautomeric structure to the anions.¹⁷

The calculated hyperfine splittings for both the 7 H and 9 H tautomers of purine given in the table predict that positions 3(N), 6(H), and 8(H) are the positions of large splitting with the largest splitting arising from the 6 position. Since substitution of the cyano group at the 6 position of purine showed this position to be the site of the 10.4-G hydrogen splitting, the calculation is in agreement with experiment. The remaining larger splittings of 4.4 G due to a nitrogen and a hydrogen can therefore be assigned to positions 3 and 8 with confidence. Closer examination of the calculated splittings shows that the calculation for the 9 H tautomer is in much better agreement with the individual magnitudes of the larger splittings. The smaller splittings of 1.8 G (H) and 1.2 G (N) are also in better agreement with the calculation for the 9 H tautomer and have been assigned accordingly. The improvement for the 9 H calculation is sufficient to suggest that the 9 H tautomer may be the anion species which predominates in the spectrum of purine anion.

The calculated hyperfine splittings for the 6-cyanopurine 7 H and 9 H tautomers are quite similar; so similar that the same assignment of splittings to positions results for each calculation. In addition, the agreement between the calculated results and experiment is excellent. The largest splitting is in better agreement with the calculation for the 9 H tautomer, but from the overall agreement it is not possible to differentiate between the two calculations. A comparison of the calculated results for purine and 6-cyanopurine predicts that the effect of the cyano group on the larger splittings is small. This is confirmed by the experimental results. The theoretical results predict that the splittings at positions 2, 3, and 8 will be lowered while that at position 1 will be raised by the

substitution of the cyano group. This is also in agreement with the experimental results.

It is apparent that in this case an indication of which tautomer is the more stable cannot be obtained from the calculation of hyperfine splittings. Another method to obtain such an indication may be the calculation of the total HMO π -electron energy for the two tautomers. The total energy of such a system cannot be expected to be predicted accurately but simple MO theory often correctly predicts qualitative differences in results¹⁸ and might be expected to do so in this case. This calculation was performed and shows the 9 H tautomer is favored by 1.6 kcal ($\beta = 50$ kcal) over the 7 H tautomer.

Summary

Comparison of theory and experiment for purine and 6-cyanopurine shows that McLachlan MO computations of the spin density are in reasonable agreement with experiment. In addition, this comparison suggests that the 9 H tautomer may be favored for the purine anion. Simple HMO calculations of the total electron energy also suggest that the 9 H tautomer may be favored for 6-cyanopurine as well.¹⁹

The theoretical and experimental results for pyrimidine and 5-methylpyrimidine are also in reasonable agreement. The experimental results for 5-methylpyrimidine and possibly pyrimidine show that dimerization and aromatization can occur through electrolysis. The mechanism of aromatization is unknown; however, it is known that in alkali metal reductions an excess of alkali metal catalyzes the aromatization of the dimer.³ In electrolysis, catalysis at the metal electrode surface must certainly be considered.

Acknowledgment. The author wishes to express his thanks to Richard Holcyd for many helpful discussions and to Kay Medeiros for her aid in programming the McLachlan SCF-MO theory.

(17) It should be noted that a rapid conversion between the two tautomeric forms of the purines is not considered likely since an aprotic solvent has been employed.

(18) A. Streitwieser, Jr., "Molecular Orbital Theory for Organic Chemists," John Wiley & Sons, New York, N. Y., 1961.

(19) It should be noted that in the crystalline state the neutral purine molecule has been shown to be the 7 H tautomer (D. G. Watson, R. M. Sweet, and R. E. Marsh, *Acta Cryst.*, 19, 573 (1965)). The results found here are not considered to be in disagreement with those reported by Watson, *et al.*, since the species observed here is the anion in solution, not the neutral molecule in a crystalline state.

Substituent Effects on Aromatic Proton Chemical Shifts. VII.

Further Examples Drawn from Disubstituted Benzenes¹

by William B. Smith, Arthur M. Ihrig,² and James L. Roark

Department of Chemistry, Texas Christian University, Fort Worth, Texas 76129 (Received August 1, 1969)

The nmr parameters for a series of 2-substituted anilines, 2-substituted toluenes, 1-perdeuteriophenyl-2-X-benzenes, and several 9-substituted fluorenes have been determined. The chemical shifts are considered in relation to the Q parameters for the various substituents. Substituent interactions due to size and intramolecular hydrogen bonding are discernible in the ring proton spectra. The Q values for a variety of substituents are summarized, and some further insights into the meaning of the Q parameter are offered.

Introduction

Interest in the role which aromatic ring substituents play in determining the chemical shifts of protons attached to the ring has continued over the years in the hope that nmr data could be used to garner more information on ground state electronic properties and chemical reactivities of these molecules. While a variety of rationalizations have been put forth to explain the nmr data,^{1c} it would appear that *ortho* effects of the substituent are best correlated by means of the parameter Q .

First defined as an empirical parameter, Schaefer and coworkers³ have suggested that Q is a measure of the paramagnetic shielding produced by the mixing of excited states of the substituent with the ground state of the electrons in the C-H bond. From the original definition one can calculate Q values only for hydrogen and the halogens. Subsequently, an experimental method for ascertaining Q values was developed, and a number of these are now available.^{1c,d} It has been observed that groups which do not have cylindrical symmetry about the bond to the aromatic ring usually require two Q values to correlate completely their *ortho* effects; Q (1) values apply when the substituent is flanked only by hydrogens while the Q (2) values apply when an *ortho* substituent is present.

In a logical extension of the work previously reported on a series of *ortho*-substituted phenols,^{1d} the nmr parameters for a similar series of anilines have been determined in both carbon tetrachloride and in dimethyl sulfoxide (DMSO). Since the work in both the phenol and aniline series consisted of substituents to which the hydroxyl and amino groups might potentially hydrogen bond, a group of *ortho*-substituted toluenes have been examined, and these nmr parameters are also reported below.

Finally, the role of substituent magnetic anisotropy in determining proton chemical shifts should be at a maximum at the *ortho* position. This effect has been proposed to account for the odd *ortho* effects of the

halogens.⁴ However, to date no consistent set of magnetic anisotropies has been produced for the halogens which lead to meaningful results in aromatic systems. Undoubtedly the group with most reliably known magnetic anisotropy is the phenyl group. Nmr results on a series of substituted biphenyls have been obtained and are reported here. As a complement to these data, a series of 9-substituted fluorenes have also been examined. Here the geometric relation between the two phenyl rings is fixed by the bridging carbon.

Experimental Section

Materials. The various anilines and toluenes used in this study were all commercially available. Those which gave any indication of impurities were distilled or recrystallized before use.

The method of Wanscheidt⁵ was used to prepare 9-iodofluorene, while 9-methoxyfluorene was synthesized by the method of Kliegel.⁶ Fluorene and the remaining 9-substituted fluorenes were commercially available. Dibiphenylene ethylene was prepared from 9-bromofluorene by the method of Bethell.⁷ A sample of 9-dichloromethylenefluorene was kindly provided by Dr. C. G. Venier.

The Elks, Hawthorne, and Hey modification of the Gomberg reaction was used to prepare a series of 1-

(1) For previous papers in this series see (a) W. B. Smith and G. M. Cole, *J. Phys. Chem.*, **69**, 4413 (1965); (b) W. B. Smith and S. Chiranjeevi, *ibid.*, **70**, 3505 (1966); (c) W. B. Smith and J. L. Roark, *J. Amer. Chem. Soc.*, **89**, 5018 (1967); (d) J. L. Roark and W. B. Smith, *J. Phys. Chem.*, **73**, 1043 (1969); (e) J. L. Roark and W. B. Smith, *ibid.*, **73**, 1046 (1969); and (f) W. B. Smith and J. L. Roark, *ibid.*, **73**, 1049 (1969).

(2) T. C. U. Research Foundation Postdoctoral Fellow, 1968-1969.

(3) (a) F. Hruska, H. M. Hutton, and T. Schaefer, *Can. J. Chem.*, **43**, 2392 (1965); (b) T. Schaefer, F. Hruska, and H. M. Hutton, *ibid.*, **45**, 3143 (1967).

(4) (a) H. Spiesecke and W. G. Schneider, *J. Chem. Phys.*, **35**, 731 (1961); see also (b) J. S. Martin and B. P. Dailey, *ibid.*, **39**, 1722 (1963).

(5) A. Wanscheidt, *Ber.*, **59**, 2092 (1926).

(6) A. Kliegel, *ibid.*, **62**, 1327 (1929).

(7) D. Bethell, *J. Chem. Soc.*, 666 (1963).

perdeuterio-2-X-benzenes where X is fluoro, chloro, bromo, and nitro.⁸ The same procedure was used to prepare 4-chloro-1-perdeuteriophenylbenzene from *p*-chloroaniline. The procedure for the 2-chloro compound is typical.

A solution was prepared from 2.14 g of *o*-chloroaniline in 5.3 ml of concentrated hydrochloric acid and 3 ml of water. The mixture was cooled in ice, and the diazotization reaction carried out by the slow addition of 1.21 g of sodium nitrite dissolved in 2.5 ml of water. The solution of diazonium salt solution and 35 ml of perdeuteriobenzene was chilled in a reaction vessel equipped with a high-speed stirrer. While this mixture was chilled and stirred, a solution of 5.35 g of sodium acetate trihydrate in 12 ml of water was slowly added (1.5 hr). After 6 hr the reaction mixture was allowed to come to room temperature, and stirring was continued for 2 days. The reaction mixture was steam distilled, and the benzene layer was separated, dried, and the unreacted benzene recovered by distillation. The viscous brown residue was purified by washing through an alumina column with Skellysolve A and ethyl ether. A crystallization from ethanol-water gave 1.04 g of 1-perdeuteriophenyl-2-chlorobenzene, mp 33.5–34.0° (lit.⁸ 34°). The melting points of all of the perdeuteriophenylated compounds prepared in this fashion agreed closely with the literature values of the appropriate nondeuterated biphenyls. The bromo and iodo compounds (prepared as below) were liquids and not purified beyond the alumina chromatography step. Their nmr spectra were normal, and all bands were fitted.

The 2-iodo, 2-cyano, and 2-hydroxy derivatives were prepared by the standard Sandmeyer reaction from 1-perdeuteriophenyl-2-aminobenzene.⁹ The latter substance was prepared by the catalytic hydrogenation of the 2-nitro compound in ethanol using palladium (5%) on carbon as the catalyst and room temperature with 3 atm pressure of hydrogen. The amine was crystallized from Skellysolve A in 82% yield, mp 47.0–48.5° (lit.¹⁰ 49–50°).

The *o*-terphenyl and 4-nitrobiphenyl were commercially available and were used without further purification.

Nmr Determinations. All nmr spectra were determined on a Varian HA-100. Solutions (10% w/v) in carbon tetrachloride and containing a small amount of tetramethylsilane were degassed and sealed under vacuum. The anilines were also examined in deuterated DMSO as previously with the phenols;¹⁴ the chemical shifts in DMSO were estimated from the completely analyzed spectra in carbon tetrachloride.

The methyl group of the toluenes, the *t*-butyl methyls in the *t*-butylbenzene derivatives, and the proton(s) at C-9 in the fluorenes were spin decoupled with the aid of a Hewlett-Packard 200 CD audio oscillator.

The fluorine spectrum of 1-perdeuteriophenyl-2-

fluorobenzene was determined at 94.1 MHz using 1,1,2,2-tetrachloro-3,3,4,4-tetrafluorocyclobutane (TC-TFB) as an internal standard. This spectrum was treated as an ABCDX system, and all five spins were fitted using both the proton and fluorine spectra.

All spectra were taken four to six times and the line positions averaged. The parameters were determined using the precepts stated before.^{1a,c,11} The LAOCOON program¹² was employed throughout. In several cases where iterated parameters seemed suspicious, the 60-MHz spectrum was calculated and checked against that produced on a Varian A-60A. Line assignments were altered if the 60-MHz fit was unsatisfactory. In general, the spectra of the compounds studied here provided 28–40 lines out of a possible maximum of 56. All lines were used in the computer program for fitting the spectra. The root-mean-square deviations for the calculated and experimental lines were routinely 0.05 Hz or less.

Results

The chemical shifts and coupling constants for the various series and a selection of miscellaneous disubstituted benzenes are given in Tables I–V.¹³ For the *ortho*-disubstituted benzenes proton chemical shifts for protons nonadjacent to substituents were assigned on the basis of the rules of Martin and Dailey.^{4b} In moderately perturbed systems, protons adjacent to substituents were assigned on the basis of splitting patterns, long-range couplings if observed, or so as to give the most consistent data pattern if no other criterion existed. The published chemical shift values for biphenyl in carbon tetrachloride were used to determine the substituent constants for the phenyl group as $d_o - 0.17$ ppm, $d_m + 0.01$ ppm, and $d_p + 0.11$ ppm.¹⁴

Several of the *ortho*-substituted anilines gave broadened spectra due to coupling with the amine protons. Weil, *et al.*,¹⁵ have reported a stereospecific coupling

(8) J. Elks, J. W. Hawthorne, and D. H. Hey, *J. Chem. Soc.*, 369 (1940).

(9) D. A. Shirley, "Preparation of Organic Intermediates," John Wiley & Sons, New York, N. Y., 1951.

(10) H. A. Scarborough and W. A. Waters, *J. Chem. Soc.*, 89 (1927).

(11) W. B. Smith and J. L. Roark, *J. Chem. Eng. Data*, 12, 587 (1967).

(12) S. Castellano and A. A. Bothner-By, *J. Chem. Phys.*, 41, 3863 (1964).

(13) We are well aware that studies of aromatic proton chemical shifts are preferred in a more "inert" solvent such as cyclohexane (see P. Laszlo in "Progress in Nuclear Magnetic Resonance Spectroscopy," Vol. 3, Ed. J. W. Emsley, J. Feeney, and L. H. Sutcliffe, Pergamon Press, New York, N. Y., 1967, p 243, *et seq.*; B. Richardson and T. Schaefer, *Can. J. Chem.*, 46, 2:95 (1968); and T. Schaefer, B. Richardson, and R. Schwenk, *ibid.*, 46, 2775 (1968)). We have reinvestigated many of the compounds reported in carbon tetrachloride from our earlier studies.¹ In cyclohexane the proton chemical shifts are routinely 0.05–0.1 ppm downfield from the carbon tetrachloride results. However, the results in carbon tetrachloride are internally self-consistent and offer the possibility of studying many compounds which are insoluble in the hydrocarbon solvents.

(14) F. A. Bovey, F. P. Hood, E. Pier, and H. E. Weaver, *J. Amer. Chem. Soc.*, 87, 2061 (1965).

(15) J. A. Weil, A. Blum, A. H. Heiss, and J. K. Kinnaird, *J. Chem. Phys.*, 46, 3132 (1967).

Table I: Parameters for the *ortho*-Substituted Anilines^a

<i>ortho</i> substituent	τ_3	τ_4	τ_5	τ_6	J_{34}	J_{35}	J_{36}	J_{45}	J_{46}	J_{56}
OCH ₃	3.43	3.43	3.43	3.43
	3.40	3.40	3.40	3.40
Cl	2.86	3.43	3.07	3.42	8.00	1.43	0.31	7.35	1.46	8.00
	2.86	3.49	3.02	3.20
Br	2.68	3.49	3.01	3.39	8.07	1.45	0.27	7.32	1.53	8.06
	2.47	3.64	2.99	3.42	7.92	1.45	0.29	7.29	1.50	8.03
I	2.49	3.69	2.96	3.23
	2.71	3.36	2.77	3.31	7.87	1.61	0.44	7.27	0.96	8.48
CN	2.72	3.41	2.79	3.19
	1.93	3.35	2.70	3.21	8.67	1.60	0.44	7.00	1.30	8.41
NO ₂	2.06	3.39	2.64	2.97	8.74	1.60	0.41	6.93	1.33	8.60

^a Coupling constants are in Hz. The first entry for each compound is for carbon tetrachloride; the second is for DMSO.

Table II: Parameters for Some 2-X-Toluenes^a

<i>ortho</i> substituent	τ_3	τ_4	τ_5	τ_6	J_{34}	J_{35}	J_{36}	J_{45}	J_{46}	J_{56}
NH ₂	3.57	3.13	3.45	3.12	7.88	1.24	0.46	7.44	1.49	7.46
OH	3.41	3.08	3.27	3.01	8.06	1.27	0.42	7.40	1.73	7.44
OCH ₃	3.34	2.99	3.28	3.01	8.23	1.18	0.35	7.50	1.74	7.32
Cl	2.76	2.98	2.96	2.89	7.97	1.49	0.29	7.54	1.64	7.60
Br	2.56	3.05	2.91	2.87	8.00	1.16	0.52	7.64	1.58	7.73
CN	2.50	2.77	2.58	2.73	7.87	1.42	0.57	7.69	1.28	7.81
NO ₂	2.13	2.71	2.56	2.71	8.26	1.37	0.48	7.46	1.49	7.72

^a Solutions in carbon tetrachloride. Coupling constants in Hz.

Table III: Parameters for Some 1-Perdeuteriophenyl-2-X-benzenes^a

<i>ortho</i> substituent	τ_3	τ_4	τ_5	τ_6	J_{34}	J_{35}	J_{36}	J_{45}	J_{46}	J_{56}
NH ₂	3.47	3.02	3.33	3.02	7.99	1.16	0.47	7.35	1.60	7.50
OH	3.17	2.89	3.16	2.90	8.09	1.19	0.37	7.41	1.73	7.61
F ^b	2.96	2.83	2.93	2.67	8.27	1.19	0.41	7.47	1.77	7.70
Cl	2.62	2.84	2.81	2.76	8.09	1.28	0.39	7.45	1.73	7.62
Br	2.42	2.92	2.77	2.77	8.00	1.28	0.38	7.41	1.73	7.64
I	2.13	3.08	2.73	2.79	7.95	1.25	0.40	7.35	1.73	7.61
CN	2.36	2.68	2.49	2.59	7.74	1.39	0.56	7.53	1.18	7.96
NO ₂	2.29	2.64	2.52	2.67	8.09	1.36	0.35	7.43	1.52	7.68
C ₆ H ₅ ^c	2.73	2.69	2.69	2.73	7.76	1.41	0.40	7.29	1.41	7.76

^a Solutions in carbon tetrachloride. Coupling constants are in Hz. ^b The chemical shift of the fluorine was 3.72 ppm upfield from TCTFB. Values for the coupling constants to fluorine are J_{3F} 10.27 Hz, J_{4F} 4.97 Hz, J_{5F} -0.29 Hz, and J_{6F} 7.83 Hz. ^c *o*-Terphenyl.

between NH and H₅ in N-acetyl-2,4-dinitroaniline. It is not clear that the couplings observed here are stereo-specific since, in cases where resolution was possible, the spectral lines appeared as triplets implying that the ring protons are coupled to both amino protons. No consistent pattern of ring broadening was noted, *i.e.*, the chloro and bromo anilines showed broadened spectra while the *o*-iodoaniline did not.

While the methyl groups in the toluenes are coupled to all ring protons, the *t*-butyl methyl protons appear to couple only to protons *ortho* to the *t*-butyl group. It

should be mentioned also that in the various aromatic nitro compounds which we have studied there is a slight broadening of the lines of protons *ortho* to the nitro group.

During the course of this investigation the parameters for fluorene were reported by Bartle and Jones,¹⁶ who substantiated the assignment of chemical shifts with the aid of a ring-substituted fluorene. Our results agree extremely well with theirs.

(16) K. D. Bartle and D. W. Jones, *J. Mol. Struct.*, **1**, 131 (1967-1968).

Table IV: Parameters for Fluorene and Derivatives^a

Compound	τ_1	τ_2	τ_3	τ_4	J_{12}	J_{13}	J_{14}	J_{23}	J_{24}	J_{34}
Fluorene	2.61	2.84	2.76	2.36	7.45	1.18	0.8	7.45	1.17	7.53
9-Chloro	2.46	2.78	2.73	2.48	7.68	0.98	0.71	7.55	1.10	7.72
9-Bromo	2.42	2.75	2.70	2.43	7.68	0.82	0.77	7.43	1.18	7.75
9-Iodo	2.44	2.80	2.75	2.46	7.76	1.03	0.75	7.61	1.06	7.85
9-Methoxy	2.49	2.79	2.72	2.44	7.49	1.15	0.78	7.58	1.17	7.61
9-Dichloromethylene	1.78	2.80	2.73	2.46	8.10	1.21	0.77	7.56	1.37	7.65
Dibiphenylene ethylene	1.62	2.87	2.77	2.39	8.26	1.02	0.78	7.55	1.19	7.85

^a For solutions in carbon tetrachloride. Coupling constants in Hz.**Table V:** Parameters for Various Disubstituted Benzenes^a

Substituents	τ_2	τ_3	τ_4	τ_5	τ_6	J_{34}	J_{35}	J_{36}	J_{45}	J_{46}	J_{56}
1-Br, 2- <i>t</i> -Bu	...	2.65	2.88	3.08	2.51	7.75	1.71	0.26	7.11	1.38	7.61
1-Cl, 2-CCl ₃	...	1.86	2.73	2.69	2.52	7.43	1.84	0.31	7.06	1.25	7.71
1- <i>t</i> -Bu, 2- <i>t</i> -Bu	...	3.04	2.54	2.54	3.04	8.33	1.73	0.00	7.10	1.73	8.33
							J_{23}	J_{25}	J_{26}	J_{35}	
1-C ₆ D ₅ , 4-Cl	2.61	2.70	...	2.70	2.61	8.30	0.46	2.30	2.30		
1-C ₆ D ₅ , 4-NO ₂	2.34	1.78	...	1.78	2.34	8.60	0.42	3.45	2.07		
1-Cl, 4-OH	2.86	3.32	...	3.32	2.86 ^b						
1-Cl, 4-CF ₃	2.49	2.52	...	2.52	2.49 ^b						
1-Cl, 4-CCl ₃	2.64	2.14	...	2.14	2.64 ^b						
1-Br, 4- <i>t</i> -Bu	2.70	2.84	...	2.84	2.70 ^b						

^a Solutions in carbon tetrachloride. Coupling constants in Hz. ^b These AA'BB' systems were analyzed for chemical shifts only.

Finally, it seemed desirable that we bring together in one place all the Q values from previous work and those derived from this study. All empirical Q (2) values have been determined from the H_3 chemical shifts for either the 1-chloro-2-X-benzene or 1-bromo-2-X-benzene and the least-squares plot of Q vs. chemical shifts for the various dihalobenzenes and including benzene itself as described previously.^{1a,c,d} Similarly, the data for a variety of 4-chloro-1-X-benzenes (largely taken from the work of Martin and Dailey¹⁷) have been used to determine Q (1) values. These values are given in Table VI.

Discussion

An Application of the Q (1) Values. In Figure 1 are plotted the H_3 chemical shifts for a series of *para*-substituted anilines and nitrobenzenes. These data were taken from the work of Martin and Dailey¹⁷ with the exception of *p*-diaminobenzene, which was estimated from their additivity rules.^{4b} Similar plots have been obtained for a variety of *para*-disubstituted benzenes and for the monosubstituted benzenes. In each case, the Q (1) values of hydroxyl, amino, and nitro are required.

The implication of these observations is that there is no appreciable ground state electronic interaction between the 1,4-substituents in these systems. Figeys and Flammung¹⁸ have calculated the decrease in ring current effect caused by a variety of substituents on the

Table VI: Summary of Q Values

Substituent	Q (1)	Q (2)
NH ₂	-0.67	-0.03
OH	0.30	1.20
OCH ₃	0.54	0.54
H	2.28 ^b	<i>a</i>
F	1.04 ^b	<i>a</i>
Cl	2.55 ^b	<i>a</i>
Br	3.16 ^b	<i>a</i>
I	3.98 ^b	<i>a</i>
CN	<i>a</i>	3.43
NO ₂	6.33	4.00
CH ₃	<i>a</i>	1.77
<i>t</i> -Bu	<i>a</i>	2.50
CF ₃	3.71	<i>a</i>
CCl ₃	<i>a</i>	5.15
CHO	4.90	<i>c</i>
COCH ₃	5.20	<i>c</i>
COCl	6.00	<i>c</i>

^a One value of Q seems to work for both situations. ^b Original values calculated by Schaefer, *et al.*^{3a} ^c Reasonably a different Q value would be required as Q (2) for these groups.

benzene ring. For strong electron donating or withdrawing groups this decrease was accompanied by an

(17) J. S. Martin and B. P. Dailey, *J. Chem. Phys.*, **37**, 2594 (1962).(18) H. P. Figeys and R. Flammung, *Mol. Phys.*, **12**, 581 (1967).

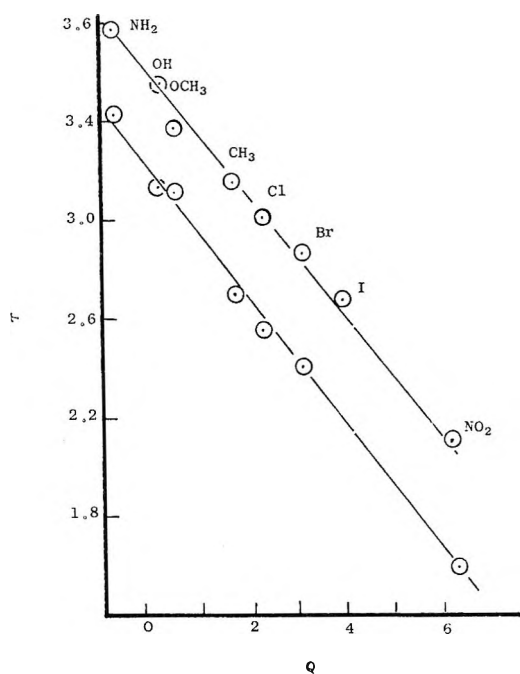


Figure 1. H_3 chemical shifts for a series of 4-substituted anilines (upper) and nitrobenzenes (lower) plotted vs. Q showing the applicability of the Q (1) values of the amino, hydroxyl, and nitro group.

increase in the importance of "quinoid" resonance structures as implied by an increase in the C_2-C_3 bond orders. If true, one might expect marked perturbations to occur in the proton chemical shifts of molecules such as *p*-nitroaniline and *p*-nitroanisole. Yet Figure 1 shows the protons adjacent to the nitro groups and those adjacent to the amino group in the aniline to behave in a pattern consistent with molecules such as *p*-aminoanisole and *p*-dinitrobenzene where "quinoid" structures reasonably play no important role. This conclusion is in accord with the observation that $J_{2,3}$ shows no evidence of enhanced bond order for either *p*-nitrophenol or *p*-nitroaniline compared to other *para*-substituted phenols or anilines.¹⁹ Further support for the contention of negligible 1,4-substituent interactions through a benzene ring has been offered by Vasil'eva²⁰ who showed that the failure of dipole moment additivity rules in these compounds could be accounted for by a slight lengthening of the dipole.

Ortho-Substituted Anilines and Toluenes. The data for the H_3 chemical shifts in the 2-X-anilines (Table I) are plotted against Q in Figure 2 for both carbon tetrachloride and DMSO. As in the case of the 2-X-phenols,^{1d} the Q (1) value of the nitro group is required in carbon tetrachloride, a result in keeping with a planar, hydrogen bonded structure for this molecule. In DMSO the hydrogen-bonded structure is disrupted, and an intermediate value of Q would be required to fit the curve. Using a series of polysubstituted *o*-nitroanilines in solutions of chloroform and DMSO, Rae²¹ concluded that an intramolecular hydrogen bond existed

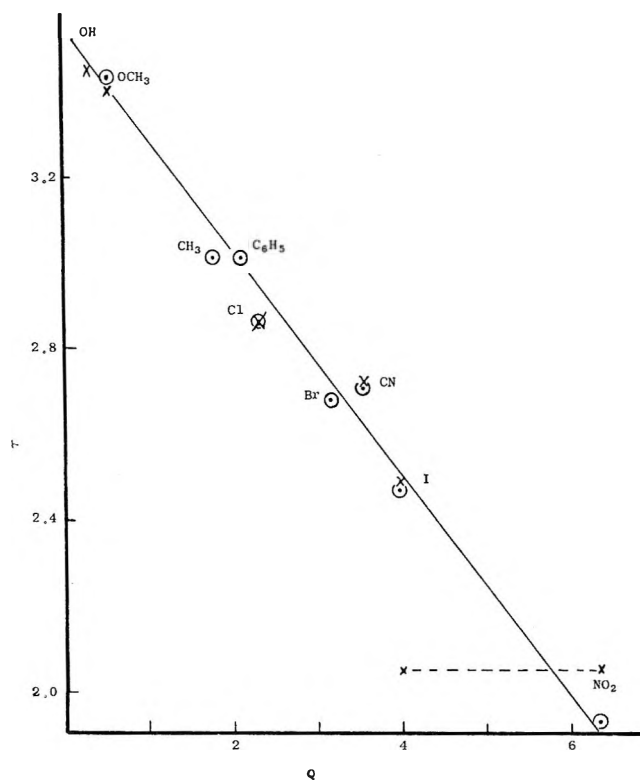


Figure 2. H_3 chemical shifts vs. Q for a series of *ortho*-substituted anilines in carbon tetrachloride (circles) and DMSO (X's). The values for *ortho*-phenyl and methyl groups were taken from Tables II and III, respectively. The line shown is a visual fit to the data in carbon tetrachloride.

between the amine and nitro groups in the former solvent but not in the latter. Later he concluded that DMSO may complex with the nitro group and effectively change its steric requirements with a variety of *ortho* substituents.²²

The general effect of changing from carbon tetrachloride to DMSO on the various ring proton chemical shifts in Table I is quite curious. In general, a change to a more polar solvent causes a downfield shift for aromatic protons.²³ Such a shift was clearly evident in the phenols, but preferential solvent effects of carbon tetrachloride or DMSO or perhaps the weaker interactions between the aniline amine group and the *ortho* substituents may account for the smaller solvent effects in the anilines than that previously observed in the phenols.

Indeed, the whole question of steric and bonding interactions in *ortho*-substituted anilines has been a matter of

(19) W. B. Smith and T. J. Kmet, *J. Phys. Chem.*, **70**, 4084 (1966). Also, it has been observed by Dr. B. A. Shoulders in these laboratories that there is no significant difference for the various J_{ortho} values in *cis*- and *trans*-4-methoxy-4'-nitrostilbene.

(20) V. N. Vasil'eva, *Tetrahedron, Suppl.*, **20**, 403 (1964).

(21) I. D. Rae, *Aust. J. Chem.*, **20**, 1173 (1967).

(22) I. D. Rae, *ibid.*, **20**, 2381 (1967).

(23) See, for instance, H. M. Hutton and T. Schaefer, *Can. J. Chem.*, **43**, 3116 (1965), and P. Laszlo in ref 13.

controversy for some time. Webster concluded from studies of the electronic spectra that steric interactions between the aniline amine group and *ortho* substituents as large as *t*-butyl were relatively slight.²⁴ In contrast, Smith²⁵ decided from dipole moment studies that even an adjacent methyl group produced a slight inhibition to resonance.

The data regarding amine hydrogen bonding to *ortho* substituents have been reviewed.²⁶ Lady and Whetsel²⁷ concluded from infrared data that N-H hydrogen bonding occurs to strong donor groups such as iodo, nitro, and keto. The question of whether such bonding maintains itself in solvents such as chloroform and carbon tetrachloride which may complex with the amine group has proven quite vexing.^{21,27,28}

We may appeal to data from earlier studies¹ combined with those from Table I to answer the question of whether the amine group is hydrogen bonded to *ortho*-substituents other than nitro in carbon tetrachloride. In Figure 3 are shown the plots of the H_3 chemical shifts in a series of 2-X-anisoles and nitrobenzenes *vs.* the appropriate Q values. It is noted that the $Q(2)$ values of the amino and hydroxyl groups are clearly called for in both plots. Since $Q(2)$ values are determined from the data on 2-X-halobenzenes and since hydrogen bonding between the amine and nitro group has been established for *o*-nitroaniline, it follows that the amine group is also hydrogen bonded to the halogen and the methoxyl group in their respective series in carbon tetrachloride solution. This point is supported by the data for the 2-X-toluenes.

The Q plot for the H_3 chemical shifts of the 2-X-toluenes (Table II) is shown in Figure 4. Of immediate interest is the observation that the point for H_3 in *o*-toluidine is far downfield from that predicted from either amine Q value. This is the only case we have observed where such anomalous behavior is displayed. Most reasonably the amine group cannot hydrogen bond to the methyl group. Moreover, the conformational requirements of the amine group are harder to assess as the conjugation of the nitrogen lone pair of electrons with the aromatic ring, the unknown state of hybridization of the nitrogen, and the ammonia-like inversion process all complicate the matter. The $Q(1)$ value of the amino group clearly characterizes the group in aniline and the *para*-substituted anilines. The $Q(2)$ value applies when the amino group is hydrogen bonded to an *ortho* substituent. The average conformation of the amine group in *o*-toluidine is observably different from these two cases, and the downfield shift of H_3 suggests that the nitrogen lone pair may be preferentially oriented toward H_3 .²⁹

The chemical shift for H_3 in 2-nitrotoluene (Figure 4) falls at a value intermediate between that given by the $Q(2)$ nitro value required for most *ortho* substituents and the $Q(1)$ value which characterizes the nitro in the plane of the aromatic ring. The situation

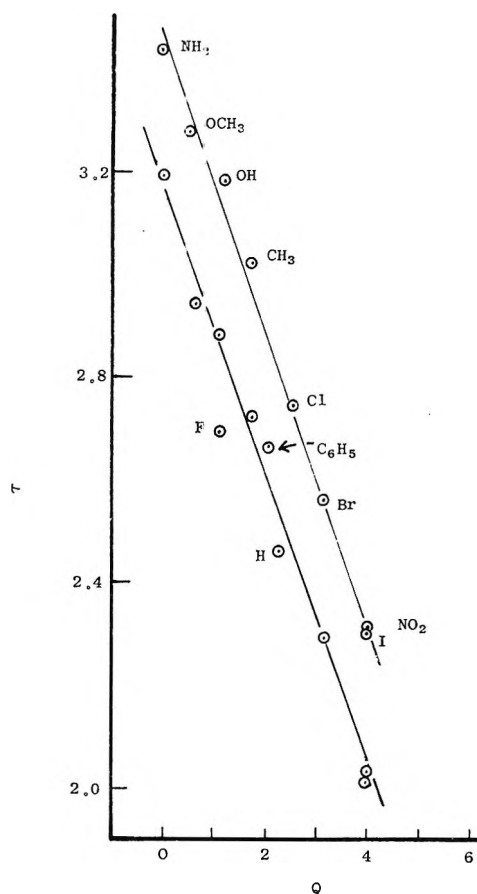


Figure 3. H_3 chemical shifts *vs.* Q for a series of *ortho*-substituted anisoles (upper) and nitrobenzenes (lower). Both lines are visual fits to data reported in this and earlier studies.¹

resembles that found previously in *o*-fluoronitrobenzene.^{1f} On the average, the nitro group finds itself somewhat out of the plane of the ring but not at the extreme right angle required by more bulky *ortho* substituents. The relatively small size of the methyl group is confirmed by the observation that the $Q(1)$ value of hydroxyl is preferred for the H_3 chemical shift in *o*-cresol (Figure 4). No hydrogen bonding to methyl occurs, and the hydroxyl is free to assume the conformation found in phenol itself.

Brief comment is merited regarding the coupling constants in Tables I and II. The additivity of substituent effects on aromatic coupling constants has

(24) B. M. Webster, "Steric Effects in Conjugated Systems," G. W. Gray, Ed., Butterworth and Co., Ltd., London, 1958, p 82.

(25) J. W. Smith in ref 24, p 141.

(26) A. N. Hambly, *Rev. Pure Appl. Chem.*, **11**, 212 (1961).

(27) J. H. Lady and K. B. Whetsel, *Spectrochim. Acta*, **21**, 1669 (1965).

(28) (a) P. J. Krueger, *Can. J. Chem.*, **40**, 2300 (1962); (b) T. Yonemoto, W. F. Reynolds, H. M. Hutton, and T. Schaefer, *ibid.*, **43**, 2668 (1965).

(29) (a) V. M. S. Gil and J. M. Murrell, *Trans. Faraday Soc.*, **60**, 248 (1964); (b) G. Fraenkel, D. G. Adams, and R. R. Dean, *J. Phys. Chem.*, **72**, 944 (1968).

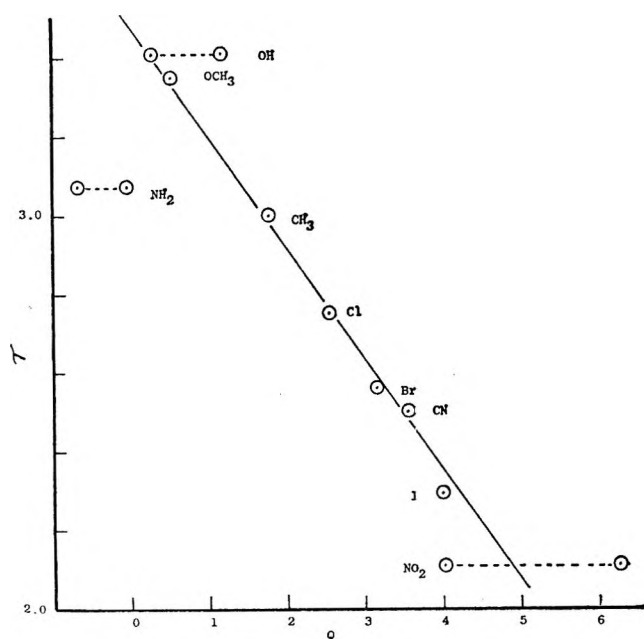


Figure 4. Plot of the H_3 chemical shifts vs. Q for the 2- X -toluenes. The range of Q values is shown for the hydroxyl, amino, and nitro groups.

been noted,³⁰ and Castellano and Kostelnik have suggested that deviations from additivity indicate *ortho* substituent interactions. The data from our previous studies and those presented here have been examined according to their rules. Most compounds show deviations of 0.1 Hz or less. The values of J_{34} , J_{45} , and J_{56} in *o*-nitrophenol and *o*-nitroaniline deviate from the predicated constants by 0.2–0.4 Hz. In each case, the sense of the deviation is to favor the enhanced importance of *ortho* “quinoid” structures in these planar, hydrogen bonded systems.^{1d}

The Biphenyls and Fluorenes. While substituent magnetic anisotropy has been offered often as a rationalization of nmr chemical shifts, the fact remains that very few, if any, reliable values exist for the anisotropy of diamagnetic susceptibility, and the experimental separation of this effect from a variety of others is difficult.³¹ The “ring current” effect in the benzene ring serves as a notable exception, and calculations of proton chemical shifts due to the “ring current” effect have proven often to be both qualitatively and quantitatively successful. The utilization of the phenyl group as a substituent offers an attractive comparison of the Q value concept and the results of the “ring current” effect. The nmr parameters for a series of substituted biphenyls and fluorene and a series of substituted fluorenes are given in Tables III, IV, and V.

As for other groups without cylindrical symmetry, the phenyl group is characterized by two values of Q . The Q (1) value (Table VI), obtained from 4-chlorobiphenyl, holds good for the *ortho* proton chemical shifts in the monosubstituted benzenes vs. Q and a

similar plot of H_3 chemical shifts in the 4- X -nitrobenzenes. Clearly, the same averaged phenyl conformation obtains in biphenyl as in 4-chloro and 4-nitro-biphenyl.

While biphenyl is a planar molecule in the solid state,³² the steric repulsions of the *ortho* hydrogens overwhelm the conjugative stabilization offered by the planar form when in solution.³³ The question of the population of the various conformers in solution is still open. Hoffman, *et al.*,³⁴ used arguments based on nmr data and magnetic anisotropy calculations using the point dipole approximation to conclude that the two rings were inclined 30–60° to each other. Kurland and Wise³⁵ studied the variation of chemical shifts with temperature for selectively deuterated biphenyl and calculated that the energy barrier to rotation was small and that an energy minimum exists at 90° rotation. Subsequently, Mayo and Goldstein³⁶ reported the chemical shifts for biphenyl to be *ortho*, 2.56 τ ; *meta*, 2.72 τ ; and *para*, 2.82 τ in tetramethylsilane and 2.42, 2.58, and 2.67 τ , respectively, in deuteriochloroform. Using a somewhat more sophisticated calculation of the ring current effect they proposed that biphenyl shows essentially free rotation at room temperature with an average dihedral angle of *ca.* 42°. Bovey, *et al.*,¹⁴ reported the chemical shifts for biphenyl in carbon tetrachloride to be 2.56 τ (*o*), 2.72 τ (*m*), and 2.84 τ (*p*) in close agreement with the results in TMS. It is curious that in their subsequent discussion of the ring conformations Mayo and Goldstein chose to use the deuteriochloroform data in spite of the fact that this solvent is known to interact with aromatic hydrocarbons.¹³

Calculations³⁶ of the magnetic anisotropy due to the ring current effect indicate that in planar biphenyl the adjacent ring will deshield the ring protons by -0.57 , -0.15 , and -0.10 ppm at *ortho*, *meta*, and *para* positions, respectively, while with the rings at right angles these values become -0.04 , -0.09 , and -0.10 ppm.³⁷ The measurement of the *para* proton chemical shift in the least reactive solvents (TMS and carbon tetrachloride) shows about a 0.1 ppm upfield shift from benzene, while the anisotropy predicts a

(30) (a) S. Castellano and R. Kostelnik, *Tetrahedron Lett.*, **51**, 5211 (1967); (b) H. B. Evans, A. R. Tarpley, and J. H. Goldstein, *J. Phys. Chem.*, **72**, 2552 (1968).

(31) See A. A. Bothner-By and J. A. Pople, *Ann. Rev. Phys. Chem.*, **16**, 42 (1965), for a recent review. Also see J. Homer and D. Callaghan, *J. Chem. Soc., A*, 518 (1968), for a description of the difficulties in separating various effects.

(32) J. Trotter, *Acta Cryst.*, **14**, 1135 (1961).

(33) E. Merkel and C. Wiegand, *Z. Naturforsch.*, **36**, 93 (1948).

(34) R. A. Hoffman, P. O. Kinell, and G. Bergstrom, *Ark. Kemi*, **15**, 533 (1960).

(35) R. J. Kurland and W. B. Wise, *J. Amer. Chem. Soc.*, **86**, 1877 (1964).

(36) R. E. Mayo and J. H. Goldstein, *Mol. Phys.*, **10**, 301 (1966).

(37) Our calculations by the Johnson and Bovey method, *J. Chem. Phys.*, **29**, 1012 (1958), are in close agreement.

similar shift but downfield. The 0.2 ppm difference is not a small substituent effect for aromatic proton chemical shifts. As will be seen shortly, the assumption that chemical shift effects of a phenyl are due only to magnetic anisotropy effects may be an oversimplification.

It has been previously noted for H_6 in a series of 2-X-chlorobenzenes^{1c} (as well as all other series examined) that chemical shifts or substituent chemical shifts (SCS)³⁸ follow σ_m . The dominant determining factor regarding the shift at H_6 is the nature of the C-1 substituent with the σ_m effect of the C-2 substituent as a perturbation. For 2-chloro, 2-bromo, or 2-iodo-1-X-benzenes, where X is chloro, bromo, or iodo, the SCS at H_6 are all *ca.* -0.11 ppm. This is because the σ_m values for these halogens are all about the same. The chemical shifts of H_6 in 2-chloro, 2-bromo, and 2-iodo-1-phenylbenzene are 2.76, 2.77, and 2.79 τ , respectively. Application of the corrector for SCS of the halogens suggests that biphenyl itself with the rings at right angles would have an *ortho* chemical shift at *ca.* 2.9 τ . Similar results are obtained using such functional groups as hydroxyl and amino. The conclusion is that effects other than simple magnetic anisotropy dictate the *ortho* effect of a phenyl substituent on an adjacent proton.

The Q (2) value for the phenyl characterizes the H_6 chemical shifts for the 1-perdeuteriophenyl-2-X-benzenes in all of the series which we have previously examined. This is true for 1-perdeuteriophenyl-2-fluorobenzene, and points out the difference in steric requirements of the phenyl group which strongly interacts with the adjacent fluorine and the nitro group which does not.^{1f} Furthermore, the chemical shift for the *ortho* fluorine falls well on the appropriate Q plot for fluorine chemical shifts while the fluorine in 2-nitrofluorobenzene does not.³⁹ A further argument against the importance of magnetic anisotropy emerges from these data. Given the phenyl to be essentially at right angles to the plane of the benzene ring in the fluorobiphenyl, one would expect the fluorine chemical shift to appear *ca.* the same as fluorobenzene since the fluorine is located on or very near the zero shielding line of the ring current effect. The experimental fact is that it appears 5.2 ppm upfield from fluorobenzene, a result in keeping with the Q value determined from proton chemical shift data.

Fluorene may be considered as a planar form of a substituted biphenyl. Using Johnson-Bovey calculations³⁷ one arrives at H_1 2.57 τ , H_2 2.65 τ , H_3 2.61 τ , and H_4 2.32 τ .⁴⁰ The agreement between the predicted and experimental chemical shifts at H_1 and H_4 are quite good though H_2 and H_3 appear nearly 0.2 ppm upfield from the predicted values. These values ignore any contribution from the bridging methylene which may be estimated from the ring proton chemical shifts of toluene and diphenyl methane to be about 0.2

ppm. Application of this correction improves the fit at H_2 and H_3 but at the expense of the agreement at H_1 and H_4 .

The ring current effect of the two rings on one side of the central double bond in dibiphenylene ethylene were applied to the experimental values of the ring proton chemical shifts of fluorene to yield calculated chemical shifts of H_1 1.3 τ , H_2 2.6 τ , H_3 2.7 τ , and H_4 2.3 τ . While the agreement with the experimental values in Table IV is reasonably good, the result may be largely fortuitous as it is known that the molecule is not quite planar⁴¹ and no account was taken of the diamagnetic anisotropy of the central double bond.

In summary, while the ring current effect appears to give reasonable answers in some cases; it is clearly evident, to quote Bovey,⁴² that "some important contribution has been overlooked." That something will be discussed in the last section.

An examination of the geometric terms, $(1 - 3 \cos^2 \theta) / 3r^3$, from the McConnell equation⁴³ for the 9-halo-fluorenes to H_1 and for the *ortho* protons in the halobenzenes shows them to be very nearly the same. While the span in chemical shifts in going from chloro to iodobenzene is 0.4 ppm at the *ortho* proton, there is no real difference at H_1 in going from 9-chloro to 9-iodofluorene. The failure of diamagnetic anisotropy (at least in the form of the McConnell equation) to explain the *ortho* effect in the halobenzenes has drawn comment before,^{4b} and recently Nomura and Takeuchi⁴⁴ have provided additional evidence that the effect must be small or nonexistent in aromatic systems. It is evident that the H_1 chemical shifts in the 9-substituted fluorines do not follow Q , a result in keeping with the evidence that Q operates through the π -electron system.^{3b} The insensitivity of H_1 to substituent changes at C-9 might be explained by an accidental cancellation of two or more effects. However, it seems best at this juncture to admit the insufficiencies of current nmr theory.

Further Comments on Q. In their original definition of Q , Schaefer and coworkers³ considered the effect to arise from a paramagnetic interaction of excited states of the substituent with the ground state of the electrons in the C-H bond. The effect was shown to be transmitted through the π -electron system.^{3b} Correlations were found for protons adjacent to hydrogen and the halogens in the monosubstituted ben-

(38) In this case the SCS would be determined by subtracting the H_6 chemical shift for chlorobenzene from that of the appropriate 2-X-chlorobenzene.

(39) See ref 1f, Figure 2.

(40) Dreiding models were used for the dimensions. The point dipole calculation gives virtually the same result.

(41) S. C. Nyberg, *Acta Cryst.*, **7**, 779 (1954).

(42) F. A. Bovey, "Nuclear Magnetic Resonance Spectroscopy," Academic Press, New York, N. Y., 1969, p 69.

(43) H. C. McConnell, *J. Chem. Phys.*, **27**, 226 (1957).

(44) Y. Nomura and Y. Takeuchi, *Tetrahedron Lett.*, **54**, 5665 (1968).

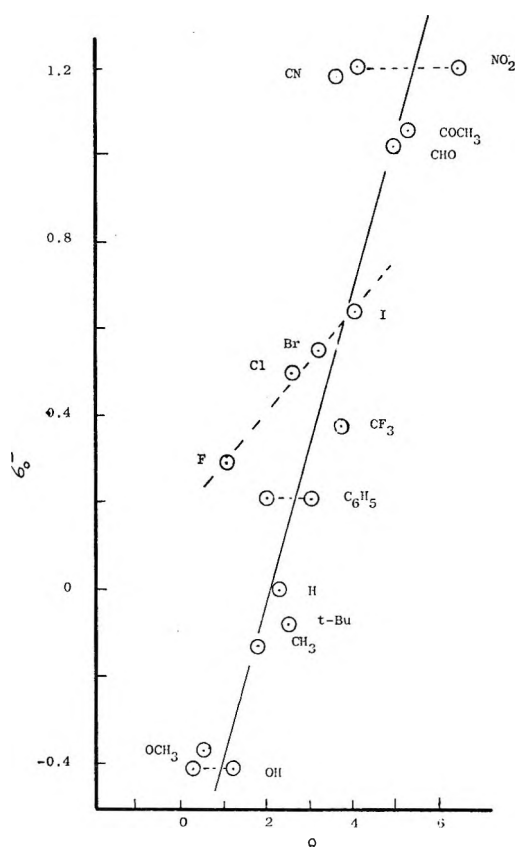


Figure 5. Plot of Q values vs. σ_0^- . Q (1) and Q (2) values are both shown where pertinent. The lines shown are merely suggestive.

zenes, *cis* and *trans* to the substituents in the vinyl series, and for fluorines in the 2-X-fluorobenzenes. Subsequently, a number of sets of empirical Q values have been obtained (Table VI) and applied successfully both to the original and many additional systems.¹ Deviations from the Q correlation have been used to draw conclusions about intramolecular hydrogen bonding and steric interactions between substituents.

It has been known for some time that aromatic protons *ortho* to a series of substituents correlate fairly well with such measures of electron density in the ring as σ_p .⁴⁵ Exceptions to such correlations were invariably the halogens, and a variety of effects have been proposed to account for their behavior.^{1c} The Q relation has the virtue of removing this anomaly.

Recently, Tribble and Traynham⁴⁶ have developed a σ_0^- scale which seems to measure electronic substituent effects at the *ortho* position. The relation between Q and σ_0^- is shown in Figure 5. The line shown is merely suggestive as it is not completely clear in all cases whether Q (1) or Q (2) values should be used. Again the halogens are seen to go their own way. A similar plot is given by σ_p , and the whole system parallels the observations made by Diehl on his substituent constants a number of years ago.⁴⁷ Clearly the empirical values of Q are mainly measuring the electronic

effect of the substituent plus some other factor which is inherent in the Q concept of Schaefer.

The chemical shifts of twelve chlorobenzenes are summarized in Table VII for convenience. All values but one were taken from this or previous papers in this series. The chemical shifts for this and most of our other various series have been subjected to a multiple regression analysis resulting in the equations shown in Table VIII. The purpose here was not

Table VII: Chemical Shifts of 2-X-Chlorobenzenes

X	τ_1	τ_4	τ_5	τ_6
NH ₂	3.42	3.07	3.43	2.86
OH	3.03	2.89	3.21	2.75
OCH ₃	3.19	2.90	3.20	2.74
H ^a	2.71	2.76	2.83	2.76
F	2.93	2.84	2.99	2.66
Cl	2.63	2.88	2.88	2.63
Br	2.47	2.99	2.86	2.62
I	2.21	3.16	2.79	2.63
CH ₃	2.87	2.96	2.98	2.75
CN	2.36	2.62	2.47	2.50
NO ₂	2.18	2.59	2.51	2.46
C ₆ H ₅	2.76	2.81	2.84	2.62

^a K. Hayamizu and O. Yamamoto, *J. Mol. Spectrosc.*, **28**, 89 (1968).

Table VIII: Correlation Equations for 2-X-Chlorobenzenes

Equation	r
$\tau_6 = -0.187\mathfrak{F} - 0.230\mathfrak{R} + 0.0009Q + 2.703$	0.946
$\tau_6 = -0.186\mathfrak{F} - 0.227\mathfrak{R} + 2.705$	0.946
$\tau_3 = -0.157\mathfrak{F} - 0.736\mathfrak{R} + 0.034Q + 2.906$	0.992
$\tau_5 = -0.200\mathfrak{F} - 0.845\mathfrak{R} + 2.830$	0.988
$\tau_4 = -0.257\mathfrak{F} - 0.815\mathfrak{R} + 0.147Q + 2.501$	0.860
^a $\tau_4 = -0.212\mathfrak{F} - 0.295\mathfrak{R} + 0.086Q + 2.830$	0.954
$\tau_4 = -0.072\mathfrak{F} - 0.341\mathfrak{R} + 2.830$	0.649
$\tau_4 = -0.101\mathfrak{F} - 0.110\mathfrak{R} - 0.253Q + 3.304$	0.997
^a $\tau_3 = -0.275\mathfrak{F} - 0.971\mathfrak{R} - 0.088Q + 2.732$	0.956
$\tau_3 = -0.418\mathfrak{F} - 0.924\mathfrak{R} + 2.732$	0.904

^a Calculated using only the Q values for the halogens.

merely to provide chemical shift correlations but to explore the various factors which contribute to the substituent effects. Consequently, we chose to use the \mathfrak{F} and \mathfrak{R} constants recently derived by Swain and Lupton to correlate some 43 sets of various type σ

(45) The parameter σ_p is determined from kinetic or equilibrium measurements and need not reflect electronic substituent effects in the ground state. However, several MO calculations of substituent electronic effects show electron density and σ_p to vary in a linear fashion. Thus, while the relation might not be causal, it seems to be well established empirically.

(46) M. T. Tribble and J. G. Traynham, *J. Amer. Chem. Soc.*, **91**, 379 (1969).

(47) P. Diehl, *Helv. Chim. Acta*, **49**, 829 (1961).

constants.⁴⁸ These authors present a convincing argument that \mathcal{F} and \mathcal{R} represent a separation of field (or inductive) and resonance effects while σ_p includes both effects. Similar equations resulted with σ_p and the correlation coefficients were about the same.

Strictly speaking one can not draw causal relations from correlation equations, but here we are seeking a model to help understand the effect of substituents on aromatic proton chemical shifts. Ideally we should do *ad hoc* calculations using the fundamental shielding equation of Ramsey. With this understanding, the equations in Table VIII offer some insights of interest.

Positions 4 and 6 are *meta* to the varying substituent. Clearly the Q effect is not important at H_6 . However, the addition of the Q factors clearly improves the correlation at H_4 . Furthermore, the Q effect is most important for the halogens. Note too that the coefficient for Q is positive here while negative at both *ortho* and *para* positions. This pattern repeated itself in all our series though the theoretical implications remain unclear.

Consistently, the addition of a Q term improved slightly the correlation at the *para* position H_5 . The effect, however, is much more prominent at the *ortho* position. Reasonably the experimental Q values include not only the electronic effects of the substituent but also the paramagnetic effect approximated in the calculated Q values of Schaefer, *et al.* Furthermore, the ionization potentials of the halogens vary as do their values of σ_p . Thus, something of the electronic effects of the halogens is inadvertently included in the calculation of their Q values.

Finally, linear correlations of \mathcal{F} , \mathcal{R} , and Q of the type shown in Table VIII have been made in other systems. The chemical shifts of the fluorines in a series of

ortho, *meta*, and *para*-substituted fluorobenzenes show correlation coefficients of 0.990, 0.941, and 0.986, respectively, for a series of sample sets of nine substituents. Spiesscke and Schneider⁴⁹ found little evident correlation between the *ortho*-carbon chemical shifts and *ortho*-proton chemical shifts. However, a seven point set gives an excellent fit to \mathcal{F} , \mathcal{R} , and Q for the *ortho*-carbon chemical shifts ($r = 0.990$). The point for the nitro group was omitted as it is found at an unexplainable high field position with reference to benzene.

Many questions regarding substituent effects on nmr parameters in aromatic systems remain to be clarified. Since the Q effect seems to operate through the π system, it is not clear why the effect at H_6 is blocked from variations at C_2 by a substituent at C_1 . Specific van der Waals interactions of the type discussed by Richardson and Schaefer⁵⁰ are not incorporated in Q though there is a trend for Q values to increase with the size of the substituent. In any event, the model evoking field, resonance, and paramagnetic effects as measured by \mathcal{F} , \mathcal{R} , and Q seems to be an improvement over earlier models.

Acknowledgment. We wish to acknowledge the help of Edith K. Rowntree in synthesizing and tabulating the data for several of the 9-substituted fluorenes. The Varian HA-100 was made available by a grant from the National Science Foundation. This work was generously supported by The Robert A. Welch Foundation, to whom we express our appreciation.

(48) C. G. Swain and E. C. Lupton, *J. Amer. Chem. Soc.*, **90**, 3328 (1968).

(49) H. Spiesscke and W. G. Schneider, *J. Chem. Phys.*, **35**, 731 (1963).

(50) B. Richardson and T. Schaefer, *Can. J. Chem.*, **46**, 2195 (1968).

A Nuclear Magnetic Resonance Study of the Effect of Hydrogen

Bonding and Protonation on Acetone^{1a}

by W. H. de Jeu^{1b}

*Laboratorium voor Technische Natuurkunde, Technische Hogeschool, Delft, the Netherlands
(Received August 12, 1969)*

With the aid of ¹³C resonance and the ¹³C satellites in ¹H resonance the following nmr parameters of acetone are obtained: carbonyl $\delta(^{13}\text{C})$, methyl $\delta(^{13}\text{C})$, $^1J_{\text{CH}}$ and $^4J_{\text{HH}}$. Measurements are reported for the solvent dependence of these quantities for acetone at various concentrations in water and for 20 mol % acetone in various concentration ratios of sulfuric acid–water. Both $^1J_{\text{CH}}$ and $^4J_{\text{HH}}$ increase due to hydrogen bonding of the carbonyl group with the solvent, and for the acidic solutions also due to protonation of the acetone molecule. The carbonyl ¹³C is shifted to a lower field, while the methyl $\delta(^{13}\text{C})$ remains almost constant. The iterative extended Hückel theory and the CNDO method are used for theoretical calculations of the changes in the acetone molecule. The direction and the order of magnitude of the changes in the chemical shifts are in general predicted very well; the results for the coupling constants are less satisfactory. Both for hydrogen bonding and for protonation there is an electron displacement away from the carbonyl carbon (which explains the shift of carbonyl $\delta(^{13}\text{C})$ to a lower field qualitatively) and away from the methyl hydrogen atoms. The methyl carbon is hardly affected, which is in agreement with the near constancy of methyl $\delta(^{13}\text{C})$.

Introduction

During the last decades nmr has appeared to be a powerful tool, not only for analytical purposes, but also for gaining insight into the structure of molecules. The chemical shifts and coupling constants provide valuable information about the electronic structure of the molecule and form an important test on the accuracy of the wave functions. Both chemical shifts and coupling constants are solvent dependent.² From these solvent shifts additional information can be obtained about possible solute–solvent interactions and accompanying electronic displacements.

In this paper a systematic study of some of the nmr parameters of acetone in various solvents is presented. From the proton spectrum the chemical shift of the methyl protons can be obtained. As 1.1% of all carbon atoms is a carbon-13 ($I = 1/2$), two satellites with a spacing of $^1J_{\text{CH}}$ occur in the proton spectrum. With one methyl ¹²C replaced by a ¹³C the two methyl groups are no longer equivalent and each of the satellites is a quadruplet with an equal spacing of $^4J_{\text{HH}}$.³ Furthermore, in ¹³C resonance the chemical shifts of the methyl and carbonyl carbon atoms can be measured. Christ and Diehl⁴ have obtained the chemical shift of the carbonyl oxygen by ¹⁷O resonance (natural abundance 0.037%; $I = 5/2$). More parameters exist, but the attention will be focused on the ones mentioned.

The chemical shifts as well as the coupling constants depend highly on the nature of the solvent.^{3b–5} The carbonyl group is able to form H bonds with proton donating solvents, which causes electronic displacements in the molecule. In strongly acidic solutions even protonation of the acetone molecule occurs.⁶ The

chemical shift of the carbonyl proton can be measured at about -60° .⁷ These effects are also apparent in other spectroscopic methods. In uv spectroscopy the $n-\pi^*$ frequency of acetone and other ketones is well known to shift to higher values (blue shift) in solvents with increasing proton donating properties.^{8,9} In acidic solutions, *e.g.*, more than 65 wt % sulfuric acid, the transition disappears gradually. From this a $\text{p}K_a$ value of -7.2 has been established for acetone.⁶ Furthermore, changes are found in the carbonyl stretching frequency $\nu_s(\text{CO})$ in infrared and Raman spectroscopy.^{10,11} $\nu_s(\text{CO})$, and thus the strength of the CO bond, decreases with increasing H bonding. However, this effect is accompanied by an increase in strength of the CC and CH bonds.¹¹ A Raman study of acetone in sulfuric acid confirms the $\text{p}K_a$ value of -7.2 .¹²

(1) (a) Part of the Ph.D. Thesis of the author. A copy of the complete thesis is available upon request. (b) School of Molecular Sciences, University of Sussex, Brighton, England.

(2) P. Laszlo, "Progress in NMR Spectroscopy," J. W. Emsley, J. Feeney, and L. H. Sutcliffe, Ed., Vol. III, 1967, p 231.

(3) (a) J. R. Holmes and D. Kivelson, *J. Amer. Chem. Soc.*, **83**, 2959 (1961); (b) W. H. de Jeu, H. Angad Gaur, and J. Smidt, *Rec. Trav. Chim.*, **84**, 1621 (1965).

(4) H. A. Christ and P. Diehl, *Helv. Phys. Acta*, **36**, 170 (1963).

(5) G. E. Maciel and J. J. Natterstad, *J. Chem. Phys.*, **42**, 2752 (1965).

(6) H. J. Campbell and J. T. Edward, *Can. J. Chem.*, **38**, 2109 (1960).

(7) C. MacLean and E. L. Mackor, *J. Chem. Phys.*, **34**, 2207 (1961).

(8) A. Balasubramanian and C. N. R. Rao, *Spectrochim. Acta*, **18**, 1337 (1962).

(9) W. P. Hayes and C. J. Timmons, *ibid.*, **21**, 529 (1965).

(10) L. J. Bellamy and R. L. Williams, *Trans. Faraday Soc.*, **55**, 14 (1959).

(11) P. G. Puranik, *Proc. Ind. Acad. Sci.*, **37A**, 499 (1953).

Many of the properties mentioned depend on the polarity of the carbonyl group of the ketone under investigation. Several relations have been proposed, often assuming a nonpolar, nonpolarizable core of σ bonds and a polar carbonyl π bond. Nagakura¹³ and Sidman¹⁴ studied $\nu_{n \rightarrow \pi^*}$ and other electronic transitions in relation to the π bond polarity. Maciel^{5,15} did the same for $\delta(^{13}\text{C})$. Cook¹⁶ established two linear relations between $\nu_s(\text{CO})$ and the ionization potential I for conjugated and unconjugated carbonyl compounds, respectively. Figgis, Kidd and Nyholm¹⁷ found a general linear relation between $\delta(^{17}\text{O})$ and $\nu_{n \rightarrow \pi^*}$, which was extended to solvent effects on these two quantities by de Jeu.¹⁸ Savitsky, Namikawa, and Zweifel¹⁹ tried to correlate $\delta(^{13}\text{C})$ and $\nu_{n \rightarrow \pi^*}$. However, in this case there is no strict linearity.¹⁸ Finally, Ito, Inuzuka, and Imanishi²⁰ established a linear relation between the increase of $\nu_{n \rightarrow \pi^*}$ and the decrease of $\nu_s(\text{CO})$ for ketones in various solvents.

General calculations on all valence electrons of a molecule with a carbonyl group, that in principle take all properties into consideration, are still rare. There are some notable nonempirical MO calculations on formaldehyde.²¹ Contrary to general opinion about the carbonyl bond, a polar σ bond as well as a polar π bond is found. For a further discussion we refer the reader to the review paper by Berthier and Serré.²¹ We used some semiempirical methods for all valence electrons in order to see if the qualitative predictions of the effects of H bonding and protonation on acetone are confirmed. The results of the Hückel-type method of Pople and Santry^{22,23} and the extended Hückel theory of Hoffmann²⁴ are given elsewhere.²⁵ Here we restrict ourselves to the iterative extended Hückel method²⁶ and the CNDO method^{27,28} (most simple SCF method for all valence electrons). These latter methods can be expected to give a reasonable account of the expected charge redistribution.

Experimental Section

The proton measurements were carried out on a Varian DA-60 spectrometer, equipped with an internal lock. The samples were in spinning Pyrex tubes of 5 mm outer diameter. All the reported values are averages of 6 to 12 spectra. For the acetone concentrations below 3 mol %, spectrum accumulation was applied using a Varian C-1024 time averaging computer.

The ^{13}C resonance was carried out on the same spectrometer provided with a 15.08-MHz transmitter, built in this laboratory. For detection the appropriate 60-MHz circuits were retuned at 15.08-MHz. The 5-MHz intermediate frequency (normally obtained by mixing the 60-MHz with a 55-MHz signal) was generated by mixing the 15.08-MHz with the signal from a 10.08-MHz oscillator. As an external reference about 50% carbonyl ^{13}C enriched acetic acid was used. The

reference was kept in a small concentric inner tube in the nonspinning 15-mm outer diameter sample tube. The necessary bulk susceptibility corrections were made. We observed 2-kHz side bands and suppressed the center band. Calibration was performed by sweeping from the first lower to the first upper side band and counting the 4-kHz separation accurately. The spectra were obtained using the adiabatic rapid passage technique.^{29,30} The reported values are averages of six spectra, each consisting of a scan increase and decrease in order to avoid transient shifts.

The acetone was obtained from E. Merck AG (uvasol) and used without further purification. The water used was distilled several times. The sulfuric acid was 95.2% Baker Analyzed reagent from J. T. Baker Chemical Co.

Theoretical Section

A. Molecular Wave Functions. In the extended Hückel theory of Hoffmann²⁴ a Hückel matrix is constructed in an empirical way. The diagonal elements α_μ are taken as the negative valence state ionization potentials of the corresponding orbitals. The off-diagonal elements are approximated by

$$\beta_{\mu\nu} = 1.75S_{\mu\nu}(\alpha_\mu + \alpha_\nu)/2 \quad (1)$$

Further, in solving the eigenvalue equations, overlap is taken into account. As the ionization potentials depend on the atomic charges,³¹ the diagonal elements α_μ are a function of the charges too. We used

$$\alpha_\mu = \alpha_\mu^0 + \Delta\alpha q_A \quad (2)$$

(12) N. C. Deno and M. J. W'isotsky, *J. Amer. Chem. Soc.*, **85**, 1735 (1963).

(13) S. Nagakura, *Bull. Chem. Soc. Jap.*, **25**, 164 (1952).

(14) J. W. Sidman, *J. Chem. Phys.*, **27**, 429 (1957).

(15) G. E. Maciel, *ibid.*, **42**, 2746 (1965).

(16) D. Cook, *J. Amer. Chem. Soc.*, **80**, 49 (1957).

(17) B. N. Figgis, R. G. Kidd, and R. S. Nyholm, *Proc. Roy. Soc.*, **A269**, 469 (1962).

(18) W. H. de Jeu, *Mol. Phys.*, **18**, 31 (1970).

(19) G. B. Savitsky, K. Namikawa, and G. Zweifel, *J. Phys. Chem.*, **69**, 3105 (1965).

(20) M. Ito, K. Inuzuka, and S. Imanishi, *J. Amer. Chem. Soc.*, **82**, 1317 (1960).

(21) G. Berthier and J. Serré, "The Chemistry of the Carbonyl Group," S. Patai, Ed., Interscience, New York, N. Y., 1966, p 1.

(22) J. A. Pople and D. P. Santry, *Mol. Phys.*, **7**, 269 (1964).

(23) J. A. Pople and D. P. Santry, *ibid.*, **9**, 301 (1965).

(24) R. Hoffmann, *J. Chem. Phys.*, **39**, 1397 (1963).

(25) W. H. de Jeu, Ph.D. Thesis, Delft University of Technology, 1969.

(26) R. Rein, N. Fukuda, E. Win, G. A. Clark, and F. E. Harris, *J. Chem. Phys.*, **45**, 4743 (1966).

(27) J. A. Pople and G. A. Segal, *ibid.*, **43**, S136 (1965).

(28) J. A. Pople and G. A. Segal, *ibid.*, **44**, 3289 (1966).

(29) G. E. Pake, "Paramagnetic Resonance," W. A. Benjamin, Inc., New York, N. Y., 1962 p 26.

(30) P. C. Lauterbur, *J. Amer. Chem. Soc.*, **83**, 1838 (1961).

(31) L. C. Cusachs and J. W. Reynolds, *J. Chem. Phys.*, **43**, S160 (1965).

where μ refers to an AO χ_μ on atom A with excess charge q_A . In this iterative extended Hückel method (IEH) iterations are performed until the charges at the output do not differ more than about 0.001 au from the charges at the input.²⁶

In the CNDO method^{27,28} a Hartree-Fock matrix F is constructed with elements

$$F_{\mu\mu} = -1/2(I_\mu + A_\mu) + \{(P_{AA} - Z_A) - 1/2(P_{\mu\mu} - 1)\}\gamma_{AA} + \sum_{B(\neq A)} (P_{BB} - Z_B)\gamma_{AB} \quad (3)$$

$$F_{\mu\nu} = \beta_{AB}^0 S_{\mu\nu} - 1/2 P_{\mu\nu} \gamma_{AB} \quad (\mu \text{ on A, } \nu \text{ on B}) \quad (4)$$

$P_{\mu\nu}$ is an element of the ordinary charge and bond order matrix; P_{AA} is the total electron density on atom A with core charge Z_A . For the Mulliken electronegativity $1/2(I_\mu + A_\mu)$, for β_{AB}^0 , and for γ_{AB} , the average Coulomb integral between valence AO's on A and B, the CNDO/2 parametrization of Pople and Segal²⁸ is used. The calculation is considered to be self-consistent if the total energy agrees with that of the last iteration to within 10^{-5} au. Trial vectors are obtained from a Hückel-type calculation retaining only the first terms of eq 3 and 4. In solving the eigenvalue equations for F , overlap is ignored by setting $S_{\mu\nu} = \delta_{\mu\nu}$.

B. Coupling Constants. In the theory of nuclear spin-spin coupling of Pople and Santry^{32,33} the Fermi contact contribution to the coupling constant is

$$J_{AB} = C_{AB} s_A^2(0) s_B^2(0) \pi_{s_A, s_B} \quad (5)$$

C_{AB} is a constant for a specific pair of nuclei AB; $s^2(0)$ is the density of the relevant s orbital at the nuclear position. Furthermore

$$\pi_{s_A, s_B} = -4 \sum_i^{\text{occ}} \sum_a^{\text{unocc}} (\epsilon_a - \epsilon_i)^{-1} c_{i s_A} c_{i s_B} c_{a s_A} c_{a s_B} \quad (6)$$

is the atom-atom polarizability. For the CNDO method $(\epsilon_a - \epsilon_i)$ is replaced by $(\epsilon_a - \epsilon_i - \gamma_{ia})$, where γ_{ia} is the Coulomb integral between the MO's ψ_i and ψ_a . For $s^2(0)$ of carbon we used the atomic SCF value of 2.767 au.³² For hydrogen 0.550 au was used which value is consistent with the orbital exponent of 1.2. In the derivation of eq 5 only one-center integrals are retained.

This type of theory of nuclear spin-spin coupling has been applied by various authors, using the Hückel-type theory of Pople and Santry³²⁻³⁶ and the extended Hückel theory of Hoffmann.^{37,38} A comparison between these two approaches has been made by de Jeu and Beneder.³⁹ CNDO calculations of coupling constants have been carried out by Ditchfield and Murrell.^{40,41}

C. Chemical Shifts. For the calculation of the ¹³C and ¹⁷O screening constants we use the MO theory of localized contributions to the screening.⁴²⁻⁴⁴ The most important approximations are the neglect of differential overlap and the neglect of electronic cur-

rents on neighbor atoms. The diamagnetic contribution to the screening of atom A is

$$\sigma_d = \frac{e^2}{3mc^2} \sum_\mu P_{\mu\mu} \langle r^{-1} \rangle_\mu \quad (7)$$

For a Slater-type orbital (STO) with exponent ζ_μ

$$\langle r^{-1} \rangle_\mu = \zeta_\mu / a_0 \quad (8)$$

In agreement with Pugmire and Grant⁴⁵ we take as our starting point for the paramagnetic contribution the formula of Karplus and Das.⁴³ Neglecting again differential overlap and the neighbor anisotropy term, we arrive at

$$\sigma_p = - \frac{2e^2 \hbar^2}{3m^2 c^2 \Delta E} \left\{ \sum_{\mu=x,y,z} P_{\mu A \mu A} R_{\mu\mu} + \frac{1}{4} \sum_{\substack{\mu, \nu=x,y,z \\ (\mu \neq \nu)}} \sum_B P_{\mu A \nu B} P_{\nu A \mu B} - P_{\mu A \mu B} P_{\nu A \nu B} \right\} R_{\mu\nu} I_{\mu\nu} \quad (9)$$

The summation B runs over all atoms, including the atom A under investigation; the index μA refers to an STO χ_μ on A; ΔE is the average excitation energy. Furthermore the following substitutions are made for the radial integrals on one atom

$$R_{\mu\nu} = \langle R(\mu) | r^{-3} | R(\nu) \rangle = \frac{(\zeta_\mu \zeta_\nu)^{5/2}}{6a_0^3 (\zeta_\mu + \zeta_\nu)^2} \quad (10)$$

$$I_{\mu\nu} = \langle R(\mu) | R(\nu) \rangle = \frac{32(\zeta_\mu \zeta_\nu)^{5/2}}{(\zeta_\mu + \zeta_\nu)^5} \quad (11)$$

$R(\mu)$ is the radial part of STO χ_μ . Using a simple Slater screening concept the exponent ζ_μ is defined, for instance, for a carbon atom by

$$\zeta_\mu = 3.25\beta - 0.35 \sum_{\nu(\neq \mu)}^A (q_\nu - 1) \quad (12)$$

q_ν is the electron density in STO χ_ν ; β is a parameter describing the contraction of an STO in a molecule.⁴⁶

(32) J. A. Pople and D. P. Santry, *Mol. Phys.*, **8**, 1 (1964).

(33) J. A. Pople and D. P. Santry, *ibid.*, **9**, 311 (1965).

(34) J. A. Pople and A. A. Bothner-By, *J. Chem. Phys.*, **42**, 1339 (1965).

(35) J. N. Murrell and V. M. S. Gil, *Theoret. Chim. Acta*, **4**, 114 (1966).

(36) R. Ditchfield, J. T. Jones, and J. N. Murrell, *ibid.*, **9**, 253 (1968).

(37) R. C. Fahey, G. C. Graham, and R. L. Piccioni, *J. Amer. Chem. Soc.*, **88**, 193 (1966).

(38) A. T. Amos, *Colloq. Intern. Centre Nat. Rech. Sci. (Paris)*, **164**, 283 (1964).

(39) W. H. de Jeu and G. P. Beneder, *Theoret. Chim. Acta*, **13**, 349 (1969).

(40) R. Ditchfield and J. N. Murrell, *Mol. Phys.*, **14**, 481 (1968).

(41) R. Ditchfield, *ibid.*, **17**, 33 (1969).

(42) A. Saika and C. P. Slichter, *J. Chem. Phys.*, **22**, 26 (1954).

(43) M. Karplus and T. P. Das, *ibid.*, **34**, 1683 (1961).

(44) J. A. Pople, *ibid.*, **37**, 53 (1962).

(45) R. J. Pugmire and D. M. Grant, *J. Amer. Chem. Soc.*, **90**, 697 (1968).

β is given. The value 1.05 for a π electron and 1.15 for a σ electron.

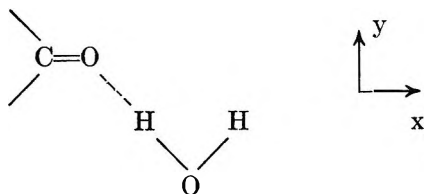
Equation 9 for the paramagnetic screening reduces to the well-known formula of Karplus and Pople,⁴⁷ if all electron densities q_ν in eq 12 are equal. Then $R_{\mu\nu} = \langle r^{-3} \rangle$ and $I_{\mu\nu} = 1$. However, we shall not use these simplifications.

Table I: Parameters for the IEH calculations (eV)

	H(1s)	C(2s)	C(2p)	O(2s)	O(2p)
$-\alpha^\circ$	13.60	21.40	11.40	32.30	15.84
$-\Delta\alpha$	14.00	11.90	11.90	15.95	15.95

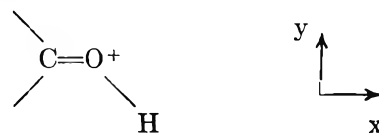
D. Numerical Evaluations. All overlap integrals were calculated using a basis of STO's, with exponents according to Slater's rules. For hydrogen we used $\zeta = 1.2$. In the IEH method where overlap is not ignored, solutions of the eigenvalue equations were obtained by the method of two successive diagonalizations. The necessary parameters are given in Table I. In this method the usual problem to obtain convergence was met and overcome by using in the successive iterations only a fraction of the charge predicted by the former iteration cycle. The diagonal elements are made consistent with the atomic charges as defined by Löwdin.⁴⁸ This does not automatically imply self-consistency for other charge definitions.⁴⁹ In the application to eq 9 the charge and bond order matrix over the orthogonal Löwdin orbitals is used; so eq 9 and the wave functions are consistent with each other with respect to the neglect of differential overlap. Nevertheless, the integrals $R_{\mu\nu}$ and $I_{\mu\nu}$ are calculated with the normal basis of STO's. In all the calculations, ΔE in eq 9 is chosen equal to 7 eV. A small increase that might be expected for H bonding¹³ would not affect our conclusions seriously.

In the calculations, the experimental geometry used for acetone is $r_{CO} = 1.23 \text{ \AA}$, $r_{CC} = 1.56 \text{ \AA}$, and $r_{CH} = 1.09 \text{ \AA}$.⁵⁰ All the carbon atoms and the oxygen lie in one plane; $\angle CCC = 120^\circ$. Each of the methyl groups can have a position with a CH bond eclipsed or staggered to the carbonyl bond (barrier $0.78 \text{ kcal mol}^{-1}$). For the calculations on acetone H-bonded to water the following model is used



Thus the water molecule is put in the plane of the acetone skeleton and a linear H bond is assumed making an angle of 120° with the carbonyl bond. The water

geometry ($r_{OH} = 0.96 \text{ \AA}$, $\angle HCH = 105^\circ$) is modified by taking in the H bond $r_{OH} = 1.05 \text{ \AA}$. Furthermore $r_{OO} = 2.50 \text{ \AA}$. These values give a minimum for the total energy of the acetone-water complex in a CNDO calculation.⁵¹ For protonated acetone we used



$r_{OH} = 0.985 \text{ \AA}$ and $\angle COH = 120^\circ$. Furthermore r_{CO} is increased from 1.23 \AA to 1.27 \AA . These values give an energy minimum for protonated formaldehyde in a nonempirical MO calculation by Ros.⁵²

Results

The ^{17}O , ^{13}C , and ^1H chemical shifts of pure acetone, relative to some reference compound, are given in Table II. The methyl ^{13}C is much more shielded than the carbonyl ^{13}C . Without calculations on the reference

Table II: Experimental Chemical Shifts for Pure Acetone

Chemical shift		Relative to
Carbonyl ^{17}O	-572^a	Water
Carbonyl ^{13}C	-12.4	Carbon disulfide
Methyl ^{13}C	162.9	Carbon disulfide
Methyl ^1H	-2.03	TMS

^a Reference 4.

compounds, the only chemical shift accessible to numerical calculation is the difference between methyl and carbonyl ^{13}C . We shall denote this quantity by Δ .

In Figure 1 the concentration dependence is shown for the ^1H chemical shifts in acetone-water.^{53,54} In Table III the same concentration dependence is given for $^1J_{CH}$, $^4J_{HH}$, carbonyl $\delta(^{13}\text{C})$, and methyl $\delta(^{13}\text{C})$ of acetone. The coupling constants increase with increasing H bonding (decreasing molar % acetone). The carbonyl ^{13}C is shifted to lower field (deshielded) with increasing H bonding, while the methyl ^{13}C is hardly affected. $\delta(^{17}\text{O})$ data are given for the purpose of comparison; we see that the ^{17}O resonance shifts in the

(46) C. A. Coulson, *Trans. Faraday Soc.*, **38**, 433 (1942).

(47) M. Karplus and J. A. Pople, *J. Chem. Phys.*, **38**, 2803 (1963).

(48) P.-O. Löwdin, *ibid.*, **18**, 365 (1950).

(49) E. W. Stout and P. Politzer, *Theoret. Chim. Acta*, **12**, 379 (1968).

(50) L. Sutton, Ed., "Tables of Interatomic Distances," The Chemical Society, London, 1958.

(51) W. H. de Jeu, to be published.

(52) P. Ros, *J. Chem. Phys.*, **49**, 4902 (1968).

(53) I. Satake, M. Arita, H. Kimizuka, and R. Matuura, *Bull. Chem. Soc. Jap.*, **39**, 597 (1966).

(54) I. Satake, private communication.

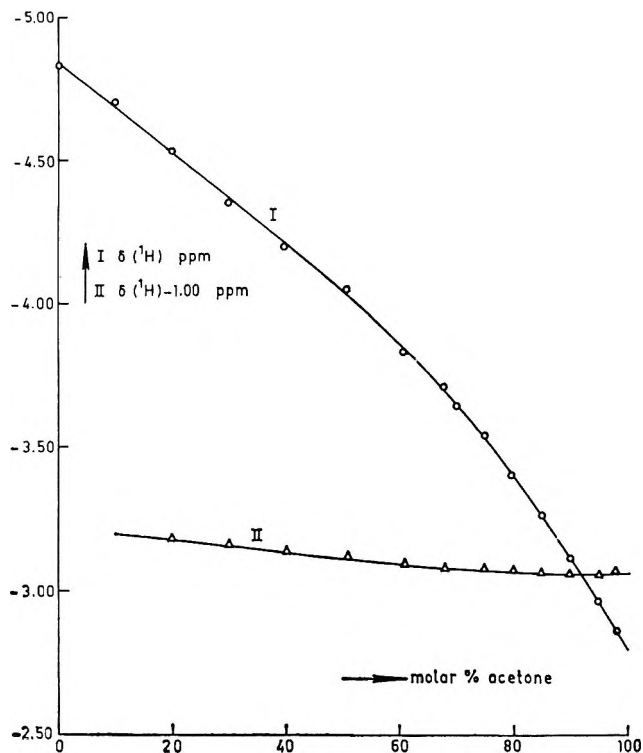


Figure 1. Proton chemical shifts for acetone-water. I, water protons (ref 53); II, acetone protons (ref 54).

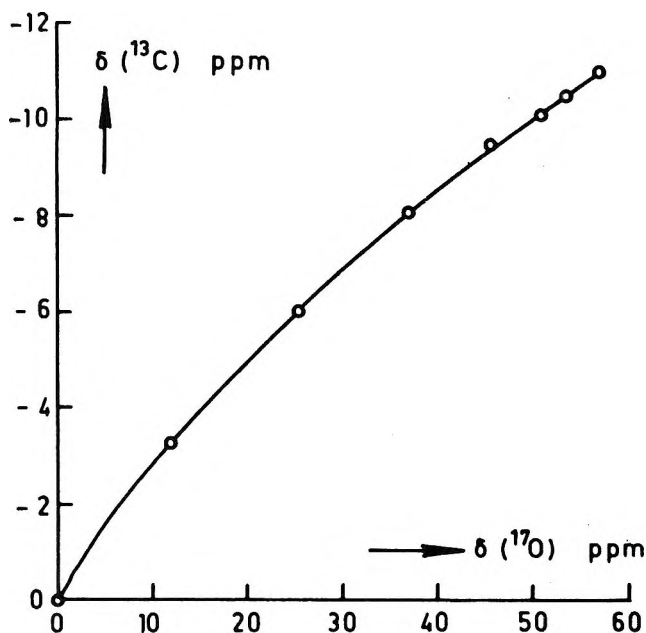


Figure 2. Carbonyl ^{13}C vs. ^{17}O chemical shift for acetone at various concentrations in water.

opposite direction as the carbonyl ^{13}C . From Figure 2 we see that the absolute changes in carbonyl $\delta(^{13}\text{C})$ and $\delta(^{17}\text{O})$ are not strictly linear with each other. In Figure 3 it is shown that within the experimental errors $^1J_{\text{CH}}$ and $^4J_{\text{HH}}$ vary linear with carbonyl $\delta(^{13}\text{C})$.

In Table IV the same coupling constants and chemical shifts (except $\delta(^{17}\text{O})$) are given for 20 mol % ace-

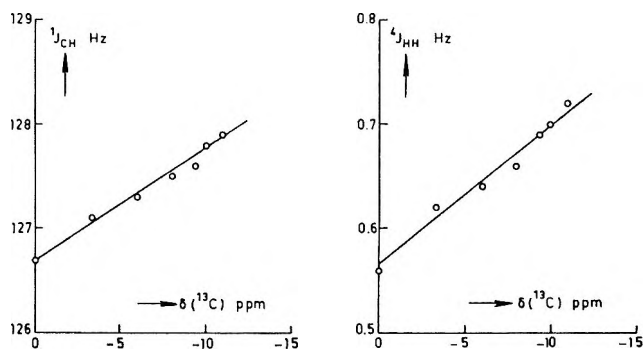


Figure 3. $^1J_{\text{CH}}$ and $^4J_{\text{HH}}$, vs. $\delta(^{13}\text{CO})$ for acetone at various concentrations in water.

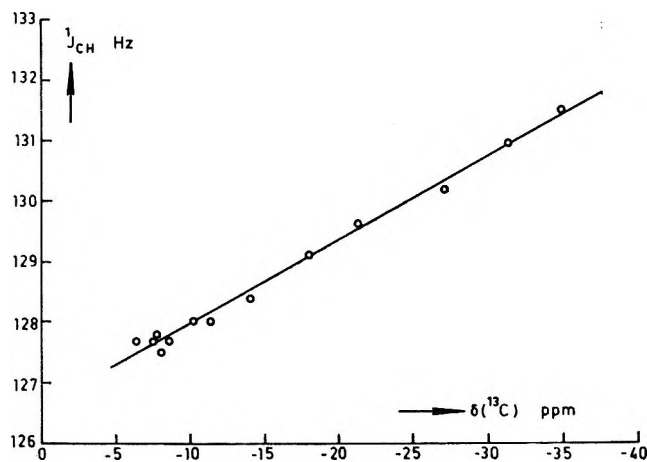


Figure 4. $^1J_{\text{CH}}$ vs. $\delta(^{13}\text{CO})$ for 0.2 M acetone in various concentration ratios of sulfuric acid-water.

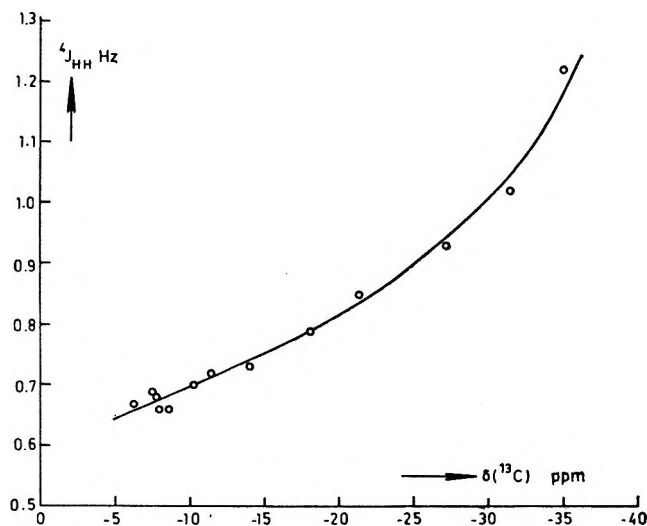


Figure 5. $^4J_{\text{HH}}$, vs. $\delta(^{13}\text{CO})$ for 0.2 M acetone in various concentration ratios of sulfuric acid-water.

tone in various sulfuric acid-water concentration ratios. Thus the sulfuric acid concentration varies from 0 to 80 mol % in the total solution. The increase in $^1J_{\text{CH}}$ and $^4J_{\text{HH}}$ is now much more. The methyl ^{13}C chemical

Table III: Concentration Dependence of Coupling Constants (Hz) and ^{17}O and ^{13}C Chemical Shifts (ppm) for Acetone in Water

Mol % acetone	Coupling constants		Chemical shifts		
	$^1J_{\text{CH}}^a$	$^4J_{\text{HH}}^b$	Carbonyl $^{17}\text{O}^c$	Carbonyl $^{13}\text{C}^d$	Methyl $^{13}\text{C}^d$
100	126.7	0.56	0.0	0.0	0.0
65	127.1	0.62	12.0	-3.3	-0.4
35	127.3	0.64	25.5	-6.0	-0.4
20	127.5	0.66	37.1	-8.0	-0.6
10	127.6	0.69	45.7	-9.4	-0.9
5	127.8	0.70	51.1 ^e	-0.0	-0.9
2.5	127.9	0.71	53.8 ^e	-0.4	-1.3
1.0	127.8	0.71			
0.5	127.8	0.70			
0.2	127.9	0.72			
0	127.9 ^e	0.72 ^e	57.0 ^e	-10.9 ^e	-1.2 ^e

^a Standard deviation 0.05 Hz. ^b Standard deviation 0.005 Hz. ^c ± 1.0 ppm (ref 4). ^d Standard deviation 0.2 ppm. ^e Extrapolated from the higher concentrations.

Table IV: Coupling Constants (Hz) and Chemical Shifts (ppm) for 20 Mol % Acetone in Various Concentration Ratios of Sulfuric Acid-Water

Mol % sulfuric acid	Coupling constants		Chemical shifts			
	$^1J_{\text{CH}}^a$	$^4J_{\text{HH}}^b$	Carbonyl $^{13}\text{C}^c$	Methyl $^{13}\text{C}^c$	Methyl $^1\text{H}^d$	Solvent $^1\text{H}^e$
0	127.5	0.66	-8.0	-0.6	-2.24	-4.56
2	127.7	0.67	-6.3	-0.6	-2.29	-5.10
3	127.7	0.69	-7.5	-0.6		
6	127.7	0.66	-8.6	-0.5	-2.29	-6.23
8	127.8	0.68	-7.8	-0.5	-2.31	-7.13
12	128.0	0.70	-10.2	-0.5	-2.35	-8.19
16	128.0	0.72	-11.4	-0.5	-2.37	-8.40
23	128.4	0.73	-14.0	-0.5	-2.43	-9.86
32	129.1	0.79	-18.0	-0.1	-2.54	-11.00
40	129.7	0.85	-21.3	0.2	-2.68	-11.57
49	130.2	0.93	-27.1	0.8	-2.80	-12.02
55	130.9	1.02	-31.4	-0.7		
63	131.5	1.22	-35.0	-1.3	-2.96	-12.26

^a Standard deviation 0.05 Hz; ^b Standard deviation 0.005 Hz. ^c Relative to pure acetone; standard deviation 0.5 ppm. ^d Relative to TMS; standard deviation 0.02 ppm. ^e Relative to TMS; standard deviation 0.1 ppm.

shift still does not change appreciably, while the carbonyl ^{13}C is shifted to a much lower field by protonation rather than by H bonding. The variations in $^1J_{\text{CH}}$ and carbonyl $\delta(^{13}\text{C})$ are again linear with each other (Figure 4). For $^4J_{\text{HH}}$ a large deviation from linearity occurs (Figure 5).

The results of the theoretical calculations with aid of the methods described in the previous section, are given in the Tables V, VI and VII; H bonded refers to the calculation on acetone H bonded to water. In Table V the excess charges on the atoms are given, in Table VI the theoretical coupling constants together with the experimental values (when available), and in Table VII the diamagnetic and paramagnetic screening constants together with the values for Δ . All theoretical values are averages over the three rotational isomers.

Discussion

A. General Considerations. The two theoretical methods both reproduce the energetical order of the rotational isomers. The conformation with both methyl groups eclipsed to the CO bond is the most favorable; with both staggered is the least favorable. The expected polarity of the carbonyl group is also found in both methods, while the excess charges on the methyl carbon and hydrogen atoms are very slight (Table V). In the orbital populations (not given in the tables) the $2p_y$ lone pair on oxygen is clearly present; the $2s$ lone pair is more mixed up with the other AO's. From the $2p_x$ and $2p_z$ populations we learn that both the carbonyl σ and the carbonyl π bond are polar; in the IEH method the σ bond is more polar while in the CNDO method the π bond is the more polar.

Table V: Theoretical Excess Charges for Acetone (au)

		Carbonyl			Methyl	
		H	O	C	C	H
IEH ^a	Pure		-0.240	0.093	0.003	0.024
	H-bonded		-0.190	0.144	0.014	0.030
	Protonated	0.240	0.022	0.281	0.059 ^b	0.056 ^b
CNDO	Pure		-0.263	0.251	-0.071	0.026
	H-bonded		-0.270	0.275	-0.074	0.033
	Protonated	0.268	-0.113	0.415	-0.090 ^b	0.101 ^b

^a Löwdin charges (ref 48). ^b There is a slight difference between the two methyl groups, which is disregarded here.

Table VI: Experimental and Theoretical Coupling Constants for Acetone (Hz)

		CC	CH	HCH	HCC	HCCC	HCCCH
Exptl	Pure	40.6 ^a	126.8	-14.9 ^b	-5.9 ^c	2.2 ^d	0.56 ^d
	H-bonded		127.9				0.72
	Protonated		131.5				1.22
IEH	Pure	26.5	67.3	-21.3	-5.1	0.4	-0.1
	H-bonded	26.5	66.7	-21.1	-4.9	0.4	0.1
	Protonated	26.6	64.4	-20.2	-4.4	0.4	1.8
CNDO	Pure	11.2	55.6	0.4	0.1	1.2	-1.8
	H-bonded	10.8	54.8	0.3	0.3	1.0	-1.2
	Protonated	9.1	58.4	-0.1	0.8	0.8	-0.4

^a F. J. Weigert and J. D. Roberts, private communication. ^b H. S. Gutowsky, M. Karplus, and D. M. Grant, *J. Chem. Phys.*, **31**, 1278 (1959); negative sign assumed in analogy with the same coupling in methane (ref 34). ^c G. J. Karabatsos and C. E. Orzech, *J. Amer. Chem. Soc.*, **86**, 3574 (1964); negative sign assumed in analogy with the same coupling in acetaldehyde, E. Sackmann and H. Dreeskamp, *Spectrochim. Acta*, **21**, 2005 (1965). ^d H. Dreeskamp, *Z. Phys. Chem.*, **59**, 321 (1968); W. H. de Jeu and H. Angad Gaur, *Mol. Phys.*, **16**, 205 (1969).

Table VII: ¹⁷O and ¹³C Screening Constants for Acetone (ppm)

		Carbonyl C		Carbonyl C		Methyl C		Δ^a
		σ_d	σ_p	σ_d	σ_p	σ_d	σ_p	
Exptl	Pure							175.3
	H-bonded							185.0
	Protonated							209.0
IEH	Pure	419.9	-1238.6	266.4	-526.2	268.8	-482.2	46.4
	H-bonded	418.7	-1190.2	265.8	-538.0	269.2	-485.5	55.9
	Protonated	414.1	-1176.1	264.5	-581.7	268.2	-499.7	85.7
CNDO	Pure	420.0	-1287.3	264.6	-580.1	269.7	-473.5	111.8
	H-bonded	419.9	-1253.5	264.4	-585.1	269.8	-473.5	117.0
	Protonated	416.2	-1128.2	263.3	-622.7	269.9	-478.9	150.6

^a $\Delta = \delta(^{13}\text{CH}_3) - \delta(^{13}\text{CO})$.

For H bonding and for protonation we notice a considerable decrease of charge on the carbonyl carbon (Table V). The oxygen atom is much less affected although some decrease of electron density is predicted in the case of protonation. For H bonding some charge is transferred to the water molecule.⁵¹ Generally we see that there is a drift of electrons in the direction of the oxygen atom for H bonding and to the carbonyl proton for protonation. This is mainly at the expense of the carbonyl carbon. Furthermore, the methyl protons together lose some electrons while the methyl carbons are much less affected. These changes cause an increase in carbonyl π bond polarity; the polarity of the σ bond changes much less.

B. Coupling Constants. From Table VI we see that for pure acetone the sign and the order of magnitude of the directly bonded CC and CH coupling constants are rather well reproduced in both methods. As expected, the theoretical values are smaller than the experimental ones because of the fact that simple MO theory underestimates electron correlation.⁵⁶ Recent calculations⁵⁶ seem to indicate that the atomic SCF value we used for $s_C^2(0)$ is too low for molecules. Consequently, agreement in absolute magnitude with experiment is probably better than is apparent from Table VI. The CNDO method is not very successful for the prediction of the two-bond coupling constants. Probably the inclusion of the one-center exchange integrals (INDO method) is essential to get the negative value.^{41,56} π -Electron contributions which are not included in Table VI may be of importance for the long-range coupling constants. Using a valence bond formalism, Holmes and Kivelson^{3a} calculated for acetone a π -electron contribution to $^4J_{HH}$ of -0.6 Hz. This value decreases in absolute magnitude with increasing π -bond polarity. In order to obtain the experimental value, we have to postulate a positive contribution through the σ bonds and/or through space⁵⁷ of $+1.2$ Hz. However, both calculations give a negative value. Nevertheless we may hope that the substituent effects can be predicted with more reliability.³⁴

From Table VI we see that the increase in $^1J_{CH}$ for H-bond formation and for protonation is in general not reproduced by the calculations. However, the increase in $^1J_{CH}$ is qualitatively in accordance with the well-known theory in which it is emphasized that $^1J_{CH}$ in CH_3X is proportional to the amount of carbon s character in the CH bonds.^{55,58} A change in electronegativity of X is supposed to cause a rehybridization of the carbon atom. With increasing electronegativity of X the CX bond becomes more polar (more p character), leaving more s character for the CH bonds; thus $^1J_{CH}$ increases. In our case the carbonyl group gets an increased electron attracting power when an H bond is formed and even more for protonation. This means an effective increase in electronegativity, and the increase in $^1J_{CH}$ is as expected.^{3b} There are several ways to

obtain a quantitative estimate of the amount of s character from the calculations. Assuming that a transformation to highly localized MO's is possible, we can use the squares of the bond orders.⁵⁹ In this way we get CNDO values for the amount of carbon s character of 0.249 (pure acetone), 0.250 (acetone H bonded to water), and 0.260 (protonated acetone). So for H bonding a small and hardly significant increase of s character is found despite the predicted decrease of $^1J_{CH}$ (Table VI). For protonation the predicted increase of $^1J_{CH}$ is in agreement with the increase of carbon s character in the CH bonds.

For $^4J_{HH}$ the experimental increase when an H bond is formed and for protonation is relatively much more than for $^1J_{CH}$. As the π -bond polarity increases, we can expect a decrease in absolute magnitude of the π electron contribution to $^4J_{HH}$.^{3a} The calculations also predict a change in positive direction for the contribution *via* the σ skeleton (Table VI). Thus the changes in both contributions reinforce each other to give the more positive value of $^4J_{HH}$. This is consistent with a simple MO picture of substituent effects on $^4J_{HH}$ in which a shift in positive direction is predicted when electrons are withdrawn from the central carbon atom.^{60,61}

Laszlo² has expressed his doubt about the explanation given above. The main argument is that changes with solvent of $^4J_{HH}$ in monochloroacetone can be explained by a change in preference for eclipsed and staggered rotational isomers.⁶² We know of no evidence to support this view in the case of acetone, as the energetical differences between the isomers are very slight. Moreover, both calculations on acetone give differences in the coupling constants of the different isomers that are less than 0.2 Hz. Only the π -electron contribution to $^4J_{HH}$ depends on the orientation of the methyl groups.

C. Chemical Shifts. Looking at the chemical shifts (Table II and VII) we see, as expected, that the major part of the difference in shielding between carbonyl and methyl ^{13}C arises from variations of σ_p . The CNDO method gives the right order of magnitude for Δ ; the value of the IEH calculation is far too low. The shift to lower field of carbonyl $\delta(^{13}C)$ when an H bond is formed and for protonation is very well reproduced by the calculations. This is also true for the near constancy of methyl $\delta(^{13}C)$. So even the IEH method

(55) J. N. Murrell in "Progress in NMR Spectroscopy," J. W. Emsley, J. Feeney, and L. H. Sutcliffe, Ed., in press.

(56) J. A. Pople, J. W. McIVER, and N. S. Ostlund, *J. Chem. Phys.*, **49**, 2965 (1968).

(57) W. H. de Jeu, R. Deen, and J. Smidt, *Rec. Trav. Chim.*, **86**, 33 (1967).

(58) N. Muller and D. E. Pritchard, *J. Chem. Phys.*, **31**, 768, 1471 (1959).

(59) C. Trindle and O. S. Nanoglu, *J. Amer. Chem. Soc.*, **91**, 853 (1969).

(60) D. J. Sardella, *J. Mol. Spectrosc.*, **31**, 70 (1969).

(61) M. Barfield and B. Chakrabarti, *Chem. Rev.*, in press.

(62) K. Takahashi, *Bull. Chem. Soc. Jap.*, **37**, 291 (1964).

which gives a bad result for Δ reflects the changes rather well. For the carbonyl ^{17}O the experimental shift of 57.0 ppm to a higher field when an H bond is formed is also found in the calculations. Thus here we find a shift to a higher field despite the fact that no appreciable increase of the electron density on oxygen is predicted. Unfortunately, no experimental ^{17}O chemical shifts are available for protonated acetone.

A shift to a lower field is normal for H-bonded protons.⁶³ For the water protons in acetone-water we have two competing types of H bonds, water-acetone and water-water. The shift to a lower field with increasing water concentration (Figure 1) suggests that the H bonds water-water are stronger than water-acetone.⁶³ The near constancy of the acetone ^1H chemical shift when an H bond is formed is probably due to a cancellation of several factors. As in both calculations the charges on the methyl protons decrease when an H bond is formed (and even more for protonation), we can expect a decreased diamagnetic screening. This is more or less compensated by a greater neighbor anisotropy effect. For the acidic solutions the changes in the ^1H chemical shift of the solvent (Table IV) are more difficult to explain. We observe a weighted average of the protons in the species H_2SO_4 , HSO_4^- , H_3O^+ , H_2O , $(\text{CH}_3)_2\text{CO}^+\text{H}$, and higher order complexes.

The deviation from linearity in the relation between the changes in carbonyl $\delta(^{17}\text{O})$ and $\delta(^{13}\text{C})$ when an H

bond is formed (Figure 2) can be attributed to the fact that the carbon atom has an opportunity to compensate for the loss of electrons at the cost of the methyl groups. Therefore the change in $\delta(^{13}\text{C})$ is not as rapid as in $\delta(^{17}\text{O})$, whereby we get the curve. The linear relation between the changes in $^1J_{\text{CH}}$ and carbonyl $\delta(^{13}\text{C})$ (Figures 3 and 4) can be understood by the direct way in which both depend on the increased electron attracting power of the carbonyl oxygen when an H bond is formed and for protonation. In the light of the more complicated mechanisms for $^4J_{\text{HH}}$ the linear relation between the changes in $^4J_{\text{HH}}$ and carbonyl $\delta(^{13}\text{C})$ when an H bond is formed (Figure 3) must be more or less fortuitous. This is confirmed by the fact that this linearity does no longer hold in the case of protonation (Figure 5).

Acknowledgment. The author wishes to express his gratitude to G. P. Beder for carrying out the measurements on acetone in sulfuric acid-water, and to Professor L. L. van Reijen (Chemistry Department) and Professor J. Smidt and several other members of the group of magnetic resonance (Physics Department) for valuable discussions and technical assistance. The CNDO program was kindly provided by G. A. Segal (Pittsburgh).

(63) J. A. Pople, W. G. Schneider, and H. J. Bernstein, "High Resolution Nuclear Magnetic Resonance," McGraw-Hill Book Co., Inc., New York, N. Y., 1959, p 400.

On the Oxyiodine Radicals in Aqueous Solution

by O. Amichai and A. Treinin

*Department of Physical Chemistry, Hebrew University, Jerusalem, Israel
(Received July 15, 1969)*

The flash photolysis of IO_3^- and IO^- provides evidence for the following primary processes: $\text{IO}_3^- \xrightarrow{h\nu} \text{IO}_2 + \text{O}^-$ and $\text{IO}^- \xrightarrow{h\nu} \text{I} + \text{O}^-$. These are followed by secondary reactions involving the parent ions. O^- (or OH) reacts with IO_3^- and IO^- to yield IO_3 and IO , respectively; the rate constants of these reactions could be determined by studying the O_3^- decay in alkaline solutions containing O_2 . IO_2 and I_2^- (produced from I in presence of I^-) react with IO_3^- and IO^- , respectively, to yield IO . The spectra and decay kinetics of the oxyiodine radicals were also studied by pulse radiolysis. The two techniques lead to the same conclusions.

The flash photolysis and pulse radiolysis techniques have yielded some basic information on the oxybromine radicals BrO_2 and BrO in solution.^{1,2} The analogous chlorine radicals are well known. On the other hand, very little is known on the oxyiodine radicals. Such information is essential for understanding the photochemistry of the oxyiodine anions.

The oxybromine anions were shown to undergo two radical types of photo-dissociation to yield O^- and O atom, respectively, which can react with the parent

(1) G. V. Buxton and F. S. Dainton, *Proc. Roy. Soc.*, **A304**, 427, 441 (1968).

(2) O. Amichai, G. Czapski, and A. Treinin, *Israel J. Chem.*, **7**, 351 (1969).

ion.^{2,3} These findings have refuted the previous interpretation of their photochemistry.^{4,5} The present work shows that the O^- type of dissociation is a major primary process also in the case of IO_3^- and IO^- and that some of the subsequent secondary processes involve the parent ion.

Experimental Section

The flash photolysis setup was as described elsewhere,⁶ but the energy of the flash was increased to 600 J. The monitoring light source was a 120-W tungsten projecting lamp, and the optical path length 5 cm. For pulse radiolysis a Varian linear accelerator was used which delivered pulses of 5 MeV, 200 mA, 1.5- μ sec duration. Full details of the experimental conditions will be published in "Pulse Radiolysis at the Hebrew University Accelerator, Internal Report, Dept. of Physical Chemistry, The Hebrew University." R 136 and IP 28 photomultipliers were employed with two Bausch and Lomb monochromators, Type 567 AB. By multiple reflections the monitoring light passed through effective optical path lengths of 6 or 12 cm. The mean dose per pulse was determined with air-saturated solution of $K_4Fe(CN)_6$ as dosimeter, taking $\epsilon_{Fe(CN)_6^{3-}} = 10^3 M^{-1} cm^{-1}$ at 420 nm and $G_{Fe(CN)_6^{3-}} = 2.7$. All the spectra recorded were measured at intervals of 5 nm; splitting of the monitoring light beam⁶ was used to overcome irreproducibility of the flashes and pulses. (The experimental points are scattered within less than 5% from the recorded absorption curves.)

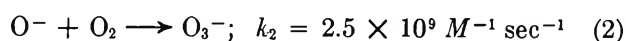
The materials used were of Spectrograde or analytical grade. Dilute solutions of $NaIO$ (10^{-3} to $10^{-4} M$) were prepared by rapidly dissolving solid I_2 in solutions containing 0.4 M NaOH. (Under these conditions their disproportionation rate was relatively slow.) Matheson's $O_2 + N_2$ mixtures, He, or N_2O , were bubbled through the solutions. N_2O was purified by passing through solutions of pyrogallol in alkali. Unless otherwise stated the solutions were neutral, air-free (saturated with He), at $23 \pm 2^\circ$.

Results

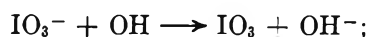
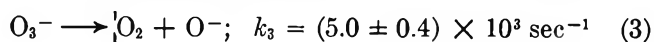
A. Flash Photolysis. The flash photolysis of alkaline solutions of IO_3^- and IO^- in presence of O_2 gave rise to transient absorption peaking at 430 nm, identical with that of O_3^- (Figure 1). Its decay rate obeyed the law

$$-\frac{d(O_3^-)}{dt} = \frac{(IO_3^-)}{p(IO_3^-) + q(O_2)} (O_3^-) \quad (1)$$

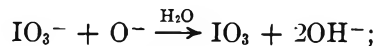
which has the same form as the corresponding law for O_3^- produced from the oxybromine systems.² This suggests a similar mechanism for the generation and decay of O_3^- . From the experimental values of p and q , the dependence of q on pH, and the known² rate constant of the reaction



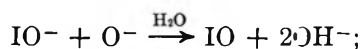
the following rate constants could be determined



$$k_4 = (9.2 \pm 0.8) \times 10^8 M^{-1} sec^{-1} \quad (4)$$



$$k_5 = (2.0 \pm 0.3) \times 10^8 M^{-1} sec^{-1} \quad (5)$$



$$k_6 = (4.6 \pm 0.6) \times 10^9 M^{-1} sec^{-1} \quad (6)$$

(The reaction of IO^- with OH could not be studied because the hypiodite solutions were unstable below pH ~ 13.5 .) The value of k_3 is in good agreement with previous data (summarized in ref 2).

Flash photolysis of oxygen containing solutions did not give rise to the 260-nm band of O_3 . This was done with comparable concentrations of IO_3^- and O_2 so that O_2 could effectively compete with the oxyiodine anions³ on $O(^3P)$. We conclude that IO_3^- and IO^- do not photodissociate to yield $O(^3P)$ at λ above ~ 200 nm.

Some other transients were observed but they could be better investigated in absence of O_2 with neutral solutions. Figure 2 shows the results of such experiments with IO_3^- solutions. Three absorption bands

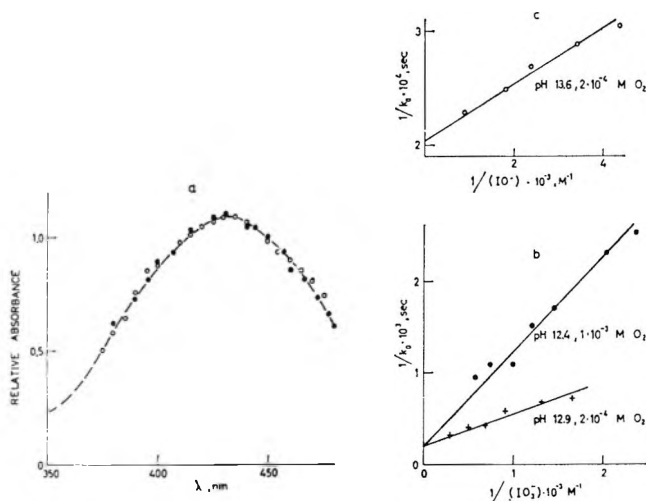


Figure 1. Absorption spectra (a) and kinetics of decay (b and c) of O_3^- produced in alkaline solutions of IO_3^- and IO^- containing O_2 . Curve (a) dashed curve, spectrum of O_3^- (ref 2); ●, $10^{-3} M IO_3^-$, $10^{-3} M O_2$, pH 12.4, 1 msec after flash; ○, $4.2 \times 10^{-4} M IO^-$, $2 \times 10^{-4} M O_2$, pH 13.6, 0.6 msec after flash. k_0 is the pseudo-first-order rate constant of the ozonide decay.

(3) O. Amichai and A. Treinin, *Chem. Phys. Lett.*, **3**, 611 (1969).

(4) L. Farkas and F. S. Klein, *J. Chem. Phys.*, **16**, 886 (1948).

(5) N. K. Bridge and M. S. Matheson, *J. Phys. Chem.*, **64**, 1280 (1960).

(6) D. Behar and G. Czapski, *Israel J. Chem.*, **6**, 43 (1968).

Table I: Rate Constants for the Reactions of the Oxyiodine Radicals at $23 \pm 2^\circ$

Transient	Proposed reaction	Rate constant $M^{-1} \text{sec}^{-1}$ ^a	Conditions and method ^b
A(IO_3)	$\text{IO}_3 + \text{IO}_3 \rightarrow \text{prod.}$	$(5.1 \pm 0.5) \times 10^6 \times \epsilon_{\text{max}}(\text{IO}_3)$ $(4.6 \pm 0.3) \times 10^6 \times \epsilon_{\text{max}}(\text{IO}_3)$	fp $(0.07-5.0) \times 10^{-2} M \text{IO}_3^-$ pr $(1.0-8.0) \times 10^{-2} M \text{IO}_3^-$
C(IO_2)	$\text{IO}_2 + \text{IO}_3^- \rightarrow \text{IO} + \text{IO}_4^-$	$(3.5 \pm 0.5) \times 10^6$	pr $(1.0-8.0) \times 10^{-2} M \text{IO}_3^-$ fp $\sim 10^{-2} M \text{IO}_3^-$
C(IO_2)	$\text{IO}_2 + \text{ethanol} \rightarrow \text{IO} + \text{prcd.}$	$(1.6 \pm 0.3) \times 10^6$	fp $2 \times 10^{-3} M \text{IO}_3^- + (0.5-17.0) \times 10^{-2} M \text{ethanol}$ pr $10^{-2} M \text{IO}_3^- + (3.5-17.0) \times 10^{-2} M \text{ethanol}$
B(IO)	$\text{IO} + \text{IO} \rightarrow \text{prod.}$	$(4.4 \pm 0.2) \times 10^6 \times \epsilon_{\text{max}}(\text{IO})$ $(4.8 \pm 0.5) \times 10^6 \times \epsilon_{\text{max}}(\text{IO})$ $(4.3 \pm 0.2) \times 10^6 \times \epsilon_{\text{max}}(\text{IO})$ $(4.5 \pm 0.4) \times 10^6 \times \epsilon_{\text{max}}(\text{IO})$ $(4.2 \pm 0.5) \times 10^6 \times \epsilon_{\text{max}}(\text{IO})$ $(4.3 \pm 0.3) \times 10^6 \times \epsilon_{\text{max}}(\text{IO})$	pr $1.2 \times 10^{-3} M \text{IO}_3^-$, pH 13.6 pr $(1.0-8.0) \times 10^{-2} M \text{IO}_3^-$ pr $1.1 \times 10^{-2} M \text{IO}_3^- + \text{ethanol}$ (up to 0.17 M) fp $1.1 \times 10^{-3} M \text{IO}_3^-$, pH 13.6 fp $(0.8-5.0) \times 10^{-2} M \text{IO}_3^-$ fp $(0.8-5.0) \times 10^{-2} M \text{IO}_3^- + \text{ethanol}$ (up to 0.17 M)
D(I_2^-)	$\text{I}_2^- + \text{IO}^- \rightarrow \text{IO} + 2\text{I}^-$	$(5.0 \pm 0.6) \times 10^7$	fp $(1.0-3.0) \times 10^{-4} M \text{IO}_3^-$, pH 13.6 fp $(1.0-3.0) \times 10^{-4} M \text{IO}_3^- + (1.0-3.0) \times 10^{-4} M \text{I}^-$, pH 13.6

^a $2k$ is recorded for reactions involving two radical molecules. From our work the values of ϵ_{max} ($M^{-1} \text{cm}^{-1}$) obtained were 900, 220, and 400 for IO, IO_2 , and IO_3 , respectively. ^b fp and pr stand for "flash photolysis" and "pulse radiolysis," respectively.

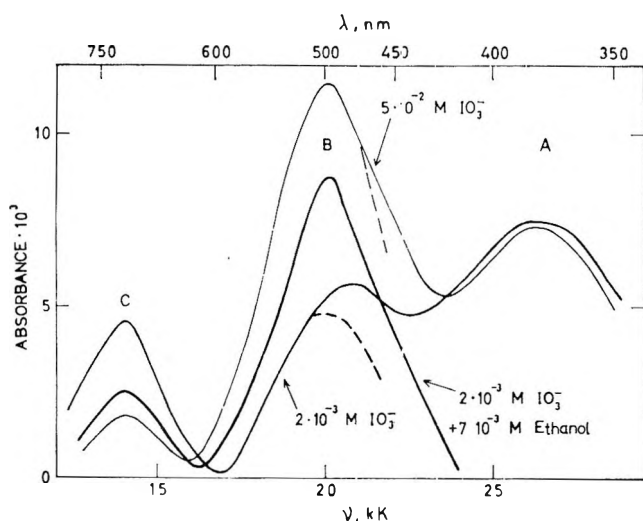


Figure 2. Absorption spectra of the transients produced by flash photolysis in solutions of IO_3^- , alone and in presence of ethanol. The absorbance was measured 110 μsec after start of flash. Resolution of the spectra to component bands (Gaussian type of analysis) is shown by the dashed curves.

emerge, designated A, B, and C, which peak at 380 nm, 490 nm, and 715 nm, respectively. (λ_{max} was determined by Gaussian type of analysis; see dashed curves in Figure 2).

Transient A undergoes a second-order decay which does not depend on IO_3^- concentration (Table I). The decay of C appeared to be first order with respect to IO_3^- , which suggests a reaction of C with IO_3^- (Figure 3). (More accurate kinetic data on this reaction were derived from the pulse experiments; see later.) This reaction appears to produce transient B, since shortly after flash the ratio between the intensities of bands B and C, respectively, markedly increased with IO_3^- (Fig-

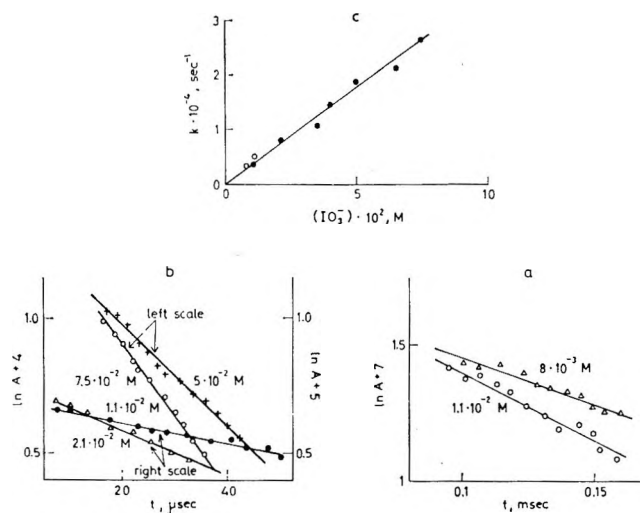


Figure 3. The pseudo-first-order decay of transient C (IO_2) in presence of IO_3^- ; a (flash) and b (pulse), the absorbance A at 710 nm vs. time for various IO_3^- concentrations; c, the dependence of the first order rate constant on (IO_3^-) as derived from the flash (O) and pulse (●) experiments. In the pulse experiments (b) the optical path lengths were 12 cm (left scale) and 6 cm (right scale).

ure 2). At $\text{IO}_3^- \gtrsim 8 \times 10^{-2} M$ band C could hardly be detected. At $(\text{IO}_3^-) \geq 0.1 M$ the generation of B was relatively fast ($\tau_{1/2} \leq 20 \mu\text{sec}$), so its decay could be readily measured starting 100 μsec after flash. It was found to be second order with k independent of (IO_3^-) (Table I). In presence of C the decay of B became slower. This is probably due to the parallel generation of B by the reaction of C with IO_3^- .

No effect of N_2O was obtained by flashing $2.7 \times 10^{-3} M \text{IO}_3^- + 1.5 \times 10^{-2} M \text{N}_2\text{O}$. (Under these conditions N_2O should effectively compete with IO_3^- on any solvated electrons if present.⁷) On the other

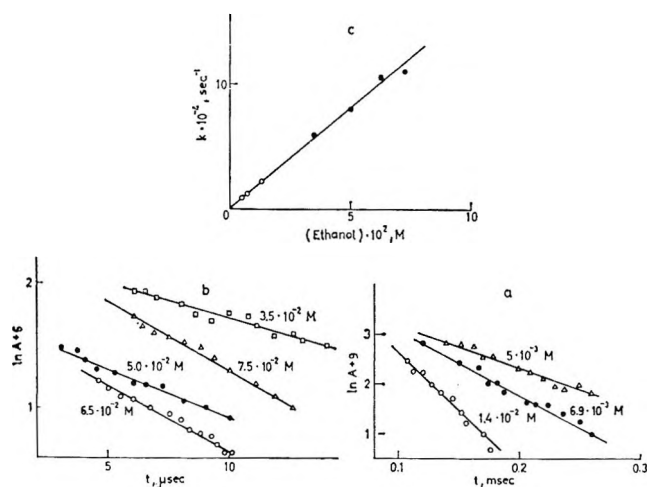


Figure 4. The pseudo-first-order decay of transient C (IO_2) in presence of ethanol; a (flash), the absorbance A at 710 nm vs. time for solutions containing $2 \times 10^{-3} M \text{IO}_3^-$ and various concentrations of ethanol; b (pulse, 12 cm optical path length), the same with $1.1 \times 10^{-2} M \text{IO}_3^-$; c, the dependence of the first order rate constant on ethanol concentration as derived from the flash (O) and pulse (●) experiments.

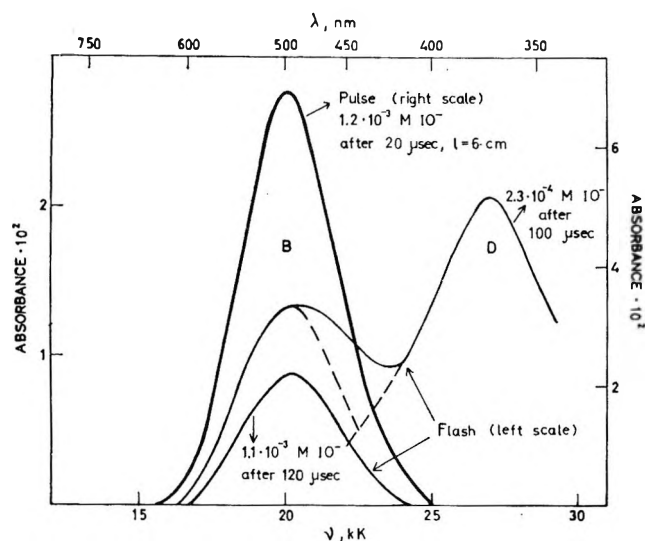


Figure 5. Absorption spectra of the transients produced by flash and pulse in solutions of IO^- with equivalent amount of I^- , pH 13.6.

hand, ethanol had a pronounced effect. Addition of ethanol to IO_3^- led to suppression of band A and to weakening and intensification of bands C and B, respectively (Figure 2). The decay of C became faster; a pseudo-first-order reaction involving C and ethanol appeared to occur (Figure 4), with transient B being the product of this reaction too.

In air-free solutions of $1.1 \times 10^{-3} M \text{IO}^-$ the flash produced a transient band peaking at 490 nm (Figure 5). This and the decay kinetics (Table I) prove its identity with transient B. On lowering the concentration of IO^- a new band grew at 370 nm, designated by D (Figure 5). It showed a first-order decay rate with

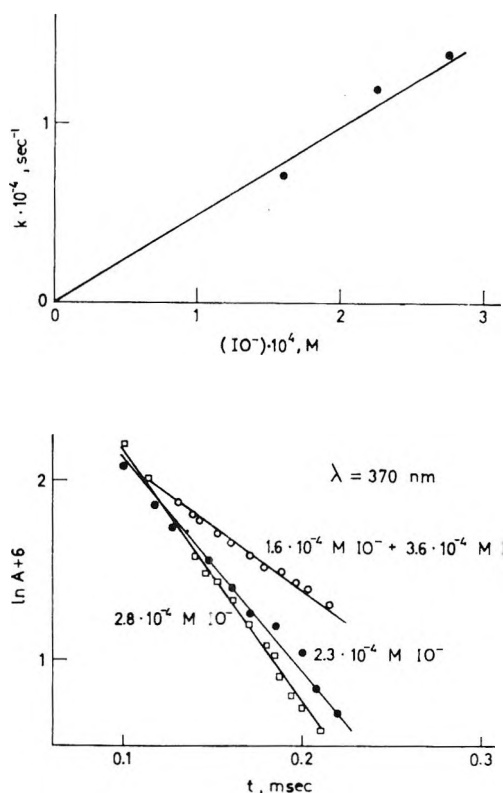


Figure 6. The pseudo-first-order decay of transient D (I_2^-) in the presence of IO^- (with equivalent amount of I^- , unless otherwise stated) pH 13.6.

k being proportional to (IO^-) (Figure 6 and Table I). In the presence of D the decay of B became slower and deviated from second order in a way which suggests further generation of B after the flash.

B. Pulse Radiolysis. The pulse radiolysis of $10^{-2} M \text{IO}_3^-$ solution clearly showed bands A, B, and C (Figure 7). Ethanol had the same influence as in the flash photolysis experiments, but now N_2O also had a pronounced effect: in the presence of $1.5 \times 10^{-2} M \text{N}_2\text{O}$, band A intensified whereas bands B and C became weaker. (N_2O and IO_3^- scavenge e_{aq}^- at comparable rates.⁷ To obtain detectable yields of radicals we could not make (IO_3^-) much lower than the concentration of N_2O .)

With IO^- solutions the pulse produced band B (Figure 5), but band D could not be detected.

The identity of the three transients produced by pulse with A, B, and C was verified by detailed study of their kinetics. The pseudo-first-order decay of C, with and without ethanol, is illustrated in Figures 4 and 3, respectively. Table I records all the rate constants obtained by the two techniques. In the case of IO^- , since transient D was not present in the pulsed solution, no deviations from the normal decay of B were observed.

(7) M. Anbar and P. Neta, *Intern. J. Appl. Radiat. Isotopes*, **18**, 493 (1967).

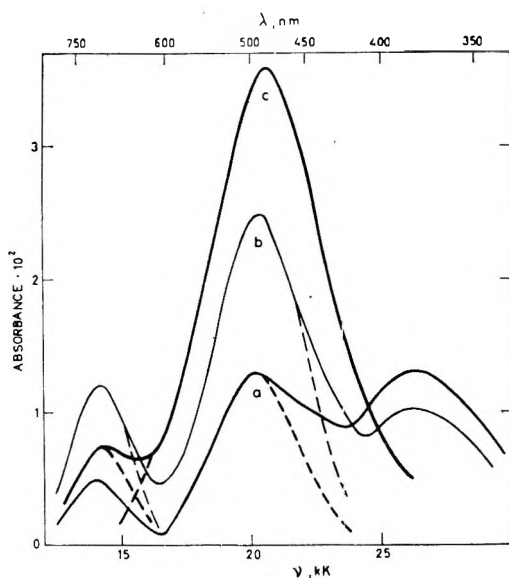
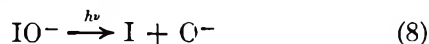
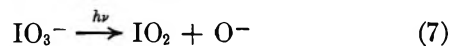


Figure 7. Absorption spectra of the transients produced by pulse radiolysis in $1.1 \times 10^{-2} M$ solutions of IO_3^- , alone (b) and in presence of $1.5 \times 10^{-2} M \text{N}_2\text{O}$ (a) and $3.5 \times 10^{-2} M$ ethanol (c). The absorbance was measured 23 μsec after pulse; 6 cm optical path length. Resolution of the spectra to component bands (Gaussian type of analysis) is shown by dashed curves.

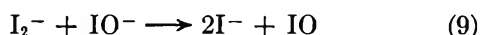
Discussion

The detection of O_3^- in alkaline solutions and the analysis of its decay kinetics prove that O^- radicals are produced by photolysis of both IO_3^- and IO^- . In analogy with the oxybromine anions,² the generation of O^- should involve the following primary processes



Thus IO_2 and IO_3 (the latter from reactions 4 or 5) are expected to result from the photolysis of IO_3^- , whereas IO^- should yield IO radicals through reaction 6. Therefore we assign band B to IO . The absorption spectrum of IO in the gas phase displays a band structure with maximum intensity at $\sim 450 \text{ nm}$; environmental shift of $\sim 1800 \text{ cm}^{-1}$ is not unreasonable.

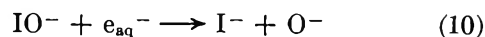
The iodine atom produced by reaction 8 could yield I_2^- , since the IO^- solutions always contained equivalent amounts of I^- . I_2^- has a very intense band peaking at 370 nm ⁸ and so we identify transient D with I_2^- . The pseudo-first-order decay of I_2^- suggests the reaction



which is analogous to the reaction¹ of Br_2^- with BrO^- . Reaction 9 is responsible for the generation of IO after flash and hence to the apparent decrease in its rate of decay. From our results we could calculate k_9 (Table I).

In pulsed IO^- solutions IO is produced by reactions 6. (At pH 13.6 very little OH is present.) However,

G_{IO} should equal $G_{\text{OH}} + G_e$ since O^- is produced by the reaction

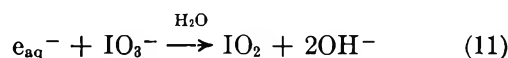


as the case¹ is with BrO^- . By extrapolating the IO absorbance to zero time and using the dosimetry results, we obtained $G_{\text{IO}} \times \epsilon_{490} = (5.0 \pm 0.7) \times 10^3$, *i.e.*, $\epsilon_{\text{max}}(\text{IO}) = 900 \pm 130 M^{-1} \text{ cm}^{-1}$. No I_2^- was formed in the pulsed solution since the reaction of O^- with I^- is probably much slower⁹ than reaction 6.

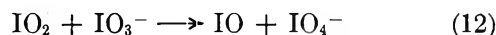
IO is also produced from IO_3^- . However, here it seems to result not from a primary process but from reaction of transient C with IO_3^- . The following results lead us to identify transients C and A with IO_2 and IO_3 , respectively.

(a) Ethanol which scavenges OH and O^- radicals could completely suppress band A both in the pulsed and flashed IO_3^- solutions. This shows that transient A results from reactions 4 or 5, and indeed, in the pulse experiment when N_2O is present to convert e_{aq}^- to OH , the amount of A increases. Thus we identify A with IO_3 . By extrapolating the IO_3 absorbance to zero time and using the dosimetry results with $G_{\text{IO}_3} = G_{\text{OH}}$ we obtained $G_{\text{IO}_3} \times \epsilon_{380} = (0.85 \pm 0.12) \times 10^3$; *i.e.*, $\epsilon_{\text{max}}(\text{IO}_3) = 400 \pm 60 M^{-1} \text{ cm}^{-1}$.

(b) In the pulsed solutions the reaction of e_{aq}^- with IO_3^- is expected to yield IO_2



in analogy with the corresponding reaction¹ of BrO_3^- . Since N_2O suppresses both bands C and B they should be related to IO_2 . Thus we are led to assign band C to IO_2 and attribute the generation of IO to the reaction



(Compare with the reaction¹⁰ $\text{IO}_2^- + \text{IO}_3^- \rightarrow \text{IO}^- + \text{IO}_4^-$.) Ethanol is also oxidized by IO_2 and here too IO is the product. (Under the conditions employed, in presence of ethanol the reaction of IO_2 with IO_3^- could be ignored; see Table I.) From the absorbance ratio $A_{\text{IO}_2}/A_{\text{IO}_3}$ at zero time (derived by extrapolation) we obtained from both techniques, flash and pulse, the ratio $\epsilon_{\text{max}}(\text{IO}_2)/\epsilon_{\text{max}}(\text{IO}_3) = 0.55 \pm 0.08$, *i.e.*, $\epsilon_{\text{max}}(\text{IO}_2) = (220 \pm 30) M^{-1} \text{ cm}^{-1}$.

(c) Our identification of the oxyiodine radicals puts their transition energies $h\nu_{\text{max}}$ in the sequence $\text{IO}_3 > \text{IO} > \text{IO}_2$. A similar order is displayed by the oxychlorine radicals¹¹ and by the known¹ oxybromine

(8) L. I. Grossweiner and M. S. Matheson, *J. Phys. Chem.*, **61**, 1089 (1957).

(9) By analogy with the behavior of the chloride⁷ and bromide anions (B. Cercec, M. Ebert, J. P. Keene, and A. J. Swallow, "Pulse Radiolysis," Academic Press, New York, N. Y., 1965, p 83). This can also be inferred from other works, *e.g.*, F. S. Dainton and S. A. Sills, *Proc. Chem. Soc.*, 223, 1962.

(10) O. Haimovich (Amichaj) and A. Treinin, *J. Phys. Chem.*, **71**, 1941 (1967).

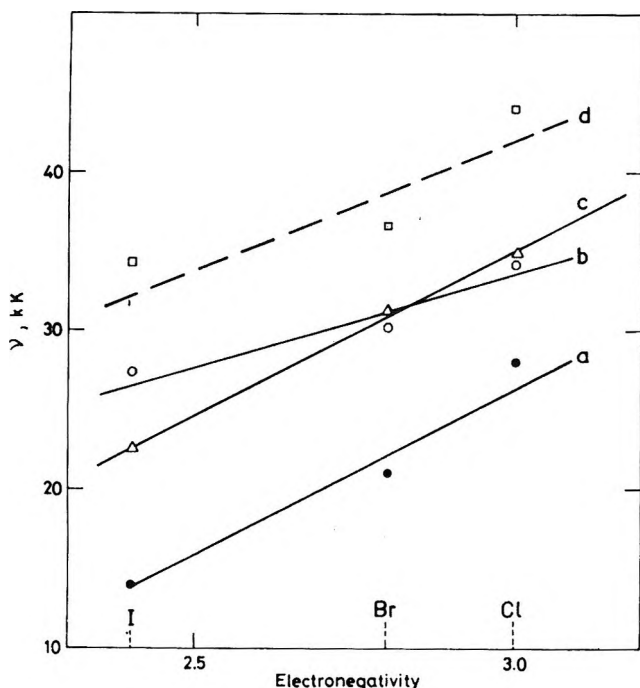


Figure 8. Transition energies of the oxyhalogen compounds vs. electronegativities of the halogen atoms. a, XO_2 in aqueous solution (ref 1, 11b and present work); b, XO^- in aqueous solution (ref 12); c, XO in the gas phase (ref 11a); d, XO_3^- in aqueous solutions (ref 13). (In the latter case the transition energies at $\epsilon = 1$ are recorded).

radicals BrO and BrO_2 . Another regularity is shown in Figure 8: the transition energy $h\nu$ of analogous oxyhalogen compounds increases almost linearly with the electronegativity of the halogen atom. The pairs ClO_3^- - IO_3^- ($\lambda_{\text{max}} = 278 \text{ nm}$ ^{11c}—in the gas phase—and 380 nm , respectively) and ClO_2^- - BrO_2^- ($\lambda_{\text{max}} = 260$ ^{11b} and 290 nm ,¹² respectively) follow the same order.

From these data we estimate that BrO_3 and IO_2^- both have absorption peaks at $\sim 340 \text{ nm}$. For BrO_3 the interpolation was based on $\lambda_{\text{max}}(\text{ClO}_3^-) \sim 300 \text{ nm}$ in aqueous solution, assuming that the red shift is close to that displayed by BrO , IO_2 , and ClO_2 on passing from gas phase to water. The value predicted for BrO_3 is close to that assigned to it in aqueous solution.^{5,14,15}

As in the case of BrO_2^- ¹ and NO_2 ,¹⁵ the decay of IO and IO_3 may involve dimerization as the first stage with the dimer further reacting with OH^- or water (in the case of IO_3 we detected a pH effect on the rate constant but this needs further investigation). The final products of the decay are probably $\text{IO}^- + \text{IO}_2^-$ (from $\text{IO} + \text{IO}$), and $\text{IO}_3^- + \text{IO}_4^-$ (from $\text{IO}_3 + \text{IO}_3$). IO^- is known to react with IO_3^- to produce IO_4^- . (IO_2^- probably being the reactive intermediate in this reaction¹⁰). IO_4^- is also produced by reaction 12, so altogether periodate should be a major product of the photolysis of IO_3^- . Some preliminary experiments have shown that this is really the case. Further work on the steady photolysis of IO_3^- will show if a single primary process (reaction 7) can account for all the results.

Acknowledgment. We are indebted to Dr. J. Rabani and Mr. D. Zehavi for their assistance in the pulse-radiolysis experiments, and to Professor G. Czapski for valuable discussions.

(11) (a) R. A. Durie and D. A. Ramsay, *Can. J. Phys.*, **36**, 35 (1958); (b) F. Stitt, S. Friedlander, H. J. Lewis, and F. E. Young, *Anal. Chem.*, **26**, 1478 (1954); (c) C. F. Coodeve and F. D. Richardson, *Trans. Faraday Soc.*, **33**, 453 (1937).

(12) Our own data.

(13) A. Treinin and M. Yaacobi, *J. Phys. Chem.*, **68**, 2487 (1964).

(14) M. S. Matheson and L. M. Dorfman, *J. Chem. Phys.*, **32**, 1870 (1960).

(15) M. Ottolenghi and J. Rabani, *J. Phys. Chem.*, **72**, 593 (1968).

The Flash Photolysis of Mercaptans in Aqueous Solution

by Günter Caspari and Albrecht Granzow

Department of Chemistry, Boston University, Boston, Massachusetts 02215 (Received June 17, 1969)

The flash photolysis of 2-mercaptoethanol, benzenethiol, and cysteine hydrochloride in deoxygenated aqueous solutions of various pH values was studied. Transient spectra ($\lambda_{\max} \sim 420$ nm) were observed which were identified as arising from the $\text{RS}\ddot{\text{S}}\text{R}^-$ radical anion. The transient decay was first order with approximately equal rate constants for cysteine and 2-mercaptoethanol; the benzenethiol decayed about ten times faster. It is proposed that the formation of $\text{RS}\ddot{\text{S}}\text{R}^-$ from flash photolysis is *via* the fast reaction of the primary $\text{RS}\cdot$ radical with an RS^- anion. The validity of the mechanism is supported by the effect of added allyl alcohol on the decay rates of the transient.

Introduction

The primary reaction in the photolysis of mercaptans in the gas¹⁻³ and liquid⁴ phase is the formation of $\text{RS}\cdot$ radicals to which has been attributed the strong absorption ($\lambda_{\max} \sim 420$ nm) observed when alkylmercaptans are photolyzed at 2537 Å in a rigid EPA matrix.⁵ Similar absorptions have resulted from the γ radiolysis of mercaptans in rigid matrices at 77°K.⁶ However, pulse radiolytic studies of cysteine^{7,8} and 2-mercaptoethanol⁹ have indicated that the absorbing species is not the $\text{RS}\cdot$ radical but rather the $\text{RS}\ddot{\text{S}}\text{R}^-$ radical anion. There is support for this proposal from the analysis of the esr spectra of such trapped radicals.¹⁰

In the radiolysis cases, the primary process is the generation of transients from the attack of solvated electrons or OH radicals on the mercaptan. The question must be raised concerning the nature of the transient produced in the photolysis and toward this end the flash photolysis study was directed.

Experimental Section

2-Mercaptoethanol (K & K Laboratories), benzenethiol (Matheson Coleman and Bell), and allyl alcohol (Fisher) were purified by distillation. Cysteine hydrochloride (Fisher, research grade) was used without further purification.

Solutions of the mercaptans were prepared with deionized water that had been deoxygenated by a stream of purified nitrogen for at least 1 hr. The mercaptan was then added with a syringe. The pH value was adjusted using perchloric acid and sodium hydroxide and measured with a Leeds and Northrup pH meter. A fresh solution was used for each flash delivered.

The flash apparatus (Xenon Corp., Medford, Mass.) delivered a flash with an energy of up to 250 J from xenon-filled flash lamps. The flash exhibited a rise time of 5 μsec , a half-peak duration of 20 μsec , and a total duration of 50 μsec . The decay of the transients was monitored using a Hilger-Engis 0.6-m combination spectrograph-monochromator, an RCA 1P28 photomultiplier and dynode chain, and a Tektronix 564 stor-

age oscilloscope. A Vycor filter restricted the flash to $\lambda > 230$ nm and a Pyrex filter in front of the analyzing lamp was used to prevent unwanted photolysis. The quartz irradiation vessel was 22 cm long with a 2-cm diameter and had optically flat quartz windows at both ends.

The absorption spectra of the mercaptan solutions were determined using a Cary 14 recording spectrophotometer.

Results and Discussion

In the spectral region $\lambda > 230$ nm, mercaptans show absorption bands which are attributed to $n \rightarrow \sigma^*$ or $n \rightarrow \pi^*$ transitions of the free electrons at the sulfur atom. The ultraviolet absorption spectra of the mercaptan solutions show that, whereas these bands are quite strong in basic solution, no absorption occurs in neutral or acid medium except for benzenethiol. The spectrum of 2-mercaptoethanol in aqueous solution at various pH values is shown in Figure 1. The spectrum of cysteine is reported to show a similar pH dependence.¹¹ In both cases the extinction coefficient at the band maximum is directly proportional to the anion concentration as is seen by a comparison with the titration curves of these compounds.¹¹ For benzenethiol this anion

(1) M. Meissner and H. W. Thompson, *Trans. Faraday Soc.*, **34**, 1238 (1938).

(2) N. P. Skerret and H. W. Thompson, *ibid.*, **37**, 81 (1941).

(3) T. Inaba and B. deB. Darwent, *J. Phys. Chem.*, **64**, 1431 (1960).

(4) W. E. Haines, G. L. Cook, and J. S. Ball, *J. Amer. Chem. Soc.*, **78**, 5213 (1956).

(5) K. J. Rosengren, *Acta Chem. Scand.*, **16**, 1418 (1962).

(6) J. Wendenburg, H. Moeckel, A. Granzow, and A. Henglein, *Z. Naturforsch.*, **B**, **21**, 632 (1966).

(7) G. E. Adams, G. S. McNaughton, and B. D. Michael, "The Chemistry of Ionization and Excitation," Taylor and Francis Ltd., London, 1967, p 281.

(8) G. E. Adams, "Symposium on Radiation Research," North-Holland Publishing Co., Amsterdam, 1967, p 195.

(9) G. Meissner, A. Granzow, and A. Henglein, unpublished results.

(10) F. K. Truby, *J. Chem. Phys.*, **40**, 2768 (1964).

(11) R. E. Benesch and R. Benesch, *J. Amer. Chem. Soc.*, **77**, 5877 (1955).

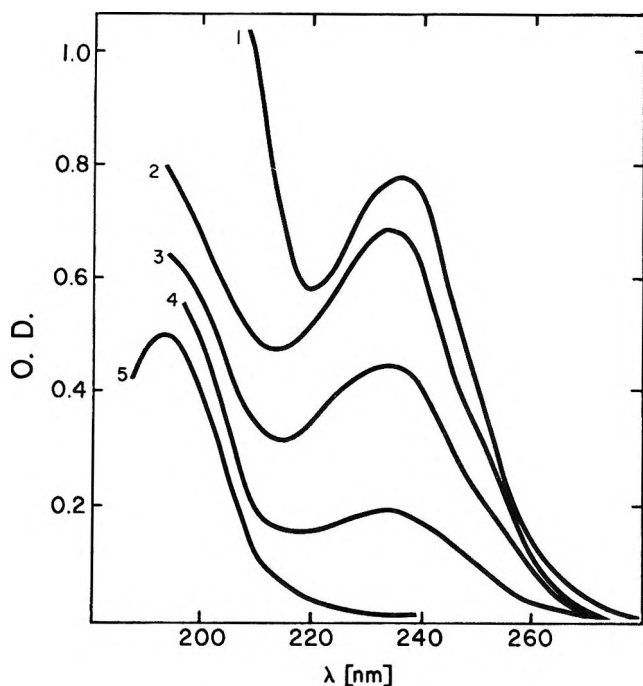


Figure 1. The uv absorption spectra of aqueous solutions of 2-mercaptoethanol: [mercaptan] = $2.0 \times 10^{-4} M$; cell path length = 1 cm; pH of solutions: 1, 13.0; 2, 10.5; 3, 9.7; 4, 9.0; 5, 6.0.

band is shifted to about 260 nm, but at low pH values another absorption at 235 nm is observed which is due to the undissociated form (Figure 2).

In all three systems strongly absorbing transients are observed after the flash. The absorption maxima are at 420 nm for 2-mercaptoethanol and cysteine and at 470 nm for benzenethiol. The spectra of the transients in Figure 3 are measured at those pH values where the highest intensity of the transient absorption is obtained. If the solutions are flash photolyzed without the Vycor filter so that $\lambda < 230$ nm radiation is also absorbed, no noticeable change in the shape or the intensity of the transient bands is observed. This fact suggests that only the long wavelength absorption band of the mercaptans is responsible for the formation of the transients.

In the case of cysteine and 2-mercaptoethanol the wavelengths of the transient absorption maxima are identical with those observed in pulse radiolytic studies⁷⁻⁹ and are accordingly attributed to the corresponding $R\dot{S}SR$ radical anions. Nothing has yet been reported on the transient arising from benzenethiol, but it is doubtless due to the formation of the analogous $C_6H_5\dot{S}SC_6H_5$ radical anion. The higher intensity and the bathochromic shift of the transient absorption for this compound are readily explained by the influence of the benzene rings.

The decay of the transients is first order; the rates are about the same for cysteine and 2-mercaptoethanol, whereas the benzenethiol transient decays more rapidly. The rate constants are listed in Table I. The addition

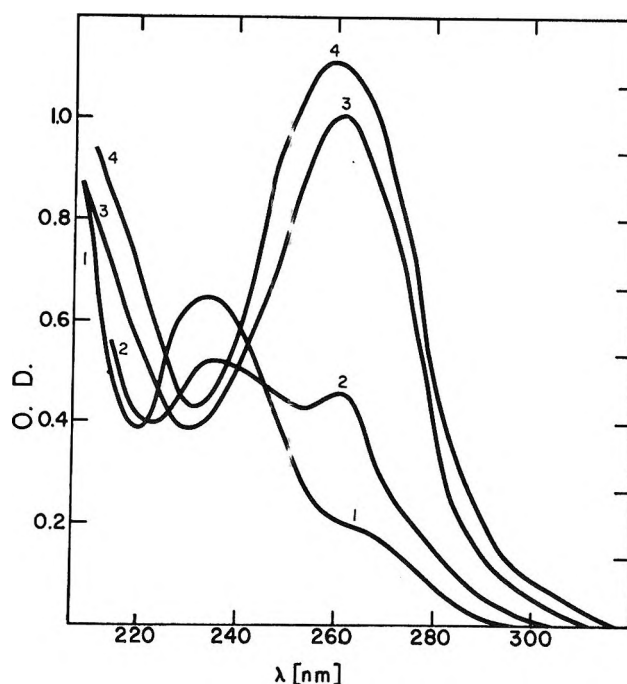


Figure 2. The uv absorption spectra of aqueous solutions of benzenethiol: [mercaptan] = $1.25 \times 10^{-4} M$; cell path length = 1 cm; pH of solutions: 1, 5.9; 2, 6.6; 3, 8.9; 4, 12.5.

Table I: Rate Constants for the Decay of $R\dot{S}SR$ Radical Anion Transient Spectra

Compound	Concn, M	pH	k , sec^{-1}	λ_{max} , nm
2-Mercaptoethanol	1.0×10^{-3}	12.2	4.9×10^3	420
Cysteine	1.0×10^{-3}	8.1	2.7×10^3	420
Benzenethiol	5.0×10^{-4}	10.6	3.8×10^4	470

of methanol or acetone has no effect on the intensity or decay constant of the transient absorption. On the other hand, the transient spectra are not observed in the presence of oxygen.

When allyl alcohol is added, the intensity of the transient absorption decreases and the decay constants increase proportionally with the concentration of the alcohols. From the slope of these straight lines the second-order rate constants for the reaction of the transients with allyl alcohol can be calculated (Table II). In the case of benzenethiol the decay constant is already so large that any additional enhancement in the presence of allyl alcohol cannot be determined.

Table II: Rate Constants for the Reaction of Transient $R\dot{S}SR$ Radical Anions with Allyl Alcohol. Concentration of the Mercaptans, $1.0 \times 10^{-3} M$

Compound	Concn range, M	pH	k , $M^{-1} sec^{-1}$
2-Mercaptoethanol	$1-2.0 \times 10^{-3}$	12.2	1.0×10^6
Cysteine	$2-5 \times 10^{-3}$	8.1	1.4×10^6

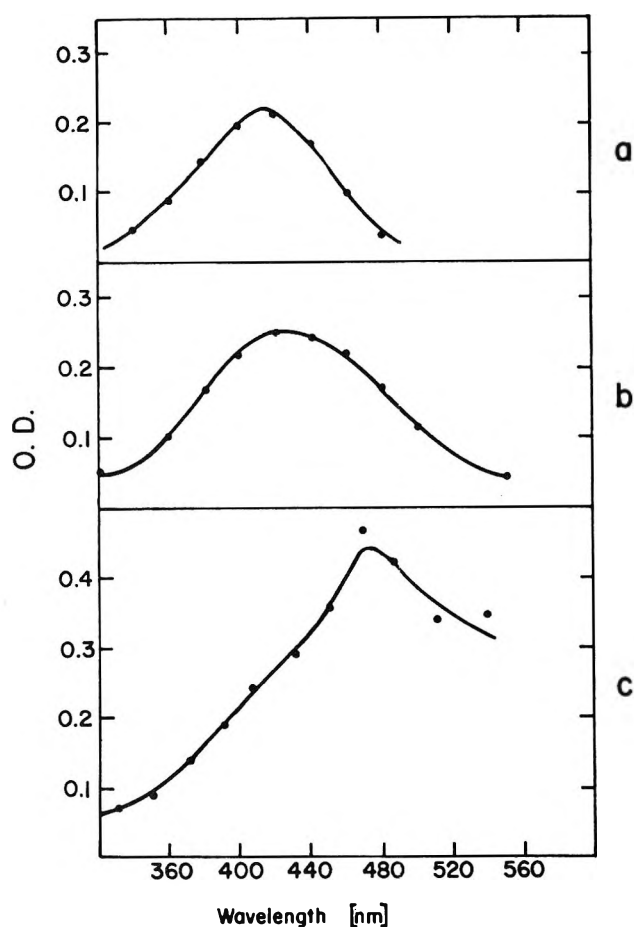


Figure 3. Absorption spectra of transients: (a) cysteine, $1.0 \times 10^{-3} M$; pH 8.7; (b) 2-mercaptoethanol, $5.0 \times 10^{-3} M$, pH 10.5; (c) benzenethiol, $5.0 \times 10^{-4} M$; pH 11.8.

Since the intensity and wavelength of the uv absorption of the mercaptan solutions show a strong dependence on the pH, the effect of pH on the transient absorption was examined (Figure 4). For cysteine and 2-mercaptoethanol, no transient absorption is observed in acid and neutral solution because in this pH range, these two compounds do not show substantial uv absorption at $\lambda > 230$ nm. On the other hand, the undissociated benzenethiol has an absorption maximum at 235 nm. Therefore, in this case, the absorbing transient is also formed in acidic solution and the intensity of the transient absorption increases with increasing pH, reaching a constant value at pH ~ 8.5 . In all cases the decay constants of the transients do not show a noticeable dependence on the mercaptan concentration or the pH of the solution.

For mercaptoethanol, the intensity of the transient absorption decreases again at pH > 12 . It appears that the formation of the absorbing $R\dot{S}SR$ radical anion is inhibited by high OH^- concentrations. As in the case of the pulse radiolysis experiments,⁹ a weak transient absorption with a maximum at $\lambda < 300$ nm is observed in solutions of pH > 12 . This short wavelength transient absorption may be tentatively attributed to the

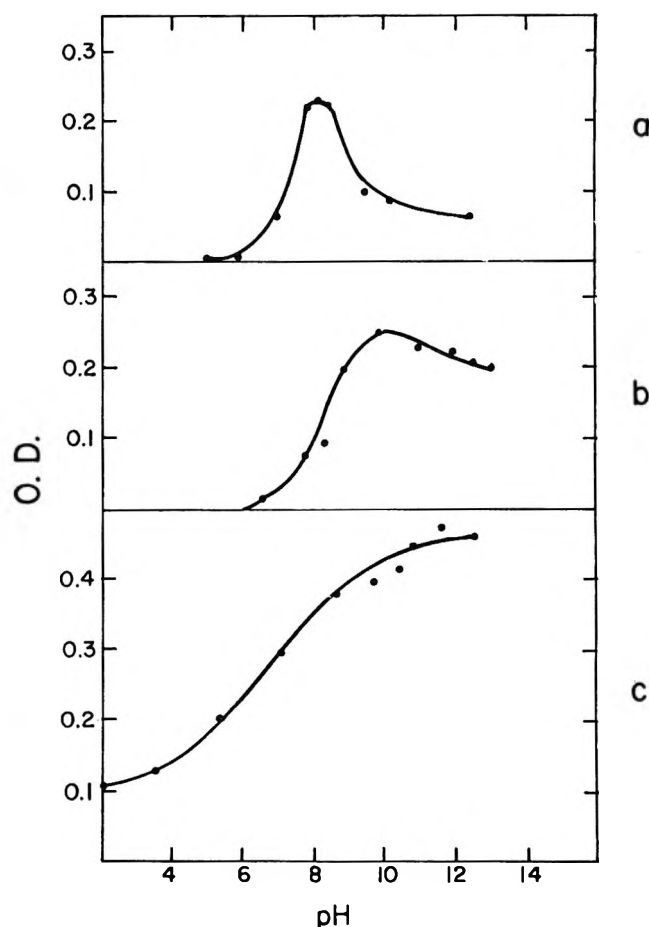


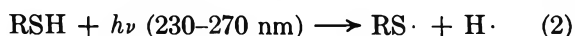
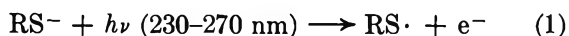
Figure 4. pH dependence of the transient absorption: (a) cysteine, $1.0 \times 10^{-3} M$, λ 420 nm; (b) 2-mercaptoethanol, $5.0 \times 10^{-3} M$, λ 420 nm; (c) benzenethiol, $5.0 \times 10^{-4} M$; λ 470 nm.

$RS\cdot$ radical, since mercaptan radicals in the gas phase are known to absorb in this region.¹² The fact that this transient is only observed in solutions at high pH can be explained in terms of the inhibition of the radical anion formation in a strongly basic medium. This should result in an enhanced lifetime for the primary $RS\cdot$ radicals.

In the case of cysteine, the intensity of the transient absorption has a distinct maximum at pH ~ 8.5 . This behavior can be explained in terms of the different steps in the dissociation of cysteine. In the pH range 8–10, cysteine exists mostly as a mixture of $HSC_2H(NH_2)COO^-$ and $S-CH_2CH(NH_3^+)COO^-$, whereas at higher pH the doubly negative $S-CH_2CH(NH_2)COO^-$ anion is formed.¹¹ Therefore, in this latter pH region the formation of the absorbing $R\dot{S}SR$ radical anion would have to take place *via* the reaction of two particles, each of which carries two negative charges. Since a reaction of that kind is energetically unfavorable, this may account for the observed decrease of the transient formation at high pH.

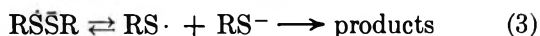
(12) R. G. W. Norrish and A. P. Zeelenberg, *Proc. Roy. Soc. (London)*, **A240**, 293 (1967).

The reaction mechanism which leads to the formation of the absorbing $R\dot{S}SR$ transients may be assumed to be similar to the one established for the formation of the same species by pulse radiolysis.^{7-9,13} The first step is the formation of a $RS\cdot$ radical by photodetachment of an electron from a RS^- anion. In the case of benzenethiol, a photodissociation of the neutral mercaptan must also be considered if the transient is produced in neutral or acidic solution



The uv absorption bands of the mercaptan solutions in the region of 230-270 nm correspond to the energy of 105-125 kcal mol⁻¹. The dissociation energies of alkylmercaptans in the gas phase have been determined to about 88 kcal mol⁻¹¹⁴ making reactions 1 and 2 energetically feasible and leaving enough excess energy available to account for differences in solvation energies.

The second step is the fast reaction of a primary $RS\cdot$ radical with a RS^- anion forming the $R\dot{S}SR$ radical anion that is responsible for the observed transient absorption. The decay of the transient complex probably takes place by reaction 3 with the stable end product being mainly the corresponding disulfide



The equilibrium position in reaction 3 has to be far to the left to account for the first-order decay kinetics. The structure of the $R\dot{S}SR$ species is expected to be similar to that of the dihalide radical anion, such as Cl_2^- .⁷

The validity of this two-step mechanism is supported by the effect of added allyl alcohol on the decay constants of the radical anions. It is well established that $RS\cdot$ radicals are efficiently scavenged by compounds with olefinic double bonds, the addition leading to the formation of an anti-Markovnikov product.^{15,16} Therefore, the addition of allyl alcohol shifts the equilibrium of reaction 3 to the right, in agreement with the observed enhancement of the decay constants. The much faster decay of the benzenethiol transient as compared to the aliphatic mercaptans can also be understood by a shift of the equilibrium to the right due to the higher stability of the aromatic thieryl radical.

Acknowledgment. The authors wish to thank Professor M. Z. Hoffman for his interest in this work. The flash photolysis apparatus was purchased with funds from NSF Grant GP 7048.

(13) W. Karmann, G. Meissner, and A. Henglein, *Z. Naturforsch. B*, **22**, 273 (1967).

(14) J. L. Franklin and H. E. Lumpkin, *J. Amer. Chem. Soc.*, **74**, 1023 (1952).

(15) M. S. Kharash, A. T. Read, and F. R. Mayo, *Chem. Ind. (London)*, **51**, 752 (1938).

(16) R. H. Pallen and C. Sivertz, *Can. J. Chem.*, **35**, 723 (1957).

Ionization of Liquids by Radiation Studied by the Method of Pulse

Radiolysis. III. Solutions of Galvinoxyl Radical

by C. Capellos

Explosives Laboratory, Feltman Research Laboratory, Picatinny Arsenal, Dover, New Jersey 07801

and A. O. Allen

Chemistry Department, Brookhaven National Laboratory, Upton, New York 11973 (Received August 4, 1969)

The yield of galvinoxyl anion, found by pulse radiolysis of dilute solutions of galvinoxyl radical in various hydrocarbon solvents, was equal to the total yield of ion pairs formed by irradiation in the same solvents, as determined by electrical methods. Galvinoxyl radical thus being shown to be an excellent electron scavenger, the method was applied to determine ion yields formed by radiation in other liquids, including alcohols and nitro compounds. From the ion yields, relative values of the mean charge-separation distances were calculated and were found to be smaller the more polar the liquid.

Introduction

Knowledge of the yield of free ions produced by radiation in liquids is essential to the understanding of the behavior of free electrons in liquid systems and the mechanisms of radiolysis of liquids. The ionic yield is best determined by electrical methods in liquids of low inherent conductivity but cannot be applied to polar liquids. We therefore turn to the use of charge scavengers or materials which will readily accept positive or negative charge from the original ions formed in the solvent to produce an ion of distinctive light absorption, which, though it may be of short lifetime, can be quantitatively estimated by the method of pulse radiolysis. We have shown¹ that the positive charge acceptor trityl chloride can be used in this way in certain solvents when present in concentrations of the order of $10^{-4}M$, as it forms the trityl carbonium ion, but it cannot be used in solvents such as alcohols in which the carbonium ion is destroyed. In the present paper we turn to the use of the negative charge scavenger galvinoxyl or Coppinger's radical, a stable neutral free radical soluble in organic solvents, which readily accepts an electron to form a negative ion² having a distinctive and very large absorption peak in the visible. By the use of this radical, we have determined the yields of free ions formed in a wide variety of solvents.

Experimental Section

Details of our methods of pulse radiolysis with 2-MeV electrons, using either a pulsed Van de Graaff generator or a Febetron Model 705 generator have been described in previous papers.^{1,3} Most of the data for the present paper were obtained from the Van de Graaff using 5- μ sec pulses, but data on the rate of buildup of the galvinoxyl anion and some of the data on the decay of the anion and of the galvinoxyl radical

were obtained using the shorter pulses from the Febetron.

The absorption spectrum of the galvinoxyl anion transient formed by pulsing dilute solutions of galvinoxyl radical in various solvents was determined separately for all the solvents used except for two of the alcohols. The results for 2,2,4-trimethylpentane (a nonpolar solvent) and nitrobenzene (a highly polar solvent) are shown in Figure 1, normalized to the same height for the main peak. The spectra in all the solvents were very similar except for slight shifts in the position of the two peaks. Estimation of the quantity of anion present was made on the assumption that the extinction coefficient at the longer wavelength maximum was equal to that reported by Kharasch and Joshi² for stable solutions of the ion in ethanol, namely, $220,000 M^{-1} \text{ cm}^{-1}$. The decrease of the galvinoxyl radical concentration after the pulse, determined by the loss of its extinction between 4000 and 4700 Å, was generally found to be much larger than the amount of the anion produced and always appeared to be kinetically first order. It was ascribed to reaction of the galvinoxyl radical with the neutral free radicals produced in the solvent by the radiation pulse, which are considerably more numerous than the free ions. At wavelengths near 5750 Å where the anion transient was determined, this destruction of the free radical sometimes resulted in considerable decrease in the optical density of the solution at the end of the anion decay as compared to its absorption at the beginning of the run. Correction for this change in absorption had to be made in analyzing the kinetics of the anion decay.

(1) C. Capellos and A. O. Allen, *J. Phys. Chem.*, **73**, 3264 (1969).

(2) M. S. Kharasch and B. S. Joshi, *J. Org. Chem.*, **22**, 1435 (1957).

(3) C. Capellos and A. O. Allen, *J. Phys. Chem.*, **72**, 4265 (1968).

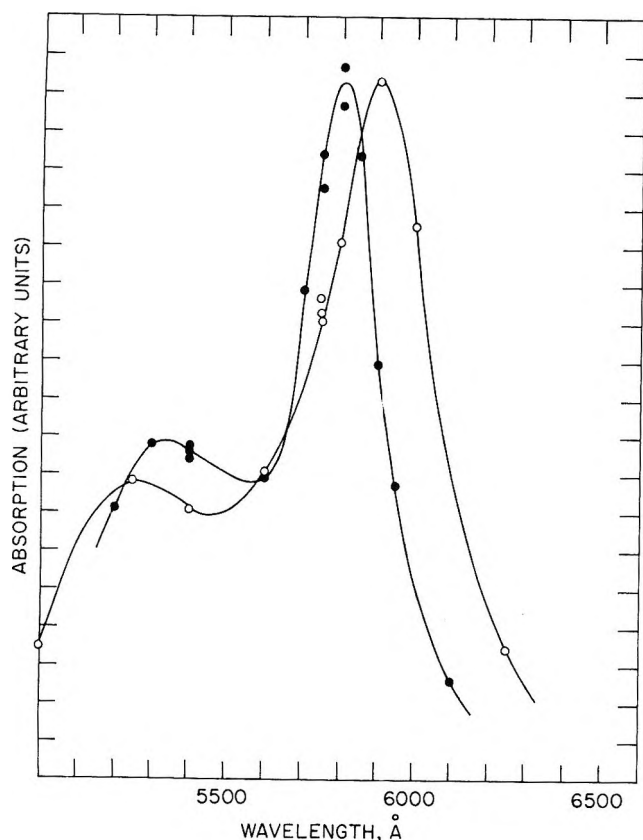


Figure 1. Spectra of the galvinoxyl anion transient obtained by pulse radiolysis in 2,2,4-trimethylpentane, ●, and in nitrobenzene, ○.

It was found that the decay of the galvinoxyl anion was second order in nonpolar solvents, as expected for its disappearance by recombination with a positive ion, but in the more polar solvents its disappearance was first order. Apparently in the polar solvents it disappears more rapidly by reaction with the solvent than by combination with a positive ion. In the case of second order decay, the optical density due to the anion is $OD_a = OD_0 / (1 + (k_2/\epsilon L)OD_0 t)$. The observed optical density is decreased by the destruction of the galvinoxyl radical, which gives a term $-OD_\infty(1 - e^{-k_r t})$. The observed optical density is given by the sum of these two expressions and the equation may be rearranged to give

$$\frac{1}{OD_{\text{obsd}} + OD_\infty(1 - e^{-k_r t})} = \frac{1}{OD_0} + \frac{k_2 t}{\epsilon L}$$

where OD_{obsd} is the observed optical density, OD_∞ is the optical density at the end of the reaction, k_r is the first-order decrease in absorption of the radical as determined at shorter wavelengths, k_2 is the actual second-order decay constant of the anion, ϵ is its extinction coefficient, L is the optical path length, t is the time after the end of the pulse, and OD_0 is the optical density at $t = 0$. It was found indeed in the nonpolar solutions that a plot of the expression on the left-hand side was

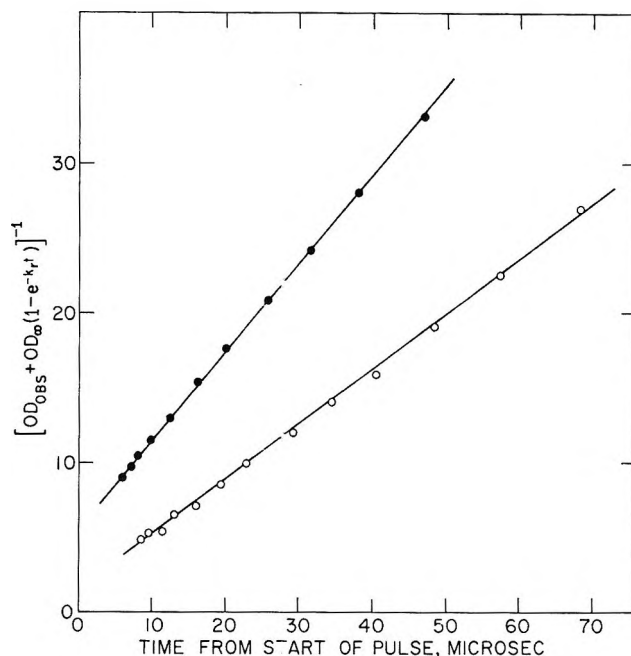


Figure 2. Second-order decay plots for the galvinoxyl anion in 2,2,4-trimethylpentane; data obtained at 5400 Å, ●, and 5750 Å, ○.

linear in time, and values of k_2 were obtained. Figure 2 shows the plots obtained from following the decay of the anion in 2,2,4-trimethylpentane in two runs made, respectively, at 5750 and 5400 Å. The lower line represents data obtained at 5750 Å where the extinction coefficient was taken, by comparison with the assumed maximum value of 2.2×10^5 , to be equal to $1.92 \times 10^5 M^{-1} \text{ cm}^{-1}$. The upper curve was for data taken at 5400 Å where the extinction coefficient was assumed to be 1.033×10^5 . In both cases the path length was 6.1 cm. The respective calculated rate constants were 4.2×10^{11} and $3.8 \times 10^{11} M^{-1} \text{ sec}^{-1}$, which are in fair agreement considering the uncertainties in the assumptions regarding the extinction coefficients.

In the polar solvents the decay of the anion was first order and the change in optical density due to this decay is given by $OD_a = OD_0 e^{-k_r t}$. Addition of the correction term due to the destruction of the radical results in the equation

$$\log [OD_{\text{obsd}} - OD_\infty(1 - e^{-k_r t})] = \log OD_0 - 2.303k_1 t$$

Thus k_1 is readily obtained by a plot of the function shown on the left-hand side against time. Very good first-order plots were in fact obtained.

The rate of formation of galvinoxyl anion was studied in polar solvents in which its rate of decay was first order. The reaction scheme can be represented as $X^- + G\cdot = G^-$ with rate constant k_b (where X^- is the negative ion originally produced in the solvent, $G\cdot$ is galvinoxyl, and G^- its anion), followed by $G^- = \text{product}$, with rate constant k_1 . Let y = the concentration of G^- and $K = k_b(G\cdot)$. If X_0^- is the total nega-

Table I: Rate Constants for Formation and Decay of Galvinoxyl Anion in Various Solvents

Solvent ^a	Order	Decay reaction		Formn rate const, k_b , $M^{-1} \text{sec}^{-1}$
			Rate constant	
2,2,4-Trimethylpentane	2		$4.2 \times 10^{11} M^{-1} \text{sec}^{-1}$...
Cyclohexane	2		$4.6 \times 10^{11} M^{-1} \text{sec}^{-1}$...
Benzene	2		$6.4 \times 10^{11} M^{-1} \text{sec}^{-1}$...
Toluene	2		$4.3 \times 10^{11} M^{-1} \text{sec}^{-1}$...
Neopentyl alcohol (64°)	1		$1.44 \times 10^4 \text{sec}^{-1}$...
<i>n</i> -Pentyl alcohol (64°)	1		$1.15 \times 10^4 \text{sec}^{-1}$...
<i>n</i> -Pentyl alcohol (25°)	1		$2.9 \times 10^3 \text{sec}^{-1}$...
<i>t</i> -Butyl alcohol	1		$6.0 \times 10^3 \text{sec}^{-1}$...
<i>n</i> -Butyl alcohol	1		$1.05 \times 10^4 \text{sec}^{-1}$	1.8×10^9
Ethanol	1		$2.1 \times 10^4 \text{sec}^{-1}$	1.08×10^{10}
Nitrobenzene	1		$8.5 \times 10^3 \text{sec}^{-1}$	2.8×10^9
Nitromethane	1		$2.2 \times 10^6 \text{sec}^{-1}$	

^a Determinations made at 25° unless otherwise stated.

tive ion concentration in the system, we then have $X^- = X_0^- e^{-Kt}$ and

$$dy/dt = KX_0^- e^{-Kt} - k_1 y$$

The solution to this equation is

$$y = (KX_0^- / (K - k_1)) (1 - e^{-(K-k_1)t}) e^{-k_1 t}$$

In practice the formation of G^- requires a few microseconds, while the decay lasts hundreds of microseconds. Traces are obtained of the optical density vs. time, first on a time scale of microseconds, then on a longer time scale. At longer times the expression in parentheses reduces to unity and the slope of the line gives k_1 ; the extrapolated intercept $I = KX_0^- / (K - k_1)$. The optical densities obtained for various short times are then divided by $Ie^{-k_1 t}$ and the result, subtracted from 1, is then plotted against time on semilog paper. From the slope of this line $K - k_1$ is obtained, which gives K , and by dividing by the concentration of galvinoxyl radical we finally get k_b , the desired rate constant for formation of the galvinoxyl anion.

Results

Table I gives the decay constants of the galvinoxyl anion in the various solvents; also the rates of formation of the anion from the galvinoxyl radical, for the cases in which this quantity was determined. The rate of disappearance of the galvinoxyl radical is not presented here since it is not a true constant but depends upon the dose per pulse used in the experiment. Under our conditions the time constant of this first-order disappearance varied from 10^4 to 10^5sec^{-1} . The second-order rate constants for disappearance of the anion found in the hydrocarbon solvents are of the same order as those found for disappearance of the ions reported in our previous publications^{1,3} and are of the order expected for recombination of oppositely charged ions in solvents of low dielectric constant. In the solvents of higher dielectric constant, the ion recombination is slower and first-order processes take over—presumably

reaction of the anion with the solvent, perhaps to give NO_2^- in the nitro compounds and alkoxide ions in the alcohols.

The main purpose of the work was to obtain the G values for the formation of the galvinoxyl anion, which are shown in Table II. The values were obtained from the Van de Graaff data on the concentration of anion existing at the end of the pulse, with the appropriate correction made for the small amount of decay occurring during the 5- μsec pulse.³

As in previous studies,^{1,3} the concentration of charge scavenger in the solution did not affect the yield of ions formed, over the concentration range 10^{-4} – $10^{-3} M$, in hydrocarbon solvent. In the higher alcohols, however, the yield increased between 1×10^{-4} and $6 \times 10^{-4} M$ solute, probably because the reaction between the solvated electron and the galvinoxyl is relatively slow in these solvents. The "best value" of $G(\text{ion})$ listed is an average of runs made at concentrations of galvinoxyl thought to be high enough to trap all free negative charges.

No galvinoxyl anion was seen in a carbon tetrachloride solution of galvinoxyl, which indicates that the anion first formed in this solvent cannot transfer an electron to this solute. By contrast, the anions formed in nitromethane and nitrobenzene cannot compete with galvinoxyl for the electron, since the yield of solute anion is not increased by increasing the solute concentration.

Ion yield values which have been obtained for some of the solvents by other methods are shown in Table II. Table II also lists the dielectric constants of the various solvents and the ion yield of these same materials in the vapor phase, together with a series of derived quantities which will now be discussed.

Discussion

The G values determined for the galvinoxyl anion agree well with the ion yields determined by other methods both for hydrocarbons and for ethanol; so it

Table II: Yields of Galvinoxyl Anion in Various Solvents, and Some Derived Quantities

Solvent ^a	Concn of galv radical, $M \times 10^4$	No of detns	Av dev, %	$G(\text{anion})$ best value	$G(\text{free ions})$ by other methods	Dielec const	r_0 , Å	$W(\text{vap})$, ^b eV/ion pair	d , g/cc	$P = \frac{GW}{100}$	b/r_0	b , Å	b_d
2,2,4-Trimethyl-pentane	1.0	5	2.5	0.392	0.39	1.933	289.9	23.3	0.687	0.0916	0.355	102.9	70.7
Cyclohexane	0.5	4	1.2	0.139	0.150	2.015	278.1	22.7	0.775	0.0340	0.234	65.1	50.5
	1.0	4	4.2	0.147									
	5.0	3	2.4	0.162									
	10.0	3	2.8	0.153									
Benzene	1.28	4	3.4	0.055	0.055	2.204	244.3	(24.5)	0.874	0.0135	0.175	42.8	37.4
Toluene	1.44	3	0.5	0.051	0.051	2.379	235.5	(24.5)	0.862	0.0125	0.171	40.3	34.7
Neopentyl alcohol (64°)	1.64	2	9.3	0.21	0.21	8.3 ± 0.3 ^f	59.7	(24)	0.812	0.0504	0.272	16.2	13.2
<i>n</i> -Pentyl alcohol (64°)	1.64	3	2.8	0.46	0.46	10.0	49.6	(24)	(0.784)	0.1104	0.390	19.4	15.2
<i>n</i> -Pentyl alcohol (25°)	1.64	3	4.2	0.447	0.485	14.2	39.5	23.9	0.811	0.1160	0.401	15.9	12.9
<i>t</i> -Butyl alcohol	4.0	3	1.3	0.457									
	6.0	3	1.8	0.519									
	8.0	3	3.0	0.482									
	1.64	3	4.6	0.608	0.67	12.3	45.6	(24)	0.781	0.1608	0.486	22.2	17.3
	4.0	3	1.8	0.656									
	6.0	3	3.9	0.691									
<i>n</i> -Butyl alcohol	1.64	3	7.6	0.345	0.63	17.1	32.8	24.1	0.806	0.1518	0.469	15.4	12.4
	3.0	4	7.4	0.495									
	6.0	4	3.5	0.644									
	10.0	4	9.1	0.612									
Ethanol	1.0	4	2.0	1.013	1.0 ^g	24.3	23.06	25.1	0.785	0.2535	0.675	15.6	12.2
Nitrobenzene	1.0	1	0.46	0.43		34.82	16.09	(30)	1.199	0.129	0.426	6.86	8.25
	2.5	3	3.6	0.42									
Nitromethane	1.0	2	0.347	0.31		37.8	14.82	30.5	1.131	0.094	0.360	5.34	6.0
	2.0	3	12.2	0.272									

^a Temperatures were 25° unless otherwise stated. ^b Data from P. Adler and K. Bothe, *Z. Naturforsch.*, **20a**, 1700 (1965); G. G. Meisels, *J. Chem. Phys.*, **41**, 51 (1964); C. Biber, P. Huber, and A. Muller, *Helv. Phys. Acta*, **28**, 503 (1955). Values in parentheses are estimates. ^c Reference 7. ^d Reference 1. ^e Solvated electron yield: M. C. Sauer, S. Arai, and L. M. Dorfman, *J. Chem. Phys.*, **42**, 708 (1965). ^f Determined in our laboratory by W. F. Schmidt. ^g Elevated temperature required by the high melting point of the substance.

seems reasonable to assume that in the other solvents also we are measuring authentic G values for formation of free ions.

Ion-pair yields in liquids are discussed⁴⁻⁶ in terms of the Onsager formula⁷ for the probability P of eventual diffusion apart of a pair of oppositely charged ions separated by a distance r in a medium of dielectric constant ϵ : $P = e^{-r_c/r}$, where $r_c = e^2/\epsilon kT$, with e in the latter case being the charge on the electron and kT the Boltzmann energy. A glance at the G values in Table II shows that the dielectric constant of the solvent does indeed have a pronounced effect on the free ion yield. Other factors are, however, involved; thus, the nitro compounds, with a higher dielectric constant than ethanol, nevertheless show a smaller value of the ion yield. It would seem that the average value of the escape distance r must be less in the nitro compounds than in the alcohols. The initial ionization acts will be similar in all these solvents, but the electrons set free will interact more strongly with the solvent molecules and lose energy more rapidly in some of the solvents, will become thermalized at a shorter distance r from the parent positive ion, and hence have a smaller probability of escaping. Ion yield determinations by the charge collection method have shown⁶ that there are great differences among hydrocarbons in their interaction with the free charges, the ion yields being much larger for hydrocarbons containing quaternary carbon atoms in the molecule. The presence of chlorine atoms in the molecule greatly decreases the free ion yield, presumably because free electrons not yet completely thermalized can react to yield chloride ions while still comparatively close to the positive ion.

We seek a quantitative measure of the relative reactivity of the free charges with the various solvents. For this purpose it is necessary to assume a distribution law for the values of r among the various ion pairs produced in the solvents by high-energy radiation. Schmidt and Allen⁶ have found that in a number of hydrocarbons the temperature coefficient of the free ion yield can be correctly predicted on the assumption that the distribution of r is random or Gaussian. Although in theory the distribution cannot be exactly Gaussian, we are dealing here only with the more widely separated ion pairs and an approximate random distribution of separations among these seems not unreasonable. Since all that is sought here is an approximate measure of the relative interaction rates for the free charges in the various solvents, we believe the Gaussian approximation is sufficient for the present purpose. We assume then that in all the solvents the probability of finding an ion pair thermalized at a distance r is given by the three-dimensional Gaussian distribution function

$$(4\pi r^2/\pi^{3/2}b^3)e^{-r^2/b^2}$$

To get the total probability of escape P we must multi-

ply this Gaussian by the escape probability $e^{-r_c/r}$. Substituting x for r/b we find

$$P = (4/\pi^{1/2}) \int_0^\infty x^2 e^{-x^2 - r_c/bx} dx$$

P is thus a function of b/r_c only. Values of the function $P(b/r_c)$ have been calculated.⁶

If the ion pairs occur in part in groups or "spurs," the distance r should relate only to the last ion pair remaining after all the others in the group have combined. The probability P thus should be the ratio of the yield of free ion pairs to the yield of groups of ions produced by the radiation. The total number of ion pairs initially formed in the liquid is presumably equal or at least proportional to the number formed in irradiation of the same material in the vapor phase. Since the number of groups of ions is not accurately known and since all we seek here is a comparison between different solvents, we have assumed that the value of P given by the above formula may be set equal to the ratio of the measured ion-pair yield in our liquids to the total number of ions formed in the irradiation of the vapors. The function $P(b/r_c)$ being known, we obtain for each solvent values of b/r_c and hence values of b . This is proportional to the mean distance that the charges travel in the particular medium before becoming thermalized. Since in any medium the distance traveled must vary inversely with the density, the best parameter to use for comparing the various solvents would seem to be the product of b and the density d . This quantity, given in the last column of Table II, is believed to afford a relative measure of the rate of energy loss by subexcitation electrons moving through the various media, or alternatively of the cross section for capture of the electron by interaction with the solvent molecules. Once the electron is either converted into a negative ion or is trapped by a coordinated group of molecules and thereby converted to a solvated electron, it will lose all effective momentum and if still within the sphere of action of its parent positive ion will diffuse toward this ion and recombine with it.

Looking at the values of bd we see first as already found^{1,6} that the values are larger for the saturated hydrocarbons than for other liquids, with the largest value for the one containing a quaternary carbon atom. Values are considerably lower for the aromatics, indicating a specific interaction between the free charges and the π electrons of the aromatic ring. A still stronger interaction exists with hydroxyl groups, as shown by the low bd values for the alcohols. Here the electron is trapped by the collective motion of a num-

(4) G. R. Freeman, *J. Chem. Phys.*, **39**, 1580 (1963).

(5) A. Hummel, A. O. Allen, and F. H. Watson, Jr., *ibid.*, **44**, 3431 (1966).

(6) W. F. Schmidt and A. O. Allen, *J. Phys. Chem.*, **72**, 3730 (1968).

(7) L. Onsager, *Phys. Rev.*, **54**, 554 (1938).

ber of molecules to form a solvated electron. The branched compound *t*-butyl alcohol seems to have a somewhat higher *bd* than the straight-chain alcohols. Neopentyl alcohol did not show the expected high *bd*; unfortunately it was studied only at a low concentration, and it is possible that the true value of *G* (free ions) may not have been attained in this case. The escape distances for the nitro compounds are much lower than for the other liquids, as was obvious simply for the lower values of *G*(free ions) in these compounds when compared with their high dielectric constants. The indicated strong interaction of these compounds with

the free charges is presumably connected with their very high dipole moments.

The nature of electronic states and behavior of free charges in liquids are not at all well understood. Data of the kind presented here offer a foundation on which an understanding of this important subject can be built.

Acknowledgments. We are grateful to Dr. W. F. Schmidt for determination of the dielectric constant of liquid neopentyl alcohol. This research was performed under the auspices of the U. S. Atomic Energy Commission.

Photoreduction of 1-Nitronaphthalene by Protonation

in the Excited State

by W. Trotter and A. C. Testa

Department of Chemistry, St. John's University, Jamaica, New York 11432 (Received July 2, 1969)

Photolysis of 1-nitronaphthalene at 366 nm in 50% isopropyl alcohol and water with varying concentrations of hydrochloric acid results in photoreduction with formation of 4-chloro-1-naphthylamine. The highest disappearance quantum yield measured was 1.28×10^{-2} for 6 *M* HCl with 50% isopropyl alcohol-water, while in pure isopropyl alcohol there is no detectable photochemistry. The results are interpreted in terms of protonation of the nitronaphthalene triplet.

Introduction

In contrast to the observed photoreduction of nitrobenzene at 366 nm in isopropyl alcohol, 1-nitronaphthalene exhibits no detectable photochemical activity under the same conditions.¹ The photoreduction of 1-nitronaphthalene, however, has been reported using tri-*n*-butylstannane.² To explore protonation in the excited state as a method to enhance photochemistry, similar to the report on nitrobenzene,³ it became interesting to investigate this effect on 1-nitronaphthalene. Consequently, this study was made to evaluate the photochemical behavior of 1-nitronaphthalene triplets in the presence of protons. Experiments were conducted in 50% isopropyl alcohol-water solutions with varying concentrations of HCl.

Experimental Section

Materials. Reagent grade 1-nitronaphthalene was recrystallized twice from hexane and reagent grade HCl was used as received. Solutions were made up with spectrograde isopropyl alcohol and quartz-distilled water. 4-Chloro-1-naphthylamine was obtained from

Aldrich Chemical Co. and recrystallized from aqueous alcoholic solutions containing decolorizing carbon. The amine hydrochloride was prepared by addition of a saturated solution of HCl gas in ether to an ether solution containing the chloronaphthylamine. The amine salt precipitated as a white solid and was recovered by filtration.

Apparatus. Photochemical quantum yields measurements were determined in 1-cm spectrophotometric cells with equipment described previously.⁴ Samples were degassed by three or more freeze-pump-thaw cycles at $<10^{-3}$ mm and sealed off from the vacuum line. Light intensities at 366 nm were 1.6×10^{16} quanta/sec as determined by the ferrioxalate actinometer.⁵ Large-scale photolyses were performed with a

- (1) R. Hurley and A. C. Testa, *J. Amer. Chem. Soc.*, **90**, 1949 (1968).
- (2) W. Trotter and A. C. Testa, *ibid.*, **90**, 7044 (1968).
- (3) R. Hurley and A. C. Testa, *ibid.*, **89**, 6917 (1967).
- (4) R. Hurley and A. C. Testa, *ibid.*, **88**, 4330 (1966).
- (5) C. G. Hatchard and C. A. Parker, *Proc. Roy. Soc. (London)*, **A235**, 518 (1956).

450-W Hanovia high-pressure quartz mercury arc (no. 679A-36) and a Pyrex sleeve to limit the region of excitation to wavelengths greater than 290 nm. Optical densities at 366 nm, before and after photolysis, were measured with a Beckman DU spectrophotometer. The following extinction coefficients of 1-nitronaphthalene at this wavelength in 50% isopropyl alcohol-water were used for calculations: 3.09×10^3 (1 M), 3.17×10^3 (2 M), 3.18×10^3 (3 M), 3.28×10^3 (4 M), and 3.35×10^3 (6 M). The values in parentheses represent HCl concentrations. Absorbance at 366 nm due to the amine hydrochloride formed photochemically was negligible.

Procedures. Monochromatic excitation for the quantum yield determinations was achieved with a 10-nm half-band-width interference filter. In a typical large-scale (broad wavelength range) experiment 0.574 g of 1-nitronaphthalene in 800 ml of 50% isopropyl alcohol-water, 2 M in HCl, was photolyzed under a nitrogen atmosphere for 4 hr. Flash evaporation after photolysis yielded a solid which was characterized by its uv absorption, fluorescence, and infrared spectra. A Beckman IR-8 spectrophotometer was used to record the infrared spectra. Samples were run as KBr pellets at 1% concentration. A Bausch and Lomb 505 spectrophotometer was used to record the uv spectra of the amine hydrochloride generated photochemically.

Results

Although 1-nitronaphthalene exhibits no photochemistry in isopropyl alcohol, addition of protons to a 50% isopropyl alcohol-water mixture resulted in its disappearance by a process involving photoreduction. Identification of the photoproduct from large-scale photolyses was made by comparison of the infrared spectrum with an authentic sample of 4-chloro-1-naphthylamine as the hydrochloride. Strong absorption bands were observed at 3.6 and 3.9 μ , characteristic of the amine hydrochloride, and at 8.3, 10.7, 12.2, and 13.2 μ . The fluorescence spectrum of the photoproduct was also identical with that of 4-chloro-1-naphthylamine. In addition, the characteristic three-peak structure of the amine hydrochloride with peaks at 279, 289, and 298 nm was observed in its uv absorption spectrum.

Determination of the disappearance quantum yield was made by measuring the optical density changes at 366 nm, where the photoproduct shows no significant absorption. There was no evidence for side effects; consequently, the formation yield of 4-chloro-1-naphthylamine is the same as the disappearance yield of 1-nitronaphthalene. In Figure 1 the dependence of the disappearance quantum yield of 1-nitronaphthalene as a function of HCl concentration is presented. Each data point in Figure 1 is the average of two or more experiments. It is evident that there is a proportionality between the two parameters from 0 to 6 M HCl, keeping the solvent constant at 50% isopropyl alcohol-

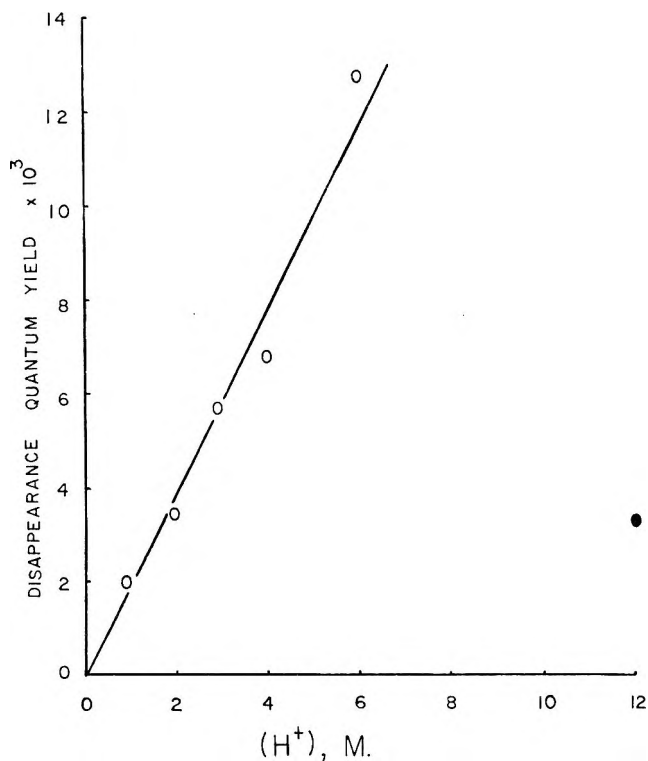


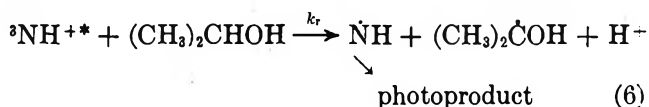
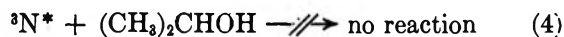
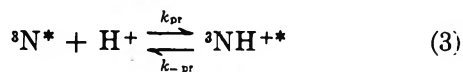
Figure 1. Photochemical disappearance quantum yields for 1-nitronaphthalene in 50% isopropyl alcohol-water with varying concentrations of HCl. Excitation was at 366 nm and all samples were vacuum degassed. The data point at 12 M HCl is included to illustrate the sharp decrease in quantum yield upon removal of isopropyl alcohol. (Concentration of 1-nitronaphthalene was 6×10^{-4} M.)

water. Beyond 6 M HCl the alcohol content is decreasing in concentration, and despite the increase in (H⁺) in going to 12 M HCl, the quantum yield falls off considerably due to the absence of hydrogen donor. This data point is included in Figure 1. It should be noted that approximately 2% isopropyl alcohol was present in concentrated HCl to solubilize the 1-nitronaphthalene; consequently, the small quantum yield of 3.3×10^{-3} at this concentration is the result of the alcoholic content. The decrease in quantum yield beyond 6 M HCl for 1-nitronaphthalene is in sharp contrast to the results for nitrobenzene where the quantum yield continues to increase. In 12 M HCl nitrobenzene exhibits its largest disappearance yield of 0.30.³

Discussion

In view of the proportionality between the disappearance quantum yield and acid concentration it appears that the protonated triplet state is the species responsible for photoreduction. Although protonation of the singlet or triplet can account for the observed results, the former is probably not involved because of the very short-lived singlet state of 1-nitronaphthalene, which does not fluoresce, and the general involvement of the

triplet state in hydrogen abstraction processes.⁶ The following scheme is suggested to explain the observed photochemical behavior of 1-nitronaphthalene (N) in the presence of protons



Completion of the hydrogen abstraction process by the protonated triplet in reaction 6 would involve electron transfer.⁷ The steady-state expression for the disappearance yield of 1-nitronaphthalene according to the above scheme is

$$\Phi = \phi_T \frac{k_r({}^3NH^{+*})(IPA)}{[k_r({}^3NH^{+*})(IPA) + k_{dt}]} \quad (I)$$

where ϕ_T is the triplet yield and (IPA) is the concentration of isopropyl alcohol. In view of the observation that the quantum yields are small in all experiments performed, it is reasonable to consider $k_{dt}({}^3N^*) \gg k_r({}^3NH^{+*})(IPA)$, since the triplet yield of 1-nitronaphthalene has been measured to be 0.63.¹ Imposing the condition that $k_{-pr} \gg k_r(IPA)$, *i.e.*, deprotonation of the triplet limits photochemical activity, the quantum yield expression becomes

$$\Phi = \frac{\phi_T K k_r}{k_{dt}} (IPA)(H^+) \quad (II)$$

which satisfactorily describes the experimental results from 0 to 6 M HCl in 50% isopropyl alcohol-water. In eq II the quantity $K = (k_{pr}/k_{-pr})$ defines the equilibrium constant for formation of the protonated triplet.

Using the slope from the plot in Figure 1, the rate constant for triplet deactivation for 1-nitronaphthalene determined previously,¹ *i.e.*, $k_{dt} < 4 \times 10^5 \text{ sec}^{-1}$, and the approximation that the rate constant for reaction 6, involving electron transfer, is diffusion controlled, the equilibrium constant for the formation of the protonated triplets is $< 10^{-8} M^{-1}$. The dependence of quantum yield on the concentration of isopropyl alcohol is reflected by the low quantum yield measured in 12 M HCl (see Figure 1). Our results with nitrobenzene indicated a ratio $k_{pr}/k_H \approx 44$,³ and including the rate constant for hydrogen abstraction, $k_H = 10^6 M^{-1} \text{ sec}^{-1}$,² the value of $k_{pr} \approx 4.4 \times 10^7 M^{-1} \text{ sec}^{-1}$. Although a direct comparison of nitrobenzene and 1-nitronaphthalene cannot be made without knowledge of k_{-pr} , the experimental results and the small equilibrium constant for protonation of the triplet of 1-nitronaphthalene indicates that the photochemical enhancement by protonation in the excited state is greater for nitrobenzene than for 1-nitronaphthalene. It is tempting to suggest that a faster triplet-state protonation occurs in the former; however, another explanation may be the lower reactivity of the protonated triplet of 1-nitronaphthalene relative to that for nitrobenzene. It has been shown that the lowest triplet is π, π^* for 1-nitronaphthalene and n, π^* for nitrobenzene.¹ The disappearance quantum yield continues to increase for nitrobenzene up to 12 M HCl while a low yield occurs for 1-nitronaphthalene under the same condition. This observation suggests that the hydrogen abstraction process is different for the two molecules.

Acknowledgments. Support of this research by a Frederick Gardner Cottrell Grant from the Research Corporation and a Fellowship for Graduate Education and Fundamental Research from the Petroleum Research Fund, American Chemical Society, is gratefully acknowledged.

(6) N. J. Turro, "Molecular Photochemistry," W. A. Benjamin, Inc., New York, N. Y., 1965, p. 37.

(7) The hydrogen atom abstraction is a combination of a protonation and an electron transfer.

The Radiolysis of Gaseous Trifluoroiodomethane in the Presence of Nitric Oxide

by I. McAlpine and H. Sutcliffe

Chemistry Department, University of Salford, Salford M6 4WT, Lancashire, England (Received June 10, 1969)

Nitric oxide reduces the 100-eV yields of tetrafluoromethane and difluorodiodomethane and increases the yield of iodine in the radiolysis of trifluoroiodomethane. The products nitrogen, nitrogen dioxide, trifluoronitrosomethane, trifluoronitromethane, and hexafluoroethane are also identified. A radical-chain mechanism involving an intermediate diazonium nitrate is proposed to explain the formation of these products and the high value of $G(-NO)$. It is suggested that nitric oxide is acting as a scavenger of excited radicals.

Nitric oxide has been used as a radical scavenger in the radiolysis of hydrocarbons, notably by Yang.^{1,2} Yang presents a cogent argument that nitric oxide is a true radical scavenger during methane radiolysis and does not interfere with any ionic or molecular reactions that may be proceeding. This argument is based on a comparison of the effect of nitric oxide and other radical scavengers on $G(H_2)$ in methane radiolysis.

The radiolysis of trifluoroiodomethane in the presence of oxygen as a radical scavenger reduces the 100-eV yields of tetrafluoromethane and difluorodiodomethane indicating that these products are formed largely by radical processes.³ Unfortunately the presence of oxygen results in a number of secondary reactions which make a complete interpretation of the results difficult. It was with a view to clarifying this situation regarding the radical nature of the reaction that the present work was initiated.

Experimental Section

Except where otherwise stated, the preparation of trifluoroiodomethane, gas chromatographic analysis, infrared spectroscopic analysis, dosimetry, and radiolysis were carried out as previously described.³ Nitric oxide was prepared by the reaction of acidified ferrous sulfate with sodium nitrite.⁴

In a typical experiment trifluoroiodomethane (45.45 mmol) and nitric oxide (45.73 mmol) were condensed into a 2.2-l. bulb and irradiated, in the gas phase, on the ⁶⁰Co source at a dose rate of *ca* 0.73 Mrad/hr for 15 hr. After irradiation the nitrogen was transferred by means of an automatic Toepler pump⁵ into a vessel of known volume and measured. The purity of the nitrogen was checked by gas chromatographic analysis and found to contain only a slight trace of nitric oxide. The condensable gases which remained frozen down during the removal of nitrogen were fractionated *in vacuo* through traps cooled to -63 , -96 , -131 , and -196° , respectively. The fraction condensed at -63° contained iodine together with a trace of nitrogen dioxide. The iodine was determined by titration with sodium thiosulfate solution after destroying the nitrogen dioxide by addition of sulfamic acid. The fraction

condensed at -96° was nitrogen dioxide; this was determined by allowing it to react with excess standard sodium hydroxide solution and back-titrating with standard hydrochloric acid. The fraction condensed at -131° consisted mainly of trifluoroiodomethane together with a small amount of trifluoronitromethane. The relative proportions of these two compounds were determined by gas chromatography using an 8 m \times 4 mm i.d. column of 30% w/w Kel F oil No. 10 (F & M Scientific Corp.) on 80–120 mesh Celite. The fraction condensed at -196° contained trifluoroiodomethane, tetrafluoromethane, carbonyl fluoride, nitric oxide, hexafluoroethane, and trifluoronitrosomethane. Since nitric oxide has almost the same retention time as tetrafluoromethane, direct analysis of this mixture by gas chromatography was not possible. Oxygen was added to the mixed gases to oxidize the nitric oxide to nitrogen dioxide. Excess oxygen was removed, and the nitrogen dioxide was separated from the other gases by trap-to-trap fractionation *in vacuo* and determined by titration. The remainder of this fraction was analyzed by gas chromatography.

Other experiments using different proportions of reactants and different irradiation times were also carried out. The results are shown in Table I together with results of the radiolysis of trifluoroiodomethane alone for comparison.

Results and Discussion

Examination of the results in Table I shows that the most notable features of this reaction are (a) the high values and dependence of $G(N_2)$ and $G(-NO)$ on the initial pressure of nitric oxide, (b) the marked increase in the value of $G(I_2)$ relative to the value in the absence of nitric oxide, and (c) the marked reduction of $G(CF_4)$ and $G(CF_2I_2)$ compared with the corresponding values for trifluoroiodomethane alone.

- (1) K. Yang and P. J. Manno, *J. Amer. Chem. Soc.*, **81**, 3507 (1959).
- (2) K. Yang, *J. Phys. Chem.*, **65**, 42 (1961).
- (3) I. McAlpine and H. Sutcliffe, *ibid.*, **73**, 3215 (1969).
- (4) *Inorg. Syn.*, **2**, 126 (1946).
- (5) I. McAlpine and H. Sutcliffe, *Chem. Ind. (London)*, 1170 (1967).

Table I

Expt no.	Ratio CF ₃ I:NO	G values								
		I ₂	CF ₄	C ₂ F ₆	CF ₃ NO	N ₂	NO ₂	CF ₃ NO ₂	-NO	CF ₂ I ₂
1 ^a	0.25	12.3	478	1092	...
2 ^a	1	10.1	0.2	0.02	0.32	150	251	3.3	571	...
3 ^a	16.6	12.1	0.03	0.03	27.7	...	1.3	...	83	...
4 ^b	∞	0.13	1.08	0.82

^a This work. ^b See ref 3.

The last point substantiates the conclusions from work in the presence of oxygen, namely, that tetrafluoromethane and difluorodiiodomethane are formed mainly by radical reactions. The value of $G(\text{CF}_4) = 0.03$ is much less and the value of $G(\text{I}_2) = 12$ higher than the corresponding values observed when trifluoroiodomethane is irradiated alone or in the presence of oxygen. This suggests that nitric oxide is a better radical scavenger than either oxygen or iodine, which is in agreement with the work of Yang on hydrocarbons.

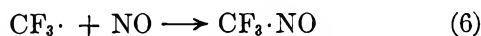
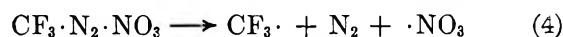
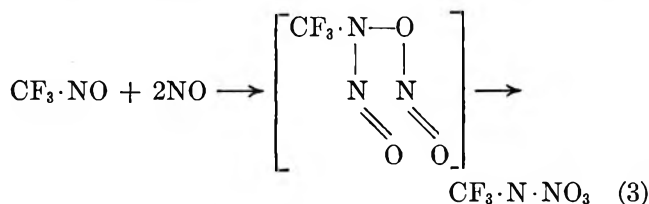
The scavenging of trifluoromethyl radicals by nitric oxide prevents the formation of tetrafluoromethane and $\cdot\text{CF}_2\text{I}$ radicals by the reaction



Hence no difluorodiiodomethane can be formed as is observed in the presence of nitric oxide. The scavenging reaction will form trifluoronitrosomethane



but the yield of trifluoronitrosomethane will depend on the relative abilities of nitric oxide and iodine as radical scavengers and on the reactivity and environment of trifluoronitrosomethane. In the presence of 5% molar nitric oxide and at low dose $G(\text{CF}_3\text{NO}) = 27.7$ whereas at higher dose and 50% molar nitric oxide $G(\text{CF}_3\text{NO}) = 0.3$. Also under the latter conditions $G(\text{N}_2)$ and $G(-\text{NO})$ are markedly increased. The reaction thus has two stages: first scavenging of trifluoromethyl radicals by nitric oxide to give trifluoronitrosomethane, followed by reaction of trifluoronitrosomethane with nitric oxide to give nitrogen, nitrogen dioxide, and trifluoronitromethane. The following chain reaction is suggested



which can lead to the formation of nitrogen and nitrogen dioxide in high yield.

The reaction of monomeric nitroso compounds with nitric oxide was first observed by Bamberger⁶ for nitrosobenzene and has subsequently been reported by other workers using nitric oxide as a radical scavenger in photolytic and pyrolytic studies.⁷⁻¹⁴ This is the first report of a reaction of this type occurring when nitric oxide is used as a radical scavenger in radiolysis work. The length of each chain will depend on how much nitric oxide is available. Once the concentration of nitrogen dioxide becomes appreciable, the chain-termination reaction



begins to compete with and may eventually take precedence over the scavenging reaction 2. This is probably what is happening in the later stages of expt 2 (Table I) since trifluoronitromethane is produced with $G(\text{CF}_3\text{NO}_2) = 3.3$. The main over-all effect of this chain reaction is the disproportionation of nitric oxide into nitrogen and nitrogen dioxide



and so the ratio $G(-\text{NO}):G(\text{NO}_2):G(\text{N}_2)$ should be 4:2:1. The observed ratio in expt 2 of 3.8:1.7:1.0 is of this order and suggests that the chain mechanism outlined above is operating. In expt 1, where an excess of nitric oxide is present, the proportion of nitrogen present in the products is low. It would appear that some other mechanism is operating when nitric oxide is present in excess, and further work is in progress to clarify this point. It should be noted that the value of $G(-\text{NO})$ is limited by the initial concentration of nitric oxide, indicating that a small amount of trifluoroiodomethane can act as an initiator for the radiolytic disproportionation of nitric oxide. The

(6) E. Bamberger, *Ber.*, **30**, 506 (1897).

(7) L. Batt and B. G. Gowenlock, *Trans. Faraday Soc.*, **56**, 682 (1960).

(8) M. I. Christie, *Proc. Roy. Soc.*, **A249**, 258 (1958).

(9) M. I. Christie, C. Gillbert, and M. A. Voisey, *J. Chem. Soc.*, 3147 (1964).

(10) D. A. Barr, R. N. Haszeldine, and C. J. Willis, *ibid.*, 1351 (1961).

(11) J. F. Brown, Jr., *J. Amer. Chem. Soc.*, **79**, 2480 (1957).

(12) L. G. Donaruma and D. J. Carmody, *J. Org. Chem.*, **22**, 635 (1957).

(13) A. N. Nesmeyanov and S. T. Ioffe, *J. Gen. Chem. USSR*, **11**, 392 (1941).

(14) J. Heicklen, *J. Phys. Chem.*, **70**, 112 (1966).

irradiation of nitric oxide alone has been carried out by other workers using fission fragments and γ rays,^{15,16} but in both cases the $G(-NO)$ value was much lower than when trifluoroiodomethane was present.

The occurrence of this chain reaction propagated by a regenerated trifluoromethyl radical casts doubt on the usefulness of nitric oxide as a radical scavenger in radiolysis work. In the present work the inference is that nitric oxide scavenges the initially formed excited or "hot" trifluoromethyl radicals followed by a chain reaction involving thermalized trifluoromethyl radicals. It has been suggested in the previous work that only excited trifluoromethyl radicals can abstract fluorine

from trifluoroiodomethane to give tetrafluoromethane, and this is now substantiated. The eventual fate of the thermal trifluoromethyl radicals is to form trifluoronitromethane, trifluoronitrosomethane, or some as yet unidentified product.

Acknowledgments. I. McAlpine wishes to thank the Science Research Council for a maintenance award, during the tenure of which this work was carried out.

(15) P. Harteck and S. Dondes, *J. Chem. Phys.*, **27**, 546 (1957).

(16) M. T. Dmitriev and L. V. Saradzhev, *Russ. J. Phys. Chem.*, **35**, 354 (1961).

Mechanism of Reaction of Hydroxyl Radicals with Benzene

in the γ Radiolysis of the Aerated Aqueous Benzene System

by I. Balakrishnan and M. P. Reddy

Communication No. 1367 from the National Chemical Laboratory, Poona, India (Received June 24, 1969)

The reaction of hydroxyl radicals with benzene in aerated aqueous solutions under γ radiolysis produces phenol and β -hydroxymucondialdehyde (β HMD). The respective G values are 1.7 and 1.2, in 0.8 N H_2SO_4 , and 1.78 and 0.7, in neutral solutions, the sum of the two yields accounting for all the OH radicals in each instance. The enhancing effect of ferrous ions on these yields has been correlated with the peroxide chain mechanism advanced originally to account for the influence of organic impurities on the $G(Fe^{2+})$ of the Fricke dosimeter. At a benzene concentration of $10^{-2} M$ and a ferrous ion concentration of $10^{-3} M$, $G(Fe^{3+})$ is ~ 48 ; $G(\text{phenol})$ and $G(\beta\text{HMD})$ are 8.8 and 6.6, respectively. This corresponds to a chain length of ~ 2 .

Introduction

A program of study of the formation of phenolic compounds under radiolysis required reexamination of the aerated aqueous benzene system. Earlier work¹⁻⁶ has reported the formation of phenol in the γ radiolysis of this system. Three other products, "mucondialdehyde" with a G value ranging from 0.2 to 1.7,⁷⁻¹⁰ an unknown phenol-like compound, and an acid, have been notably described. In a previous communication¹¹ it was shown that these three products are one and the same, *i.e.*, β -hydroxymucondialdehyde (β HMD). Interference due to β HMD accounts for the wide variation in the values of $G(\text{phenol})$ reported earlier.^{1-6,9,10,12} This problem has here been solved by effecting a separation of the two compounds before analyzing them, and reliable $G(\text{phenol})$ and $G(\beta\text{HMD})$ values have been obtained.

Ferrous ions have been observed to enhance the yields of phenol and the dial.⁹ This effect has been restudied and correlated with the peroxide chain mechanism advanced originally by Kolthoff and Medalia¹³ in the

case of Fenton's reagent and later by Dewhurst^{14,15} to explain the influence of organic impurities on the G

(1) G. Stein and J. Weiss, *J. Chem. Soc.*, 3245 (1949).

(2) T. J. Sworski, *J. Chem. Phys.*, **20**, 1817 (1952).

(3) P. V. Phung and M. Burton, *Radiation Res.*, **7**, 199 (1957).

(4) J. Goodman and J. Steigman, *J. Phys. Chem.*, **62**, 1020 (1958).

(5) J. H. Baxendale and D. Smithies, *J. Chem. Soc.*, 779 (1959).

(6) H. C. Christensen, Aktiebolaget Atomenergie Stockholm, AE 142, 1964, p 34; *Chem. Abstr.*, **61**, 12829 (1964).

(7) M. Daniels, G. Scholes, and J. Weiss, *J. Chem. Soc.*, 832 (1956).

(8) I. Loeff and G. Stein, *ibid.*, 2623 (1963).

(9) L. I. Kartasheva and A. K. Pikaev, *Dokl. Akad. Nauk SSSR*, **163**, 1155 (1965).

(10) L. I. Kartasheva and A. K. Pikaev, *Russ. J. Phys. Chem.*, **41**, 1534 (1967).

(11) T. K. K. Srinivasan, I. Balakrishnan, and M. P. Reddy, *J. Phys. Chem.*, **73**, 2071 (1969).

(12) I. Balakrishnan and M. P. Reddy, *ibid.*, **72**, 4609 (1968).

(13) I. M. Kolthoff and A. I. Medalia, *J. Amer. Chem. Soc.*, **71**, 3784 (1949).

(14) H. A. Dewhurst, *J. Chem. Phys.*, **19**, 1329 (1951).

(15) H. A. Dewhurst, *Trans. Faraday Soc.*, **48**, 905 (1952).

(Fe^{3+}) of the Fricke dosimetric system. This in turn helps to evolve a mechanism for the formation of the two products, taking the clue from the pulse radiolysis study of this system produced by Dorfman.¹⁶

Experimental Section

Materials. A BDH sample of benzene, washed with pyrosulfuric acid, alkali, and water, dried over sodium sulfate, and purified by five crystallizations, was used. *p*-Nitroaniline, laboratory grade, was purified by recrystallization from alcohol. *o*-Phenanthroline, pure, colorless, BDH sample, was used as such. Ferrous ammonium sulfate, a pure grade, was recrystallized from the triply distilled water used for all solutions in this study.

Solvent ether, B.P., was further purified by washing with 1 *N* NaOH, water, 0.8 *N* H_2SO_4 , and distilled water, before it was used for extraction. This was found to be essential for proper coupling of aqueous solutions containing dissolved ether.

Procedures. A kilocurie ^{60}Co γ source was used on the basis of the 15.6 value for the Fricke dosimeter. The solutions studied were 0.8 *N* in sulfuric acid, for the most part. Some were neutral. Analyses were made using a Perkin-Elmer 350 spectrophotometer, as well as a Beckmann 378E ratio recording spectrophotometer.

1. **Phenol.** *p*-Nitrobenzenediazonium chloride reagent (PNDC) forms deeply colored indicator dyes with phenols which are useful for unequivocal qualitative identification¹⁷ of these compounds in many cases. The dyes have high extinction coefficients and are recommended for quantitative analysis of phenols. The procedure for the analysis of phenol given in Snell's treatise¹⁸ was used, but the addition of sodium acetate was not essential. The irradiated solution was extracted four times with ether and the extract was washed five times with 0.1 *N* NaOH. The alkali layer was made barely acidic to litmus before coupling. The absorption maximum at 475 $m\mu$ was measured against a reagent blank. The absorption of the latter at 475 $m\mu$ is negligible and there is no interference due to it. The ether extraction method was applied to a standard phenol solution of comparable strength and gave quantitative results.

2. **β HMD.** PNDC also couples with β HMD to give a yellow dye. To estimate the product, the irradiated solution after ether extraction at a pH of 7 (pure sodium bicarbonate), to remove phenol, was made acidic to litmus and treated with sodium acetate (1 ml of a 25% solution) and then with PNDC (twice the theoretical amount). After 1 hr the yellow test solution was run against a practically colorless blank containing only sodium acetate, acid and PNDC, and the broad absorption maximum at 370 $m\mu$ (*cf.* curve D in the inset in Figure 1) was measured. Coupling in sodium carbonate solution gives curve E of Figure 1, but this is

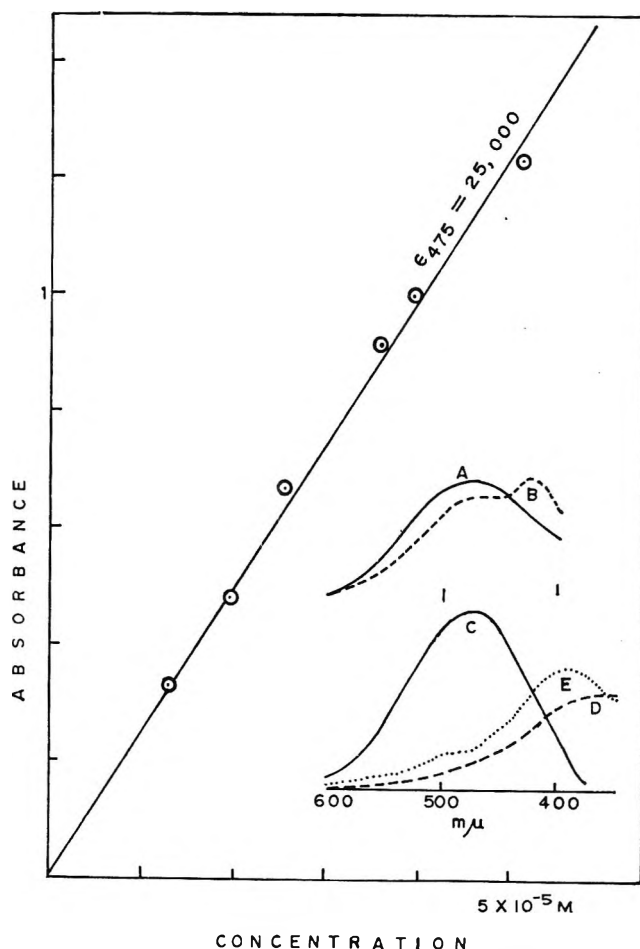


Figure 1. Standardization of the PNDC method for phenol: a, spectrum of irradiated aqueous solution of benzene treated with small excess of PNDC; b, the same, treated with large excess of PNDC; c, spectrum of PNDC dye of pure phenol; d, spectrum of β HMD solution treated with PNDC at pH \sim 5 (acetate buffer); e, spectrum of β HMD solution treated with PNDC at pH \sim 10 (sodium carbonate).

not recommended because of interference due to the strong color developed by the blank. The extinction coefficient for the maximum at 370 $m\mu$ was obtained using milligram quantities of the dye isolated from a large volume of solution irradiated intermittently to a high dose. At each interruption, benzene and air were dissolved to compensate for depletion. The ether solution of the dye was washed twice with small amounts of water and evaporated. The solid dye was dried at 80°. A weighed amount was dissolved in a little alcohol and diluted to a suitable volume with water and 1 ml of acetate-acid buffer (pH \sim 5) ($\epsilon_{370 m\mu}$ 7850). In sodium carbonate solution $\epsilon_{390 m\mu}$ is 9950.

(16) L. M. Dorfman, I. A. Taub, and R. E. Bühler, *J. Chem. Phys.*, **36**, 3051 (1962).

(17) S. Palkin and H. Wales, *J. Amer. Chem. Soc.*, **46**, 1488 (1924).

(18) F. D. Snell and C. T. Snell, "Colorimetric Methods of Analysis," Vol. III, D. Van Nostrand Co., Inc., Princeton, N. J., 1953, pp 117, 127.

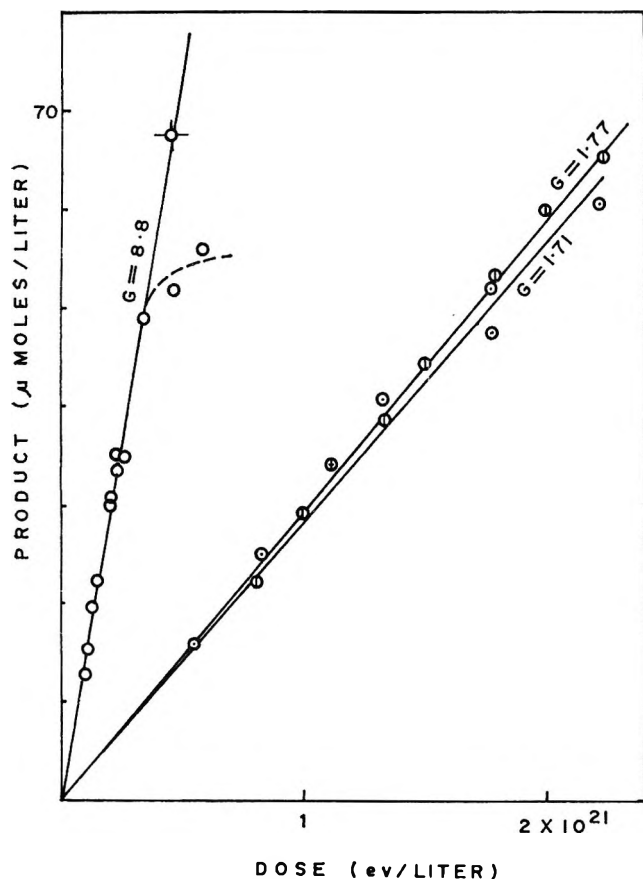


Figure 2. Yields of phenol in the γ radiolysis of aerated aqueous benzene: \circ , $0.8 N H_2SO_4$; \square , neutral; \triangle , in presence of $10^{-3} M$ ferrous ion; \diamond , oxygenated.

Irradiated solutions above pH 4 show an absorption maximum at $345 m\mu$,⁴ which is entirely due to β HMD and has an ϵ of 4080 in solutions neutralized with pure bicarbonate. The value is about 2% lower at pH 5 and 5% higher at pH 10. This value was obtained by matching the $345\text{-}m\mu$ peak with that of the dye at $370 m\mu$. The order of magnitude of this ϵ value proves that the OH is situated β to an aldehyde group, as pointed out earlier.¹¹ Figure 5 describes the pH dependence of the complete spectrum of β HMD and contrasts it with the behavior of a few related ketonols.¹⁹⁻²¹

The $345\text{-}m\mu$ peak is particularly useful in determining the effect of ferrous ions upon the yield of β HMD. For this purpose, the iron was precipitated at about pH 9 using sodium hydroxide and centrifuged and the absorption compared at the same pH with that of irradiated solutions containing no iron.

In neutral solutions the formation of 2,4-dinitrophenylhydrazone from β HMD was found to be linear up to a very large dose. Assuming this to be a trihydrazone, a G value of 0.7 was obtained (see inset in Figure 3) in agreement with the PNDC method. The implied proof that the derivative is a trihydrazone is crucial to the identification of the compound as β -hydroxyacetaldehyde.¹¹

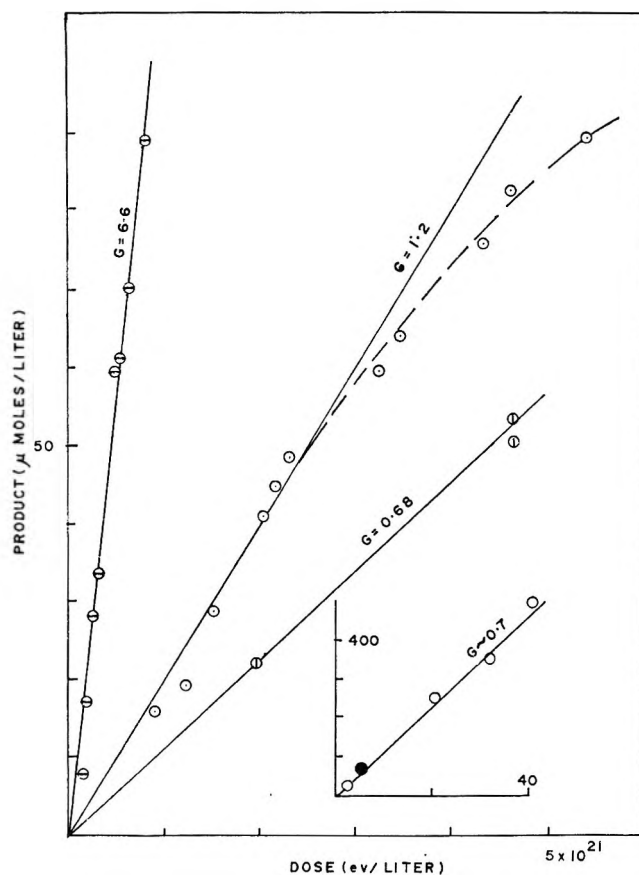


Figure 3. Yields of β HMD in the γ radiolysis of aerated aqueous benzene: \circ , $0.8 N H_2SO_4$ in absence of ferrous ion; \square , the same in presence of $10^{-3} M$ ferrous ion; \triangle , neutral; \diamond , neutral (by weighing the dinitrophenylhydrazone); \bullet , the p -nitrophenyl hydrazone.

3. *Polyhydroxybenzenes.* Sensitive color tests for quinol and quinone,²² catechol, and all the higher polyhydroxybenzenes¹⁸ showed the absence of these compounds in the irradiated solution. Resorcinol gives a deep purple color with PNDC which was never observed with irradiated solutions.

4. *Ferrous Ion.* Ferrous ion oxidation in the Fricke system saturated with benzene was followed using the *o*-phenanthroline method²³ standardized excluding acetate or citrate. With a large excess of reagent (~ 30 times the ferrous content), even in $0.8 N H_2SO_4$ the extinction coefficient is only slightly lower than the reported value, provided a reaction time of 1 hr is allowed. Acetate seems to interfere with color formation in the case of irradiated solutions and the results are erratic.

(19) C. J. Cavallito, C. M. Martini, and F. C. Nachod, *J. Amer. Chem. Soc.*, **73**, 2546 (1951).

(20) G. Schwarzenbach, K. Lutz, and E. Felder, *Helv. Chim. Acta*, **27**, 579 (1944).

(21) Y. Kojima, N. Itada, and O. Hayaishi, *J. Biol. Chem.*, **236**, 2227 (1961).

(22) R. J. Lacoste, J. R. Covington, and G. J. Frisone, *Anal. Chem.*, **32**, 990 (1960).

(23) M. Lefort and J. Pucheault, *J. Chim. Phys.*, **50**, 580 (1953).

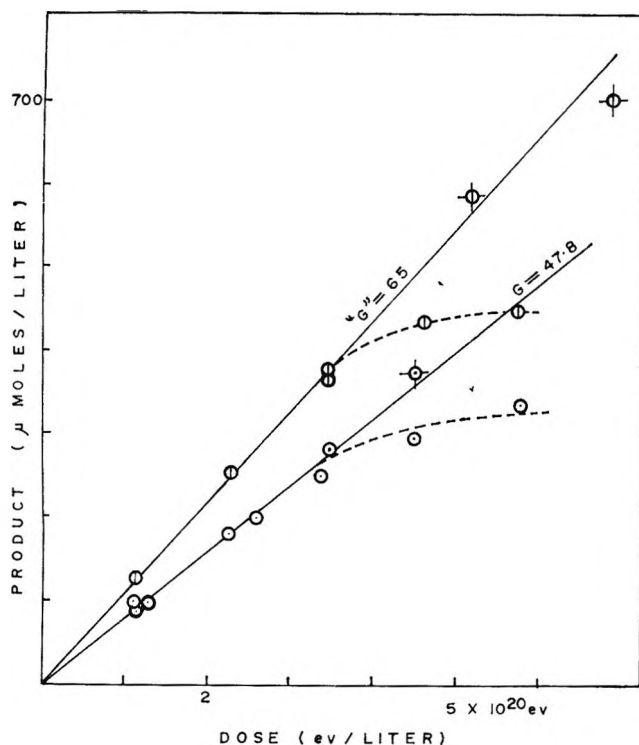


Figure 4. The disappearance of ferrous ion in the γ radiolysis of aerated aqueous benzene containing $10^{-3} M$ ferrous ion: \ominus , disappearance of ferrous ion; \ominus , appearance of 305- $m\mu$ peak; \ominus - \odot and \ominus - \odot , oxygenated.

Results

Figure 1 shows the standardization of the PNDC method for phenol ($\epsilon_{475 m\mu}$ 25,000). Curve C of the inset is the spectrum of the phenol dye. Curve B is the absorption of the irradiated solution upon treatment with an excess of PNDC. In the present work it was this two-peak spectrum which first revealed the formation of the two products. When the excess of reagent is reduced progressively, the 475- $m\mu$ peak rises and the spectrum resembles that of the phenol dye. The G (phenol) value of 1.54 reported earlier¹² is the highest obtainable by this procedure, which was abandoned when it was later realized that ether extraction removes the phenol exclusively.

Figure 2 describes phenol formation in the presence and absence of ferrous ion in 0.8 N H_2SO_4 solution. The yield in neutral benzene solution is practically indistinguishable from that in 0.8 N H_2SO_4 , the values quoted being the least-squares figures for the experimental points in each case.

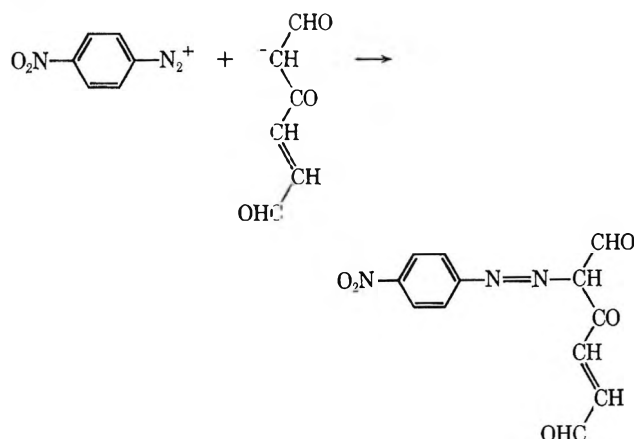
Figure 3 describes the formation of β HMD. Comparison with Figure 2 shows that the ferrous ion increases the yield of the two products by the same factor. At large doses, in acid solutions, the G value of the two compounds drops.

Figure 4 describes the effect of benzene on $G(Fe^{3+})$ of the Fricke dosimetric system at a ferrous ion concentration of $10^{-3} M$, saturated with benzene. The

lower curve represents the actual ferrous ion disappearance (*o*-phenanthroline method) while the upper gives the absorption at 305 $m\mu$ comprising evidently the β HMD contribution and the ferric ion contribution. The few points obtained with oxygenated solutions clearly indicate restored linearity. Oxygen consumption in this system is very large.

Discussion

The Mechanism of Reaction of Hydroxyl Radicals with Benzene. In continuation of the various observations on β HMD reported previously¹¹ a reliable method of quantitative determination has been developed here based upon its reaction with PNDC²⁴ which, according to present views²⁵ on such compounds coupling with diazonium salts, can be written



With the use of this method it now becomes evident that the assignment $G(\text{phenol}) = G(\text{OH})$, originally made by Phung and Burton,³ should read $G(\text{phenol}) + G(\beta\text{HMD}) = G(\text{OH})$. The values in Table I, for 0.8 N H_2SO_4 and neutral water, bear this out very clearly. The table also contains values taken from earlier work^{8,10} after applying a correction to the molar extinction of the hydrazone. It may be mentioned here that, in the present work, acid solutions gave precipitates whose weights varied in an erratic manner, in complete contrast to neutral solutions. The reason was not investigated.

The ratio of phenol to β HMD remains the same in the presence of ferrous ions as in their absence, in spite of the profound change in the mechanism and the onset of a chain reaction. Clearly, therefore, the two products are from the same primary source (*i.e.*, the OH radical). In addition, the mechanisms of their formation must have other features in common so that ferrous ions could influence them both identically. The mechanism given in Scheme I, involving the formation of the HO_2 radical together with phenol or β HMD, meets these requirements.

(24) A. P. Altshuller and I. R. Cohen, *Anal. Chim. Acta*, **24**, 61 (1961).

(25) S. Hunig and O. Boes, *Liebigs Ann. Chem.*, **579**, 28 (1953).

Table I: The Yields of Phenol and β -Hydroxymuconialdehyde in the γ Radiolysis of Aerated Aqueous Solutions of Benzene

Dose rate, eV ml ⁻¹ min ⁻¹	Neutral					Acid					Ref
	pH	Phenol	β HMD	Sum	G(OH)	pH	Phenol	β HMD	Sum	G(OH)	
5×10^{16}	7	1.77 \pm 0.05	0.68 \pm 0.04	2.45	2.4 ^a	0.4 ^b	1.71 \pm 0.1	1.20 \pm 0.07	2.91	2.9 ^a	Present study
13.8×10^{16}	7	2.00	0.87 ^c	2.87		0.4 ^b	2.20	1.23 ^c	3.43		10
7.644×10^{16} (200 kVp X-rays)	5.4	1.87	0.70 ^d	2.57		2.2	1.87	1.29 ^d	3.16		8

^a Standard values from A. O. Allen, "The Radiation Chemistry of Water and Aqueous Solutions," D. Van Nostrand Co., Inc., Princeton, N. J., 1961, Chapter 4. ^b 0.8 N H₂SO₄. ^c After correction using $\epsilon_{650 \text{ m}\mu}$ of 44,000 obtained in this study for β HMD in place of 35,000 reported in ref 9 for muconialdehyde dinitrophenylhydrazone. ^d After correction using $\epsilon_{390 \text{ m}\mu}$ of 9400 obtained here for the *p*-nitrophenylhydrazone of β HMD, in place of the value of 8240 for that of muconialdehyde reported in ref 8. We may add that when mass spectrometry of the two hydrazones was attempted, they decomposed at 250–280° and did not yield the peak of the parent ion. The PNDC dye did likewise.

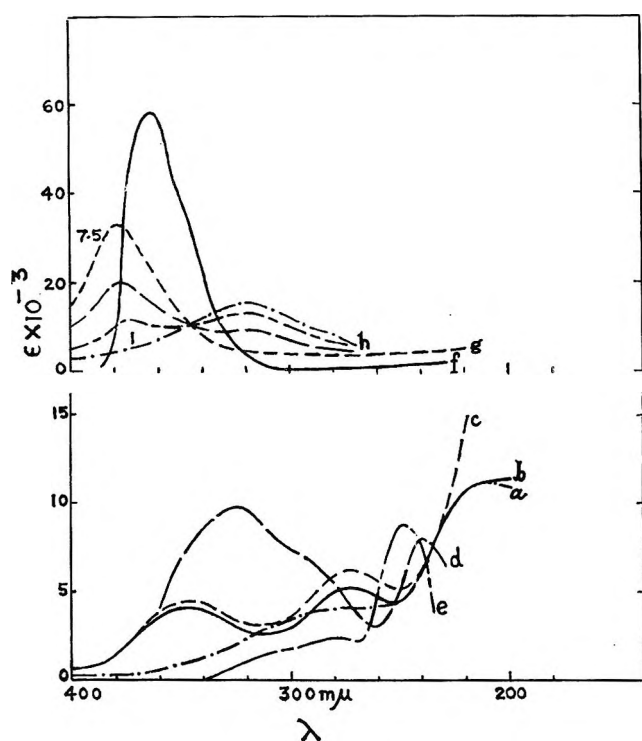


Figure 5. Spectra of ketoenols conjugated with C=O (see ref 19–21). β HMD: a, pH 1; b, pH 7–8; c, pH 12.5; benzoyl acetaldehyde: d, 95% alcohol; e, pH 2; glutaconic aldehyde: f, sodium salt; α -hydroxymuconicsemialdehyde: g, pH 7.5; h, pH 6.5, 5.5, and 1. The ϵ for the peak in the 350 m μ region for β hydroxy α,β -unsaturated aldehydes (lower set of curves) is one order of magnitude lower than for δ hydroxy $\alpha,\beta,\gamma,\delta$ -unsaturated aldehydes (upper curves).

The Effect of Ferrous Ions. Proskurnin²⁶ and Kartasheva⁹ measured the "catalytic" effect of ferrous ions upon the aerated aqueous benzene system and found an enhancement of $G(\text{phenol})$ and $G(\text{"muconialdehyde"})$. On the other hand, Vermeil²⁷ and others^{28,29} studied systems made up of benzene and other hydrocarbons, aromatic and aliphatic, dissolved in acid ferrous sulfate solution and found in all cases a large increase in $G(\text{Fe}^{3+})$. The two effects are evidently related, and quantitative correlation should be possible.

A situation similar to the above arises in the case of the Fenton system, in which hydroxyl radicals are produced in a reaction between ferrous ions and hydrogen peroxide.^{30–32} When benzene is added to this system, the yield of ferric ion is greatly enhanced,³³ an effect obtainable by the addition of many other organic compounds. To account for this, Kolthoff and Medalia¹³ suggested a mechanism in which the hydroxyl radicals react with the organic compound in preference to the ferrous ion, to produce radicals which pick up oxygen and become peroxy radicals which either oxidize two ferrous ions and carry a chain reaction or yield three ferric ions before becoming a product. Dewhurst^{14,15} first studied the Fricke dosimetric system in presence of a series of alcohols and used the above chain mechanism to account for the high yields of ferric ions. He did not measure the products arising from the organic impurity for correlation with the yield of ferric ion.

Scheme I incorporates the chain mechanism of Kolthoff and Medalia, modifying it to include an important reaction visualized by Dorfman,¹⁶ in which the organic peroxy radicals decompose to yield HO₂ instead of attacking ferrous ions. The result is that the identical influence of ferrous ions upon the yields of the two products finds a natural explanation.

The number of ferrous ions required to convert the primary species into OH radicals and reduce the latter in the chain-terminating step is 15.6. The remaining ferric yield is formed in the propagation of the chain

(26) E. V. Barelko, L. I. Kartasheva, P. D. Novikov, and M. A. Proskurnin, *Proc. All-Union Conf. Radiat. Chem.*, 1st, 1957, 2, 84 (1957).

(27) C. Vermeil, *J. Chim. Phys.*, 52, 587 (1955).

(28) H. Le Bail and J. Sutton, *ibid.*, 53, 430 (1956).

(29) K. C. Kurien, P. V. Phung, and M. Burton, *Radiat. Res.*, 11, 283 (1959).

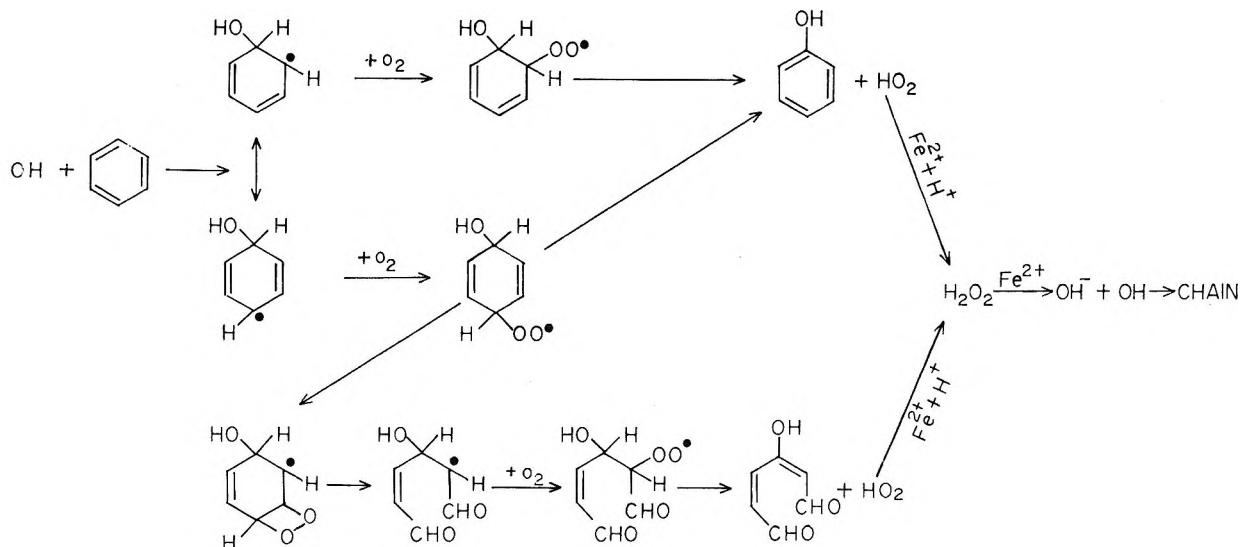
(30) F. Haber and J. Weiss, *Proc. Roy. Soc.*, A147, 332 (1934).

(31) W. G. Barb, J. H. Baxendale, P. George, and K. R. Hargrave, *Trans. Faraday Soc.*, 47, 462 (1951).

(32) W. Taylor and J. Weiss, *J. Chem. Phys.*, 21, 1419 (1953).

(33) J. H. Baxendale and J. L. Magee, *Discussions Faraday Soc.*, 14, 160 (1953).

Scheme I



and should be twice the total yield of organic product, *i.e.*, $G(\text{phenol}) + G(\beta\text{HMD})$. The two values for saturated solutions of benzene in 10^{-3} M ferrous sulfate are 32.2 and 15.4, respectively. Allowing for errors, the agreement with the requirements of Scheme I is satisfactory. Per 100 eV, the number of cycles of the chain is 15.4 while the number of hydroxyl radicals participating in the initiation is 7.4 (*i.e.*, $2.9 + 3.7 + 0.8$, being the sum of the yields of OH, HO_2 , and H_2O_2 , since the last two are converted to OH by the ferrous ion, as shown in Scheme I). Thus, each OH radical on an average gives rise to 2.1 cycles of the chain before it is reduced by a ferrous ion.

The virtual absence of an effect on the $G(Fe^{3+})$ upon addition of phenol to the Fricke dosimetric system has a simple explanation. It has been shown^{34,35} that the attack of OH on phenol produces the phenoxy radical. Understandably, the ferrous ion simply reduces this radical back to phenol and there is no chain in this case.

The Homolytic Hydroxylation of Benzene. In connection with the hydroxylation of naphthalene,¹² it has been pointed out that oxygen plays an important part. The HO_2 elimination visualized by Dorfman¹⁶ has

further support from the present work. The inclusion of this step in the mechanism of formation of β HMD is justifiable on the ground that there is a substantial gain in resonance energy in the formation of β HMD as in the case of phenol. Such a reaction has been recently suggested in the case of the α -hydroxyisopropylperoxy radical³⁶ which is an intermediate in the formation of acetone in the radiolysis of 2-propanol solutions.

There is a striking pH effect upon the course of the hydroxylation reactions (Table I). The only plausible explanation for it is a steric effect caused by the protonation of the OH adduct in the more acidic solutions and solvation of the $\cdot OH_2^+$. The *ortho* positions are thus rendered less accessible to O_2 addition and the phenol yield is reduced relative to that of β HMD.

Acknowledgment. We wish to express thanks to K. G. Deshpande and V. K. Bhalerao for numerous spectra taken toward this work.

(34) J. H. Merz and W. A. Waters, *J. Chem. Soc.*, 2427 (1949).

(35) M. Ebert and E. J. Land, *Trans. Faraday Soc.*, **63**, 1181 (1967).

(36) G. Hughes and H. A. Makada, *ibid.*, **64**, 3276 (1968).

Dye-Sensitized Photopolymerization in the Presence of Reversible Oxygen Carriers^{1a}

by Nan-Loh Yang and Gerald Oster^{1b}

Department of Chemistry, Polytechnic Institute of Brooklyn, Brooklyn, New York 11201 (Received July 11, 1969)

Addition of cobalt(II) ion to dye-sensitized photopolymerization systems changes the kinetic characteristics of the system. The induction period can be eliminated. The rate is higher than that in the absence of cobalt and remains constant throughout prolonged irradiation. Furthermore, the monomer conversion is much greater than for the conventional systems. The cobalt ion forms a reversible oxygen carrier with the electron donor and thus serves as an oxygen buffer. It is demonstrated that oxygen is necessary for the initiation process in dye-sensitized photopolymerization. The reversible oxygen carrier also enhances the rate of photoreduction of dye in the absence of monomer.

Introduction

Since the discovery of dye-sensitized photopolymerization² considerable effort has been expended to improve its quantum efficiency (for review see Section J of ref 3). The polymerization system consists of a vinyl monomer in aqueous solution and is sensitized with a photoreducible dye in the presence of an electron donor for the light-excited dye. The dye may be a member of the acridine, xanthene, or thiazine families. The electron donor may be a mild reducing agent such as ascorbic acid or may be a secondary or tertiary nitrogen compound such as ethylenediaminetetraacetic acid. The reaction is sensitive to visible light in the spectral region which the dye absorbs.

The light-excited dye is converted into a metastable species, presumably the triplet state, which thereupon abstracts an electron from the electron donor.⁴ The reduced dye, as the semiquinone, may react with ambient oxygen to give the initiating radical and the dye is regenerated.^{2a} An alternative suggestion is that the semiquinone and the oxidized electron donor serve as the initiating species.⁵⁻⁷ However, in the rigorous absence of oxygen, the dye is photoreduced to its leuco form but no polymer is produced.² Some authors⁷ contend oxygen is not necessary for dye-sensitized photopolymerization since the oxygen level was reduced to $10^{-7} M$ by flushing the system with helium and still the reaction proceeded. In the present paper it will be shown, however, that oxygen is a necessary component for the reaction.

The photopolymerization reaction, like all radical-initiated chain reactions, is inhibited by oxygen. The induction period is reduced by lowering the concentration of oxygen. If oxygen were not necessary for the initiation process, then one should remove as much of the oxygen as possible to improve the over-all efficiency. If, on the other hand, oxygen is necessary for initiation, there should exist an optimum range of oxygen concen-

tration for the greatest efficiency. The optimum range would then be where the oxygen level is low enough to eliminate the induction period and yet is sufficient to maintain the initiating processes. The best dye-sensitized photopolymerization system will be the one where the oxygen is maintained at the optimum level even as oxygen is being consumed during the course of the reaction. This would require a system in which there is a continuous supply of free oxygen in just the right amount to compensate for the oxygen being consumed in the initiation of polymerization.

In the present work the proper level of oxygen is maintained with a reversible oxygen carrier. A reversible oxygen carrier is a complex which combines with molecular oxygen when its environment is rich in oxygen and releases it when the oxygen concentration is low.⁸ In our system, the reversible oxygen carrier is a cobalt(II) complex. Many of the ligands for cobalt-oxygen carrier complexation are also electron donors for light-excited dyes.⁹ Thus, such substances may serve in dye-sensitized photopolymerization both as an electron donor and as a cobalt-complexing agent

(1) (a) Taken in part from the Ph.D. dissertation of N. L. Yang, Polytechnic Institute of Brooklyn, June 1969. Work was supported by the National Institute of Health on Grant GM 13823. (b) Address correspondence to the author at Mount Sinai School of Medicine of the City University of New York, New York, N. Y. 10029.

(2) (a) G. Oster, *Nature*, **173**, 300 (1954); (b) G. K. Oster, G. Oster, and G. Prati, *J. Amer. Chem. Soc.*, **79**, 595 (1957).

(3) G. Oster and N. L. Yang, *Chem. Rev.*, **68**, 125 (1968).

(4) G. Oster and A. H. Adelman, *J. Amer. Chem. Soc.*, **78**, 913 (1956).

(5) S. Toppet, G. Delzenne, and G. Smets, *J. Polym. Sci.*, **A2**, 1539 (1964).

(6) C. S. H. Chen, *ibid.*, **A3**, 1807 (1965).

(7) S. Chaberek and R. J. Allen, *J. Phys. Chem.*, **69**, 647 (1965); S. Chaberek, A. Shepp, and R. J. Allen, *ibid.*, **69**, 641 (1965).

(8) E. Bayer and P. Schretzmann, *Struct. Bonding* (Berlin), **2**, 181 (1967).

(9) G. Oster and N. Wotherspoon, *J. Amer. Chem. Soc.*, **79**, 4836 (1957).

for reversible oxygen binding. Since the ligand which is complexed with metal loses its electron-donating character,^{10,11} the ligand must be in excess of the cobalt(II) ion concentration.

The purpose of the present work is to demonstrate the advantages of the use of reversible oxygen carriers in dye-sensitized photopolymerization. The second purpose is to show the role of oxygen in the initiating process.

Results and Discussion

As a model system for dye-sensitized photopolymerization in the presence of reversible oxygen carriers, we have chosen methylene blue as the sensitizer, acrylamide as the monomer, and triethylenetetramine (TETA) as both the electron donor and the ligand for Co(II). Two molecules of Co^{II}(TETA) combine with one molecule of oxygen to form the oxygenated species (TETA)₂Co^{II}O₂Co^{II}(TETA) with an association constant K_{O_2} given by:

$$K_{O_2} = \frac{[(TETA)Co^{II}O_2Co^{II}(TETA)]}{[(TETA)Co^{II}]^2[O_2]} \quad (1)$$

and is observed¹² to be equal to 10^9 . Other chelating agents such as diethylenetriamine, glycylglycine, and histidine whose Co(II) complexes are known to be reversible oxygen carriers,⁸ have likewise been found by us to serve as electron donors when present in excess of the cobalt concentration.

Methylene blue was chosen because its absorption spectrum does not overlap with that of the oxygenated form of the oxygen carrier which is yellowish. Other dyes such as rose bengal are also sensitizing dyes but, because of their color, their use complicates the photometry of the system.

The photopolymerization reactions were carried out in two different conditions of oxygen control. In one series (the "closed system"), before Co(II) is added the solution is saturated with air and sealed off from the ambient atmosphere, both during the introduction of Co(II) and during the entire course of the photopolymerization. In the other series (the "aerobic system"), the solution is saturated with air after Co(II) is added. In the aerobic system the air stream also serves to oxygenate the Co^{II}(TETA) complex. In the closed system the total oxygen concentration $[O_2]_t$ is the solubility of oxygen in the aqueous solution under 1 atm of air and is taken as $2.5 \times 10^{-4} M$. After Co(II), of final concentration C , is introduced, the total oxygen concentration $[O_2]_t$ is the sum of free oxygen $[O_2]_f$ and bound oxygen $[O_2]_b$, from which, using eq 1

$$K_{O_2} = \frac{[O_2]_b}{\{C - 2[O_2]_b\}^2[O_2]_f} = 10^9 \quad (2)$$

Here we have assumed that all of the cobalt ions are complexed to the ligand which is in large excess. In

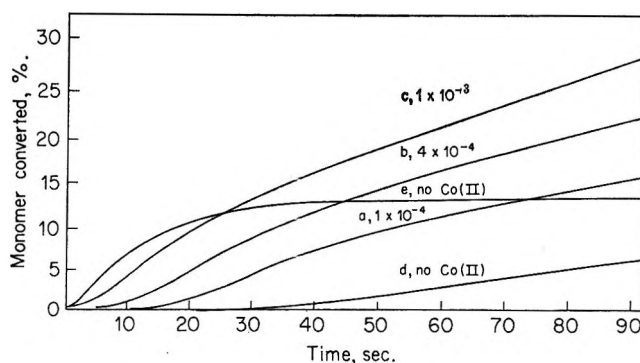


Figure 1. Monomer conversion curve for closed system. Methylene blue $5.5 \times 10^{-5} M$, acrylamide $3.8 M$, triethylenetetramine $2.0 \times 10^{-2} M$ at pH 9.6. Intensity of red light absorbed initially, 5.45×10^{-8} einstein $cm^{-2} sec^{-1}$. Numbers on curves indicate molar concentration of Co(II). See text for conditions for curve e.

the aerobic system $[O_2]_f$ is taken as being $2.5 \times 10^{-4} M$; thus

$$[O_2]_t = 2.5 \times 10^{-4} + [O_2]_b \quad (3)$$

Closed System Photopolymerization. The course of photopolymerization of the cobalt-containing system with varying amounts of the metal ion under closed-system conditions is illustrated by curves a, b, c of Figure 1. These curves differ considerably from those for the conventional (*i.e.*, Co(II) absent) system, curves d and e of Figure 1. The conventional system when not deoxygenated (curve d) exhibits a long induction period of 35 sec and even after 50 sec of irradiation achieves only 2% monomer conversion. When Co(II) is added to the conventional system, the induction period is shortened and the rate of polymerization is increased (curves a, b, and c). At a cobalt concentration of $10^{-3} M$ (curve c) the induction period is practically eliminated and after 50 sec of irradiation the monomer conversion is 20%, *i.e.* tenfold that for the conventional system under the same conditions (curve d). For the conventional system which has been deoxygenated by passing a stream of helium through the solution for 30 min just prior to the irradiation, there is also no induction period (curve e) but the rate of polymerization quickly levels off. Here after 35 sec of irradiation the extent of conversion reaches its limiting value, namely, 13%. This is in contrast to the cobalt-containing system where the polymerization proceeds with a relatively constant rate over an extended period of time of irradiation. Thus for a Co(II) concentration of $1 \times 10^{-3} M$ (curve c) in 35 sec the monomer conversion is 16% and at 90 sec the monomer conversion is 27% and continues upward thereafter. Only in the

(10) G. K. Oster and G. Oster, *J. Amer. Chem. Soc.*, **81**, 5543 (1959).

(11) J. Jousset Dubien and G. Oster, *Bull. Soc. Chim. France*, 343 (1960).

(12) O. Bekaroglu and S. Fallab, *Helv. Chim. Acta*, **46**, 2125 (1963).

very earliest stages of the reaction is the rate of conversion for the deoxygenated conventional system higher than that for the cobalt-containing system.

For the examples given in Figure 1 the ligand concentration is more than an order of magnitude greater than the Co(II) concentration. When Co(II) and triethylenetetramine are at comparable concentrations, polymerization does not take place since then the ligand ceases to function as an electron donor.

The differences in the kinetic behavior between the conventional system and the cobalt-containing system can be explained in terms of the action of oxygen in the initiation process. The conventional system which has not been subjected to deoxygenation (curve d) exhibits a long induction period due to the inhibitory effect of the excess oxygen. The conventional system which has been deoxygenated by passing helium through it (curve e) immediately polymerizes on irradiation due to the low level of oxygen initially present. The polymerization ceases, however, when all available traces of molecular oxygen are consumed in the initiating step. The cobalt-containing system, on the other hand, is equipped with an *in situ* oxygen reservoir, so to speak. Now there is no or only a short induction period (curves a, b, and c) since most or part of the total oxygen, $[O_2]_t$, is bound to the $Co^{II}(TETA)$ complex. As free oxygen $[O_2]_f$ is being depleted in the initiating step, the oxygenated complex releases its bound oxygen to the system for participation in further initiation.

The oxygen carrier functions as an oxygen buffer. In the context of the present work we define the oxygen buffer capacity as the number of moles of oxygen released from the complex per mole of free oxygen consumed in the polymerization process or, from eq 2

$$\frac{\partial [O_2]_b}{\partial [O_2]_f} = \frac{[O_2]_b}{[O_2]_f} \frac{1}{1 + 10^4 \{10 [O_2]_b [O_2]_f\}^{1/2}} \quad (4)$$

Hence as $[O_2]_f$ decreases there is an increasing tendency to release oxygen. For dilute systems the buffer capacity is approximately proportional to the concentration of the oxygenated carrier.

Aerobic Photopolymerization. In the aerobic series (Figure 2) each run has a different concentration of bound oxygen which depends upon the concentration of Co(II) the higher the limiting value of monomer conversion and the greater the steady-state rate of polymerization (curves a-d of Figure 2). In all cases, there is induction period due to the high initial free oxygen concentration. On irradiation the free oxygen is consumed in the course of the induction period and in the initiation, however, the bound oxygen is concurrently being released. The reaction ceases when all the oxygen, whether free or stored in the complex, has been consumed. The higher the cobalt concentration, the higher is the limiting monomer conversion since more oxygen is stored. Since the buffer capacity is

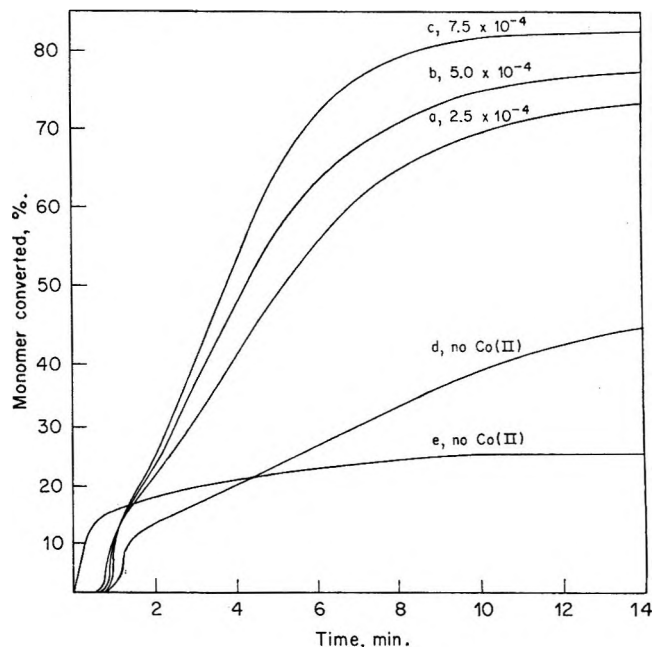


Figure 2. Monomer conversion curve for aerobic system. Concentrations and intensity of light as in Figure 1.

greater at more concentrated cobalt solutions, the steady-state rate will likewise be higher.

In the absence of cobalt, the helium-purged system (curve e) exhibits no induction period. For the air-saturated case (curve d), however, there is, of course an induction period, which has a lower rate in the early stages of the polymerization but eventually overtakes the former system since there is more available oxygen and reaches a higher monomer conversion. Here again oxygen appears to be necessary for dye-sensitized photopolymerization.

Photobleaching. In order to learn more of the role of the initiation process in photopolymerization, studies on the photobleaching (*i.e.*, photoreduction) of methylene blue in the absence of monomer were carried out. In the closed system the addition of cobalt not only greatly accelerates the initial rate of fading but also eliminates the induction period (compare curves a, b, and c with curves d of Figure 3). The rate increases with increasing amount of Co(II) when TETA is in large excess but, parallel to the polymerization studies, the reaction does not proceed when the metal ion exceeds the concentration of the ligand.¹⁰

The elimination of the induction period and the enhancement of the rate on addition of Co(II) to the closed system are due to the ability of the cobalt complex to bind free oxygen which would otherwise convert the leuco (reduced) dye back to the blue form. Indeed, the $Co^{II}(TETA)$ complex is a very effective oxygen remover in that, for example, Co(II) at a concentration of $5 \times 10^{-3} M$ lowers the concentration of free oxygen to less than $10^{-7} M$ (see eq 2). In comparison, flushing the air-saturated system with helium for 40 min is

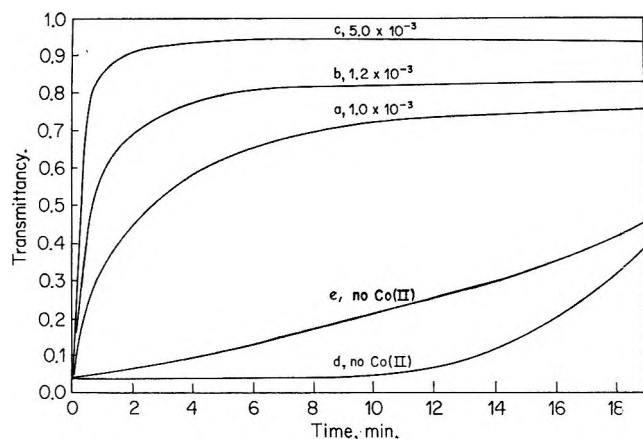


Figure 3. Photobleaching of methylene blue in closed system. Methylene blue $2.75 \times 10^{-5} M$, triethylenetetramine $7.50 \times 10^{-2} M$ at pH 7.3. Numbers on curves indicate molar concentration of Co(II). For comparison, see the Co(II)-free system purged with helium for 30 min (curve e).

two orders of magnitude less effective in removing oxygen.⁶ This is manifested in photobleaching as illustrated in curves c and e of Figure 3.

The hypothesis that the cobalt complex functions as an oxygen buffer is further borne out from observations of the spectral changes of this complex during both photobleaching and photopolymerization. The yellow color associated with the oxygenated carrier bleaches concurrently with the photobleaching of methylene blue. This is an indication of the release of oxygen from the carrier.

If, as has been contended^{6,7} the semiquinone species of the sensitizing dye and the oxidized electron donor are the initiating species, then the course of photopolymerization should parallel the course of photobleaching since these species are the primary photochemical products. That this is not the case can be readily seen by comparing the aerobic photopolymerization (Figure 2) with the aerobic photobleaching (Figure 4). For aerobic photobleaching, the addition of cobalt decreases both the rate and the limiting extent of reaction whereas the reverse is the case for photopolymerization. Increasing the cobalt concentration increases the oxygen buffer capacity and hence provides more oxygen for the reoxidation of the leuco dye; thus the rate of photobleaching is decreased. With photopolymerization, on the other hand, the reaction is enhanced since there is more oxygen available for reacting with the leuco dye to produce the initiating species.

Conclusions

The new dye-sensitized photopolymerization system is unique in that the free oxygen concentration is maintained in an optimum range for an extended period during the course of the reaction. The closed system polymerizes immediately upon irradiation without the need for usual cumbersome degassing procedures. The reaction proceeds with a constant high rate and the

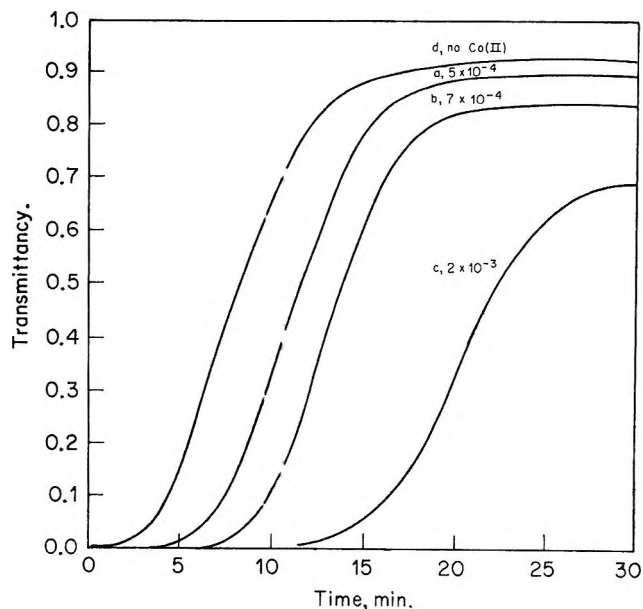


Figure 4. Photobleaching of methylene blue in aerobic system. Concentrations (but no monomer) and intensities as in Figure 1.

conversion is greater than for the conventional system. A constant rate over long irradiation time implies that if our new system is used for photography the image produced is a faithful replication of the exposure (*i.e.*, dosage of light). Still further, the new system under aerobic conditions yields much higher monomer conversions than does the conventional system. The behavior of the cobalt-containing systems clearly demonstrates that oxygen is essential for the dye-sensitized photopolymerization system described in this paper and may be the case for similar systems.

Experimental Section

Materials. Technical grade triethylenetetramine obtained from Fisher Scientific Co. was purified by vacuum distillation over sodium metal. The purified TETA was standardized by conductometric titration with standard perchloric acid.

Acrylamide from Eastman Kodak Co. was recrystallized from chloroform and stored in a refrigerator.

Methylene blue (zinc free) and cobalt(III) chloride were of reagent grade obtained from Merck Co. A stock solution of Co(II) was standardized by titration with disodium ethylenediaminetetraacetate (disodium EDTA, 0.1 M, Fisher Certified reagent) using murexide as the indicator. Helium was purified by passing the gas through a chromic chloride solution to remove trace amounts of oxygen. All other chemicals were analytical reagent grade.

Procedure. A 500-W tungsten lamp in a slide projector was used as the light source. To eliminate light below about $475 \text{ m}\mu$, a pale yellow glass filter was interposed and a heat glass filter was used to reduce radiation of wavelength above about $700 \text{ m}\mu$. To ensure uniform

illumination of the sample cell a ground-glass plate was inserted in the usual slide position of the projector. The sample was fixed 10 cm from the front of the projector. The lamp was stabilized with a constant-voltage transformer. The intensity of light falling on the sample was determined with a calibrated thermopile (Epply Laboratories).

The polymerization was followed by the thermal-rise method² and the adiabatic heat rise was followed with a thermistor unit (Yellow Spring Model 73) in conjunction with a recorder. The temperature rise was converted into monomer converted into polymer by means of a conversion factor predetermined gravimetrically. For a 20-ml aqueous solution in a cylindrical test tube 2

cm in diameter a rise of 1° corresponds to a conversion of acrylamide of 1.25×10^{-3} mol. For the aerobic system where the time of irradiation is long the sample cell was insulated to maintain adiabatic conditions.

The rate of photobleaching was followed photometrically using a red-sensitive silicon solar cell (Hoffman), the same light beam being used for the radiation and for the transmission measurements. An interference filter which transmitted maximally at 665 m μ , corresponding to the absorption maximum of methylene blue, was interposed between the sample and the light detector. An optical cell with optical path of 1 cm was used as the reaction cell.

On the Mechanism of Decomposition of Dithiocarbamates^{1a,b}

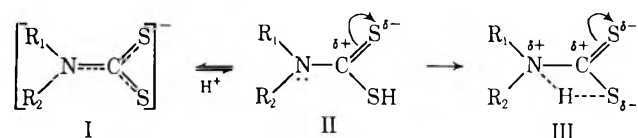
by Serge J. Joris,^{1c} Keijo I. Aspila, and Chuni L. Chakrabarti^{1d}

Department of Chemistry, Carleton University, Ottawa 1, Ontario, Canada (Received July 7, 1969)

The titration of the dithiocarbamates and the kinetics of their decomposition indicate that an intramolecular hydrogen bond exists between the sulfur and the nitrogen atoms of the dithiocarbamic (DTC) acid molecule. This intramolecular hydrogen bond is formed as soon as the sulfur atom of the dithiocarbamate ion protonates. The fractional charges resulting from the intramolecular hydrogen bond introduce a high internal energy in the DTC acids and are responsible for their great instability. This is proven by the kinetics of decomposition in mixed solvents, which also reveals the existence of a large steric effect on the solvation and on the related stability of the DTC acids. Specific solvation of the DTC acids was also detected in mixed solvents. It is also shown that the activated complex for decomposition cannot be very different from the acid form of the dithiocarbamates.

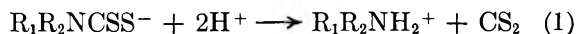
Introduction

In a previous paper² some erroneous conclusions found in the literature concerning the acidic properties of the dithiocarbamic (DTC) acids were corrected. It was proven that these acids are definitely monobasic (with the proton located on the sulfur atom) and differ therefore from the usual amino (or dithioamino) acids which are dibasic. This difference was explained² by the delocalization of the free electrons of the nitrogen in the DTC anion (model I) and by the possible formation of an intramolecular hydrogen bond in the acid molecule (see model III).



The kinetic profiles for the decomposition of the dithiocarbamates indicate that only the acid form of the

molecule decomposes. The overall equation for the decomposition is

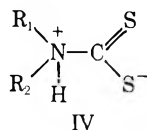


The proximity of the fractional positive charges on the nitrogen and carbon atoms in model III is obviously responsible for the decomposition of the molecule into carbon disulfide and an amine (this amine further protonates to form an ammonium ion). The zwitterion IV, which is an extreme case of model III, was initially proposed by Zahradnik and Zuman to represent the DTC acids in solution and the reactive form for their de-

(1) (a) This paper was partly presented at the 52nd Canadian Chemical Conference, Montreal, Canada, May 25-28, 1969. (b) This paper will constitute part of the Ph.D. thesis of K. I. A. (c) Postdoctorate research fellow. (d) Author to whom all correspondence should be addressed.

(2) S. J. Joris, K. I. Aspila, and C. L. Chakrabarti, *Anal. Chem.*, **41**, 1441, 1969.

composition.³ However no experimental evidence was given.



It has been reported more recently, that the steric effects in the kinetics of decomposition are difficult to explain.⁴ In this paper we discuss further the existence of an intramolecular hydrogen bond between the nitrogen and the sulfur atoms. By interpreting the kinetic data for the decomposition of the DTC molecule in mixed solvents, the present authors have established the dipolar ion (model III) as the reactive intermediate for the decomposition of the DTC molecule. This analysis has also indicated the significance of the steric effect, especially, in regard to the solvation of the DTC molecule.

Experimental Section

Reagents. The dithiocarbamic acids considered in this study were generated from their sodium salt. The diethyl-, dimethyl-, and di-*n*-butyldithiocarbamates were commercial products. The other derivatives were prepared and purified according to the procedure described in the literature.⁵⁻⁷ AR grade methanol and dioxane were used for the preparation of the water-methanol and the water-dioxane mixtures. The values of dielectric constants corresponding to these mixtures are given in Table I. The variation of the dielectric

Table I: Dielectric Constants of Mixed Solvents at 25.0°

% water in the mixed solvent	Dielectric constant for water-methanol mixtures ⁸	Dielectric constant for water-dioxane mixtures ⁹
100	78.49	78.49
90	74.21	69.75
80	70.01	61.50
60	60.92	45.10
40	51.71	28.75
20	42.60	12.40
0	32.64	2.21

constant as a function of the composition of these mixed solvents is essentially linear.^{8,9} All percentage values considered in this paper are weight percentages.

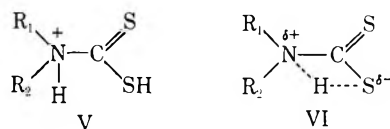
Apparatus. A modified Bausch and Lomb Spectronic 505 recording spectrophotometer was used to study the kinetics of decomposition in mixed solvents. Matched silica cells of 10-mm path length were used and maintained at a constant temperature of 25.0 ± 1°.

Procedure. Solutions of 10⁻³-10⁻⁴ M DTC acid were prepared by adding a measured amount of an unbuffered solution of the DTC salt to the mixed solvent kept in the silica cell. The mixed solvent was made

0.05 N in HCl in order to generate the DTC acid from the DTC sodium salt. At 98% methanol, the spectrum of the acid form⁴ of the dithiocarbamates was still observed. The solutions were mixed with a Teflon stirrer or a pipet bubbler; the mixing was completed within an average time of 6 sec, and the absorbance was measured immediately after mixing. In the concentration range used, the plot of log concentration *vs.* time was found to be linear and gave reproducible rate constants to within ±2%. The absorbance was measured at about 275 mμ; the actual wavelength of measurement depended on the derivative used.

Intramolecular Hydrogen Bonding in the DTC Acids

The importance of the positive charge on the nitrogen atom during the decomposition process was pointed out in the Introduction. This positive charge can only arise as a result of (1) protonation of the nitrogen atom by a proton from the solvent (model V) or (2) an intramolecular hydrogen bond by means of the proton of the sulfur acid group (model VI).



However, there is experimental evidence for the existence of structure VI; potentiometric titration and polarographic analysis have definitively shown² that the DTC molecule is monobasic and that the nitrogen atom does not accept a proton from the solution even though the decrease of the resonance in the molecule caused by protonation of the sulfur makes the nitrogen atom basic (see models I and II). An intramolecular hydrogen bond between the sulfur atom and the proximate nitrogen atom most probably prevents the free electrons of the nitrogen from being oriented toward the solvent. Thus, further protonation of the molecule is prevented. In addition, if model V were the actual reactive species, one would expect that at high pH values (*e.g.*, pH ≫ pK_s and [DTC⁻] ≫ [H⁺]), the rate of decomposition would be proportional to the square of the proton concentration since two proton atoms would be required prior to the decomposition of the DTC ion (DTC⁻) (see model V). Actually, the rate of decomposition at high pH values depends only on the first power of the

(3) R. Zahradnik and P. Zuman, *Collect. Czech. Chem. Commun.*, **24**, 1132 (1959).

(4) D. M. Miller and R. A. Latimer, *Can. J. Chem.*, **40**, 246 (1962).

(5) K. I. Aspila, V. S. Sastri, and C. L. Chakrabarti, *Talanta*, **16**, 1099 (1969).

(6) H. L. Klöpping and G. J. Van Der Kerk, *Rec. Trav. Chim.*, **70**, 917 (1951).

(7) D. J. Halls, A. Townshend, and P. Zuman, *Anal. Chim. Acta*, **40**, 459 (1968).

(8) T. Shedlowsky and R. L. Kay, *J. Phys. Chem.*, **60**, 151 (1956).

(9) S. K. Garg and C. P. Smyth, *J. Chem. Phys.*, **43**, 2959 (1965).

hydrogen concentration.²⁻⁵ The evidence²⁻⁵ is conclusive that only one protonation is required for the decomposition of the DTC anion. The requirement of single protonation on the sulfur atom and the need for a positive charge on the nitrogen to explain the decomposition can only be satisfied by the intramolecular hydrogen bond of model VI (the second proton of eq 1 is included only for the protonation of the amine released by the decomposition). Also, the anomalous acidic properties² of the dithiocarbamates suggest that the intramolecular proton bridge would be formed as soon as the sulfur atom of the DTC anion is protonated. Similar observations were made in the case of several other acids.¹⁰⁻¹⁵

One should also recognize that the zwitterion (model IV) which had been proposed by earlier workers³ is too extreme a representation for the dithiocarbamic acid in solution. Indeed, the charge on the sulfur atom would give the molecule a dibasic character and the zwitterion IV would have a much higher solubility than the DTC anion.^{16,17} Such an increase in the solubility has not been observed.¹⁸

The Transition State

The charge distribution in the dipolar acid molecule explains why only the acid form of the dithiocarbamates decomposes. A high internal energy is introduced in the DTC acids by the presence of the fractional charge on the nitrogen atom as a result of the formation of the intramolecular hydrogen bond. Therefore, one can consider that from the energetical and structural points of view, the transition state for the decomposition of the dithiocarbamates cannot be very different from the DTC acid molecule. The proximity of the fractional positive charges in the DTC acid molecule should elongate the vibrations on the N-C bond axis to such an extent that the critical bond distance for decomposition is more easily exceeded causing rupture of the N-C bond.

With the above considerations in mind, one would expect that the analogous carbamic acids would decompose even more rapidly than these dithiocarbamates. The reason for this enhanced decomposition rate is the presence of the more electronegative oxygen atom,¹⁹ which should increase the magnitude of the fractional charge on the carbon atom in the activated complex. Table II which presents the rate constants for decomposition of the DTC acids shows that they do not decompose at the same rate. As indicated by the following discussion on the solvation of the DTC acids, steric factor is responsible, to a large extent, for the wide variation in the decomposition rate.

Solvation of the Dithiocarbamic Acids

Table II shows that the rate of decomposition of the dithiocarbamic acids generally increases as a function of the bulkiness of the substituents R₁ and R₂ on the ni-

Table II: Rate Constant (sec⁻¹) for Decomposition of the DTC Acids in Aqueous Solution at pH 1.0⁶ and 25.0⁹

DTC acid	Rate constant
Monomethyl	3.50×10^{-4}
Pyrrolidine	3.55×10^{-4}
Dimethyl	4.90×10^{-2}
Di- <i>n</i> -butyl	5.76×10^{-2}
Di- <i>n</i> -propyl	6.61×10^{-2}
Diethyl	1.00×10^{-1}
Diisopropyl	1.66×10^{-1}

trogen atom. This steric effect can be explained in several ways. The increasing size of R₁ and R₂ can introduce a strain on the N-C bond as a result of an interaction with the relatively large sulfur atoms in the molecule (see Figure 1). However, such a strain should decrease, in the same manner, the stability of the DTC anion. This is not observed, probably because of the stabilization by resonance in the anion. Another point to consider is the inductive effect of the bulky alkyl groups which would enhance the nucleophilic character of the nitrogen atom. However, the very large difference in the decomposition rates of the dithiocarbamic acids listed in this paper must be due to factors more important than just mechanical strain and inductive effects. Indeed, the solvation of the fractional positive charges in the acid molecule must have a significant effect on the stability.²⁰⁻²⁷ For example, in aqueous solutions the negative end of the dipole of the solvent molecule will be located between the fractional positive charges on the nitrogen and the carbon atoms (Figure 1). This will represent the most favorable state for the

(10) S. Patai, "The Chemistry of the Amino Group," Interscience Publishers, London, 1968.

(11) R. Kuhn and K. Geider, *Chem. Ber.*, **101**, 3587 (1968).

(12) L. Ebersson, *Acta Chem. Scand.*, **13**, 224 (1959).

(13) L. Ebersson and I. Wadsö, *ibid.*, **17**, 1552 (1963).

(14) R. P. Jensen, E. M. Eyring, and W. M. Walsh, *J. Phys. Chem.*, **70**, 2264 (1966).

(15) H. M. Cardwell, J. D. Dunitz, and L. E. Orgel, *J. Chem. Soc.* **3740** (1953).

(16) E. J. Cohn and J. T. Edsall, "Proteins, Amino Acids and Peptides," Hafner Publishing Co., New York, N. Y., 1965.

(17) J. P. Greenstein and M. Winitz, "Chemistry of the Amino Acids," John Wiley and Sons, New York, N. Y., 1961.

(18) K. I. Aspila, S. J. Joris, and C. L. Chakrabarti, unpublished results, 1969.

(19) J. Hinze and H. H. Jaffé, *J. Amer. Chem. Soc.*, **84**, 540 (1962).

(20) F. E. Condon, *ibid.*, **87**, 4494 (1965).

(21) J. B. Hyne and H. S. Golinkin, *Can. J. Chem.*, **41**, 3139 (1963).

(22) D. Bethell and V. Gold, "Carbocation Ions," Academic Press, London, 1967.

(23) A. J. Parker, *Chem. Rev.*, **69**, 1 (1969).

(24) D. J. G. Ives and P. D. Marsden, *J. Chem. Soc.*, 649 (1965).

(25) L. W. Clark, *J. Phys. Chem.*, **65**, 180 (1961).

(26) M. S. Newman, "Steric Effects in Organic Chemistry," John Wiley and Sons, New York, N. Y., 1956.

(27) N. B. Chapman, J. Shorter, and J. H. P. Utley, *J. Chem. Soc.*, 1291 (1963).

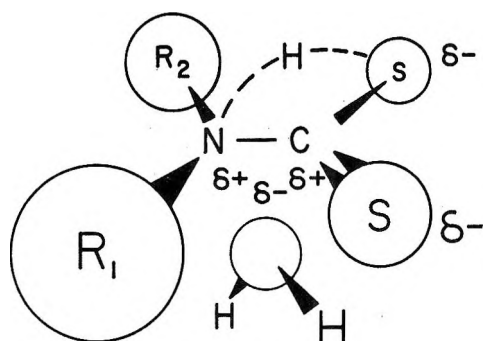


Figure 1. Masking of the fractional positive charges in the DTC acids by the solvent (H_2O) during the solvation process.

electrostatic system, composed of two positive charges attracting a negative charge²⁸ thereby lowering the potential energy of the acid molecule and would thus increase the activation energy for the decomposition, which will stabilize the acid molecule. Although such solvation is energetically favorable, one would expect the size of the substituents on the nitrogen to hinder, more or less, the solvent molecules from occupying the stabilizing position. Of all the DTC acids that have been considered, monomethyldithiocarbamic acid (MeHDTCH) should permit the most favorable approach of the solvent to the positive sites of the molecule. Indeed, this compound is observed to be the most stable. On the other hand, diisopropyldithiocarbamic acid (*i*-Pr₂DTCH) represents an extreme case of steric hindrance which prevents the solvent from solvating the fractional charges in the acid molecule. This is reflected in the very low stability of this acid. Even though in aqueous solutions the stabilization by the solvent makes the MeHDTCH almost 500 times more stable than the *i*-Pr₂DTCH, such solvent stabilization does not completely prevent these acids from decomposing (*e.g.*, MeHDTCH has a half-life of 32 min).

The importance of the stabilization of the DTC acids by solvent is substantiated by the values for activation energies⁹ which are 21.7 kcal mole⁻¹ and 12.7 kcal mole⁻¹ for MeHDTCH and *i*-Pr₂DTCH, respectively, and by the kinetic study of decomposition of these acids in mixed solvents.

Mixed Solvent Analysis

A study of the decomposition of DTC acids in mixed solvents should indicate how the repelling positive charges in model III influence the decomposition rate. The results of such a study of several dithiocarbamic acids are presented in Figures 2-4.

A decrease in the dielectric constant (ϵ) of the solvent should increase, theoretically, the stability of the DTC acids since these compounds would have lower dipole moments in a solvent of lower dielectric constant. In such cases, the activation energy to reach the transition state would be increased. Actually, an increase in the

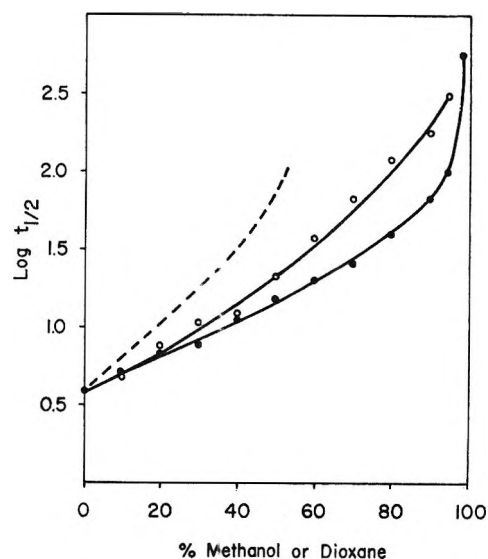


Figure 2. Variation of the logarithm of the half-life for decomposition of diisopropyl DTC acid as a function of the composition of the mixed solvent at 25.0°: ●, water-methanol mixtures; ○, water-dioxane mixtures; —, expected increase of $\log t_{1/2}$ in water-dioxane mixtures.

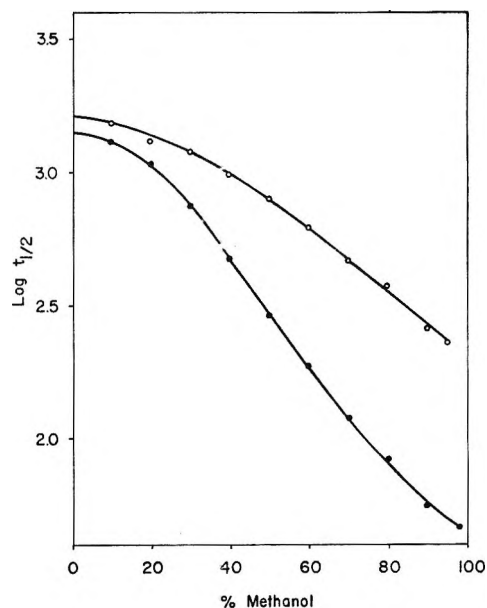


Figure 3. Variation of the logarithm of the half-life for decomposition of DTC acids as a function of the composition of the water-methanol mixed solvent at 25.0°: ○, monomethyl DTC acid; ●, pyrrolidine DTC acid.

stability corresponding to a decrease of ϵ is observed only for *i*-Pr₂DTCH (Figure 2). For other dithiocarbamates, the expected increase in the half-life for decomposition is preceded by a decrease in stability of the compounds (Figure 4). For the MeHDTCH and pyrrolidinedithiocarbamic acid (PyrDTCH), only a decrease of the stability of the acid is observed (Figure 3).

(28) R. A. Robinson and R. H. Stokes, "Electrolyte Solutions," Butterworth and Co. Ltd., London, 1959.

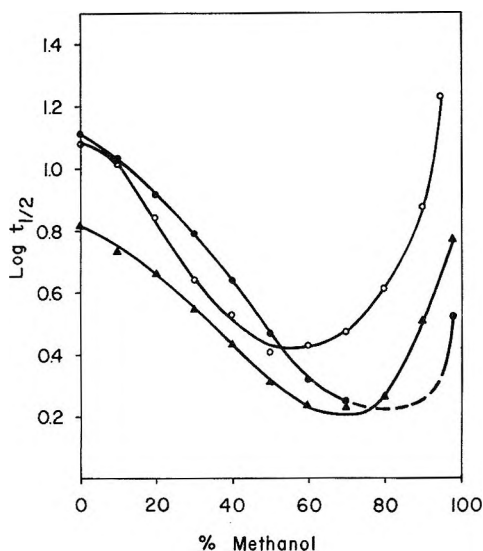


Figure 4. Variation of the logarithm of the half-life for decomposition of DTC acids as a function of the composition of the water-methanol mixed solvent at 25.0°: ●, dimethyl DTC acid; ○, di-*n*-butyl DTC acid; ▲, diethyl DTC acid.

These observations indicate, that depending on the degree of steric hindrance in the dithiocarbamates, the variation in the solvent dielectric constant can result in two different effects: stabilization or destabilization of the acid molecule. The former effect is seen in the decomposition of *i*-Pr₂DTCH; this compound is very unstable because of the lack of stabilization of the acid form by the solvent. In this case, the lowering of ϵ results only in a decrease of the dipolar charges in the DTC acid molecule by means of an inductive effect (the inductive effect would operate mainly on the fractional negative charges of the sulfur atoms since the positive centers are sterically hindered for this compound). On the other hand, for less sterically hindered compounds which enable very efficient solvent stabilization (e.g., MeHDTCH and PyrDTCH),²⁹ the lowering of ϵ affects mainly the stabilizing ability of the solvent, which is directly related to the magnitude of the dipole moment in the solvent molecule. One would notice however, that for these less sterically hindered compounds, only a decrease in the stability is observed despite the fact that the decrease of ϵ also affects the magnitude of the fractional charges in the acid molecule itself. It is therefore concluded that the stabilization of the DTC acids by solvent is the most critical factor in the decomposition process of these acids.

The result of opposing effects of ϵ on the decomposition rate is best seen in the case of the DTC acids which illustrate both effects because of their intermediate degree of steric hindrance (see Figure 4). Initially, the decrease of ϵ reduces the solvent stabilization of the acid. However, the reduction of the dipolar charges in the acid molecule gradually becomes predominant and stabilizes the acid. The location of the minimum in the

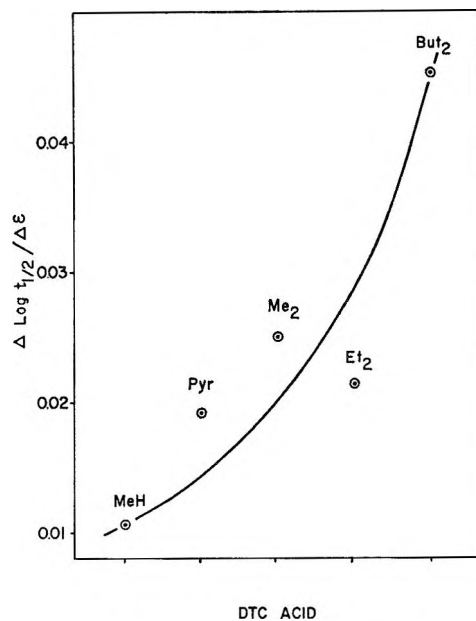


Figure 5. Influence of the bulkiness of the substituents in the DTC acids on the initial slope of the graph $\log t_{1/2}$ vs. ϵ at 25.0°.

three curves (see Figure 4) is probably determined by the effect of increasing steric hindrance to solvation. The steric hindrance increases in the order MeHDTCH < Et₂DTCH < Bu₂DTCH. The more these compounds are sterically hindered, the lower is the methanol content required (1) to nullify the stabilization by solvent and (2) to increase the half-life by reducing the dipolar charges in the acid molecule.

Specific Solvation

The initial slope of the graph $\log t_{1/2}$ vs. ϵ depends on the compound considered (see Figures 3 and 4). Figure 5 presents the values of these slopes ($\Delta \log t_{1/2} / \Delta \epsilon$) calculated, for example, between 10 and 20 wt % methanol. One qualitatively observes that the more bulky the alkyl substituents are, the higher is the value of $\Delta \log t_{1/2} / \Delta \epsilon$. In keeping with the previous conclusions, this variation indicates a more efficient decrease of the stabilization by solvent in the case of bulky substituents as ϵ is lowered. Although the slope must be related to the steric factors, one cannot ignore the possibility of the specific solvation effect that is inherent in the use of mixed solvents.³⁰⁻³⁵

(29) R. E. Marsh and J. Donohue, *Adv. Protein Chem.*, **22**, 235 (1967).

(30) C. D. Ritchie, B. A. Bierl, and R. J. Honour, *J. Amer. Chem. Soc.*, **84**, 4687 (1962).

(31) C. D. Ritchie and A. L. Pratt, *ibid.*, **86**, 1571 (1964).

(32) J. B. Hyne, *ibid.*, **82**, 5129 (1960); **85**, 304 (1963).

(33) J. B. Hyne, R. Wills, and R. E. Wonkka, *ibid.*, **84**, 2914 (1962).

(34) J. B. Hyne and R. Wills, *ibid.*, **85**, 3650 (1963).

(35) J. B. Hyne, H. S. Golinkin, and W. G. Laidlaw, *ibid.*, **88**, 2104 (1966).

It is expected that the less sterically hindered dithiocarbamic acids would favor specific solvation, since in the case of these compounds the solvent molecules can approach closely the dipoles of the solute molecule and can interact strongly with them. However, in the case of the dithiocarbamates with a high degree of steric hindrance, the forces between the solute dipoles and the solvent are less.

Some effect of specific solvation is observed in the case of *i*-Pr₂DTCH. One would expect that in water-dioxane mixtures the change in the stability of this DTC acid should be greater than in water-methanol mixtures, because of a larger change in the dielectric constant (Table I). Actually, the results in water-dioxane mixtures indicate (see Figure 2) that the increase of the stability of *i*-Pr₂DTCH in these mixtures is not as large as the increase expected from the values of dielectric constant for these mixtures (the expected increase is represented by the dashed line in Figure 2). This can be rationalized in terms of the dielectric constant around the molecule which is different from that in the bulk of the solution. In the case of *i*-Pr₂DTCH, the specific solvation most probably occurs at the sulfur atoms of the molecule since the fractional positive charges in this compound are sterically hindered by the substituents.

Further experimentation of specific solvation of the dithiocarbamic acids is in progress.

Conclusions

It has been proven that the DTC acids contain an intramolecular hydrogen bond between the nitrogen and one of the sulfur atoms of the molecule. The

intramolecular hydrogen bond is formed immediately after the dithiocarbamate ion protonates and is therefore responsible for the anomalous acidic properties of these dithioamino acids. The above definitive account clarifies the recently reported uncertainty on the nature of the DTC acids in solution.³⁶

The repelling fractional positive charges inherent in the intramolecular hydrogen-bonded structure make the acid form of the dithiocarbamates very unstable. Both energetically and structurally, the acid form of the DTC molecule cannot be very different from the transition state. However, the DTC acids can be stabilized to some extent by the solvation of their fractional charges. The stabilization caused by solvent depends largely on the size of the alkyl substituents on the nitrogen atom. The analysis of the decomposition rates in mixed solvents indicates that the dielectric constant of the medium influences the rate of decomposition in two opposing ways—(1) destabilization, by reduction of the solvation efficiency, or (2) stabilization, by reduction of the fractional charges in the acid molecule. The balance between these two effects is determined by the size of the substituents on the nitrogen atom.

This study also indicates some specific solvation of the DTC acids. Further investigation in this field is in progress.

Acknowledgment. The authors are grateful to the National Research Council of Canada and to the Ontario Department of University Affairs, for research grants.

(36) D. J. Halls, *Mikrochim. Acta*, 62 (1969).

Comparison of the Reactions of Atomic and Molecular Halogens with Silver

by R. J. McIntyre and F. K. McTaggart

Division of Mineral Chemistry, CSIRO, Port Melbourne, Victoria, Australia, 3207 (Received August 11, 1969)

Atomic chlorine, bromine, and iodine were produced in a flow system by an electric discharge. An optical interference method was developed for measuring the rate of halide film formation on silver and was used to compare the reactivity of the molecular and atomic species. This procedure enabled the existence of iodine atoms, downstream from a discharge, to be established. In contrast to the protective nature of silver halide films to halogen molecules, the rates of growth produced by halogen atoms were found to be independent of film thickness. Low activation energies and high collision efficiencies were found for the reactions with halogen atoms.

Introduction

Chlorine and bromine atoms were first produced by electrical discharge¹ in 1933 but their rapid recombination on the reaction tube walls discouraged experimentation until stimulus for further studies was provided by the realization of Ogryzlo² of the advantages of wall "poisoning" with oxyacids, and by the development of an isothermal calorimeter³ suitable for use in halogen gases.

Rosner and Allendorf^{4,5} have studied the kinetics of chlorination of nickel, molybdenum, and boron by chlorine atoms and molecules at temperatures where the reaction products are volatile. A high reaction probability was found for nickel above 1000°K but no difference was detected between the rates with chlorine atoms and molecules. With molybdenum in the temperature range 700–1100°K the reaction probability with atomic chlorine was two orders of magnitude greater than for the molecular reaction. In the same temperature range the activation energy for the molecular reaction was 13.7 kcal mol⁻¹ and for the atomic reaction was less than 5 kcal mol⁻¹. In the case of boron the rate of chlorine atom attack exceeded that of molecular chlorine 10-fold in the temperature range 1100–2200°K while the activation energies were similar for both reactions (52 kcal mol⁻¹), a result attributed to a higher sticking probability of Cl than Cl₂ on chlorine-covered boron.

The reactions of the molecular halogens with silver have been extensively reported in the literature in connection with corrosion, etc. On the other hand, silver foil has been used to detect the presence of chlorine and bromine atoms and Gurman, *et al.*,⁶ investigated the reaction of the former with silver with a view to the measurement of chlorine atom concentration. They found that the velocity of the atomic reaction was independent of the thickness of the silver chloride film produced on the surface and proportional to the concentration of chlorine atoms. The method used in these experiments involved measuring the decrease in the level of radioactivity of a silver sample when the

film of silver chloride was removed by washing. Chlorine atoms were produced by photolysis using a mercury lamp as a light source.

The following work compares the reactions of atomic and molecular chlorine, bromine, and iodine with silver using a light reflectance method for determining the thickness of the halide film produced. Because the method of study required the supply of a constant concentration of atoms for periods up to 1 hr, a preliminary investigation was undertaken to determine the operating conditions necessary to achieve this.

Experimental Section

(a) *Film Thickness Measurement.* The rate of growth of halide films on silver surfaces was followed by recording the variation in the intensity of a beam of monochromatic light reflected from the surface. Changes in intensity occur due to interference between rays reflected from the film and from the silver substrate, during growth. The change in film thickness, x , associated with the change from a maximum to a minimum of intensity is given by

$$x = \frac{\lambda}{4} (\mu^2 - \sin^2 \phi)^{-1/2} \quad (1)$$

where ϕ is the angle of incidence, λ is the wavelength of the light, and μ is the refractive index of the film.

This relationship does not apply to the first-order interference which occurs at a film thickness dependent upon the magnitude of the phase jumps occurring at the film interfaces.⁷ The phase jumps are unchanged for subsequent orders and so the increments in thickness,

(1) W. H. Rodebusch and W. C. Klingelhoefer, *J. Amer. Chem. Soc.*, **55**, 130 (1933).

(2) E. A. Ogryzlo, *Can. J. Chem.*, **39**, 2556 (1961).

(3) L. Elias, E. A. Ogryzlo, and H. I. Schiff, *ibid.*, **37**, 1680 (1959).

(4) D. E. Rosner and H. D. Allendorf, *J. Phys. Chem.*, **69**, 4290 (1965).

(5) D. E. Rosner and H. D. Allendorf, *ibid.*, **72**, 4259 (1968).

(6) V. S. Gurman, V. A. Lishnevskii, and G. B. Sergeev, *Izv. Vyssh. Ucheb. Zaved. Khim. Khim. Tekhnol.*, **1**, 29 (1960).

(7) A. B. Winterbottom, *Trans. Faraday Soc.*, **42**, 487 (1946).

given by eq 1, are constant. As the main concern of this work has been to compare rates of film growth, no correction has been made for this effect on the total film thickness. The magnitude of the correction would be about 200 Å; *i.e.*, the first order interference occurs at a film thickness approximately 200 Å less than shown on the graphs. The growth of AgI films up to 2.2 μ, AgBr up to 0.8 μ, and AgCl up to 0.4 μ thick could be monitored by this method provided the rate of growth was not too rapid. This is hereafter referred to as the interference method.

The above method was not entirely satisfactory for measurements of the rate of formation of AgBr and AgCl films because of their greater opacity, especially when film formation was rapid. An alternative method used the experimentally established fact that the change in reflectivity to polychromatic light during film growth could be represented by a simple exponential expression of the form

$$I = I_0 e^{-kt}$$

Where I is the reflected light intensity, k is a constant, and $I = I_0$ where $t = 0$, *i.e.*

$$\frac{d \ln \frac{I}{I_0}}{dt} = -k \quad (2)$$

where k is the specific reaction rate.

In cases where a linear rate of growth had been established by the interference method, the interference curves were used to obtain a relationship between I/I_0 and the film thickness

$$\frac{d \ln \frac{I}{I_0}}{dx} = -\alpha \quad (3)$$

from which the velocity of film growth v was calculated

$$v = \frac{dx}{dt} = \frac{k}{\alpha} \quad (4)$$

This is hereafter referred to as the reflection method.

(b) *Chemicals. Silver.* The silver used was made from AR silver nitrate fused at low pressure with AR sodium chloride and cast into $\frac{3}{8}$ -in. diameter rods. Spectroscopic examination indicated that, Ni, Cu, Ca, Fe, Si, and Na were present in concentrations of less than 10 ppm. Mg, Zn, Pb, Cr, Sb, As, Sn, Cd, and B were not detected.

Two methods of surface preparation were used: (1) mechanical polishing with fine abrasive and (2) abrasion down to 600 mesh paper followed by electropolishing.⁸

Argon. Welding grade argon was purified by passing over zirconium powder at 800°.

Chlorine. Commercial chlorine was passed suc-

cessively over glass wool at -30°, silica gel, and magnesium perchlorate.

Bromine. AR bromine was dried by passing the gas over phosphorus pentoxide.

Iodine. AR iodine was melted through a sintered glass disk and resublimed under vacuum.

Traces of organic impurities remaining in the gases were removed by using an auxiliary discharge applied by means of two external electrodes connected to the tuned circuit of a self-excited oscillator operating at 18 MHz, upstream from the main discharge to bring about dissociation and polymerization. This method also removed traces of oxygen from iodine by producing solid iodine oxides.⁹

Apparatus. The apparatus consisted of a Pyrex vacuum flow system coupled *via* a trap to a vacuum pump. Gases were admitted to the system through glass capillaries and could be directed either to a by-pass tube or the reaction tube by means of a three-way stopcock. Before entering the reaction tube the gases were passed through the section of tube where trace impurities were removed.

Figure 1 shows the reaction tube used for following the growth of films on the flat section of a silver rod. The main radiofrequency generator¹⁰ was a vacuum tube power amplifier excited by a crystal-controlled generator at 29 MHz. Power was controlled by a variac in the primary of the high voltage supply and the radiofrequency was coupled to the reaction tube by inserting the latter into the tuning coil of the plate circuit of the power amplifier. This coil could be moved over a distance of 20 cm. The reaction tube was supplied with a water jacket and an earth shield between the coil and the side arms holding the sample and atom detector.

Two atom detectors were used, one similar to that described by Ogryzlo,² and the other consisting of a coil of 150 cm of 40 s.w.g. nickel wire. The latter was employed for the detection of low atom concentrations. The bridge circuit was automatically balanced by means of a dc amplifier and servo motor driving a resistance in series with the bridge. A viton "O" ring seal enabled the detector coil, mounted on a glass rod, to be positioned in the reaction zone or withdrawn into the branch arm. Chlorine and bromine atom concentrations were measured satisfactorily but iodine atom concentrations were too low to measure by this method.

The sample consisted of a flat surface machined on the end of a $\frac{5}{16}$ -in. diameter silver rod which fitted into a branch arm *via* an "O" ring seal. A thermocouple passed through a small hole drilled down the

(8) W. J. McG. Tegart, "The Electrolytic and Chemical Polishing of Metals," Pergamon Press Ltd., London, 1959, p 68.

(9) D. I. Walton and L. F. Phillips, *J. Phys. Chem.*, **70**, 1317 (1966).

(10) F. K. McTaggart, "Plasma Chemistry in Electrical Discharges," Elsevier Publishing Co., Amsterdam, 1967, p 40.

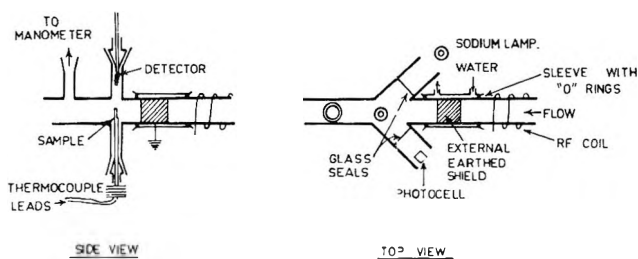


Figure 1. Reaction tube.

center of the rod to within $\frac{1}{8}$ in. of the flat surface and the sample could be heated or cooled by placing flanges attached to the end of the rod in a suitable bath. The surface of the sample was illuminated through a side arm at 45° to the reaction tube axis and the reflected light was received through an opposite branch by a cadmium sulfide photoconductive cell (Philips Type ORP60). The change in potential across a resistance in series with this cell and a battery was recorded on a chart recorder. Portions of the reaction tube and the branch arms were painted black to prevent light, other than that from the sodium lamp and the discharge, from reaching the reaction zone. An alternative arrangement enabled the sample surface to be placed parallel to the axis of the reaction tube so that light from the discharge did not strike the surface. Preliminary experiments with various sources of illumination and with the silver sample facing the discharge and at right angles to this direction, failed to reveal any evidence that photolysis was affecting the rate of film growth. In the case of atomic iodine, uneven films were produced when the sample surface was parallel to the reaction tube axis due to the already low iodine atom concentration being depleted by reaction with the leading edge.

Gases leaving the reaction zone passed through a liquid nitrogen trap and then into a second trap which also received the gases from the by-pass tube. When using Cl_2 and Br_2 the pressure in the reaction tube was measured by a sulfuric acid manometer connected between this tube and the vacuum pump. The flow rates of argon used as a diluent for I_2 and of chlorine were measured with floating ball type flowmeters and those of bromine and iodine by weighings. The flow rates of Br_2 and I_2 were controlled by using thermostated reservoirs of these elements. All joints and stopcocks were lubricated with Kel-F grease.

For work with chlorine and bromine the walls of the reaction tube, including the discharge region, were poisoned by coating with 5% phosphoric acid solution followed by heating under vacuum to 200° for 1 hr.

(d) *Conditions for Constant Atom Concentration.* Experiments with chlorine and bromine indicated that the number of atoms reached a maximum at between 0.4 and 0.5 Torr. A rapid decrease occurred when the pressure was lowered below 0.4 Torr and a slower

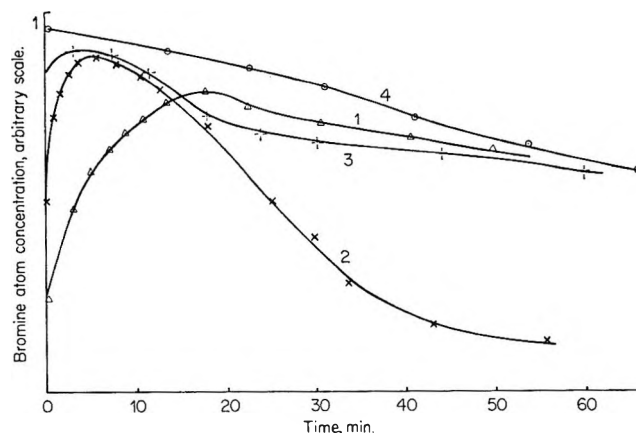


Figure 2. Effect of operating conditions on Br yield: curve 1, no pump down period, water cooled; curve 2, 5-min pump down, no water cooling; curve 3, 30-min pump down, cooling on 18 min after start of discharge; curve 4, 60-min pump down, water cooled.

decrease when the pressure was increased above 0.5 Torr. Also, the number of atoms increased with flow rate and power input. These results are similar to those found for hydrogen by Shaw;¹¹ however, with chlorine and bromine significant dissociation occurred with very low levels of power input (*e.g.*, atom concentrations were measurable with power inputs as low as 2 W). In addition, variations in the yield due to wall effects occurred which were illustrated by experiments in which the pumping down period (before initiating the discharge) and the temperature of the reaction tube walls were varied.

These experiments were carried out with chlorine and bromine, the tube being opened to the atmosphere between each run. The results for bromine at a flow rate of 4 l. hr^{-1} , pressure of 0.5 Torr, power input of 15 W, with the detector 20 cm from the end of the visible discharge, are represented in Figure 2.

An initial atom yield in proportion to the duration of the pump down period will be noted. The yield increased with time in all except curve 4 which was preceded by a 60-min pump down period. The decrease in yield following the initial increase was greatest for curve 2 in which no cooling water was used. The opening of the tube to the atmosphere always restored the original condition presumably by restoring water to the acid.

The production of a reasonably steady concentration of atoms for extended periods therefore involved operating under conditions which enabled the wall poison to retain a near-optimum water content with a low rate of evaporation, *i.e.*, a low input, low atom concentration, and cooling of the discharge tube.

(11) T. M. Shaw in "Formation and Trapping of Free Radicals," A. M. Bass and H. P. Broida, Ed., Academic Press, New York, N. Y., 1960, p. 58.

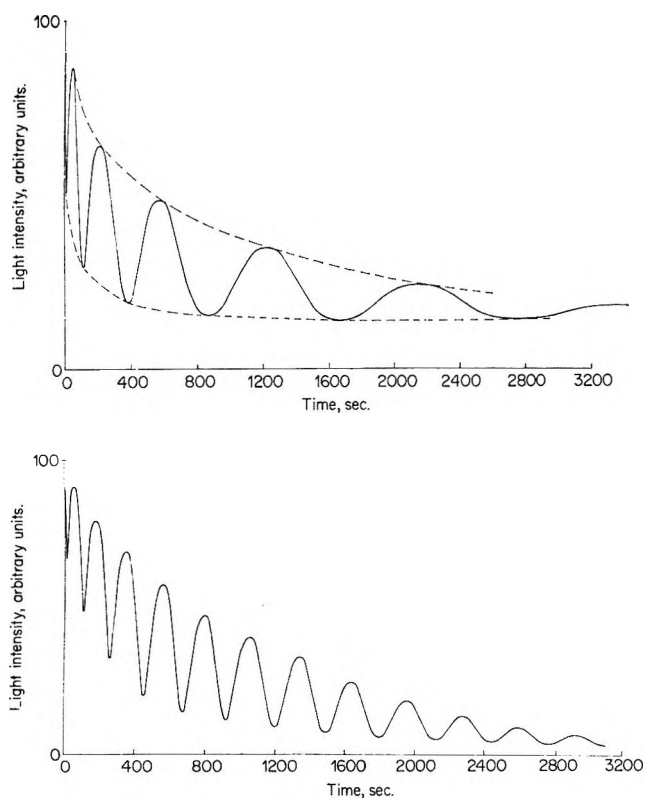


Figure 3. Variations in reflected light intensity due to interference during the growth of AgI films on silver exposed to: (a) molecular iodine, top; (b) atomic and molecular iodine, bottom.

Results

1. *Comparison of Molecular and Atomic Iodine Attack on Silver.* Using argon as a carrier gas at a flow rate of 1 l. hr⁻¹ (0.9 Torr), iodine vapor was passed over silver at 25°. Recorder traces, showing the variation in the intensity of light as AgI films formed on the surface, were made first in the absence of a discharge and then with the discharge turned on. Typical results obtained with an iodine flow rate of 0.17 g hr⁻¹ ($p_{I_2} = 0.0315$ Torr) are shown in Figures 3a and b.

The increment in AgI thickness causing a change from constructive to destructive interference was calculated from eq 1 to be 710×10^{-8} cm ($\mu = 2.2$). A correction for the asymmetry of the trace was made by taking the points of contact of the dotted curve (see Figure 3a) with the trace, for the measurement of the time at which integral increases in thickness occurred. Rate curves for the above results are shown in Figure 4.

In contrast to the simple parabolic form of the molecular rate curves, the atomic rate curves consisted of parabolic and linear components. At a certain film thickness which depended upon p_{I_2} , the contribution by I₂ to the rate of growth became negligible compared with I and interference peaks at this stage recurred at regular intervals. Further evidence for this effect was obtained by turning off the discharge

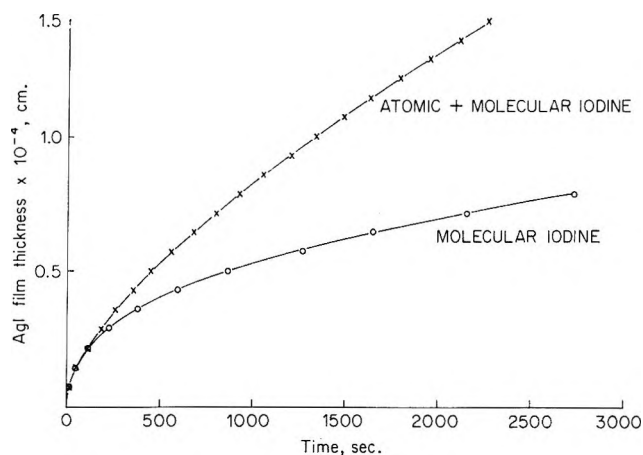


Figure 4. AgI film thickness plotted against time for molecular iodine and atomic and molecular iodine, I₂, at 0.17 g hr⁻¹.

at this point which resulted in a negligibly small rate of film growth due to I₂. The slope of the straight portion of the curve, see Figure 4, was therefore taken as the velocity of film growth due to I.

The differences between the rates of growth due to I₂ and I became more marked at lower I₂ flow rates, e.g., at an I₂ flow rate of 0.002 g hr⁻¹, $p_{I_2} = 3.16 \times 10^{-4}$ Torr, rate curves were obtained as shown in Figure 5. Assuming that all the I₂ is dissociated and the density of the AgI film is 6.01 g cm⁻³, we may calculate the reaction probability (ϵ_I) defined as the ratio of the I flux effective in producing AgI (Z_{AgI}) to the I collision flux with the film surface (Z_I) where Z_{AgI} is found from the velocity of film growth and Z_I is given by the equation

$$Z_I = p_I(2\pi MRT)^{-1/2} \text{ mol cm}^{-2} \text{ sec}^{-1} \quad (5)$$

where M is the atomic weight of I₂.

The value of 0.73 obtained for ϵ_I under the above conditions will be higher if less than 100% dissociation is assumed. It may therefore be regarded as a minimum value. The highest velocity of film growth measured for I was 11.6×10^{-8} cm sec⁻¹ obtained when the I₂ flow rate was 1.5 g hr⁻¹. Atoms were detected and the concentration was approaching that required to give 1 mW of power, the lower limit of measurement of the isothermal detector. If 1 mW of power is assumed, a maximum value of reaction probability of 0.8 is obtained. While it may be argued that both values of ϵ_I calculated above would be decreased by lower values of density due to porosity in the film, it is apparent that the reaction probability is high and that it remains high during film growth. Also the degree of dissociation of I₂ at low iodine pressures must be high.

Although generally the I₂ contributed significantly to the initial film growth rate during reaction in the presence of I, the contribution of I₂ was less than that

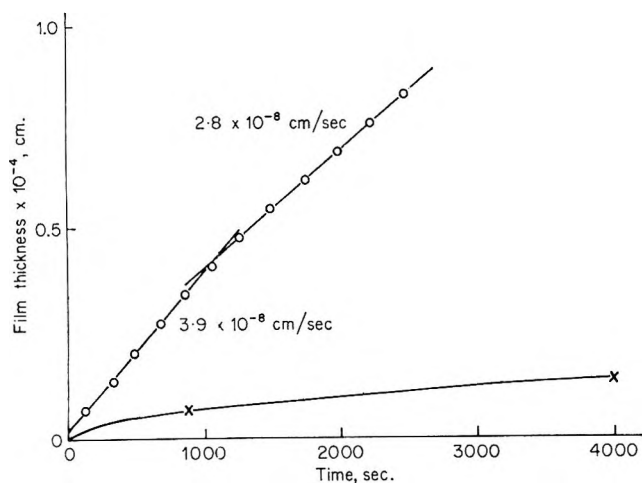


Figure 5. AgI film thickness plotted against time at a low iodine flow rate, I_2 at 0.002 g hr^{-1} .

to be expected from a simple addition of the molecular rate to the atomic rate. The further observation was made that a thick film ($5 \times 10^{-5} \text{ cm}$) produced by reaction with I_2 commenced to thicken at a constant rate when exposed to I , the rate being similar to that found for continuous growth in the presence of I at a comparable thickness.

The rate of the reaction indicated by the slope of the lines in Figure 5 appeared to change at a film thickness of approximately 4000 \AA . A similar apparent change in the parabolic rate constant k_p , defined by the equation $x^2 = k_p t$, where x is the film thickness at time t , was also noted and is illustrated by plotting film thickness against $t^{1/2}$ as in Figure 6.

Effect of Temperature. A small negative temperature coefficient was found for the parabolic rate constant in the temperature range $0\text{--}50^\circ$. No significant variation in the rate of the atomic reaction could be detected over a similar range. This result was also obtained when both I_2 and I contributed to the growth of films and may be illustrated by the three typical rate curves shown in Figure 7. These curves represent the combined action of I_2 and I on silver at the same iodine flow rate and at three different temperatures. In the initial stages of film growth the parabolic rate law predominates and the differences in the film thickness after a given time indicates the effect of temperature on the parabolic rate. As the film thickness increases, the rate of growth approaches a constant value, indicated by the slope of the nearly straight portion of the curves, which is determined mainly by the reaction of I . The negligible effect of temperature on the linear rate is consistent with the high reaction probability found for I .

Effect of Pressure. (a) *Molecular Iodine.* Measurements of k_p at a series of iodine flow rates corresponding to partial pressures in the range $0.001\text{--}0.23 \text{ Torr}$, indicated a direct proportionality with pressure.

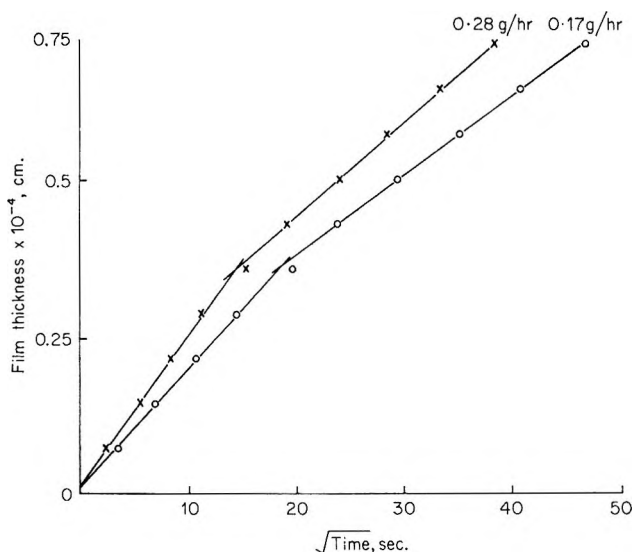


Figure 6. AgI film thickness plotted against the square root of the time for molecular iodine at different I_2 flow rates, I_2 at 0.28 and 0.17 g hr^{-1} .

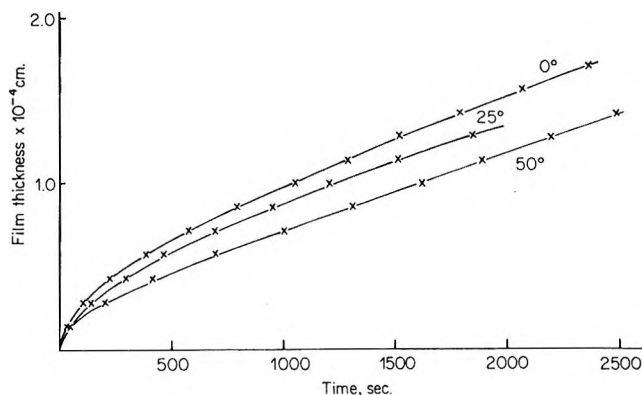


Figure 7. AgI film thickness plotted against time at constant iodine flow rate and at temperatures of 0 , 25 , and 50° , with atomic and molecular iodine, I_2 at 0.73 g hr^{-1} .

(b) *Atomic Iodine.* The I concentration was too low to measure directly by isothermal calorimeter; however the linear rate of AgI film growth, taken to be due to I , was found to increase with p_{I_2} , from a value of 3.3×10^{-8} to $11.6 \times 10^{-8} \text{ cm sec}^{-1}$ in the pressure range $0.001\text{--}0.23 \text{ Torr}$. This increase with pressure was more rapid at low than at high values of p_{I_2} .

2. *Comparison of Molecular and Atomic Bromine Attack on Silver.* Most of the experiments with bromine were performed without the use of argon as a carrier gas. The interference curves obtained were similar to those obtained with iodine in that they showed a parabolic rate law for molecular bromine and a linear rate law for atomic bromine. It was noted that below 10° , uneven film growth occurred with bromine when the auxiliary discharge was not used to remove trace impurities. In these cases the surface acquired a patchy appearance and rate curves of sigmoid form, typical of lateral growth, were recorded.

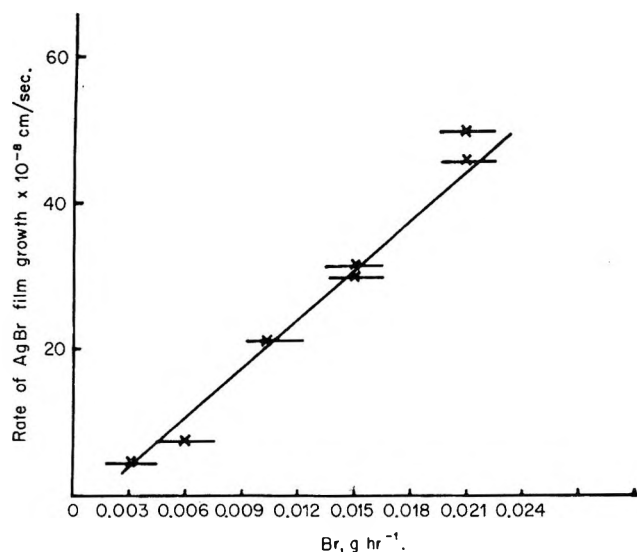


Figure 8. Linear rate constant v for the reaction of atomic bromine on silver plotted against bromine atom flow rate.

Effect of Bromine Atom Concentration on Rate on Film Growth. The use of argon-bromine gas mixtures enabled stable low atom concentrations to be obtained which were measured by means of a sensitive detector coil capable of responding to a few milliwatts placed at the position normally occupied by the sample. Having established the required bromine atom concentration the detector coil was then replaced by the silver sample and the rate of film growth measured. The results shown in Figure 8 were obtained using an argon flow rate of 1 l. hr⁻¹, Br₂ at 0.43 g hr⁻¹, total pressure 1.0 Torr, and the silver at 25°.

Assuming a density of 6.47 g cm⁻³ for the AgBr in the film, the average value of the Br reaction probability (ϵ_{Br}), defined similarly to ϵ_I , is calculated to be 0.52. After allowing for porosity we are still left with a high ϵ_{Br} and this value was maintained during film growth up to a thickness of 0.8×10^{-4} cm. Assuming 20% porosity in the film and a uniform thickness over the sample area, the rates of growth found at these low Br atom concentrations account for all the available Br. Above a Br flow of 0.1 g hr⁻¹ the rate of growth showed no further increase with Br atom concentration and a steady value of film growth was obtained; *i.e.*, excess Br atoms were being supplied.

Effect of Temperature. (a) *Molecular Bromine.* The parabolic rate constants k_p were determined at temperatures in the range 25–125° and at a pressure of 0.5 Torr by the interference method. An Arrhenius plot of the results is shown in Figure 9 from which an activation energy of 15 kcal mol⁻¹ was calculated.

(b) *Atomic Bromine.* The rate of the atomic reaction was measured in the temperature range -20 to 50° by the reflection method. The Br₂ pressure was 0.5 Torr, linear flow rate 580 cm sec⁻¹, and the Br partial pressure 0.03 Torr. This corresponded to a

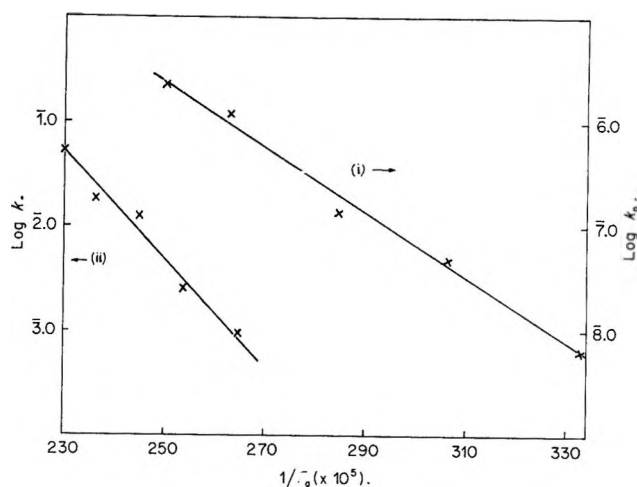


Figure 9. Arrhenius plot of the (i) parabolic rate constant (k_p) for the reaction of molecular bromine on silver and (ii) the specific reaction velocity l for molecular chlorine on silver.

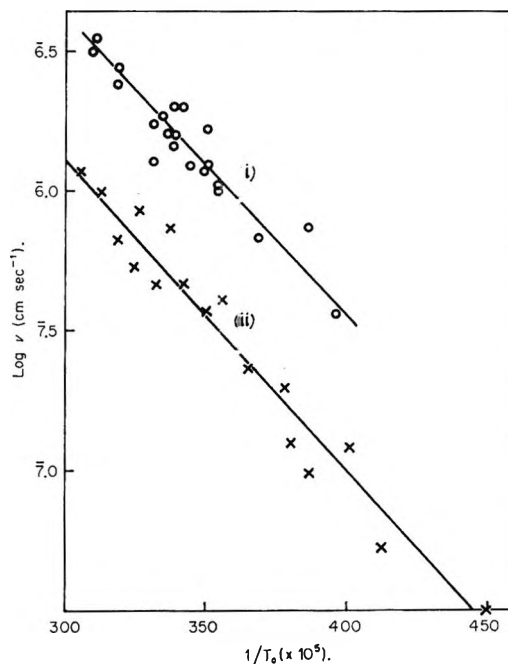


Figure 10. Arrhenius plots of the linear rate constant v for the reaction of (i) atomic bromine on silver and (ii) atomic chlorine on silver.

supply of Br of approximately 15 times the number required to produce the maximum rate of film growth observed. Values of the linear rate constants v for the atomic reaction were used to obtain the Arrhenius plot shown in Figure 10. The activation energy calculated from these results was 5 kcal mol⁻¹.

3. *Comparison of Molecular and Atomic Chlorine Attack on Silver.* Interference curves produced during the growth of silver chloride films by the action of molecular and by atomic chlorine are shown in Figures 11a and b.

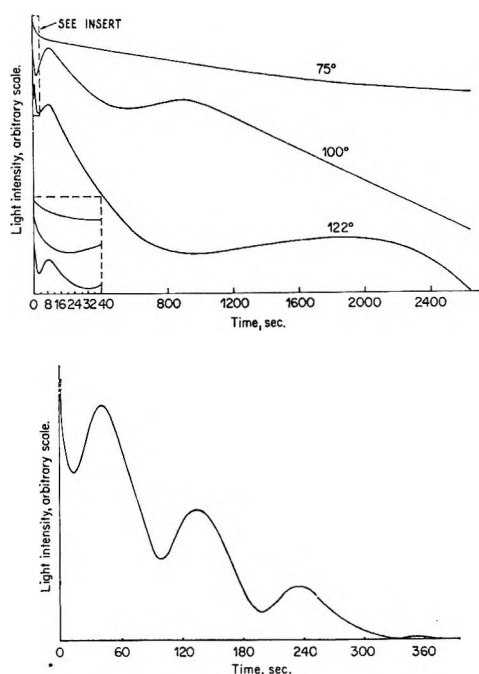


Figure 11. Variations in reflected light intensity due to interference during the growth of AgCl films on silver exposed to: (a) molecular chlorine, top; (b) atomic chlorine, bottom.

While the rate of film growth produced by Cl was again constant as found with I and Br, the molecular reaction at temperatures between 100 and 150° appeared to obey a direct logarithmic law of the form

$$x = c \ln(at + 1) \quad (6)$$

where x is the thickness at time t and c and a are constants. Values of x and t taken from the curves representing reaction at 100 and 122°, respectively, in Figure 11a were used to obtain the plots shown in Figure 12. Changes in P_{Cl_2} in the range 0.5–500 Torr did not significantly alter the rate found at several given temperatures in this range.

Effect of Chlorine Atom Concentration on Rate of Film Growth. Using a similar procedure as described for low Br concentrations, the rate of AgCl film growth was measured at low Cl concentrations. Unlike Br and I the rate of film growth for low [Cl] was found to decrease as the film thickness increased. The initial rate of growth however was proportional to the atom concentration and like Br and I indicated a high reaction probability; e.g., $\epsilon_{\text{Cl}} = 0.25$ assuming a density of 5.56 g cm^{-3} for AgCl. Above a Cl flow of approximately 0.06 g hr^{-1} the rate of AgCl film growth became steady indicating an excess of Cl atoms. Measurements of film growth rate made in the presence of an excess of Cl showed a constant rate up to thickness of 0.4μ .

Effect of Temperature. (a) *Molecular Chlorine.* No visible film was observed on the silver surface exposed to Cl_2 at room temperatures for lengthy periods at 0.5 Torr pressure. However changes in the reflectivity

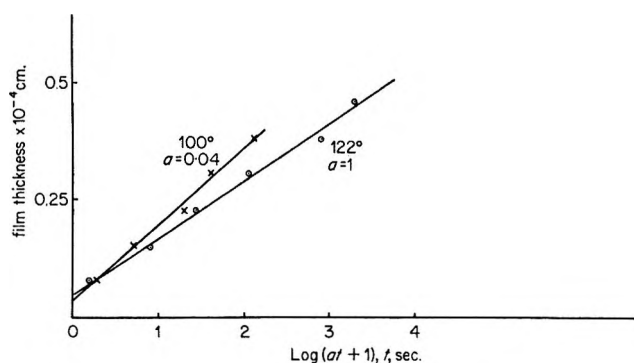


Figure 12. Values of AgCl film thickness x and time t obtained from the curves shown in Figure 11(a) representing reaction at 100 and 122° are shown plotted in the form x vs. $\log(at + 1)$.

were recorded which indicated the formation of a thin highly protective film within a few minutes of exposure. The reflectivity method was used to measure changes in the rate of film formation in the temperature range 100–160°. An activation energy of 22 kcal mol^{-1} was obtained from these results; see Figure 9.

(b) *Atomic Chlorine.* The growth rate of AgCl was measured when p_{Cl_2} was 0.45 Torr, linear flow rate 190 cm sec^{-1} , and p_{Cl} 0.02 Torr, corresponding to a fivefold excess of Cl over that required to produce the maximum rate of film growth observed. An Arrhenius plot of the results is shown in Figure 10.

An activation energy of approximately 5 kcal mol^{-1} was calculated for this reaction.

General Observations. In the foregoing results the measurements of film growth rate were made on surfaces prepared by mechanically polishing and by electropolishing. The type of surface preparation made no significant difference to the rate of growth the halide films.

The films produced by atomic halogens gave the surface a more matte appearance than those produced by molecules.

Discussion

Wall Poisoning. Wall "poisons" such as water, oxyacids, "Drifilm," etc., have long been recognized as effective agents for increasing the downstream concentration of various atoms obtained from electrical discharges. Also traces of impurities in the gas stream are often found to increase the yield of atoms substantially above those obtained from highly pure gases. Earlier theories as to the mechanism of the latter effect assumed the formation of short-lived intermediate compounds, but more recently Kaufman, *et al.*,¹² have ascribed the influence of such impurities to their adsorption on the walls and the subsequent change in the surface recombination efficiency; *i.e.*, they func-

(12) F. L. Kaufman, *et al.*, "Chemical Reactions in Electrical Discharges," American Chemical Society, Washington, D. C., 1969, Chapter 3.

tion as wall poisons. In the case of the halogen atoms it has been established that water molecules are efficient third bodies for atom recombination in the gas phase and that oxyacids on the walls act as poisons.

Our results pointed to there being an optimum value of water content in the oxyacid used *above* which water molecules evaporating into the gas phase became significant as third bodies for gas-phase recombination, and *below* which the wall-poisoning effect decreased. Loss of water molecules was caused initially by pumping at the working pressure and the atom yield rose with time to a maximum value. Thereafter further loss could result from heating due to atom recombination and the atom yield slowly decreased. Cooling of the reaction tube resulted in an almost uniform atom yield for periods sufficiently long for experimental runs. It appears reasonable therefore to conclude that the efficacy of the oxyacids as wall poisons depends on the hydrophilic character they confer to the surface thus enabling a relatively high surface concentration of water species to coexist with a low gas-phase concentration.

Formation of Halide Films. Early work on the growth of halide films on silver at temperatures of 200–400° established that a parabolic rate law applied and provided evidence to support the cationic diffusion mechanism proposed by Wagner.¹³ More recently it has been claimed that this mechanism is also operative down to room temperature,^{14,15} although the supporting data are less convincing. In the present work the rate law for Cl₂ is a logarithmic rather than a parabolic one and the activation energy we found for the reaction (22 kcal mol⁻¹, 100–150°) is substantially higher than the activation energy of cationic conduction in AgCl calculated from results obtained by Compton¹⁶ (8.4 kcal mol⁻¹) for the same temperature range and indicates that a different mechanism becomes effective below 150°. This change could be due to impurities which are known to have a marked effect on the diffusion mechanism in silver halides and are reported to become more effective in AgCl below 150°C.¹⁷ While the rate of growth of AgBr and AgI films follow parabolic laws, the films are polycrystalline and porous and as the ionic conductivity at low temperatures is a structure-sensitive property¹⁸ any comparison of parabolic rate constants with values calculated from Wagner's theory would need to take account of this fact. From this and other considerations the similarity in the values of activation energy of the bromine reaction at temperatures of 25–125° to that of the cationic conductivity of Ag in AgBr¹⁷ does not necessarily support a Wagner-type mechanism. On the other hand the direct proportionality between the parabolic rate constant and I₂ pressure would appear to contradict the existence of this type of mechanism in the case of AgI film formation at low temperatures.

We observed an apparent small change in the rate

during the growth of AgI films at a thickness of approximately 0.4×10^{-4} cm (see Figures 5 and 6) which is accompanied at a slightly greater thickness by an increase in the light-scattering coefficient of the film. The rate change may be an apparent one due to structural changes in the film affecting the optical method of measurement or such changes could be responsible for actual variations in rate. Similar behavior was indicated with AgBr films but could not be established unequivocally due to the greater opacity of the films.

The only linear film growth rates previously noted for molecular halide reactions with silver occurred when traces of H₂O and CCl₄ were present¹⁴ and much smaller rates than those for the pure halogen vapors were obtained. In these cases the rate-determining factor was attributed to phenomena occurring at the film-gas interface. The results presented here for the halogen atoms show that linear rate laws apply for Cl, Br, and I, respectively. At low atom concentrations, first-order kinetics appear to be obeyed and the reaction probability of the atoms is close to unity; furthermore, this very high value is maintained over considerable film thickness except for a relatively small decrease in the case of Cl. At high atom concentrations the rates for Cl and Br are independent of film thickness up to the limits allowed by the method and are several orders of magnitude greater than those obtained at any appreciable film thickness for the molecules. Despite the slight difference in appearance of films formed by atoms and molecules, respectively, the rates of film growth do not depend on the species used for the initial film formation. Thus all films afford considerable protection to further attack by halogen molecules but are penetrated with considerable ease by halogen atoms, and the kinetics suggest control at the silver-silver halide interface.

Previously it was noted that halide films formed by molecular halogens on silver are porous. It is probable that the films formed at lower temperatures and more rapidly by atomic attack are no less porous and that the passage of atoms occurs through the labyrinth of crystallite boundaries, subboundaries, and other structural imperfections which account for the porosity. The Pilling-Bedworth¹⁹ ratios for AgCl, AgBr, and AgI are 2.5, 2.8, and 4.0, respectively, and the growth of films from the *metal* surface with the

(13) C. Wagner, *Z. Phys. Chem.*, **32B**, 447 (1936).

(14) D. M. Smythe and M. Cutler, *J. Electrochem. Soc.*, **106** (2), 107 (1959).

(15) J. L. Weininger, *ibid.*, **105**, 577 (1958).

(16) W. D. Compton, *Phys. Rev.*, **101**, 1209 (1956).

(17) R. J. Friauf, *ibid.*, **105**, 843 (1957).

(18) J. W. Mitchell in "Chemistry of the Solid State," W. E. Garner, Ed., Butterworth and Co. London, Ltd., 1955, p 316.

(19) N. B. Pilling and R. E. Bedworth, *J. Inst. Metals*, **29**, 529 (1923).

resulting intrusion of large volumes of products at this location might be expected to cause considerable disruption of the film compared with growth from the film-gas interface which would occur if a Wagner-

type mechanism prevailed. Further work which should establish whether in the case of halogen *molecules*, the growth occurs at the halogen-silver halide or the silver halide-silver interface, is planned.

Mass Spectrometric Investigation of the Fragmentation Pattern and the Pyrolysis of Borane Carbonyl¹

by O. Herstad,² G. A. Pressley, Jr., and F. E. Stafford

Department of Chemistry and the Materials Research Center, Northwestern University, Evanston, Illinois 60201
(Received July 14, 1969)

Borane carbonyl, BH_3CO , and its pyrolysis have been investigated using a mass spectrometer as the detector of a molecular beam issuing from a flow reactor. The high resolution of the instrument and a movable beam defining slit made it possible to distinguish between residual background, background caused by the effluent from the reactor, and the molecular beam molecules (*i.e.*, pyrolysis effects in the ion source were eliminated) and also to discern reactive intermediates. The first mass spectrum of BH_3CO free of pyrolysis products is reported as well as a clear-cut identification of borane, BH_3 , formed in the pyrolysis. Pressures of BH_3 about six times greater than that of the other product, B_2H_6 , were obtained. This confirms the identification and the mass spectrum of BH_3 formed from B_2H_6 . The ion BHO^+ was observed at high temperature and may be due to BH_2OH .

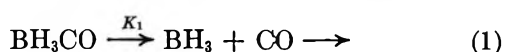
Introduction

Borane, BH_3 , has long been postulated as a reactive intermediate in formation and dissociation processes for polyboranes and other borane compounds.³⁻⁶ However, the only direct identifications of BH_3 have been by mass spectrometry.⁷⁻⁹ Of these, only one paper reports a mass spectrum of BH_3 , in that case produced from B_2H_6 .⁹

To our knowledge, at least three laboratories have attempted to use various optical spectrometric techniques including matrix isolation to identify BH_3 produced by pyrolysis or flash techniques from a variety of compounds; none has yet been successful enough to publish.

In addition, mass spectrometry involves ionization, fragmentation, and possibly excitation. In particular, the process B_2H_6^* (excited) $\rightarrow \text{BH}_3^+$ could account for the results of Baylis, *et al.*⁹ Therefore, means were sought to produce BH_3 in high yield and to replicate the mass spectrum of BH_3 produced from a source other than B_2H_6 .

Borane carbonyl has been extensively investigated^{8,10-14} and seemed to be a propitious starting material because of its reported pyrolysis mechanism¹⁰⁻¹⁴



and because of a previous mass spectrometric study⁸ of its pyrolysis from which was reported formation of BH_3 .

Neither a mass spectrum of BH_3CO free of pyrolysis

(1) Supported by the United States Atomic Energy Commission, Document No. COO-1147-31. The acquisition and maintenance of the mass spectrometer facility was made possible by grants from the Materials Research Center, the AEC, and the University. Presented at 3rd Great Lakes Regional Meeting of the American Chemical Society, Northern Illinois University, DeKalb, Ill., June 5, 1969.

(2) Institute of Inorganic Chemistry, Technical University of Norway, Trondheim, Norway.

(3) R. M. Adams, "Boron, Metallo-Boron Compounds and Boranes," Interscience Publishers, New York, N. Y., 1964.

(4) R. T. Holzmann, "Production of the Boranes and Related Research," Academic Press, New York, N. Y., 1967.

(5) W. N. Lipscomb, "Boron Hydrides," W. A. Benjamin, Inc., New York, N. Y., 1963.

(6) A. E. Stock, "Hydrides of Boron and Silicon," Cornell University Press, Ithaca, N. Y., 1933.

(7) T. P. Fehlner and W. S. Koski, *J. Amer. Chem. Soc.*, **86**, 2733 (1964).

(8) T. P. Fehlner and W. S. Koski, *ibid.*, **87**, 409 (1965).

(9) A. B. Baylis, G. A. Pressley, Jr., and F. E. Stafford, *ibid.*, **88**, 2428 (1966).

(10) A. B. Burg, *ibid.*, **74**, 3482 (1952).

(11) S. H. Bauer, *ibid.*, **78**, 5775 (1956).

(12) Y. C. Fu and G. R. Hill, *ibid.*, **84**, 353 (1962).

(13) M. E. Garabedian and S. W. Benson, *ibid.*, **86**, 176 (1964).

(14) G. W. Bethke and M. K. Wilson, *J. Chem. Phys.*, **26**, 1118 (1957).

or other impurities (except for a preliminary result from this laboratory¹⁵) nor that of BH_3 produced from it has been reported.

Subsequent to the start of our work Fehlner and Mappes¹⁶ reported a reinvestigation of the BH_3CO pyrolysis at higher pressures and longer contact times than those to be reported on below. Diborane was observed in large quantities, but BH_3 was barely discernible.

In this paper is reported a reinvestigation of the pyrolysis of BH_3CO in a flow reactor. The dissociation of BH_3CO and the reaction products, including intermediates, have been studied as a function of temperature by means of molecular beam mass spectrometry. In addition to the study of the dissociation process, the molecular beam fragmentation pattern (*i.e.*, that free of effects of pyrolysis) of BH_3CO has been determined and is reported for the first time.

Experimental Section

Borane carbonyl was synthesized using the method of Burg and Schlesinger,¹⁷ as modified by J. C. Carter,¹⁸ by treating B_2H_6 with CO at 20 atm. Diborane (96% ^{10}B and 4% ^{11}B) was prepared by the LiAlH_4 reduction of $^{10}\text{BF}_3 \cdot \text{Et}_2\text{O}$. Borane carbonyl thus produced was purified by trap-to-trap distillation in an all-glass apparatus and stored at -196° (liquid N_2). During the experiments, the sample was kept in a Pyrex container at -160.5° (isopentane slush), at which temperature the pressure of BH_3CO is 4×10^{-2} Torr.¹⁷ At the entrance of the inlet system the pressure was reduced by a metering valve to 7×10^{-4} Torr, as determined from the ratio of ion intensities at the opening used and at the full opening of the valve. The rest of the inlet system, the furnace, the movable beam defining slit (called the "shutter"), and the ion source region were the same as described earlier.⁹ The only change was that the reactor in this case was made of molybdenum (instead of stainless steel) and had a lid with a knife-edged slit of 0.2 cm^2 , giving a calculated¹⁹ contact time of 1.8 msec.

The molecular beam effusing from the reactor usually was ionized by 70-eV electrons except when appearance potential measurements were made. The ions formed were accelerated through 4000 V, mass analyzed, accelerated through an additional 3200 V, and detected by a 20-stage Cu-Be secondary electron multiplier.

Appearance potentials (AP) were measured by the vanishing current method, using ionization efficiency curves made automatically with an X-Y recorder.²⁰ Argon, leaked directly into the mass spectrometer, was used as the calibrant.

Identifications of ions and their neutral progenitors were accomplished using mass number, mass defect, isotopic ratios, shutter effect,^{21,22} and intensity variation as a function of temperature.

All ion current readings at "centered" and "displaced" shutter settings were time averaged. These averages and the instrument settings were read directly into a DEC (Digital Equipment Corporation, Maynard, Mass.) PDP-8/S digital computer which was programmed to calculate total ion current (amperes), net molecular beam ion current, shutter percentage,²¹ "grid" currents, and gain. These data were immediately printed out on a Teletype, and were also stored in core or on a disk memory so they could later be put out on tape for further calculations in the University's central computer facility.

Data and Results

Fragmentation Pattern of BH_3CO . The fragmentation pattern of $^{10}\text{BH}_3\text{CO}$ was determined from the mass spectra obtained with the reactor at temperatures of 290–450°K, over which range it remained nearly constant and where no thermal decomposition could be observed.

Shutterable mass peaks were observed in three mass regions: (1) $m/e = 42, 41, 40, 39$, and 38; (2) $m/e = 24, 23$, and 22; (3) $m/z = 13, 12, 11$, and 10. That part of the mass spectrum assigned to BH_3CO , and in some cases stripped of contributions from trace amounts of B_2H_6 , is given in Table I.

The entire mass range $m/e = 43$ to 75 was searched. No peaks were observed our detectability limit was 0.05% of the reference peak.

Region (1) can then be assigned to the ions BH_3CO^+ , BH_2CO^+ , BHCO^+ , and BCO^+ . The major molecular beam mass peak in this group is at $m/e = 39$ (mainly $^{10}\text{BHCO}^+$); $m/e = 42$ is due to the ion species $^{11}\text{BH}_3$ - $^{12}\text{CO}^+$ and $^{10}\text{BH}_3$ - $^{13}\text{CO}^+$. The measured ratio $I(42^+)/I(41^+)$ was 0.047, compared to 0.049 calculated from the isotopic contributions of $^{11}\text{B}^{23}$ and $^{13}\text{C}^{24}$ (4% ^{11}B and 1.1% ^{13}C).

(15) Private communication. Earlier measurements on BH_3CO done at this laboratory by S. M. Schilderout.

(16) Private communication. Preliminary report on the thermal decomposition of borane carbonyl, BH_3CO , by T. P. Fehlner and G. W. Mappes, Aug 1968; *J. Phys Chem.*, **73**, 873 (1969).

(17) A. B. Burg and H. I. Schlesinger, *J. Amer. Chem. Soc.*, **59**, 780 (1937).

(18) J. C. Carter, Ph.D. Thesis, University of Michigan, Ann Arbor, Michigan, 1961.

(19) S. Dushman, "Scientific Foundations of Vacuum Technique," 2nd ed, revised by J. M. LaFerty, John Wiley & Sons, Inc., New York, N. Y., 1962.

(20) R. J. Loyd and F. E. Stafford in "Mass Spectrometry in Inorganic Chemistry," Advances in Chemistry Series, No. 72, American Chemical Society, Washington, D. C., 1968, pp 127–136.

(21) The movable beam defining slit ("shutter"), located between the crucible orifice and the ion source, permitted differentiation of species originating from the crucible, the crucible lip, the radiation shields, and the residual background gases. The ratio of molecular beam to total ion intensity at a given mass peak is called the "percentage shutter effect." Highly reactive species, which are expected to be destroyed by every collision with the vacuum chamber walls, have high shutter effects (~100%), while stable species have small ones (*e.g.*, 5–10% for Ar at these temperatures).

(22) F. E. Stafford, G. A. Pressley, Jr., and A. B. Baylis, ref 20, pp 137–152.

Table I: Observed and Stripped Molecular Beam Mass Spectra of BH_3CO

m/e	96% ^{10}B , rel intensity	Ion	Rel int ^a
42	2.6		
41	62.0	$^{10}\text{BH}_3\text{CO}^+$	59.
40	83.0	BH_2CO^+	79.
39	100.0	BHCO^+	100.
38	0.86	BCO^-	0.86
24	0.15	BH_2C^+	0.10
23	1.2	BHC^+	1.2
22	0.6	BC^+	0.6
13	1.1	BH_3^+	$\sim 0^b$
12	28.1	BH_2^+	28.
11	14.5	BH^+	14.3
10	6.4	B^+	6.4

^a Calculated from column 2 assuming 4% ^{11}B . See ref 23.

^b See text.

Mass peak 23 was the most intense peak in mass region (2). The intensity of mass peak 25 was not measurable except during the first experiment after changing to a new sample of $^{10}\text{BH}_3\text{CO}$. Since mass peak 25 is the major peak in the molecular beam mass spectrum of $^{10}\text{B}_2\text{H}_6$,⁹ this behavior indicates that a small amount of diborane was present initially as an impurity. Consequently mass peaks 24, 23, and 22 were assigned to the ionic species $^{10}\text{BH}_2\text{C}^+$ (isoelectronic with CN^+ and C_2), $^{10}\text{BHC}^+$, and $^{10}\text{BC}^+$, respectively. These assignments agree with those of Fehlner and Koski,⁸ who were unable to report relative intensities. In mass region (3), the ratios $I(10^+)/I(39^+)$, $I(11^+)/I(39^+)$, $I(12^+)/I(39^+)$, and $I(13^+)/I(39^+)$ were nearly constant below 500°K, indicating that these mass peaks are due to the fragments B^+ , BH^+ , and BH_2^+ from BH_3CO . The BH_3^+ ion seems not to be formed by fragmentation of BH_3CO since the measured ratio $I(13^+)/I(12^+) = 0.037$ is smaller than that calculated from the nominal isotopic contribution of 4% ^{11}B , specified by the supplier.²³ The monoisotopic molecular beam mass spectrum calculated, assuming 4.0% ^{11}B , of $^{10}\text{BH}_3\text{CO}$ is given in Table I, column 4.

Thermal Dissociation of BH_3CO . The thermal dissociation of BH_3CO started at about 500°K, as seen from the drop in the intensity of $m/e = 39$ ($^{10}\text{BHCO}^+$) in Figure 1. Above this temperature the intensities of the mass peaks 38, 39, 40, 41, and 42 all dropped steadily with increasing temperature. However, a slight change (Figure 2) in the ratio $I(41^+)/I(39^+)$ was observed just below the temperature where the pyrolysis started, dropping from 0.62 (the value obtained in the low temperature range) to about 0.55 in the pyrolysis range. Similar changes were not observed for the other intensity ratios as seen from Figure 2.

Above 500°K, where the intensities of the fragments from BH_3CO were decreasing, the intensities of the mass peaks 22, 23, 24, 25, and 26 increased, reached a maxi-

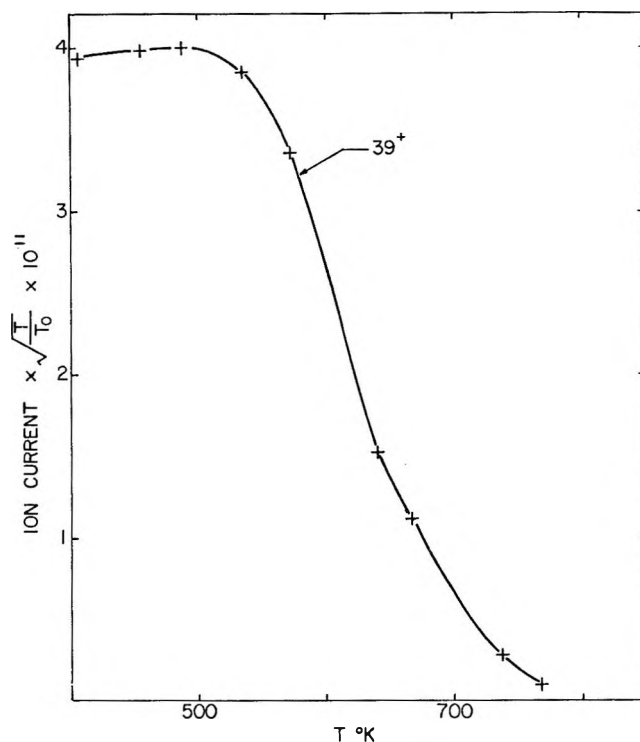


Figure 1. Variation in ion current $\times \sqrt{T/T_0}$ with reactor temperature. T is the variable temperature and T_0 is a reference temperature (404°K). The factor $\sqrt{T/T_0}$ is introduced to correct for changing molecular beam velocity with temperature.

um at about 700°K, and fell off rapidly at higher temperatures as shown in Figure 3. The measured ratios $I(24^+)/I(25^+) = 0.48$ and $I(22^+)/I(25^+) = 0.56$ are in fair agreement with the respective values 0.44 and 0.52 obtained for diborane at this laboratory.⁹

The observed ratio $I(26^+)/I(25^+) \cong 0.2$ over the range 500–740°K. This is about three times that reported for diborane,⁹ indicating possibly that a small amount of another neutral species contributed to mass peak 26. However, the low absolute intensity of mass peak 26 makes measurement of its relative intensity uncertain. Thus, the molecular beam ion intensities at mass peaks 22, 23, 24, 25, and probably 26 are assigned to ion fragments from diborane in the pyrolysis region above 500°K.

Mass peak 27 also was shutterable above 500°K, and increased rapidly with temperature without reaching a maximum at 700°K as shown in Figure 3 (see also the figure caption). The ratio $I(27^+)/I(26^+)$ increased from about 2 at 500°K to 23 at 739°K at which temperature it has a 30% shutter effect. This shows that the neutral species giving rise to the ion current at m/e

(23) Analysis given by the supplier, United States Atomic Energy Commission, Oak Ridge, Tenn., claims a minimum of 96% ^{10}B . Therefore, the concentration of ^{11}B may be less than 4% in some samples.

(24) "Chart of the Nuclides," Knolls Atomic Power Laboratory, Naval Reactors, U. S. Atomic Energy Commission 9th ed, Revised to July 1966.

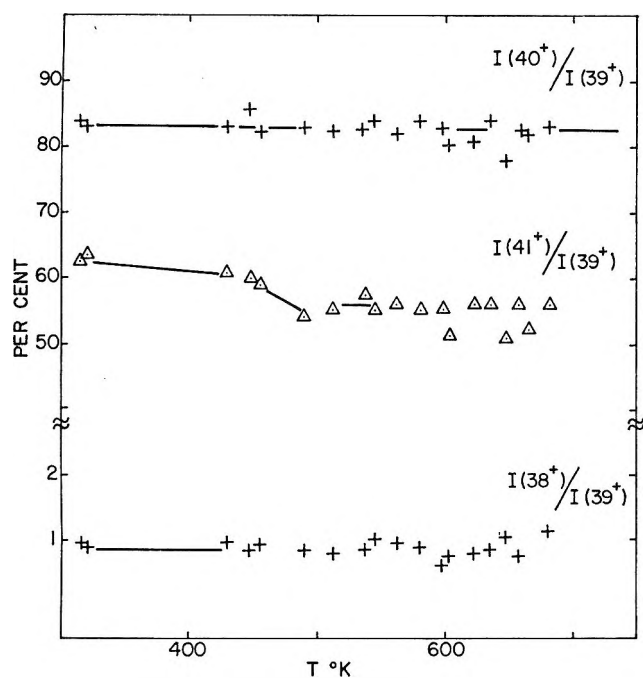


Figure 2. Relative ion intensities at m/e 38, 40, and 41 as percentages of m/e 39 vs. temperature.

27 makes little or no contribution to the current at mass peak 26. In experiments in which $^{10}\text{BH}_3\text{CO}$ and $^{11}\text{B}_2\text{H}_6$ were admitted simultaneously (see below), this peak was observed to grow in just down of mass $^{11}\text{B}_2\text{H}_5^+$. Accordingly, this peak at m/e 27 formed from a pyrolysis product of $^{10}\text{BH}_3\text{CO}$ is assigned to the ion $^{10}\text{BHO}^+$. The excess intensity observed at $m/e = 26$ (relative to $I(25^+)$) may be due to $^{10}\text{BO}^+$, but this must be formed independently of $^{10}\text{BHO}^+$.

The molecular beam intensities at m/e 10, 11, 12, and 13 increased both absolutely and relatively. The ratio $I(13^+)/I(12^+)$ increased from 0.037 to 0.36. Since the only known borane that gives any appreciable BH_3^+ on fragmentation is BH_3 , this is strong evidence for the formation of monoborane.

In addition to the increasing intensities of the mass peaks in the monoborane region, their shutter percentages²¹ increased strongly with temperature as shown in Figure 4. This also points clearly to BH_3 neutral. The shutter percentage for mass peak 13 is expected to be 100% if no other ion species contribute to that peak. In this case, however, $^{11}\text{BH}_2^+$ from BH_3CO was not resolved from the $^{10}\text{BH}_3^+$.

By using the known mass spectra of B_2H_6 and BH_3CO to subtract out the contributions due to fragmentation of BH_3CO and B_2H_6 we deduce the mass spectrum of BH_3 . The monoisotopic mass spectrum of $^{10}\text{BH}_3$ is obtained by further subtracting out a 4% isotopic²³ contribution from ^{11}B . These residual intensities of $^{10}\text{BH}^+$, $^{10}\text{BH}_2^+$, and $^{10}\text{BH}_3^+$ are shown in Figure 5 as a function of temperature. The average mass spectrum of BH_3 , obtained for the temperature range 640–740°K,

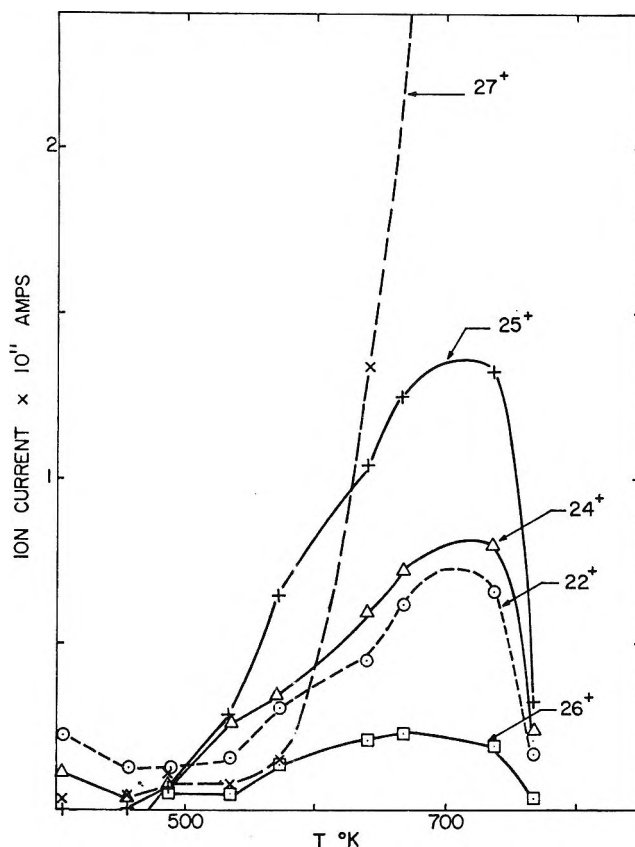


Figure 3. Variation in the ion currents at m/e 22, 24, 25, 26, and 27 as a function of temperature. Not shown on the graph is the ion current for 27^+ equal to 4.5×10^{-11} A at 739°K; % shutter effect = 30%, while for m/e 22–26 it is 6–7% at this temperature.

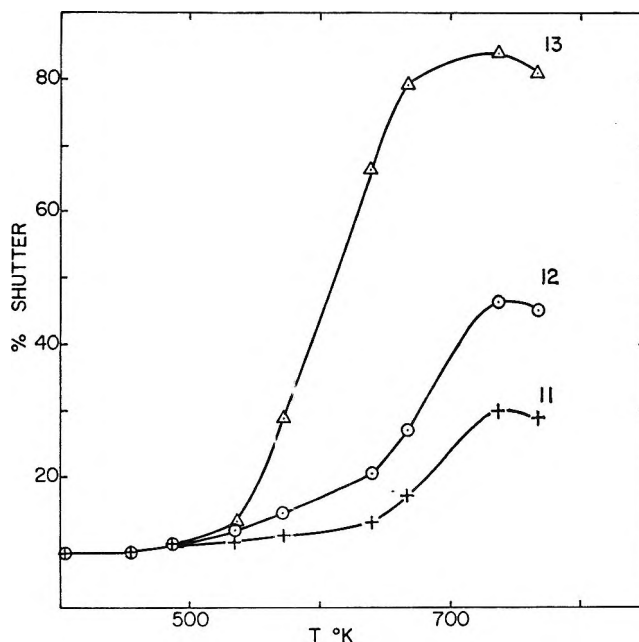


Figure 4. Shutter percentages for m/e 11, 12, and 13 as a function of temperature.

is given in Table II. As shown in the table, this mass spectrum of $^{10}\text{BH}_3$ is in good agreement with the only other reported mass spectrum.

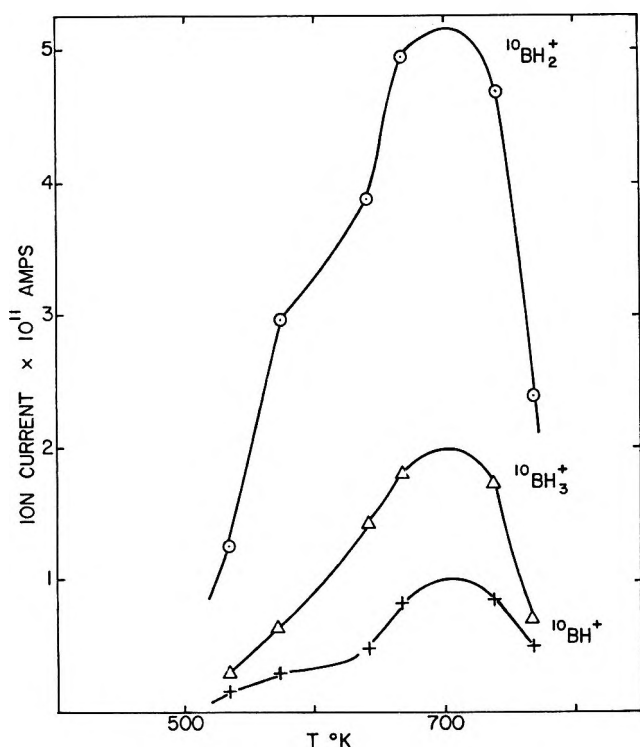


Figure 5. Ion currents of $^{10}\text{BH}^+$, $^{10}\text{BH}_2^+$, and $^{10}\text{BH}_3^+$ as a function of temperature. The contributions due to fragmentation of BH_3CO and B_2H_6 at these masses have been subtracted out. Note that these ion currents are substantially higher than those in the diborane region as shown in Figure 3.

Table II: Comparison of Monoisotopic Molecular Beam Mass Spectrum of $^{10}\text{BH}_3$ Formed from BH_3CO and from B_2H_6

Ion	Starting material	
	BH_3CO	B_2H_6^a
$^{10}\text{BH}_3^+$	37	31
$^{10}\text{BH}_2^+$	100	100
$^{10}\text{BH}^+$	16	16
$^{10}\text{B}^+$	9	8

^a Reference 9. See this paper for a comparison with BX_3 ($\text{X} = \text{halogen}$) and other M^{11}X_3 mass spectra.

It now must be shown that the BH_3 spectrum reported above does indeed come from BH_3 neutral produced from BH_3CO , and not from the B_2H_6 produced as a side product in the reaction. In order to resolve this important problem, $^{11}\text{B}_2\text{H}_6$, containing the normal isotopic composition of boron²⁴ (20% ^{10}B and 80% ^{11}B), was leaked into the mass spectrometer together with $^{10}\text{BH}_3\text{CO}$ (96% ^{10}B) at 769°K (the highest temperature used in the earlier experiments). Since the major peak in the mass spectrum of $^{11}\text{B}_2\text{H}_6$ is at $m/e = 27$ and $^{11}\text{BH}_3$ from it is observed at $m/e = 14$, it was possible to study the pyrolysis of $^{11}\text{B}_2\text{H}_6$ in presence of the pyrolysis products from $^{10}\text{BH}_3\text{CO}$.

From the mass spectra of $^{10}\text{B}_2\text{H}_6$ (96% ^{10}B) and $^{11}\text{B}_2\text{H}_6$ it can be calculated that at equal ratios of $^{10}\text{BH}_3/^{10}\text{B}_2\text{H}_6$ and $^{11}\text{BH}_3/^{11}\text{B}_2\text{H}_6$ for the respective diboranes, the intensity ratio $I(14^+)/I(27^+)$ (for $^{11}\text{B}_2\text{H}_6$) should be 1.6 times that of $I(13^+)/I(25^+)$ (for $^{10}\text{B}_2\text{H}_6$, 96% ^{10}B).

Mass peak 27 from $^{11}\text{B}_2\text{H}_6$ was observed at the high mass side of $^{10}\text{BHO}^+$ from the pyrolysis of $^{10}\text{BH}_3\text{CO}$, and the two ion peaks were completely resolved. $^{11}\text{B}_2\text{H}_6$ was admitted in such an amount that its shutterable intensity at m/e 27 was about the same as that for $^{10}\text{B}_2\text{H}_6$ at m/e 25.

The measured ratio $I(14^+)/I(27^+) = 4.05 \times 10^{-2}$ for the pyrolysis of $^{11}\text{B}_2\text{H}_6$ is to be compared with $I(^{10}\text{BH}_3^+)/I(25^+) = 2.1$, the latter obtained for the pyrolysis of $^{10}\text{BH}_3\text{CO}$ just before $^{11}\text{B}_2\text{H}_6$ was introduced. The small value for $I(14^+)/I(27^+)$ shows that very little BH_3 is being formed from B_2H_6 under the experimental conditions (reactor, material, pressures, contact time) used. Therefore, the BH_3 observed is formed directly from the pyrolysis of BH_3CO . The agreement between the mass spectra for BH_3 obtained in this work and that reported⁹ earlier confirms that the latter also was due to BH_3 neutral.

The appearance potential for BH_3^+ was measured using higher resolution than usual. With the exit slit 12×10^{-3} in., the ions $^{10}\text{BH}_3^+$ and $^{11}\text{BH}_2^+$ were resolved. The electron energy scale was calibrated by setting the measured $\text{AP}(\text{Ar}^+) = \text{IP}(\text{Ar}) = 15.75$ eV.²⁵ The corrected value for $\text{AP}(\text{BH}_3^+)$ was found to be 14.0 ± 2 eV. The large uncertainty is due to the low molecular beam intensity of BH_3^+ .

The obtained $\text{AP}(\text{BH}_3^+)$ is 2–2.5 eV higher than earlier reported values, 11.4 ± 0.27 and 12.32 ± 0.1 ,²⁶ and probably is due to the low beam intensity.

Yield of BH_3 and B_2H_6 . The ratio between mono- and diborane is nearly constant in the pyrolysis region, as shown in Figure 6 (top) where the ratio $b = \sum_{i=10}^{13} I(i^+)/\sum_{i=22}^{26} I(i^+)$ is plotted vs. temperature. If the secondary electron multiplier gains are equal and the cross section²⁷ for the ionization of diborane is about twice that of monoborane, the ratio $p(\text{BH}_3)/p(\text{B}_2\text{H}_6)$ is about 5.6. If anything, the secondary electron multiplier gain for B_2H_6^+ ions is greater than that for BH_3^+ ions, changing this ratio in favor of BH_3 .

The formation of BH_3 and B_2H_6 relative to the loss of BH_3CO is shown in Figure 6 (bottom), where

(25) C. E. Moore, "Atomic Energy Levels," Vol. 1 and 2, National Bureau of Standards, Circular 467, U. S. Government Printing Office, Washington, D. C., 1949, 1952.

(26) J. H. Wilson and H. A. McGee, Jr., *J. Chem. Phys.*, **46**, 1444 (1967).

(27) S.-S. Lin and F. E. Stafford, *ibid.*, **47**, 4664 (1968); the arguments of this paper show that the arguments given by F. E. Stafford (ref 20, p 153) for the validity, and for the small deviations from the "additivity rule" for cross sections are roughly valid also for the $\Sigma(r, r')$ method of calculating cross sections.

$$a = \frac{\left[\sum_{i=10}^{13} I(i^+) + \sum_{i=22}^{26} I(i^+) \right] \sqrt{\frac{T}{T_0}}}{I(39^+)_{T_0} - I(39^+) \sqrt{\frac{T}{T_0}}}$$

is plotted *vs.* temperature. T is the variable temperature, and $T_0 = 404^\circ\text{K}$ is a reference temperature. As seen from Figure 6, the loss of BH_3CO to products other than mono- and diborane rapidly increases up to about 600°K , and then becomes constant up to 740°K . By assuming 100% yield at 535°K , we find that at the maximum intensity of BH_3 and B_2H_6 , at about 700°K , the yield is only 20% or less. The maximum yield of boranes from the total amount of BH_3CO introduced is obtained at about 740°K , also being 20% or less.

This low yield shows that other products must be formed. One possibility was indicated in an earlier result from our laboratory,¹⁵ when some evidence for the formation of higher boranes was observed using higher inlet pressure and contact time for the reactor, which in that case was made of stainless steel.

In the present work, attempts were made to replicate the earlier result using the same experimental conditions, except that the reactor was made of molybdenum. No or very little evidence for higher boranes was observed, even when a mixture of B_2H_6 and BH_3CO was introduced and reacted at temperatures between 450 and 600°K .

The earlier result¹⁵ may be due to a catalytic effect from stainless steel (<0.08% C, 2% Mn, ~8% Ni, 18–20% Cr) not obtained with molybdenum.

Thus, the observed, but unexplained loss of borane supports earlier work,¹⁶ which reports free hydrogen (not recorded in the present work) as a significant pyrolysis product from BH_3CO , as well as the invariable observation in this laboratory and others of dark deposits on the reactor walls. Longer contact times for the reactor results in a larger yield of B_2H_6 in agreement with the observations of other workers.^{15,16}

A referee has asked us to comment about why a molecule that decomposes measurably rapidly at 0°C is observed here to decompose only at 500°K (227°C), as shown in Figure 1. The preexponential factor of the rate constant for reaction 1 has been estimated by Garabedian and Benson¹³ to be $10 \exp(14.4 \pm 0.5)$ and the activation energy to be less than 23.7 kcal/mol. This leads to characteristic $(1/e)$ decomposition times of $10 \exp(0 \pm 1)$ msec, in good agreement with the flow time of the reactor of 1.8 msec. The problem, however, is more complicated. Under the present conditions, the mean free path is long compared to reactor dimensions and gas-wall collisions predominate. The reactor surface, created by decomposition of the borane carbonyl, is at best poorly characterized, as indicated by the review of Newkirk;²⁸ we have mentioned above that higher molecular weight products of the reaction seem to depend on whether a stainless steel or molyb-

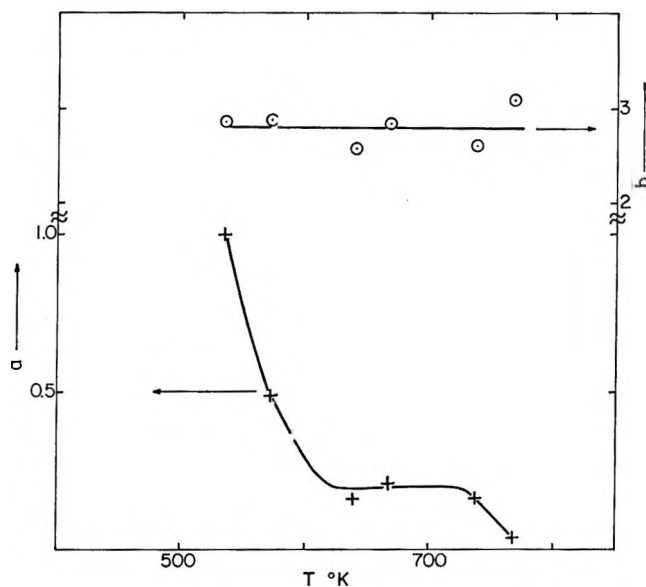


Figure 6. Crosses (bottom curve), left-hand ordinate: Yield of BH_3 and B_2H_6 *vs.* loss of BH_3CO as a function of temperature. The quantity a gives the yield as the total amount of mono- and diborane relative to the loss of borane carbonyl. The intensities of m/e 10, 11, 12, and 13 are stripped of the contributions due to fragmentation of BH_3CO . Circles (top curve), right-hand ordinate: Ratio between mono- and diborane intensities as a function of temperature. The intensity ratios, b , average to 2.8, indicating that there is about six times as much BH_3 as B_2H_6 present; see text for definitions of a and b .

denum substrate is used. Furthermore, the question is more general and involves the ability of a gas to equilibrate with a surface. It thus involves all "double Knudsen cell" experiments in which a sample is vaporized from one compartment held at a constant temperature and caused to dissociate in a second held at a higher, variable temperature. The most extreme cases where the equilibration problem is recognized are those in which BH_3 , BH_2R , and/or various hydrocarbons seem to be formed by gas phase reactions and then survive many collisions with surfaces at $\sim 2000^\circ$.^{29,30} Discrepancies, however, between double Knudsen cell results and other results seem to indicate that this problem is more widespread and serious than previously believed.

Since this paper was completed and submitted, Ganguli and McGee³¹ have reported an electron impact study of borane produced by pyrolysis of BH_3CO . They do not, however, report a mass spectrum of BH_3 . Borane and BH_3^+ both are believed to be planar, while

(28) A. E. Newkirk, "Preparation and Chemistry of Elemental Boron," *Advances in Chemistry Series*, No. 32, "Borax to Boranes," American Chemical Society, Washington, D. C., 1961, p. 35.

(29) S. J. Steck, G. A. Pressley, Jr., and F. E. Stafford, *J. Phys. Chem.*, **73**, 1000 (1969).

(30) S. J. Steck, G. A. Pressley, Jr., S.-S. Lin, and F. E. Stafford, *J. Chem. Phys.*, **50**, 3196 (1963).

(31) P. S. Ganguli and H. A. McGee, Jr., *ibid.*, **50**, 4658 (1969).

the -BH_3 groups in both diborane and borane carbonyl are not planar. The BH_3^+ ions formed by fragmentation of these molecules, therefore, are likely to have appreciable internal and translational energy. Consequently the value $D(\text{BH}_3\text{-BH}_3) = 59$ kcal/mol derived from appearance potentials³¹ must be taken as an upper limit.

Mappes and Fehlner³² report a high absolute yield synthesis of borane from the carbonyl. The BH_3 mass spectrum reported by them is in excellent agreement with those given in the present Table II.

Conclusion

The molecular beam mass spectrum of BH_3CO believed to be free of pyrolysis products and other impurities has been obtained for the first time and is shown to have fragments of the type BH_xC^+ in addition to BH_yCO^+ ($y = 0, 1, 2, 3$) and BH_x^- ($x = 0, 1, 2$); BH_3^+ not formed in measurable amounts.

Pyrolysis of BH_3CO under the specific conditions used in this investigation, low inlet pressure and short contact time for the reactor, gave a high enough concentration of BH_3 that it could be identified clearly and its molecular beam mass spectrum obtained. This spectrum agrees with that obtained earlier from B_2H_6 ⁹ and used in

interpreting results obtained for the high-temperature reaction of B_4C with H_2 ,²⁹ thus confirming the identification and quantitative estimates of BH_3 concentration in the latter²⁹ case.

Destruction of BH_3CO to products other than BH_3 and B_2H_6 takes place through the whole temperature range where the pyrolysis is studied, and is in disagreement with the assumptions of a previous kinetic study.⁸ The ion BHO^+ as well as hydrogen and black deposits in the reactor also were observed. Porter reports³³ that evidence for BH_2OH is observed when BH_3CO is decomposed by flowing through a hot quartz tube and the products are condensed in a rare gas matrix. Our observation of BHO^+ is consistent with the previous observation of BH_2OH .³⁴

Acknowledgments. The authors wish to thank R. E. Hollins for preparing the samples, and S. M. Schilderout¹⁵ and A. B. Baylis for valuable information from their preliminary study of this subject. Professor T. P. Fehlner gave us manuscripts^{16,32} in advance of publication as did Professor R. F. Porter.³³

(32) G. W. Mappes and T. P. Fehlner, private communication.

(33) R. F. Porter, private communication.

(34) R. F. Porter and S. K. Gupta, *J. Phys. Chem.*, **68**, 2732 (1964).

The Hydrogen-Deuterium Exchange of Benzene at a Fuel Cell Electrode

by H. J. Barger, Jr., and A. J. Coleman

Energy Conversion Research Division, U. S. Army Mobility Equipment Research and Development Center, Fort Belvoir, Virginia 22060 (Received June 11, 1969)

The hydrogen-deuterium exchange of benzene at a fuel cell electrode was studied at 0.30 V. After electrochemical pretreatment the electrode was potentiostatically held at 0.30 V as benzene passed over the electrode surface. The amount of exchange increased rapidly for 1–2 min then abruptly diminished. The percentage of the various deuteriobenzenes ranging from $\text{C}_6\text{H}_5\text{D}$ to C_6D_6 suggests at least two types of exchange reactions, both of which occur concurrently.

Elucidation of the anodic oxidation reaction mechanism of hydrocarbons has been of interest for several years as a key step in the development of practical fuel cells which directly oxidize logistic fuels such as combat gasoline and kerosene. An important part in the overall mechanism is the initial adsorption and bonding of the hydrocarbon to the electrocatalyst. Recently hydrogen-deuterium exchange has been used to study the adsorption of propane on a fuel cell electrode.¹ Most of the material removed from the electrode by the cathodic pulse was completely deuterated. These

results suggested that the intermediate species on the surface were highly mobile and that carbon-catalyst and carbon-hydrogen bonds could be made and broken very easily. In this paper, the isotopic exchange of benzene at a fuel cell electrode is reported. Benzene is a common component of many logistic fuels and has been shown to be extremely detrimental to the oxidation of alkanes on platinum electrodes.² By studying

(1) H. J. Barger, Jr. and A. J. Coleman, *J. Phys. Chem.*, **72**, 2285 (1968).

the hydrogen-deuterium exchange of benzene under conditions similar to those of an actual fuel cell, it was hoped that some information could be obtained as to how benzene adsorbed, what its structure on the surface was, and thus the reason why benzene acts as an electrocatalyst poison. In addition, the many nonelectrochemical exchange studies of benzene on platinum could be compared to exchange at the electrode and would perhaps aid in the interpretation of these results.

Experimental Section

Apparatus and Materials. The electrochemical cell and circuitry used in these experiments have been described previously.³ The working electrode was an American Cyanamid Type LAA 25 consisting of 25 mg/cm² of platinum pressed together with 25 wt % Teflon on a tantalum screen. A Teflon film was applied to the gas side of the electrode for wet-proofing. The helium carrier gas used in these experiments was 99.99% minimum purity and was used as received. The benzene, Fisher spectroquality, and the electrolyte, Brinkmann Instruments 85% perdeuteriophosphoric acid with a 99% deuterium content, were also used as received. The flow system diagrammed in Figure 1 was connected to a CEC 21-130 mass spectrometer equipped with a CEC 5-124 oscillograph which allowed scans between mass 76 and 100 to be made in 2 sec or at the rate of 30 per min. By manipulation of valves 1, 2, and 3, helium could be passed over the working electrode or through a benzene saturator and the resulting mixture used as the reactant. Flow rates, 0.5 to 2.0 ml/sec, were controlled with a capillary flow meter and a precision needle valve, which were calibrated with a bubble flow meter. A benzene concentration of 2.8×10^{-7} mol/ml was used most often since this represented the best compromise between good mass spectrometer sensitivity and electrode life. Reactant concentrations were determined by weighing the amount of benzene collected at liquid nitrogen temperature for 10 min at each flow and saturator temperature. The benzene saturator and cell temperatures were controlled to $\pm 0.1^\circ$, and were monitored continuously with calibrated iron-constantan thermocouples connected to a Hewlett-Packard 7100 B dual channel strip chart recorder with a full scale range of 1 mV.

Experimental Procedure. Before conducting an experiment, a pretreatment procedure⁴ was followed to prepare a reproducible catalyst surface and to determine the electrochemical surface area.⁵ While sweeping with helium, the working electrode was held for 25 min at 1.35 V vs. the dynamic hydrogen electrode,⁶ dhe, in the same medium whereby the catalyst surface and species on the surface were oxidized. The potential was then lowered to 0.05 V for 3-5 min to reduce the platinum oxide. Next the potential was raised to 1.35 V for 5 min followed by cathodically pulsing the working electrode at a constant current of 1.0 A. A Hewlett-

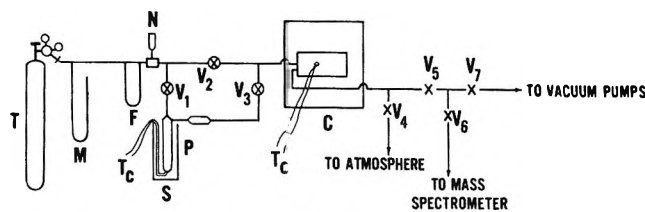


Figure 1. Diagram of flow system: T, helium supply; M, mercury manometer; N, needle valve; F, capillary flow meter; S, benzene supply and constant-temperature bath; P, preheater; V, valves; C, electrochemical cell and oven; T_c, thermocouples.

Packard 7001A time based X-Y recorder was used to record the cathodic charging curve from which the surface area was calculated assuming 210 $\mu\text{coul}/\text{real cm}^2$ for a monolayer of hydrogen.⁷ Then the potential was held at 0.3 V, the potential of interest, until the deposited deuterium from the cathodic pulse had been oxidized (1-2 min). The adsorption potential, 0.30 V, was chosen for this study because it represented a point where benzene readily adsorbed but oxidized little.⁸ An exchange experiment was started by opening valves 1 and 3 while simultaneously closing valve 2 and starting the mass scan. A low ionization voltage (9.45 V) was used to minimize fragmentation of the hydrocarbons. After 2-5 min, the cell was flushed with helium until no peaks were seen on the oscillogram. The electrode was cathodically pulsed to remove any adsorbed hydrocarbons¹ after which the pretreatment could be started again.

Results and Discussion

The measured values of the peaks comprising the mass spectra were treated with a Mathatron computer-calculator to correct for naturally occurring isotopic contributions to the deuteriobenzenes, to calculate the percentage concentration of each deuteriobenzene with and without C₆H₆, and to calculate ϕ .⁹ No correction for differences in mass spectrometric sensitivities for the various deuteriobenzenes was made in these calculations.¹⁰ The quantity ϕ , mentioned above equals $i\sum\% \text{C}_6\text{H}_{6-i}\text{D}_i$ and reflects the number of hydrogen-deuterium exchanges per 100 molecules of benzene,

(2) (a) E. Luksha and E. Y. Weissman, *J. Electrochem. Soc.*, **116**, 120 (1969); (b) J. F. Lennon, E. Luksha, and E. Y. Weissman, *ibid.*, **116**, 122 (1969).

(3) H. J. Barger, Jr., and M. L. Savitz, *ibid.*, **115**, 686 (1968).

(4) (a) S. Gilman, *J. Phys. Chem.*, **67**, 78 (1963); (b) S. E. Brummer and M. J. Turner, *ibid.*, **71**, 2825 (1967).

(5) B. E. Conway and D. Gilroy, *Can. J. Chem.*, **46**, 875 (1968).

(6) J. Giner, *J. Electrochem. Soc.*, **111**, 376 (1964).

(7) S. B. Brummer, *J. Phys. Chem.*, **69**, 562 (1965).

(8) (a) W. Heiland, E. Gileadi, and J. O'M. Bockris, *ibid.*, **70**, 1207 (1966); (b) M. L. Savitz and A. L. Hubbard, *J. Electrochem. Soc.*, **116**, 714 (1969).

(9) J. R. Anderson and C. Kemball, *Advan. Catal.*, **9**, 51 (1957).

(10) S. Meyerson, H. M. Grubb, and R. W. Van der Harr, *J. Chem. Phys.*, **39**, 1445 (1963).

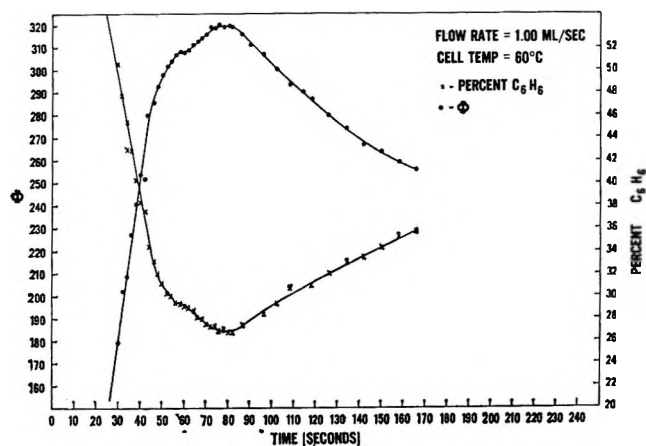


Figure 2. Plot of ϕ and per cent C_6H_6 vs. time.

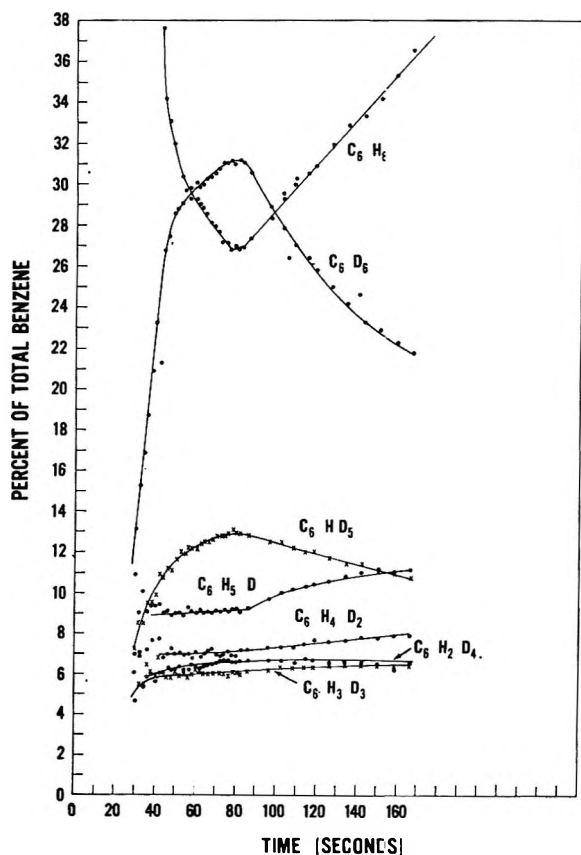


Figure 3. Distribution of benzene isomers vs. time at 1.00 ml/sec and 60° .

i.e., ϕ divided by 600 gives the fraction of hydrogens that underwent exchange. Figure 2 is a typical plot of ϕ and percentage C_6H_6 vs. time, zero seconds occurring when valves 1 and 3 were opened and valve 2 was closed. This figure illustrates the facile nature of the exchange reaction of benzene on a fuel cell electrode at 0.3 V. This is in marked contrast to results using propane as the reactant¹ where no deuterated compounds could be detected until the working electrode was cathodically pulsed. There are three distinct

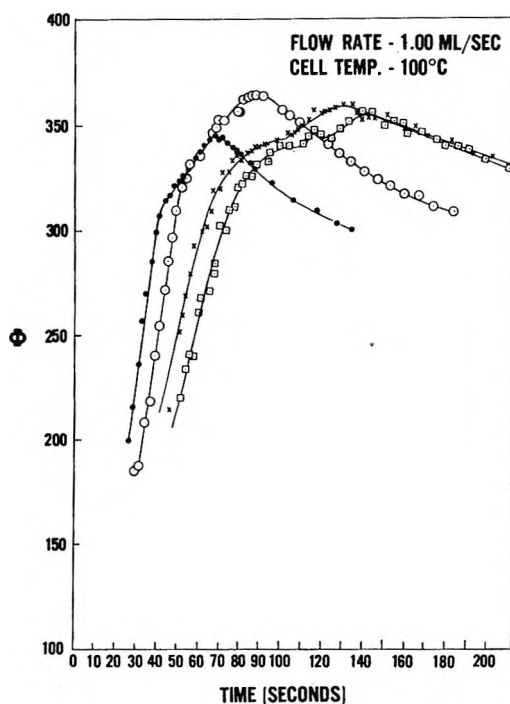


Figure 4. Variations of ϕ at various benzene concentrations (in mol/ml $\times 10^7$): 4.2, \bullet ; 2.8, \circ ; 2.1, \times ; 1.7, \square .

regions in the ϕ vs. time plot (Figure 2). In the first region, ϕ increases linearly. After 10–25 sec, depending on flow rate, a slope change occurs and sometimes even a hump results. This hump is quite prominent at 60 and 70° . After this break in the initial slope, ϕ continues to increase but at a slower rate until the maximum is reached whereupon ϕ declines. Figure 2 also shows the nearly symmetrical relationship between ϕ and % C_6H_6 as a function of time. The change with time of the concentrations of all the benzenes under the same reaction conditions is seen in Figure 3. As would be expected from the large weighting factor of 6, the shape of the percentage C_6D_6 plot closely follows the shape of the ϕ plot (Figure 2). The percentage of C_6HD_5 increases with C_6D_6 but at a slower rate, and its decline after ϕ_{max} is more gradual. The absolute percentages of the $C_6H_4D_2$, $C_6H_3D_3$, and $C_6H_2D_4$ compounds change very little with time although the relative percentage increase of each shows some increase after ϕ_{max} . The percentage of C_6H_5D slowly increases after ϕ_{max} as C_6D_6 declines.

The rapidly increasing and decreasing benzene percentages as a function of time suggested a complex and changing process. Additional information was needed to gain more of an understanding of these reactions, so the process was studied as a function of benzene concentration, flow rate, and reaction temperature. In Figure 4, the effect of benzene concentration on the shape of the ϕ -time plots is shown where the flow rate and reaction temperature were not varied. At the higher benzene concentrations, the maximum value of

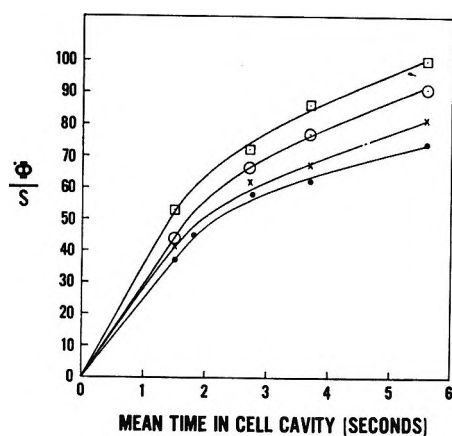


Figure 5. ϕ_{\max} per m^2 vs. the mean time in the cell at 60° , \bullet ; 70° , \times ; 90° , \circ ; and 100° , \square .

ϕ occurred sooner than at the lower benzene concentrations. Generally, the reaction temperature and the flow rate caused only minor variations in the ϕ -time plots. The time to reach the maximum of ϕ -time plot and the time at which measurable amounts of deuterated compounds came off the electrode decreased as the flow rate increased.

The initial, rapid increase in ϕ as a function of time followed by a slower increase and finally a decline was observed for all reaction conditions. Thus during the course of these experiments, steady state was not attained. In one extended run in which benzene was passed over the working electrode for 1 hr, ϕ decreased continuously after the maximum. There are 2 unique points in time for all experiments, $d\phi/dt = 0$ or ϕ_{\max} and at the first break on the upward slope, $d\phi/dt \neq \text{constant}$. A plot of the value of ϕ at ϕ_{\max} divided by the surface area vs the mean time in the electrochemical cell (volume of the cell gas cavity divided by the flow rate) gave a family of curves seen in Figure 5. The terms contact time and residence time are not used to avoid confusion relating to the length of time the reactant spends on the catalyst. It was necessary to normalize ϕ for surface area because the surface area of the working electrode as measured by deuterium deposition varied as the electrode aged and with temperature, the reason for which is beyond the scope of this paper. These data (Figure 5 and Table I) were plotted according to the first-order equation $k\tau = 1/S \ln [1/(1 - \phi/600)]$ where S is the surface area. The rate constants at the various temperatures were obtained from the slopes of the lines in Figure 6; the logarithms of these rate constants when plotted against the reciprocal temperature gave the line in Figure 7. Treatment of the data for ϕ at the first break in the ϕ vs. time plots gave similar results. The Arrhenius plots gave activation energies of $2.85 \text{ kcal mol}^{-1}$ for the point in time at ϕ_{\max} and $1.57 \text{ kcal mol}^{-1}$ for the point at the first break. Table II lists rate constants for the process at both points. These rate constants may be expressed as $\ln k = -2847/RT + 0.838$

Table I

$T, ^\circ\text{K}$	Mean time in cell, sec	Surface area, m^2	ϕ at ϕ_{\max}	ϕ at break
333	5.6	5.77	425	397
333	3.7	5.69	351	332
333	2.7	5.52	320	280
333	1.5	5.58	205	170
343	5.7	5.26	427	
343	3.6	5.41	362	326
343	2.7	5.25	327	240
343	1.5	5.25	222	192
363	5.6	4.93	447.5	410
363	3.5	4.84	372	330
363	2.7	4.87	321	280
363	1.5	5.11	226.5	207
373	5.7	4.71	470	415
373	3.7	4.61	395	347
373	2.7	4.50	324	281
373	1.5	4.71	250	211

Table II

$T, ^\circ\text{K}$	k (at ϕ_{\max}), $\% \text{ sec}^{-1} \text{ m}^{-2}$	k' (at break), $\% \text{ sec}^{-1} \text{ m}^{-2}$
333	5.23	3.02
343	5.42	3.30
363	4.46	3.68
373	5.06	3.80

and $\ln k' = -1574/RT - 1.13$ for the points at ϕ_{\max} and the first break in the ϕ vs. time plot, respectively. The low values of the energy of activation at these two points in time compared to 10 – 19 kcal mol^{-1} previously obtained for hydrogen-deuterium exchange of benzene on platinum^{9,11} suggest a diffusion controlled reaction.^{11,12} Diffusion control in a system of this sort is not surprising.¹³ The data were subjected to least-square fits in determining the slopes.

We have used the word process to describe the hydrogen-deuterium exchange occurring in these experiments because there seem to be at least two and perhaps more types of reactions taking place. One type involves 6 site multiple exchange and occurs during one residence of the benzene on the catalyst. This reaction probably accounts for the formation of the C_6D_6 , C_6HD_5 , and some of the $\text{C}_6\text{H}_2\text{D}_4$. The latter two deuteriobenzenes occur because the deuterium concentration on the catalyst surface is less than 100%, especially after the reaction has been in progress for some time. Support for this suggestion is seen in Figure 3 where the C_6HD_5 benzene percentage declines much slower than that of

(11) J. L. Garnett and W. A. Solllich, *J. Catal.*, **2**, 339 (1963).

(12) A. M. North, "The Collision Theory of Liquids," John Wiley & Sons, Inc., New York, N. Y., 1964.

(13) G. C. Bond, "Catalysis by Metals," Academic Press, New York, N. Y., 1962.

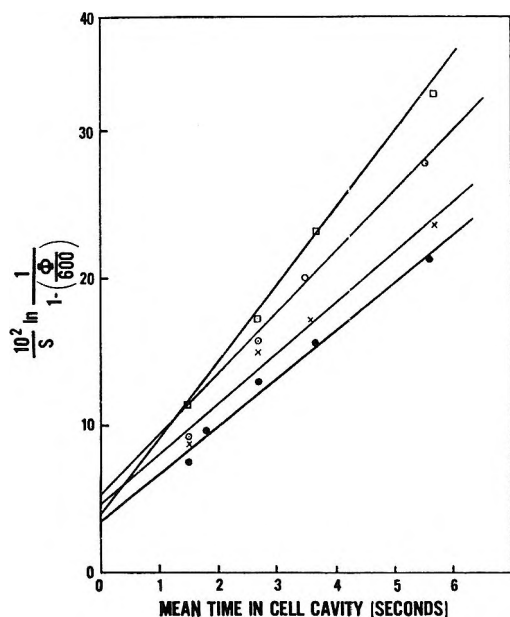


Figure 6. First-order plot of data in Table I at ϕ_{\max} .

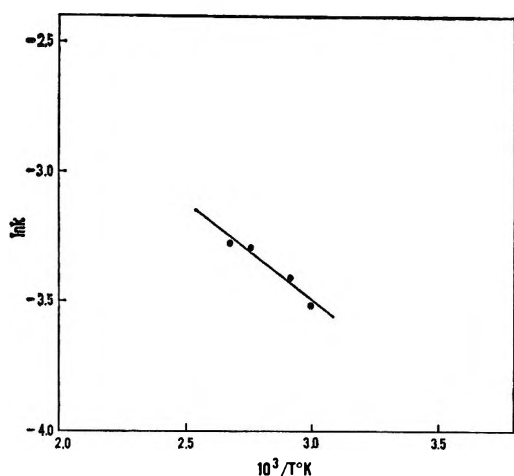


Figure 7. Arrhenius plot of data in Table II at ϕ_{\max} .

C_6D_6 after ϕ_{\max} . The other type of reaction involves single stepwise exchange and gives rise to the C_6H_5D , $C_6H_4D_2$, $C_6H_3D_3$, and the remainder of the $C_6H_2D_4$. Successive adsorptions on the catalyst or perhaps two, three, or four stepwise exchange reactions during one residence on the surface could account for $C_6H_4D_2$, $C_6H_3D_3$, and $C_6H_2D_4$. The second possibility might occur after benzene σ bonded to the catalyst; the resulting unpaired electron or charge could be localized at the *ortho* or *para* positions allowing subsequent exchange at these positions. If these suggestions are correct, there must be at least two different types of reaction sites on the surface, one type site for each reaction. Multiple exchange would most likely occur when the plane of the benzene ring is parallel to the catalyst surface; stepwise, single exchange would occur on those sites where benzene adsorbed normal to the catalyst surface. Possible modes

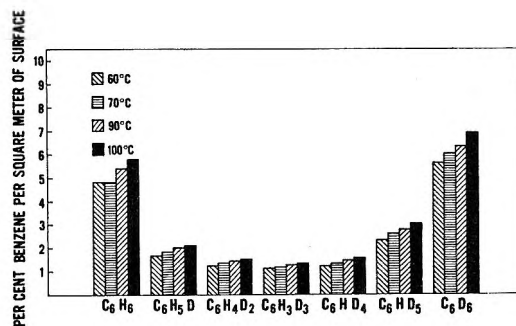


Figure 8. Distribution at ϕ_{\max} at a flow rate of 1.00 ml/sec.

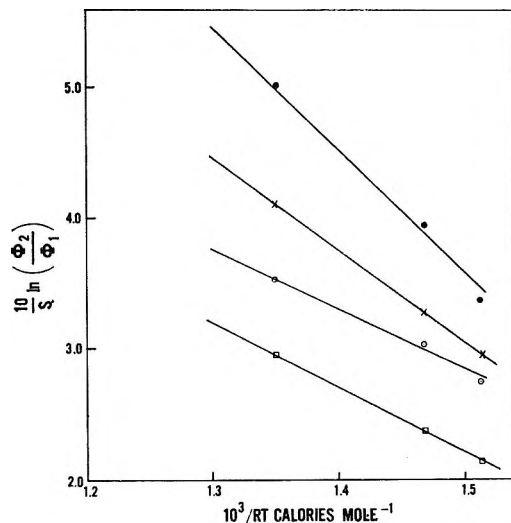


Figure 9. Booser-Lewis treatment for data at ϕ_{\max} at flow rates of 0.48, \bullet ; 0.73, \times ; 1.00, \circ ; and 1.78, \square .

of bonding and structures of the reaction intermediates have been suggested previously.^{9,14-16}

The percentage distribution of the various benzenes at ϕ_{\max} normalized on a per square meter basis is seen in Figure 8 for a "medium" flow. At faster flows, there was considerably more C_6H_6 , and conversely at slow flow rates the percentage concentrations of C_6D_6 and C_6HD_5 were larger than at faster flows. It is apparent that the time in the cell is more important than temperature in determining the product composition. For all flows, a U-shaped distribution was obtained with the minima at $C_6H_3D_3$. At the slow flow rate, there was a marked shift toward C_6D_6 because there was a greater chance for additional residences of the benzene on the surface. Wei¹⁷ has pointed out that distributions of this sort suggest diffusion controlled reactions and noted the pitfalls inherent in drawing mechanistic

(14) (a) J. L. Garnett and W. A. Sollich, *J. Catal.*, **2**, 350 (1963); (b) J. L. Garnett and W. A. Sollich-Baumgartner, *J. Phys. Chem.*, **68**, 3177 (1964).

(15) F. Hartog, J. H. Tebben, and C. A. M. Weterings, *Proc. Int. Congr. Catal.*, 3rd, Amsterdam, **2**, 1199 (1964).

(16) J. J. Rooney, *Chem. Brit.*, **2**, 242 (1966).

(17) J. Wei in "Applied Kinetics," American Chemical Society Publications, Washington, D. C., 1967, p 71.

conclusions about a mechanism involving two types of catalyst sites such as suggested above. Support for two types of reactions is seen in Figure 9. Using the treatment of Lewis and Boozer,¹⁸ the logarithm of the rate constant ratio was plotted against the reciprocal of the reaction temperature. The method and the rationale for this procedure are briefly outlined below. When different products result from the same reactant, the ratio of the yield of these products under certain circumstances equals the ratio of the respective rate constants. In this treatment, we assumed some of the benzene exchanged by one reaction to give C_6D_6 , C_6HD_5 , and one-half the $C_6H_2D_4$ and by another reaction to give the remainder of the deuteriobenzenes. Placement of half the $C_6H_2D_4$ in each category was arbitrary but seemed reasonable on the basis of the isotopic distributions (Figure 8). The fraction of hydrogens undergoing exchange by the former process $\phi_2/600$, equals $4 \times \% C_6H_2D_4/2 + 5 \times \% C_6HD_5 + 6 \times \% C_6D_6$, and similarly the fraction of hydrogens that exchanged by the latter process equals $\phi_1/600$ or $1 \times \% C_6H_5D + 2 \times \% C_6H_4D_2 + 3 \times \% C_6H_3D_3 + 4 \times \% C_6H_2D_4/2$. The value of ϕ as used earlier thus equals $\phi_1 + \phi_2$. The rate of both reactions may be written as $d\phi_1/dt = k_1f_1 \cdot (C_6H_6)$ and $d\phi_2/dt = k_2f_2 \cdot (C_6H_6)$. Division of one rate by the other gives $d\phi_2/d\phi_1 = k_2f_2/k_1f_1$. Assuming the same dependence on benzene concentration for both reactions, on integration we have $\phi_2/\phi_1 = k_2/k_1$. When the logarithm of ϕ_2/ϕ_1 at the ϕ_{max} point in time, corrected for surface area, was plotted against the reciprocal of RT (Figure 9), the slopes of the resulting lines equal the difference in activation energy of the two reactions. A least-squares fit gave lines with slopes corresponding to 0.93, 0.70, 0.45, and 0.44 kcal mol⁻¹ respectively at flows of 0.50, 0.75, 1.00, and 1.75 ml/sec. The larger energy of activation differences at the slower flows may result from consecutive ϕ_1 type reactions which would appear at ϕ_2 . In any case, these plots suggest that two types of reactions are occurring and that their energies of activation differ very little.

First-order plots of ϕ_2 normalized for surface area resulted in the lines (Figure 10) which were reasonably linear except for the points at the slow flow. This deviation is ascribed to two effects. At the slow flow, more of the reactant benzene exchanges than at the faster flow creating an appreciable concentration of hydrogen on or near the catalyst surface. In addition because of the long time in the cell, second and third readsorptions probably occur. Thus instead of shifting the distribution of the deuteriobenzenes overwhelmingly toward C_6D_6 , there may be some back reactions of the sort $C_6D_6 \rightarrow C_6HD_5$, etc. The fact that the deviation from linearity is less at 90 and 100° than at the lower temperatures may be explained by the faster diffusion of hydrogen into the bulk electrolyte at these temperatures. When the logarithms of the slopes from the linear portion of the lines in Figure 10 were plotted

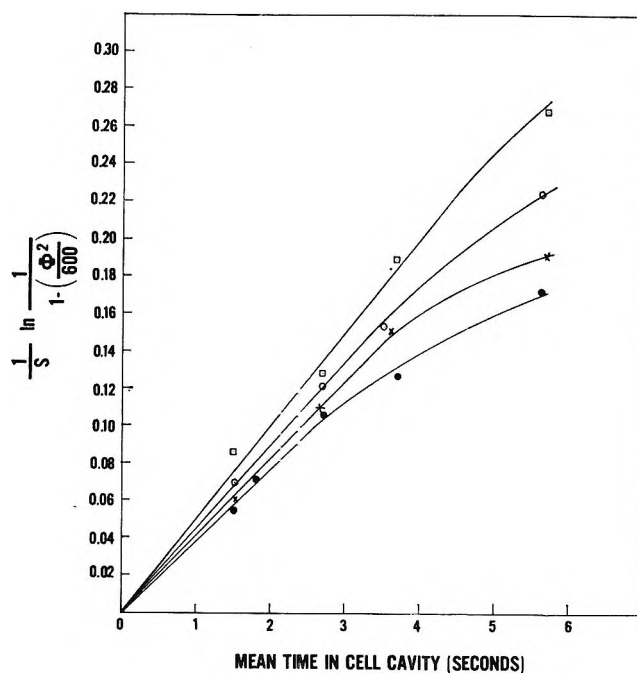


Figure 10. First-order plot of ϕ_2 at ϕ_{max} for temperature 60°, ●; 70°, ×; 90°, ○; 100°, (□).

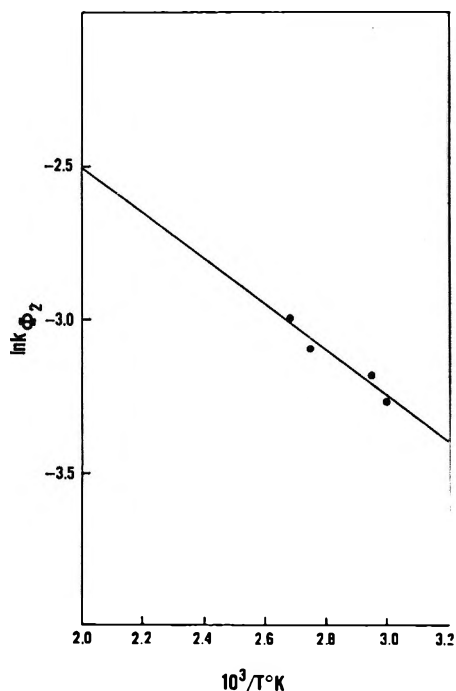
against the reciprocal of RT , a line (Figure 11) with a least-squares slope equivalent to an activation energy of 1.45 kcal mol⁻¹ was obtained. The values of ϕ_1 were not plotted because they showed little change with temperature and flow (Table III).

Evidence suggesting two types of reaction sites was obtained on considering the cause for the decline in ϕ after the maximum. Figure 3 showed that the decline can be attributed to the decrease in C_6D_6 and C_6HD_5

Table III

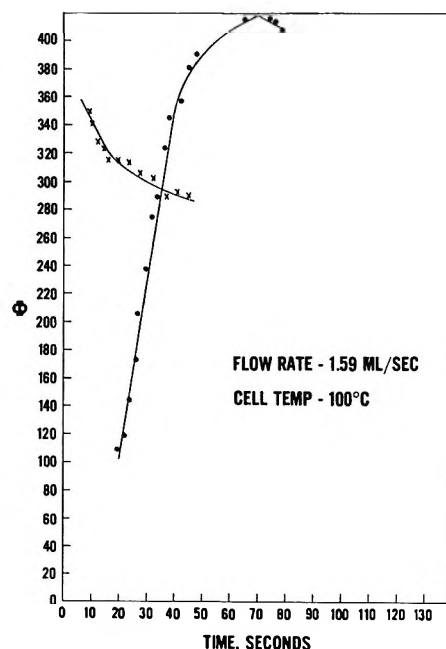
T , °K	Mean time in cell, sec	ϕ_1
60	1.5	47.8
	1.8	50.8
	2.7	54.8
	3.7	54.3
	5.6	48.6
70	1.5	49.3
	2.7	55.3
	3.6	55.4
	5.7	48.8
90	1.5	52.0
	2.7	55.8
	3.5	54.8
	5.6	46.2
100	1.5	49.7
	2.7	54.7
	3.7	51.4
	5.7	40.6

(18) E. S. Lewis and C. E. Boozer in "Technique of Organic Chemistry," Vol. VIII, Part II, A. Weissberger, Ed., Interscience Publishers, New York, N. Y., 1963.

Figure 11. Arrhenius plot of ϕ_2 .

because the other deuteriobenzenes have about the same concentrations after the maximum or actual increase. The decrease in yield of the ϕ_2 reaction was probably caused by tightly bound carbon moieties acting as poisons on the ϕ_2 reaction sites alone. Evidence supporting this contention is seen in Figure 12. In this experiment after the electrode pretreatment, benzene was passed across the catalyst surface as usual. Then the gas space above the electrode was swept with helium until benzene could no longer be detected. On reintroducing benzene to the working electrode, ϕ rapidly climbed to a point close to where it was at the beginning of the helium sweep, taking much less time than when the catalyst surface was clean at the beginning of the experiment. When the gas space and lines were again swept free of benzene with helium and the working electrode cathodically pulsed, only deuterated cyclohexanes and a small amount of C_6D_6 and C_6HD_5 were observed. (This reaction will be reported in detail later.) Thus the only species on the catalyst surface giving a detectable product still had a six-membered ring intact.

Many of the suggestions in this paper must be regarded as tentative until more is known about these reactions. The dangers of being too certain about kinetics and mechanisms in a system of this sort have been amply stressed.^{17,19} In the future, we plan to study the effect of potential on these reactions and hope to determine whether one of the reactions may be

Figure 12. Plot of ϕ vs. time.

specifically inhibited by poisons. Meaningful comparisons to earlier work on the hydrogen-deuterium exchange of benzene should be delayed until some of these results have been obtained.

Discussion of Errors. Temperatures and flow rates were measured with 0.5% precision and, because of calibration procedures, within 1.0% of their true values. The parameter ϕ contributes more to the uncertainty of the rate constants and activation energies reported here. It is recognized that when sampling a continuous gas stream, it is desirable to sample all components simultaneously. In this particular system, this was impossible. Each group of seven peaks for a calculation ϕ was scanned in 0.7 sec and repeated every 2 sec. The error incurred from changing benzene concentrations during this 0.7 sec is quite difficult to assess. From the ϕ vs. time plots most values fell within $\pm 2\%$ of the line drawn through the points and in the most extreme case were only 5% off. It was calculated that an error of the latter magnitude would give an uncertainty in the rate constants and energies of activation of ± 8 and $\pm 13\%$, respectively.

Acknowledgments. The support of Dr. J. R. Huff and the help of Mr. D. H. Bomkamp in programming the Mathatron computer-calculator are gratefully acknowledged.

(19) J. M. Thomas and W. J. Thomas, "Introduction to the Principles of Heterogeneous Catalysis," Academic Press, New York, N. Y., 1967.

Tautomeric and Protolytic Properties of *o*-Aminobenzoic

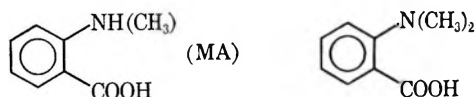
Acids in Their Lowest Singlet and Triplet States

by A. Tramer¹

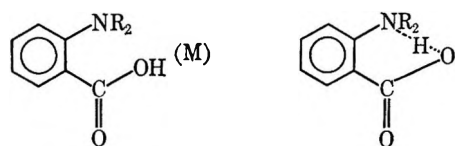
Institute of Physics, Polish Academy of Science, Wa-saw, Poland (Received June 2, 1969)

Absorption, fluorescence (in water at 293°K), and phosphorescence (in ethanol rigid glasses at 77°K) spectra of bications, cations, neutral molecules, and anions of *N*-methylantranilic and *N,N*-dimethylantranilic acids have been recorded. pK values in the excited singlet S_1 and triplet T_1 states have been evaluated by means of the Förster cycle. The constants K_t of the tautomeric equilibria between the molecular (M) $Ar(NH_2)(COOH)$ and quasizwitterionic (Z) $Ar(NH_3^+)(COO^-)$ forms of amino acids in both states have been determined. The solvent effects on the absorption and fluorescence spectra in nondissociating solvents and the kinetics of the $Z \rightleftharpoons M$ transition in excited states are discussed.

In the first part of the present work,² the structures of the tautomeric forms of the *o*-aminobenzoic acid derivative *N*-methylantranilic acid (MA) and *N,N*-dimethyl-



antranilic acid (DMA) were investigated by infrared and ultraviolet spectroscopy in their ground electronic state. It was shown that in the molecular (M) form, an intramolecular hydrogen bond between the carboxyl and amino groups is not formed, while in the quasizwitterionic form (Z) a strong intramolecular hydrogen bond ($-COO \cdots H \cdots NR_2$) changes the conformation of the amino group and removes the conjugation between the nitrogen lone electron pair and the ring π -electron system.



The equilibrium constant of the $M \rightleftharpoons Z$ reaction

$$K_t = \frac{[Z]}{[M]}$$

was evaluated and shown to be strongly solvent dependent. In all solvents, the K_t values are much higher in the case of DMA.

In this work, the problem of the tautomeric equilibria $M \rightleftharpoons Z$ in the lowest excited singlet and triplet states is discussed. The acidity constants K_a of the amino and carboxyl groups conjugated to the aromatic systems are known to change by many orders of magnitude and in opposite directions in the lowest excited singlet state (S_1).^{3a,b} Similar, though less pronounced, changes occur on excitation of a molecule to the lowest excited triplet state T_1 .⁴ It may, therefore,

be expected that K_t , related to the K_a values of interacting groups by Mason's equations,⁵ will be drastically changed in S_1 and T_1 states. If the direct determination of excited state K_t values (pK_t^S and pK_t^T) is impossible, they can be evaluated by combining the equilibrium constants pK_a^S or pK_a^T of protolytic reactions.^{5,6}

In this purpose absorption, fluorescence, and phosphorescence spectra were recorded for bicationic (B), cationic (C), molecular (M), and zwitterionic (Z) forms of neutral molecules and anions (A) of MA and DMA. The difference of the acidity constants in the excited (pK_a^e) and ground (pK_a^0) state of the AH acid was estimated from the spectral shift of the electronic transition in the acid AH and its conjugated base A^- .^{3a,7}

$$pK_a^e - pK_a^0 = \frac{hc}{kT} (\nu_{AH} - \nu_{A^-})$$

When it was possible, ΔpK_a was evaluated from the shift of the (0,0) band, determined as the intersection of normalized absorption and fluorescence bands. In other cases (nonfluorescent forms, S-T transitions) a similar reasoning may be based exclusively on the shift of the absorption or luminescence band, but the errors in the pK_a^e values are then certainly much greater.

From ΔpK_a and from the ground-state pK_a^0 values evaluated² for M and Z forms, the pK_a^S and pK_a^T constants and hence the pK_t^S and pK_t^T have been estimated. The conclusions are confirmed by a study of

(1) Laboratoire de Photophysique Moléculaire, Faculté des Sciences, 91, Orsay, France.

(2) A. Tramer, *J. Mol. Structure*, **4**, 313 (1969).

(3) (a) A. Weller, "Progress in Reaction Kinetics," Vol. I, Pergamon Press, Oxford, 1961, p 188; (b) H. Beens, H. Grellmann, M. Gurr, and A. H. Weller, *Disc. Faraday Soc.*, **39**, 183 (1965).

(4) G. Jackson and G. Porter, *Proc. Roy. Soc.*, **A260**, 15 (1961).

(5) S. F. Mason, *J. Chem. Soc.*, 675 (1958).

(6) R. E. Ballard and J. W. Edwards, *ibid.*, 4868 (1964).

(7) T. Förster, *Z. Elektrochem.*, **54**, 42, 531 (1950).

Table I: Absorption Spectra of Anthranilic Acids in Ethanol Solutions.

Form and solvent	Anthranilic acid		N-Methylantranilic acid		N,N-Dimethylantranilic acid	
	ν	ϵ	ν	ϵ	ν	ϵ
Neutral (M or Z) ethanol	29,500	5,200	28,100	5,900	29,500	20
					35,000	900
					36,000	1,000
	40,350	8,800	39,050	9,800		
	44,750	18,000	44,150	23,000	42,100	9,000
Cation (C) 1 N H ₂ SO ₄ in ethanol	35,650	900	35,600	750	35,200	800
	36,550	1,000	36,500	800	36,100	900
	44,250	13,000	43,850	14,000	42,700	11,800
Bication (B) concd H ₂ SO ₄	35,700	1,300	35,700	1,600	35,500	1,800
	41,950	9,800	41,750	10,750	42,200	12,600
Anion (A) 0.1 N NaOH in ethanol	31,150	4,000	29,750	1,900	32,700	1,750
	40,750	9,800	39,150	8,600	37,900	7,000
	43,850	10,000

Table II: Characteristics of the First ($S_1 \leftrightarrow S_0$ and $T_1 \rightarrow S_0$) Electronic Transitions for Differently Protonated Forms of N-Methylantranilic (MA) and N,N-Dimethylantranilic (DMA) Acids in Water

	B	C	MA	M	Z	A
ν_{abs}	35,800	36,600	28,400	28,400	37,000	30,250
ν_{fl}	22,500	22,500	...	23,900
ν_{00}	25,000 ^a	25,000 ^a	...	26,400 ^a
			25,450 ^b	25,450 ^b		27,200 ^b
ν_{ph}	24,100	24,400	21,600	21,600	...	21,900
			DMA			
ν_{abs}	35,700	36,400	31,000	31,000	37,000	33,100
ν_{fl}	27,200	...	22,700	22,700	...	23,700
ν_{00}	32,500 ^a	...	25,600 ^a	25,600 ^a	...	27,300 ^a
	31,450 ^b	...	26,850 ^b	26,850 ^b	...	28,400 ^b
ν_{ph}	23,900	24,400	20,100	20,100	24,700	21,600

^{a,b} (00) frequencies evaluated as: ^a frequencies of intersection points of absorption and fluorescence bands and ^b as $\nu_{00} = 1/2(\nu_{abs} + \nu_{fl})$.

the solvent effect on the absorption and fluorescence spectra of aminobenzoic acids and of their hydrogen-bonded complexes in nonaqueous solutions.

Experimental Section

The methods of purification of chemical compounds and the apparatus used for absorption measurements have been described.² The fluorescence spectra were recorded by means of a spectrofluorimeter composed of an SPM-1 Zeiss-Jena monochromator, an EMI 6256B photomultiplier, a UNIPAN 202 and 203 narrow-band amplifier and phase-sensitive detector, and an MAV recorder. The system was equipped with a 176-Hz chopper which could work also as a one-disk phosphoscope. The spectral sensitivity distribution was determined by recording the fluorescence spectra of standard compounds.⁸ The fluorescence was excited by the groups of Hg lines at 3650, 3130, and 2750 Å from an HBO 500 high-pressure mercury lamp isolated by means of Schott glass filters or a Zeiss 2750 Å interference filter.

The phosphorescence was excited either with the entire Hg spectrum or with selected wavelengths.

The fluorescence spectra were measured at the room temperature. The spectra of deaerated and non-deaerated solutions were found to be identical. The phosphorescence spectra were studied in ethanol rigid glasses at 77°K with silica cells immersed in liquid nitrogen in a silica dewar vessel equipped with optical windows. All solvents were nonfluorescent or very weakly fluorescent; when necessary, the background of the solvent fluorescence was taken into account.

Acid-Base Equilibria. To evaluate the pK_a^S values, absorption and fluorescence spectra of anthranilic acid, MA, and DMA were studied in water and in aqueous H₂SO₄ and NaOH solutions. The principal absorption bands of differently protonated forms are listed in Table I. More detailed data concerning the first $S_1 \leftrightarrow$

(8) E. Lippert, W. Nägele, I. Seibold-Blankenstein, H. Steiger, and W. Voss, *Z. Anal. Chem.*, **170**, 1 (1959).

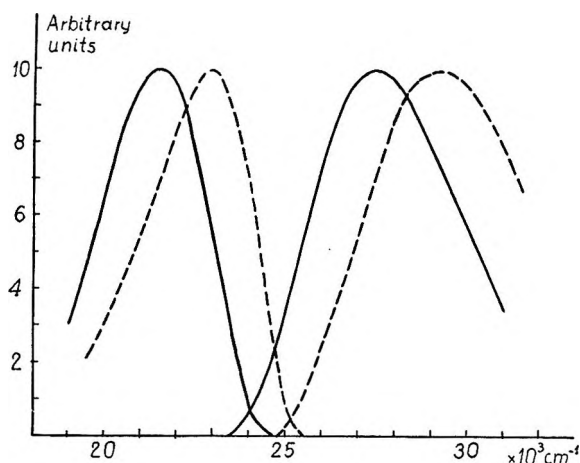


Figure 1. Absorption and fluorescence spectra of N-methylanthranilic acid: solid line, neutral molecule in water; broken line, anion (A) in 0.1 *N* NaOH_{aq}.

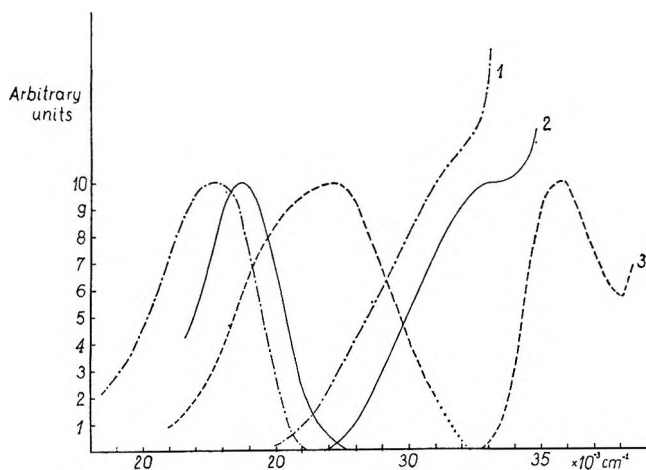


Figure 2. Absorption and fluorescence spectra of N,N-dimethylanthranilic acid: 1, neutral molecules (M + Z) in water; 2, anion (A) in 0.1 *N* NaOH_{aq}; 3, bication (B) in 35.7 *N* H₂SO₄.

S_0 and $T_1 \rightarrow S_0$ transitions in MA and DMA are given in Table II; absorption and fluorescence spectra are presented in Figures 1 and 2. The absorption spectra of neutral M and Z forms of MA and DMA were reproduced and discussed in ref 2.

The C forms (cations) of both acids are not fluorescent in 1–5 *M* H₂SO₄ solutions. In view of the close analogy of their absorption spectra with those of non-fluorescent *o*-alkylbenzoic acids, this fact is not astonishing. No fluorescence which could be ascribed as corresponding to the Z form of MA or DMA (close analogs of *o*-alkylbenzoate anions) was detected; the DMA fluorescence spectrum is always the mirror image of the absorption band of the M form, even when excited in the spectral region where all quanta are absorbed by the Z form.

A characteristic feature of both acids is a very small (as compared to the benzoic acid) red shift of the order of a few hundred cm^{-1} on protonation of the carboxyl

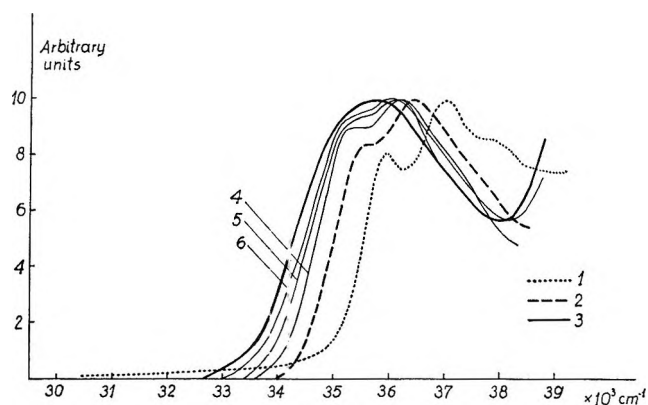


Figure 3. Absorption spectra of N,N-dimethylanthranilic acid: 1, M and Z forms in water; 2, cation (C) in 2 *N* H₂SO_{4(aq)}; 3, bication (B) in 35.7 *N* H₂SO₄; 4, 17.8 *N* H₂SO₄; 5, 28.4 *N* H₂SO₄; 6, 33.0 *N* H₂SO₄.

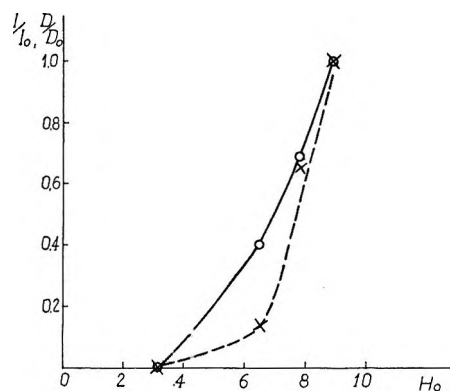


Figure 4. Relative optical densities (O) and fluorescence intensities (X) of the bication (B) of N,N-dimethylanthranilic acid vs. the H_0 acidity function of H₂SO₄ solutions.

group in concentrated sulfuric acid solutions. The process $B \rightleftharpoons C + H^+$ was studied in more detail in the case of DMA (Figure 3). The absorption spectrum is continuously red-shifted without any change in the band shape when the H₂SO₄ concentration is increased from 1 *N* to 20 *N*. This shift may be considered due to the solvent dielectric effects. A pronounced change in the band shape suggesting the formation of a new species (bication) occurs only in 25–35 *N* H₂SO₄ and is accompanied by the appearance of a violet fluorescence which is assigned to the B form. The optical densities D at 34,250 cm^{-1} (where the intensity changes are the most distinct) are taken as a measure of the bication concentration. In Figure 4, D/D_0 (where D_0 is the optical density at 34,250 cm^{-1} in 35.7 *N* H₂SO₄) is plotted against H_0 , the acidity function of H₂SO₄ solutions (H_+ would be more correct in this case, but we do not have reliable H_+ values for this concentration range⁹). In the same plot relative intensities of the bication fluorescence excited with λ 2750 Å, I/I_0 (where I_0 is its intensity in 35.7 *N* H₂SO₄), vs. H_0 are given. More con-

(9) M. A. Paul and F. A. Long, *Chem. Rev.*, **57**, 1 (1957).

concentrated acids would be needed for exact pK determinations but it seems that pK_{BC}^0 and pK_{BC}^S are very close to each other and amount to ~ -8 or less.

The phosphorescence of differently protonated forms was studied in ethanol rigid glass solutions: in pure ethanol (neutral molecules), in 1 *N* ethanolic H_2SO_4 (cations), and in 0.1 *N* ethanolic NaOH (anions). The bication spectrum was studied in concentrated H_2SO_4 rigid solution. For the first three forms the solvent shift need not be taken into account but the shift from B to C may be due to the solvent as well as to the protonation effect.

In the case of MA the phosphorescence spectra of B, C, M, and A forms may be easily identified. As might be expected, no *Z*-form phosphorescence was observed, the *Z* form being virtually nonexistent in ethanolic solutions. The phosphorescence of the B, C, and A forms of DMA resemble closely those of the analogous forms of MA, but quite specific effects are found in the case of neutral molecules. Here the spectrum when excited with unfiltered mercury light, consists of two bands: a weak band in the $25,000\text{-cm}^{-1}$ region, characteristic of B and C (protonated in the amino group) forms of both acids and a stronger band at $20,100\text{ cm}^{-1}$ which is red-shifted with respect to the M-form emission of MA (Figures 5, 6). When the phosphorescence is excited with Hg 3650-Å lines (absorbed only by the M form of DMA) the first band disappears. When the excitation is carried out with 2750-Å lines (*i.e.*, mainly the *Z* form is excited), the relative intensity of the first band increases. It seems reasonable to assign the first band to the phosphorescent transition in the *Z* form and the second to that in the M form of the neutral molecule. The dependence of the emission spectra on the wavelength of the exciting light shows that the *Z* \rightleftharpoons M transitions may take place during the lifetime of the excited species and that this process is an irreversible one.

From the spectra of different protonated forms, the spectral shifts $\nu_{AH} - \nu_A$ may be determined but the accuracy of the $\Delta\nu$ measurement varies a great deal from one case to another. The most reliable data may be obtained from the $S_1 \leftrightarrow S_0$ transition in the fluorescent compounds, *i.e.*, for M and A forms of both acids and the B form of DMA. The (0-0) transition is defined either as the average of the absorption and fluorescence band maxima or as the intersection point of normalized absorption and fluorescence band contours. The errors are somewhat greater in the case of DMA, where the $S_1 \leftarrow S_0$ absorption bands appear as shoulders of stronger absorption bands. The *Z* and C forms are not fluorescent but since their absorption bands possess a similar vibrational structure, the shifts of the corresponding maxima may be taken as very closely to that of the (0-0) transition. $\nu_C - \nu_M$ must be approximated also by the shift absorption maxima and, since the shapes of the bands

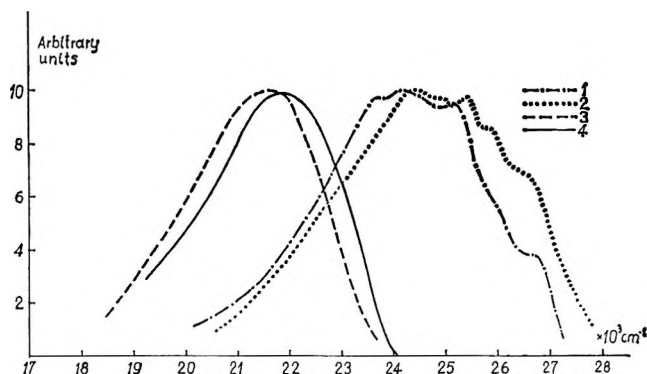


Figure 5. Phosphorescence spectra of N-methylanthranilic acid at 77°K: 1, B in 35.7 *N* H_2SO_4 ; 2, C in 1 *N* H_2SO_4 in ethanol; 3, M in ethanol; 4, A in 0.1 *N* NaOH in ethanol.

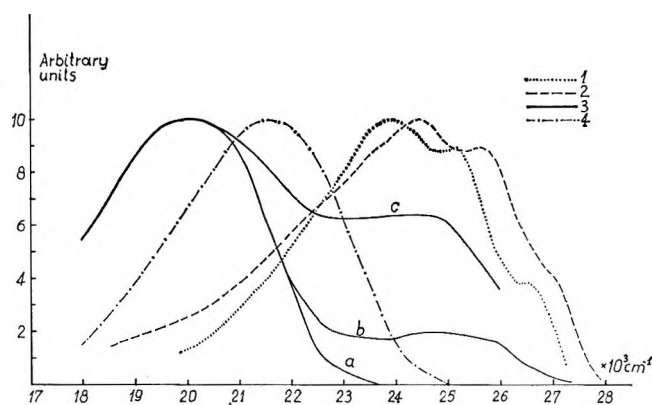


Figure 6. Phosphorescence spectra of N,N-dimethylanthranilic acid at 77°K: 1, B in 35.7 *N* H_2SO_4 ; 2, C in 2 *N* H_2SO_4 in ethanol; 3, M and *Z* in ethanol excited with (a) 3650-Å Hg lines (b) unfiltered Hg spectrum (c) 2750-Å Hg lines; 4, A in 0.1 *N* NaOH in ethanol.

are different, the errors in this case may be much greater. In evaluating the $\nu_H - \nu_C$ value the solvent shift from water to concentrated H_2SO_4 must be taken into account: $\Delta\nu$ is considered as being equal to the frequency difference between the absorption maxima of B and C in concentrated sulfuric acid solutions.

The data concerning the triplet state are deduced from the shifts in the phosphorescence spectra of ethanol rigid glass solutions. This procedure may be subjected to strong criticism. First of all, the shift of the band maximum may be not equal to that of the (0-0) transition, especially when the band shapes are different as it is for the M and C forms. A more serious objection is that the frequency shifts measured in ethanol rigid medium are applied to estimate the pK values in liquid water solutions where the energy of the phosphorescing species may be strongly influenced by the relaxation of solvent molecules.¹⁰

(10) A. Grabowska and B. Pakula, *Photochem. Photobiol.*, **9**, 339 (1969).

Table III: pK Values of *N*-Methylantranilic (MA) and *N,N*-Dimethylantranilic (DMA) Acids in S_0 (pK^0), S_1 (pK^S), and T_1 (pK^T) Electronic States

	MA			DMA		
	pK^0	pK^S	pK^T	pK^0	pK^S	pK^T
$pK_{BC} - pK_{BC}^0$...	1.7	0.65	...	1.5	1.1
pK_{CM}	2.61	-15	-3.4	4	-11.5	-7.5
pK_{CZ}	2.03	2.9	...	1.4	2.7	2.0
pK_{MA}	4.66	8.5	5.3	6	10	9
pK_{ZA}	5.48	-6.7	...	8.58	0.3	2
pK_t	-0.58	17.5	...	-2.6	9.8	6

pK_a^T values must be, therefore, considered only as rough approximations.

From the frequency differences $\nu_x - \nu_y$ deduced in this way the ΔpK values $pK_{zy}^S - pK_{zy}^0$ and $pK_{zy}^T - pK_{zy}^0$ may be calculated by means of the Weller equation^{3a}

$$pK^{\text{exc}} - pK^0 = \frac{0.625}{T} \Delta\nu$$

if the entropy of the protolytic reaction is assumed to be equal in the ground and in the excited state and pK_{zy} characterize different protolytic processes listed in Figure 7. pK_{zy}^0 values (except for pK_{BC}^0) were evaluated previously.¹ The values of pK^S and pK^T are given in Table III; for the $B \rightleftharpoons C + H^+$ equilibrium only ΔpK values are available.

Since the constant of the tautomeric equilibrium, K_t , is related to the acidity constants⁵

$$K_t = \frac{[Z]}{[M]} = K_{CZ}/K_{CM} = K_{MA}/K_{ZA}$$

K_t in S_1 state (K_t^S) for both acids and in T_1 state (K_t^T) for DMA only (in MA the phosphorescence of the *Z* form was not detected and K_{CZ}^T and K_{ZA}^T constants could not be determined) may be evaluated in two independent ways. The results differ by 2-3 pK units in all cases, and this may be taken as evidence that the errors in pK^{exc} estimations do not greatly exceed ordinary error limits in pK evaluations based on the Förster cycle.

From the data given in Table III, important conclusions concerning the structure of excited molecules may be deduced. (a) The $M \rightleftharpoons Z$ equilibrium is strongly displaced to the left in the S_1 and T_1 states. This would be expected on general considerations of the acid-base properties of aromatic amines and acids in the excited states. That the excitation of the *Z* form of DMA leads, in a variety of solvents, to the fluorescence emission of the *M* form is direct evidence of the stabilization of the *M* form in the S_1 state. This problem will be discussed in a more detailed way in the last section of this paper. (b) The acid properties of the $-NR_2H^+$ group are strongly increased in both excited states. As in the case of aromatic amines¹¹

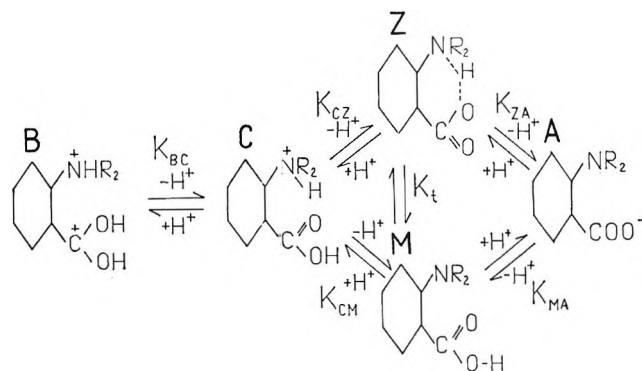


Figure 7. Scheme of protolytic reactions.

the change in pK is very high for the $S_1 \leftarrow S_0$ transition but is different for two processes involving the acid dissociation of the $-NR_2H^+$ group: $C \rightleftharpoons M + H^+$ and $Z \rightleftharpoons A + H^+$. The corresponding ΔpK values are -17.6 and -11.5 in the former case and -12.2 and -8.3 in the latter for MA and DMA, respectively. This difference probably exceeds the error limits and may be explained by the influence of the intramolecular hydrogen bond. The proton of the ammonium group is more strongly bonded to the $-COO^-$ group in *Z* than in the case of *C* which contains a more acidic $-COOH$ group.¹² In the excited state, increased basic properties of the carboxyl cancel to some extent the enhancement of the acid strength of the amino group. It should be pointed out that the pK increase in the T_1 state although considerably weaker than that in the S_1 state, is relatively large compared to aniline and naphthylamines.⁴ (c) Similar but more pronounced effects due to the presence of intramolecular hydrogen bonds are observed in the case of protolytic processes involving the carboxyl group. The acidity of the *M* form is lowered in the S_1 state ($\Delta pK \approx 4$) as for other aromatic acids.^{13,14} In contrast, the

(11) T. Förster in "Photochemistry in Liquid and Solid States," F. Daniels, Ed., John Wiley and Sons, New York, N. Y., 1960.

(12) E. Czarnecka and A. Tramer, submitted for publication.

(13) E. L. Wehry and L. B. Rogers, *J. Amer. Chem. Soc.*, **88**, 351 (1966).

(14) E. van der Donck and G. Porter, *Trans. Faraday Soc.*, **64**, 3215 (1968).

Table IV: Absorption (ν_{abs}) and Fluorescence (ν_{fl}) Band Maxima Frequencies, Frequencies of the (00) Transitions (ν_{00}), Stokes Shifts ($\delta\nu$), and Equilibrium Constants of Complex Formation in the Ground (K_g) and Excited S_1 (K_e) States of N-Methylantranilic Acid (MA)

Solvent	Base	ν_{abs}	ν_{fl}	ν_{00}	$\delta\nu$	K_g	K_e
Cyclohexane (monomer)	None	27,750	24,400	26,100	3350
Cyclohexane (dimer)	None	27,300	23,850	25,550	3450	7.5×10^3	8.5×10^4
Cyclohexane	Dioxane	28,050	24,300	26,250	3750	30	15
Cyclohexane	TEA	28,300	24,650	26,450	3650	900	100
Cyclohexane	Ethanol	28,100	24,000	26,000	4100
Dioxane	None	28,000	24,000	26,000	4000
Ethyl acetate	None	27,950	23,650	25,800	4300
Acetonitrile	Dioxane	27,800	23,350	26,100	4450
Ethanol	None	28,100	23,300	25,700	4800
Water	None	28,400	22,500	25,450	5900

equilibrium constants K_{CZ} and K_{BC} are less sensitive to the electronic excitation (ΔpK is 0.9 and 1.3 in the former and 1.7 and 1.5 in the latter case for MA and DMA, respectively) than the pK of the protonation of benzoic acid (an analog of the $\text{B C} + \text{H}^+$ reaction) which is increased in the S_1 state by +7 pK units.^{3b} The low values of ΔpK_{BC} and ΔpK_{CZ} as compared to ΔpK_{MA} may be explained by the effect of the $\text{NR}_2^+ \cdots \text{H} \cdots \text{O}=\text{C}$ hydrogen bond in Z (whose existence was shown by infrared spectroscopy²) and in C. As the acidity of the ammonium group increases in the S_1 state, the hydrogen bond is strengthened and this may counterbalance the enhancement of basic properties of the carboxyl group. Very poor proton-acceptor properties of the C form of DMA, stabilized probably by the intramolecular hydrogen bond, are directly evidenced by direct measurements of the absorption and fluorescence as a function of the acid concentration (Figure 4). For DMA, $pK_{\text{BC}}^0 \approx pK_{\text{BC}}^{\text{S}} \approx -8$ while, for the benzoic acid, $pK^0 = -7.4$ ¹⁵ and $pK^{\text{S}} = -1.2$.^{3b}

The results may be summarized by saying the effects of the electronic excitation on the acid-base properties of amino and carboxyl groups in the *ortho* position are qualitatively the same as in the case of isolated groups but they may be attenuated by the influence of the intramolecular hydrogen bond.

Solvent Effects in Nondissociating Solvents. Absorption and fluorescence of MA and DMA were studied in a series of solvents (cyclohexane, dioxane, ethyl acetate, aceto-nitrile, dimethylformamide, and ethanol) as well as in mixed solvents (cyclohexane-dioxane, cyclohexane-ethanol, cyclohexane-triethylamine (TEA), dimethylformamide-TEA). The solvent effects are due to a superposition of the dielectric solvent shift and of the spectrum changes resulting from the formation of hydrogen-bonded complexes with basic compounds. The effects of the second kind were studied in more detail for MA in cyclohexane solutions; the frequencies of absorption and fluorescence bands and the equilibrium constants of complex

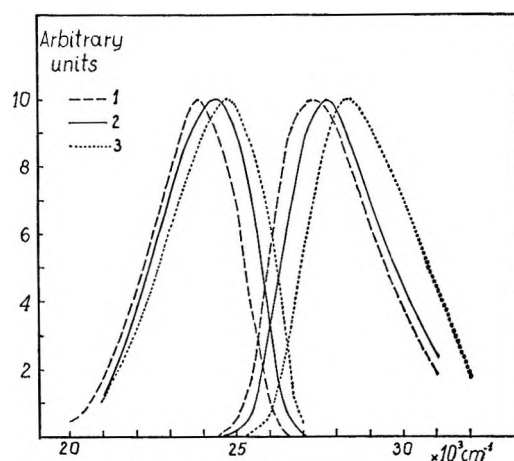


Figure 8. Absorption and fluorescence spectra of N-methylantranilic acid: 1, 5×10^{-4} mol/l. in cyclohexane (dimer); 2, 5×10^{-6} mol/l. in cyclohexane (monomer); 3, 10^{-6} mol/l. in 10^{-3} mol/l. TEA in cyclohexane (TEA complex).

formation in the ground state (K_g) and in the excited S_1 state of the amino acid molecule (K_e) are given in Table IV. K_g values were evaluated from the dependence of optical densities on the base concentration by means of the simplified Benesi-Hildebrand equation;¹⁶ K_e from the shift of the (0-0) band on complex formation by a procedure analogous to the Förster cycle.¹⁷ Some examples of the spectra are given in Figures 8 and 9.

As was previously shown,² MA is present in cyclohexane solutions solely in the M form. The dimer formation in more concentrated solutions is accompanied by a red shift of absorption and fluorescence bands. This effect seems to be quite general and its explanation was given by Hochstrasser in his study of 1-naphthoic acid solutions.¹⁸ The dimer composed

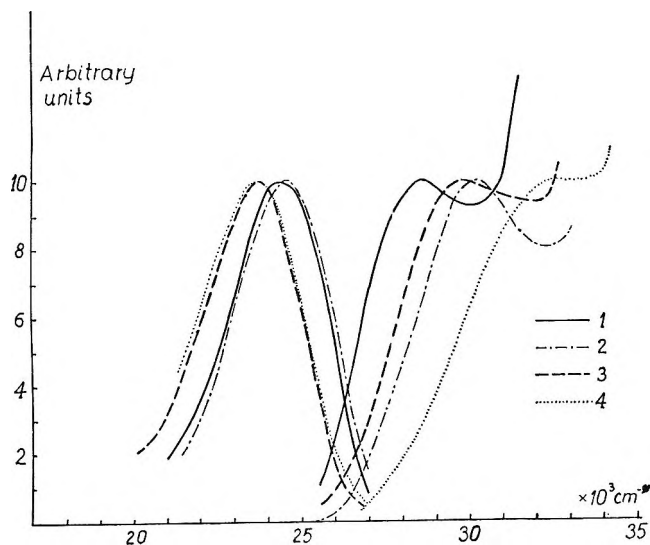
(15) L. A. Flexsner, L. P. Hammett, and A. Dingwall, *J. Amer. Chem. Soc.*, **57**, 2103 (1935).

(16) K. Szczepaniak, M. Golinska, and J. Mikolajczyk, *Acta Phys. Pol.*, **34**, 431 (1968).

(17) N. Mataga and Y. Kaifu, *Mol. Phys.*, **7**, 137 (1964).

Table V: Absorption and Fluorescence Maxima (ν_{abs} and ν_{fl}), Band Shifts ($\Delta\nu_{\text{abs}}$ and $\Delta\nu_{\text{fl}}$), and Stokes Shifts ($\delta\nu$) for *N,N*-Dimethylanthranilic Acid (DMA) Solutions

Solvent	Base	ν_{abs}	ν_{fl}	$\Delta\nu_{\text{abs}}$	$\Delta\nu_{\text{fl}}$	$\delta\nu$
Cyclohexane	Ncne	28,600	24,500	0	0	4100
Acetonitrile	Ncne	28,900	23,700	+300	-800	5200
Tetrahydrofuran		29,600	23,900	+1000	-600	5700
Cyclohexane	TEA	30,100	24,600	+1500	+100	5500
Dimethylformamide		30,200	23,800	+1600	-700	6400
Dimethylformamide	TEA	32,600	23,700	+4000	-800	8900

**Figure 9.** Absorption and fluorescence spectra of 10^{-4} mol/l. *N,N*-dimethylanthranilic acid in: 1, cyclohexane; 2, 0.7 mol/l. TEA in cyclohexane; 3, dimethylformamide; 4, 0.7 mol/l. TEA in dimethylformamide.

of one excited and one ground-state molecule is stabilized by the increased basic properties of the excited species and by the excitonic effects; hence, $K_g < K_e$ and $\Delta\nu < 0$.

In contrast, in the hydrogen-bonded complexes with basic (proton-acceptor) compounds, a weakening of intermolecular interactions in the excited state should be expected. The spectra of MA in the presence of dioxane, TEA, etc., are blue-shifted as anticipated, the shift being stronger for the absorption than for the fluorescence band. This effect is more pronounced in DMA, which is a very weak acid in the S_1 state ($pK = 9.6$). While the absorption spectrum of the M form is very sensitive to small quantities of TEA added to cyclohexane solution,² the fluorescence remains practically unchanged even at the TEA concentration of 1 mol/l. In strongly polar solvents (dimethylformamide, acetonitrile) where the absorption spectrum of the DMA-TEA complex, quite similar to that of the DMA anion, points to the formation of hydrogen-bonded ion pairs,² the emission spectrum is almost identical with that of free (bonded to solvent) DMA molecules (Figure 9). The acidity of DMA in the

excited state is so strongly reduced that hydrogen bonds are broken or extremely weakened.

The dielectric solvent effects are thus obscured by those of specific intermolecular interactions. It seems, however, possible to estimate their magnitude (in the case of MA only) if the choice of solvents is limited to those of similar basicity (dioxane, ethyl acetate) and to the nearly inert solvents containing a small amount of the base (dioxane) sufficient to ensure the bonding of almost all MA molecules. When the values of the Stokes shift $\delta\nu = \nu_{\text{abs}} - \nu_{\text{fl}}$ are plotted against the values of the Lippert-Mataga function of the solvent,^{19,20} the points corresponding to this group of solvents (marked by crosses in Figure 10) lie almost on a straight line, the slope of which is similar to that found by Mataga²⁰ for anthranilic acid. The difference between the ground-state (μ_g) and excited-state (μ_e) dipole moments of MA may be roughly estimated from the Lippert-Mataga equation

$$\delta\nu = \delta\nu_0 + \frac{(\mu_e - \mu_g)^2}{hca^3} F(n, \epsilon)$$

where

$$F(n, \epsilon) = \frac{\epsilon - 1}{2\epsilon + 1} - \frac{n^2 - 1}{2n^2 + 1}$$

as equal to $\mu_e - \mu_g = 1.75$ D, if the Onsager radius of the molecule is taken as $a = 3.5$ Å.

The Stokes shifts in other solvents are either smaller (monomer and dimer in cyclohexane) or much greater (ethanol, water). It seems that in the last case the strong solvent shifts may be due to the re-forming of the hydrogen-bonded system, solvent-solute, in the excited state (breaking of the $\text{ROH} \cdots \text{NR}_2^-$ and strengthening of the $\text{RO}-\text{H} \cdots \text{O}=\text{C}$ bonds).

In view of specific effects due to intermolecular interactions, the estimation of dielectric shifts in the case of DMA was not possible.

The Z \rightleftharpoons M Transitions in Excited States. As mentioned above, the excitation of the Z form of DMA results in a fluorescence emission corresponding to the

(18) R. M. Hochstrasser, *Can. J. Chem.*, **39**, 1776 (1961).

(19) E. Lippert, *Z. Elektrochem.*, **61**, 962 (1957).

(20) N. Mataga, *Bull. Chem. Soc. Jap.*, **36**, 654 (1963).

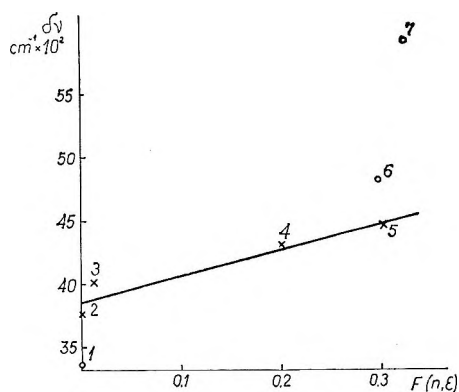


Figure 10. The Stokes shift in N-methylanthranilic acid spectra plotted vs. the $F(n, \epsilon)$ function of solvents.

M form. When the Z form is excited in rigid solutions, the phosphorescence consists of two bands assigned to Z and M forms, while the excitation of the M forms yields only the M form phosphorescent emission. The $Z \rightarrow M$ radiationless transition may thus take place during the lifetime of the excited species, but the process is irreversible as might be expected in view of the energy differences between corresponding S_1 and T_1 levels and of the values of the K_t^S and K_t^T equilibrium constants.

In Figure 11, possible ways of energy degradation in the case of the Z form excited to the S_1 state are listed. Relatively inefficient $S_1 \rightarrow S_0$ transitions²¹ are omitted. The T_1 level of the M form may be populated by two different ways, $S_1^Z \xrightarrow{k_7} T_1^Z \xrightarrow{k_8} T_1^M$ and $S_1^Z \xrightarrow{k_9} S_1^M \xrightarrow{k_6} T_1^M$. The first way is certainly effective since the (8) process is responsible for the M-form fluorescence excited in the Z form absorption region. Since the intersystem crossing in Z (7) and the $Z \rightarrow M$ transition are competitive, k_8 must be of a similar order of magnitude to k_7 . No data concerning k_7 in aromatic acids are available, but values of 10^{10} – 10^{12} sec^{-1} seem to be reasonable (cf. ref 22). If $k_8 = k_7$, the lifetime of the excited Z form would exceed by 2–3 orders of magnitude the period of O–H··N stretching vibrations. The analogous process in the lowest triplet state, the $T_1^Z \rightarrow T_1^M$ transition, if it occurs at all, is an extremely slow one. Its rate constant (k_9) must be comparable to $k_4 + k_5$ which is of the order of 1 sec^{-1} (in the case of $k_9 \gg k_4 + k_5$ the T_1^Z level would be rapidly depopulated and the Z-form phosphorescence would be quenched).

These estimations point to the existence of potential

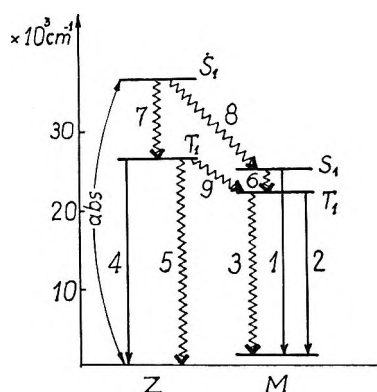


Figure 11. Scheme of lowest electronic levels and transitions in the neutral N,N-dimethylantranilic acid molecule.

energy barriers for $Z \rightarrow M$ processes very important in the T_1 , much lower in the S_1 state, although the energy differences between the Z and M forms are similar in both excited states. This barrier could be considered as corresponding to the proton transfer in the hydrogen bond but this explanation seems to be highly improbable. The potential energy barrier for the proton transfer in the much weaker and more symmetric hydrogen bond in the excited molecule of salicylic ester was shown to be very low.^{3b} In our case we are certainly concerned with a very strong, short (the $N \cdots O$ distance may be estimated to be $\sim 2.5 \text{ \AA}$) hydrogen bond. The other explanation that can be proposed is based on the assumption (discussed in more detail in ref 1) that the conformation of the dimethylamino group is different in the M form (the symmetry plane of the NR_2 group perpendicular to the ring plane—the nitrogen lone-electron pair conjugated with the ring π -electron system) and in the Z form (the symmetry plane of NR_2 in the ring plane). If this is the case, the $Z \rightarrow M$ transition would necessitate the rotation of the dimethylamino group around the C_{ar} –N bond, which would be the rate-determining step of the process.

In any case, the difference between the rates of the (8) and (9) processes is puzzling. More detailed studies of the fluorescence and phosphorescence yields and lifetimes and of their solvent and temperature dependence are needed to elucidate this problem and they are now in progress in this laboratory.

(21) V. L. Ermolaev and E. B. Sveshnikova, *Acta Phys. Pol.*, **34**, 771 (1968).

(22) M. A. El-Sayed, *ibid.*, **34**, 649 (1968).

A Calculation of the Energy Barriers Involved in the Isomerization Processes of Ethylene in Its Excited and Ionized States

by A. J. Lorquet^{1a}

Institut de Chimie, Université de Liège Sart-Tilman par Liège I, Belgium (Received August 1, 1969)

The lowest singlet and triplet electronic states of the ethylene molecule and the lowest doublet and quartet electronic states of its positive ion have been studied by a semiempirical quantum chemical method. For each state, the energy of several nuclear configurations has been calculated, in order to determine the preferred pathways of evolution. In the case of the triplet state, there are two low-energy processes. One of them is the *cis-trans* isomerization, and the second is a rearrangement process involving the ethylidene configuration (CH_2CH). The results agree with the accepted views concerning the sensitized photochemistry of ethylene.

Introduction

In a previous paper,^{1b} the C_2H_4^+ ion in its ground doublet state was studied by a semiempirical SCF calculation. It was shown that the equilibrium configuration of this ion was twisted, and that the potential function corresponding to the twisting motion had a double minimum and was remarkably flat. The exchange phenomenon occurring among hydrogen atoms (scrambling process) was also studied in the case of C_2H_4^+ , and it was concluded that this process took place through the asymmetrical configuration CH_2CH^+ .

The purpose of this paper is to report a similar study for the mechanisms involved in the evolution of the first triplet state. A comparative study will be made of the properties of the lowest electronic states of singlet and triplet multiplicity of the ethylene molecule and of doublet and quartet multiplicity of the ethylene ion. The method of calculation has been described elsewhere.^{1b} It is the CNDO/2² version of the self-consistent field molecular orbital method, with slight semiempirical modifications.

Results

The calculations have been made in the neighborhood of particular geometrical configurations, depicted in Figure 1, and conventionally designated as the "planar," "twisted," "perpendicular," "bridged," "doubly-bridged," "asymmetrical" (ethylidene), and "asymmetrically bridged" configurations. The latter configuration corresponds to the intermediate state postulated by Whalley³ in a study of the mercury-sensitized photochemistry of ethylene. Table I gives the energy of the most stable structure for each state and configuration, determined by varying every internuclear distance and angle, and measured from the ground state of the neutral molecule.

The method is found to overestimate the internuclear distances, but in a rather uniform way (20–25% increase).

Several experimental results are available to enable us to determine the accuracy of the calculations. They are summarized in Table II.^{4–8}

We conclude that, in general, the method is capable of giving fairly reliable estimates of at least qualitative significance.

A. The Twisting Motion. The corresponding potential function has already¹ been discussed in great detail for the doublet state of the ion. For the triplet state of the molecule and the quartet state of the ion, one notices from Table I that this motion does not involve the angle of twist θ only, but is accompanied by an appreciable variation of internuclear distances and angles, especially in the case of the quartet state.

Calculations were also made for intermediate values of the angle of twist (not reported here for the sake of brevity). They show that the potential function for the twisting motion is remarkably flat, especially in the neighborhood of the minimum.

B. The Flapping Distortion. Walsh⁹ has suggested that in its first excited state, the C_2H_4 molecule should

(1) (a) Chercheur qualifié du Fonds National Belge de la Recherche Scientifique; (b) A. J. Lorquet and J. C. Lorquet, *J. Chem. Phys.*, **49**, 4955 (1968).

(2) J. A. Pople and G. A. Segal *ibid.*, **44**, 3289 (1966).

(3) E. Whalley, *Can. J. Chem.*, **35**, 565 (1957).

(4) D. F. Evans, *J. Chem. Soc.*, 1735 (1960).

(5) J. E. Douglas, B. S. Rabinovitch, and F. S. Looney, *J. Chem. Phys.*, **23**, 315 (1955).

(6) D. P. Chong, and G. B. Kistiakowsky, *J. Phys. Chem.*, **68**, 1793 (1964).

(7) A. J. Merer and L. Schoonveld, *J. Chem. Phys.*, **48**, 522 (1968).

(8) W. C. Price and W. T. Tuttle, *Proc. Roy. Soc.*, **A174**, 207 (1940).

(9) A. D. Walsh, *J. Chem. Soc.*, 2325 (1953).

Table I: Energies of the Different Configurations of C_2H_4 and $C_2H_4^+$

Species	Configurations	Geometrical parameters	Energy, eV
Neutral molecule, singlet state	Planar	$\angle CCH = 122^\circ$; $R(CH) = 1.37 \text{ \AA}$; $R(CC) = 1.61 \text{ \AA}$; $\theta = 0^\circ$	0
	Perpendicular	$\angle CCH = 122^\circ$; $R(CH) = 1.37 \text{ \AA}$; $R(CC) = 1.67 \text{ \AA}$; $\theta = 90^\circ$	3.93
	Bridged	$R(C_1H_2) = 1.35 \text{ \AA}$; $R(C_1H_1) = 1.59 \text{ \AA}$; $R(CC) = 1.81 \text{ \AA}$	8.91
	Doubly bridged	$R(CC) = 1.71 \text{ \AA}$; $R(CH) = 1.71 \text{ \AA}$;	8.09
	Asymmetrical	$R(C_1H) = 1.36 \text{ \AA}$; $R(C_2H) = 1.38 \text{ \AA}$; $R(CC) = 1.70 \text{ \AA}$; $\angle C_2C_1H = 180^\circ$; $\angle C_1C_2H = 105^\circ$	3.27
	Asymmetricaly bridged	$R(CC) = 1.85 \text{ \AA}$; $R(CH_1) = 1.58 \text{ \AA}$; $R(CH_2) = 1.39 \text{ \AA}$; $R(H_1H_4) = 2.52 \text{ \AA}$; $\angle C_2C_1H_2 = 104^\circ$	2.90
Neutral molecule, triplet state	Planar	Vertical transition	4.52
	Planar	$\theta = 0^\circ$; $\angle CCH = 120^\circ$; $R(CH) = 1.36 \text{ \AA}$; $R(CC) = 1.78 \text{ \AA}$;	3.55
	Perpendicular	$\theta = 90^\circ$; $\angle CCH = 121^\circ$; $R(CH) = 1.37 \text{ \AA}$; $R(CC) = 1.72 \text{ \AA}$;	2.60
	Bridged	$R(CH_1) = 1.57 \text{ \AA}$; $R(CH_2) = 1.34 \text{ \AA}$; $R(CC) = 1.78 \text{ \AA}$	9.91
	Doubly bridged	$R(CC) = 1.66 \text{ \AA}$; $R(CH) = 1.77 \text{ \AA}$	8.62
	Asymmetrical	$R(CC) = 1.70 \text{ \AA}$; $R(C_1H) = 1.34 \text{ \AA}$; $R(C_2H) = 1.36 \text{ \AA}$; $\angle C_2C_1H = 180^\circ$; $\angle C_1C_2H = 107^\circ$	3.24
Ion, doublet state	Asymmetricaly bridged	$R(CC) = 1.60 \text{ \AA}$; $R(CH_1) = 2.19 \text{ \AA}$; $R(CH_2) = 1.38 \text{ \AA}$; $R(H_1H_4) = 0.96 \text{ \AA}$; $\angle C_2C_1H_2 = 133^\circ$	7.03
	Twisted	$\angle CCH = 120^\circ$; $R(CH) = 1.38 \text{ \AA}$; $R(CC) = 1.69 \text{ \AA}$; $\theta = 37^\circ$	11.44
	Planar	$\angle CCH = 120^\circ$; $R(CH) = 1.38 \text{ \AA}$; $R(CC) = 1.70 \text{ \AA}$; $\theta = 0^\circ$	11.54
	Perpendicular	$\angle CCH = 120^\circ$; $R(CH) = 1.38 \text{ \AA}$; $R(CC) = 1.68 \text{ \AA}$; $\theta = 90^\circ$	12.34
	Bridged	$R(C_1H_2) = 1.37 \text{ \AA}$; $R(C_1H_1) = 1.78 \text{ \AA}$; $R(CC) = 1.53 \text{ \AA}$	15.25
	Doubly bridged	$R(CC) = 1.7 \text{ \AA}$; $R(CH) = 1.7 \text{ \AA}$	16.70
Ion, quartet state	Asymmetrical	$R(CC) = 1.69 \text{ \AA}$; $R(C_1H) = 1.37 \text{ \AA}$; $R(C_2H) = 1.39 \text{ \AA}$; $\angle C_2C_1H = 180^\circ$; $\angle C_1C_2H = 104^\circ$	12.23
	Asymmetricaly bridged	$R(CC) = 1.64 \text{ \AA}$; $R(CH_1) = 1.66 \text{ \AA}$; $R(CH_2) = 1.39 \text{ \AA}$; $R(H_1H_4) = 2.44 \text{ \AA}$; $\angle C_2C_1H_2 = 135^\circ$	13.76
	Planar	$\angle CCH = 128^\circ$; $R(CH) = 1.41 \text{ \AA}$; $R(CC) = 1.72 \text{ \AA}$; $\theta = 0^\circ$	18.20
	Perpendicular	$\angle CCH = 104^\circ$; $R(CH) = 1.38 \text{ \AA}$; $R(CC) = 1.8 \text{ \AA}$; $\theta = 90^\circ$	17.57
	Bridged	$R(C_1H_2) = 1.36 \text{ \AA}$; $R(C_1H_1) = 1.59 \text{ \AA}$; $R(CC) = 1.86 \text{ \AA}$	19.32
	Doubly bridged	$R(CC) = 1.62 \text{ \AA}$; $R(CH) = 1.80 \text{ \AA}$	21.98
Ion, quartet state	Asymmetrical	$R(CC) = 1.80 \text{ \AA}$; $R(C_1H) = 1.41 \text{ \AA}$; $R(C_2H) = 1.39 \text{ \AA}$; $\angle C_2C_1H = 180^\circ$; $\angle C_1C_2H = 94^\circ$	18.90
	Asymmetricaly bridged	$R(CC) = 1.87 \text{ \AA}$; $R(CH_1) = 1.60 \text{ \AA}$; $R(CH_2) = 1.38 \text{ \AA}$; $R(H_1H_4) = 2.56 \text{ \AA}$; $\angle C_2C_1H_2 = 128^\circ$	18.07

Table II: Comparison between Calculated and Experimental Energies

Process	Energy, eV		Ref
	Calcd	Exptl	
(1) Vertical singlet-triplet transition	4.52	4.6	4
(2) Planar ground state to 90° twisted perpendicular ethylene in its singlet state	3.93	2.8 ^a	5
(3) Planar ground state to lowest level of the triplet state (perpendicular)	2.6	2.3	6
(4) Planar ground state to asymmetrical triplet state (ethylidene)	3.24	3.0 ^b	6
(5) Twisting motion of the $C_2H_4^+$ ion in its doublet state (two barriers) ^b	0.1	0.05	7
	0.8	0.3	7
(6) Adiabatic ionization	11.5	10.5	8

^a Activation energy of the *cis-trans* isomerization reaction involving no spin multiplicity change. ^b Estimated from bond dissociation energies and heats of hydrogenation.

have a pyramidal arrangement of the bonds about each C atom.

We have investigated this possibility by calculating the energy of the system as a function of the angle between the molecular plane before distortion and the plane $H_1C_1H_2$ after distortion, which we call δ .

In the case of the singlet state of the molecule and the doublet state of the ion, in the planar and perpendicular configurations, the minimum of energy corresponds to a value of δ equal to zero (no distortion takes place).

In the case of the triplet state, this kind of distortion stabilizes both the planar and the perpendicular con-

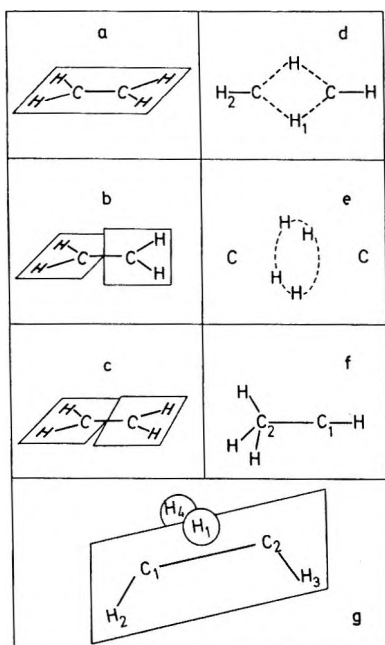
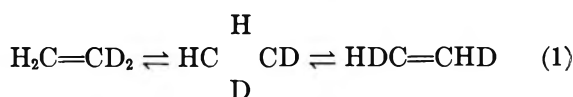


Figure 1. Geometrical configurations of ethylene and its ion: a, planar; b, perpendicular; c, twisted; d, bridged; e, doubly bridged; f, asymmetrical; and g, asymmetrically bridged.

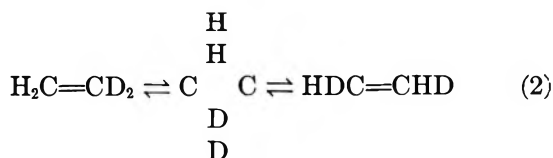
figurations, but to a small extent. When the molecule is *trans*-bent, the largest gain in energy is equal to 0.13 eV for a value of δ equal to 33° ; when it is *cis*-bent, the gain is equal to 0.4 eV for a value of δ of 42° . When the perpendicular configuration is distorted, the maximum gain in energy is equal to 0.09 eV ($\delta = 31^\circ$). The latter distortion leads to the most stable configuration of the triplet ($E = 2.51$ eV).

Our calculations agree with Walsh's predictions, but they also show that the gain in energy obtained by the flapping distortion is rather small.

C. *The Scrambling Process.* Four possible mechanisms for exchange phenomena among hydrogen atoms have been studied.



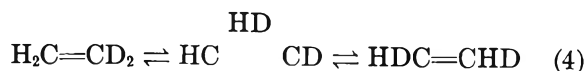
The intermediate form is the "bridged" structure represented in Figure 1d.



The intermediate form is the "doubly bridged" structure represented in Figure 1e.



The intermediate form is the "asymmetrical" structure represented in Figure 1f.



The intermediate form is the "asymmetrically bridged" structure proposed by Whalley³ and represented in Figure 1g.

The energy difference between each of the possible intermediate forms and the lowest energy configuration was calculated by the CNDO method for the lowest state of each multiplicity. Again, the geometrical configurations giving the lowest energy were determined by varying all the internuclear distances and angles. The results are summarized in Table III.

Table III: Energy Barriers for the Different Rearrangement Mechanisms^a

Process	E_{mol} , eV		E_{ion} , eV	
	Singlet	Triplet	Doublet	Quartet
(1)	8.9	7.3	3.8	1.8
(2)	8.1	6.0	5.3	4.4
(3)	3.3	0.6	0.8	1.3
(4)	2.9	4.4	2.3	0.5

^a This table gives, for each state, the energy difference between each intermediate structure and the lowest energy configuration. In the case of the neutral molecule, the lowest energy configuration is, for the singlet state, the planar configuration, and, for the triplet state, the perpendicular one (the small gain in energy realized by the flapping motion has not been taken into account). In the case of the ion, the lowest energy configuration is, for the quartet state the perpendicular configuration, and, for the doublet state, the twisted configuration.

Process 3 (*via* asymmetrical ethylidene) is therefore seen to be responsible for the rearrangement occurring in the ionic doublet and molecular triplet states, whereas in the case of the quartet state of the ion, a similar rearrangement process should probably occur through process 4.

A question now arises concerning the exact significance of the energy differences given in Table III—to what extent can these numbers be assimilated to activation energies? It is not evident that the energy variation along the reaction path will be of the type depicted in Figure 2a. A second possibility is depicted in Figure 2b; in that case, our calculations would indicate only a lower limit to the activation energies.

It is very difficult to investigate this by means of calculations because the number of geometrical parameters to optimize for a distorted intermediate calculation is very large. We tried it, however, in a favorable case.

One finds that the energy variation along the reaction path is uniform, as in Figure 2a. The calculation was made in the case of the doublet state of C_2H_4^+ passing from the planar to the bridged configuration. It was supposed that during the whole reaction the molecule was planar and had a center of symmetry.

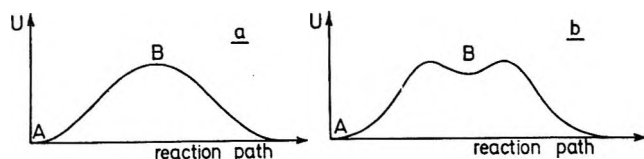


Figure 2. Two possible variations of the energy along the reaction path.

The progression of the reaction was measured by the value of α , the angle between the C_2C_1 bond and the C_1H_1 bond. The values of the other geometrical parameters were determined by successive approximations to obtain, for each value of α , the minimum value of the energy. The results are given in Table IV, where the

Table IV: Energy Variation along a Possible Reaction Path in the Case of the Doublet State of $C_2H_4^+$ Passing from the Planar to the Bridged Configuration

α	β	$R(C_1H_2)$, Å	$R(C_1H_1)$, Å	$R(CC)$, Å	E , eV
120°	120°	1.38	1.38	1.70	11.54
90°	131°	1.37	1.40	1.73	13.05
70°	161°	1.37	1.53	1.62	14.75
64° 33'	180°	1.37	1.78	1.53	15.25

energies are measured from the ground state of the neutral molecule, and β is the angle between the bonds C_2C_1 and C_1H_2 .

In the other cases, a similar calculation is practically impossible. In the intermediate steps, the symmetry of the molecule is very low. The number of possible reaction paths becomes very large, and the number of geometrical parameters to optimize for each point of a given path becomes prohibitively large.

But this very difficulty makes it reasonable, although by no means certain, to generalize our previous result, and to argue that the number of possible different paths leading from A to B (Figure 2) is so large that it will always be possible to find at least one with no secondary maximum.

The Sensitized Photochemistry of C_2H_4

The mechanism proposed by Callear and Cvetanović¹⁰ for the mercury sensitized reaction of ethylene is generally accepted. According to this mechanism, C_2H_4 is first converted into a vibrationally excited triplet state molecule (designated as $C_2H_4^*$), which can undergo *cis-trans* isomerization by deactivation. This state ($C_2H_4^*$) cannot decompose directly to acetylene and hydrogen, but can isomerize to another triplet state ($C_2H_4^{**}$) which can so decompose. The latter state ($C_2H_4^{**}$) is also capable of undergoing extensive hydrogen rearrangement. For that reason, Callear and Cvetanović suggested that the $C_2H_4^{**}$ state might have the ethylidene structure (CH_3CH ; see Figure 1f).

Our calculations agree with Callear and Cvetanović's mechanism, since they show that there are two low energy processes for the evolution of C_2H_4 in its triplet state: (1) *cis-trans* isomerization, with possible transformation into a quasi-free rotor, or (2) isomerization to triplet ethylidene. The other processes are characterized by much higher energy barriers (see Table III). In particular, the state suggested by Whalley³ (asymmetrical bridge, Figure 1g) as an alternative possibility for the structure of $C_2H_4^{**}$ is probably ruled out.

From Table I, one sees that the most stable configuration of the triplet state is the perpendicular one (2.6 eV above the ground state). Next comes the asymmetrical ethylidene at about 3.2 eV, and then the planar configuration at about 3.5 eV above the ground state. The energy necessary to convert the molecule into a free rotor is thus, according to our calculations, slightly greater than that required to induce the hydrogen migration.

cis-trans isomerization of deuterated species is, however, always possible even if the energy of the sensitizer is reduced down to about 2.6 eV, because the formation of the perpendicular triplet by collision need not be a vertical one. Collisional deactivation of the perpendicular triplet should give either isomer with equal probability, at least in the case of ethylene- d_2 , where there is no difference in energy between the two isomers in their ground state.

On the other hand, hydrogen rearrangement, evidenced by the formation of *anti-CH₂=CD₂* from *CHD=CHD*, is only possible if the sensitizer provides an amount of energy which we calculate as about 3.2 eV. This agrees with a recent experimental work,¹¹ where it is stated "This leads us to speculate that when the energy transferred to the vibrationally excited triplet state from a sensitizer is lower than the energy of the lowest triplet of benzene (*i.e.*, 3.6 eV), it does not always cross over to E^{**} even if it is not collisionally stabilized, but has a possibility to change to another state (probably another vibrationally excited state) which undergoes only *cis-trans* isomerization."

Finally, there appears to be a certain probability for the scrambling process to occur in the singlet state, this time probably by process (4), *i.e.*, the mechanism suggested by Whalley (ref 3 and last paragraph of ref 13).

Remarks on the Ethylene Decomposition Reaction. It has been pointed out by Cundall¹² that the decomposition reaction



is endothermic even in the mercury photosensitization experiments.

(10) A. B. Callear and R. J. Cvetanović, *J. Chem. Phys.*, **24**, 873 (1956); R. J. Cvetanović in "Progress in Reaction Kinetics," Vol. 2, G. Porter, Ed., Pergamon Press Ltd., London, 1964.

(11) S. Hirokami and S. Sato, *Can. J. Chem.*, **45**, 3182 (1967).

(12) R. B. Cundall, private communication.

Another possibility, however, would be that C_2H_2 is formed in the singlet state, either from a spin-forbidden predissociation or from the vibrationally excited singlet ground state of ethylene.

The second mechanism has been recently advocated by Hunziker,¹³ who has introduced a third intermediate state ($C_2H_4^\dagger$) in addition to the other two already postulated by Callear and Cvetanović.¹⁰ This new state would decompose into acetylene and hydrogen and would be produced from the triplet ethylidene by an intersystem crossing to some vibrationally excited singlet state.

What would be the geometrical configuration of this new intermediate state, postulated by Hunziker?

According to our calculations there are three possibilities corresponding to the three possible low-energy configurations of C_2H_4 in its singlet ground state: (1)

the planar configuration, (2) the asymmetrical ethylidene, and (3) the asymmetrical bridge proposed by Whalley.³ Concerning the latter, an independent observation by Hunziker in the isotopic scrambling might provide some possible evidence for the occurrence of the third possibility.

Acknowledgment. The author wishes to thank Dr. G. R. De Maré for suggesting the problem, and for a critical reading of the manuscript. She is also indebted to Professor R. B. Cundall for a fruitful correspondence. It is a pleasure to thank Professor L. D'Or for his interest in this work. The financial support of the Fonds de la Recherche Fondamentale Collective and of the Fonds National de la Recherche Scientifique of Belgium is gratefully acknowledged.

(13) H. E. Hunziker, *J. Chem. Phys.*, **50**, 1288 (1969).

Determination of the Equilibrium Constants of Associating Protein Systems. V. Simplified Sedimentation Equilibrium Boundary Analysis for Mixed Associations

by P. W. Chun and S. J. Kim

Department of Biochemistry, College of Medicine, University of Florida, Gainesville, Florida 32601
(Received August 25, 1969)

A simplified procedure for the determination of equilibrium constants for mixed associations of the type $iA + jB \rightleftharpoons A_iB_j$ or $nA + mB \rightleftharpoons A_iB_j + A_hB_l$, where $i + h = n$, and $j + l = m$, are described. The procedure is applied to a thermodynamically ideal situation, but its application in the analysis of reaction boundaries of any mixed association in a biological system is also considered. The equations outlined are based on concentration as a function of radial distance at sedimentation equilibrium.

In recent years, the theoretical treatment of associating protein systems of the type $nA + mB \rightleftharpoons C$ has been based on the interpretation of data obtained by various physical techniques.¹⁻⁵

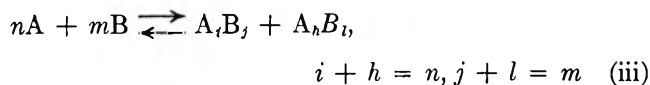
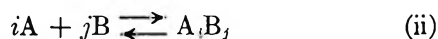
Nichol and Ogston⁶ and Adams⁷ have described procedures for analyzing mixed associations of this type in an ideal system from sedimentation equilibrium boundary experiments. Adams, *et al.*,⁸ describe the equilibrium constants and nonideal term B_{ij} evaluated from mixed associations using osmometric measurements (\bar{M}_{napp}).

The principal drawback of these earlier procedures for determination of the apparent equilibrium constant and composition of the complex is the cumbersome manipulation of the data involved.

This communication describes a greatly simplified procedure for quantitative evaluation of the equilibrium constants of any mixed type of association in an ideal

- (1) R. F. Steiner, *Arch. Biochem. Biophys.*, **49**, 71 (1954).
- (2) G. A. Gilbert, *Proc. Roy. Soc.*, **A250**, 377 (1959).
- (3) J. L. Bethune and G. Kegeles, *J. Phys. Chem.*, **65**, 1755 (1961).
- (4) G. A. Gilbert and R. C. Li. Jenkins in "Ultracentrifugal Analysis in Theory and Experiment," J. W. Williams, Ed., Academic Press, New York, N. Y., 1963, p 59.
- (5) L. W. Nichol, A. G. Ogston, and D. J. Winzor, *Arch. Biochem. Biophys.*, **121**, 517 (1967).
- (6) L. W. Nichol and A. G. Ogston, *J. Phys. Chem.*, **69**, 4365 (1965).
- (7) E. T. Adams, Jr., New York Academy of Science Conference on Advances in Ultracentrifugal Analysis, Feb 15, 1968.
- (8) E. T. Adams, Jr., A. H. Pekar, D. A. Soucek, L. H. Tang, and G. Barlow, *Biopolymers*, **7**, 5 (1969).

situation. Application of column matrix transformation is used in determining concentration as a function of radial distance at sedimentation equilibrium. Associations of the following three types are considered



Column Matrix Transformation for Evaluation of the Equilibrium Constant and Composition of the Complex

Basic Equations and Assumptions. The assumptions that are used in the analysis of mixed associations of all types based on sedimentation equilibrium experiments are (1) that the partial specific volumes of all species are the same, (2) that the refractive index increments of all species are equal, (3) that the system is ideal in that the activity coefficient of each solute species is unity, and (4) it is assumed that the system undergoes no volume change on chemical reaction. As the result of these assumptions, the differential equation for sedimentation equilibrium⁹ is given by

$$\frac{d \ln C_{ij}}{dr^2} = \frac{w^2(\partial \rho / \partial C_i) M_{ij}}{2RT} = LM_{ij} \quad (1)$$

where C_{ij} is the concentration of the component A_iB_j and $M_{ij} = iM_A + jM_B$, the partial differential, $\partial \rho / \partial C_i$, at constant concentration of all other species equals $(1 - \nu_i \rho)$. Equation 1 is integrated between any two limits, a and r , provided that $r_m \leq a$ and $r \leq r_b$ where r_m and r_b refer to meniscus and bottom of cell, respectively.

$$\ln \left[\frac{C_{ij}(r)}{C_{ij}(a)} \right] = LM_{ij}(r^2 - a^2) = L(iM_A + jM_B)(r^2 - a^2) \quad (2)$$

Substitution of $\ln [C_{A(r)}/C_{A(a)}] = LM_A(r^2 - a^2)$ and $\ln [C_{B(r)}/C_{B(a)}] = LM_B(r^2 - a^2)$ into eq 2 yields

$$\ln \left[\frac{C_{ij}(r)}{C_{ij}(a)} \right] - i \ln \left[\frac{C_{A(r)}}{C_{A(a)}} \right] - j \ln \left[\frac{C_{B(r)}}{C_{B(a)}} \right] = 0 \quad (3a)$$

$$\ln \left\{ \frac{C_{ij}(r)}{[C_{A(r)}]^i [C_{B(r)}]^j} \right\} = \ln \left\{ \frac{C_{ij}(a)}{[C_{A(a)}]^i [C_{B(a)}]^j} \right\} = \text{constant} \quad (3b)$$

Equation 3b can be written as

$$C_{ij} = K_{ij} C_A^i C_B^j \quad (4)$$

The equilibrium constant, K_{ij} , for reactions of the type $iA + jB \rightleftharpoons A_iB_j$ is given by eq 4 and the total concentration at r as

$$C = \sum_i \sum_j C_{ij} \quad (5)$$

Equations 1, 4, and 5 are fundamental expressions in the evaluation of equilibrium constants and composition of the complex for mixed association. Both Nichol and Ogston⁶ and Adams⁷ determined the apparent weight, average molecular weight, and concentration at each radial distance (r). Knowing these quantities, it is possible to evaluate C_A , C_B , and K for a mixed association of the type $A + B \rightleftharpoons C$ (see Appendix); however, the necessary calculations are burdensome. In contrast, the simplified procedure described here provides all necessary data for evaluation of equilibrium constants and composition using only the determination of $C = C(r)$.

Case I. $A + B \rightleftharpoons AB$

Method 1. The total concentration at r is given by

$$C_r = C_{A(r)} + C_{B(r)} + C_{AB(r)} \quad (6)$$

From eq 1 and 4

$$C_{A(r)} = C_{A(a)} e^{LM_A(r^2 - a^2)} \quad (7a)$$

$$C_{B(r)} = C_{B(a)} e^{LM_B(r^2 - a^2)}$$

$$C_{AB(r)} = KC_{A(r)}C_{B(r)} \quad (7b)$$

Substitution of eq 7a and 7b into 6 gives

$$C_r = C_{A(a)} e^{LM_A(r^2 - a^2)} + C_{B(a)} e^{LM_B(r^2 - a^2)} + KC_{A(a)}C_{B(a)} e^{L(M_A + M_B)(r^2 - a^2)} \quad (8)$$

In order to solve eq 8 and evaluate $C_{A(r)}$, $C_{B(r)}$, and $C_C(r) = C_{AB(r)}$,¹¹⁻²¹ the curve of C vs. r^2 obtained from either Schlieren²⁰ or Rayleigh fringe data¹¹⁻¹² must be constructed. In general, the C vs. r^2 ¹³ curve for mixed association will not be linear.

When three species are involved in equilibrium, the curve is bisected by three r^2 lines, each equidistant from the next. When four species coexist, four r^2 lines are plotted, and four simultaneous equations set up, etc.

(9) T. Svedberg and K. O. Pedersen in "Ultracentrifuge," Oxford University Press, London, 1940.

(10) E. F. Casassa and H. Eisenberg, *Advan. Protein Chem.*, **19**, 287 (1964).

(11) E. G. Richard and H. K. Schachman, *J. Phys. Chem.*, **63**, 1578 (1959).

(12) D. A. Yphantis, *Biochemistry*, **3**, 297 (1964).

(13) S. M. Klainer and G. Kegeles, *J. Phys. Chem.*, **59**, 952 (1955).

(14) L. D. Harris, "Numerical Methods using FORTRAN," Charles E. Merrill Books, Columbus, Ohio, 1964, p 149.

(15) E. T. Adams, Jr., *Biochemistry*, **4**, 1646 (1965).

(16) G. K. Ackers and T. E. Thompson, *Proc. Nat. Acad. Sci. U. S.*, **53**, 342 (1965).

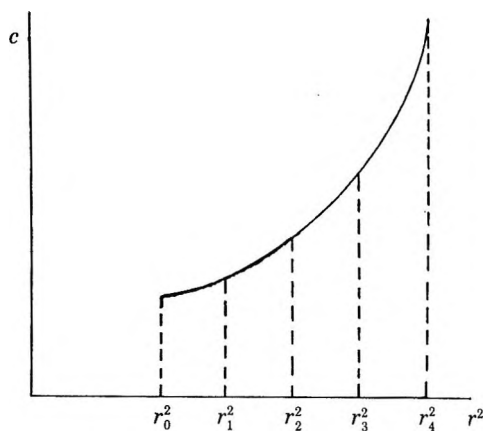
(17) P. W. Chun, S. J. Kim, C. A. Stanley, and G. K. Ackers, *Biochemistry*, **8**, 1625 (1969).

(18) P. W. Chun and S. J. Kim, *ibid.*, **8**, 1633 (1969).

(19) E. T. Adams, Jr., *ibid.*, **4**, 1655 (1965).

(20) D. J. Winzor, J. P. Loke, and L. W. Nichol, *J. Phys. Chem.*, **71**, 4492 (1967).

(21) O. Bryugdahl and S. Ljunggren, *ibid.*, **64**, 1264 (1960).



In this case, $r_2^2 - r_0^2 = 2(r_1^2 - r_0^2)$ and $r_3^2 - r_0^2 = 3(r_1^2 - r_0^2)$ where $a < r_0 < b$. Letting $(r_1^2 - r_0^2) = \Delta Z$, C_{r_1} , C_{r_2} , and C_{r_3} can be expressed in terms of eq 8.

$$\begin{aligned}
 C_{r_1} &= C_{A_{r_0}} e^{LM_A(r_1^2 - r_0^2)} + C_{B_{r_0}} e^{LM_B(r_1^2 - r_0^2)} + \\
 &\quad KC_{A_{r_0}B_{r_0}} e^{L(M_A + M_B)(r_1^2 - r_0^2)} \\
 &= C_{A_{r_0}} e^{LM_A(\Delta Z)} + C_{B_{r_0}} e^{LM_B(\Delta Z)} + \\
 &\quad KC_{A_{r_0}B_{r_0}} e^{L(M_A + M_B)(\Delta Z)} \\
 C_{r_2} &= C_{A_{r_0}} e^{LM_A 2(r_1^2 - r_0^2)} + C_{B_{r_0}} e^{LM_B 2(r_1^2 - r_0^2)} + \\
 &\quad KC_{A_{r_0}B_{r_0}} e^{L(M_A + M_B) 2(r_1^2 - r_0^2)} \\
 &= C_{A_{r_0}} e^{LM_A(2\Delta Z)} + C_{B_{r_0}} e^{LM_B(2\Delta Z)} + \\
 &\quad KC_{A_{r_0}B_{r_0}} e^{L(M_A + M_B)(2\Delta Z)} \quad (9) \\
 C_{r_3} &= C_{A_{r_0}} e^{LM_A 3(r_1^2 - r_0^2)} + C_{B_{r_0}} e^{LM_B 3(r_1^2 - r_0^2)} + \\
 &\quad KC_{A_{r_0}B_{r_0}} e^{L(M_A + M_B) 3(r_1^2 - r_0^2)} \\
 &= C_{A_{r_0}} e^{LM_A(3\Delta Z)} + C_{B_{r_0}} e^{LM_B(3\Delta Z)} + \\
 &\quad KC_{A_{r_0}B_{r_0}} e^{L(M_A + M_B)(3\Delta Z)}
 \end{aligned}$$

The evaluations which follow are arrayed in matrix form, due to the adaptability of matrices to computer

$$\begin{bmatrix} C_{r_1} \\ C_{r_2} \\ C_{r_3} \end{bmatrix} = \begin{bmatrix} \alpha & \beta & \alpha\beta \\ \alpha^2 & \beta^2 & \alpha^2\beta^2 \\ \alpha^3 & \beta^3 & \alpha^3\beta^3 \end{bmatrix} \begin{bmatrix} C_{A_{r_0}} \\ C_{B_{r_0}} \\ C_{C_{r_0}} \end{bmatrix} \quad (10a)$$

analysis and ease of application to various model systems. By determinants¹⁴ the solution to eq 9 is given by eq 10a. Note that ε matrix array is distinguished from some other array by the brackets as shown here. Here $\alpha = e^{LM_A \Delta Z}$, $\beta = e^{LM_B \Delta Z}$, and by Cramer's rule, eq 10b may be set up. Thus the concentration term $C_{A_{r_0}}$, $C_{B_{r_0}}$, and $C_{C_{r_0}}$ becomes

$$\begin{aligned}
 C_{A_{r_0}} &= D_{A/D} = \frac{C_r \alpha \beta^2 - C_{r_2} \beta (\alpha + 1) + C_{r_3}}{\alpha^2 (\beta - \alpha) (\beta - 1)} \\
 C_{B_{r_0}} &= D_{B/D} = \frac{C_{r_1} \beta \alpha^2 - C_{r_2} \alpha (\beta + 1) + C_{r_3}}{\beta^2 (\alpha - \beta) (\alpha - 1)} \quad (11) \\
 C_{C_{r_0}} &= D_{C/D} = \frac{C_{r_1} \alpha \beta - C_{r_2} (\alpha + \beta) + C_{r_3}}{\alpha^2 \beta^2 (\alpha - 1) (\beta - 1)}
 \end{aligned}$$

Having shown how to obtain the quantities $C_{A_{r_0}}$, $C_{B_{r_0}}$, and $C_{C_{r_0}}$, we evaluate the equilibrium constant from

$$K = \frac{C_{C_{r_0}}}{C_{A_{r_0}} C_{B_{r_0}}} = \frac{C_{C_r}}{C_{A_r} C_{B_r}} \quad (12)$$

The composition of the reacting boundary of the complex is determined by the expressions

$$\begin{aligned}
 C_{A_r} &= C_{A_{r_0}} e^{LM_A(r^2 - r_0^2)} \\
 C_{B_r} &= C_{B_{r_0}} e^{LM_B(r^2 - r_0^2)} \\
 C_{C_r} &= C_{C_{r_0}} e^{L(M_A + M_B)(r^2 - r_0^2)}
 \end{aligned}$$

The value of the equilibrium constant may be reconfirmed by selecting three new equidistant points r_1^2 , r_2^2 , and r_3^2 and repeating the procedure. The resulting value should be identical with the first.

Method 2. A modification of associations of the type $iA + jB \rightleftharpoons A_i B_j$. When i and j are known, eq 8 takes the form

$$C_r = C_{A_{r_0}} e^{LM_A(r^2 - r_0^2)} + C_{B_{r_0}} e^{LM_B(r^2 - r_0^2)} + KC_{A_{r_0}} C_{B_{r_0}}^j e^{L(iM_A + jM_B)(r_1^2 - r_0^2)} \quad (13)$$

$$D = \begin{vmatrix} \alpha & \beta & \alpha\beta \\ \alpha^2 & \beta^2 & \alpha^2\beta^2 \\ \alpha^3 & \beta^3 & \alpha^3\beta^3 \end{vmatrix} = \alpha^2\beta^2 \begin{vmatrix} 1 & 1 & 1 \\ \alpha & \beta & \alpha\beta \\ \alpha^2 & \beta^2 & \alpha^2\beta^2 \end{vmatrix} = \alpha^3\beta^3(\beta - \alpha)(\alpha - 1)(\beta - 1) \quad (10b)$$

$$C_{A_{r_0}} = D_{A/D}, \quad C_{B_{r_0}} = D_{B/D}, \quad \text{and} \quad C_{A_{r_0}B_{r_0}} = KC_{A_{r_0}}C_{B_{r_0}} = D_{C/D}$$

$$D_A = \begin{vmatrix} C_{r_1} & \beta & \alpha\beta \\ C_{r_2} & \beta^2 & \alpha^2\beta^2 \\ C_{r_3} & \beta^3 & \alpha^3\beta^3 \end{vmatrix} = \alpha\beta^2 \begin{vmatrix} C_{r_1} & 1 & 1 \\ C_{r_2} & \beta & \alpha\beta \\ C_{r_3} & \beta^2 & \alpha^2\beta^2 \end{vmatrix} = \alpha\beta^3(\alpha - 1)[C_{r_1}\alpha\beta^2 - C_{r_2}(\alpha + 1)\beta + C_{r_3}]$$

$$D_B = \begin{vmatrix} \alpha & C_{r_1} & \alpha\beta \\ \alpha^2 & C_{r_2} & \alpha^2\beta^2 \\ \alpha^3 & C_{r_3} & \alpha^3\beta^3 \end{vmatrix} = \alpha^2\beta \begin{vmatrix} 1 & C_{r_1} & 1 \\ \alpha & C_{r_2} & \alpha\beta \\ \alpha^2 & C_{r_3} & \alpha^2\beta^2 \end{vmatrix} = -\alpha^3\beta(\beta - 1)[C_{r_1}\alpha^2\beta - C_{r_2}\alpha^2(\beta + 1) + C_{r_3}]$$

$$D_C = \begin{vmatrix} \alpha & \beta & C_{r_1} \\ \alpha^2 & \beta^2 & C_{r_2} \\ \alpha^3 & \beta^3 & C_{r_3} \end{vmatrix} = \alpha\beta \begin{vmatrix} 1 & 1 & C_{r_1} \\ \alpha & \beta & C_{r_2} \\ \alpha^2 & \beta^2 & C_{r_3} \end{vmatrix} = \alpha\beta(\beta - \alpha)[C_{r_1}\alpha\beta - C_{r_2}(\beta + \alpha) + C_{r_3}]$$

where r_0 is the reference point and $r_m < r_0 < r_b$. Choosing equidistant points r_1 and r_2 , $(r_2^2 - r_0^2) = 2(r^2 - r_0^2)$. Letting $(r_1^2 - r_0^2) = \Delta Z$ and $C_{tjr} = KC_{A_0}^i C_{B_0}^j$, the following set of simultaneous equations may be set up

$$\begin{aligned} C_{r_0} &= C_{A_0} + C_{B_0} + KC_{A_0}^i C_{B_0}^j = C_{A_0} + C_{B_0} + C_{tjr_0} \\ C_{r_1} &= C_{A_0} e^{LM_A(r_1^2 - r_0^2)} + C_{B_0} e^{LM_B(r_1^2 - r_0^2)} + \\ &\quad KC_{A_0}^i C_{B_0}^j e^{L(iM_A + jM_B)(r_1^2 - r_0^2)} \\ &= C_{A_0} e^{LM_A(\Delta Z)} + C_{B_0} e^{LM_B(\Delta Z)} + \\ &\quad C_{tjr_0} e^{L(iM_A + jM_B)(\Delta Z)} \quad (14) \end{aligned}$$

$$\begin{aligned} C_{r_2} &= C_{A_0} e^{LM_A 2(r_1^2 - r_0^2)} + C_{B_0} e^{LM_B 2(r_1^2 - r_0^2)} + \\ &\quad KC_{A_0}^i C_{B_0}^j e^{L(iM_A + jM_B) 2(r_1^2 - r_0^2)} \\ &= C_{A_0} e^{LM_A(2\Delta Z)} + C_{B_0} e^{LM_B(2\Delta Z)} + \\ &\quad C_{tjr_0} e^{L(iM_A + jM_B)(2\Delta Z)} \end{aligned}$$

By determinants, the solution to equation set 14 in matrix form is

$$\begin{bmatrix} C_{r_0} \\ C_{r_1} \\ C_{r_2} \end{bmatrix} = \begin{bmatrix} 1 & 1 & 1 \\ \alpha & \beta & \alpha^i \beta^j \\ \alpha^2 & \beta^2 & \alpha^{2i} \beta^{2j} \end{bmatrix} \begin{bmatrix} C_{A_0} \\ C_{B_0} \\ C_{tjr_0} \end{bmatrix} \quad (15)$$

where $\alpha = e^{LM_A \Delta Z}$, $\beta = e^{LM_B \Delta Z}$. By Cramer's rule, eq 15 becomes $C_{A_0} = D_{A/D}$, $C_{B_0} = D_{B/D}$, $C_{C_0} = D_{C/D}$, where

$$D = \begin{vmatrix} 1 & 1 & 1 \\ \alpha & \beta & \alpha^i \beta^j \\ \alpha^2 & \beta^2 & \alpha^{2i} \beta^{2j} \end{vmatrix} = \alpha \beta (\beta - \alpha) (\alpha^{i-1} \beta^j - 1) \cdot (\alpha^i \beta^{j-1} - 1)$$

$$D_A = \begin{vmatrix} C_{r_0} & 1 & 1 \\ C_{r_1} & \beta & \alpha^i \beta^j \\ C_{r_2} & \beta^2 & (\alpha^i \beta^j)^2 \end{vmatrix} = \alpha^{2i} \beta^{2j} (\beta C_{r_0} - C_{r_1}) - \alpha^i \beta^j (\beta^2 C_{r_0} - C_{r_2}) + \beta (\beta C_{r_1} - C_{r_2})$$

$$D_B = \alpha^{2i} \beta^{2j} (\alpha C_{r_0} - C_{r_1}) - \alpha^i \beta^j (\alpha^2 C_{r_0} - C_{r_2}) + \alpha (\alpha C_{r_1} - C_{r_2})$$

$$D_C = (\beta - \alpha) [\alpha \beta C_{r_0} - (\alpha + \beta) C_{r_1} + C_{r_2}]$$

Knowing C_{A_0} , C_{B_0} , and C_{C_0} , we may evaluate the equilibrium constant for this system from

$$K = \frac{C_{C_0}}{(C_{A_0})^i (C_{B_0})^j} = \frac{C_{C_0}}{(C_{A_0})^i (C_{B_0})^j} \quad (16)$$

and the composition of the reaction boundary is determined from the expression

$$\begin{aligned} C_{A_r} &= C_{A_0} e^{LM_A(r^2 - r_0^2)} \\ C_{B_r} &= C_{B_0} e^{LM_B(r^2 - r_0^2)} \\ C_{C_r} &= C_{C_0} e^{L(iM_A + jM_B)(r^2 - r_0^2)} \end{aligned}$$

In solving for K , a number of values for i and j are assumed until the resulting K value remains constant. Note that when $i = j = 1$, equation set 14 becomes identical with equation set 9 of method 1; and when $j =$

0, $i = 2$, the result of analysis is similar to $2P_1 \rightleftharpoons P_2$. This method can be readily applied to a monomer- n -mer self-associating system.^{15-18, 20}

Case II. $nA + mB \rightleftharpoons A_n B_j + A_h B_l$;

$$i + h = n, j + l = m$$

When four species are involved in chemical equilibrium, the following simultaneous equations similar to equation set 8 may be set up

$$\begin{aligned} C_r &= C_{A_0} e^{LM_A(r^2 - r_0^2)} + C_{B_0} e^{LM_B(r^2 - r_0^2)} + \\ &\quad K_{tj} C_{A_0} C_{B_0} e^{L(iM_A + jM_B)(r^2 - r_0^2)} + \\ &\quad K_{hl} C_{A_0}^h C_{B_0}^l e^{L(hM_A + lM_B)(r^2 - r_0^2)} \quad (17) \end{aligned}$$

Here $r_m < r_0 < r_b$. Choosing equidistant points r_1 , r_2 , and r_3 , $r_2^2 - r_0^2 = 2(r_1^2 - r_0^2)$ and $r_3^2 - r_0^2 = 3(r_1^2 - r_0^2)$. Letting $(r_1^2 - r_0^2) = \Delta Z$, $C_{tjr_0} = K_{tj} C_{A_0}^i C_{B_0}^j$ and $C_{hlr_0} = K_{hl} C_{A_0}^h C_{B_0}^l$, four simultaneous equations result

$$\begin{aligned} C_{r_0} &= C_{A_0} + C_{B_0} + K_{tj} C_{A_0}^i C_{B_0}^j + K_{hl} C_{A_0}^h C_{B_0}^l \\ C_{r_1} &= C_{A_0} e^{LM_A(r_1^2 - r_0^2)} + C_{B_0} e^{LM_B(r_1^2 - r_0^2)} + \\ &\quad K_{tj} C_{A_0}^i C_{B_0}^j e^{L(iM_A + jM_B)(r_1^2 - r_0^2)} + \\ &\quad K_{hl} C_{A_0}^h C_{B_0}^l e^{L(hM_A + lM_B)(r_1^2 - r_0^2)} \quad (18) \end{aligned}$$

$$\begin{aligned} C_{r_2} &= C_{A_0} e^{LM_A 2(r_1^2 - r_0^2)} + C_{B_0} e^{LM_B 2(r_1^2 - r_0^2)} + \\ &\quad K_{tj} C_{A_0}^i C_{B_0}^j e^{L(iM_A + jM_B) 2(r_1^2 - r_0^2)} + \\ &\quad K_{hl} C_{A_0}^h C_{B_0}^l e^{L(hM_A + lM_B) 2(r_1^2 - r_0^2)} \\ C_{r_3} &= C_{A_0} e^{LM_A 3(r_1^2 - r_0^2)} + C_{B_0} e^{LM_B 3(r_1^2 - r_0^2)} + \\ &\quad K_{tj} C_{A_0}^i C_{B_0}^j e^{L(iM_A + jM_B) 3(r_1^2 - r_0^2)} + \\ &\quad K_{hl} C_{A_0}^h C_{B_0}^l e^{L(hM_A + lM_B) 3(r_1^2 - r_0^2)} \end{aligned}$$

Equation 18 becomes

$$\begin{aligned} C_{r_0} &= C_{A_0} + C_{B_0} + C_{tjr_0} + C_{hlr_0} \\ C_{r_1} &= C_{A_0} \alpha + C_{B_0} \beta + C_{tjr_0} \alpha^i \beta^j + C_{hlr_0} \alpha^h \beta^l \\ C_{r_2} &= C_{A_0} \alpha^2 + C_{B_0} \beta^2 + C_{tjr_0} \alpha^{2i} \beta^{2j} + C_{hlr_0} \alpha^{2h} \beta^{2l} \\ C_{r_3} &= C_{A_0} \alpha^3 + C_{B_0} \beta^3 + C_{tjr_0} \alpha^{3i} \beta^{3j} + C_{hlr_0} \alpha^{3h} \beta^{3l} \end{aligned} \quad (19)$$

where $\alpha = e^{LM_A \Delta Z}$, $\beta = e^{LM_B \Delta Z}$. By determinants, the solution to equation set 19 is

$$\begin{bmatrix} C_{r_0} \\ C_{r_1} \\ C_{r_2} \\ C_{r_3} \end{bmatrix} = \begin{bmatrix} 1 & 1 & 1 & 1 \\ \alpha & \beta & \alpha^i \beta^j & \alpha^h \beta^l \\ \alpha^2 & \beta^2 & (\alpha^i \beta^j)^2 & (\alpha^h \beta^l)^2 \\ \alpha^3 & \beta^3 & (\alpha^i \beta^j)^3 & (\alpha^h \beta^l)^3 \end{bmatrix} \begin{bmatrix} C_{A_0} \\ C_{B_0} \\ C_{tjr_0} \\ C_{hlr_0} \end{bmatrix} \quad (20)$$

Application of Cramer's rule gives values for C_{A_0} , C_{B_0} , C_{tjr_0} , and C_{hlr_0} , and the quantities C_{A_r} , C_{B_r} , C_{tjr} , C_{hlr} , K_{tj} , and K_{hl} are evaluated as before.

When $m = j = l = 0$, then three species $qP_1 \rightleftharpoons SP_i + rP_h$ coexist at chemical equilibrium, where $h > i > l$, for the self-associating system.¹⁵⁻¹⁹ In addition to the mixed associations described here, this method could be extended to indefinite mixed associations or associations of the type $nA + mB + lC \rightleftharpoons$

$A_nB_mC_l$. Thus it is widely applicable to the association of biological systems which exhibit multiple equilibria through the construction of the $C = C(r)$ curve.

Acknowledgment. This work was supported by National Institutes of Health Research Grant NIH FR 05362-06, 07.

Appendix

The abbreviated outline of procedures for determination of equilibrium constants developed by Nichol and Ogston⁶ and Adams⁷ is given below for contrast with our simplified method.

1. Nichol and Ogston Method.⁶

$$C_{r_0}(M_c - M_{wr_0})e^{LM_A(r^2 - r_0^2)} - C_r(M_c - M_{wr}) = (M_c - M_A)C_{A_{r_0}}[e^{LM_A(r^2 - r_0^2)} - e^{LM_B(r^2 - r_0^2)}] \quad (1')$$

$$C_{r_0}(M_c - M_{wr_0})e^{LM_B(r^2 - r_0^2)} - C_r(M_c - M_{wr}) = (M_c - M_B)C_{B_{r_0}}[e^{LM_B(r^2 - r_0^2)} - e^{LM_A(r^2 - r_0^2)}] \quad (2')$$

From eq 1' and 2', $C_{A_{r_0}}$ and $C_{B_{r_0}}$ may be evaluated. $C_{C_{r_0}}$ is determined from the equation

$$C_{C_{r_0}} = C_{r_0} - C_{A_{r_0}} - C_{B_{r_0}}$$

knowing $C_{A_{r_0}}$, $C_{B_{r_0}}$, and $C_{C_{r_0}}$, we may determine the composition of the boundary complex from

$$C_{A_r} = C_{A_{r_0}}e^{LM_A(r^2 - r_0^2)}$$

$$C_{B_r} = C_{B_{r_0}}e^{LM_B(r^2 - r_0^2)}$$

$$C_{C_r} = C_{C_{r_0}}e^{LM_C(r^2 - r_0^2)}$$

The equilibrium constant is then evaluated from $K = C_{C_r}/C_{A_r}C_{B_r}$.

2. Adams Method.⁷

$$C\left(\frac{M_w}{M_A} - 1\right) = C_{B_{r_0}}e^{\phi_B}\left(\frac{M_B}{M_A} - 1\right) + KC_{A_{r_0}}^m C_{B_{r_0}}^n \left(\frac{M_C}{M_A} - 1\right)e^{m\phi_A + n\phi_B} \quad (3')$$

Dividing eq 3' by e^{ϕ_B} [which is $\ln [C_{B_r}/C_{B_{r_0}}] = LM_B \cdot (r^2 - r_0^2)$]

$$y_B = C\left(\frac{M_w}{M_A} - 1\right)/e^{\phi_B} = C_{B_{r_0}}\left(\frac{M_B}{M_A} - 1\right) + KC_{A_{r_0}}^m C_{B_{r_0}}^n \left(\frac{M_C}{M_A} - 1\right)e^{m\phi_A + (n-1)\phi_B}$$

where

$$\phi_A = \ln \left[\frac{C_{A_r}}{C_{A_{r_0}}} \right] = LM_A(r^2 - r_0^2)$$

Similarly

$$y_A = C\left(\frac{M_w}{M_B} - 1\right)/e^{\phi_A} = C_{A_{r_0}}\left(\frac{M_A}{M_B} - 1\right) + KC_{A_{r_0}}^m C_{B_{r_0}}^n \left(\frac{M_C}{M_B} - 1\right)e^{(m-1)\phi_A + n\phi_B}$$

plotting y_B vs. $e^{[m\phi_A + (n-1)\phi_B]}$ yields $C_{B_{r_0}}[(M_B/M_A) - 1]$ as the hypothetical y_B intercept where the exponential function is zero and $KC_{A_{r_0}}^m C_{B_{r_0}}^n [(M_C/M_A) - 1]$ is the slope. A value for $C_{A_{r_0}}$ is determined from a plot of y_A vs. $e^{[(m-1)\phi_A + n\phi_B]}$ at the intercept. Then knowing $C_{A_{r_0}}$, $C_{B_{r_0}}$, and $C_{C_{r_0}}$, we may evaluate the composition of the complex and the equilibrium constant.

Estimation of the Excess Thermodynamic Functions of Nonelectrolyte Solutions from the First-Order Perturbation of a Hard-Sphere System¹

by T. Boublik² and G. C. Benson

Division of Pure Chemistry, National Research Council of Canada, Ottawa, Canada (Received March 17, 1969)

Expressions for the excess functions of a binary mixture of nonpolar molecules were derived from a first-order perturbation treatment using the equation of state and distribution function for a system of hard spheres and assuming a square-well interaction potential. Application of the equations to data for the system cyclopentane-carbon tetrachloride at 25° provided a satisfactory correlation between the excess thermodynamic functions and properties of the pure component liquids.

Introduction

Recently,³⁻⁵ relations were formulated for calculation of the thermodynamic functions of a pure liquid, assuming the effect of the attractive part of the intermolecular forces (together with the contribution due to softness of the repulsive part) to be a perturbation of a system of hard spheres. The equation of state and radial distribution of the latter is relatively well known either from the solution of the Percus-Yevick equation^{6,7} or from the scaled-particle theory.⁸

Yosim^{9,10} used the results of the scaled particle theory to calculate the heat of vaporization of the pure liquid and the excess entropy of a binary solution. These calculations exploited the idea of a thermodynamic cycle in which "charging" and "discharging" of the hard spheres by intermolecular forces occurred. This is also the starting point of the following treatment.

Theoretical Considerations

The process of mixing the pure components (numbers of molecules N_i) to form a mole of solution at constant temperature T and pressure p can be imagined to take place in five isothermal steps. (i) The pure components (molar volumes V_i) are "discharged" to hard-sphere systems at constant volume. (ii) Each hard-sphere system is expanded from volume V_i to some large volume V^* for which the behavior is ideal ($p^*V^* = RT$). (iii) The components are mixed at constant pressure p^* . (iv) The solution of hard spheres is compressed to volume V_s where V_s is the molar volume of the real solution with composition $x_i = N_i/N_A$ (N_A is Avogadro's number) at temperature T and pressure p . (v) The hard spheres are "charged" with attractive forces at constant volume V_s .

The entropy of mixing per mole, ΔS^M , calculated from these steps is

$$\Delta S^M = \sum_i x_i(S_i^0 - S_i) + \sum_i x_i \int_{V_i}^{V^*} \left(\frac{\partial S_i}{\partial V} \right)_T dV + \Delta S^0 + \int_{V^*}^{V_s} \left(\frac{\partial S_s}{\partial V} \right)_T dV + S_s - S_s^0 \quad (1)$$

where S_i and S_s are the entropies of component i and of the solution, respectively. The superscript zero denotes the hard sphere system and ΔS^0 is the molar entropy of mixing of the hard sphere components at high dilution. Similarly, the energy change associated with the mixing (*i.e.*, the excess energy, essentially at constant pressure) is given by

$$U^E = \sum_i x_i(U_i^0 - U_i) + \sum_i x_i \int_{V_i}^{V^*} \left(\frac{\partial U_i}{\partial V} \right)_T dV + \Delta U^0 + \int_{V^*}^{V_s} \left(\frac{\partial U_s}{\partial V} \right)_T dV + U_s - U_s^0 \quad (2)$$

where U_i and U_s are the energies per mole of component i and of the solution, respectively. ΔU^0 is the energy of mixing of the hard sphere systems (at $V^* \rightarrow \infty$) and is obviously equal to zero. Also since for hard spheres the ratio p/T is a function only of the volume it follows that $(\partial U/\partial V)_T^0$ vanishes and that $T(\partial S/\partial V)_T^0$ is equal to the pressure. Thus eq 1 and 2 can be simplified to the forms

$$TS^E = T[S_s - S_s^0 - \sum_i x_i(S_i - S_i^0)] + \sum_i x_i \int_{V_i}^{V^*} p_i^0 dV - \int_{V_s}^{V^*} p_s^0 dV \quad (3)$$

and

$$U^E = U_s - U_s^0 - \sum_i x_i(U_i - U_i^0) \quad (4)$$

(1) Issued as NRCC No. 11194.

(2) National Research Council of Canada Postdoctorate Fellow, 1967-1968. Institute of Chemical Process Fundamentals, Czechoslovak Academy of Science, Prague, Czechoslovakia.

(3) R. W. Zwanzig, *J. Chem. Phys.*, **22**, 1420 (1954).

(4) J. A. Barker and D. Henderson, *ibid.*, **47**, 2856 (1967).

(5) J. A. Barker and D. Henderson, *ibid.*, **47**, 4714 (1967).

(6) J. L. Lebowitz, *Phys. Rev.*, **133**, A895 (1964).

(7) J. S. Rowlinson, *Mol. Phys.*, **7**, 349 (1964).

(8) H. Reiss, *Advan. Chem. Phys.*, **9**, 1 (1965).

(9) S. J. Yosim and B. B. Owens, *J. Chem. Phys.*, **39**, 2222 (1963).

(10) S. J. Yosim, *ibid.*, **43**, 286 (1965).

In preparation for evaluating the molecular parameters of the pure components, we consider two different isothermal processes for evaporating a pure liquid initially at pressure p_i^{sat} (saturation vapor pressure) to produce a gas at very high dilution (pressure $p^* \rightarrow 0$). In the first process the liquid is "discharged" at constant volume to produce a hard-sphere system and then expanded to volume V^* ($p^*V^* = RT$). In the second process, the liquid is evaporated at constant pressure p_i^{sat} and then expanded to volume V^* . From a comparison of the changes in energy, and of the changes in entropy, associated with these processes, it follows that

$$U_i - U_i^0 = -\Delta U_{i,\text{coh}} \quad (5)$$

and

$$-(S_i - S_i^0) + \int_{V_i}^{V^*} \left(\frac{\partial p}{\partial T} \right)_V dV = \frac{\Delta H_{i,\text{vap}}}{T} + \int_{p^*}^{p_i^{\text{sat}}} \left(\frac{\partial V_{i,g}}{\partial T} \right)_p dp \quad (6)$$

Here, $\Delta U_{i,\text{coh}}$ is the cohesion energy, $\Delta H_{i,\text{vap}}$ the heat of vaporization, and $V_{i,g}$ the vapor phase volume, of component i .

Assuming that the energy due to attractive forces is a sum of pair interactions which can be treated as a perturbation of the potential of hard spheres, it has been shown⁴ that the Helmholtz free energy of a pure component is given by

$$F_i/N_A kT = F_i^0/N_A kT + (N_A/2V_i kT) \int_{\sigma_{ii}}^{\infty} u_{ii}(r) g_{ii}^0(r) 4\pi r^2 dr \quad (7)$$

where only the first-order term in the perturbation treatment is retained and the proper choice of hard-sphere diameter d_{ii} is used.¹¹ In this equation, k is the Boltzmann constant, $u_{ii}(r)$ is the potential between a pair of molecules of species i with centers separated by a distance r , $g_{ii}^0(r)$ is the radial distribution function of the unperturbed system, *i.e.*, the hard-sphere system, and σ_{ii} is the separation for which $u_{ii}(r)$ vanishes. It can be seen from differentiation of eq 7 with respect to temperature that

$$S_i = S_i^0 \quad (8)$$

and hence that

$$U_i/N_A kT = U_i^0/N_A kT + (N_A/2V_i kT) \int_{\sigma_{ii}}^{\infty} u_{ii}(r) g_{ii}^0(r) 4\pi r^2 dr \quad (9)$$

Following arguments similar to those given for pure liquids it is possible to obtain first-order perturbation relations for the solution. Thus

$$F_s/N_A kT = F_s^0/N_A kT + (N_A/2V_s kT) \sum_{i,j} x_i x_j \int_{\sigma_{ii}}^{\infty} u_{ij}(r) g_{ij}^0(r) 4\pi r^2 dr \quad (10)$$

$$\mathcal{L}_s = S_s^0 \quad (11)$$

and

$$U_s/N_A kT = U_s^0/N_A kT + (N_A/2V_s kT) \sum_{i,j} x_i x_j \int_{\sigma_{ii}}^{\infty} u_{ij}(r) g_{ij}^0(r) 4\pi r^2 dr \quad (12)$$

It is clear from eq 3, 8, and 11 that the excess entropy of mixing is given by the hard sphere contribution.

$$TSE = \sum_i x_i \int_{V_i}^{V^*} p_i^0 dV - \int_{V_s}^{V^*} p_s^0 dV \quad (13)$$

This expression is identical with that derived by Yosim¹⁰ but has been obtained as a consequence of the limitation to first-order perturbation terms, without recourse to the original assumption that the "charging" and "discharging" terms cancel.

The pressure of a system of hard spheres at given temperature, volume, and numbers of molecules of different kinds is a function of the radii R_1, R_2, \dots of the hard spheres. For a binary mixture, Lebowitz, Helfand, and Praestgaard¹² derived the following equation of state from the scaled particle theory

$$\frac{p_s^0}{kT} = \frac{6}{\pi} \left[\frac{\xi_0}{(1 - \xi_3)} + \frac{3\xi_1\xi_2}{(1 - \xi_3)^2} + \frac{3\xi_2^3}{(1 - \xi_3)^3} \right] \quad (14)$$

where the variables ξ_n are defined by

$$\xi_n = \frac{\pi N_A}{6 V_s} \sum_i x_i (2R_i)^n \quad (15)$$

In the case of a one-component system, eq 14 becomes

$$\frac{p_i^0}{kT} = \frac{N_A}{V_i} \left[\frac{1}{1 - y_i} + \frac{3y_i}{(1 - y_i)^2} + \frac{3y_i^2}{(1 - y_i)^3} \right] \quad (16)$$

where

$$y_i = \frac{\pi N_A}{6 V_i} (2R_i)^3 \quad (17)$$

The integrals in eq 13 can be evaluated after substituting the hard-sphere pressures from eq 14 and 16. The formula for the excess entropy can then be written

$$TSE = RT \sum_i x_i \left\{ \ln \frac{V_s(1 - \xi_3)}{V_i(1 - y_i)} + 3 \left[\frac{y_i}{1 - y_i} - \frac{\xi_2(2R_i)}{1 - \xi_3} \right] + \frac{3}{2} \left[\frac{y_i^2}{(1 - y_i)^2} - \frac{\xi_2^2(2R_i)^2}{(1 - \xi_3)^2} \right] \right\} \quad (18)$$

The hard-sphere integral in eq 6 can be handled in a

(11) Cf. ref 5, eq 12.

(12) J. L. Lebowitz, E. Helfand, and E. Praestgaard, *J. Chem. Phys.*, **43**, 774 (1965).

similar manner. Evaluation of the second integral in eq 6 is based on the simple virial expression

$$V_i^g = \frac{RT}{p} + B_{ii} \quad (19)$$

where B_{ii} is the second virial coefficient. Using Haggmacher's formula¹³ to estimate the temperature variation of B_{ii} , the formula for the heat of vaporization becomes

$$\Delta H_i^{\text{vap}} = 2B_{ii}p_i^{\text{sat}} - RT \left[\ln \frac{p_i^{\text{sat}} V_i (1 - y_i)}{RT} - \frac{3 y_i (2 - y_i)}{2 (1 - y_i)^2} \right] \quad (20)$$

The radial distribution functions are needed for determining the excess energy (or free energy). The form of these functions is known from the scaled particle theory only for particles at closest approach; thus in a binary solution

$$g_{ij}^0(R_i + R_j) = \frac{1}{1 - \xi_3} + \frac{6\xi_2}{(1 - \xi_3)^2} \frac{R_i R_j}{R_i + R_j} + \frac{12\xi_2^2}{(1 - \xi_3)^3} \left(\frac{R_i R_j}{R_i + R_j} \right)^2 \quad (21)$$

which becomes

$$g_{ii}^0(2R_i) = \frac{1}{1 - y_i} + \frac{3}{2} \frac{y_i}{(1 - y_i)^2} + \frac{3}{4} \frac{y_i^2}{(1 - y_i)^3} \quad (22)$$

for a one-component system. Equations 21 and 22 are sufficient for considering those cases in which interactions which are significantly different from those of hard spheres occur only at intermolecular distances differing very slightly from closest approach; in other cases, the solution of the Percus-Yevick equation is required.

In the present treatment, the interactions are represented by the simple square-well potential

$$\left. \begin{aligned} u_{ij}(r) &= +\infty & r < \sigma_{ij} \\ &= -\epsilon_{ij} & \sigma_{ij} < r < \sigma_{ij} + a \\ &= 0 & r > \sigma_{ij} + a \end{aligned} \right\} \quad (23)$$

where

$$\sigma_{ij} = d_{ij} = R_i + R_j \quad (24)$$

and it is assumed that the distance a is very small. The integrals in eq 10 and 12 can then be approximated

$$\int_{\sigma_{ij}}^{\infty} u_{ij}(r) g_{ij}^0(r) 4\pi r^2 dr = -\epsilon_{ij} g_{ij}^0(R_i + R_j) 4\pi (R_i + R_j)^2 a \quad (25)$$

Defining the molecular parameter ω_{ij} by

$$\omega_{ij} = \epsilon_{ij} a / kT \quad (26)$$

eq 9 can be rearranged to

$$\frac{U_i^0 - U_i}{RT} = \frac{\Delta U_i^{\text{coh}}}{RT} = \omega_{ii} (N_A/V_i) 2\pi (2R_i)^2 g_{ii}^0(2R_i) \quad (27)$$

and eq 12 becomes

$$\frac{U_s^0 - U_s}{RT} = (N_A/V_s) \sum_{i,j} x_i x_j \omega_{ij} 2\pi (R_i + R_j)^2 g_{ij}^0(R_i + R_j) \quad (28)$$

The expression for the excess energy, obtained by combining eq 4, 21, 27, and 28 is

$$U^E = RT \left(\sum_i x_i \frac{\Delta U_i^{\text{coh}}}{RT} - \frac{2\pi N_A}{V_s} \sum_{i,j} x_i x_j \omega_{ij} \left[\frac{1}{(1 - \xi_3)} (R_i + R_j)^2 + \frac{6\xi_2}{(1 - \xi_3)^2} R_i R_j (R_i + R_j) + \frac{12\xi_2^2}{(1 - \xi_3)^3} R_i^2 R_j^2 \right] \right) \quad (29)$$

It appears unlikely that the contributions of hard spheres and of the attractive forces to the volumetric behavior of the system can be separated and derived from the thermodynamic cycle described above. Thus, in subsequent numerical calculations, eq 18 and 29 are used to express TS^E and U^E as functions of the temperature, volume, and certain molecular parameters R and ω .

Numerical Calculations

The utility of the equations derived in the preceding section was investigated by applying them to the system cyclopentane-carbon tetrachloride. This system was chosen because the component molecules are approximately spherical, and because data for the thermodynamic functions H^E , V^E , and G^E (i.e., the excess enthalpy, volume, and Gibbs free energy) at 25° are available.¹⁴ "Experimental" values of TS^E and U^E can be obtained from these results using the thermodynamic relations

$$TS^E = H^E - G^E \quad (30)$$

and

$$U^E = H^E - pV^E \quad (31)$$

The term pV^E is relatively small in the present case, and for practical purposes it is unnecessary to distinguish between U^E and H^E .

Several different ways of establishing the values of the molecular parameters (R_i and ω_{ij}) of the pure component liquids were investigated. In all cases, the semiempirical mixing rule

$$\omega_{12}^2 = \omega_{11}\omega_{22} \quad (32)$$

(13) J. E. Haggmacher, *J. Amer. Chem. Soc.*, **68**, 1123 (1946).

(14) T. Boublik, V. T. Lam, S. Murakami, and G. C. Benson, *J. Phys. Chem.*, **73**, 2356 (1969).

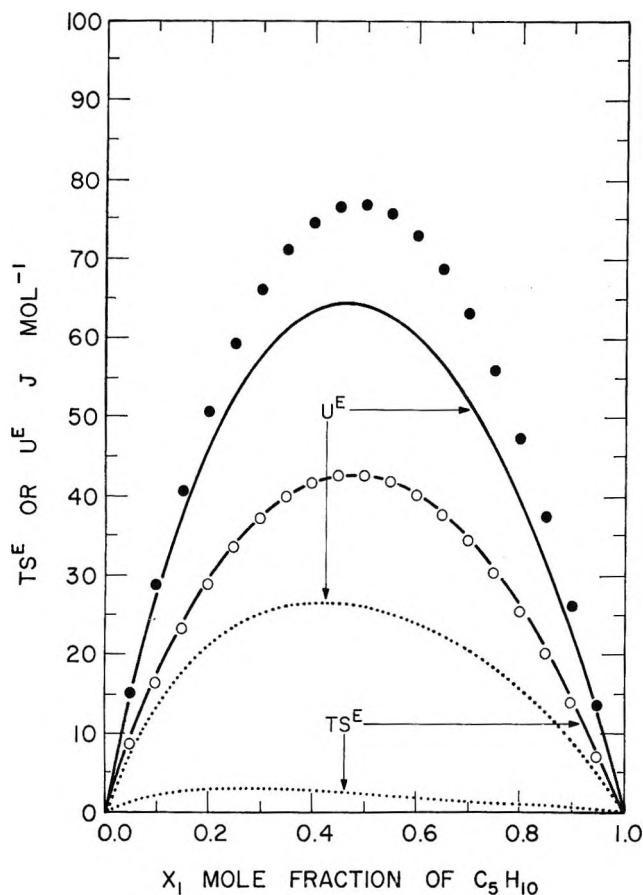


Figure 1. Comparison of theoretical and experimental values of excess functions of system cyclopentane (1)-carbon tetrachloride (2) at 25°. Dotted and solid curves correspond, respectively, to calculations (a) and (b) described in the text. Points represent experimental data: O, TSE^E ; ●, U^E .

was used to evaluate the cross coefficient ω_{12} , and theoretical values of the excess functions TSE^E and U^E were computed from eq 18 and 29 for volumes of the mixture given by

$$V_s = \sum_i x_i V_i + V^E \quad (33)$$

The values adopted for the properties of the pure component liquids are summarized in Table I. The heats of vaporization and cohesion energies were estimated from the temperature derivative of the vapor pressure (represented by an Antoine form) with correction for nonideality of the vapor phase approximated by the second virial contribution (again, the temperature variation of B_{ii} was obtained from Haggmacker's formula¹³).

In our initial calculation (a), R_i for each component was computed from eq 20 using the data for ΔH_i^{vap} from Table I. The corresponding ω_{ij} was then obtained from eq 27, using the values of R_i and ΔU_i^{coh} . The resulting molecular parameters are listed in Table II. Using these values, the dotted curves for TSE^E and U^E in Figure 1 were computed from eq 18 and 29. The points plotted in Figure 1 at mole fraction intervals of

0.05 were calculated from the equations representing the smoothed experimental data.¹⁴ It appears from comparison of these values that the theoretical estimates of both the excess energy and entropy are too small.

Table I: Properties of the Component Liquids at 25°

	Cyclopentane	Carbon tetrachloride
p_i^{sat} , Torr	317.5 ^a	113.8 ^b
V_i , cm ³ mol ⁻¹	94.71	97.10
B_{ii} , cm ³ mol ⁻¹	-1054 ^c	-1675 ^d
ΔH_i^{vap} , J mol ⁻¹	28540 ^e	32450 ^e
ΔU_i^{coh} , J mol ⁻¹	26200 ^e	30050 ^e

^a American Petroleum Institute Research Project 44. "Selected Values of Properties of Hydrocarbons and Related Compounds," Carnegie Press, Carnegie Institute of Technology, Pittsburgh, Pa., 1953, and later revisions. ^b J. A. Barker, I. Brown, and F. Smith, *Discussions Faraday Soc.*, **15**, 142 (1953). ^c R. W. Hermesen and J. M. Prausnitz, *Chem. Eng. Sci.*, **18**, 485 (1963). ^d P. G. Francis and M. L. McGlashan, *Trans. Faraday Soc.*, **51**, 593 (1955). ^e Calculated by method described in the text.

Table II: Values of the Molecular Parameters^a

Calculation ^b	R_1	ω_{11}	R_2	ω_{22}
(a)	2.6530	1.4687	2.7114	1.4666
(b)	2.6417	1.5353	2.7270	1.3736

^a R_i and ω_{ij} in Å. ^b Calculations (a) and (b) described in the text.

However, the results computed for the excess functions are fairly sensitive to the values employed for the radii. This is illustrated by the solid curves in Figure 1 which were obtained in calculation (b). The values of R_i used in the latter were altered to achieve a least-squares fit of the experimental TSE^E results, instead of being determined from ΔH_i^{vap} ; the ω_{ij} were obtained from ΔU_i^{coh} as in calculation (a). The fit of TSE^E in this case is within the uncertainty of the experimental results, and the agreement between the theoretical and experimental excess energies is much better than that obtained in calculation (a). It can be seen from Table II that this improvement has been achieved by changes of less than 1% in the radii. Using eq 20, it can be shown that the changes in R_i correspond to variations of between 1 and 2% in ΔH_i^{vap} ; these are similar in magnitude to estimates of the accuracy of ΔH_i^{vap} .

Discussion

The agreement between experiment and theory found for calculation (b) shows that the real behavior of a system of simple nonpolar molecules can be obtained quite well from the perturbation of a hard-sphere system. Advantages of this treatment are the relative

simplicity of the expressions obtained and the small number of molecular parameters required. Since only first-order perturbation terms are retained and an oversimplified model of the molecular interactions is assumed, it appears that the theory should work better for energetical functions than for functions derivable more directly from the equation of state. The latter equation can be obtained from the Helmholtz function (eq 10), but attempts to use it to formulate a description of the volumetric behavior of the system, and to

calculate V^E (at constant pressure), were unsuccessful. It seems likely that this failure is due to the neglect of higher order perturbation terms and to the assumption that the attractive forces are independent of the separation between the molecules over some range a .

Application of the present expressions is limited to systems composed of nearly spherical nonpolar molecules. Extension of the equations to consider multi-component systems is straightforward.

Coal-Like Substances from Low-Temperature Pyrolysis at Very Long Reaction Times

by R. A. Friedel, J. A. Queiser, and H. L. Retcofsky

U. S. Department of the Interior, Bureau of Mines, Pittsburgh Coal Research Center, Pittsburgh, Pennsylvania 15213
(Received September 2, 1969)

The importance of long reaction times in the coalification process has been demonstrated in the laboratory. Samples of cellulose and pine sawdust in evacuated, sealed glass vials have been heated at 200° for 2 years. Black coal-like chars were produced; conventional heating at 200° for hours produces very little chemical change. The chars were characterized by infrared and electron spin resonance spectra and by ultimate analysis. The infrared spectra of the pine sawdust char and of a subbituminous coal are nearly identical, except for differing carbonyl absorption. The spectrum of the cellulose char is also similar to that of the subbituminous coal. The electron spin resonance (esr) results show that g values, line widths, and spin concentrations are very similar for the two chars, and resemble closely the corresponding values for subbituminous coal. 200° is considered a reasonable coalification temperature; a feasible depth of burial can provide such temperatures. The experimental coalification obtained in only 2 years supports the hypothesis that geologic time could produce all ranks of coals, from lignite to anthracite, at temperatures below 200°.

Introduction

In the study of the structure and properties of coal, attempts have been made to prepare synthetic coals, principally by pyrolysis methods. Chars having properties identical with those of coals have not been produced. Initial attempts at studying the infrared spectra of coal-like chars prepared by pyrolysis of pure materials were carried out several years ago.^{1,2} The pyrolysis method used was that of Smith and Howard, who had prepared from cellulose, chars that had some of the properties of coals.³ We studied the infrared spectra of chars prepared from cellulose over a range of temperatures; the spectrum of a 400° cotton char somewhat resembled that of high-volatile bituminous coal.^{1,2} The spectrum of this char showed a definite carbonyl absorption band which is not present, except as a weak shoulder, in infrared spectra of coals. Carbohydrate chars prepared at 300, 400, and 500° produced absorption

bands in the aromatic region that were identical with the aromatic bands produced, respectively, by lignite, high-volatile bituminous, and anthracite coals; less similarity was observed in other parts of the spectra.⁴ Similarities of reaction of coal and the carbohydrate, sucrose, were illustrated by the nearly identical spectra of products obtained in hydrogenation studies.⁵ Friedman and coworkers studied many coal-like chars prepared by the pyrolysis of pure oxygenated compounds, mostly at 400° and reaction times of 1 hr; several

(1) R. A. Friedel and M. G. Pelipetz, *J. Opt. Soc. Amer.*, **43**, 1051 (1953).

(2) R. A. Friedel and J. A. Queiser, *Anal. Chem.*, **28**, 22 (1956).

(3) R. C. Smith and H. C. Howard, *J. Amer. Chem. Soc.*, **59**, 234 (1937).

(4) R. A. Friedel, *Proceedings of the Fourth Carbon Conference*, University of Buffalo, Pergamon Press, New York, N. Y., 1960, p 321.

(5) M. G. Pelipetz and R. A. Friedel, *Fuel*, **38**, 8 (1959).

properties of these chars, including infrared spectra, have some resemblance to the corresponding properties of coals.⁶ Broido has studied the thermal behavior of cellulose in the presence of additives and found that decomposition begins 80° lower if 1.5% KHCO₃ is present.⁷ Urbanski has carried out infrared studies of the carbonization of lignin and cellulose and found that decomposition is greatest at 300–350°.⁸

Pure hydrocarbons have been charred in the presence and absence of molecular oxygen; only when oxygen was present did the infrared spectra of the chars resemble those of coals, particularly in the 1600-cm⁻¹ region.^{4,9} Unless oxygen is involved, the 1600-cm⁻¹ band is weak or nonexistent; thus it is believed that the structure producing the strong absorption at 1600 cm⁻¹ contains carbonyl groups.^{4,9}

In another study, chars were prepared from ¹⁸O-labeled compounds in an attempt to ascertain whether an isotopic shift would occur at 1600 cm⁻¹ and would thus indicate that carbonyl groups are involved. No isotopic shift was obtained; the infrared spectrum of an ¹⁸O-labeled chelate, dibenzoylmethane, demonstrated that if a C=O group is very strongly chelated the C=O vibration becomes completely delocalized and no isotopic shift occurs.^{10,11}

In attempting to simulate coal, the following principal variables are available: starting material, temperature, rate of heating, reaction time, and pressure. The effect of pressure is considered minor compared to the effect of temperature.^{12–14} The effect of pressure during many runs may be important; temperature during many runs is certainly important. Though presumptuous, it was assumed that some slight indication of the effect of geologic time might be observable in the laboratory. Pyrolysis experiments involving reaction times of years, rather than hours or days, were planned. A temperature of 200° was chosen. The spectral methods selected for investigation of the coal-like properties of the chars were infrared and electron spin resonance spectrometry.

Experimental Procedure

Pyrolyses. In initial experiments, pyrolytic oxidation of cotton and pine wood sawdust were carried out at low temperatures. Two sets of samples were heated in air at 150 and 200° for 10 months; the chars produced were investigated by infrared spectrometry.

Then, pyrolysis experiments in the absence of air were carried out. Samples of cotton, 0.43 g, and pine wood sawdust, 0.20 g, were placed in heavy-walled Pyrex tubes, evacuated, and sealed. The sample tube volumes were 3.1 cc. The samples were heated at 200° for 2 years. The cotton char was sampled in two different places and the pine sawdust char in three places, and infrared spectra were obtained. The spectra for each char were identical. These results

indicate, but do not prove, that the two chars were homogeneous.

Instrumental Investigation. The principal methods of characterizing the pyrolysis products were infrared (Perkin-Elmer Model 521)^{14b} and electron spin resonance (esr) spectrometry (Varian Associates Model 4300). Preliminary examinations of the chars were also made on a high-resolution mass spectrometer (Consolidated 21-110B); many aromatic structures found in coals were identified. Analysis of gases and other volatile components was carried out on a Consolidated 103C mass spectrometer. Ultimate microanalyses of the chars were performed by the Huffman Laboratories.

Results and Discussion

Low pyrolysis temperatures and reaction times of several months were decided on in an attempt to simulate mild coalification conditions. Temperatures in the 200° range are considered realistic; many coals have been subjected to such temperatures due to depth of burial. Initially, pyrolytic oxidation runs were made on cellulose and on pine sawdust at 150° in the presence of air. Pyrolysis of these materials for 10 months gave black, insoluble solids having infrared spectra which indicated extensive oxidation. The second set of investigations was carried out at 200° in the presence of air; as expected, greater pyrolytic oxidation was produced. Then pyrolysis runs in the absence of air were initiated with samples of cotton and of pine sawdust sealed in evacuated, heavy-wall glass tubes. The samples were heated at 200° for 2 years. Tarry products were observed during the early stages of pyrolysis; these became solid char long before 2 years elapsed. The gas produced in the pyrolysis of the cotton sample was lost at the end of 2 years by an explosion; most of the char was salvaged. The vial containing the pine sawdust char was then opened, with release of considerable pressure of gas (6.3 atm). A thin film of colorless liquid, mostly water, vaporized completely into the evacuated gas-handling system. The gas analysis in Table I shows mainly H₂O and CO₂. Both the cotton

(6) S. Friedman, R. Raymond, L. Reggel, I. Wender, and R. A. Friedel, Abstracts of Papers, 129th National Meeting of the American Chemical Society, April 1956.

(7) A. Broido, *Pyrodynamics*, **4**, 243 (1966).

(8) T. Urbanski, W. Hofmar, T. Ostrowski, and M. Witanowski, *Bull. Acad. Polon. Sci., Ser. Sci., Chim., Geol. Geogr.*, **7**, 851, 861 (1959).

(9) R. A. Friedel, *Appl. Opt.*, **2**, 1109 (1963).

(10) R. A. Friedel, R. A. Durie, and Y. Shewchuk, *Carbon*, **5**, 559 (1967).

(11) R. A. Durie, Y. Shewchuk, and R. A. Friedel, *Spectrochim. Acta*, **24A**, 1543 (1968).

(12) M. Teichmueller and R. Teichmueller, Chapter in "Coal Science," R. F. Gould, Ed., Advances in Chemistry Series No. 55, American Chemical Society, Washington, D. C., 1966, p 133.

(13) J. Karweil, *Z. Deut. Geol. Ges.*, **107**, 132 (1956).

(14) (a) W. Francis, "Coal," E. Arnold, Ltd., London, 1961 p 573. (b) Reference to trade names is made for identification only and does not imply endorsement by the Bureau of Mines.

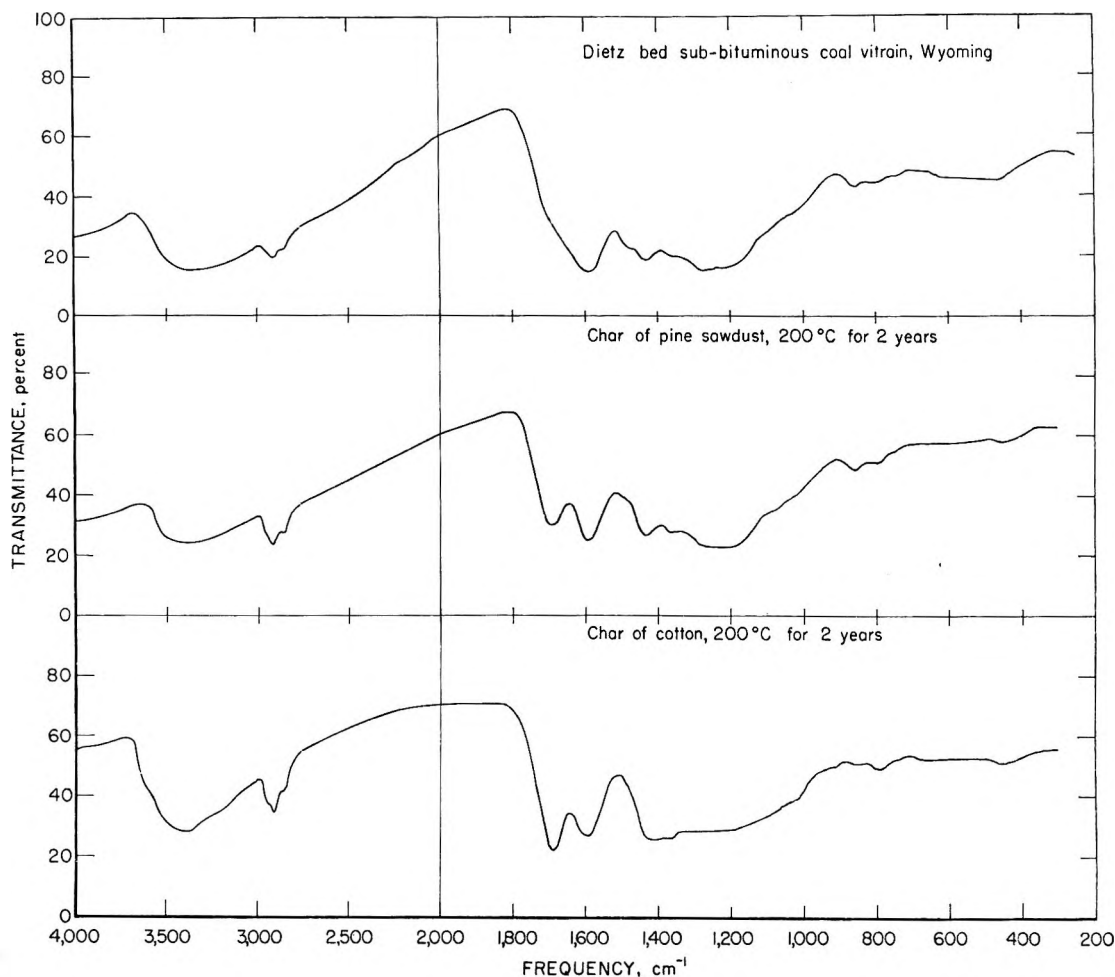


Figure 1. Infrared spectra of Dietz bed subbituminous coal vitrain, 200° char of pine sawdust and 200° char of cotton.

Table I: Spectrometric Analysis of Gases from 200° Pyrolysis of Pine Sawdust

	Per cent	Weight, mg
Carbon dioxide	25.8	9.7
Water	57.9	8.9
Methanol	3.9	1.1
Dimethyl ether	12.4	4.9
	100	
Estimate of total carbonyl compounds, by infrared		5.0
		29.6

Table II: Ultimate Analyses of Cotton Char, Pine Sawdust Char, and Dietz Bed Subbituminous Coal (Big Horn Mine, Wyoming)

	Dietz subbituminous coal	Cotton char	Pine sawdust char
C	70.83	76.5	67.6
H	5.06	5.1	4.9
S	1.02		
N	0.59	18.4 ^a	27.5 ^a
O	22.50 ^a		
C/H	1.16	1.24	1.16

^a By difference.

and sawdust chars were completely black; the yield of char from pine sawdust was about 53%. By contrast the char produced from cellulose by Smith and Howard⁴ at 190° gave a yield of 89% of brown material; the infrared spectrum of this substance closely resembled that of unchanged cellulose. The infrared spectra of both samples are shown in Figure 1, along with a spectrum of a subbituminous coal (Dietz bed, Wyoming, 70.8% C, m.a.f.). Ultimate analyses and C/H ratios, given in Table II, demonstrate the close similarity of

coal and chars. The spectra of the coal and the sawdust char are remarkably similar. In addition to the more obvious spectral similarities at 1600, 1440, 1370, 1280, 3400, 2950, 2920, 2860, and 1180 cm^{-1} , there is a considerable similarity at the aromatic band positions, 860, 810, and 750 cm^{-1} . The aromatic bands are weak in the spectra of subbituminous coals, but the similarity of the coal and char absorption patterns in this region is impressive. It is apparent from these spectra that

Table III: Relative Absorption Intensities in the Infrared Spectra of 300, 400, and 500° Cellulose Chars at 1700 cm⁻¹ (Carbonyl Compounds) and 1600 cm⁻¹ (Presumably Chelated, Conjugated Carbonyl Groups)

Cellulose char, preparation temp, °C	Relative intensities, per cent	
	1700 cm ⁻¹	1600 cm ⁻¹
300	78	22
400	59	41
500	0	100

Table IV: Electron Spin Resonance Data for Chars and a Coal Vitrain

Sample	Spins/g	<i>g</i>	Line width, G
Cotton char	7 × 10 ¹⁸	2.00314	5.6
Pine sawdust char	2.3 × 10 ¹⁹	2.00321	6.3
Dietz subbituminous vitrain	1.8 × 10 ¹⁹	2.00381	8.0
Range of values for 15 bituminous and subbituminous coals	6 × 10 ¹⁸ to 4 × 10 ¹⁹	2.00274 to 2.00381	6.1 to 8.0

bonyl structures which can produce the intense 1600-cm⁻¹ absorption band observed in infrared spectra of coals and chars. Substantiation of such a conversion may exist in the behavior of carbonyl groups in chars that were prepared from cellulose at 300, 400, and 500°. In the spectrum of the 300° char the carbonyl absorption is greater than the unknown absorption at 1600 cm⁻¹. (Relative intensities are given in Table III.) For the 400° char the intensities are reversed. The spectrum of the 500° char exhibits no simple carbonyl absorption; only the 1600-cm⁻¹ band remains. These changes may be attributable to conversion into a modified carbonyl-containing structure. This structure could be the conjugated chelated structure, such as the enol form of acetylacetone, that has been proposed previously as the source of the 1600-cm⁻¹ absorption band. It is interesting that the same kind of change, though more subtle, occurs in coals; infrared spectra of lignites and low-rank coals have weak absorption shoulders at 1700 cm⁻¹ which gradually disappear from spectra of higher rank coals. For the coals the conversion of carbonyl compounds to the presumed conjugated chelated carbonyls may be farther advanced than it is in these chars which were prepared at reaction

Table V: Variation of ESR Parameters for Carbohydrate Chars Prepared at Differing Temperatures and Reaction Times

Char	Pyrolysis temp, °C	Reaction time	Spins/g	<i>g</i> Value	Line width, G
Cotton	200	2 years	7 × 10 ¹⁸	2.00314	5.6
Pine sawdust	200	2 years	2.3 × 10 ¹⁹	2.00321	6.3
Cellulose ^a	200	>12 hr	5 × 10 ¹⁷	2.0047	8.7
Cellulose ^a	300	>12 hr	1 × 10 ¹⁹	2.0036	6.6
Sucrose ^b	350	8 hr	~2 × 10 ¹⁹	~2.0030	~7.0
Sucrose ^b	400	8 hr	~4 × 10 ¹⁹	~2.0029	~7.0

^a B. Milsch, W. Windsch, and H. Heinzelman, *Carbon*, **6**, 807 (1968). ^b L. S. Singer, W. J. Spry, and W. H. Smith, Proceedings of the 3rd Carbon Conference, 1959, p 121.

it is possible over a long period of time to approach a coal-like spectrum, even at a low temperature. Heating from room temperature to 190° in 1 hr, Smith and Howard's cellulose⁴ had produced a brown char but the infrared spectrum, as well as the elemental analysis, resembled those of cellulose with only minor differences. No coal-like spectral features were observed.

The usual 1700-cm⁻¹ carbonyl band occurs in the spectrum of the sawdust char, but, for the first time in spectra of chars prepared at low temperature the 1600-cm⁻¹ band is more intense than the 1700, as in coal spectra. Thus the very long heating time has produced a definite decrease in carbonyl-containing structures absorbing at 1700 cm⁻¹. It is feasible that simple carbonyl groups are first formed in the early stages of pyrolysis (and coalification) and then are gradually converted to other structure(s) during elapsed time. Possibly the carbonyl groups are converted to modified car-

times of only 1 hr.

Electron spin resonance (esr) spectrometry has also been applied to the study of the cotton and pine sawdust chars. Values for the esr spectral parameters (Table IV) are comparable to values for subbituminous coal.¹⁹ As with the infrared, the results for the chars are closely similar to those for the coal vitrain. The fact that a signal is detected is of interest for it demonstrates that stable free radicals can be formed in natural materials on exposure to very mild heating conditions. There

(15) J. K. Brown, *J. Chem. Soc.*, 744 (1955).

(16) S. Fujii and F. Yokoyama, *J. Fuel Soc. Jap.*, **37**, 267 (1959).

(17) R. A. Friedel in "Applied Infrared Spectroscopy," D. N. Kendall, Ed., Reinhold Publishing Corp., New York, N. Y., 1966, p 312.

(18) R. A. Friedel, H. L. Retcofsky, and J. A. Queiser, U. S. Bureau of Mines Bulletin 640, U. S. Government Printing Office, Washington, D. C., 1967.

(19) H. L. Retcofsky, J. M. Stark, and R. A. Friedel, *Anal. Chem.*, **40**, 1699 (1968).

are not many examples of free radical signals obtained from chars produced at temperatures as low as 200°. It is probable that even lower temperatures will produce free radicals in carbonaceous materials over long periods of time. The relative effects of temperature and reaction time are further demonstrated in Table V. Cellulose at 200° for 2 years produces esr data equivalent to those obtained with short reaction times at 300 and 350°. Also, cellulose charred at 200° for 2 years contains more than an order of magnitude greater concentration of unpaired electrons than cellulose charred at 200° for 12 hr.

The striking importance of time in pyrolysis reactions has been demonstrated. If chars as coal-like as these can be produced in 2 years, at temperatures that have little effect during short times, then it appears that in geologic times coal could be produced at temperatures much lower than 200° as proposed by various people.¹²⁻¹⁴ Future experiments will be carried out using longer times and lower temperatures, in an effort to simulate coal spectra even more closely. Also, attempts will be made by this process to convert plant materials into high-rank coals, and to convert low-rank coals into higher rank coals.

Carbon-13 Nuclear Magnetic Resonance Spectroscopy.

Solvent Effects on Chemical Shifts^{1a}

by Robert L. Lichter and John D. Roberts

Gates and Crellin Laboratories of Chemistry,^{1b} California Institute of Technology, Pasadena, California 91109
(Received June 16, 1969)

The ¹³C chemical shift of chloroform has been measured in a variety of solvents. Relative to dilute solution in cyclohexane, all of the solvents studied resulted in downfield shifts which, with the exceptions of benzene and acetonitrile, correlate linearly ($r = 0.982$) with the changes in proton shifts in the same solvents. The results, taken with the variation of the ¹³C-H coupling constant with solvent, suggest that the solvent effects arise from changes in the average distance of the bonding electrons in the chloroform C-H bond as the result of intermolecular association. Contributions from the anisotropy of benzene and acetonitrile indicate that measurements of the chemical shift of more than one nucleus in the same molecule may allow detection and estimation of neighbor anisotropy contributions to chemical shifts.

Introduction

In contrast to the extensive investigations of solvent effects on proton chemical shifts,² comparatively little attention has been paid to such effects on the chemical shifts of other nuclei. This is partly because of the difficulty of observing the resonances of some of the nuclei under conditions where meaningful conclusions about solvent-solute interactions can be drawn, but also because changes in molecular structure affect the chemical shifts of nuclei other than proton to a far greater extent than changes in medium. Consequently, particularly in structure elucidation problems, choice of solvent has generally been dictated by practical rather than theoretical considerations. There have been exceptions, most notably in the case of ¹³C where Maciel and coworkers³⁻⁷ examined the shifts of carbons of carbonyl groups as a function of solvent. Also, Beconsall and Hampson⁸ have reported a solvent shift on the ¹³C resonance of methyl iodide.

We have studied solvent effects on the ¹³C chemical shift of chloroform. That such shifts should be solvent sensitive was anticipated both by the well-documented behavior of chloroform as a hydrogen-bonding acid⁹ and, more directly, by the observation¹⁰ that the ¹³C-proton coupling constant in chloroform is solvent dependent.

(1) (a) Supported by the Public Health Service, Research Grant GM-11072-07 from the Division of General Medical Sciences and the National Science Foundation; (b) Contribution No. 3875.

(2) For an excellent review, see P. Laszlo in "Progress in N.M.R. Spectroscopy," Vol. 3, J. W. Emsley, J. Feeney, and L. H. Sutcliffe, Ed., John Wiley & Sons, Inc., New York, N. Y., 1968, p 231 ff.

(3) G. E. Maciel and G. C. Ruben, *J. Amer. Chem. Soc.*, **85**, 3903 (1963).

(4) G. E. Maciel and R. V. James, *ibid.*, **86**, 3893 (1964).

(5) G. E. Maciel, *J. Chem. Phys.*, **42**, 2746 (1965).

(6) G. E. Maciel and J. J. Natterstad, *ibid.*, **42**, 2752 (1965).

(7) G. E. Maciel and D. D. Traficante, *J. Amer. Chem. Soc.*, **88**, 220 (1966).

(8) J. K. Beconsall and P. Hampson, *Mol. Phys.*, **10**, 21 (1965).

Experimental Section

Reagent grade chloroform was freed from ethanol by passage through alumina, after which it was distilled under a nitrogen atmosphere and stored for short times in the dark in the refrigerator. No impurities were detectable by glpc or by pmr spectroscopy. Reagent grade cyclohexane was extracted with a 1:1 mixture of nitric and sulfuric acids until the acid layer was no longer yellow. The organic layer was then washed to neutrality with distilled water, dried over potassium carbonate, and distilled under a nitrogen atmosphere through a 25-cm Vigreux column. All other solvents were either freshly opened bottles of Matheson Coleman and Bell Spectroquality solvents or were purified by standard methods; in no case were impurities detected by pmr spectroscopy.

Solutions were prepared volumetrically using standardized pipets, except that the shift reported for boron trifluoride is that of chloroform saturated with the gas. The mole ratio of chloroform-solvent-cyclohexane (used as internal standard for both ^{13}C and ^1H measurements) was 1:9:1. The ^{13}C shifts were measured in natural abundance with a Varian DFS-60 spectrometer operating at 15.1 MHz (14,100 G) as previously described,¹¹ with the aid of complete proton decoupling achieved by noise modulation of the proton-decoupling frequency.¹² The sample temperatures under these conditions were estimated to be 45–50°. Each chemical shift is an average of at least three independent measurements and is estimated to be accurate to ± 0.8 Hz (0.05 ppm). Proton spectra were taken on a Varian A56/60 spectrometer at ambient probe temperature (ca. 35°) and were calibrated by the usual audio sideband method. Chemical shifts are the average of at least three upfield and three downfield sweeps and are estimated to be accurate to ± 0.1 Hz (0.002 ppm).

Results

The carbon and proton chemical shifts, measured with respect to internal cyclohexane, are presented in Table I, together with the ^{13}C -H coupling constants reported by Evans.¹⁰ With the exception of benzene, each solvent induces a downfield shift of both the carbon and proton resonances with respect to cyclohexane as solvent. The proton shifts span a range of about 2 ppm, whereas the carbon shifts cover more than 4 ppm. Figure 1 shows the correlation between the two shifts (correlation coefficient 0.982, not including benzene); the slope of the least-squares line is 2.02 ± 0.09 ppm/ppm. In Figure 2 the ^{13}C -H coupling constants are shown to correlate linearly with the ^{13}C chemical shifts in the same solvents (correlation coefficient 0.979, slope = 3.84 ± 0.23 Hz/ppm). Entries 1 and 4 of Table I show that dilution of chloroform with cyclohexane induces a small upfield shift,¹³ agreeing in direction, but hardly in magnitude, with the 7.3-ppm upfield shift experienced by methyl iodide on dilution with

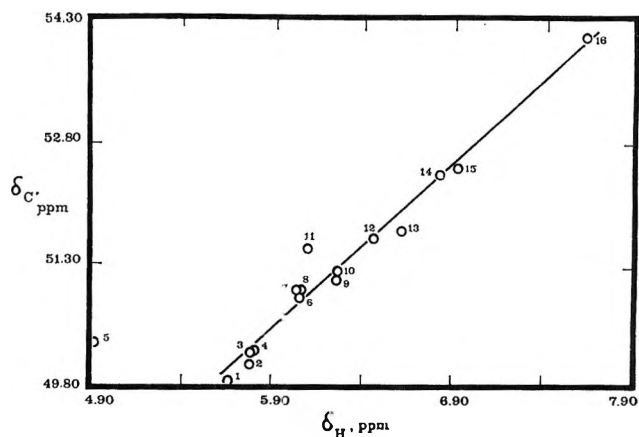


Figure 1. Correlation between ^{13}C and ^1H chemical shifts of chloroform. Numbers correspond to numbers in Table I. Point 5 (benzene) was not included in the calculation of the slope by least squares.

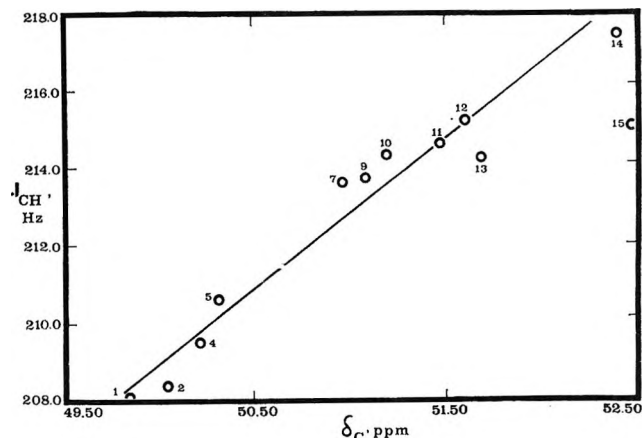


Figure 2. Correlation between ^{13}C chemical shift and $J_{13\text{CH}}$ of chloroform. Numbers correspond to numbers in Table I. Points 13 (triethylamine) and 15 (pyridine) were not included in the least-squares calculation.

cyclohexane.¹⁴ Part of the deviations from linearity evident in Figures 1 and 2 may be ascribed to the differences among the temperatures of measurement; nevertheless, the general trends are not expected to be greatly affected.

Discussion

Though the existence of a solvent shift is perhaps not surprising, the linearity of the correlation with the

(9) (a) For some leading references to recent and older literature, see L. Lunazzi and F. Taddei, *Spectrochim. Acta*, **24A**, 1479 (1968); (b) H. Suhr, *J. Mol. Structure*, **1**, 295 (1967).

(10) D. F. Evans, *J. Chem. Soc.*, 5575 (1963).

(11) F. J. Weigert and J. D. Roberts, *J. Amer. Chem. Soc.*, **89**, 2967 (1967).

(12) F. J. Weigert, M. Jaute at, and J. D. Roberts, *Proc. Nat. Acad. Sci.*, **60**, 1152 (1968).

(13) At 0.5 mole fraction in cyclohexane, the chloroform ^{13}C chemical shift is 50.07 ppm.

(14) H. Spiesscke and W. G. Schneider, *J. Chem. Phys.*, **35**, 722 (1961).

Table I: Nmr Parameters of Chloroform as a Function of Solvent^a

No.	Solvent	δ_C , ppm	$\Delta\delta_C$, ppm	δ_H , ppm	$\Delta\delta_H$, ppm	J^{13C-H} , Hz ^b
1	Cyclohexane	49.85	0.00	5.660	0.00	208.1
2	Carbon tetrachloride	50.05	0.20	5.780	0.120	208.4
3	Boron trifluoride ^c	50.20	0.35	5.787	0.127	...
4	Neat ^d	50.22	0.37	5.807	0.147	209.5
5	Benzene	50.32	0.47	4.913	-0.747	210.6
6	Acetic acid	50.87	1.02	6.060	0.400	...
7	Nitromethane	50.97	1.12	6.042	0.382	213.6
8	Nitrobenzene	50.97	1.12	6.070	0.410	...
9	Diethyl ether	51.09	1.24	6.265	0.605	213.7
10	Methanol	51.20	1.35	6.271	0.611	214.3
11	Acetonitrile	51.48	1.63	6.105	0.445	214.6
12	Acetone	51.61	1.76	6.472	0.812	215.2
13	Triethylamine	51.70	1.85	6.627	0.967	214.2
14	Dimethylformamide	52.40	2.55	6.842	1.182	217.4
15	Pyridine	52.48	2.63	6.942	1.282	215.0 ^e
16	Hexamethylphosphoramide	54.09	4.24	7.655	1.995	...

^a Downfield from carbon and proton resonances, respectively, of internal cyclohexane. ^b Data taken from ref 10. The mole fraction of chloroform was 0.16. ^c Chloroform saturated with gaseous boron trifluoride. ^d Contained 10 mol % cyclohexane. ^e From ref 2, p 335.

proton shift is striking. Not unexpectedly, there is no apparent correlation with macroscopic properties of the medium, *i.e.*, with any of a variety^{2,15-21} of "reaction field" or solvent polarity functions.²² Becconsall and Hampson⁸ attempted to explain their observed downfield shift in these terms; in their case the carbon shifts extended over 7.7 ppm in going from neat methyl iodide to dilute solution in TMS, contrasting sharply with the limited 0.18 ppm range of the proton shifts. However, though the correlation between the carbon and proton shifts for methyl iodide is monotonic, it is not linear, suggesting that there are several factors influencing the chemical shift of this particular, highly polarizable, solute.

If benzene and, possibly, acetonitrile are for the moment excluded from consideration, it would seem unlikely that solvent magnetic anisotropy can account for the observed relative magnitudes and linearity of the shifts.²³ The contribution of neighbor anisotropy to shielding should depend only on the anisotropic center and not on the nucleus being observed; the effect should decrease as the distance between the interacting centers increases.²⁴ In any kind of a specific solvation complex, the chloroform proton ought to be closer to an anisotropic center than the carbon, thus experiencing a greater change in shielding than the carbon. The data here show that this is not the case, suggesting that anisotropy is not the source of the solvent shift.

We choose to interpret this effect in terms of the known hydrogen-bonding properties of chloroform.^{9,25} The linear correlation thus reflects the fact that changes in screening of the carbon nuclei parallel the change at the hydrogen nuclei, which should be true if there is only one dominant interaction, in this case along the $\geq C-H \cdots B$ bond. It is somewhat more difficult to

understand the direction of the shift. Certainly a simple electrostatic argument based on polarization of the chloroform C-H bond in the sense $C-H^+$ would seem to imply a diamagnetic shift. A clue may lie in the $^{13}C-H$ coupling constant variations. The apparently linear correlation between these values and the carbon chemical shifts (Figure 2) suggests that similar mechanisms are operating. Evans¹⁰ interpreted the increase in terms of mutual electronic repulsion between the electrons on the hydrogen-bonded base and those in the C-H bonding orbital. He argued that such a repulsion corresponds to an increase in the s character of the orbital at the carbon atom without affecting the bond length (evidenced from infrared spectroscopic measurements) and suggested that the coupling constant, dominated by the Fermi contact mechanism, should increase proportionately to the strength of the hydrogen bond. Though this explanation is likely to be oversimplified,²⁶ it may possibly provide a conceptual explanation of the

(15) A. D. Buckingham, *Can. J. Chem.*, **38**, 300 (1960).

(16) A. D. Buckingham, T. Schaefer, and W. G. Schneider, *J. Chem. Phys.*, **32**, 1227 (1960).

(17) F. Hruska, G. Kotowycz, and T. Schaefer, *Can. J. Chem.*, **43**, 3188 (1965).

(18) F. Hruska, D. W. McBride, and T. Schaefer, *ibid.*, **45**, 1081 (1967).

(19) G. Kotowycz and T. Schaefer, *ibid.*, **45**, 1093 (1967).

(20) H. M. Hutton and T. Schaefer, *ibid.*, **45**, 1111 (1967).

(21) J. Homer, *Tetrahedron*, **23**, 4065 (1967).

(22) C. Reichardt, *Angew. Chem. Intern. Ed. Engl.*, **4**, 29 (1965).

(23) *Cf.* ref 7, p 24.

(24) J. A. Pople, W. G. Schneider, and H. J. Bernstein, "High-resolution Nuclear Magnetic Resonance," McGraw-Hill Book Co., Inc., New York, N. Y., 1959, p 176 ff.

(25) It is noteworthy that Becconsall and Hampson⁸ rejected hydrogen bonding as the source of the shift in their study, asserting that the effect should be larger on the proton shift than on the carbon.

solvent shift. In the Ramsey formulation of the chemical shift,²⁷ carbon chemical shifts are dominated by the paramagnetic term σ_p , which in turn is approximately proportional to the expression $(1/\Delta E) \langle 1/r^3 \rangle_{av}$, where ΔE is an "average" electronic excitation energy and $\langle 1/r^3 \rangle_{av}$ is the average of the inverse cube of the effective orbital radius.²⁸ Clearly a change in either one of these terms will change the average electronic screening experienced by the nucleus. We suggest that repulsion of the C-H bonding electrons toward the nucleus results in a shortening of the average radius of that orbital,²⁹ thus increasing the term $\langle 1/r^3 \rangle_{av}$ and inducing a paramagnetic shift. Alternatively, several investigators²⁸ have shown that the $\langle 1/r^3 \rangle_{av}$ term increases with the orbital effective nuclear charge; in a similar manner, Grant and Litchman^{26a} have suggested a correlation between substituent-induced increases in the ¹³C-H coupling constants of substituted methanes and increases in the values of the effective nuclear charge. It is thus possible that the solvent-induced paramagnetic shifts observed here may be interpreted in these terms. The shift is indeed small, so that only a small perturbation need be invoked. Perhaps detailed calculation of the effects of a directed electric field on the electron distribution in the C-H bond may provide an insight into the mechanism.³⁰

It has been suggested³¹ that interactions at the C-Cl bond may also contribute to the observed solvent shifts. Carbon tetrachloride, for example, is known to effect both proton² and carbon³ resonance line positions, but these effects are smaller than the shifts reported here, and, for proton shifts, seem to correlate better with changes in reaction field than with any specific solvation complex.² Nevertheless, further experimental evidence seemed desirable and in Table II we

Table II: ¹³C Chemical Shift of Carbon Tetrachloride as a Function of Solvent^a

Solvent	$\delta_C^{CCl_4}$, ppm	$\delta_C^{CHCl_3}$, ppm	$\Delta\delta_C^{CCl_4}$, ppm	$\Delta\delta_C^{CHCl_3}$, ppm
Cyclohexane	69.38	49.85	0.00	0.00
Benzene	69.29	50.32	-0.09	0.47
Nitromethane	69.19	50.97	-0.19	1.12
Acetonitrile	69.13	51.48	-0.25	1.65
Triethylamine	69.29	51.70	-0.09	1.85
Pyridine	69.44	52.48	0.06	2.63
Hexamethylphosphoramide	69.33	54.09	-0.05	4.24

^a Downfield from carbon resonance of internal cyclohexane. Mole ratio of carbon tetrachloride-solvent-cyclohexane = 1:9:1.

show the shifts induced by a few representative solvents on the ¹³C chemical shift of carbon tetrachloride, along with the corresponding solvent shifts for chloroform for comparison. The small and randomly varying solvent

shifts of carbon tetrachloride, some of which are within the experimental error of measurement, indicate it is unlikely that Cl...solvent interactions play an important role in the solvent shifts observed for chloroform. There is, however, a possible ambiguity in that carbon tetrachloride, though polarizable, has no dipole moment. The dipole in chloroform could induce Cl...solvent interactions which would not be present with carbon tetrachloride as a model.

Recently, other workers have reported the effects of hydrogen bond formation and disruption on the chemical shifts of other nuclei. Dilution with organic solvents³² or a temperature increase of about 200°³³ induces upfield shifts in the ¹⁷O resonance of liquid water of about 10 ppm. Furthermore, the ¹⁷O resonance of water vapor lies about 36 ppm to higher applied field than that of the liquid.³³ Litchman, Alei, and Florin³⁴ reported similar changes in the ¹⁵N resonance of liquid ammonia and a 17.2 ppm difference between the chemical shifts of the liquid and gas (gas at higher field). In both cases, hydrogen bonds can form with O-H and N-H bonds on the one hand, and unshared electron pairs on the other, and contributions may be expected to arise from both sources.³⁵

Effects of Anisotropy. It is of special interest to consider the exceptions to the proton-carbon solvent

(26) (a) D. M. Grant and W. Litchman, *J. Amer. Chem. Soc.*, **87**, 3994 (1965); (b) See also A. W. Douglas and D. Dietz, *J. Chem. Phys.*, **46**, 1214 (1967).

(27) J. W. Emsley, J. Feeney, and L. H. Sutcliffe, "High Resolution Nuclear Magnetic Resonance Spectroscopy," Vol. 1, Pergamon Press, Ltd., Oxford, 1965, p 65 ff.

(28) (a) B. V. Cheney and D. M. Grant, *J. Amer. Chem. Soc.*, **89**, 5319 (1967), have presented a valence-bond formulation in which structural effects on these parameters are clearly discussed; (b) M. Karplus and J. A. Pople, *J. Chem. Phys.*, **38**, 2803 (1963); (c) J. A. Pople, *Mol. Phys.*, **7**, 301 (1964).

(29) It is necessary to assume, of course, that to a first approximation the effect on the carbon-chlorine orbitals can be neglected.

(30) The upfield shift observed on dilution of chloroform with cyclohexane is consistent with the interpretation presented here. Chloroform is known to be weakly self-associated; if complex formation induces a downfield shift, then disruption of the self-association complexes by an inert solvent should produce the opposite effect. It should also be emphasized that the proton-carbon shift correlation automatically corrects for any residual self-association under the experimental conditions.

(31) W. M. Litchman, private communication.

(32) Z. Luz and G. Yagil, *J. Phys. Chem.*, **70**, 554 (1966).

(33) A. E. Florin and M. Alei, Jr., *J. Chem. Phys.*, **47**, 4268 (1967).

(34) W. M. Litchman, M. Alei, Jr., and A. E. Florin, *ibid.*, **50**, 1031 (1969).

(35) (a) The ¹³C chemical shift of methanol is solvent dependent; dilution of neat methanol with water to 90% induces a downfield shift of about 1.5 ppm. Unpublished results of D. E. Dorman; (b) After this paper was submitted, W. M. Litchman, M. Alei, Jr., and A. E. Florin, *J. Amer. Chem. Soc.*, **91**, 6574 (1969), reported paramagnetic solvent-induced shifts of the ¹⁵N resonance of ammonia in various solvents, relative to the gas as reference. Their statistical analysis of the various possible contributions to the solvent shifts indicates that while interactions between the nitrogen lone pair and hydrogen-bonding acids induce large paramagnetic shifts, those between the N-H bond and hydrogen-bonding bases induce small diamagnetic shifts. The apparent discrepancy between these conclusions and the interpretation presented here is difficult to rationalize and may arise from some overlooked factor in the qualitative explanations proposed, or in differences in the systems studied.

shift correlation. Whereas δ_H and δ_C of chloroform in benzene do not correlate, nor do δ_H and $J_{1,CH}$, δ_C and $J_{1,CH}$ fall nicely on the least-squares line. This is consistent with the well-known anisotropy of the benzene ring and suggests that the effect of the latter, to a first approximation, may be negligible at the carbon nucleus of the solute. From the equation of the least-squares line a "correct" proton shift of 5.82 ± 1.19 ppm can be calculated. The 0.91 ppm difference between this and the experimental value may be interpreted as the contribution from the benzene ring-current anisotropy. Using the Johnson-Bovey tables³⁸ and assuming the chloroform C-H bond to be perpendicular to the ring and directly over the center, the difference corresponds to a distance of about 3.8 Å between the center of the ring and the proton. This value is to be compared with the value of 3.1 Å calculated by Reeves and Schneider³⁷ in their classic pmr investigation of the hydrogen-bonding properties of chloroform. From dipole moment studies Young, Holt, and Walker³⁸ estimated an upper limit of about 5.5 Å as the corresponding distance in the chloroform-*p*-xylene complex, and Homer and Huck,³⁹ using pmr data, calculate a value of 2.93 Å in the nitroform-benzene complex. The value estimated here is at least of the right magnitude. In like manner, the 0.27 ppm difference between the calculated (6.38 ppm) and experimental (6.11 ppm) proton chemical shifts of acetonitrile compares reasonably well with the value of about 0.4 ppm for the anisotropy contribution to the association shift of the complex estimated by Howard, Jumper, and Emerson.^{40,41} These results seem to suggest that chemical shift measurements of different nuclei in the same molecule may possibly be useful in detecting contributions from neighbor magnetic anisotropy.

The correlation shown in Figure 2 does not include the points for pyridine and triethylamine. In each

case the experimentally determined coupling constant falls below the line. For triethylamine, Evans¹⁰ ascribes this to partial cancellation of the expected increase by a lengthening of the C-H bond, indicated by infrared measurements. No corresponding measurements are available for pyridine, so that it is impossible to assess the validity of this argument here. Moreover, Howard, Jumper, and Emerson,⁴⁰ and Berkeley and Hanna⁴¹ suggest that the measured proton shift in that solvent arises only in part from hydrogen bonding at nitrogen, the rest of the (downfield) shift arising from ring-current anisotropy. Yet if this were the case, and the above argument for benzene is valid, there ought not be the good correlation between the carbon and proton shifts which is observed. The sources of the discrepancy are unclear.⁴²

(36) Reference 27, p 595 ff.

(37) L. W. Reeves and W. G. Schneider, *Can. J. Chem.*, **35**, 251 (1957).

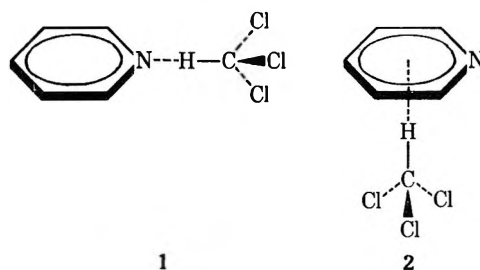
(38) R. P. Young, A. Holt, and S. Walker, *Tetrahedron*, **20**, 2351 (1964).

(39) J. Homer and P. J. Huck, *J. Chem. Soc., A*, 277 (1968).

(40) B. B. Howard, C. F. Jumper, and M. T. Emerson, *J. Mol. Spectrosc.*, **10**, 117 (1963).

(41) However, P. J. Berkeley and M. W. Hanna, *J. Amer. Chem. Soc.*, **86**, 2990 (1964), have estimated the anisotropy contribution of cyclohexyl cyanide to be about 0.6 ppm.

(42) One possibility is that the anisotropy-induced paramagnetic shift experienced by the chloroform proton in conformation 1 is counterbalanced by an anisotropy-induced diamagnetic shift experienced by the proton in conformation 2.



The Decay of Radicals in Ammonia-Oxygen-Nitrogen Flames

by Melvin P. Nadler, Victor K. Wang, and Walter E. Kaskan

Department of Chemistry, State University of New York at Binghamton, Binghamton, New York 13901
(Received August 25, 1969)

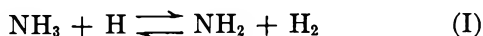
Measurements have been made of the concentrations of OH and NH, and the relative concentrations of NH₂, in the flame gases from two fuel rich flat NH₃-O₂-N₂ flames as a function of the distance from the burner surface. The technique involved the measurement of light absorption by an individual rotational level in the electronic ground state of each radical. [OH] was found to be at equilibrium, but [NH] was present in higher than equilibrium amounts. All three radicals decayed with flow downstream. Evidence is presented to show that during the decay, the reaction NH₂ + OH ⇌ NH + H₂O is in dynamic equilibrium. This equilibration allows the calculation of an *f* number for the NH₂ line. The implications of the findings for the analysis of the kinetics of radical decay are discussed.

Introduction

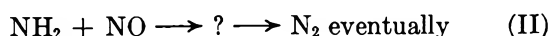
Flames burning in H₂-O₂-N₂ or H₂-CO-O₂-N₂ are known to produce radical concentrations in excess of equilibrium amounts, which then decay by recombination at measurable rates. In the analysis of the kinetics of recombination, the concept of the equilibration of fast reactions has proven to be very useful. According to this concept, due originally to Bulewicz, James, and Sugden,¹ certain reactions which are fast relative to the recombination reactions are maintained in dynamic equilibrium during the recombination process. Hence radical concentrations may be quantitatively related to each other through thermochemical quantities, the equilibrium constants for the equilibrated reactions, and the kinetic analysis of recombination simplified considerably.

A program of study of the flame gases from NH₃-O₂-N₂ flames has been initiated in this laboratory. The technique employed is the use of space resolved spectroscopic probing of stationary flat laminar premixed flames. In view of the utility of the equilibration concept in other flames, it was felt that the first step should be a test of equilibration among the radicals in ammonia flames.

Two earlier studies of ammonia flames are related to the present work. Fenimore and Jones² studied low-pressure flames containing ammonia, using gas sampling techniques in the reaction zone and into the burned gases. They suggested that the reaction



was equilibrated. They also noted that the NO which was formed in the reaction zones of their flames tended to react further if NH₃ was present, presumably due to an incompletely specified reaction



and tended to not react further in lean flames where NH₃ disappears more or less completely at the end of

the reaction zone. MacLean and Wagner³ made a similar experimental study of NH₃-O₂ flames at reduced pressure, but in addition obtained measures of OH and NH by optical absorption. Their experimental findings resembled those of Fenimore and Jones, but led them to disagree with the suggested importance of reaction II.

Earlier experiments by one of us⁴ had established that all three of the radicals, OH, NH, and NH₂, could be observed in absorption in atmospheric pressure flames of the proper fuel-oxygen ratio. Since the H₂O concentration can be calculated with little error in such flames, it seemed feasible to test the reaction



for equilibration. The oscillator strengths of both OH²Σ⁺-²Π and NH³Π-³Σ⁻ are known^{5,6} so that OH and NH concentrations can be determined absolutely. The NH₂ A-X oscillator strength is not accurately known, only an estimate having been reported,⁷ so that only relative measurements of NH₂ can be made.

Equilibration of reaction III would be considered to be established insofar as the concentration function *F*₃

$$F_3 = \frac{[\text{NH}][\text{H}_2\text{O}]}{[\text{NH}_2][\text{OH}]} \quad (1)$$

exhibited the expected temperature dependence of the equilibrium constant *K*₃, independent of the values of the radical concentrations. In this work only the

- (1) E. M. Bulewicz, C. G. James, and T. M. Sugden, *Proc. Roy. Soc.*, **A235**, 89 (1956).
- (2) C. P. Fenimore and G. W. Jones, *J. Phys. Chem.*, **65**, 298 (1961).
- (3) D. I. MacLean and H. G. Wagner, Eleventh Symposium (International) on Combustion, Combustion Institute, 1967, p 871.
- (4) Unpublished work of W. E. Kaskan, performed at the General Electric Research Laboratory, Schenectady, N. Y.
- (5) D. M. Golden, F. P. Del Greco, and F. Kaufman, *J. Chem. Phys.*, **39**, 3034 (1963).
- (6) R. G. Bennett and F. W. Dalby, *ibid.*, **40**, 1414 (1964); **32**, 1716 (1960).
- (7) O. Schnepf and K. Dressler, *ibid.*, **32**, 1682 (1960).

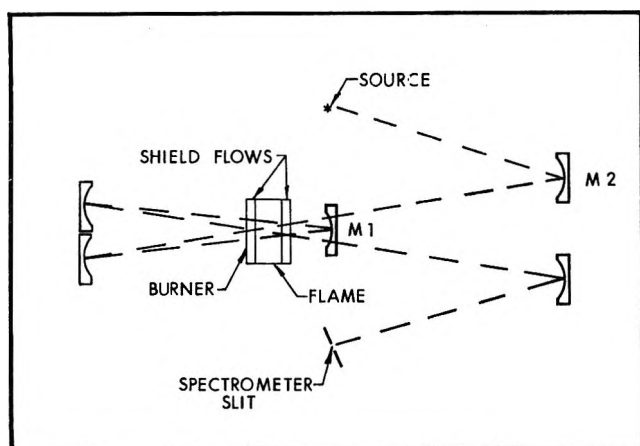


Figure 1. Experimental arrangement, top view, not to scale (see text).

ratio of F_3 to f_i , an oscillator strength for NH_2 , can be determined. This paper describes the test of reaction III for equilibration in the flame gases from two fuel rich $\text{NH}_3\text{-O}_2\text{-N}_2$ flames burning at atmospheric pressure.

Experimental Method

A. Apparatus. The apparatus consisted of a gas handling system, the flat flame burner, and an optical system, depicted in Figure 1.

Commercial gases in cylinders were used without purification. Metering was accomplished by the use of critical flow orifices. The flow through each orifice was calibrated using a wet-test meter and with the individual gases used, except for ammonia. For the ammonia orifice, the flow was measured using nitrogen and the ammonia flow was calculated from the nitrogen flow and the orifice equation. The specific heat of ammonia, as well as all other thermochemical data required in this work, was taken from the JANAF tables.

The burner was a flat flame burner, whose surface was a $7.5 \times 10 \times 0.6$ -cm brass plate through which about 2000 0.1-cm holes were drilled in a regular array. The plate was mounted on a water cooled three-compartmented box in such a way that an inner section, 5×10 cm, was fed the desired $\text{NH}_3\text{-O}_2\text{-N}_2$ mixture, and two outer 1.2×10 -cm sections could be fed a shielding flow (see Figure 1). Since the flames used were fuel rich, the shielding flow was N_2 so as to prevent a diffusion flame from forming between ambient air and the still combustible flame gases. The area of the holes comprised about one-fourth of the burner surface. Even so, the flames were flat, homogeneous (to the eye) sheets rather than arrays of cones. This was presumably due to the fact that rather low gas velocities were employed, so that the combustible mixture "diffused" (in a hydrodynamic sense) around the edges of the holes to form a uniform stream before burning. A perforated, water-cooled brass plate was situated about an inch above the flame, in order to stabilize the flow of the hot

gas stream. The burner plus stabilizing plate were moveable in the vertical direction, enabling the fixed optical system to observe the flame gases at varying distances from the burner surface.

The optical system consisted of several light sources, a White multiple-pass system, and a 0.75 m SPEX Czerny-Turner grating spectrometer equipped with photoelectric recording. The sources were a 1000-W Hanovia 976C-1 high-pressure Xe arc lamp for providing a continuum in the uv and visible, and a tungsten strip filament lamp for sodium reversal measurements.

Light from a source was directed into the multiple-pass system as indicated in Figure 1. All of the mirrors were spherical, with 150-cm focal lengths. The burner was placed as near (about 15 cm) from mirror M1 at which the image is focused, in order to enhance the spacial resolution in the flame gases. To improve this resolution further, mirror M2 was stopped down in the vertical direction to a height of about 1 cm. The resulting spacial resolution was about 2 mm. Care was taken to make all beams parallel to the burner surface and equidistant from it in order to ensure that the entire gas volume sampled by the optical system was at the same stage of reaction. From 12 to 20 passes of the light beam over the burner were used, depending on the strength of absorption.

B. Free Radical Measurements. The free radical measurements were made on the isolated spectral lines listed in Table I, by absorption on the Xe continuum. For OH and NH, the third order of a 100-mm, 625 line/mm grating was employed, and for NH_2 , the second order of the same grating was used. The grating blaze was at 1μ . All measurements were made with straight $10\text{-}\mu$ entrance and exit slits, 5 mm long, giving a resolution of roughly 0.1 \AA . The NH_2 line, actually an unresolved doublet,⁸ was chosen on the basis of its being the strongest feature which could be observed in flames in absorption out of the three strongest vibrational bands listed by Dressler and Ramsay.⁸ The strength of this line as observed in this work seemed anomalously high in comparison to intensities suggested by the above authors. Moreover, our spectrum showed additional weaker lines, some of which may be among the unassigned lines apparent in the photograph of Dressler and Ramsay. In order to ascertain that the line was properly identified, an Fe emission line at 5167.49 \AA was superposed on a scan of the absorption spectrum of NH_2 by reflecting light from a Westinghouse Fe hollow-cathode lamp from an inclined glass plate onto the slit. This provided an accurate wavelength calibration approximately 1 \AA away from the ${}^3Q_{0,4}$ line. By combining this with a measure of the dispersion, also from the Fe hollow cathode spectrum, a very satis-

(8) K. Dressler and D. A. Ramsay, *Phil. Trans. Roy. Soc. London*, **A251**, 553 (1959).

Table I

Species	Transition	Line	Wavelength, Å
OH	$^2\Sigma^+ \leftarrow ^2\pi, 0-0$	P ₁₅	3101
NH	$^3\pi \leftarrow ^3\Sigma^-, 0-0$	P ₃₇	3385
NH ₂	$A \leftarrow X, (0,12,0) \leftarrow (0,0,0)$	R _{Q_{0,4}}	5166

factory identification of the lines from R_{Q_{0,4}} through R_{Q_{0,4}} was made. This rather laborious procedure was necessitated by the fact that the dispersion of the combination spectrometer plus recorder varied by several per cent in consecutive scans over Fe lines, 30 Å apart, and one could be sure of the identification only by obtaining a wavelength fix quite close to the desired line. There is no doubt that the NH₂ line employed is R_{Q_{0,4}}, but it is possible that this rotational branch bends back so as to place a higher rotational line on top of R_{Q_{0,4}}. Since the band has only been analyzed out to R_{Q_{0,4}}, this point is obscure. In what follows, it is assumed that the R_{Q_{0,4}} line is not overlapped.

The curve of growth⁹ method was used to obtain concentrations from measurements of the absorption on a continuum. This method allows one to correct for that failure of Beer's law which occurs when the band pass of the spectrometer is wider than the absorption line width. A curve of growth is a log-log plot, for a particular value of the collision broadening parameter α , of the ordinate

$$[(\ln 2)^{1/2}/\Delta\nu_D] \int (1 - e^{-k\nu l}) d\nu \equiv [(\ln 2)^{1/2}/I_0\Delta\nu_D] \int (I_0 - I) d\nu \quad (2)$$

in which k_ν is the absorption coefficient at wave number ν , l is the optical path, $\Delta\nu_D$ is the full width at half-intensity of a Doppler line, I_0 is the incident intensity, and I is the transmitted intensity at ν , against the abscissa $N_i f_i l (\ln 2)^{1/2} / c\pi\Delta\nu_D$ in which N_i is the number density of absorbers, f_i is the line oscillator strength, and c is the velocity of light.

The molecular data required for this method are the f numbers and the broadening parameters; only an estimate of the f number for NH₂ was available,⁷ so that parameter was assumed unknown initially. In the last section of this paper a value for it will be deduced. For both OH and NH, individual line f numbers were calculated using an equation of the form

$$f_i = F \left(\frac{S_i}{2J_i + 1} \right) \quad (3)$$

in which F is the band oscillator strength, and S_i is a rotational line strength. For OH, the S_i were taken to be the A_K values of Dieke and Crosswhite,¹⁰ as corrected by Learner,¹¹ and F_{OH} was taken as 1.74×10^{-4} .⁵ For NH, S_i were calculated from equations given by Budo,¹²

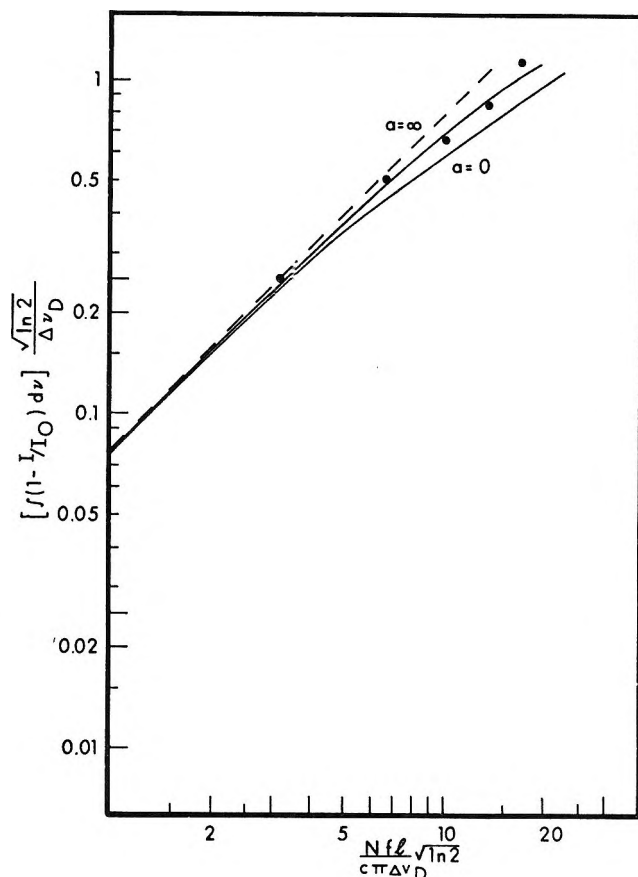


Figure 2. Portion of curve of growth for NH.

which gave a value of 3.07 for the P₃₇ line, and F_{NH} was taken as 8.0×10^{-3} .⁶

The line broadening parameter, α , for OH was calculated from the data of Engleman,¹³ assuming the presence of only N₂, H₂, and H₂O. These data have been verified in this laboratory under flame conditions.¹⁴ Broadening data for NH and NH₂ were not available. Therefore portions of the curves of growth for both NH and NH₂ were constructed by making absorption measurements at a single position in a single flame (*i.e.*, fixed N_i) at 4, 8, 12, 16, and 20 passes. The results for NH are shown in Figure 2; those for NH₂ were similar. The deviation from a straight line (Beer's law) at high I is clearly apparent. These data could be fit by translation along the abscissa to a curve of growth with a collision broadening parameter α equal to approximately 1. This value of α has essentially no significance, since not nearly enough of the curve was con-

(9) S. S. Penner, "Quantitative Molecular Spectroscopy and Gas Emissivities," Addison-Wesley, Reading, Mass., 1959, Chapter 4.

(10) G. H. Dieke and H. M. Crosswhite, *J. Quant. Spectrosc. Radiat. Transf.*, **2**, 97 (1962).

(11) R. C. M. Learner, *Proc. Roy. Soc.*, **A269**, 311 (1962).

(12) A. Budo, *Z. Physik*, **105**, 579 (1937).

(13) R. Engleman, Jr., *J. Quant. Spectrosc. Radiat. Transf.*, **9**, 391 (1969).

(14) M. P. Nadler and W. E. Kaskan, *ibid.*, **10**, 25 (1970).

structed to allow a reliable determination. However, it served the function of allowing the ordinate and therefore $N_i f_i$ to be specified absolutely to within 10–20%. Then given f_i from eq 3, N_i could be determined. A similar procedure was followed for NH_2 , except in this case only the product $N_i f_i$ was determined.

The application of the procedures above gives N_i (or $N_i f_i$), the concentration in the absorbing level. From these total concentrations N_T of OH and NH were obtained from

$$N_T = g \frac{N_i Q_{r,v} e^{E_i/kT}}{(2J+1)} \quad (4)$$

in which $Q_{r,v}$ is the rotation-vibration partition function, E_i is the energy of the absorbing state, and g is an electronic degeneracy of the ground state, having the value 4 for OH and 3 for NH. In the case of NH_2 the expression employed was

$$N_T f_i = \frac{4}{3} \frac{(N_i f_i) Q_{r,v} e^{E_i/kT}}{\sigma(2N+1)} \quad (5)$$

in which $\sigma = 2$ is the symmetry number, and N is both the rotational quantum number without spin and the average of J , for the two unresolved levels which contribute to the absorption of ${}^R Q_{0,4}$. The factor $4/3$ arises because of the nuclear spin of the H atoms. Briefly it accounts for the fact that the measurement is made on a level in the *ortho*, or high statistical weight modification of NH_2 , but N_T includes both modifications. The rotational part of $Q_{r,v}$ is the high temperature limiting form for an asymmetric rotor with neither nuclear nor electronic spin degeneracy. Molecular data for NH_2 came from the JANAF tables; those for NH and OH from Herzberg.¹⁵

The experiments were conducted at atmospheric pressure. Temperatures were determined by sodium line reversal. Table II contains the essential data on the two flames studied, including Na D-line reversal temperatures, the nominal burned gas composition, assuming only N_2 , H_2 , and H_2O as products, and the calculated temperature gradients (see below).

Table II

Flame no.	T at		V_{25} , cm/sec	X_{N_2}	X_{H_2}	$X_{\text{H}_2\text{O}}$	dT/dz , °K/cm
	0.5 cm, °K						
1	2033		14.0	0.302	0.313	0.385	44
2	2173		13.5	0.347	0.149	0.504	61

Results and Discussion

A. *Equilibration.* Figure 3 shows the concentrations of the three radicals in flame 1. The results for flame 2 are similar both in the trend of the values and in the actual concentrations. Figure 4 shows the func-

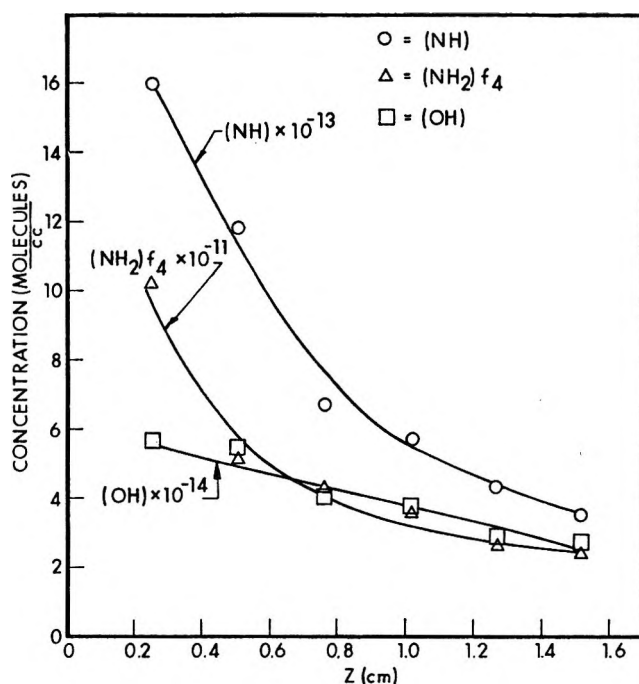


Figure 3. Data on concentrations as a function of Z , the distance from the burner, for flame 1.

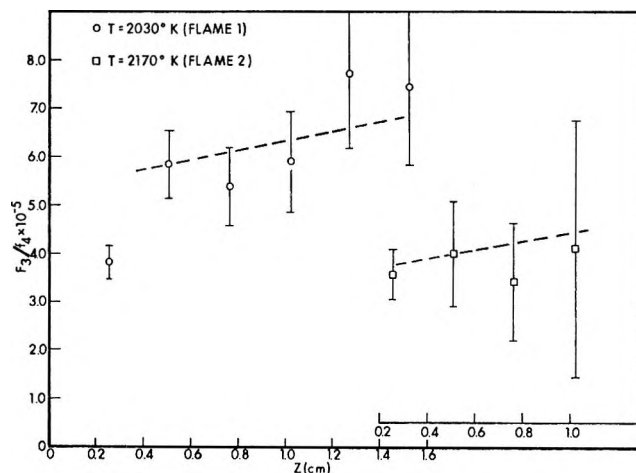


Figure 4. Data on behavior of F_3/f_4 as a function of Z , the distance from the burner. Data for flame 2 displaced 1.2 cm for clarity. Dotted lines were drawn through points at 0.5 cm and show expected temperature dependence of K_3 .

tion F_3/f_4 as a function of distance from the burner for both flames. f_4 is the oscillator strength of $\text{NH}_2 {}^R Q_{0,4}$, to be discussed in more detail later. In Figure 4 the error bars indicate the uncertainty introduced by signal noise. Both relative and absolute error increase with distance from the burner because all three radicals are decaying and the absorption is decreasing. The data from flame 2 do not extend as far as those from flame 1 because the NH_2 signal disappeared in the noise, typically 3%, beyond 1 cm from the burner.

(15) G. Herzberg, "Spectra of Diatomic Molecules," 2nd ed, D. Van Nostrand Co., Inc., 1950.

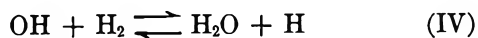
Before interpreting these data in terms of equilibration, the temperature dependence of reaction III should be considered. This should be done not only because the measured temperatures of the two flames were different, but also because it is to be expected that the gases cool in the direction of flow through radiation by H₂O, which is a major constituent. During preliminary experiments it was found that the measured reversal temperature decreased slightly with increasing distance from the burner, but the amount of decrease over the approximately 1-cm region of measurement was not much larger than the experimental uncertainty in the temperature determination, $\pm 15^\circ\text{K}$. Hence, temperatures were measured at only the one position of 0.5 cm in each case. In addition, a temperature gradient was calculated using data on the total emissivity of water vapor,¹⁶ extrapolated to the totally transparent case, and the knowledge of the gas composition (assuming complete combustion to H₂O, H₂, and N₂), the heat capacity, and the hot gas velocity. The contribution of chemical heat loss from the deduced net reaction (to be discussed below) was only 20% of the heat loss by radiation. This method of calculating temperature gradients had been found previously to give results in good agreement (within 10%) with temperature gradients obtained by the use of fine silica coated thermocouples in lower temperature H₂-O₂-N₂ flames.¹⁷

Given the temperature gradients, the straight lines in Figure 4 were drawn through the points at 0.5 cm, at which the temperatures were measured, to represent the variation of K_3 with distance. Two points can now be made. First, the upward drift of the experimental points with distance from the burner in each flame is in rough accord with the expected increase of K_3 . Second, the ratio of the observed F_3/f_4 values in the two flames at 0.5 cm is in good agreement with that calculated from the JANAF tables.

The agreement displayed in Figure 4 between the behavior of the experimental function F_3/f_4 and the equilibrium constant K_3 is very strong evidence for the equilibration of reaction III. In the following it will be considered to have been established.

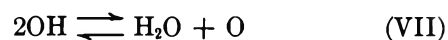
The demonstration of equilibration has two immediate consequences. First, some statements can be made about the reactions occurring in the flame gases, and second, an f number for the observed transition in NH₂ can be calculated. These are discussed separately in the next two sections.

B. Mechanism of Radical Decay. In the H₂-O₂-N₂ system, in which N₂ is a nonreactive diluent, the reactions



have been shown to be equilibrated at temperatures at

least as low as 1500°K.¹³ Other bimolecular reactions may occur between species, notably

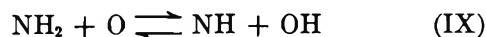
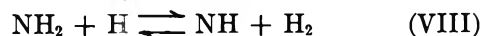


but these are linear combinations of the complete linearly independent set IV-VI and can only serve to make more complete the equilibration of the entire system. The result of this equilibration is that in H₂-O₂-N₂ flames all of the radical concentrations, present initially at greater than equilibrium amounts, decay together.

In the flames discussed here, there is an interesting departure from this behavior in that the measured NH (and therefore NH₂) is in excess of the equilibrium, relative to N₂ + H₂ as final products, but the measured OH is the equilibrium value. Since the H₂-O₂ system would on the basis of previous experience be equilibrated in these flames the finding that [OH] is the equilibrium value means that [H], [O], and [O₂] are also at equilibrium. Note here that H₂ and H₂O, being in excess, have essentially calculable concentrations whether or not the system is exactly at equilibrium. Further evidence that OH is at equilibrium comes from the fact that the decay of OH agrees well with that which would be expected if OH were simply following the falling temperature, as calculated above. Hence, what is being observed is the decay of N-H species in an equilibrium H₂-O₂ system.

Equilibration depends on the reaction in question being sufficiently fast in both directions, one criterion for which being that the activation energy in the endothermic direction not be too high. Sugden¹⁹ has discussed this criterion and has suggested that reactions with activation energies less than 40-50 kcal/mol might be equilibrated at typical flame temperatures. Reaction III is a simple H atom transfer, for which the activation energy in the reverse direction should not be too different from its endothermicity of 26 kcal/mol. Its equilibration is thus not surprising.

The same argument applies to two similar reactions



In fact, given the equilibration of (III)-(IV), those of (VIII) and (IX) follow. But since (VIII) and (IX) are both simple H atom transfers, they both probably occur with a facility equal to that of (III), and all three contribute to the equilibration of each.

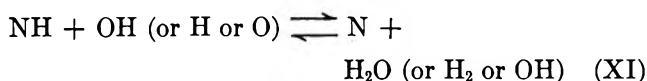
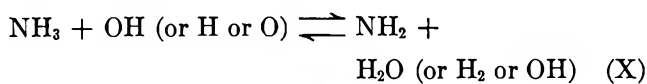
If these arguments are valid, then it is obvious that two other sets of reactions

(16) W. H. McAdams, "Heat Transmission," 3rd ed, McGraw-Hill Book Co., Inc., New York, N. Y., 1954, pp 83, 85.

(17) W. E. Kaskan, Sixth Symposium (International) on Combustion, Reinhold Publishing Corp., New York, N. Y., 1957, p 134.

(18) W. E. Kaskan, *Combust. Flame*, **3**, 49 (1959).

(19) T. M. Sugden, *Trans. Faraday Soc.*, **52**, 1465 (1956).



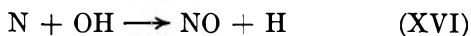
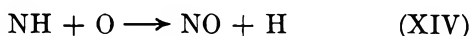
would be equilibrated, (X) more easily than (XI) on thermochemical grounds. Note that reaction X, with H and H₂ as reaction partners, is the same as (I), postulated by Fenimore and Jones² to be equilibrated. Again, as with reactions VIII and IX, the equilibration of (X) and (XI) together with the previous reactions implies the equilibration of a set of hydrogen atom transfer reaction which can be represented by



but since these are simple H-atom transfers, they can be expected to occur and to contribute to the general equilibration of the system.

The picture that emerges then for what is occurring in the flame gases of NH₃-O₂-N₂ flames is one of a radical-catalyzed thermal decomposition of NH₃, with NH₂, NH, and N present in equilibrated amounts throughout. The only thing which is lacking is the set of reactions which convert the nitrogen in these species to the final products.

At this point one can only speculate, especially since it is known that other species, principally NO, exist in these flames. Among the reactions which appear, qualitatively at least, to be capable of explaining the observed behavior are



These are all atom-transfer reactions which are very exothermic as written, and can thus be expected to be fast and irreversible.

The proposed equilibration of reactions II-XII suggests that the appropriate way to treat the kinetics of radical decay is through the use of the concentration function F_N

$$F_N = [\text{NH}_3] + [\text{NH}_2] + [\text{NH}] + [\text{N}] \quad (6)$$

which represents the total nitrogen not yet in the form of NO or N₂. For example if reactions III-XVII comprised the entire mechanism, one could write

$$dF_N/dt = \sum_{(\text{XIII})}^{(\text{XVII})} R_i \quad (7)$$

in which the R_i are the forward rates of (XIII)-(XVII), assumed irreversible. The only unknown concentration

in this equation is [NO]. Preliminary calculations, using suggested values for the rate constants²⁰ for (XIII)-(XVII) and the dF_N/dt which can be deduced from the data in this paper, result in a value for NO which appears consistent with previous work.^{1,2}

The obvious conclusion to be drawn from the above considerations is that other species, especially NO, should be measured. Attempts at measurements of additional species are currently in progress.

Even though the mechanism (III)-(XVII) is speculative, the point should be made that this mechanism appears to be at least in qualitative agreement with previous findings concerning the fate of the NO formed in the reaction zone.^{1,2} Thus, in rich flames in which NH₃ persists downstream, both the formation, through reactions XIV, XVI, and XVII, and the destruction, through (XV) of NO should occur. On the other hand, in lean flames the decay of F_N will be much more rapid, by reactions XIV, XVI, and XVII, due to the greatly increased concentrations of oxygen containing species. Once F_N has become very small, so also will the rate of (XV) and the NO remaining will react further at only a very low rate.

C. f Number for NH₂ R_{Q,4}. Given the equilibration of reaction III, F_3 can be equated to K_3 and a value of f_4 deduced from the observed value of $F_3/f_4 = K_3/f_4$. This has been done for the datum at 0.5 cm in flame 1, which is a relatively reliable point in that the observed signals were relatively large, and also the temperature was measured directly. At the observed temperature of 2033°K, $K_3 = 2.32 \times 10^2$ and $K_3/f_4 = 5.8 \times 10^6$ leading to $f_4 = 4 \times 10^{-4}$. This is an entirely reasonable value, but depends on the thermochemical data used, and as pointed out previously, on the assumption that the $R_{Q,4}$ is not overlapped by any other line.

This line f number is of the same order of magnitude as that reported previously,⁷ and also as those of the OH and NH lines used for observation in this work. It applies of course only to the $R_{Q,4}$ line in the (0,12,0)-(0,0,0) band. Inasmuch as the same ground state level of this transition is connected by optical transitions to a number of other vibrational levels in the upper electronic state, the total intensity of the electronic transition is probably an order of magnitude higher than indicated by f_4 .

Given a set of relative line strengths for transitions of the type, NH₂ A ← X, it would be possible to deduce a band oscillator strength for NH₂. However, the authors are not aware of any such compilation.

Acknowledgment. This work was supported by the National Science Foundation.

(20) D. Garvin, Ed., "A Compendium of Evaluated and Estimated Rate Coefficients," National Bureau of Standards Report 9884, U. S. Government Printing Office, Washington, D. C., 1968.

Isotopic Exchange Reactions in Nitrogen Oxides

by H. D. Sharma,

Department of Chemistry, University of Waterloo, Waterloo, Ontario, Canada

R. E. Jervis, and K. Y. Wong

*Department of Chemical Engineering and Applied Chemistry, University of Toronto, Toronto, Ontario, Canada
(Received July 25, 1969)*

The kinetics of the oxygen self-exchange in $N^{16}O_2 + N^{18}O_2 \rightleftharpoons 2N^{16}O^{18}O$ reaction has been studied in a fast-flow gas-phase tubular reactor in conjunction with a time-of-flight mass spectrometer. The reaction is found to be second order and has a rate constant of $3.0 \pm 0.1 \times 10^6 \text{ l. mol}^{-1} \text{ sec}^{-1}$ at 25° . The rate constant has no measurable temperature dependence between 25 and 82° . The rate constant for oxygen atom exchange in $^{14}NO + ^{15}NO_2 \rightleftharpoons N_2O_3$ reaction is $4.9 \pm 0.8 \times 10^7 \text{ l. mol}^{-1} \text{ sec}^{-1}$ at room temperature. The kinetics of exchange in the NO_2 - NO_2 system indicates that a cyclic structure $O-N \begin{matrix} \diagup \\ \text{O} \\ \diagdown \end{matrix} N-O$ exists either in the transition state or as

an intermediate. Similarly the exchange in the NO - NO_2 system takes place through $O-N \begin{matrix} \diagup \\ \text{O} \\ \diagdown \end{matrix} N-O$. Other exchange studies in the systems NO_2 - $^{18}O_2$ and NO - NO_2 - $^{18}O_2$ indicate that the rapid self-exchange in the $N^{16}O_2$ - $N^{18}O_2$ and ^{14}NO - $^{15}NO_2$ systems does not take place through any dissociative mechanism.

Introduction

Numerous studies exist on gas phase isotopic exchange reactions involving the oxides of nitrogen, sulfur, and carbon.¹⁻¹⁰ Of all oxides of nitrogen, N_2O is the least reactive. It does not undergo exchange with any of the other nitrogen oxides under ordinary conditions. Similarly, no exchange occurs in a mixture of $^{14}N^{18}O$ and $^{16}N^{16}O$.³ However, NO_2 exchanges oxygen rapidly with NO with a rate constant of $2.16 \times 10^7 \text{ l. mol}^{-1} \text{ sec}^{-1}$.^{2,3} $^{15}NO_2$ and $^{14}N_2O_5$ are known to exchange nitrogen atom which is postulated to take place by a dissociative mechanism of $N_2O_5 = NO_2 + NO_3$.⁴ In $S^{16}O_2$ and $S^{18}O_2$ system, exchange of oxygen atoms is postulated through the formation of a dimer having a cyclic structure either in the transition state or as an intermediate.^{5,6} No exchange is observed between SO_2 and SO_3 ⁷ and also in CO , CO_2 , and O_2 systems at room temperature.⁸⁻¹⁰ It is of interest to examine whether oxygen atom exchange takes place in NO_2 - NO_2 system via N_2O_4 having a cyclic structure formed either in the transition state (an excited intermediate) or as an intermediate. Similarly, direct kinetics data on the transfer of oxygen atom in NO - NO_2 system would indicate a comparison of the rates in the two systems. In this paper are reported the results of the study of kinetics of oxygen-atom exchange in the two systems. The exchange of oxygen atom in NO_2 - NO_2 systems would indicate whether N_2O_4 can have a cyclic or bridged structure as proposed by Longuet-Higgins¹¹ even as an unstable excited intermediate, since N_2O_4 is known to have other unstable isomers.¹²

Experimental Section

Preparation of Gases. NO_2 was prepared by the

thermal decomposition of dry $Pb(NO_3)_2$. The gas thus generated was dried by 3 or 4 passes over P_2O_5 . NO_2 containing NO was treated with dry oxygen and N_2O_4 condensed at -78° and purified till no coloration due to N_2O_3 was observed. Initially, $N^{18}O_2$ was prepared and purified in a similar manner from labeled $Pb(NO_3)_2$ supplied by Yeda Research and Development, the Weizmann Institute, Rehovoth, Israel. Later, $N^{18}O_2$ containing 92 atom per cent of oxygen-18 was obtained from Miles Laboratories Inc., Elkhart, Ind. and stored along with $^{18}O_2$ to prevent the formation of $N^{18}O$. $^{15}NO_2$ was prepared by the reduction of $H^{15}NO_3$ with Fe^{2+} ions, and subsequent purification and oxidation of NO with dry oxygen. NO was prepared by heating a mixture of KNO_2 , KNO_3 , Cr_2O_3 , and Fe_2O_3 according to the method of Ray and Ogg.¹³

- (1) K. Y. Wong, Ph.D. Thesis, University of Toronto, Toronto.
- (2) E. Leifer, *J. Chem. Phys.*, **8**, 301 (1940).
- (3) F. S. Klein, W. Spindel, and M. J. Stern, *J. Chim. Phys.*, **60**, 148 (1963).
- (4) A. R. Amell and F. Daniels, *J. Amer. Chem. Soc.*, **74**, 6209 (1952).
- (5) J. L. Huston, *J. Phys. Chem.*, **63**, 389 (1959).
- (6) N. N. Lichtin, I. Laulich, and S. Pinchas, *Inorg. Chem.*, **3**, 537 (1964).
- (7) H. H. Volge, *J. Amer. Chem. Soc.*, **61**, 1032 (1939).
- (8) C. A. Bank and E. A. Th. Verdurmen, *J. Inorg. Nucl. Chem.*, **25**, 667 (1963).
- (9) C. A. Bank and E. A. Th. Verdurmen, *ibid.*, **25**, 667 (1963).
- (10) E. A. Th. Verdurmen, *J. Phys. Chem.*, **71**, 678 (1967).
- (11) H. C. Longuet-Higgins, *Nature*, **153**, 408 (1944).
- (12) R. V. St. Louis and B. C. Crawford, Jr., *J. Chem. Phys.*, **42**, 857 (1965).
- (13) J. D. Ray and R. A. Ogg, Jr., *J. Amer. Chem. Soc.*, **78**, 5993 (1956).

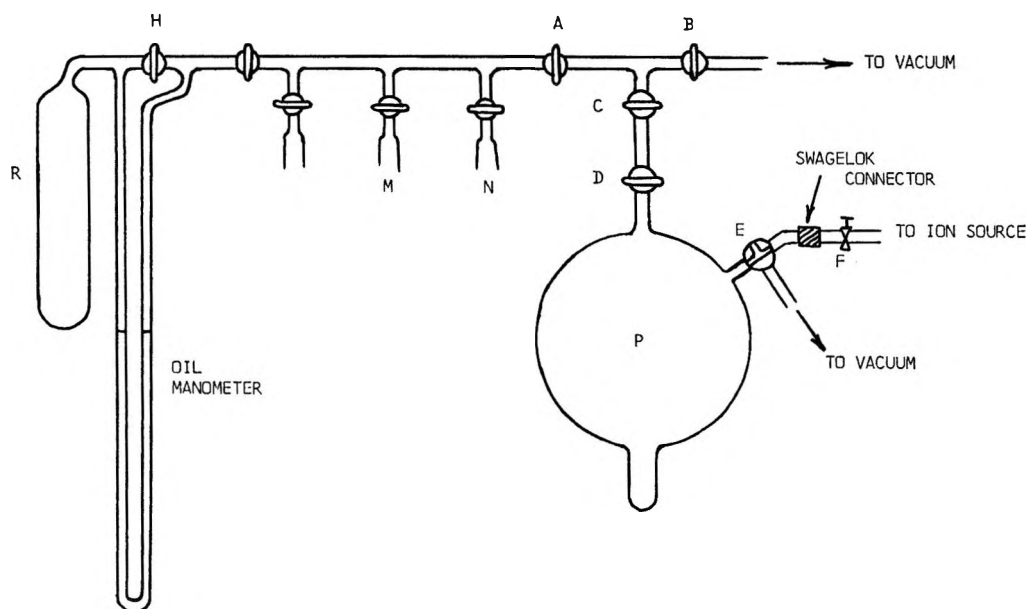


Figure 1. The static reactor.

Gas mixtures of $\text{NO}_2\text{-Ar}$, $\text{NO}_2\text{-O}_2$, NO-He , NO-N_2 , and $\text{O}_3\text{-Ar}$ were prepared by admitting a less volatile component (NO , NO_2 , or O_3) into a 5-l. flask and measuring its pressure. A mercury manometer was used with NO while a fluorosilicone oil manometer was used with NO_2 and O_3 . The gas was then condensed in a cold finger in the flask and an appropriate amount of the second gas (Ar , He , O_2 , or N_2) was added. In the case of NO_2 , equilibrium data of Giauque and Kemp was used to determine the composition of NO_2 in the mixture¹⁴ since NO_2 dimerizes to N_2O_4 .

Static Reactor Experiments. The vacuum line used in all static reactor experiments is shown in Figure 1. A 1-l. reaction vessel P was connected to the regular sample inlet port of the mass spectrometer by means of a Swagelok glass to metal connector. Gas flow into the ion source was controlled by a Hoke 2PY-281 stainless steel fine control needle valve F, equipped with Teflon packings. The gas "pipet" volume between stopcocks C and D and that between A, B, and C were determined precisely by filling them with mercury and weighing it. Inaccuracies in pressure readings due to slow degassing (gas evolution) in the reference limb of the oil manometer were avoided by attaching a 300-ml expansion bulb to that limb.

Tubular Flow Reactor. The design of the reactor was adapted from that of Arrington, *et al.*¹⁵ An important consideration in the present design was the size of the flow tube. Since the amount of labeled gas required for the experiment would increase as the square of the flow tube diameter, a narrow flow tube should be used. However, pressure drop and possible flow turbulence placed a limit on its dimension. Experiments in a 0.5 cm id flow tube proved to be unsuccessful. In the final design, a 1.0 cm id flow tube was used.

A schematic drawing of the tubular reactor is shown in Figure 2. Isotopically "normal" reactants, together with their carrier gas, were admitted at the side arm, after passing through a needle valve and a calibrated capillary flowmeter. The reaction mixture was sampled through a $75\text{-}\mu$ pinhole in a gold foil mounted at the end of the 1 cm id flow tube, a few mm away from the electron beam in the ion source of Bendix time-of-flight mass spectrometer. A precision Model D-75 two-stage mechanical pump, with a rated pumping capacity of 75 l. min^{-1} , maintained a high linear flow velocity in the flow tube. The flow could be "throttled" by means of the large stopcock at the exhaust end of the flow system, thereby changing the linear flow velocity as well as the pressure in the reactor.

The difficult problem of maintaining a constant flow of labeled NO_2 through the reactor, from a limited amount, was overcome by evaporating the labeled gas from its solid condensed in a small glass thimble attached to the jet and maintained at bromobenzene slush (prepared by slowly pouring liquid nitrogen into liquid bromobenzene in a small dewar and stirring until a malt-like consistency was obtained) temperature (-31°). At this temperature NO_2 had a vapor pressure of 22 mm, which was constant as long as there was solid N_2O_4 in the cold thimble. The size of the jet was such that the constant vapor pressure maintained a small, desired rate of flow through it.

The distance between the jet and the pinhole leak was taken to be the length of the reactor. This was varied by sliding the jet toward or away from the

(14) W. F. Giauque and J. D. Kemp, *J. Chem. Phys.*, **6**, 40 (1938).

(15) C. A. Arrington, W. Brennen, G. P. Glass, J. V. Michael, and H. Nikki, *ibid.*, **43**, 525 (1965).

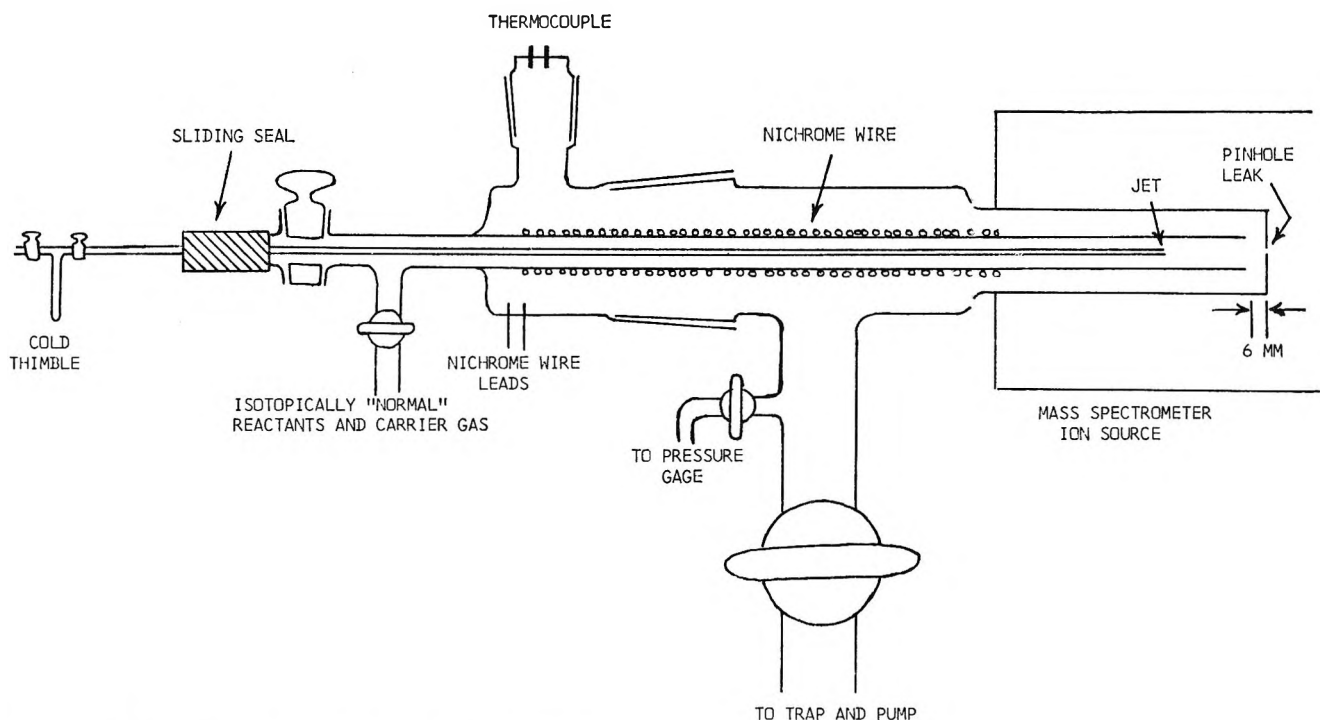


Figure 2. Schematic of gas phase fast flow tubular reactor.

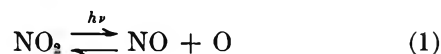
pinhole. A vacuum-tight double O-ring sliding seal ensured smooth movement of the jet. Reactor pressures varied between 0.15 and 1 mm. Pressure measurements were made with a Pace Engineering Model P90D variable reluctance pressure transducer (Baker Instruments, Toronto) having a full range of 1.5 mm. A digital read-out device provided reading accuracies of ± 0.002 mm. The pressure-sensing elements were made of nonmagnetic, corrosion resistant stainless steel. Heating of the tubular reactor was provided by a heating tape wrapped around the ion source of the mass spectrometer and by nichrome heating wire windings around the flow tube. The nichrome wire wound section began about 11 cm from the end of the flow tube. This unusual mode of heating was adopted because preliminary experiments showed that if the flow tube was heated by nichrome wire alone, with the windings extended to the end of the flow tube, radiant energy trapped inside the stainless steel fast reaction chamber caused the temperature of that section of the flow tube inside the chamber to rise much above the outside section. The situation was not improved by judicious spacing of the windings. A temperature profile uniform to $\pm 2.0^\circ$ along the length of the flow reactor was recorded using copper-constantan in thermocouple probe.

Results and Discussion

(a) *Exchange between $^{18}\text{O}_2$ and Nitrogen Oxides.* No observable exchange occurred between N^{16}O_2 and $^{18}\text{O}_2$ kept in a darkened vessel for 4 days at NO_2 pressures as high as 60 mm. When the reaction mixture was

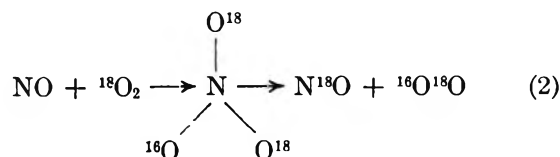
exposed to sunlight, a very slow exchange process took place. About 20% of the ^{18}O in $^{18}\text{O}_2$ was transferred to NO_2 in 2 days. There was also some scrambling among the O_2 species. In one run, the ratio $[\text{N}^{16}\text{O}^{18}\text{O}]^2/[\text{N}^{16}\text{O}_2][^{18}\text{O}_2]$ was found to be 0.7 after 2 days, as compared to the equilibrium value of 4.0.

The reactive intermediate in the presence of sunlight was O atoms produced in the photolysis (by sunlight) of NO_2



Subsequent exchange and scrambling took place via the reactions caused by oxygen atoms with O_2 molecules through the formation of O_3^* .

In the oxidation of NO with $^{18}\text{O}_2$, if the initial step is the formation of NO_3^* having the symmetrical nitrate ion structure, rapid oxygen atom scrambling in O_2 would occur as follows



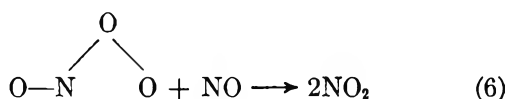
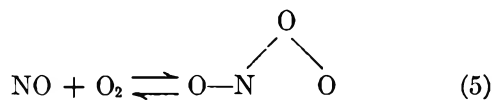
No such scrambling was observed in a darkened reaction vessel. The alternative oxidation mechanisms



and

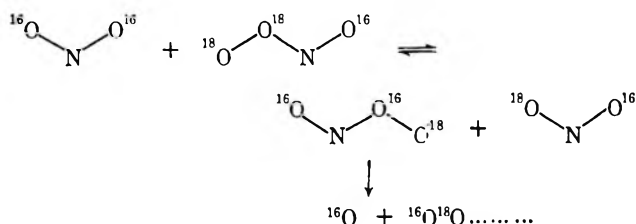
Table I: Summary of Experimental Data and Processed Results— $N^{16}O_2 + N^{18}O_2$ Self-Exchange

Run no.	Composition of F	Temp. °C	\bar{P} , mm	\bar{v} , cm/sec	$F \times 10^4$, mol/sec	$F^* \times 10^4$, mol/sec	$[NO_2] \times 10^4$, mol/l.	$R' \times 10^4$, mol/l. sec	$R \times 10^4$, mol/l. sec	$k \times 10^{-6}$, l./mol-sec
1	9.6% NO_2 in O_2	23	0.35	495	6.86	0.56	0.312	0.300	0.304	3.12
2	9.6% NO_2 in O_2	23	0.52	330	6.80	0.55	0.462	0.615	0.632	2.96
3	9.6% NO_2 in O_2	23	0.445	381	6.71	0.54	0.396	0.483	0.495	3.26
4	9.6% NO_2 in O_2	23	0.585	285	6.59	0.53	0.518	0.752	0.780	2.90
5	9.9% NO_2 in O_2	23	0.65	253	6.49	0.53	0.580	0.975	1.02	3.04
6	9.6% NO_2 in O_2	23	0.72	226	6.41	0.52	0.644	1.20	1.27	3.04
7	22.3% NO_2 in O_2	23	0.49	296	5.64	0.55	0.777	1.72	1.83	3.03
8	22.3% NO_2 in O_2	23	0.61	234	5.55	0.53	0.967	2.46	2.68	2.88
9	22.3% NO_2 in O_2	23	0.735	190	5.45	0.53	1.16	3.53	4.00	2.98
10	22.3% NO_2 in O_2	23	0.82	167	5.33	0.51	1.30	4.32	5.05	3.0
11	22.3% NO_2 in O_2	23	0.885	153	5.29	0.50	1.39	4.75	5.68	2.94
12	22.3% NO_2 in O_2	23	0.97	141	5.31	0.52	1.54	5.56	6.79	2.87
13	22.3% NO_2 in O_2	23	0.92	146	5.21	0.52	1.46	5.26	6.40	3.00
14	22.3% NO_2 in O_2	23	0.86	153	5.10	0.52	1.38	4.52	5.38	2.84
15	22.3% NO_2 in O_2	23	0.78	166	5.0	0.52	1.26	3.87	4.52	2.86
16	22.3% NO_2 in O_2	23	0.68	186	4.92	0.48	1.08	3.02	3.44	2.96
17	22.3% NO_2 in O_2	74	0.655	226	4.92	0.44	0.870	2.24	2.50	3.3
18	22.3% NO_2 in O_2	74	0.685	226	4.82	0.80	1.06	2.72	3.02	2.71
19	22.3% NO_2 in O_2	74	0.68	224	4.75	0.79	1.05	2.68	2.98	2.70
20	22.3% NO_2 in O_2	82	0.63	245	4.71	0.80	0.960	2.30	2.52	2.74
21	22.3% NO_2 in O_2	82	0.68	210	4.64	0.44	0.890	2.13	2.40	3.02
22	22.3% NO_2 in O_2	82	0.72	194	4.55	0.44	0.950	2.32	2.64	2.93
23	22.3% NO_2 in O_2	82	0.58	254	4.50	0.78	0.880	1.90	2.06	2.66
24	18.1% NO_2 in Ar	23	0.69	132	3.36	0.53	1.10	2.63	3.20	2.68
25	18.1% NO_2 in Ar	23	0.77	117	3.33	0.53	1.23	3.37	4.30	2.84
26	18.1% NO_2 in Ar	23	0.61	147	3.32	0.51	0.962	2.12	2.50	2.71
27	18.1% NO_2 in Ar	23	0.53	164	3.22	0.50	0.837	1.83	2.13	3.03
28	No Carrier Gas	23	0.14	190	0.68	0.47	0.76	1.17	1.58	2.7

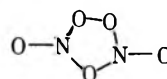


are consistent with the above observation. Guillory and Johnston¹⁶ recently found evidence for the peroxy NO_3^* in the infrared spectrum of a mixture of NO and O_2 . The intensity of the absorption band (1840 cm^{-1}) assigned to it was shown to be first order with respect to both NO and O_2 . The present experiment is unable to differentiate between the two mechanisms but support the peroxy structure of NO_3^* rather than symmetrical nitrate ion one.

The following oxygen transfer reactions, which would also produce scrambling in O_2 , through NO_3^* (peroxy), do not take place



A bridged structure such as



may also be ruled out as an intermediate.

(b) $N^{16}O_2 + N^{18}O_2$ Self-Exchange Reaction. Table I summarizes the experimental data and processed results for the NO_2 self-exchange reaction studied in the fast flow tubular reactor. A typical plot of peak height vs. x , the distance of the jet from the pinhole, is shown in Figure 3. The change in the m/e 48 peak is twice that in the m/e 46 or m/e 50 peak; all calculations are therefore based on the m/e 48 peak. Since the sensitivity of the mass spectrometer does vary slightly in the course of an experiment, the progress of the reaction is better presented as a plot of f_{46} , f_{48} , f_{50} vs. x (Figure 4).

In Table I, \bar{P} is the average pressure in the reactor. Since $\Delta P/\bar{P}$ over the length of the reactor is less than 3% for most runs, the effect of pressure drop is negligible. F^* is the molar flow rate of $N^{18}O_2$, determined by using the equation

$$F^* = \alpha F [f_{18}/f_{18}^0 - f_{18}]$$

(16) W. A. Guillory and H. S. Johnston, *J. Chem. Phys.*, **42**, 2457 (1965).

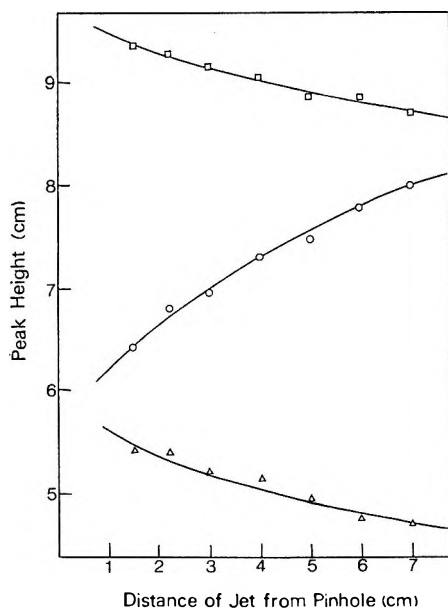


Figure 3. Peak height vs. distance of jet from pinhole, NO_2 self-exchange: run no. 23; \square , m/e 46; \circ , m/e 48; \triangle , m/e 50.

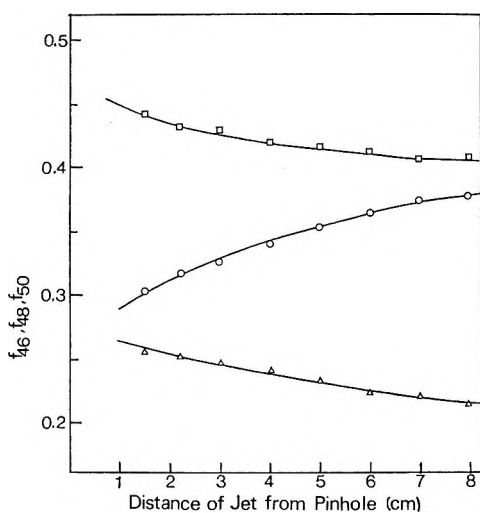


Figure 4. f_{46} , f_{48} , f_{50} vs. distance of jet from pinhole, NO_2 self-exchange: run no. 23; \square , f_{46} ; \circ , f_{48} ; \triangle , f_{50} .

where F^* is the flow rate of labeled gas (mol sec^{-1}), F the flow rate of 'normal' gases ($\text{N}^{16}\text{O}_2 + \text{carrier gas}$), f_{18}^0 the fraction of ^{18}O in the labeled gas, f_{18} the fraction of ^{18}O in NO_2 in the reaction mixture, and α the mol fraction of NO_2 in $\text{N}^{16}\text{O}_2 + \text{carrier gas}$ mixture.

Typical plots of $\ln(f_{48}^\infty - f_{48})$ vs. the distance of the jet from the pinhole x are shown in Figure 5. The slopes of the plots are obtained by least-squares fitting. The exchange rate R' , uncorrected for diffusion, is determined from the slope according to equation

$$f_{48}^\infty - f_{48} = \text{const. exp}(-R'x/[\text{NO}_2]\bar{v})$$

where f_{48}^∞ is the mole fraction of $\text{N}^{16}\text{O}^{18}\text{O}$ at equilibrium, f_{48} is the mole fraction $\text{N}^{16}\text{O}^{18}\text{O}$ at distance x between the jet and the pinhole, and \bar{v} is the average velocity

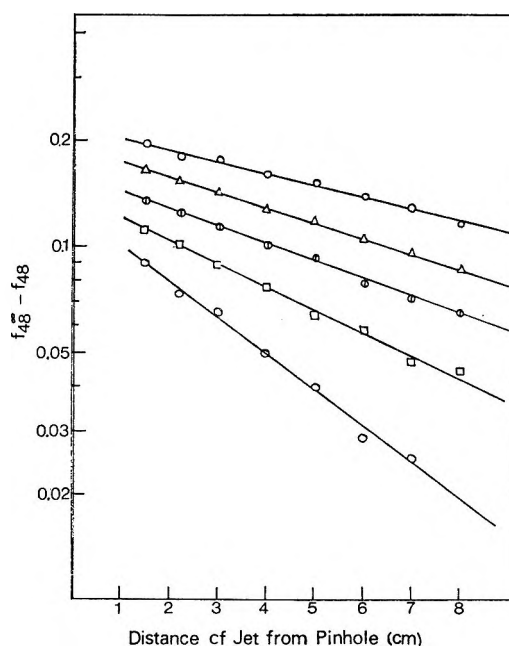


Figure 5. $\ln(f_{48}^\infty - f_{48})$ vs. distance of jet from pinhole, NO_2 self-exchange; run no.: \circ , 7; \triangle , 20; \odot , 21; \square , 26; and \circ , 13.

of gases in the flow-tube. R , corrected for back diffusion, is calculated according to an equation (see Appendix I)

$$R = R' \left(1 + \frac{R'D}{[\text{NO}_2]\bar{v}^2} \right)$$

where D is the diffusion coefficient of NO_2 . Binary diffusion coefficients for the $\text{NO}_2\text{-O}_2$ and $\text{NO}_2\text{-Ar}$ pairs are calculated as shown in Appendix II, using the recently obtained¹⁷ Lennard-Jones parameters for NO_2 . It is readily seen from Table I that the back-diffusion correction is not negligible. For some runs, it may change R' by as much as 20%. This correction is more important at low linear flow velocities and low pressures.

The exchange rate law may be written as $R = k[\text{NO}_2]^n$. Figure 6 is the plot of $\log R$ vs. $\log [\text{NO}_2]$ for data taken at 23° with O_2 as the carrier gas (runs 1 to 16). From the slope of the plot, the order of the reaction is found to be 1.96 ± 0.01 . Taking n as 2.0, the exchange rate constant k , corrected for back diffusion, is calculated for different experimental conditions (Table II).

Over the temperature range studied, the rate constant is not significantly temperature dependent. The activation energy for the reaction is nearly zero. The use of different carrier gases (O_2 and Ar) does not seem to have any effect on the rate constant. Run no. 28 is not as reliable as the other ones because the pressure was measured with an oil manometer instead of the more accurate pressure transducer. Also,

(17) R. S. Brokaw and R. A. Svehla, *J. Chem. Phys.*, **44**, 4643 (1966).

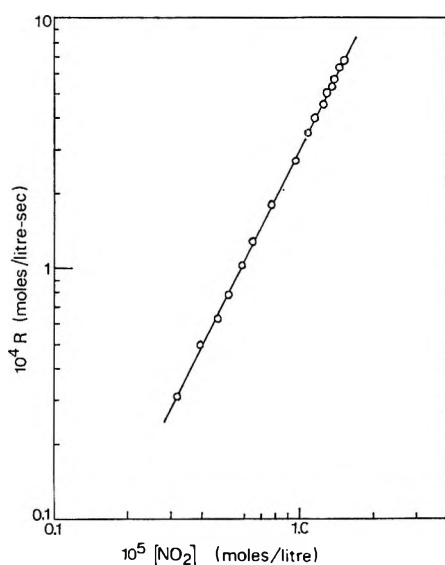


Figure 6. Log R vs. log $[\text{NO}_2]$, NO_2 self-exchange.

Table II: Second-Order Rate Constant for NO_2 Self-Exchange

T , °C	Number of runs	Carrier gas	k , l. mol ⁻¹ sec ⁻¹
23	16	O ₂	$(3.0 \pm 0.1) \times 10^6$
74	3	O ₂	$(2.9 \pm 0.3) \times 10^6$
82	4	O ₂	$(2.8 \pm 0.2) \times 10^6$
23	4	Ar	$(2.8 \pm 0.2) \times 10^6$
23	1	No carrier gas used	2.7×10^6

the very low pressure (1.5 mm of oil) and low linear flow velocity (190 cm/sec) in the reactor necessitate a rather large back-diffusion correction. Nevertheless, the run indicates that essentially the same rate constant is obtained in the absence of an inert carrier gas.

Because of the rapidity of the NO_2 self-exchange process, it is unlikely to be heterogeneous. Even the rate constant for wall recombination of oxygen atoms (in a 2 cm diameter flow tube at a total pressure of 1 mm) is only about 1 sec⁻¹ to 5 sec⁻¹.¹⁸ This corresponds to a reaction half-time of 1–0.2 sec, a time already much too large compared to the reaction time of the exchange experiment. Surface recombination reactions involving atoms and free radicals are expected to be first-order processes and to exhibit some temperature dependence.¹⁹ The exchange reaction is second order and involves practically no activation energy. Moreover, the lower limit to the NO_2 self-exchange rate constant (1×10^6 l. mol⁻¹ sec⁻¹) estimated from the static reactor experiment, where the surface to volume ratio S/V is 0.48 cm⁻¹, is not very different from k obtained in the flow reactor (3.0×10^6 l. mol⁻¹ sec⁻¹), where S/V is 4.0 cm⁻¹. If the reaction is heterogeneous, one would expect it to be significantly slower in the static reactor. As

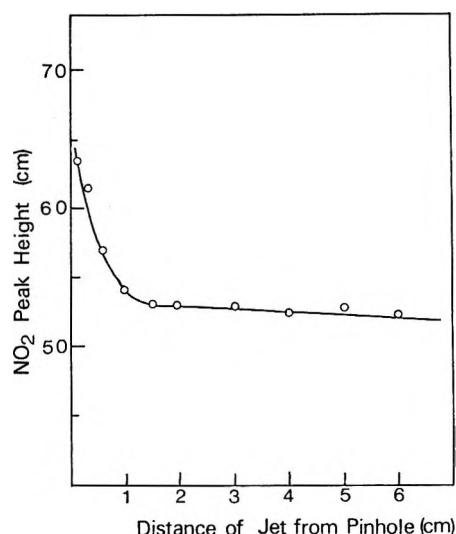


Figure 7. Variation of NO_2 concentration with distance of jet from pinhole: a gas mixing study.

noted before, the presence of an inert carrier gas has no effect on the exchange rate. In addition, the chemically very similar nitrogen exchange between NO and NO_2 ³ has been shown to be homogeneous. It appears that the NO_2 self-exchange reaction is also a homogeneous one.

The performance of the reactor was checked by determining the rate constant for the reaction $\text{NO} + \text{O}_3 \rightarrow \text{NO}_2 + \text{O}_2$ (Appendix III). The precision of the exchange data is very good. This is so because there is no change in the total NO_2 concentration. The quantities that change along the length of the flow reactor are the mole fractions of the three NO_2 species f_{46} , f_{48} , and f_{50} . These can be calculated accurately from the adjacent mass peaks m/e 46, 48, 50 at any jet position. Individual calibrations of reactant and product concentrations against peak height, which constitute a major source of error in flow-reactor experiments, are not required in the present experiment. The equilibrium value F_{48}^∞ , required in calculating k , is also determined. Major systematic errors are (i) *flow rate measurements and flow fluctuations*: reproducibility of the flow calibrations for NO_2 - O_2 gas mixtures is only slightly better than 5%. The flow of N^{18}O_2 from the jet is not perfectly constant at room temperature, as can be seen in Table I under the column F^* . In addition, gas depletion from the 5-l. supply bulb, which amounts to about 2% for the average run, causes a very slight, gradual decrease in flow rate over the duration of the run.

(ii) *Incomplete Mixing*. The reactants are assumed to be perfectly mixed within 1 to 2 cm from the jet. This mixing distance is estimated from gas mixing

(18) F. Kaufman, *Progr. Reaction Kinetics* 1, 1 (1961).

(19) K. J. Laidler, "Chemical Kinetics," 2nd ed, McGraw-Hill Book Co., Inc., New York, N. Y., 1965, p 284.

Table III: Summary of Experimental Data and Processed Results— $^{14}\text{NO} + ^{15}\text{NO}_2$ Exchange at 23°

Run no.	Composition of F	\bar{p} , mm	\bar{v} , cm/sec	$F \times 10^6$, mol/sec	$F^* \times 10^6$, mol/sec	$[\text{NO}_2] \times 10^6$, mol/l.	$[\text{NO}] \times 10^6$, mol/l.	$R' \times 10^4$, mol/l. sec	$R \times 10^4$, mol/l. sec	$k \times 10^{-7}$, l./mol sec
6	13.6% NO in N ₂	0.175	550	3.55	0.55	1.28	1.12	0.60	0.73	5.10
10	8.3% NO in N ₂	0.23	734	6.75	0.55	0.95	0.97	0.47	0.515	5.60
13	8.3% NO in N ₂	0.31	525	6.34	0.55	1.33	1.27	0.70	0.805	4.75
15	8.39% NO in N ₂	0.26	744	7.65	0.55	0.94	1.10	0.395	0.42	4.08
16	8.39% NO in N ₂	0.32	590	7.50	0.55	1.18	1.36	0.62	0.685	4.29
17	8.39% NO in N ₂	0.40	465	7.36	0.55	1.50	1.68	1.08	1.28	5.10
19	8.39% NO in N ₂	0.19	936	7.05	0.55	0.744	0.805	0.345	0.37	6.01
20	8.39% NO in N ₂	0.47	372	6.88	0.55	1.88	1.98	1.18	1.44	3.86
21	8.39% NO in N ₂	0.535	320	6.80	0.55	2.18	2.26	1.98	2.74	5.55
22	8.39% NO in N ₂	0.37	454	6.62	0.55	1.54	1.55	1.07	1.30	5.50

experiments in which NO₂ flowing from the jet mixes with a stream of inert N₂. Figure 7 shows the variation of NO₂ concentration with distance. Mixing is essentially complete within about 1.5 cm.

(iii) *Back-Diffusion Corrections* The application of back-diffusion corrections to the data reduces considerably data scatter; the standard deviation of the rate constant is very small (see Tables I and II). However, the amount of correction required for some runs is as high as 20%, and if the mathematical model from which the back-diffusion formula is derived cannot be rigorously applied to the present flow reactor design, some errors may result.

(c) *Nitrogen Exchange in ^{14}NO and $^{15}\text{NO}_2$.* Experimental data and processed results are summarized in Table III. From the peak height of m/e 47 vs. x , the distance of the jet from the pinhole, similar to results shown in Figure 3 for NO₂, R' , the exchange rate, is obtained from the plot of $\ln(f_{47} - f_{47}^\infty)$ vs. x (Figure 8). R , corrected for back diffusion, is calculated from the equation given in Appendix I.

$$R = R'(1 + R'D([\text{NO}] + [\text{NO}_2])/v^2)$$

The plot of R vs. $[\text{NO}_2][\text{NO}]$ (Figure 9) shows considerable scatter. Apart from systematic errors previously discussed in connection with the NO₂ self-exchange reaction, additional sources of error arise from uncertainties in the flow of labeled gas and thus in the value of f_{47}^∞ . In the NO₂ self-exchange experiment, N^{18}O_2 flow from the jet can be calculated for each run from a mass balance of ^{18}O in NO₂. A similar procedure cannot be employed to obtain the $^{15}\text{NO}_2$ flow in the NO + NO₂ exchange experiment because there is a net transfer of ^{15}N atoms from one chemically distinct species to another. The sensitivities of the mass spectrometer for NO and NO₂ are different. The mass spectrum is further complicated by the fact that NO⁺ is a prominent peak in the fragmentation of NO₂. The value of 0.55×10^{-6} mol sec⁻¹, calibrated for NO₂ flow from the jet, is used as the flow rate for all runs. Since the flow from the jet may vary by as much as 6 or 7% between 2 runs, an additional error is introduced into the calculated data.

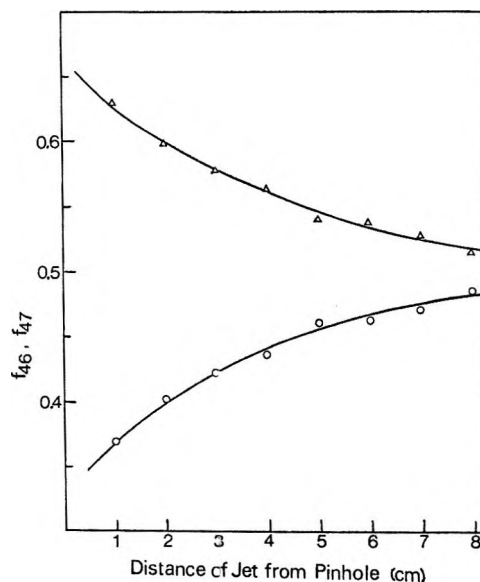
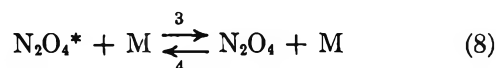
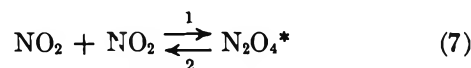


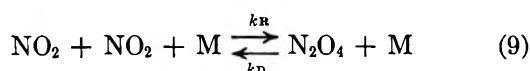
Figure 8. f_{46}, f_{47} vs. distance of jet from pinhole, NO + NO₂ exchange, run no. 13: O, f_{46} ; Δ, f_{47} .

The second-order rate constant for the NO + NO₂ exchange reaction, corrected for back diffusion, is $(4.9 \pm 0.8) \times 10^7$ l. mol⁻¹ sec⁻¹. Klein, *et al.*,³ who examined the NO₂ "catalyzed" exchange between $^{14}\text{N}^{18}\text{O}$ and $^{16}\text{N}^{18}\text{O}$, gave the value of 2.16×10^7 l. mol⁻¹ sec⁻¹ as the exchange rate constant. Because of the difference in the definitions of exchange rate, the rate constant in the present work should be twice that of Klein, *et al.*³ The discrepancy between the two sets of results, which were obtained by very different methods, is a little over 10%.

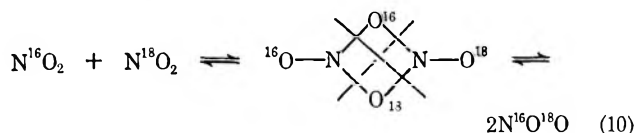
(d) *Mechanism of Exchange.* The bimolecular association of NO₂ to form N₂O₄ may be considered in the light of the so-called energy transfer mechanism



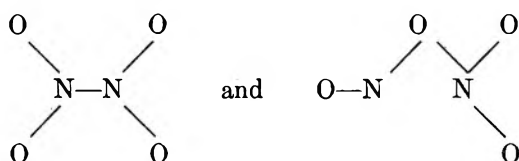
The overall reaction is



The excited intermediate (not differentiated from transition-state configuration) N_2O_4^* containing the excess energy of recombination may re-dissociate to NO_2 , or it may be stabilized to N_2O_4 through collision with a third body, M. If N_2O_4^* has the bridged structure, oxygen exchange takes place as follows



Evidence for this mechanism is the second-order concentration dependence of the rate of exchange. The other species



will not lead to oxygen-atom exchange although further rearrangement of these species may result in forming a bridged structure.

From the data of Carrington and Davidson²⁰ $k_D = 2.0 \times 10^{14} \exp(-11,000/RT) \text{ l. mol}^{-1} \text{ sec}^{-1} = 1.6 \times 10^6 \text{ l. mol}^{-1} \text{ sec}^{-1}$ at 25° ; $k_D^\infty = 1 \times 10^{16} \exp(-13,000/RT) \text{ sec}^{-1} = 3 \times 10^6 \text{ sec}^{-1}$ at 25° .

From the known equilibrium constant for the dissociation of N_2O_4 , which is $0.0059 \text{ mol l.}^{-1}$ at 25° , one

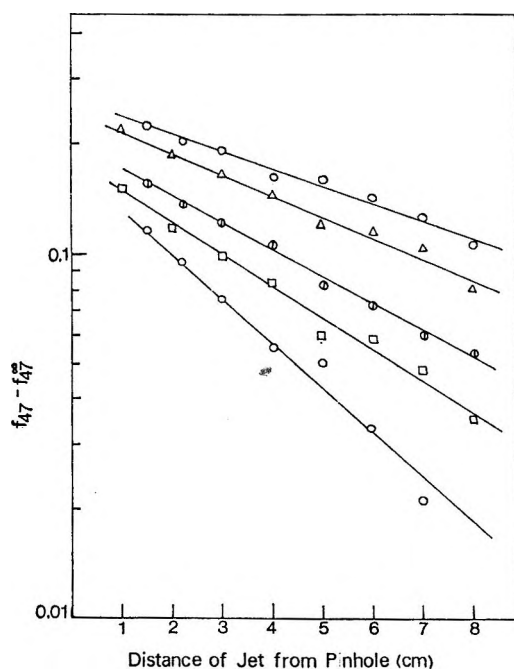


Figure 9. $\ln(f_{17} - f_{17}^\infty)$ vs. distance of jet from pinhole, $\text{NO} + \text{NO}_2$ exchange; run no: \circ , 15; \triangle , 10; \diamond , 16; \square , 13; and \circ , 17.

obtains, at 25° , $k_R = 2.7 \times 10^8 \text{ l.}^2 \text{ mol}^{-2} \text{ sec}^{-1}$, $k_R^\infty = 5 \times 10^8 \text{ l. mol}^{-1} \text{ sec}^{-1}$, where k_D is the second-order dissociation constant of N_2O_4 in the low-pressure limit at which the rate of energy transfer determines the rate of reaction, k_R is the overall third-order recombination constant of NO_2 for the low-pressure limit, k_D^∞ is the first-order dissociation constant in the high-pressure limit, and k_R^∞ is the overall second-order recombination rate constant, also for the high-pressure limit. It must be emphasized that k_D^∞ is estimated from data taken in the second-order region. It is probably accurate only to within a factor of 5.

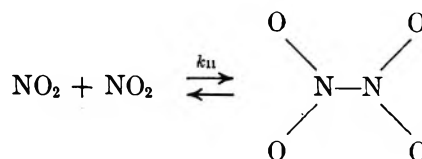
At the low pressure used in the exchange experiments, the collisional deactivation process (equation 8) may be neglected. Thus, $k_1[\text{NO}_2]^2 = k_2[\text{N}_2\text{O}_4^*]$. If N_2O_4^* has the bridged structure, the exchange rate R is

$$R = \frac{1}{2}k_2[\text{N}_2\text{O}_4^*] = \frac{1}{2}k_1[\text{NO}_2]^2 = \frac{1}{2}k_R[\text{NO}_2]^2 = 2.5 \times 10^8 \text{ l. mol}^{-1} \text{ sec}^{-1}$$

However, the observed exchange rate constant k ($3.0 \times 10^6 \text{ l. mol}^{-1} \text{ sec}^{-1}$) is about a factor of 100 smaller than $\frac{1}{2}k_R^\infty$. It may perhaps be that the probability of forming the symmetrical bridged intermediate in the association of NO_2 is only about 0.01.

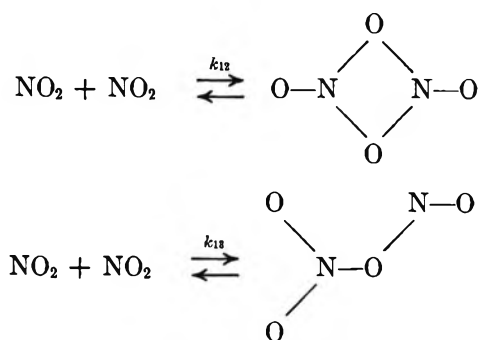
Two other structures of N_2O_4 are possible; the nitrosyl nitrate structure and the N-N bonded structure. The latter structure is the currently accepted one, mainly based on the evidence from electron diffraction and spectroscopic work, in spite of the unusual features of the N-N bond, *viz.*, its length and weakness, its planarity, and its high barrier to internal rotation.²¹ Recently, observed lines in the ir spectra of N_2O_4 at liquid nitrogen and liquid helium temperatures¹² by matrix isolation techniques were assigned to the unstable nitrosyl nitrate isomer and the staggered N-N bonded isomer with D_{2d} configuration. Perhaps a reexamination of these spectra may reveal lines that may be assigned to the bridged structure and thus provide evidence for the existence of bridged structure as an intermediate.

The excited intermediate N_2O_4^* probably consists of all three of the possible structures of N_2O_4 , in equilibrium proportions. Thus, in the gas association of NO_2 to form N_2O_4^* , the following parallel processes may be conceived



(20) T. Carrington and N. Davidson, *J. Phys. Chem.*, **57**, 418 (1953).

(21) P. Gray and A. D. Yoffe, *Chem. Rev.*, **55**, 1069 (1955).



At room temperature, k_{11} is about 5×10^8 l. mol⁻¹ sec⁻¹ and k_{12} is, from the NO₂ self-exchange experiment, 6.0×10^6 l. mol⁻¹ sec⁻¹. From the oxygen atom transfer reaction between NO and NO₂, which goes

through the $\begin{array}{c} \text{N} \quad \text{N} \\ \diagdown \quad \diagup \\ \text{O} \quad \text{O} \quad \text{O} \end{array}$ excited intermediate and has a rate constant of 4.9×10^7 l. mol⁻¹ sec⁻¹, k_{13} is estimated to have a similar value.

Since the exchange process involves essentially no activation energy, repulsion between the bridging oxygen atoms is not important. The low probability of bridge formation may be attributed to the small steric factor; the NO₂ molecules must assume certain spatial orientations relative to each other in forming the bridge.

The existence of small, equilibrium concentrations of the bridged isomer and the nitrosyl nitrate isomer of N₂O₄, provides a simple explanation for the heterolytic dissociation in liquid N₂O₄



It also seems likely that the small observed dipole moment of N₂O₄ may be due to the unstable nitrosyl nitrate isomer.¹² However, it is premature to derive any quantitative estimations.

Any dissociative mechanism that would lead to rapid self-exchange in NO₂ is implausible. The thermal decomposition of NO₂ to give NO and O₂ begins at temperatures above 200°. It is a very slow reaction with a high activation energy of 26.9 kcal mol⁻¹.²² At room temperature, the equilibrium constant $K = [\text{NO}_2]^2 / [\text{NO}]^2 [\text{O}_2]$ is 5.9×10^{12} l./mol.¹⁴ With NO₂ as low as 10⁻⁴ mol/l. the equilibrium NO concentration is 3×10^{-8} mol/l. NO₂ dissociation is certainly negligible in the presence of excess O₂ carrier gas. Another oxygen-containing species that could lead to exchange is NO₃. This is a very unstable species whose existence is suggested by the results of certain gas kinetic experiments. It is conceivable that NO₃ may be produced by the reaction $\text{NO}_2 + \text{NO}_2 \rightarrow \text{NO} + \text{NO}_3$. The standard free energies of formation of NO and NO₂ are 20.719 kcal mol⁻¹ and 12.390 kcal/mol, respectively.²² Using the standard free energy of formation of NO₃ (27.36 kcal mol⁻¹) which was calculated by Hisatsune,²³ the standard free energy change

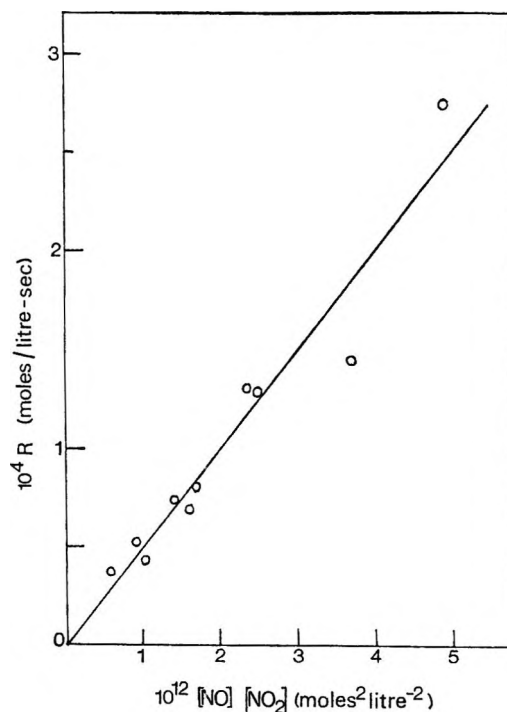


Figure 10. Exchange rate as a function of $[\text{NO}][\text{NO}_2]$, NO + NO₂ exchange.

for the above reaction is 23.30 kcal mol⁻¹, which corresponds to an equilibrium constant of 10¹⁷. At NO₂ = 10⁻⁵ mol l.⁻¹, the equilibrium NO₃ concentration is 10^{-13.5} mol l.⁻¹. This cannot account for the rapid rate of oxygen self-exchange in NO₂. Moreover, exchange data in the N¹⁶O + ¹⁸O₂ system indicate that the peroxy form of NO₃ does not exchange oxygen atoms with NO₂. Finally, the nonexchange between N¹⁶O₂ and ¹⁸O₂ shows that the extremely small amount of O atoms produced in the photolysis of NO₂ (by diffuse sunlight in the laboratory) cannot be responsible for the observed exchange.

Acknowledgments. Financial support through the provision of research grants and a National Research Fellowship to K. Y. W. by the National Research Council of Canada is gratefully acknowledged.

Appendix I

The general equation of change for the concentration of a species in a flow system is given by²⁴

$$\frac{\delta C}{\delta t} + \left(v_x \frac{\delta C}{\delta x} + v_y \frac{\delta C}{\delta y} + v_z \frac{\delta C}{\delta z} \right) = D \left(\frac{\delta^2 C}{\delta x^2} + \frac{\delta^2 C}{\delta y^2} + \frac{\delta^2 C}{\delta z^2} \right) + R''$$

(22) F. D. Rossini, *et al.*, "Selected Values of Chemical Thermodynamic Properties," National Bureau of Standards Circular No. 500, U. S. Government Printing Office, Washington, D. C., 1952; P. G. Ashmore and M. G. Burnett, *Trans. Faraday Soc.*, **58**, 253 (1962).

(23) I. C. Hisatsune, *J. Phys. Chem.*, **65**, 2249 (1961).

where v_x , v_y , and v_z are the linear velocities in the x , y , and z directions, respectively. D is the diffusion coefficient of the species and R'' is the rate of reaction for the production of the species. For a system at steady state $\delta C/\delta T = 0$. In a tubular reactor there is no bulk flow in the y and z direction. Further, if the flow in the x direction is laminar and its profile is assumed to be parabolic, the equation in cylindrical coordinates reduces to

$$v_0 \left(\frac{r^2}{r_0^2} \right) \frac{\delta C}{\delta x} = D \left(\frac{\delta^2 C}{\delta r^2} + \frac{1}{r} \frac{\delta C}{\delta r} \right) + D \frac{\delta^2 C}{\delta x^2} + R''$$

where v_0 is the velocity at $r = 0$ and r_0 is the radius of the flow tube. Assuming the radial gradient $\delta C/\delta r = 0$ (the assumption is justified since $D/R''r_0^2 > 1^{24}$) and replacing the velocity term by the average stream velocity \bar{v} , the equation simplifies to

$$\bar{v} \frac{dC}{dx} = D \frac{d^2 C}{dx^2} + R'' \quad (i)$$

For the NO_2 self-exchange reaction

$$R'' = \frac{dC_{48}}{dt} = \frac{d}{dt} f_{48}[\text{NO}_2] = R(f_{48}^\infty - f_{48})$$

where R and $[\text{NO}_2]$ are the rate constants for isotopic exchange and the total concentration of NO_2 , respectively. The total concentration of NO_2 is constant in a particular experiment and thus eq i becomes

$$\bar{v} \frac{df_{48}}{dx} = D \frac{d^2 f}{dx^2} + \frac{R}{[\text{NO}_2]} (f_{48}^\infty - f_{48})$$

The solution of the equation is

$$f_{48}^\infty - f_{48} = A \exp \left[\frac{x}{2D} \left(\bar{v} + \sqrt{\bar{v}^2 + 4DR/[\text{NO}_2]} \right) \right] + B \exp \left[\frac{x}{2D} \left(\bar{v} - \sqrt{\bar{v}^2 + 4DR/[\text{NO}_2]} \right) \right]$$

For $x \rightarrow \infty$, $f_{48}^\infty - f_{48} \rightarrow 0$ and thus $A = 0$

$$f_{48}^\infty - f_{48} = B \exp \left[\frac{x}{2D} \left(\bar{v} - \sqrt{\bar{v}^2 + 4DR/[\text{NO}_2]} \right) \right]$$

If R' is the rate constant for isotopic exchange uncorrected for back-diffusion, R is related to R' by the following expression

$$R = R' \left(1 + \frac{R'D}{[\text{NO}_2]\bar{v}^2} \right)$$

If $R'D/[\text{NO}_2]\bar{v}^2 \ll 1$, correction due to back-diffusion is negligible. It would seem that the near-ideal plug-flow reactor should be one operated at high linear velocities and at high total pressure. However, at high pressure, diffusion is slow and the radial diffusion terms may become important.

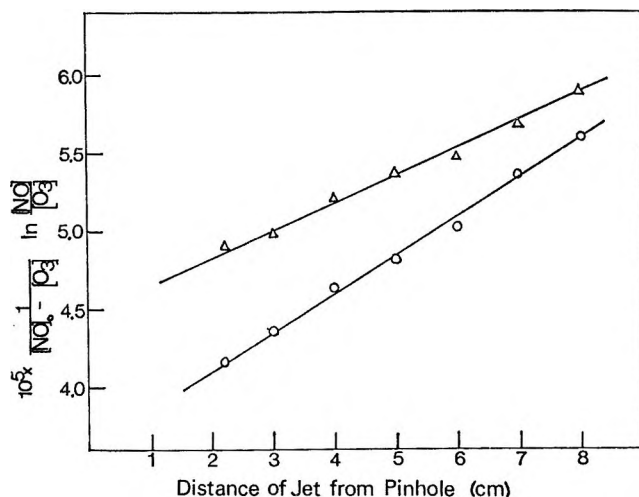


Figure 11. Extent of reaction vs. distance of jet from pinhole, $\text{NO} + \text{O}_3 \rightarrow \text{NO}_2 + \text{O}_2$ reaction.

For the second-order oxygen-atom exchange in NO_2 , the rate constant k is given by

$$k = k' \left(1 + \frac{k'D[\text{NO}_2]}{\bar{v}^2} \right)$$

where k' is the rate constant uncorrected for back-diffusion.

The corresponding equations for the exchange in $\text{NO}-\text{NO}_2$ system are

$$f_{47} - f_{47}^\infty = C \exp \left[\frac{x}{2D} \left(\bar{v} - \sqrt{\bar{v}^2 - 4kD([\text{NO}_2] + [\text{NO}])} \right) \right]$$

and $k = k' [1 + k'D([\text{NO}] + [\text{NO}_2])/\bar{v}^2]$

Appendix II

Calculation of Diffusion Coefficients for Binary Mixtures. The diffusion coefficient D_{12} in $\text{cm}^2 \text{sec}^{-1}$, for binary mixtures is given by²⁵ (Table IV)

$$D_{12} = 0.002628 \frac{\sqrt{(M_1 + M_2)T^3}}{P\sigma_{12}^2\Omega_{12}}$$

Table IV: Diffusion Coefficients of Binary Mixtures

Gas mixture	$\sigma_{12}^{17,26}$	$\epsilon/k, ^\circ\text{K}^{17,26}$	Ω_{12}^{27}	$DP, \text{cm}^2 \text{sec}^{-1} \text{mm}$
NO_2-O_2	3.653	136	1.044	118
NO_2-Ar	3.591	161	1.107	108
NO_2-N_2	3.757	129	1.028	118

(24) R. B. Bird, W. E. Stewart, and E. N. Lightfoot, "Transport Phenomena," John Wiley & Sons, New York, N. Y., 1960, p 559.

(25) J. O. Hirschfelder, C. F. Curtiss, and R. B. Bird, "Molecular Theory of Gases and Liquids," John Wiley & Sons, Inc., New York, N. Y., 1954, p 539.

Table V: Summary of Results: $\text{NO} + \text{O}_3 \rightarrow \text{NO}_2 + \text{O}_2$ at 23° (Flow of 8.35%)

Run no.	\bar{v} cm/sec	\bar{P} , mm	Flow of NO , mol/sec	O_3 in Ar, mol/sec	Slope $\times 10^{-4}$, l./mol cm	$k \times 10^{-7}$, l./mol sec
1	510	0.335	1.92×10^{-6}	5.36×10^{-6}	2.84	1.27
2	630	0.270	1.93×10^{-6}	5.40×10^{-6}	1.79	1.13
3	455	0.370	1.85×10^{-6}	5.30×10^{-6}	2.94	1.34
						Average = 1.24 ± 0.11

Table VI: Rate Constant for $\text{NO} + \text{O}_3 \rightarrow \text{NO}_2 + \text{O}_2$: Comparison with Literature

k at 23° , l./mol sec	Method	References
1.13×10^7	Stopped-flow; spectrophotometric	28
1.3×10^7	Tubular flow; mass spectrometric	29
0.86×10^7	Tubular flow; spectrophotometric	30
1.24×10^7	Tubular flow; mass spectrometric	This work

where P is the pressure in atmospheres, T is the absolute temperature in $^\circ\text{K}$, M_1 and M_2 are molecular weights of the two components, Ω_{12} is the collision integral at reduced temperature kT/ϵ_{12} , and σ_{12} and ϵ_{12} are the Lennard-Jones potential parameters in Å and $^\circ\text{K}$, respectively, obtained by the following rules and given in Table IV.^{26,27}

$$\epsilon_{12} = (\epsilon_1 \epsilon_2)^{1/2}; \quad \sigma_{12} = 1/2(\sigma_1 + \sigma_2)$$

Appendix III. Test Reaction



Results of the test reaction are given in Table V. The second-order rate constant is obtained from the plot of $1/[\text{NO}]_0 - [\text{O}_3]_0 \ln [\text{NO}]/[\text{O}_3]$ against x , the distance of the jet from the pinhole [Figure 11]. Because of the high linear flow velocities used, the correction due to back-diffusion has not been applied to the data. Comparison between the rate constant obtained and the reported values in the literature is shown in Table VI.²⁸⁻³⁰

(26) Reference 25, p 1110.

(27) Reference 25, p 1126.

(28) H. S. Johnston, and H. J. Crosby, *J. Chem. Phys.*, **22**, 689 (1954).

(29) L. F. Phillips and H. I. Schiff, *ibid.*, **36**, 1509 (1962).

(30) M. A. A. Clyne, B. A. Thrush, and R. P. Wayne, *Trans. Faraday Soc.*, **60**, 359 (1964).

Conductance of Lanthanum Hexacyanoferrate(III) Tetrahydrate in Dioxane-Formamide and Acetone-Formamide Mixtures at 25°¹

by Gyan P. Johari²

Department of Chemistry, University of Gorakhpur, Gorakhpur, India (Received April 9, 1969)

Conductance measurements are reported for $\text{LaFe}(\text{CN})_6 \cdot 4\text{H}_2\text{O}$ in dioxane-formamide and acetone-formamide mixtures at 25° over the composition range 10–50% dioxane and 10–60% acetone. The data were analyzed for Λ^0 and association constant by Shedlovsky's method. The association constant in dioxane-formamide mixtures is higher than in acetone-formamide mixtures at comparable dielectric constant. The Walden product decreases with decreasing dielectric constant in both systems but relatively more in acetone-formamide mixtures.

Introduction

This paper reports a part of our investigation of the conductance behavior of high charge symmetrical electrolytes in solvents of high dielectric constant. In previous papers we reported that several 2:2 salts are unassociated in formamide³ and in N-methylformamide.⁴ Several 3:3 salts were found to have an association constant of the order of 10^2 in formamide.⁵ Consistent values for the ion-size parameter from hydrodynamic and electrostatic approaches justified the applicability of the Fuoss-Onsager extended theory⁶ to these 3:3 salts. In this paper we report on the conductance data of $\text{LaFe}(\text{CN})_6 \cdot 4\text{H}_2\text{O}$ in two mixed solvent systems of varying dielectric constant with the particular purpose of examining the short-range ion-ion interaction in this 3:3 salt.

Experimental Section

Materials. Lanthanum hexacyanoferrate(III) was prepared by the method of James and Willard.⁷ A concentrated aqueous solution of LaCl_3 (prepared from the pure oxide) was mixed at 60° with an equimolar $\text{K}_3\text{Fe}(\text{CN})_6$ solution. Brown crystals of $\text{LaFe}(\text{CN})_6 \cdot 4\text{H}_2\text{O}$ separated on cooling. These were washed with cold water and dried over P_2O_5 to a constant weight. The dried salt had a definite tetrahydrate form as shown by a quantitative analysis for lanthanum. Acetone, dioxane, and formamide were purified as described earlier.^{3,8,9}

Equipment and Technique. The conductance equipment and the methods of measurement have been described earlier.^{3,8,9}

Results

The molar concentration, C , and the equivalent conductance, Λ , data in the two solvent systems are presented in Table I. Each set of data is headed by the dielectric constant of the mixed solvent taken from ref 8 and 9.

The phoreograms in all solvent mixtures are cata-batic; the positive deviation from the theoretical

Onsager slope increases progressively with decreasing dielectric constant.

We attempted to fit the data (at concentrations for which $\kappa_a^0 < 0.2$) to Fuoss-Onsager extended equation for an associated salt by the "y - x" method⁶

$$\Lambda = \Lambda^0 - S(C\gamma)^{1/2} + EC\gamma \log C\gamma + JC\gamma - K_A C\gamma f_{\pm}^2 \Lambda \quad (1)$$

The analysis was done on an IBM 7094 computer using a Fortran program similar to the one described by Kay.¹⁰ For most sets of data the program computation failed to converge. For sets of data for which Λ^0 , a_j , and K_A were obtained, the standard deviations were so large as to make the reliability of analysis doubtful. We also tried to analyze the available conductance data in the literature for an associated 3:3 salt. The conductance data of Dunsmore, *et al.*, for $\text{LaCo}(\text{CN})_6$ in aqueous solutions¹¹ were analyzed according to eq 1. The results obtained were $\Lambda^0 = 161.64 \pm 1.6 \text{ ohm}^{-1} \text{ cm}^2 \text{ g-equiv}^{-1}$, $K_A = 2900 \pm 627 \text{ M}^{-1}$, and $a_j = 6.3 \pm 2.3 \text{ \AA}$, in comparison to the value of $\Lambda^0 = 166.98 \text{ ohm}^{-1} \text{ cm}^2 \text{ g-equiv}^{-1}$, and $K_A = 5460 \text{ M}^{-1}$ obtained by neglecting $EC\gamma \log C\gamma$ and $JC\gamma$ terms.

The Fuoss-Onsager extended equation describes the conductance data of 1:1 and 2:2 salts^{6,8,9,12} and of

(1) Support for this work from the University Grants Commission, New Delhi, India, is gratefully acknowledged.

(2) Visiting Assistant Professor, Belfer Graduate School of Science, Yeshiva University, New York, N. Y. 10033.

(3) G. P. Johari and P. H. Tewari, *J. Phys. Chem.*, **69**, 696 (1965).

(4) P. H. Tewari and G. P. Johari, *ibid.*, **69**, 3167 (1965).

(5) G. P. Johari and P. H. Tewari, *ibid.*, **69**, 2862 (1965).

(6) R. M. Fuoss and F. Accascina, "Electrolytic Conductance," Interscience Publishers, Inc., New York, N. Y., 1959, pp 109, 136, 172, 195.

(7) C. James and P. C. Willard, *J. Amer. Chem. Soc.*, **38**, 1497 (1916).

(8) G. P. Johari and P. H. Tewari, *ibid.*, **87**, 4691 (1965).

(9) P. H. Tewari and G. P. Johari, *J. Phys. Chem.*, **69**, 2857 (1965).

(10) R. L. Kay, *J. Amer. Chem. Soc.*, **82**, 2099 (1960).

(11) H. S. Dunsmore, T. R. Kelley, and G. H. Nancollas, *Trans. Faraday Soc.*, **59**, 2606 (1963).

Table I: Molar Concentration, Equivalent Conductance Data for $\text{LaFe}(\text{CN})_6 \cdot 4\text{H}_2\text{O}$ in Solvent Mixtures at 25°

10°C	Λ	10°C	Λ	10°C	Λ
Dioxane-Formamide Mixtures					
81.4°		68.2°		55.4°	
2.686	21.628	2.308	17.817	1.686	11.680
3.673	20.523	2.651	16.990	2.460	9.466
5.315	19.198	2.998	16.713	3.930	9.163
6.885	18.189	4.860	14.867	4.840	8.749
8.715	17.398	6.337	14.051	5.970	8.283
11.207	16.465	8.082	13.331	9.746	7.416
13.503	15.907	10.629	12.537	12.901	6.946
43.2°		33.0°			
2.417	4.773	0.507	5.252		
3.487	4.355	1.353	3.501		
4.149	4.187	2.104	2.850		
5.788	3.853	2.952	1.943		
5.806	3.848	3.627	1.516		
8.631	3.529	4.504	1.113		
12.391	3.345				
Acetone-Formamide Mixtures					
97.6°		85.2°		73.5°	
1.039	34.411	0.922	38.861	0.597	44.623
2.181	32.620	2.047	36.109	1.241	41.911
3.354	31.233	3.594	33.802	1.989	39.775
4.841	30.267	4.579	32.830	2.734	38.289
7.405	29.033	5.435	32.131	3.606	37.019
8.412	28.732	7.329	30.893	5.193	34.948
10.089	28.162	9.873	29.432	5.152	34.106
62.8°		53.5°			
0.953	37.227	0.578	34.105		
1.383	34.916	1.090	29.554		
1.785	33.209	1.612	27.110		
2.458	31.211	2.197	25.009		
3.340	29.525	2.668	24.338		
4.120	28.338	3.120	24.136		
5.446	26.623	4.135	23.064		

^a Dielectric constant; see ref 8 and 9.

several 3:3 salts,⁵ which are not highly associated, fairly well. We believe that the apparent discrepancy is due to the reason that conductance data at very low concentrations where the theory is applicable may be less precise than required in the analysis according to eq 1¹³ (for example, the applicability of eq 1 for a 3:3 salt in a solvent of dielectric constant 80 at 25° is restricted to concentrations below 9×10^{-4} mol/l.). The viscosity correction term important for large ions which we have neglected may also be partially responsible.

The data were then analyzed by the limiting equation for conductance. The limiting equivalent conductance and the association constant were obtained by Shedlovsky's method.¹⁴ Instead of using the function in the usual form for the simultaneous determination of Λ^0 and K_A , which in these cases required long extrapolation, the following procedure was adapted. For a set of data, a number of Λ^0 values were chosen to make $f_{\pm}C^{1/2}$ against $(1 - \gamma/\gamma^2)^{1/2}$ plots; γ was calculated by the equation

$$\gamma = (\Lambda/\Lambda^0)S(z) \quad (2)$$

$$z = (\alpha\Lambda^0 + \beta)\Lambda^{0/2}(C\Lambda)^{1/2} \quad (3)$$

(the values of the function $S(z)$ for various values of z have been tabulated by Daggett¹⁵), and f_{\pm} from

$$-\log f_{\pm} = (0.2172ab\kappa/C^{1/2})C^{1/2}\gamma^{1/2} \quad (4)$$

The value of Λ^0 which linearized the $f_{\pm}C^{1/2}(1 - \gamma/\gamma^2)^{1/2}$ plot with zero intercept was used to calculate K_A from

$$f_{\pm}C^{1/2} = K_A^{-1/2}(1 - \gamma/\gamma^2)^{1/2} \quad (5)$$

(12) G. Atkinson and S. Petracci, *J. Amer. Chem. Soc.*, **86**, 7 (1964); G. Atkinson and H. Tsubota, *ibid.*, **87**, 164 (1965).

(13) The computer fails to resolve the terms $EC\gamma \log C\gamma$ and $JC\gamma$ for a highly associated 1:1 salt. The Λ^0 and K_A obtained by ignoring these two terms, which is usually done in such cases, are not much different from the ones obtained from the limiting law, because the $K_A C \gamma f_{\pm}^2 \Lambda$ term is overwhelmingly large. For a 3:3 salt the large size of the terms E and J (ref 5) makes their contribution comparable to that of K_A term. One would be in error if one considered the situation in a 3:3 salt the same as for a 1:1 salt. See also R. A. Matheson, *J. Phys. Chem.*, **72**, 3330 (1958).

(14) T. Shedlovsky, *J. Franklin Inst.*, **225**, 739 (1938); R. M. Fuoss and T. Shedlovsky, *J. Amer. Chem. Soc.*, **71**, 1496 (1949).

(15) H. M. Daggett, *J. Amer. Chem. Soc.*, **73**, 4977 (1951).

Table II: Derived Constants for $\text{LaFe}(\text{CN})_6 \cdot 4\text{H}_2\text{O}$ in Solvent Mixtures

% Dioxane or acetone	D^a	η (cP) ^a	Λ^0	K_A	$\Delta\eta$
Dioxane-Formamide Mixtures					
0 ^b	109.5	3.30	34.55	249	1.14
20	81.4	3.25	34.98	4,754	1.14
30	68.2	3.13	35.51	13,820	1.11
40	55.4	2.97	35.65	60,690	1.06
50	43.2	2.69	36.26	3.6×10^5	0.98
60	33.0	2.39	38	1.6×10^6	0.91
Acetone-Formamide Mixtures					
0 ^b	109.5	3.30	34.55	249	1.14
10	97.6	2.78	38.55	504	1.07
20	85.2	2.31	44.76	1,041	1.03
30	73.5	1.87	51.06	2,450	0.94
40	62.8	1.48	54.13	8,220	0.80
50	53.5	1.16	58.1	26,500	0.68

^a Taken from ref 8 and 9. ^b Taken from ref 5.

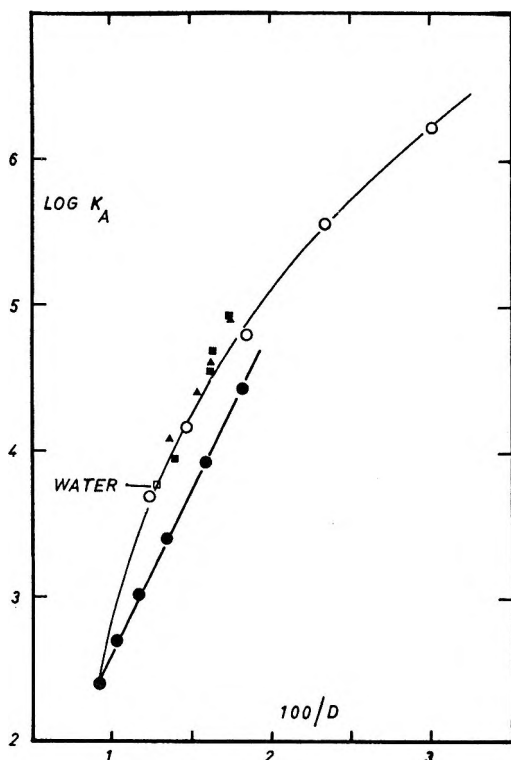


Figure 1. Dependence of the logarithm of association constant on the reciprocal dielectric constant in mixed solvents: dioxane-formamide (open circles), acetone-formamide (closed circles), dioxane-water (closed triangles), acetone-water (closed rectangles).

Table II. Logarithm of the association constant is plotted against the reciprocal dielectric constant in Figure 1. We have also included in this figure the association constant of this salt in dioxane-water and acetone-water mixtures from the literature.¹⁶

Discussion

The association constants in dioxane-water and acetone-water mixtures in Figure 1 are very close to the values in dioxane-formamide mixtures at the same dielectric constant. Strictly interpreted in terms of the Fuoss-Bjerrum equation¹⁷

$$K_A = (4\pi N a_K^3 / 3000) \exp(z_1 z_2 e^2 / a_K D k T) \quad (6)$$

it would mean that an electrostatic sphere of one size can describe the behavior of $\text{LaFe}(\text{CN})_6$ in the three solvent systems. It also indicates the absence of metal-ligand interaction in formamide solution. The $\log K_A$ vs. D^{-1} plot is concave toward the abscissa. Such nonlinearity has also been found for MgSO_4 in these mixtures.⁸ It is interesting to note that in dioxane-water mixtures also, several 1:1 salts show a concave $\log K_A$ vs. D^{-1} plot.^{18,19} The concavity may result from an increase in the size of electrostatic sphere with increasing dioxane content. Dioxane, acceptedly, is a strong hydrogen-bonding base. In mixtures with hydrogen-bonding liquids, dioxane, in addition to breaking the extensive intermolecular association, forms complexes with the liquid molecules (proton donors). This is commonly observed from the dielectric relaxation and infrared absorption studies of dioxane in mixture with proton donors.²⁰⁻²² If such complex

(16) J. C. James, *J. Chem. Soc.*, 1094 (1950).

(17) R. M. Fuoss, *J. Amer. Chem. Soc.*, **80**, 5059 (1958).

(18) J. E. Lind and R. M. Fuoss, *J. Phys. Chem.*, **65**, 999 (1961).

(19) G. Atkinson and Y. Mori, *J. Chem. Phys.*, **45**, 4716 (1966).

for each set of Λ , C data. The calculations were programmed for the IBM 360 computer. The average deviation in the K_A values obtained from the analysis was between 2 and 5 %. The values for the density, viscosity, and dielectric constant used in the calculations for these solvents were taken from ref 8 and 9.

The Λ^0 and K_A values along with the other parameters in both the solvent systems are summarized in

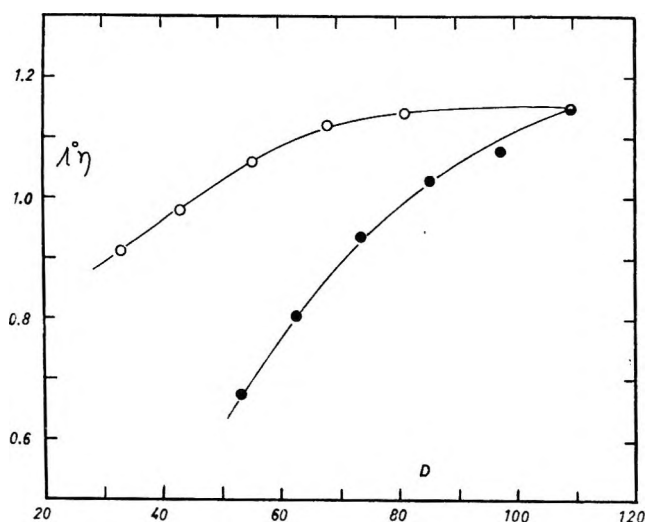


Figure 2. Dependence of the Walden product on the dielectric constant in mixed solvents. Dioxane-formamide (open circles), acetone-formamide (closed circles).

formation occurs, the solvation pattern of the ions would change with the dioxane content, because the concentration of such complexes depends upon the relative concentration of dioxane and proton donors.

The plot in acetone-formamide mixtures is linear in the limited range of dielectric constant. The value for the contact distance parameter, a_K , obtained from the slope is 10.5 Å. This is in good agreement with the values of the ion-size parameter obtained from the J term and from the limiting ionic mobilities in pure formamide.⁵ The theoretical intercept from eq 6 is 0.55 in comparison to 0.57 obtained from the plot in Figure 1. The agreement in these parameters is good enough to show that this system conforms to the Fuoss-Bjerrum behavior.

$\text{LaFe}(\text{CN})_6$ is associated to a greater extent in dioxane-formamide mixtures which are isodielectric to acetone-formamide mixtures. According to eq 6 different contact distances are required in the two solvent systems. The inclusion of the energy of ion-solvent interaction in the form $\exp(-E_s/kT)$ as introduced by Gilkerson²³ in eq 6 can also describe the behavior, but then the E_s will be found to vary with the solvent composition in dioxane-formamide systems.

The Walden product, $\Lambda^0\eta$, in Table II and Figure 2 decreases with decreasing dielectric constant in both systems. The decrease at low dielectric constant is more pronounced in the acetone-formamide system. In dioxane-water and acetone-water mixtures the $\Lambda^0\eta$ for this salt is considerably higher ($\Lambda^0\eta = 1.52$ and 1.36, respectively),¹⁶ and is independent of the dielectric constant. Fuoss²⁴ attributed the variation in $\Lambda^0\eta$ in different solvents to an additional braking on the moving ion caused by a finite time taken by the solvent dipoles to relax. The magnitude of the resulting drag on a given ion depends on the relaxation time of the

solvent dipole and the static and the optical dielectric constant of the solvent. Zwanzig²⁵ has derived an equation for the calculation of limiting ionic mobilities by taking this effect into account. Atkinson and Mori²⁶ have found that this equation, which they refer to as the FBZ equation, gives a good description of this effect in water, alcohols, and several mixed solvents. D'Aprano and Fuoss²⁷ have used this equation to elucidate the hydrodynamic behavior of TiCl_4 in dioxane-water mixtures. We believe that the application of the FBZ equation should be restricted only to those solvents in which extensive intermolecular association is absent.²⁸ However, the decrease in the Walden product for $\text{LaFe}(\text{CN})_6$ in both solvent systems is consistent with the Fuoss effect.

In solvents having extensive intermolecular association, particularly in water, aliphatic amides, and aliphatic alcohols, the electrostatic interaction between the ion and the solvent dipole produces a considerable change in the solvent structure. This is a well known fact, but unfortunately is not readily quantified because the exact changes in the liquid structure induced by the ionic field are not known. Recently, Kay and Evans²⁹ have rationalized the ionic mobility data of monovalent ions by postulating that the alkali metal ions break the structure in water (in contrast to alkyl substituted ammonium ions which "make" the structure) and consequently move in a medium less viscous than given by the bulk viscosity. Such change

(20) S. K. Garg and C. P. Smyth, *J. Chem. Phys.*, **43**, 2959 (1965), for dioxane-water complex.

(21) D. A. Ibbitson and L. F. Moore, *J. Chem. Soc., B*, 80 (1967); G. P. Johari and C. P. Smyth, *J. Amer. Chem. Soc.*, **91**, 6215 (1969), for dioxane-alcohol complex.

(22) M. D. Magee and S. Walker, *J. Chem. Phys.*, **50**, 1019 (1969), for dioxane-chloroform complex.

(23) W. R. Gilkerson, *ibid.*, **25**, 1199 (1956).

(24) R. M. Fuoss, *Proc. Natl. Acad. Sci., U. S.*, **45**, 807 (1959).

(25) R. Zwanzig, *J. Chem. Phys.*, **38**, 1603 (1963).

(26) G. Atkinson and Y. Mori, *J. Phys. Chem.*, **71**, 3523 (1967).

(27) A. D'Aprano and R. M. Fuoss, *J. Amer. Chem. Soc.*, **91**, 279 (1969).

(28) We wish to express some reservations regarding the use of the relaxation time values in the FBZ equation. In this equation, the relaxation time represents the rate of dipole reorientation as originally given by Debye (P. Debye, "Polar Molecules," Chemical Catalog Company, Inc., New York, N. Y., 1929). In hydrogen-bonded liquids, e.g., water, alcohols and amides, the main relaxation time (used in ref 26 for calculations) represents the rate of H bond breaking in the H-bonded aggregates (for water, ref 20; for alcohols, C. Brot and M. Magat, *J. Chem. Phys.*, **39**, 841 (1963). S. K. Garg and C. P. Smyth, *J. Phys. Chem.*, **69**, 1294 (1965), G. P. Johari and W. Dannhauser, *J. Chem. Phys.*, **50**, 1862 (1969); for amides, S. J. Bass, W. L. Nathan, R. M. Meighan, and R. H. Cole, *J. Phys. Chem.*, **58**, 509 (1964), W. Dannhauser and G. P. Johari, *Can. J. Chem.*, **46**, 3143 (1968)). Furthermore, the decay of macroscopic polarization in alcohols does not occur with the only one relaxation time that is representative of the life of a hydrogen bond. In many pure liquids, the relaxation characteristics are not Debye-like. The situation in mixed solvents is more complicated. Mixed solvents show two relaxation times (A. Schallamach, *Trans. Faraday Soc.*, **A42**, 180 (1946), S. K. Garg and C. P. Smyth, *J. Chem. Phys.*, **45**, 2799 (1966)) and interaction between two different solvent molecules which usually is of a donor-acceptor type (H. A. Bent, *Chem. Rev.*, **68**, 587 (1968), gives rise to more relaxation times (ref 22).

(29) R. L. Kay and D. F. Evans, *J. Phys. Chem.*, **70**, 2325 (1966).

should also be reflected in the electrostatic behavior of ions. Undoubtedly, the dielectric constant and the viscosity of a solvent in the vicinity of the ion are considerably different from the macroscopic values, and thus the ion does not move, or form ion pairs, in a medium of such properties as described by the bulk parameters; what is puzzling to us is the fact that the experimental data on conductance can still be described satisfactorily well by the equations, obtained from the most rigorous theoretical treatment on electrolytic conductance, using the macroscopic values for the solvent properties.

We conclude from this study that $\text{LaFe}(\text{CN})_6 \cdot 4\text{H}_2\text{O}$ is moderately associated in formamide. In acetone-formamide mixtures the ion association is very well described by the Fuoss-Bjerrum equation. In dioxane-formamide mixtures the dependence of ion association is strongly affected by the ion-solvent and possibly solvent-solvent interactions.

Acknowledgment. I wish to thank the Department of Engineering, Princeton University, Princeton, N. J., for providing me the computer time for these calculations.

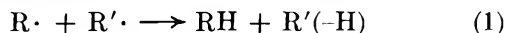
NOTES

Alkyl Radical Disproportionation

by R. L. Thommarson

*McDonnell Douglas Astronautics Company—Western Division
Santa Monica, California 90406 (Received March 25, 1969)*

Alkyl radical disproportionation reactions



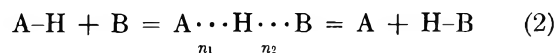
are observed when an alkyl radical larger than methyl is present in the reaction system. They are extremely efficient, proceeding with rate constants comparable to those for alkyl radical recombination. They have no apparent activation energy in contrast to the 8 ± 3 kcal/mol expected of the hydrogen abstraction reactions of alkyl radicals. Moreover, the *A* factors are about a factor of 10 higher than the "typical" *A* factors for alkyl radical hydrogen abstraction reactions. The negligible activation energy is rationalized by the high exothermicity of disproportionation and the generally observed trend of decreasing activation energy with increasing reaction exothermicity. However, the high *A* factors have led to some controversy. It has been argued that the high *A* factors and small temperature dependence of disproportionation rates suggest that the process is not closely related to ordinary radical H-abstraction reactions. Radical recombination and disproportionation were envisaged as proceeding through a common transition state involving initial formation of the excited dimer RR'^* which could decompose unimolecularly to give alkane and alkene.¹ Benson² has pointed out that such a process is incompatible with experimental results and presented arguments

favoring the "head-to-tail" model, which is similar, though necessarily looser, than the transition state assumed for normal H-abstraction reactions.

Recently, Johnston³ has offered the empirical bond energy-bond order method as a tool for calculating the activation energies and rate constants of elementary bimolecular H-transfer reactions without using adjustable parameters from kinetic data. This method has been highly successful when applied to a variety of H-transfer reactions.⁴ The purpose of this paper is to examine alkyl radical disproportionation using a rather direct modification of the bond energy-bond order method.

Computational Procedure

The generalized hydrogen abstraction reaction can be written



where n_1 and n_2 are the bond orders in the transition state of the breaking bond $\text{A}\cdots\text{H}$ and the forming bond $\text{H}\cdots\text{B}$, respectively. The total bond order is assumed to be conserved throughout the reaction so that $n_1 + n_2 = 1$. The potential energy for forming the transition state is postulated on a trial basis³ to be equal to

(1) J. A. Kerr and A. F. Trotman-Dickenson, *Progr. Reaction Kinetics*, **1**, 113 (1961); P. S. Dixon, A. P. Sefani, and M. Szwarc, *J. Amer. Chem. Soc.*, **85**, 2551 (1963).

(2) S. W. Benson, *Advan. Photochem.*, **2**, 1 (1964).

(3) H. S. Johnston, "Gas Phase Reaction Rate Theory," Ronald Press Company, New York, N. Y., 1966.

(4) (a) H. S. Johnston, *Advan. Chem. Phys.*, **3**, 131 (1961); (b) H. S. Johnston and C. Parr, *J. Amer. Chem. Soc.*, **85**, 2544 (1963); (c) S. W. Mayer, L. Schieler, and H. S. Johnston, *J. Chem. Phys.*, **45**, 385 (1966); (d) S. W. Mayer and L. Schieler, *J. Phys. Chem.*, **72**, 2628 (1968).

the energy required to break the bond A-H to A...H of bond order n_1 , less the energy supplied by forming H...B to order n_2 , plus a repulsion energy V_r arising from the parallel spins on A and B. Considering alkyl radical disproportionation specifically, the bond order increases by one in the overall reaction owing to π -bond formation in the product molecule A, and it is this factor that renders disproportionation reactions highly exothermic. This can be accounted for by assuming that when bond A-H is broken to A...H of bond order n_1 incipient π -bond formation of order n_2 occurs. Then the potential energy of formation of the transition state can be expressed as

$$V = D_{A-H} - D_{A-H}n_1^p - D_{B-H}n_2^q - D_{\pi}n_2^q + V_r \quad (3)$$

where D is the bond dissociation energy, and p and q are the slopes of the log (dissociation energy) vs. log (bond order) lines for C-H and C-C bonds, respectively. The bond indices have the values $p = 1.082$ and $q = 1.191$. Since incipient π -bond formation is being explicitly accounted for, D_{A-H} is taken to be the same as the corresponding C-H bond dissociation energy in the AH_2 molecule.

The triplet repulsion is assumed to be given by an anti-Morse function,^{4b} and is expressed in terms of bond orders as

$$V_r = D_{A-B}[(1/2)e^{-\beta\Delta R}(n_1n_2)^{0.26\beta}] \times [1 + (1/2)e^{-\beta\Delta R}(n_1n_2)^{0.26\beta}] \quad (4)$$

where β is the A-B bond Morse constant and $\Delta R(\text{\AA})$ is the sum of the A-H and B-H bond equilibrium internuclear distances less the A-B bond equilibrium internuclear distance. To a first approximation the effect of incipient π -bond formation on the triplet repulsion energy manifests itself as $D_{A-B} = D_{A-BH}n_1^q$. This correction is negligible for the bond orders of the transition state, *vide infra*, and the expediency of neglecting it was adopted for the kinetic calculations.

The calculated rate constants refer to the linear triatomic model. Some justification for using this model comes from (1) the observations² that for most atom-molecule reactions the A factors fall in the range $10^{10.5 \pm 0.5}$ l./mol sec; (2) for radical-molecule reactions the A factors may be represented by $10^{9.5 \pm 0.5}$ l./mol sec; and (3) for radical-radical disproportionation the rate constants (presumably equal to the A factors) are clustered about $10^{9.5}$ l./mol sec. This relative constancy of the preexponential factor for a given class of reactions has been attributed to the probability that most of the force constants for polyatomic A and B are not extensively altered in the transition state.³ Also, the estimation of bending force constants in the transition state is not dependable when A and B are not monatomic. Although this modification cannot be completely correct, it is believed that in many reactions the net correction arising from changes in bending force

constants of A and B in the transition state is small.^{4b} This should be particularly true of disproportionation reactions since the steric factors are *ca.* 0.1.

The equations for the force constants of the triatomic complex have been given by Johnston (ref 3, pp 339-344). The only change required by the modifications introduced here is in the force constant along the reaction path, F_p , which is the second derivative evaluated at the point of maximum V^* , where dV/dn_1 is zero

$$-F_p = \left(\frac{d^2V}{dn^2}\right)\left(\frac{dn}{dp}\right)^2 \simeq \frac{10.27}{\frac{1}{n_1^2} + \frac{1}{n_2^2}} \left[\frac{D_{A-H}p(p-1)}{n_1^{2-p}} + \frac{D_{B-H}p(p-1)}{n_2^{2-p}} + \frac{D_{\pi}q(q-1)}{n_2^{2-q}} + \frac{D_{A-B}2B\gamma}{(n_1n_2)^{1-\gamma}} \left(\frac{1}{2} + \frac{(1-\gamma)(1-2n_1)^2}{2n_1n_2} \right) \right] \quad (5)$$

where $\gamma = 0.26\beta$ and $\beta = 1/2 \exp(-\beta\Delta R)$. F_p is in dyn/cm and the dissociation energies are in cal/mol.

In terms of local bond properties, the rate constant expression takes the form (ref 3, p 224)

$$k = B_e B_\sigma B_\gamma \left[\left(\frac{R_{\neq}}{R}\right)_{A-H}^2 \left(\frac{F}{F_{\neq}}\right)_{A-H}^{1/2} \right] \times \left(\frac{\omega^*}{1000W}\right) (R_{B-H}^2 l_{B-H})_{\neq} l_{\phi}^2 \times 1.81 \times 10^{10} \exp(-V^*/RT) \text{ l./mol sec} \quad (6)$$

where R represents internuclear distances in \AA , F represents the stretching force constants in dyn/cm, l_i represents classical vibrational amplitudes ($l_i = (2\pi kT/F_i)^{1/2}$) in units of cm for the B-H stretch and radians for the A-H-B bend (denoted by l_{ϕ}); ω^* is the imaginary frequency (cm^{-1}) associated with the reaction coordinate, and $V^* = (1 - F_{12}^2/F_{11}F_{22})^{1/2}$. B_γ is the ratio of quantum corrections $((1/2u)/\sinh(u/2))$; $u = h\nu/kT$ for the real vibrations in the transition state to those for the reactants, the tunnelling correction being omitted. B_e represents the ratio of the electronic partition function of the transition state to the product of the electronic partition functions of the reactants. The value of B_e is taken to be $1/4$; the

Table I: Bond Properties^a

Bond	D_e , kcal/mol	Vibrational wave number, cm^{-1}	Bond length, \AA
CH ₃ -H	106.0	3100	1.09
Primary (C-H)	102.0	3100	1.09
Secondary (C-H)	99.0	3100	1.09
Tertiary (C-H)	95.0	3100	1.09
C-C	83.0	1000	1.54

^a S. W. Benson, "Thermochemical Kinetics," John Wiley & Sons, New York, N. Y., 1963, pp 205-215.

Table II: Disproportionation Rate Constants,^a $k_{R,R'} \times 10^{-9}$ l./mol sec

R·	R'·	C ₂ H ₆	n-C ₃ H ₇	i-C ₃ H ₇	n-C ₄ H ₉	sec-C ₄ H ₉	t-C ₄ H ₉
CH ₃		1.2 (1.9)	0.8 (1.5)	2.3	0.7	1.9	3.3
C ₂ H ₅		2.2 (3.5)	0.6	1.9	0.6	1.5	2.7
n-C ₃ H ₇		0.9	1.1	1.8	0.5	1.3	2.4
i-C ₃ H ₇		0.9	0.6	3.4 (5.2)	0.5	1.3	2.4
n-C ₄ H ₉		0.9	0.5	1.5	0.9	1.0	2.1
sec-C ₄ H ₉		0.9	0.5	1.5	0.7	2.4	2.1
t-C ₄ H ₉		0.9	0.5	1.5	0.5	1.2	4.3 (10.0)

^a Experimental values in parentheses.

electronic multiplicity of alkyl radicals is 2 and it is only the singlet transition state that leads directly to ground state products. B_σ represents the reaction path degeneracy and is equal to the number of C-H bonds adjacent to the radical head of the disproportionating radical. It is only at these sites that incipient π -bond formation can occur, thereby lowering the activation energy below the 8 ± 3 kcal/mol normally expected of alkyl radical H-abstraction reactions.

The molecular parameters used in these calculations are given in Table I. Morse parameters are obtained from the relationship^{4b}

$$\beta = (1.2177 \times 10^7) \omega_e (\mu/D_e)^{1/2} \text{ cm}^{-1} \quad (7)$$

where ω_e is the vibrational wave number in cm^{-1} , D_e is the dissociation energy in kcal/mol, and μ is the reduced mass in atomic weight units. Vibrational force constants are given by^{4c}

$$F = 1389 \beta^2 D_e \text{ dyn/cm} \quad (8)$$

with β in units of 10^8 cm^{-1} and D_e in kcal/mol.

A value of 77.5 kcal/mol is used for D_π . The π -bond accounts for 59.5 kcal/mol and the additional 18.0 kcal/mol arises from the increased strength of C-C single bonds involving sp^2 rather than sp^3 hybridization.⁵

Results and Discussion

The potential energy of the interacting radical pairs was calculated in 0.01 decrements in η_1 from 1.00 to 0.90. In all cases potential energies of activation *ca.* 1.5 kcal/mol were observed at $\eta_1 = 0.05$. The potential energy of activation differs from the observed activation energy not only by the difference in zero-point energy between reactants and complex, but also in thermal excitation of the reactants and complex. In general, potential energies of activation are slightly higher than experimental activation energies. Hence, values of $V^* = 1.5$ kcal/mol are consistent with the experimental observations that disproportionation reactions proceed with negligible activation energy.

Before proceeding to the rate constant calculations, the magnitude of the classical vibrational amplitude associated with the doubly degenerate A-H-B bend

must be ascertained to be physically realistic. When rate constant formulas are expressed using the usual partition function expressions^{4c} the ratio $l_\phi^2/4\pi$ can be identified as the solid-angle ratio for reaction, so $l_\phi^2/4\pi$ must be less than 1 to be physically realistic. Small vibration theory, on which activated complex theory is based, dictates that $l_\phi^2/4\pi$ should be much less than unity. For disproportionation $l_\phi = 1.17$ radians. While bends of this magnitude cannot be considered infinitesimal, $l_\phi^2/4\pi$ is substantially less than 1.

Table II lists the rate constants calculated for hydrogen transfer from R' to R at 400°K. This temperature was chosen in order to facilitate comparison with experimental data. The values in parentheses were obtained from the experimental $k_{\text{disp}}/k_{\text{comb}}$ ratios⁶ and the measured values (ref 5, p 104) of k_{comb} . Further comparison with experimental data can be made for cross-disproportionation/cross-combination ratios by examining $k_{R,R'}$ (H-transfer from R' to R) / $k_{R',R}$ (H-transfer from R to R'), thereby cancelling the unknown rate constant for cross-combination. Such a comparison between the calculated and experimental⁶ ratios is shown in Table III. Where experimental data

Table III: $k_{R,R'}/k_{R',R}$

R·	R'·	Calcd	Obsd
C ₂ H ₅ ·	n-C ₃ H ₇ ·	0.7	1.4
C ₂ H ₅ ·	i-C ₃ H ₇ ·	2.0	2.3
C ₂ H ₅ ·	t-C ₄ H ₉ ·	3.0	1.5
i-C ₃ H ₇ ·	t-C ₄ H ₉ ·	1.5	1.0

are available agreement within a factor of 2 is generally observed. Such agreement is within experimental error. This is particularly true of the data in Table III since experimental errors and uncertainties associated with self-disproportionation/self-combination ratios collect in the cross-disproportionation/cross-combination ratios. In view of the approximate nature of these calculations,

(5) S. W. Benson, "Thermochemical Kinetics," John Wiley & Sons, New York, N. Y., 1968, p 50.

(6) S. W. Benson and W. B. DeMore, *Ann. Rev. Phys. Chem.*, **16**, 397 (1965).

it is probably more significant that rate constants of the right order of magnitude are predicted than that agreement with existing experimental data is achieved.

The transition state structure depicted by BEBO calculations should not be interpreted too literally,³ and the results presented here do not constitute unequivocal proof that disproportionation reactions proceed *via* a "head-to-tail" transition state. However, the general picture of a loose transition state in which the disproportionating radical has developed very little π -bond character is strikingly similar to the main aspects of the model proposed by Benson.²

Acknowledgment. This work was sponsored by the MDAC Independent Research and Development Program.

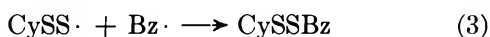
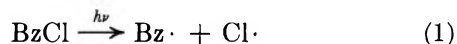
The Photolysis of Aqueous Solutions of Cystine in the Presence of Benzyl Chloride

by C. J. Dixon and D. W. Grant

Department of Pure and Applied Chemistry, Huddersfield College of Technology, Huddersfield, England (Received June 23, 1969)

Although many products from the photolysis of aqueous solutions of cystine ($\text{HOOCCH}(\text{NH}_2)\text{CH}_2\text{S}\cdot$)₂ by 254-nm radiation have been identified,¹ evidence for the nature of the intermediates involved is sparse. Electron spin resonance signals from the irradiated solid amino acid have been attributed by Bogle, *et al.*,² to the presence of $\text{HOOCCH}(\text{NH}_2)\text{CH}_2\text{S}\cdot$ ($\text{CyS}\cdot$) radicals. These authors, however, admit that the signals do not exclude the presence of $\text{CySS}\cdot$ radicals.

The present communication describes work carried out to obtain evidence for the presence of $\text{CyS}\cdot$, $\text{CySS}\cdot$, and $\text{Cy}\cdot$ radicals in aqueous solutions of cystine irradiated with 254-nm radiation. If these radicals are actually produced, then CyS -benzyl, CySS -benzyl, and Cy -benzyl might be found among the products of the photolysis of cystine in the presence of benzyl chloride (BzCl), *viz.*



Evidence for reaction 1 has been obtained by Porter and Strachan,³ who detected the characteristic benzyl radical absorption at 319 nm when benzyl chloride was irradiated with 254-nm radiation in glassy solvents at -197° .

Experimental Section

Water used was twice distilled, the second distillation being from alkaline permanganate. L-Cystine (CySSCy), L-cysteine (CySH), and DL-lanthionine (CySCy) were supplied by KCC-Light Laboratories, Bucks, England. DL- α -Alanine (CyH) and bibenzyl were supplied by British Drug Houses Ltd., Poole, England. 1-Amino-2-chloropropionic acid (CyCl),⁴ 1,1'-diaminoadipic acid (CyCy),⁵ 1-amino-2-benzylpropionic acid (CyBz),⁶ S-benzyl thio-cysteine (CySSBz),⁷ S-benzyl cysteine (CySBz),⁸ 1-amino-1'-oxo-2,2'-dithiodipropionic acid (AODT-DFA),⁹ and dialanine trisulfide (CySSSCy)¹⁰ were prepared as described in the literature.

Benzyl chloride was prepared by the chlorination of toluene, followed by fractional distillation. Gas-liquid phase chromatography revealed only one peak.

All solutions prior to irradiation were thoroughly degassed on a vacuum line which incorporated an oil diffusion pump. Irradiation of stirred solutions (50 ml) was carried out at ambient temperature in 100-ml silica flasks using a 120-W low-pressure mercury vapor lamp (Model T/M5/369E; Thermal Syndicate Ltd., Wallsend, England) operated from a stabilized power supply. Wavelengths below 254 nm were filtered out using an aqueous solution of 0.1 M acetic acid. Cystine solutions (1 mM) in 0.1 M HCl, and cystine (1 mM)-benzyl chloride (3.5 mM) solutions in 0.1 M HCl were irradiated for respective times of 60 and 187 min to ensure the same photon absorption initially by cystine in each solution.

The presence of S-benzyl cysteine and S-benzyl thio-cysteine in irradiated cystine-benzyl chloride solutions was detected in the following way. Two 10-ml aliquots were concentrated to a few drops, applied to Whatman 3MM paper, and subjected to descending chromatography ($\text{EtOH-H}_2\text{O-H}_2\text{SO}_4$, 80:20:0.5 by vol). After drying, one-half of the paper containing the products from one aliquot was developed with 0.2% ninhydrin in ethanol-acetic acid-collidine (25:5:1 by vol) to reveal a spot at R_{ala} (R_{F} value relative to alanine) of 1.25. A band at R_{ala} 1.2-1.3 was cut from the undeveloped piece of paper and eluted with glacial acetic acid. High voltage electrophoresis (20 kV, pH 1.85) of the

(1) W. F. Forbes and W. E. Savage, *Photochem. Photobiol.*, **1**, 1 (1962).

(2) G. S. Bogle, V. R. Burgess, W. F. Forbes, and W. E. Savage, *ibid.*, **1**, 277 (1962).

(3) G. Porter and E. Strachan *Trans. Faraday Soc.*, **54**, 1595 (1958).

(4) E. Fischer and K. Raske, *Eur. J. Biochem.*, **40**, 3717 (1970).

(5) A. Bertho and J. Maier, *Ann.*, **498**, 50 (1932).

(6) P. E. Gagnon and B. Nelin, *Can. J. Res.*, **27B**, 742 (1949).

(7) G. W. Stapleton and J. M. Swan, *Aust. J. Chem.*, **15**, 570 (1962).

(8) H. Suter, *Hoppe-Seyler's Z. Physiol. Chem.*, **20**, 562 (1895).

(9) C. J. Dixon and D. W. Grant, *Biochem. J.*, **105**, 8c (1967).

(10) W. E. Savage, J. Eager, I. A. Maclaren, and C. M. Roxburgh, *Tetrahedron Lett.*, 3289 (1964).

eluate yielded two ninhydrin-positive spots with mobilities relative to alanine of 0.42 and 0.44, colored brown and green, respectively. The brown and green spots were shown to be S-benzyl thiocysteine and S-benzyl cysteine, respectively, by subjecting authentic mixtures of these compounds to the above procedure.

For quantitative analysis 4-ml aliquots were evaporated to dryness, dissolved in a few drops of methanol, and applied to Whatman 3MM paper for electrophoresis (1 hr at 20 kV, pH 1.85). The paper containing the separated products was then dried at 70° for 20 min. The section of paper containing all products except alanine was sewn to another sheet of Whatman 3MM paper (46 × 57 cm) and descending chromatography (EtOH-H₂O-HCl, 80:20:0.5 by vol) was carried out in a direction at right angles to that of the electrophoresis. The products were located by the ninhydrin-cadmium acetate technique¹¹ modified by the replacement of acetone with a similar volume of ethanol-acetic acid-collidine (25:5:1 by vol). Developed spots were eluted with 10 ml of methanol and extinctions at 506 nm measured in a Unicam SP600 spectrophotometer. Since alanine is well separated from the other products by electrophoresis alone, it was determined in eluates from paper strips after spot development with the unmodified ninhydrin-cadmium acetate technique.¹¹ Amino acid concentrations in all eluates were obtained using standard extinction curves of authentic samples similarly treated.

Ammonia yields in irradiated solutions were determined by the Conway microdiffusion technique.¹²

Bibenzyl, benzyl alcohol, and benzyl chloride were determined by extraction of the appropriate solutions with 25 ml of benzene, and subsequent analysis of 1- μ l aliquots of the extracts with gas-liquid phase chromatography on a Silicone SE column operated at 175° for bibenzyl, and at 100° for benzyl chloride and benzyl alcohol.

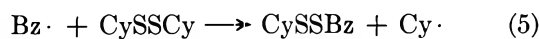
The intensity of absorbed light, determined using the ferrioxalate actinometer,¹³ was $2.0 \pm 0.15 \times 10^{16}$ photons sec⁻¹.

Results and Discussion

Thermal hydrolysis of benzyl chloride (3.5×10^{-3} M) in 0.1 M HCl was shown to be unimportant at ambient temperature by the fact that even after 48 hr only 0.2 mol % of the chloride was converted into benzyl alcohol. Irradiation of benzyl chloride (3.5×10^{-3} M) in the presence or absence of cystine (10^{-3} M) increased the rate of hydrolysis, but the concentrations of alcohol produced ($\approx 10^{-5}$ M) were not photochemically significant. It has been assumed, therefore, that hydroxyl radicals from the photolysis of benzyl alcohol³ can be ignored in the subsequent discussion.

The most significant result (Table I) is the detection of CySBz and CySSBz in irradiated cystine-benzyl chloride solutions. Although the formation of biben-

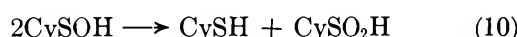
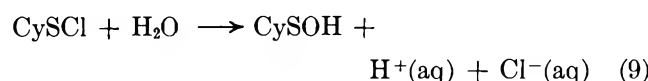
zyl is good evidence for the presence of benzyl radicals in the irradiated solutions, it might be argued that these radicals do not produce the benzyl derivatives *via* reactions 2 and 3 but rather *via* reactions with cystine itself, *e.g.*



Reactions 5 and 6 can be ruled out on the basis of their high endothermicities (≈ 92 kJ mol⁻¹). Thermal reaction between benzyl chloride and the photolysis product cysteine (CySH) to produce CySBz was shown to be unimportant at ordinary temperatures. Therefore, the production of the benzyl derivatives can be attributed with some confidence to reactions 3 and 2. However, it might also be argued that the radicals CyS· and CySS· are produced not by direct photolysis of cystine itself, but rather through reactions of chlorine atoms with cystine, *viz.*



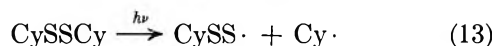
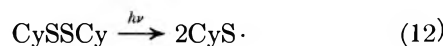
Reactions 7 and 8 cannot be eliminated from bond energy considerations, but seem unlikely because CyCl and CySO₂H were not detected in electropherograms of the irradiated solutions. If reaction 8 occurs, then the sulphenyl chloride would be expected to undergo hydrolysis to the sulfenic acid which would disproportionate to the sulfinic acid, *viz.*



The failure to detect lantionine (CySCy) in irradiated cystine solutions indicates that CySS· radicals are not produced to any significant extent in the reaction



The evidence would thus appear to favor production of CyS· and CySS· radicals in the photolytic steps



According to reaction 13 Cy· and CySS· radicals are produced in equal numbers, yet neither CyBz nor Cy-Cy was detected. This is readily explained by assuming that Cy· radicals readily abstract hydrogen atoms from cystine and/or benzyl chloride to form alanine (CyH). If all Cy· radicals are produced by reaction

(11) J. Heilmann, J. Barrolier, and E. Watzke, *Hoppe-Seylers Z. Physiol. Chem.*, **309**, 219 (1958).

(12) E. J. Conway and A. Byrne, *Biochem. J.*, **27**, 419 (1944).

(13) C. G. Hatchard and C. A. Parker, *Proc. Roy. Soc.*, **A235**, 518 (1956).

Table I: Quantum Yields of Products from 50-ml Irradiated Cystine and Cystine-Benzyl Chloride Solutions (Light Intensity $2.0 \pm 0.15 \times 10^{16}$ quanta sec^{-1})

Product ^a	CySSCy: 1.0×10^{-3} M		CySSCy: 1.0×10^{-3} M BzCl: 3.5×10^{-3} M	
	Yield, mol $\times 10^7$	Quantum yield	Yield, mol $\times 10^7$	Quantum yield
NH ₃	44	3.7×10^{-2}	65	5×10^{-2b}
AODT-DPA	6	5×10^{-3}	5	4×10^{-3b}
CyH	0.8	7×10^{-4}	0.9	8×10^{-4b}
CySSSCy	0.9	8×10^{-4}	1	8×10^{-4b}
(Bz-) ₂			43	2×10^{-2c}
CySBz			1	8×10^{-4b}
CySSBz			1	8×10^{-4b}
CyBz			$>0.1^d$	$>10^{-4b}$
H ₂	>0.06	$>4 \times 10^{-5}$		
CySCy	$>0.1^d$	$>10^{-4}$		
CyCl	$>0.1^d$	$>10^{-4}$		
(Cy-) ₂	$>0.1^d$	$>10^{-4}$		
BzH			^d	
-BzCl			650	

^a Cy- = HOOCCH(NH₂)CH₂-; Bz- = C₆H₅CH₂-. ^b Based on quanta absorbed by CySSCy. ^c Based on quanta absorbed by BzCl. ^d Not detected.

13 and react in this way, then the alanine yield is a measure of the net amount of C-S fission produced on photolysis. The formation of CySSBz and CySBz merely reflects the relatively low reactivities of CySS· and CyS· radicals compared with Cy· radicals. The unreactive character of CySS· is due to the low bond energy S₂-H, approximately 84 kJ mol⁻¹ less than that of S-H.¹⁴ In the presence of oxygen, alanine is no longer a photolytic product and is replaced by a substance whose chromatographic and electrophoretic behavior suggest that it is serine (CyOH).¹⁵ This oxygen effect is consistent with a radical mechanism for alanine production.

Since CySS· radicals do not abstract hydrogen atoms they most probably react to form the trisulfide, *viz.*



The similarity of the quantum yields of CySSSCy and alanine in the absence of benzyl chloride indicates that most CySS· radicals probably react according to reaction 14. In the presence of benzyl chloride there must be reaction(s) in addition to (13) leading to the production of CySS· radicals, since the quantum yield of alanine is significantly less than that of the sum of the quantum yields of trisulfide and CySSBz.

The total amount of noncondensable gas from 50 ml of 10^{-3} M cystine irradiated in deoxygenated solution for 85 min did not exceed 6×10^{-9} mol. If all this gas were hydrogen, then its quantum yield would not exceed 4×10^{-5} , which suggests at first sight that AODT-DPA is not produced *via* photolytic rupture of a C-H bond. However, low hydrogen yields do not necessarily mean small numbers of hydrogen atoms in the system, since abstraction reactions might be much less important than the displacement reaction



A strict comparison between the quantum yields in the presence and absence of benzyl chloride is not possible since the relatively high conversions of substrates make the absolute values of quantum yields accurate to no better than $\pm 20\%$. However, it is noteworthy that benzyl chloride would be expected to promote enhanced deamination of cystine (*cf.* Table I) since chlorine atoms generated radiolytically have been shown to deaminate cystine readily.¹⁶ If twice the bibenzyl yield is regarded as a measure of the minimum number of chlorine atoms which escape cage-recombination, the ammonia yield would increase by about 8.6×10^{-6} mol in the presence of benzyl chloride assuming all chlorine atoms attack cystine. Since the observed increase is only 2×10^{-6} mol (Table I), it would appear that only a relatively small fraction of the chlorine atoms actually attack cystine under the experimental conditions obtaining. Since AODT-DPA has been shown to be only a minor product in the radiolysis of oxygenated cystine solutions in 0.1 M HCl,¹⁷ it would appear that chlorine atoms preferentially attack the β -carbon atoms of cystine when the amino acid is in the protonated form.

It is of interest to note that the quantum yields for ammonia and alanine in cystine (Table I) compare fairly well with those of 0.04 and 0.001, respectively, reported recently by Risi, *et al.*,¹⁸ for nitrogen-saturated solutions of cystine at pH 1-2.

(14) N. J. Friswell and B. G. Gowenlock, "Advances in Free Radical Chemistry," Vol. 2, Logos Press, London, 1967, p 26.

(15) C. J. Dixon and D. W. Grant, unpublished work.

(16) W. A. Armstrong and D. W. Grant, *Can. J. Chem.*, **41**, 1882 (1963).

(17) D. W. Grant and D. J. Powles, unpublished work.

In conclusion it ought to be mentioned that Box, *et al.*,¹⁹ have obtained evidence for the presence of radical-ions in single crystals of cysteine hydrochloride irradiated with ultraviolet light at 77°K. Although the possibility of radical-ion production in irradiated cysteine itself cannot be ruled out, it would appear unlikely that CySBz and CySSBz are produced *via* radical-ion reactions in 0.1 M HCl, where rapid neutralization with hydrogen or chloride ions would occur.

Acknowledgments. The financial support of the Wool Textile Research Council and the Huddersfield Corporation is gratefully acknowledged.

(18) S. Risi, K. Dose, T. K. Rathinasamy, and L. Augenstein, *Photochem. Photobiol.*, **6**, 423 (1967).

(19) H. C. Box, H. G. Freund, and E. E. Budzinski, *J. Chem. Phys.*, **45**, 809 (1966); the authors are grateful to one of the reviewers for drawing their attention to this paper.

The Osmotic Pressure of Polyelectrolyte in Neutral Salt Solutions

by Akira Takahashi, Narundo Kato, and Mitsuru Nagasawa

Department of Applied and Synthetic Chemistry, Nagoya University, Chikusa-Ku, Nagoya, Japan (Received June 30, 1969)

Most theories^{1,2} on the second virial coefficient (A_2) of spherical colloidal electrolytes so far published predict that the second virial coefficient is proportional to $1/C_s^0$, where C_s^0 is the concentration of added salt in mol/l. in the solvent with which the sample solution is in equilibrium. Moreover, the second virial coefficient is believed to be independent of molecular weight. These predictions arise from the fact that electroneutrality must be fulfilled in both the sample solution and the solvent, and, hence, the second virial coefficient is determined primarily by the Donnan distribution of diffusible ions between them. In practice, there were several experimental studies³⁻⁵ which supported the speculation. Our recent light scattering experiment using a linear polyelectrolyte,⁶ however, showed that the invariance of A_2 with molecular weight and the linearity between A_2 and $1/C_s^0$ holds only at low ionic strengths, whereas at high ionic strengths A_2 depends on molecular weight and is linear with respect to $1/\sqrt{C_s^0}$.

The second virial coefficient of linear polyelectrolytes in the salt-added system is determined not only by the electrostatic interaction between ions, but also by the intermolecular interaction of polyion coils.⁶⁻⁸ We concluded⁶ that the deviation from the linear plot of A_2 vs. $1/C_s^0$ as well as the molecular weight dependence of A_2 observed at high ionic strengths arises from the

intermolecular interaction between coils. If the concentration of added salt is low, the expansion of the polyion coil is so high that the effect of intermolecular interaction on A_2 becomes practically independent of both molecular weight and added-salt concentration. Consequently, A_2 appears to be linear with respect to the reciprocal salt concentration and independent of molecular weight.

An ambiguity concerning the above conclusion still exists since in osmotic pressure measurements reported in the literature,⁹ A_2 was always proportional to $1/C_s^0$ though not many measurements at high salt concentrations were made. We speculated⁶ that the polymer concentration used in the osmometry may be too high to obtain A_2 .

The purpose of this work is to carry out careful measurements of osmotic pressure both in salt-free and salt-added systems of the same sample as used for light scattering and to compare the second virial coefficients determined by both methods.

Experimental Section

Polymer Sample. The F-8 fraction of sodium poly(styrenesulfonate) [Na-PS] (mol wt = 4.3×10^5) used in a previous investigation⁶ was selected in this study. A measured amount of the sample was dissolved into NaCl aqueous solutions of specified concentrations in volumetric flasks.

Osmometer. The most important criterion in the osmometry of polyelectrolyte solutions in salt-added systems is to confirm the complete Donnan equilibrium between the sample solution and solvent separated by a membrane. To this end, a Zimm-Myerson osmometer¹⁰ was modified by incorporating two magnetic stirrers inside the cell. They were swung as pendulums with a magnet operated from outside of the cell. To avoid the contamination of the solution with ions, the whole cell was made of poly(methyl methacrylate) resin, 6-10 Nylon, and glass. A stainless steel rod in the original design was replaced by a long-stem glass syringe, and the glass capillaries were fastened to the cell with synthetic rubber stoppers.

(1) F. G. Donnan and E. A. Guggenheim, *Z. Phys. Chem.*, **162**, 364 (1934).

(2) T. L. Hill, *Discussions Faraday Soc.*, **21**, 31 (1956); *J. Phys. Chem.*, **61**, 548 (1957).

(3) M. Nagasawa, A. Takahashi, M. Izumi, and I. Kagawa, *J. Polym. Sci.*, **38**, 213 (1959).

(4) Z. Alexandrowicz, *J. Polymer Sci.*, **43**, 337 (1960); **56**, 115 (1962).

(5) H. Inagaki and H. Hiram, *Z. Electrochem.*, **63**, 419 (1959).

(6) A. Takahashi, T. Kato, and M. Nagasawa, *J. Phys. Chem.*, **71**, 2001 (1967).

(7) T. A. Orofino and P. J. Flory, *ibid.*, **63**, 283 (1959).

(8) H. Eisenberg, *J. Chem. Phys.*, **44**, 137 (1966).

(9) D. T. F. Pals and J. J. Hermans, *Rec. Trav. Chim.*, **71**, 458 (1952).

(10) B. H. Zimm and I. Myerson, *J. Amer. Chem. Soc.*, **68**, 911 (1946).

Table I: Number-Average Molecular Weight, Second and Third Virial Coefficients of Na-PS-Aqueous NaCl Solution Determined from Osmotic Pressure Measurements

C_s^0 mol/l.	$(\frac{\pi}{C})_0$	$M_n \times 10^{-5}$	Δ_2	Δ_3	Δ_3/Δ_2^2	$A_2 \times 10^4$ $\frac{\text{cc. mol}}{\text{g}^2}$ (OS)	$A_2 \times 10^4$ $\frac{\text{cc. mol}}{\text{g}^2}$ (LS)	$A_3 \times 10^2$	$A_2 \times 10^4$ $\frac{\text{cc. mol}}{\text{g}^2}$ (LS)
0.500	0.792	3.194	0.513	0.118	0.448	1.60 ^a	1.45 ^b	0.369	2.47
0.100	0.776	3.259	1.428	1.258	0.616	4.38 ^a	4.36 ^a	3.86	4.34
0.050	0.792	3.194	2.20	2.50	0.516	6.88 ^a	6.47 ^b	7.82	5.52
0.020	0.792	3.194	3.95	9.40	0.602	12.36 ^a	12.38 ^b	29.43	13.0
0.010	0.792	3.194	6.65	26.60	0.601	20.82 ^a	20.59 ^b	83.28	18.6
0.005	0.792	3.194	11.35	78.88	0.612	35.53 ^a	25.45 ^b	246.96	37.4
	(Average)	3.204							

^a Evaluated by the procedure of Stockmayer and Casassa. ^b Evaluated assuming $g = 5/8$.

Measurements of Osmotic Pressure. When the polymer concentration was low, the static equilibrium method was employed. When the pressure was higher than 20 cm H₂O in salt-free systems, a dynamic method with a mercury manometer system was employed. Both the osmometer and the manometer were immersed in a thermostat regulated at $25 \pm 0.001^\circ$. Membranes used were gel Cellophane No. 600 and conditioned by the standard method.¹¹ The membrane dissymmetry pressures observed were smaller than 0.01 ± 0.005 cm H₂O and this correction was applied to all measured osmotic pressures. After the cell was filled with solution and temperature equilibrium was reached, the pressure change was recorded. Usually, the initial steep rising of pressure was observed, then it fell with time elapsed, and a steady state was reached. At this stage an inhomogeneity in the concentrations of both polymer and NaCl inside the cell was diminished by swinging the magnetic stirrers. Then, the second run followed, and the equilibrium pressure was determined. The inside solution was stirred again and the outside solvent was refreshed. Then run III was repeated. The osmotic pressures thus determined in both runs II and III agreed with each other within the experimental error. This procedure was employed in all measurements to obtain really reliable osmotic pressures.

Results

The relationship between π/C and C obtained for the sample in NaCl solutions of various concentrations is shown in Figure 1. The plots are not straight lines but curve upward. In order to determine the second virial coefficient (A_2), we assumed that the quadratic function, eq 1, is adequate to express π/C of polyelectrolytes in salt solution

$$(\pi/C) = (\pi/C)_0 [1 + \Delta_2 C + \Delta_3 C^2] \quad (1)$$

where $(\pi/C)_0 = RT/M_n$, $\Delta_2 = A_2 M_n$ and $\Delta_3 = g \Delta_2^2$.

First, the limiting value of π/C was determined by extrapolation to infinite dilution from measurements in 0.500 M solution, in which Δ_2 is low. Then, adopting the procedure of Stockmayer and Casassa,¹² the

second and third virial coefficients were evaluated from a plot of the quantity

$$[(\pi/C)/(\pi/C)_0 - 1]/C$$

against C . Very good straight lines were obtained at each ionic strength, and Δ_2 and Δ_3 were determined from intercept and from slope of the lines, respectively. The results are summarized in Table I. The values of $g = \Delta_3/\Delta_2^2$ are also shown in Table I, column 6. It is observed that g is always smaller than $g = 5/8$, and gradually decreases with the increase of C_s^0 . However, g thus determined is not much smaller than $5/8$ at lower ionic strengths since the polyion is expanded markedly. Even if we assume $g = 5/8$ and adopt Flory's procedure¹³ to determine $(\pi/C)_0$ and Δ_2 , that is, even if we determine $(\pi/C)_0$ and Δ_2 by comparing the calculated plot of the form $\log [1 + \Delta_2 C + 5/8 \Delta_2^2 C^2]$ against $\log \Delta_2 C$ with the experimental results, no appreciable difference is caused in the values of A_2 as indicated in Table I, column 8.

The values of A_2 (LS) reported previously were determined from the initial slope of Kc/R_θ vs. C plots. In order for comparisons with A_2 (OS), the light scattering data reported were treated in the same way and the results are shown in Table I, column 10. A_2 (LS) at $C_s^0 = 0.005$ previously reported was found to be a little overestimated, but no change need be given to the discussion in the previous paper. The values of A_2 (LS) at some ionic strengths are not available but can be estimated from the data for other samples of different molecular weight, since A_2 for polyelectrolytes does not depend on molecular weight except at very high ionic strengths. Remarkable agreement between A_2 (LS) (column 10) and A_2 (OS) (column 7) is manifest.

(11) R. U. Bonnar, M. Dimbat, and F. H. Stross, "Number-Average Molecular Weights," Interscience Publishers Inc., New York, N. Y., 1958.

(12) W. H. Stockmayer and E. F. Casassa, *J. Chem. Phys.*, **20**, 1560 (1952).

(13) T. G. Fox, P. J. Flory, and A. M. Bueche, *J. Amer. Chem. Soc.*, **73**, 285 (1951); W. R. Krigbaum and P. J. Flory, *J. Polym. Sci.*, **9**, 503 (1952).

In Figure 2a are shown the plots of $A_2(\text{OS})$ vs. $1/C_s^0$ together with $A_2(\text{LS})$. The linearity of A_2 with respect to $1/C_s^0$ holds over a wide range of ionic strengths, but at high ionic strengths the experimental data deviate from the linear relationship. In Figure 2b, the same data are plotted against $1/\sqrt{C_s^0}$. The linear relationship between A_2 vs. $1/\sqrt{C_s^0}$ appears to hold at high ionic strengths, although a careful examination of the data of both $A_2(\text{LS})$ and $A_2(\text{OS})$ reveals that the straight line in Figure 6 of ref 6 should have been drawn with a slightly lower slope, as shown in Figure 2b. These

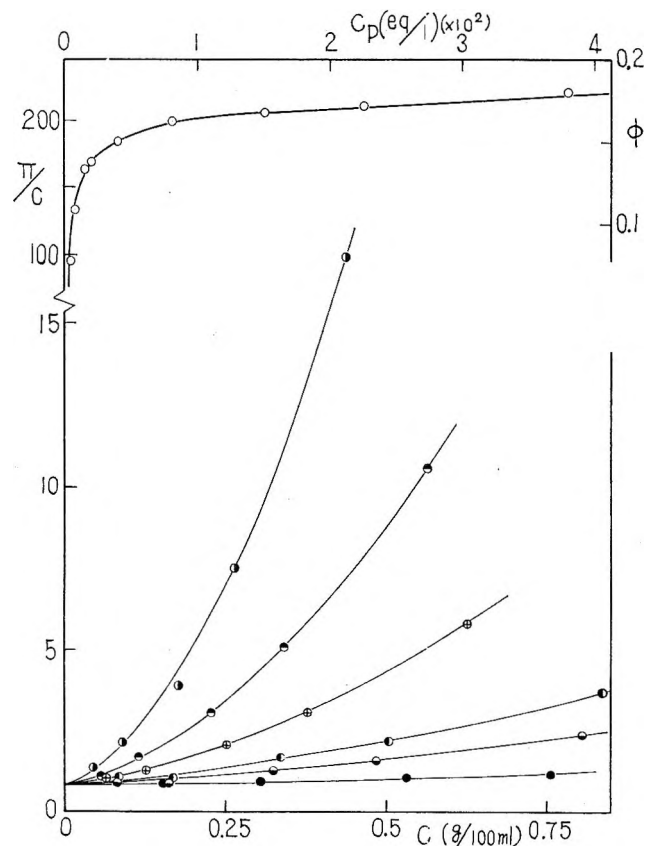


Figure 1. Plots of π/C vs. polymer concentration C for Na-PS (F-8) in aqueous NaCl Solutions. NaCl concn, O, 0; ●, 0.005; ⊙, 0.01; ⊕, 0.02; ⊙, 0.05; ⊖, 0.1; ●, 0.5 M. ϕ denotes the osmotic coefficient. The solid lines for salt-added systems denote the values calculated from eq 1 using the values of A_2 shown in Table I and assuming $g = 5/8$.

experimental data appear to support our previous conclusions better than before. Alexandrowicz¹⁴ presented a theory which accounts for the linear dependence of A_2 on $1/\sqrt{C_s^0}$. Thus, we withdraw our statement that the polymer concentrations used for osmotic pressure measurements are too high to obtain reliable second virial coefficients. If we take into account the third virial coefficient in a proper way, we can determine the second virial coefficient of polyelectrolyte solution with high reliability by osmometry.

From the osmotic pressure measurement of Na-PS in deionized water, the osmotic coefficient ϕ was calculated according to

$$\pi(\text{obsd}) = \frac{Z + 1}{M_n} \phi CRT = \phi c_p RT \quad (2)$$

where Z is the number of charges on a polyion and c_p is expressed in (equiv/l.). ϕ (or π/C) is also plotted against c_p (equiv/l.) or C (g/100 ml) in Figure 1. If c_p is lower than 0.005 equiv/l., ϕ gradually increases with increasing polymer concentration, while at concentrations higher than 0.005 equiv/l., ϕ is almost constant and about 0.17. The similar characteristic curves were obtained by Kern¹⁵ and Takahashi and Kagawa¹⁶ and Alexandrowicz¹⁷ for various polyelectrolytes in water.

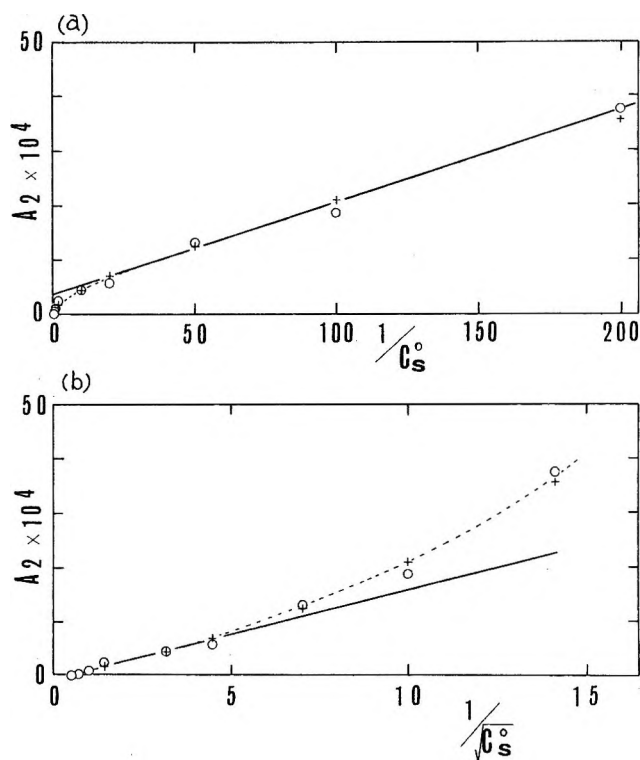


Figure 2. Plots of second virial coefficient vs. reciprocal ionic strength (a) and reciprocal square root of ionic strength (b). O, $A_2(\text{LS})$; +, $A_2(\text{OS})$.

Moreover, $\phi = 0.17$ is favorably compared with the average value of counterion activity coefficient ($\gamma_c = 0.2$) evaluated from light scattering experiments previously.

(14) Z. Alexandrowicz, *J. Polym. Sci.*, **6**, A-2, 1227 (1968).

(15) W. Kern, *Z. Phys. Chem.*, **A184**, 197 (1937).

(16) A. Takahashi and I. Kagawa, *Nippon Kagaku Zasshi*, **83**, 6, 9 (1962).

(17) Z. Alexandrowicz, *J. Polym. Sci.*, **40**, 91 (1959).

Activity Coefficients of [Co(NH₃)₄(NO₂)₂][Co(NH₃)₂(NO₂)₄] in Divalent Metal Perchlorate and Other Salt Media

by Zofia Libuś

Department of Physical Chemistry, Technical University of Gdańsk,
Gdańsk, Poland (Received July 9, 1969)

It has recently been shown that manganese(II), cobalt(II), nickel(II), and zinc(II) perchlorates display practically the same concentration dependences of the osmotic and activity coefficients up to considerable concentrations.¹ This behavior was ascribed to the existence of the corresponding metal cations exclusively in the form of octahedral hexaquo complexes, possibly with second layers of hydrogen-bonded water molecules, whose interactions with the medium are essentially independent of the nature of the central metal atom. Slightly lower activity and osmotic coefficients of the Cu(ClO₄)₂ and Mg(ClO₄)₂ solutions were interpreted as arising from an outer-sphere association of the perchlorate anion with the hydrated cations in question. However, more intimate interactions consisting in the penetration of the anions into the first coordination spheres of the cations could not be excluded definitely in this case. It seemed interesting, therefore, to examine to what extent different divalent cations of the same group of metals may differ in their interaction with an anion which, on account of its bulkiness, may be expected to be unable to penetrate into the first coordination sphere. For this purpose the activity coefficients of the complex salt [Co(NH₃)₄(NO₂)₂][Co(NH₃)₂(NO₂)₄] in aqueous solutions of several divalent metal perchlorates of varying concentration were determined using the solubility method.

Experimental Section

Materials. Solutions of Mg(ClO₄)₂, Co(ClO₄)₂, Ni(ClO₄)₂, Cu(ClO₄)₂, NaClO₄, and NaCl were prepared and analyzed as described in ref 1. The complex salt [Co(NH₃)₄(NO₂)₂][Co(NH₃)₂(NO₂)₄] was prepared from the [Co(NH₃)₄(NO₂)₂]Cl and NH₄[Co(NH₃)₂(NO₂)₄] complex compounds. The latter two had been obtained by the method of Jørgensen² and purified by repeated recrystallizations from water. Equivalent amounts of dilute aqueous solutions of the above compounds were mixed at room temperature. The precipitate was filtered off and washed with distilled water. In order to obtain as uniform crystals as possible, the material was placed in a big dish filled with water, where it remained for 2 weeks. Every 2 days, the solution was removed from over the crystals and a new portion of distilled water was added. Conductivity water was used in the two last operations. The crys-

talline material was dried under vacuum at room temperature. It was analyzed for cobalt by repeated evaporation in sulfuric acid, followed by gently heating and weighing anhydrous CoSO₄ thus obtained. *Anal.* Calcd for Co: 23.8%. Found: 23.7%.

Procedures. The investigated solutions were saturated with the [Co(NH₃)₄(NO₂)₂][Co(NH₃)₂(NO₂)₄] complex salt at 18° following the procedure described by Brønsted.³ The room temperature was always higher than 18°, thus preventing precipitation of the complex in further manipulations. The concentration of [Co(NH₃)₄(NO₂)₂][Co(NH₃)₂(NO₂)₄] in the resulting solution was determined spectrophotometrically using the Unicam SP 500 spectrophotometer. The optical density of the solution under investigation was measured at 425 and 430 mμ, while the reference cell always contained the corresponding solution without the complex salt. The necessary value of the molar extinction coefficient of [Co(NH₃)₄(NO₂)₂][Co(NH₃)₂(NO₂)₄] was found as the sum of the molar extinction coefficients of the [Co(NH₃)₄(NO₂)₂]Cl and NH₄[Co(NH₃)₂(NO₂)₄] complexes measured in their dilute aqueous solutions. The resulting value, the same within experimental error for both 425 and 430 mμ, is 752. It was found to be the same in pure water and in different salt media of varying concentrations which were used in this work. In order to avoid errors arising from the aequation of the complex salt, all operations were performed in as short a time as possible, usually within 10 to 15 min from the beginning of the saturation operation. No detectable changes in the optical densities of the solutions took place in these time intervals.

Results and Discussion

Table I lists the solubilities in mol/kg of solvent units of the [Co(NH₃)₄(NO₂)₂][Co(NH₃)₂(NO₂)₄] complex salt in water solutions of Mg(ClO₄)₂, Co(ClO₄)₂, Ni(ClO₄)₂, and Cu(ClO₄)₂ at 18°. As is seen, the solubility in pure water found in different series of experiments was slightly different, probably as a result of gradual dissolution of the smallest crystals in the solubility column.

The mean ionic activity coefficient, γ , of the complex electrolyte [Co(NH₃)₄(NO₂)₂][Co(NH₃)₂(NO₂)₄] was calculated from the equation

$$s\gamma = s_0\gamma_0$$

where s and s_0 are the solubilities in the presence of the cosolute and in pure water, respectively. The necessary value of γ_0 , the activity coefficient of [Co(NH₃)₄(NO₂)₂][Co(NH₃)₂(NO₂)₄] in its saturated solution in

(1) Z. Libuś and T. Sadowski, *J. Phys. Chem.*, **73**, 3229 (1969).

(2) S. M. Jørgensen, *Z. Anorg. Chem.*, **17**, 469, 477 (1898).

(3) J. N. Brønsted and V. K. La Mer, *J. Amer. Chem. Soc.*, **46**, 555 (1924).

Table I: Solubilities, s , of $[\text{Co}(\text{NH}_3)_4(\text{NO}_2)_2][\text{Co}(\text{NH}_3)_2(\text{NO}_2)_4]$ in Aqueous Solutions of $\text{Mg}(\text{ClO}_4)_2$, $\text{Co}(\text{ClO}_4)_2$, $\text{Cu}(\text{ClO}_4)_2$, and $\text{Ni}(\text{ClO}_4)_2$ of Varying Molalities, m , at 18°

$\text{Mg}(\text{ClO}_4)_2$		$\text{Co}(\text{ClO}_4)_2$		$\text{Cu}(\text{ClO}_4)_2$		$\text{Ni}(\text{ClO}_4)_2$	
m	$10^4 \times s$	m	$10^4 \times s$	m	$10^4 \times s$	m	$10^4 \times s$
0.0	3.130	0.0	3.130	0.0	3.083	0.0	3.077
0.0222	3.841	0.0222	3.834	0.0275	3.886	0.0251	3.801
0.0558	4.226	0.0552	4.204	0.0623	4.256	0.0532	4.165
0.0923	4.527	0.0907	4.540	0.1185	4.778	0.1068	4.571
0.1901	5.249	0.1845	5.245	0.2289	5.516	0.2069	5.299
0.3814	6.371	0.3749	6.489	0.4768	7.223	0.4106	6.673
0.5815	7.621	0.5691	7.857	0.7343	9.337	0.6482	8.428
0.7847	8.986	0.7673	9.325	0.9897	11.64	0.8734	10.26
0.9996	10.53	0.9763	11.17	1.2518	14.24	1.0984	12.50
1.3166	13.09	1.2823	14.13	1.5411	18.20	1.3503	15.01
1.7014	17.54	1.6853	19.57	1.9884	26.86	1.7066	20.08

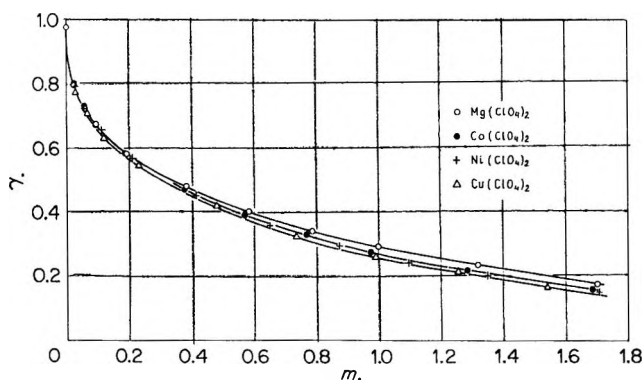


Figure 1. The dependence of the activity coefficient, γ , of $[\text{Co}(\text{NH}_3)_4(\text{NO}_2)_2][\text{Co}(\text{NH}_3)_2(\text{NO}_2)_4]$ on the molal concentrations of divalent metal perchlorates in aqueous solution, at 18° .

pure water, was calculated from the limiting Debye-Hückel equation.

Figure 1 shows plots of the activity coefficient of the complex electrolyte under investigation against the molal concentration of the cosolute, the latter being $\text{Mg}(\text{ClO}_4)_2$, $\text{Co}(\text{ClO}_4)_2$, $\text{Ni}(\text{ClO}_4)_2$, or $\text{Cu}(\text{ClO}_4)_2$. As is seen, the activity coefficient, γ , in each case decreases monotonously with increasing concentration of the metal perchlorate in the whole concentration range investigated. While this decrease may be considered as a quite general effect of the coulombic interactions between the ions when lower concentrations are concerned, it seems to be accountable only in terms of ionic association for the region of higher concentrations. For our purposes, most essential seems to be the fact that the values of the activity coefficient of the $[\text{Co}(\text{NH}_3)_4(\text{NO}_2)_2][\text{Co}(\text{NH}_3)_2(\text{NO}_2)_4]$ complex electrolyte are very nearly the same in equally concentrated solutions of the four metal perchlorates at concentrations lower than approximately $0.2 m$, and they remain approximately equal in the whole concentration range investigated, *i.e.*, up to $1.7 m$. There seems to be little doubt that, like the coincidence of the activity

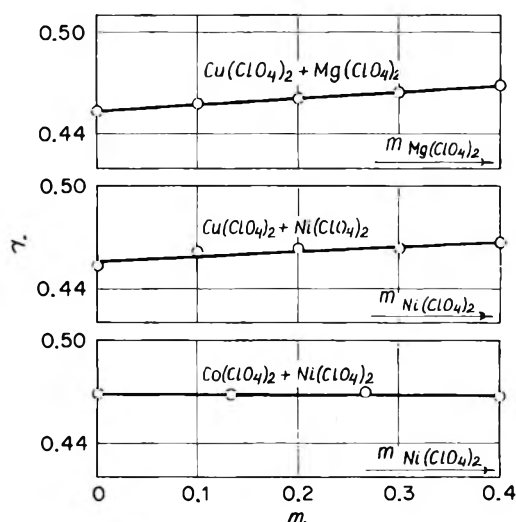


Figure 2. The dependence of the activity coefficient, γ , of $[\text{Co}(\text{NH}_3)_4(\text{NO}_2)_2][\text{Co}(\text{NH}_3)_2(\text{NO}_2)_4]$ on the composition of $0.4 m$ mixtures of different divalent metal perchlorates at 18° .

coefficients of the metal perchlorates themselves,¹ the results discussed here should be ascribed to the fact that all the metal perchlorates studied exist in the form of octahedral hexaaquo cations and coordinatively nonbonded perchlorate anions. The sequence of increasing values of γ at concentrations higher than $0.4 m$ is: $\text{Cu}(\text{ClO}_4)_2 < \text{Ni}(\text{ClO}_4)_2 \lesssim \text{Co}(\text{ClO}_4)_2 < \text{Mg}(\text{ClO}_4)_2$. It may be noted that it is the same as the sequence of increasing acidities of the hydrated cations.⁴ Hence, it seems probable that the small differences in the activity coefficients of $[\text{Co}(\text{NH}_3)_4(\text{NO}_2)_2][\text{Co}(\text{NH}_3)_2(\text{NO}_2)_4]$ in equally concentrated solutions of different divalent metal perchlorates are accountable in terms of the strength of hydrogen bonds probably formed between the hydrated cations, on one hand, and the $[\text{Co}(\text{NH}_3)_2(\text{NO}_2)_4]^-$ anions, on the other, when they form ion pairs.

(4) G. Mattock, *Acta Chem. Scand.*, **8**, 777 (1954).

In accordance with what might be expected in view of the above results, the activity coefficient of $[\text{Co}(\text{NH}_3)_4(\text{NO}_2)_2][\text{Co}(\text{NH}_3)_2(\text{NO}_2)_4]$ in equimolal mixtures of two different divalent metal perchlorates belonging to the above group remains very nearly constant, or shows only a small variation with changing composition. This is illustrated in Figure 2 showing the dependences of γ on the composition of equimolal mixtures of different divalent metal perchlorates.

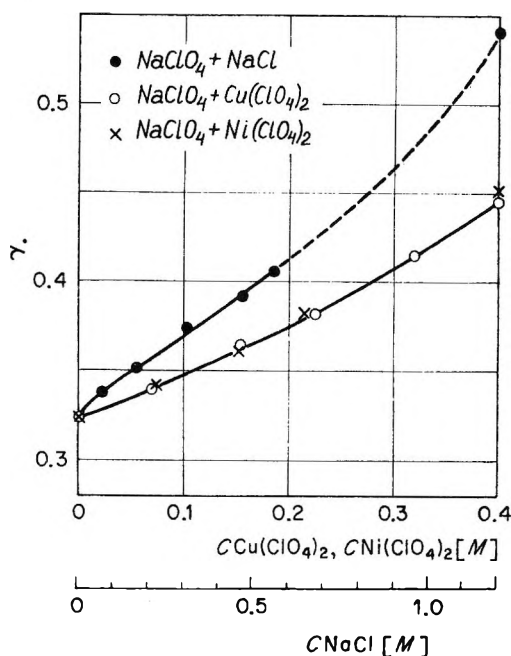


Figure 3. The dependence of the activity coefficient, γ , of $[\text{Co}(\text{NH}_3)_4(\text{NO}_2)_2][\text{Co}(\text{NH}_3)_2(\text{NO}_2)_4]$ on the composition of mixed electrolyte solutions having constant total ionic strength of 1.2 M, at 18°.

It seemed interesting to see to what extent the activity coefficient of $[\text{Co}(\text{NH}_3)_4(\text{NO}_2)_2][\text{Co}(\text{NH}_3)_2(\text{NO}_2)_4]$ may change in mixtures of two salts differing either in the nature of the anion or in the coordination state of the cation, but having constant formal ionic strength. Mixtures of NaClO_4 with NaCl , $\text{Cu}(\text{ClO}_4)_2$, or $\text{Ni}(\text{ClO}_4)_2$ having an ionic strength of 1.2 mol/l. have been investigated from this point of view. The results are shown in Figure 3. As is seen, replacement of NaClO_4 for an equivalent amount of NaCl results in a drastic increase in the activity coefficient of the complex electrolyte under investigation. A similar, though smaller, effect is observed when NaClO_4 is gradually replaced for $\text{Ni}(\text{ClO}_4)_2$ or $\text{Cu}(\text{ClO}_4)_2$. These results once more demonstrate how large may be the variations of the activity coefficients of complex ions in solutions of a constant ionic strength but of varying composition.

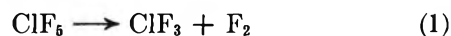
Acknowledgment. The author wishes to thank Dr. W. Libuś for many helpful discussions and suggestions, and Mrs. G. Czerwińska for technical assistance.

Kinetics of the Gas Phase Pyrolysis of Chlorine Pentafluoride¹

by A. E. Axworthy and J. M. Sullivan

Rocketdyne, A Division of North American Rockwell Corporation, Canoga Park, California 91504 (Received April 11, 1969)

The kinetics of the photochemical formation of chlorine pentafluoride from ClF_3 and F_2 has been studied by Krieger, Gatti, and Schumacher.² Herein we report the results of our investigation of the gas phase thermal decomposition of ClF_5



where,³ $\Delta H^\circ_{600^\circ\text{K}} = 18.5$ kcal/mol, $\Delta S^\circ(\text{p}) = 40.4$ gibbs/mol, and $\Delta S^\circ(\text{c}) = \Delta S^\circ(\text{p}) - R - R \ln(RT) = 30.7$ gibbs/mol.

Experimental Section

The electrically heated, stirred flow reactor (91 ml, monel) employed is described elsewhere.^{4,5} Chlorine pentafluoride vapor of 98 wt % purity (the impurities were HF , ClF_3 , and small amounts of CF_4) was passed through the reactor at an initial partial pressure of 32 Torr in a mixture with helium. The total pressure was 1 atm. The reactor was equipped with a by-pass to allow measurement of the ClF_5 concentration in the entering gas stream.

The gases leaving the reactor (or the by-pass) passed through a 10-cm nickel infrared cell with AgCl windows. The ClF_5 concentration was followed by measuring the absorbance at 12.5μ pressure. The flow rates were measured with a soap bubble flow meter connected to the exit stream. The measured flow rates and reactor volume were corrected to reactor temperature. No correction was made for the partial dissolution of reactants and products in the soap solution or for the presence of water vapor from the soap solution.

Infrared analysis of the exit gas showed ClF_3 and ClF_5 as the major absorbers. Fluorine does not absorb in this pressure range ($2\text{--}15 \mu$). The absorption bands for ClF_3 were masked by ClF_5 . However, crude estimates of the moles of ClF_3 formed per mole of ClF_5 reacted were obtained for some of the experiments by measuring the ClF_3 absorbance at 15μ . These results, presented in Table I, indicate that the stoichiometry is essentially that of eq 1. The possible de-

(1) This work was supported by the United States Air Force under Contract No. AF04(611)-10544.

(2) R. L. Krieger, R. Gatti, and H. J. Schumacher, *Z. Phys. Chem.*, **51**, 240 (1966).

(3) JANAF Thermochemical Tables.

(4) J. M. Sullivan and T. J. Houser, *Chem. Ind. (London)*, 1057 (1965).

(5) J. M. Sullivan and A. E. Axworthy, *J. Phys. Chem.*, **70**, 3366 (1966).

Table I: Experimental Kinetic Data for the Pyrolysis of Gaseous Chlorine Pentafluoride

$T, ^\circ\text{C}$	τ, sec	Fraction reacted, α	k, sec^{-1}	$(\text{ClF}_3)_{\text{calcd.}}, (\text{ClF}_3)_{\text{obsd.}}$	
				Torr	Torr
252.2	24.9	0.119	0.00542		
252.2	113.0	0.378	0.00538	12.1	10.5
252.2	281.5	0.638	0.00626	20.4	20.1
252.2	449.0	0.648	0.00409		
268.5	196.8	0.694	0.0115		
279.4	36.2	0.483	0.0254		
279.4	115.3	0.731	0.0235		
283.2	23.6	0.471	0.0378		
283.0	36.3	0.571	0.0368		
288.0	9.5	0.301	0.0452	9.6	11.7
287.4	24.4	0.551	0.0503	17.7	20.5
288.0	27.9	0.610	0.0559	19.5	22.9
288.2	40.4	0.699	0.0572	22.4	24.9
287.4	42.4	0.703	0.0558	22.5	25.6
287.6	55.0	0.772	0.0614	24.7	31.4
293.0	11.6	0.394	0.0561		
291.8	11.9	0.394	0.0546		
293.0	14.6	0.457	0.0580		
291.5	24.1	0.603	0.0610		
293.3	32.4	0.669	0.0622		
293.0	38.4	0.705	0.0620		
293.5	41.7	0.740	0.0680		
293.0	62.8	0.806	0.0663		
294.0	81.3	0.844	0.0663		
307.5	7.96	0.532	0.143	17.0	15.0
306.8	9.76	0.624	0.169	20.0	22.2
307.0	11.9	0.677	0.176	21.7	25.4
307.5	12.9	0.664	0.153	21.2	16.2

composition of ClF_3 to ClF and F_2 is limited to less than 13% by thermodynamic considerations.

Results

The experimental results^{6,7} for the thermal decomposition of ClF_5 over the temperature range 252–307° are presented in Table I. For a first-order decomposition in a stirred flow reactor, the rate constant k is given by

$$k = \alpha/\tau(1 - \alpha) \quad (2)$$

where α is the fraction reacted and τ is the average residence time in the reactor.⁸ In Figure 1, a plot of $\alpha/(1 - \alpha)$ vs. τ for the data at 293° shows that the reaction follows first-order kinetics up to at least 84% decomposition. The data in Figure 1 were obtained at 291.5–294.0° and converted to 293° using the measured activation energy of 36.8 kcal/mol. The data in Table I give a linear Arrhenius plot. A least-squares fit of the data to the Arrhenius equation gives

$$k = 10^{13.02} \exp(-36,800/RT) \text{ sec}^{-1} \quad (3)$$

The limit of error for the activation energy is

$$E = 1.0 \text{ kcal/mol} \quad (4)$$

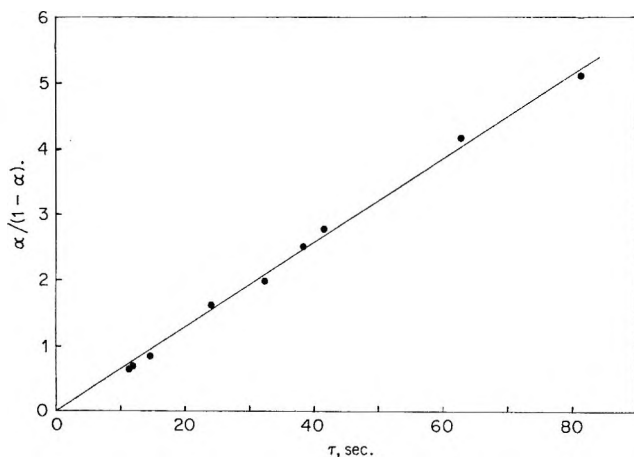
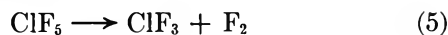


Figure 1. First-order plot at 193°.

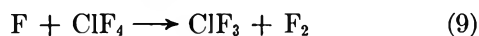
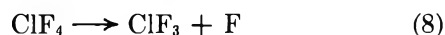
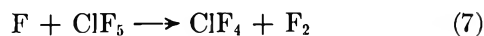
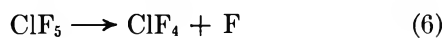
Discussion

Reaction Mechanism. Three possible mechanisms may be written which are compatible with the observed rate expression, *i.e.*, first-order in ClF_5 with no apparent inhibition as the products accumulate.

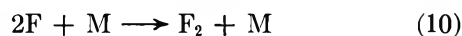
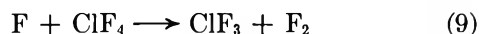
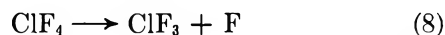
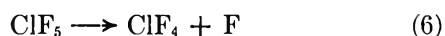
A. Unimolecular Elimination of F_2



B. Radical Chain Mechanism



C. Nonchain Radical Mechanism



It will be shown in the following discussion that none of these mechanisms can be completely eliminated on the grounds of giving unreasonable Arrhenius parameters, but the nonchain radical mechanism appears to be the most likely mechanism. The expected⁹ A

(6) The results presented herein differ from those presented in ref 7 because an error was found in the computational procedure used to convert absorbance to concentration. The amount by which this changed the reported kinetic parameters does not indicate the experimental uncertainty in these parameters.

(7) A. E. Axworthy and J. M. Sullivan, 155th National Meeting of the American Chemical Society, San Francisco, Calif., April 1968.

(8) A. A. Frost and R. G. Pearson, "Kinetics and Mechanism," John Wiley and Sons, Inc., New York, N. Y., 1956, p 185.

(9) S. W. Benson, "Thermochemical Kinetics," John Wiley and Sons, Inc., New York, N. Y., 1968.

factor for direct molecular elimination of fluorine, reaction 5, is 10^{13} to 10^{14} sec^{-1} . Three-center reactions of this type are not common, and for ClF_5 would be expected to involve a "stiff" transition state. The structure of ClF_5 is square pyramidal with the central chlorine and the four equivalent fluorine atoms approximately in a plane.¹⁰ The unique fluorine atom would probably be involved in reaction 5 since this would permit the closest approximation to the planar ClF_3 structure¹¹ in the transition state. If ClF_5 does decompose through reaction 5, the reverse of this reaction has an A factor of $10^{6.3}$ $1. \text{ mol}^{-1} \text{ sec}^{-1}$. This is unusually low for a bimolecular association reaction but is not unreasonable if the transition state is very stiff compared with ClF_5 .

Although reaction 5 cannot be ruled out on the basis of the observed A factor, it is not unlikely that the activation energy required to form the three-center transition state is considerably greater than the experimental value of 36.8 kcal/mol (the shortest distance between two F atoms in ClF_5 is 2.36 Å compared with 1.41 Å in F_2). If $A_5 \cong A_{\text{ob}} = 10^{13.0}$, the criterion for reaction 5 to be negligible (less than 1%) is $E_5 > E_{\text{ob}} + 2\theta = 41.8$ kcal/mol, where $\theta = 2.3 RT = 2.5$ kcal/mol at 550°K.

If the radical chain mechanism predominates, the following conditions obtain at steady state

$$k_{\text{ob}} = k_6 + (k_6 k_7 k_8 / k_9)^{1/2} \quad (12)$$

$$(\text{F}) = (k_6 k_8 / k_7 k_9)^{1/2} \quad (13)$$

$$(\text{ClF}_4) = (k_6 k_7 / k_8 k_9)^{1/2} (\text{ClF}_5) \quad (14)$$

$$R_6 = R_9 \text{ and } R_7 = R_8 \quad (15)$$

where R_6 represents the rate of reaction 6, etc.

At long chain length, $k_{1c} = (k_6 k_7 k_8 / k_9)^{1/2}$. If $A_7 \cong A_9$, $A_{1c} = (A_6 A_8)^{1/2} \cong (10^{14} \cdot 10^{14})^{1/2} = 10^{14}$. This is in fair agreement with A_{ob} .

The activation energy at long chain length is given by $1/2(E_6 + E_7 + E_8 - E_9)$. Because ΔH for $\text{ClF}_5 = \text{ClF}_3 + 2\text{F}$ is 57.0 kcal/mol,¹² $E_6 + E_8 = 57.0 + E_{6R} + E_{8R}$ where E_{6R} and E_{8R} are the activation energies for the reverse of reactions 6 and 8, respectively. Thus for the long-chain mechanism, $E_7 = 2E_{\text{ob}} - 57.0 - E_{6R} - E_{8R} + E_9 = 16.6 - E_{6R} - E_{8R} + E_9$. If as expected $E_{6R} \cong E_{8R} \cong E_9 \cong 0$, $E_7 \cong 16.6$ kcal/mol. $E_7/\theta = 6.6$ which is only slightly above the expected maximum value for a fast bimolecular propagation step.¹³

An additional requirement for the long-chain mechanism is that $R_6 \ll R_7 = R_{\text{ob}}$. If $A_6 \cong 10^{14}$, E_6 must be greater than about $E_{\text{ob}} + 3\theta$ or 44 kcal/mol. Thus, for a long-chain mechanism to prevail, $E_6 \geq 44$, $E_7 \cong 16.6$, and $E_8 \cong 57.0 - E_6 < 13$ kcal/mol. These values cannot, *a priori*, be considered as unreasonable; hence the long-chain mechanism cannot be eliminated.

If $39 < E_6 < 45$, a short chain mechanism could occur. This would lead to a linear Arrhenius plot only if both terms in eq 12 have the same activation energy. This would be the case, however, because it was shown above that the A factors for these two terms should be of the same magnitude, requiring that their activation energies be about the same for a short-chain mechanism to occur.

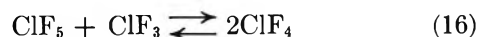
The termination process in the chain mechanism must involve the reaction of F and ClF_4 (*e.g.*, reaction 9). The occurrence of the other possible termination reactions, 10 and 11, does not give first-order kinetics. However, the termination reaction



could be added to the chain mechanism without affecting the above discussion. Krieger,² *et al.*, conclude that $R_{6R} = R_9$ under their conditions.

The major factor which determines whether the radical chain reaction occurs is, of course, the rate of the fluorine atom abstraction reaction, 7. There are indications¹³ that these types of reactions (*e.g.*,¹⁴ $\text{QF} + \cdot\text{NF}_2 \rightarrow \text{NF}_3 + \text{Q}\cdot$) have high activation energies and, therefore, do not occur. On this basis, the chain mechanism appears less likely to occur than the non-chain radical mechanism.

If the decomposition reaction proceeds *via* the non-chain radical mechanism, the observed activation energy (36.8 kcal/mol) is a measure of the bond dissociation energy for the first bond in ClF_5 —providing that, as expected, $E_{6R} \cong 0$. Hence, the dissociation energy of the second bond (eq 8) would be $57.0 - 36.8 = 20.2$ kcal/mol.² This value for ΔH_8 appears reasonable. In the first place, if we consider the reaction



then $\Delta H_{16} = \Delta H_6 - \Delta H_8 = (\Delta H_6 + \Delta H_8) - 2\Delta H_8 = 57.0 - 2\Delta H_8 = +16.6$ kcal/mol. Since ΔS_{16} should be small, $\log K_{16}^{\text{eq}} \cong -16.6/\theta$ which at 600°K gives $K_{16}^{\text{eq}} = 10^{-6.4}$. A larger value of ΔH_8 would permit the ClF_4 radical to reach very appreciable concentrations at moderate temperatures; this presumably is not the case.

Secondly, the high quantum yields (up to 0.5) obtained in the photochemical synthesis² at ~ 1 atm and 30° puts a lower limit on ΔH_8 (and thus an upper limit on ΔH_6). The half-life of ClF_4 is given by $\tau_{1/2} = 0.7 (A_8)^{-1} \times 10^{+\Delta H_8/\theta} \cong 7 \times 10^{-15} \times 10^{+\Delta H_8/1.38}$

(10) G. M. Begun, W. H. Fletcher, and D. F. Smith, *J. Chem. Phys.*, **42**, 2236 (1965).

(11) R. D. Burbank and F. N. Bensey, *ibid.*, **21**, 602 (1953).

(12) If the new value for the dissociation energy of F_2 [W. Stricker, *Z. Naturforsch.*, **22a**, 1137 (1967)] is confirmed, the sum of the first two bonds in ClF_5 will be lowered to 53.5 kcal/mol.

(13) See p 122 of ref 9.

(14) Unpublished data from this laboratory.

sec. The time required to suffer at least one collision with an F atom is $\sim 10^{-10} (X_F)^{-1}$ sec, where X_F is the mole fraction of F atoms in the photochemical reactor. Thus $\Delta H_8 > 1.36 (4.15 - \log X_F)$. An upper limit for X_F can be estimated by calculating the value at which F atom recombination, reaction 10, equals the rate of the photochemical dissociation of F_2 which was about 0.01 Torr/sec at the highest F_2 pressure. Using the smallest reported rate constant¹⁵ for k_{10} at room temperature, $5 \times 10^7 \text{ l.}^2 \text{ mol}^{-2} \text{ sec}^{-2}$, the calculated maximum value of X_F is 10^{-5} . Thus $\Delta H_8 > 12.5 \text{ kcal/mol}$.

It may be seen from the above discussion that at least three mechanisms are compatible with the observed kinetic parameters. We favor the nonchain radical mechanism on the grounds that reactions 5 and 7 might be expected to be too slow.

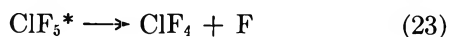
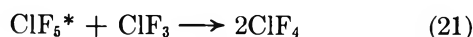
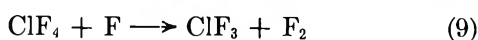
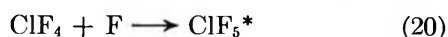
Photochemical Mechanism. Krieger, Gatti, and Schumacher² studied the kinetics of the photochemical formation of ClF_5 from ClF_3 and F_2 (365 $m\mu$, 16 to 70°) and obtained the complex rate expression

$$\frac{d(ClF_5)}{dt} = kI_{\text{abs}} \left[k' \frac{(ClF_3)}{(M)} + 1 + \frac{k''}{(M)} \right]^{-1} \quad (17)$$

where

$$(M) = (F_2) + 0.40(ClF_5) + 0.22(N_2) + 0.18(He) \quad (18)$$

They explain their results on the basis of the following reaction scheme



Reaction 21 is required to account for the observed inhibition by ClF_3 . Each of the competing paths for ClF_5^* , reactions 21, 22, and 23, occurred to an appreciable extent (>10%) in every experiment. Two consequences of the photochemical investigation are of interest to the present study (in addition to the lifetime of ClF_4 discussed above). First, from the photochemical results the average lifetime of the activated ClF_5^* is calculated to be 10^{-9} sec^{-1} . Hence, the thermal reaction should be in the pressure-dependent region. Secondly, the photochemical mechanism predicts an acceleration of the thermal reaction as the product ClF_3 accumulates. It may be seen from Figure 1 that the thermal reaction follows first-order kinetics out to at least 84% reaction, with no indication

of acceleration at higher fractions of decomposition. From the photochemical rate parameters, a 20% increase in the first-order rate constant would be predicted at 80% decomposition. Further thermal experiments at various pressures and initial ClF_3 concentrations would be required to establish definitely whether the thermal reaction is pressure dependent or inhibited slightly by ClF_3 .

The lifetime of the photochemically activated ClF_5^* is shorter than would be predicted for a thermally activated molecule of this complexity.^{16,17} Classical RRK theory predicts a lifetime¹⁸ of $10^{-5.7} \text{ sec}$ at 600°K and $10^{-4.6} \text{ sec}$ at 300°K. The fluorine atoms formed from the photochemical decomposition of F_2 at 365 $m\mu$ contain 20 kcal/mol of excess translational energy, since there are no accessible electronic states. If all of this energy were introduced into the ClF_5^* , its predicted lifetime would be reduced to $10^{-8.5} \text{ sec}$, near the observed value. This excess energy from the photochemical fluorine atom would also account for the reactivity of ClF_5^* toward ClF_3 . A major problem with this suggested difference between the thermal and photochemical reactions is that the photochemically formed F atoms should cycle through reaction 8R many times and lose their excess energy before forming ClF_5^* .

(15) R. W. Diesen, *J. Phys. Chem.*, **72**, 108 (1968).

(16) S. W. Benson, "The Foundations of Chemical Kinetics," McGraw-Hill Book Company, Inc., New York, N. Y., 1960.

(17) A. F. Trotman-Dickenson, "Gas Kinetics," Academic Press Inc., New York, N. Y., 1955.

(18) The value $c_v = c_p - 8$ was used in making the calculation. For details see p 112 of ref 9.

Calculation of Photodissociation Quantum Yields for Azoethane

by P. G. Bowers

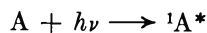
Department of Chemistry, Simmons College, Boston, Massachusetts 02115 (Received May 26, 1969)

The extent to which modern unimolecular theory can be used to interpret the dissociation of an electronically excited molecule was investigated in our previous work on ketene¹ and hexafluoroacetone.² This note reports some further calculations, chiefly on the primary photodissociation of azoethane for which we have computed the absolute quantum yield ϕ , as a function of pressure, temperature, and exciting wavelength. The results are compared to the experimental findings of Cerfontain and Kutschke³ and Worsham and Rice.⁴

(1) P. G. Bowers, *J. Chem. Soc.*, A, 466 (1967).

(2) P. G. Bowers, *Can. J. Chem.*, **46**, 307 (1968).

In azoethane, the primary dissociation is monitored by the quantum yield of nitrogen production, and its pressure dependence is satisfactorily described by a mechanism in which strong collisional deactivation competes with dissociation for the vibrationally excited $^1(n\pi^*)$ state produced by absorption



This scheme yields the familiar Stern-Volmer expression

$$\frac{1}{\phi} = 1 + \frac{k_3[A]}{k_2} \quad (1)$$

from which the rate constant k_2 is $4.0 \times 10^9 \text{ sec}^{-1}$ at 3660 Å and 28° and changes by factors of 0.66 and 1.60 at 3776 and 3519 Å, respectively. Increasing the temperature to 152° at 3660 Å increases k_2 by a factor of 3.1.

Calculation of ϕ

The dissociating molecules have a vibrational energy distribution function $g(E^*)$ which embodies both the thermal energy distribution factor $f(E)$, of the ground electronic state, and the energy profile of the absorbed light. If $k_2(E^*)$ is the specific rate constant for dissociation of a molecule with vibrational energy E^* , then instead of eq 1, we obtain⁵

$$\phi = \int_{E_{\min}}^{\infty} \frac{[k_2(E^*)][g(E^*)]}{k_2(E^*) + k_3[A]} dE^* \quad (2)$$

The Marcus expression⁶ for $k_2(E^*)$ is

$$k_2(E^*) = \frac{1}{h} \left(\frac{Z^+}{Z^*} \right) \frac{S^+(E^+)}{N^*(E^*)} \quad (3)$$

In eq 2 and 3, E^* is related to the energy of the incident light (see Figure 1) by

$$E^* = E_\lambda - E_{00} + E \quad \text{and} \quad E^+ = E^* - E_{\min}$$

The functions S^+ , N^* , and $g(E^*)$ were calculated by direct count or using the Whitten-Rabinovitch expression,⁷ from vibrational frequency assignments for the species involved. Although a complete vibrational analysis for azoethane has not been made, most of the normal-mode frequencies can be reasonably well estimated by comparison with related species such as azomethane, dimethylacetylene, ethyl radicals, etc. For the ground state, four torsional motions were treated as free rotations, and the remaining 38 frequencies (cm^{-1}) were assigned as follows: 2950 (10), 1550 (1), 1450 (6), 1300 (2), 1000 (8), 900 (2), 800 (1), 600 (1), 450 (2), 315 (2), 250 (1), 150 (2). For the excited state, those frequencies which were closely associated with the region of electronic excitation were reduced to 50% of their ground-state value (e.g., N-N stretching and

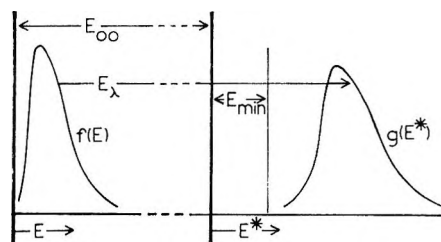


Figure 1. The Boltzmann distribution $f(E)$, of total vibrational energy in ground-state azoethane, and the nonequilibrium distribution, $g(E^*)$ in the excited $^1(n, \pi^*)$ state.

twisting), while others such as the deformation modes of the C_2H_5 groups were left unchanged. Frequencies for the activated complex were taken to be the same as those for the excited molecule, omitting the asymmetric C-N stretching mode. All vibrations and free internal rotations were taken to be active in intramolecular energy exchange. Overall rotations were assumed to be adiabatic, with Z^+/Z^* equal to unity.

Neither E_{00} or E_{\min} could be assigned definite *a priori* values, although E_{00} , judging from the absorption spectrum, is probably less than about 22,500 cm^{-1} . The experimental k_2 , obtained by applying eq 1, give an Arrhenius energy E_a of $2.1 \pm 0.4 \text{ kcal/mol}$.³ As we have previously discussed, E_{\min} must be greater than this.¹ (E_a would be equal to E_{\min} only if the excited molecules were vibrationally equilibrated.) We therefore examined the behavior of $\phi(T, \lambda, [A])$ over a range of values of E_{00} (19,000–23,000 cm^{-1}) and E_{\min} (2–14 kcal).

In most of the calculations, $g(E^*)$ was taken to have the same form as $f(E)$, i.e., assuming monochromatic excitation and neglecting effects of Franck-Condon and symmetry factors on the transition probability. The effect of polychromatic excitation (for 3660 Å) was considered as a correction, using a light profile calculated approximately from the experimental conditions described by Cerfontain and Kutschke. At 27°, the function $f(E)$ had a maximum at 800 cm^{-1} , and its width at half-height was 1200 cm^{-1} . The corresponding width for $g(E^*)$ was 1800 cm^{-1} .

Results and Discussion

Figure 2 shows the experimental data at 27°, compared with calculated Stern-Volmer lines. The values chosen for E_{00} and E_{\min} are those which reproduce the data most closely. Outside of the ranges 5000–5300 Å and 10–13 kcal for E_{00} and E_{\min} , respectively, the

(3) H. Cerfontain and K. O. Kutschke, *Can. J. Chem.*, **36**, 344 (1958).

(4) W. C. Worsham and O. K. Rice, *J. Chem. Phys.*, **46**, 2021 (1967).

(5) The symbols have the same meaning as in ref 1 and 2. A more complete discussion of the dissociation process may also be found in these papers.

(6) R. A. Marcus, *J. Chem. Phys.*, **20**, 352 (1952).

(7) G. Z. Whitten and B. S. Rabinovitch, *ibid.*, **38**, 2466 (1963); **41**, 1883 (1964).

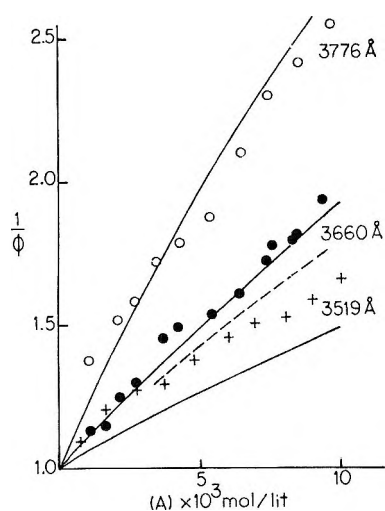


Figure 2. Calculated wavelength dependence of the primary dissociation yield in azoethane at 27°, compared with the experimental results of Worsham and Rice. The lines were calculated using $E_{00} = 5260 \text{ \AA}$ and $E_{\min} = 12.3 \text{ kcal/mol}$. Dashed line includes correction for spectral width of 3660- \AA excitation.

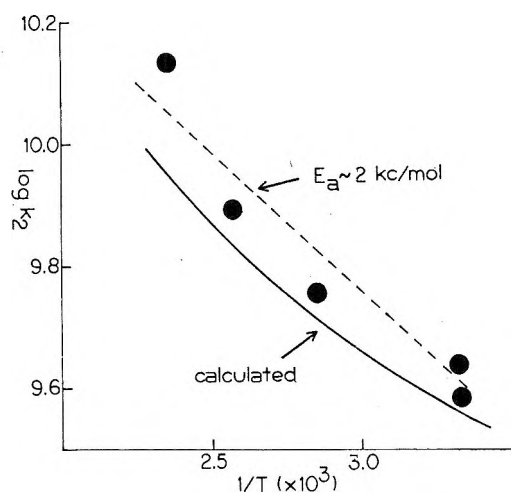


Figure 3. Temperature dependence of k_2 at 3660 \AA , calculated using the same energy parameters as in Figure 2. The lower experimental point at 27° is from ref 4; the others are from ref 3.

agreement is very poor. Curvature in the lines due to the width of $g(E^*)$ is slight: at 3660 \AA , the computed ratio of the limiting high- and low-pressure slopes is less than 1.1 and would certainly be difficult to recognize experimentally.

The effect of nonmonochromatic exciting light (from a mercury source-filter combination) is minor, as Figure 2 illustrates. The curvature is somewhat more evident because $g(E^*)$ is broader.

Calculations of the temperature dependence of ϕ at 3660 \AA are summarized on the Arrhenius diagram in Figure 3. The agreement is moderately good, except at the highest temperature. In particular, both the calculated and experimental Arrhenius lines are curved,

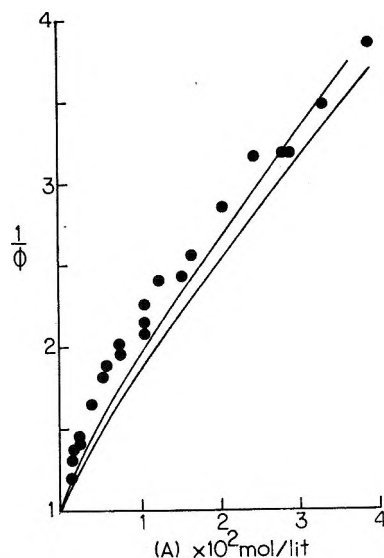


Figure 4. Calculated quantum yield for perfluoroazomethane at 3660 \AA and 30°, compared to experimental results of Wu and Rice. Respective E_{00} and E_{\min} values used were: 4650 \AA , 10.0 kcal (top line); 5000 \AA , 11.4 kcal (lower line).

with a mean "activation" energy (E_a) about six times smaller than the critical dissociation energy (E_{\min}), used in the calculation. It is clear that serious misinterpretations in this type of diagram could occur for any excited molecule or radical reaction where a reacting species has not had time to thermalize its vibrational energy.

A few calculations were carried out on the decomposition of a related molecule, perfluoroazomethane, for comparison with the interesting data reported by Wu and Rice.⁸ These authors photolyzed PFAM over a very wide pressure range at 3660 \AA and found that $1/\phi$ vs. pressure was significantly curved. Our calculation was designed to test whether the extent of this curvature and the pressure region in which it was the greatest could be explained solely on the basis of the width of the energy function $g(E^*)$. Figure 4 shows the result of two typical calculations, with E_{00} and E_{\min} chosen to fit the high-pressure slope of the experimental points. Although the limiting low-pressure slope could be approximately reproduced, the coincidence of the calculated lines in Figure 4, with the points, is poor because the predicted "falloff" in $1/\phi$ occurred mostly at much lower pressures (below $10^{-4} M$). At present, we are inclined to agree with Wu and Rice that more than one electronic state may be involved in this photodissociation, although further experimental data would be of considerable interest. The point has some importance because overall photochemical mechanisms are frequently based on the linearity or otherwise of reciprocal yield plots of this type. Campbell, Shlag, and Ristow have discussed the possible consequences in some detail.⁹

(8) E-C. Wu and O. K. Rice, *J. Phys. Chem.*, **72**, 542 (1968).

Although we believe our calculations on these and other molecules have demonstrated some interesting general features, the present uncertainties in applying RRKM theory to photodissociation are considerable and have been discussed elsewhere.²

Acknowledgment. This work was supported by the Simmons College Fund for Research.

(9) R. J. Campbell, E. W. Schlag, and B. W. Ristow, *J. Amer. Chem. Soc.*, **89**, 5098 (1967).

The Oxidation of Hypophosphorous Acid by Chromium(VI)

by J. N. Cooper

Department of Chemistry, Bucknell University, Lewisburg, Pennsylvania 17837 (Received August 25, 1969)

The report by Haight and coworkers¹ of a preliminary study of the oxidation of hypophosphorous acid by Cr(VI) in 1 *M* aqueous perchlorate media prompts us to present the results of our work. In 1 *M* perchlorate we find, in substantial agreement with Haight, *et al.*, a rate law largely first order in Cr(VI) and hypophosphorous acid, but our results differ in some details. To analyze our data more fully, we have determined the dissociation quotient of hypophosphorous acid and the formation quotient of the Cr(VI)-P(I) complex. The interpretation of data in an earlier study by Pan and Lin² of this reaction in sulfate media, proposing a rate law second order in Cr(VI), is in error. Apparently the formation of a Cr(VI)-P(I) complex was overlooked; the absorbance data given are clearly first order if their initial absorbance datum is disregarded.

Experimental Section

J. T. Baker 50% H₃PO₂ was purified by the fractional melting technique,³ stored under nitrogen, and determined iodometrically.⁴ Unused solutions of H₃PO₂ were discarded 3 weeks after preparation or when they were found to have contained more than 1% H₃PO₃. Recrystallized potassium dichromate was used as a source of Cr(VI), and water was redistilled from alkaline permanganate. Otherwise reagent grade chemicals were used without further purification. All solutions were purged with deoxygenated nitrogen before use.

On a 0.01 to 0.5 *F* scale all of the Cr(III) product was cationic and was separated from neutral and anionic products using analytical grade exchange resins. Analysis for product chromium was performed at 372 nm following alkaline oxidation with hydrogen peroxide, $\epsilon(\text{CrO}_4^{2-}) = 4.82 \times 10^3$. Coordinated P(I) and P(III) were determined by modifications of the standard iodometric procedures.⁴ Free H₃PO₂ and H₃PO₃

were removed from samples before analysis by passage through a chloride-form anion column with a large excess capacity. In the subsequent P(I) determination, the column eluent was heated to 90° for 1 hr in 3 *M* HCl purged with N₂ to hydrolyze the Cr(III) hypophosphite. Analysis was performed as usual on the cooled sample. In the P(III) determination, the sample was allowed to remain in the phosphate buffer-iodine mixture for 4 hr to assure complete reaction.

The dissociation quotient of H₃PO₂ at 25° was estimated in 1 *M* LiClO₄ using a glass electrode and saturated NaCl-calomel reference electrode calibrated against solutions of known hydrogen ion concentration in 1 *M* perchlorate. The compositions of the solutions studied are summarized in Table I. Over a sevenfold

Table I: pH of H₃PO₂ Solutions in 1 *M* LiClO₄ at 25°

H ₃ PO ₂ , <i>F</i>	Observed p[H ⁺]	Q _A (H ₃ PO ₂), ^a <i>M</i>
0.184	1.624 ± 0.004	0.099
0.123	1.140 ± 0.005	0.103
0.0925	1.234 ± 0.003	0.098
0.0615	1.262 ± 0.006	0.105
0.0308	1.620 ± 0.005	0.085
0.0246	1.681 ± 0.005	0.114

^a Q_A(H₃PO₂) = [H⁺][H₂PO₂⁻]/[H₃PO₂].

change in formal H₃PC₂ concentration, Q_A(H₃PO₂) = 0.101 ± 0.015.

The formation quotient of the Cr(VI)-P(I) complex was estimated photometrically in 1 *M* perchlorate media, [H⁺] = 0.161 *M*; reduction of Cr(VI) was negligible during the time of measurement. Haight, *et al.*,¹ observed no evidence for complex formation between H₂PO₂⁻ and Cr(VI), and we interpret the data in Table II in terms of a 1:1 complex between the prin-

Table II: Absorbance of Solutions of Cr(VI) and H₃PO₂ at 350 nm

[H⁺] = 0.161 *M*; temp, 25°, path length = 1.00 cm; Cr(VI) = 2.00 × 10⁻⁴ *F*

H ₃ PO ₂ , <i>F</i>	0.000	0.01016	0.01695	0.0339	0.0508
A ₃₅₀	0.311	0.296	0.287	0.270	0.255

cipal species, H₃PO₂ and HCrO₄⁻, corresponding to the anhydride, H₂PCrO₅⁻. Hypophosphorous acid was in large excess over Cr(VI), and its molar concentration

(1) G. P. Haight, Jr., M. Rose, and J. Preer, *J. Amer. Chem. Soc.*, **90**, 4809 (1968).

(2) K. Pan and S. H. Lin, *J. Chin. Chem. Soc. (Taipei)*, (II) **7**, 75 (1960).

(3) W. A. Jenkins and R. T. Jones, *J. Amer. Chem. Soc.*, **74**, 1353 (1952).

(4) R. T. Jones and E. H. Swift, *Anal. Chem.*, **25**, 1272 (1953).

was calculated using the $Q_A(\text{H}_3\text{PO}_2)$ obtained above. Absorbances were measured at 350 nm where HCrO_4^- , the complex, H_2CrO_4 , and $\text{Cr}_2\text{O}_7^{2-}$ absorb. The latter two species were minor contributors and the observed absorbances were adjusted using the values, $^b Q_C(\text{H}_2\text{CrO}_4) = 4.2$ for the dissociation quotient of chromic acid and $Q_D(\text{HCrO}_4^-) = 98$ for the dimerization quotient of bichromate. Molar absorptivities, $\epsilon(\text{H}_2\text{CrO}_4) = 925$ and $\epsilon(\text{Cr}_2\text{O}_7^{2-}) = 3000$, were estimated from the absorbance of $\text{K}_2\text{Cr}_2\text{O}_7$ solutions in 1 M perchlorate. In all cases the adjustment was less than 5% of the observed absorbance, and the results did not depend critically on the specific molar absorptivities chosen. The formation quotient and molar absorptivity obtained were $Q_f = 13 \pm 2$, $\epsilon(\text{complex}) = 650 \pm 100$.

Kinetics were followed at 350 nm on a Beckman DU spectrophotometer equipped with a thermostated cell holder; infinite time absorbances were less than 1% of the initial absorbances. Individual runs, flooding with hypophosphorous and perchloric acids, were cleanly first order in the absorbance and the pseudo-first-order rate constant was essentially constant over the range of initial Cr(VI) concentrations, 1.50 to $8.00 \times 10^{-4} F$.

Results and Discussion

Our value of $Q_A(\text{H}_3\text{PO}_2) = 0.101$ in LiClO_4 is compared with that reported recently for LiNO_3 media,⁶ $Q_A = 0.135$; agreement is good if the mean activity coefficient for a 1:1 electrolyte in 1 M LiClO_4 or LiNO_3 is taken approximately that for 1 M LiClO_4 or LiNO_3 , respectively.⁷ Our value of $Q_f(\text{complex}) = 13$ is in reasonable agreement with the previous kinetic estimate,¹ $Q_f = 11$.

The rate law obtained from 25 observed pseudo-first-order rate constants, $k = -d \ln(A_{350})/dt$ (sec^{-1}), is

$$\text{rate} = [\text{HCrO}_4^-][\text{H}_3\text{PO}_2]\{k_0 + k_1[\text{H}^+] + k_2[\text{H}^+]^2 + k_3[\text{H}_3\text{PO}_2]\}$$

where

$$\text{rate} = -d[\text{HCrO}_4^-]/dt$$

$$k_0 = 1.87 \times 10^{-3}, k_1 = 4.96 \times 10^{-3},$$

$$k_2 = 1.61 \times 10^{-3}, k_3 = 9.53 \times 10^{-3}$$

$$[\text{HCrO}_4^-] = [\text{Cr(VI)}]/\{1 + [\text{H}^+]/Q_C + Q_f[\text{H}_3\text{PO}_2] + 2Q_D[\text{HCrO}_4^-]\}$$

and

$$[\text{H}_3\text{PO}_2] = [\text{P(I)}]/\{1 + Q_A/[\text{H}^+]\}$$

The observed and calculated rate constants at 25° are presented in Table III. Our rate law was of the same general form as that suggested by Haight, *et al.*,¹ but the rate constants we observed were lower except for those at low $[\text{H}_3\text{PO}_2]$. In preliminary work we ob-

Table III: Pseudo-First-Order Rate Constants (25°)

[H ⁺], <i>M</i>	[H ₃ PO ₂] × 10 ³ , <i>M</i>	<i>k</i> × 10 ⁶ , sec ⁻¹	
		Obsd	Calcd ^a
1.00	4.51	21.9 ^b	21.6
1.00	2.71	14.4	14.5
1.00	4.57	22.0	21.8
1.00	9.10	35.0	34.9
1.00	1.83	10.3	10.4
1.00	0.918	5.43	5.58
0.607	4.29	14.8	14.5
0.371	3.94	10.5	10.3
0.206	3.35	7.28	7.20
0.131	2.82	5.43	5.49
0.0818	2.24	4.10 ^b	4.14
0.632	1.93	3.44 ^b	3.50
0.742	3.07	5.51 ^b	5.34
0.0569	2.62	4.54 ^b	4.50
0.300	18.07	26.2	27.5
0.272	8.78	15.7	16.4
0.260	5.21	11.3	11.0
0.247	1.72	4.45	4.33
0.368	47.4	56.0	55.0
0.325	27.6	36.3	37.1

^a Median deviation: 1.9%. ^b Average of two runs.

served that for initial H_3PO_2 concentrations greater than about 0.1 M , the rate constants increased with time elapsed since purification of the acid. We used H_3PO_2 within three weeks of purification; Haight, *et al.*, used reagent chemicals without further purification.

The mechanism proposed by Haight, *et al.*, involved formation of the anhydride complex, protonation of the complex, and abstraction of a phosphinic proton from the complex by basic species in solution with reduction to Cr(IV). This mechanism is consistent with the present rate with these modifications. The k_0 term may correspond either to reaction of the unprotonated complex involving an indeterminate number of solvent molecules or to abstraction from the neutral, protonated complex of a phosphinic proton by hydroxide ion. The second-order rate constant for this latter process would be near to or less than the diffusion-controlled limit if the acid dissociation quotient of the protonated form of the Cr(VI)-P(I) complex is less than about 10. Direct abstraction of a phosphinic proton from H_3PO_2 by HCrO_4^- is also consistent with the kinetics but is thought unlikely because of the relatively weak basicity of bichromate ions and the unfavorability of transferring another negative charge to the HCrO_4^- moiety.

The k_2 term is too large to attribute solely to the changes in activity coefficients typically found in proceeding from 1 F LiClO_4 to 1 F HClO_4 ,^{8,9} although there

(5) J. Y. Tong, *Inorg. Chem.*, **3**, 1804 (1964).

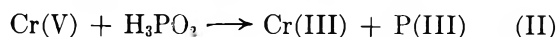
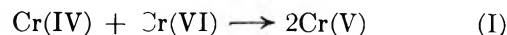
(6) J. H. Espenson and D. F. Dustin, *ibid.*, **8**, 1760 (1969).

(7) R. A. Robinson and R. H. Stokes, "Electrolyte Solutions," Butterworth and Co. Ltd., London, 1959, p 491.

may be some contribution from this effect. Mechanistically, a second-order term in hydrogen ion concentration corresponds to the formation of a doubly protonated complex $H_4PCrO_5^+$, followed by proton abstraction by water. We have no independent evidence for the formation of such a species, but studies on the exchange of the phosphinic protons in hypophosphorous acid¹⁰ show the reaction to be acid catalyzed, suggesting a transient species, $H_4PO_2^+$, whose structure would be analogous to $H_4CrPO_5^+$ formed prior to or during the rate-determining reduction of Cr(VI) in the k_2 step.

The principal phosphorus product is P(III); the ratio, total P(III)/Cr, is 1.55 ± 0.05 . The Cr(III) product is green and is not displaced from an acidic cation exchange column by barium perchlorate. The product band is somewhat spread out by cerium perchlorate but $Cr^{3+}(aq)$, when added to the column after a sample of the product, passes through the product band under cerium displacement. We interpret this as indicating complex Cr(III) products with ionic charge greater than or equal to +3.^{8,11} In all cases both P(I) and P(III) were found in the cationic product. The reaction is exothermic and the ratios of bound P(I) and P(III) were somewhat scattered as is shown in Table IV, diminishing with increasing reaction time and the

In terms of the fast steps, I and II, presumed to follow the rate-determining reduction of Cr(VI) to Cr(IV)



nonoxidative ligand capture implies that coordination of Cr(V), and perhaps Cr(IV), is as fast as or faster than reduction of Cr(V). On the basis of crystal field energies, Cr(IV) and Cr(V) ought to be substitution labile. Their high formal charges may well encourage rapid and extensive coordination, and steps I and II may involve several substituted Cr species.

Acknowledgments. The author expresses thanks to Professor G. P. Haight, Jr., for his thoughtful comments and to the Research Corporation and Bucknell University for grants in partial support of this work.

Table IV: Variation of P(I) and P(III) in the Product Cr(III) Complex

Reactant concn, F	Reaction time, hr	Temp, °C	P(I)/Cr	P(III)/Cr
0.02	3	30	1.2 ± 0.2	1.3 ± 0.1
0.02	10	30	...	1.0 ± 0.1
0.02	45	30	...	0.7 ± 0.1
0.2	1	70	0.4 ± 0.1	0.7 ± 0.1

elevated temperatures produced at higher reactant concentrations. The reported rate of hydrolysis of $Cr(H_2PO_2)^{2+}$ in acidic media⁸ suggests that the diminution of these ratios with increasing reaction time and temperature may be attributed to partial hydrolysis of the product. The apparent ionic charge of +3 or greater may be due to the formation of polynuclear complexes; or alternatively, protonated mononuclear complexes, such as have been reported for Cr(III)-acetate¹² and Cr(III)-cyanide,¹³ may be formed. The weak basicity of hypophosphite and phosphite ions does not appear to support this latter interpretation and the study of the $Cr(H_2PO_2)^{2+}$ hydrolysis showed little evidence for such a species under cation column conditions. The nonoxidative capture of a ligand during the reduction of Cr(VI) has been observed in other systems,¹⁴ specifically in the reduction with hydrazine in the presence of EDTA.¹⁵

- (8) J. H. Espenson and D. E. Binaw, *Inorg. Chem.*, **5**, 1365 (1966).
- (9) T. W. Newton and F. B. Baker, *J. Phys. Chem.*, **67**, 1425 (1963).
- (10) W. A. Jenkins and D. M. Yost, *J. Inorg. Nucl. Chem.*, **11**, 297 (1959); A. Fratiello and E. W. Anderson, *J. Amer. Chem. Soc.*, **85**, 519 (1963).
- (11) J. E. Finholt, K. G. Caulton, and J. W. Libbey, *Inorg. Chem.*, **3**, 1801 (1964).
- (12) E. Deutsch and H. Tautz, *ibid.*, **7**, 1532 (1968).
- (13) D. K. Wakefield and W. P. Schaap, *ibid.*, **8**, 512 (1969).
- (14) This was pointed out by Professor G. P. Haight, Jr.
- (15) M. T. Beck and I. Bardi, *Acta Chim. Acad. Sci., Hung.*, **29**, 3 (1961).

Medium Effects on Hydrogen-1 Chemical Shift of Benzene in Micellar and Nonmicellar Aqueous Solutions of Organic Salts^{1a}

by John E. Gordon,^{1b} J. Colin Robertson, and Robert L. Thorne

Woods Hole Oceanographic Institution, Woods Hole, Massachusetts 02543, and Department of Chemistry, Kent State University, Kent, Ohio 44240 (Received August 22, 1969)

The nature of the medium experienced by molecules in micelles is a subject of considerable interest. An elegant application of nuclear magnetic resonance to this problem has been made by Muller and Birkhahn,² who prepared systems containing appropriate fluorine tags in surfactant and solubilized nonelectrolyte molecules and used ¹⁹F spectra to study the

(1) (a) Contribution No. 2372 from the Woods Hole Oceanographic Institution. (b) Department of Chemistry, Kent State University, Kent, Ohio 44240.

(2) N. Muller and R. H. Birkhahn, *J. Phys. Chem.*, **71**, 957 (1967); **72**, 583 (1968).

medium effects. The medium effects in ^1H spectra are very much smaller. Nevertheless, Eriksson and Gillberg³ have made use of the anomalous aromatic solvent-solute shift to probe the intramicellar medium *via* ^1H spectra using the shifts of solubilized benzene.

Muller and Birkhahn² characterized the medium bathing a surfactant or solubilized molecule by a variable Z ranging between zero (pure water) and 1 (pure saturated hydrocarbon). Z is defined by eq 1 where $\delta_{\text{H}_2\text{O}}$ and δ_{hc} are the chemical shifts of a solute in water

$$Z = (\delta_{\text{mic}} - \delta_{\text{H}_2\text{O}}) / (\delta_{\text{hc}} - \delta_{\text{H}_2\text{O}}) \quad (1)$$

and alkane solvents, and δ_{mic} is that of the solute within the micelle. Results for fatty acid soaps indicate an intramicellar medium about halfway between water and saturated hydrocarbon ($Z \approx 0.5$). Eriksson and Gillberg³ did not employ a formal solvent parameter, but their benzene shifts indicate that the micelle interior in 0.1749 *M* cetyltrimethylammonium bromide is still more highly aqueous than that of the fatty acid soaps.

We have now extended the ^1H chemical shift measurements on solubilized benzene to include an anionic and a neutral surfactant and the effects of concentration and added electrolyte on the former. Particular attention has been devoted to separating the observed average shifts for solubilized benzene into intra- and extramicellar components and thus estimating Z for these systems. The dependence of δ_{obsd} on benzene concentration has been semiquantitatively accounted for. Finally, the medium experienced by benzene salted in by the lower symmetrical tetraalkylammonium bromides has been compared with that in micellar solubilization.

Experimental Section

The salts and water employed have been described previously.⁴ Sodium decanoate solutions were prepared by neutralizing Eastman White Label decanoic acid with standard sodium hydroxide. Polyoxyethylene(23) lauryl ether (Brij 35) was a gift of Atlas Chemical Industries, Inc., and was used as received. Organic liquids were Fisher Certified materials except Spectro Grade cyclohexane (Matheson Coleman and Bell). Nmr measurements were made on a Varian A-60A spectrometer whose probe temperature was 41°. Line positions were measured by the audio-sideband technique using Hewlett-Packard 200CD oscillator and 521C frequency counter. The calibration and replication routine has been described.⁵ Each benzene-reference separation has an associated precision of ~ 0.06 Hz except for the lowest benzene concentrations and the externally referenced measurements where it is no better than 0.1 Hz at 60 MHz. Externally referenced measurements were made relative to cyclohexane in a Wilmad precision coaxial

cell. Light absorption was measured using a Cary 14 spectrophotometer.

An aqueous solution of references, surfactant, and/or other addend was first prepared (solution I). The most concentrated benzene solution in each series was prepared by contacting solution I with excess benzene in a vessel which allowed withdrawal of the aqueous phase from the bottom by means of syringe, needle, and septum. The benzene concentration in this stock solution was determined from the optical density measured at 247.5, 255, and/or 259 $\text{m}\mu$. Dilutions of the stock solution with solution I were made by weight directly in the withdrawing syringe, whose contents were mixed using a minute glass-enclosed stirring bar. The resulting solution was injected into an nmr cell which was equilibrated in the probe for 20 min before measurement. Susceptibility corrections were applied to the externally referenced measurements as previously described;⁵ the benzene and references were ignored in computing the correction.

The chemical shift of benzene was measured in water and the various aqueous electrolyte and surfactant solutions relative to a battery of four internal references: $(\text{CH}_3)_4\text{N}^+$, $(\text{CH}_3)_2\text{S}\rightarrow\text{O}$ (DMSO), CH_3CN (AN), and $(\text{CH}_3)_3\text{COH}$. Previous work⁵ has shown that two of these, DMSO and AN, show normal behavior in aqueous solutions containing inorganic and organic salts, low concentrations of other nonelectrolytes, and potassium perfluorobutyrate in the region of the critical micelle concentration. These reference molecules appear not to enter the micelle phase appreciably. The other references agreed generally with AN and DMSO but showed occasional evidence of specific interactions with the other solutes as noted before.⁵ To determine the limiting shift of benzene in cyclohexane *vs.* the same referencing system, the aqueous solution of AN, DMSO, etc., was used as external reference.

Results and Discussion

The benzene shifts observed for a fivefold variation in benzene molarity within the range $0.004 \leq M^{\text{C}_6\text{H}_6} \leq 0.16$ were linear in $M^{\text{C}_6\text{H}_6}$ for all solutions studied; they were fitted to eq 2 by least squares. The limiting shifts δ_0 and the slopes a are summarized in Table I.

$$\delta = \delta_0 + aM^{\text{C}_6\text{H}_6} \quad (2)$$

Agreement between the two references is good. The observed separation, 18.20 Hz at 60 MHz, of δ_0 in water and cyclohexane agrees reasonably well with that of Eriksson and Gillberg,³ 17.1 Hz.

Z Values. We have interpreted the results of Ta-

(3) J. C. Eriksson and G. Gillberg, *Acta Chem. Scand.*, **20**, 2019 (1966).

(4) J. E. Gordon and R. L. Thorne, *J. Phys. Chem.*, **71**, 4390 (1967).

(5) J. E. Gordon and R. L. Thorne, *ibid.*, **73**, 3643 (1969).

Table I: Benzene Chemical Shift Data for Various Media

Solvent	Additive	Additive concn., M	Ref	$\delta_0^{a,b}$	$\delta^{b,c}$	$Z^{b,d}$	Z (cor) ^e
H ₂ O			AN	322.18 ± 0.25	14 ± 17		
			DMSO	283.32 ± 0.23	13 ± 15		
			H ₂ O	164.7 ^f			
H ₂ O	NaCl	1.00	AN	322.01 ± 0.04	-0.6 ± 5		
			DMSO	283.39 ± 0.01	-7 ± 2		
C ₆ H ₁₂			AN	303.99 ± 0.21	-2.23 ± 0.18		
			DMSO	265.12 ± 0.15	-2.16 ± 0.13		
			H ₂ O	147.6 ^f			
H ₂ O	Cetyltrimethylammonium bromide	0.1729	H ₂ O	162.2 ^f		0.15	0.18
H ₂ O	Sodium decanoate	0.200	AN	319.10 ± 0.01	-50.9 ± 0.5	0.17 ± 0.01	0.29
			DMSO	280.27 ± 0.02	-52.8 ± 0.8	0.17 ± 0.01	
H ₂ O	Sodium decanoate	0.400	AN	317.13 ± 0.14	-30.8 ± 1.4	0.28 ± 0.01	0.33
			DMSO	278.19 ± 0.16	-34.4 ± 1.6	0.28 ± 0.01	
H ₂ O	Sodium decanoate + NaCl	0.400	AN	312.86 ± 0.25	-47.3 ± 2.7	0.51 ± 0.02	0.55
			DMSO	273.79 ± 0.28	-51.8 ± 3.1	0.52 ± 0.02	
H ₂ O	Polyoxyethylene(23) lauryl ether	2.08 × 10 ⁻³	AN	321.80 ± 0.04	+24.0 ± 4.1	0.02 ± 0.01	0.06-
			DMSO	282.88 ± 0.07	+29.4 ± 5.1	0.02 ± 0.01	0.16
H ₂ O	(CH ₃) ₄ N ⁺ Br ⁻	1.00	AN	322.33 ± 0.10	-2.1 ± 6.3	-0.01 ± 0.01	
			DMSO	283.76 ± 0.11	+0.4 ± 6.5	+0.02 ± 0.01	
H ₂ O	(CH ₃) ₄ N ⁺ Br ⁻ + NaCl	1.00	AN	321.97 ± 0.03	+5.3 ± 2.6	+0.01 ± 0.01	
			DMSO	283.44 ± 0.03	+12.8 ± 2.4	-0.01 ± 0.01	
H ₂ O	(C ₄ H ₉) ₄ N ⁺ Br ⁻	0.500	AN	322.33 ± 0.09	-5.8 ± 4.0	-0.01 ± 0.01	
			DMSO	284.07 ± 0.04	-4.6 ± 2.0	-0.04 ± 0.01	
H ₂ O	(C ₄ H ₉) ₄ N ⁺ Br ⁻	1.00	AN	320.70 ± 0.04	-5.9 ± 0.54	+0.08 ± 0.01	
			DMSO	283.51 ± 0.04	-9.1 ± 0.52	-0.01 ± 0.01	
H ₂ O	(C ₄ H ₉) ₄ N ⁺ Br ⁻ + Na ₂ SO ₄	0.500	AN	321.25 ± 0.08	-8.5 ± 2.7	+0.05 ± 0.01	
			DMSO	283.42 ± 0.08	-10.0 ± 2.6	-0.01 ± 0.01	
H ₂ O	(C ₄ H ₉) ₄ N ⁺ Br ⁻ + NaCl	1.00	AN	318.94 ± 0.05	-8.5 ± 0.35	+0.18 ± 0.01	
			DMSO	281.92 ± 0.06	-12.5 ± 0.41	0.08 ± 0.01	

^a In hertz downfield from reference (60 MHz). ^b Precision measure is standard deviation. ^c Equation 2. ^d Equation 1. ^e See text. ^f Reference 3.

ble I in terms of the model^{6,7} of solubilization as distribution between bulk solvent and a micellar pseudo-phase. To reduce the data to Z values one needs to take into account the contribution of benzene in the aqueous phase to the observed shift, according to eq 3, where $X_1^{C_6H_6}$ is the fraction of benzene in

$$\delta_{\text{obsd}}^{C_6H_6} = X_{\text{aq}}^{C_6H_6} \delta_{\text{aq}}^{C_6H_6} + X_{\text{mic}}^{C_6H_6} \delta_{\text{mic}}^{C_6H_6} \quad (3)$$

phase i.⁸ Since our extrapolation involves measurements at low benzene concentrations, we cannot place an upper limit on $X_{\text{aq}}^{C_6H_6}$ on the basis that the observed concentrations are large multiples of the solubilize solubility in pure water as has been done in other systems;⁹ an estimate of the partition coefficient is required. The reported value of the distribution coefficient for benzene between olive oil and water, 164,¹⁰ suggests that a large fraction of the benzene will be in the micelles. We determined the benzene distribution coefficient for cyclohexane-water spectrophotometrically to be 3.2×10^2 at $M_{\text{aq}}^{C_6H_6} = 1.4 \times 10^{-4}$ and $25 \pm 1^\circ$. The distribution coefficient for micelle-water was approximated by eq 4, and

$$K_{\text{mic-aq}}^{C_6H_6} = K_{C_6H_{12}\text{-aq}}^{C_6H_6} Z \quad (4)$$

$K_{\text{mic-aq}}^{C_6H_6}$ was computed from the uncorrected values of Z in column 7 of Table I. Using or estimating surfactant partial molal volumes from the literature,¹¹ the volume ratio of the two phases and (combining with $K_{\text{mic-aq}}^{C_6H_6}$) $X_{\text{aq}}^{C_6H_6}$ and $X_{\text{mic}}^{C_6H_6}$ were computed. From these $\delta_{\text{mic}}^{C_6H_6}$ and Z could be obtained via eq 3 and 1. The new value of Z was used in eq 4 to start a second approximation, and self-consistency was achieved in ~ 5 cycles. In the case of sodium decanoate, where the cmc is large, correction was made for the effect of 0.098 M monomer on the activity

(6) M. E. L. McBain and E. Hutchinson, "Solubilization," Academic Press, New York, N. Y., 1955, p 75.

(7) P. H. Elworthy, A. T. Florence, and C. B. Macfarlane, "Solubilization by Surface Active Agents," Chapman and Hall, Ltd., London, 1968, Chapter 2, p 48 ff.

(8) Exchange of solubilize between micellar and bulk phases is rapid on the nmr time scale: T. Nakagawa and K. Tori, *Kolloid-Z.*, **194**, 143 (1964).

(9) A. S. Waggoner, O. H. Griffith, and C. R. Christensen, *Proc. Natl. Acad. Sci. U. S.*, **57**, 1198 (1967).

(10) R. Macy, *J. Ind. Hyg. Toxicol.*, **30**, 140 (1948); *Chem. Abstr.*, **42**, 6619 (1948).

(11) (a) L. Benjamin, *J. Phys. Chem.*, **70**, 3790 (1966); (b) P. Becher, *J. Colloid Sci.*, **16**, 491 (1951).

coefficient of benzene.¹²⁻¹⁴ In the sodium decanoate-NaCl solutions correction for the effect of the NaCl on $\gamma_{\text{aq}}^{\text{C}_6\text{H}_6}$ was included,¹⁴ and the concentration of monomer (=cmc) was taken as 0.02 M.¹⁵ It is difficult to estimate the success of the above procedure; eventually it may be possible to determine $K_{\text{mic-aq}}^{\text{C}_6\text{H}_6}$ more directly. However, the correction is large only for the smallest Z values; Z for polyoxyethylene(23) lauryl ether is poorly defined, but definitely small.

Although the $X_{\text{aq}}^{\text{C}_6\text{H}_6}$ values (Table III) and the uncorrected Z values for 0.2 and 0.4 M sodium decanoate are rather different, the corrected Z values, 0.29 and 0.33, are gratifyingly similar. The mean value, 0.31, differs significantly from those observed *via* ¹⁹F spectra using C₆H₅CF₃ in 0.05 M sodium dodecanoate ($Z = 0.52$) and sodium decanoate ($Z \approx 0.45$).¹⁶ Muller and Birkhahn² observed no effect of 0.2-0.6 M NaCl on the measured Z . In contrast, 1 M NaCl produces a substantial increase in Z obtained from the benzene shifts (Table I), and the effect of the salt is also reflected in the slope a (see below). We suspect that the differences in Z as observed by ¹⁹F *vs.* ¹H chemical shifts reflect inherent differences in the response of the two probes, due in part to differences in the shielding mechanisms of the two nuclei. Further, it is unlikely that Z is either precisely linear in the intramicellar medium composition ($\delta^{\text{C}_6\text{H}_5\text{CF}_3}$ is not a linear function of composition in aqueous ethanol) or dependent on medium composition alone (electrostatic effects probably contribute).

The available Z values are listed in Table II.¹⁷⁻¹⁹ The highly aqueous intramicellar medium indicated is not so surprising if one recalls that in spherical

micelles of optimum size for reduction of hydrocarbon-water contact (micelle number perhaps 50) about 75% of the surface of the sphere must be made up of the hydrocarbon portions of the surfactant molecules.²⁰ Smaller spherical micelles shield the hydrocarbon chains still less well, and larger ones in which the radius significantly exceeds the length of a surfactant molecule would result either in voids or in submergence of water or hydrated polar head groups in the micelle interior. Hydrodynamic evidence interpreted on a spherical model by Courchene²¹ indicates 33-51 vol % water in sodium dodecyl sulfate and dimethylalkylamine oxide micelles. In the traditional micelle models, which have perpetuated a static and regular picture of micellar structure, this water is assumed to be segregated in an aqueous rind at the micellar surface. Magnetic resonance data now indicate much more fluctuant aggregates⁹ undergoing rapid exchange with bulk phase monomer and solubilize, possessing short correlation times for intramicellar molecules, and, according to the Z values, displaying much more scrambling of hydrocarbon and aqueous components than heretofore supposed.

The data of Table II suggest a possible trend of increasing Z with decreasing micelle size, which can be evaluated only as more comparisons of ¹⁹F and ¹H nmr, esr, and optical measurements for the same systems become available. This could correspond to increasing water penetration with increasing micelle size. Resolution of the conflicting ¹⁹F and ¹H results may help elucidate the effect of added electrolyte on micelle structure.²

Slopes. The larger values of Z are accompanied by enhanced negative slopes, a , in eq 2. We interpret a

Table II: Values of Z and Micelle Size Parameters

Surfactant	Z	n^a	M^b
Polyoxyethylene(23) lauryl ether	0.06-0.16 ^c	40 ^d	48,800 ^d
Hexadecyltrimethylammonium bromide	0.18 ^c	80 ^e	29,000 ^e
Sodium dodecyl sulfate	0.20-0.22 ^f	62 ^g	18,000 ^g
Sodium dodecanoate	0.52 ^h	50 ⁱ	11,900 ⁱ
Sodium decanoate	0.29-0.33 ^c	~28 ^j	~5,400 ^j
Sodium decanoate-1 M NaCl	~0.45 ^h 0.55 ^c		

^a Micelle number. ^b Micellar weight. ^c Table I. ^d Reference 11b. ^e H. V. Tartar, *J. Colloid Sci.*, **14**, 115 (1959). ^f From esr coupling constants and electronic absorption maxima of solubilized nitroxide probes⁹ *via* an equation analogous to eq 1. ^g R. J. Williams, J. N. Phillips, and K. J. Mysels, *Trans. Faraday Soc.*, **51**, 728 (1955). ^h Reference 2. ⁱ For potassium dodecanoate: E. Hutchinson and J. C. Melrose, *Z. Phys. Chem.* (Frankfurt am Main), **2**, 363 (1954). ^j Estimated from log (cmc) *vs.* n plots for RSO₃⁻Na⁺, ROSO₃⁻Na⁺, and RN(CH₃)₃⁺Br⁻, the known cmc and n for potassium dodecanoate,¹ and the cmc for sodium decanoate: H. B. Klevens, *J. Phys. Chem.*, **52**, 130 (1948).

(12) The Setschenow constant for the aqueous sodium decanoate-naphthalene system,¹³ together with the relationship of Setschenow constants for benzene¹⁴ and naphthalene,⁴ was used to estimate $\gamma_{\text{aq}}^{\text{C}_6\text{H}_6}$, and $K_{\text{C}_6\text{H}_5\text{CF}_3\text{-aq}}^{\text{C}_6\text{H}_6} \times \gamma_{\text{aq}}^{\text{C}_6\text{H}_6}$ was substituted for $K_{\text{C}_6\text{H}_5\text{CF}_3\text{-aq}}^{\text{C}_6\text{H}_6}$ in eq 4.

(13) J. E. Gordon and R. L. Thorne, *Geochim. Cosmochim. Acta*, **31**, 2433 (1967).

(14) W. F. McDevit and F. A. Long, *J. Amer. Chem. Soc.*, **74**, 1773 (1952).

(15) S. H. Herzfeld, *J. Phys. Chem.*, **56**, 953, 959 (1952).

(16) From reference 2. The dodecanoate value is from C₆H₅CF₃ shifts extrapolated to zero C₆H₅CF₃ concentration (three measurements ≥ 0.014 M). The decanoate value was estimated using the measured value (0.47) at 0.063 M and the Z *vs.* M slope from the dodecanoate measurements.

(17) Another potential measure of hydrocarbon-water contact in micelles is the partial molal volume increase on micellization, ΔV_m , which is attributed to water-structure loss on transfer of hydrocarbon chains from an aqueous to a less aqueous environment. Several ΔV_m values are known^{18,19} but the expansion expected for transfer from water to hydrocarbon solvent, $\Delta V_{\text{aq} \rightarrow \text{hc}}$, can only be roughly estimated¹⁹ for chains longer than propyl, so that Z cannot be meaningfully compared with $\Delta V_m / \Delta V_{\text{aq} \rightarrow \text{hc}}$ at present.

(18) J. M. Corkill, J. F. Goodman, and T. Walker, *Trans. Faraday Soc.*, **63**, 768 (1967).

(19) G. Nemethy and H. A. Scheraga, *J. Chem. Phys.*, **36**, 3401 (1962).

(20) A. F. H. Ward, *Proc. Roy. Soc.*, **A176**, 412 (1940).

(21) W. L. Courchene, *J. Phys. Chem.*, **68**, 1870 (1964).

Table III: Concentration Dependence of Benzene Shifts in Aqueous Sodium Decanoate Solutions

	Effective $V_{mic}^0 = 178.4$ ml/mol			Effective $V_{mic}^0 = 133.8$ ml/mol		
	0.2 M NaC ₁₀	0.4 M NaC ₁₀	0.4 M NaC ₁₀ + 1 M NaCl	0.2 M NaC ₁₀	0.4 M NaC ₁₀	0.4 M NaC ₁₀ + 1 M NaCl
$X_{mic}^{C_6H_6}$ ^a	0.588	0.835	0.947	0.538	0.797	0.930
Z	0.29	0.33	0.55	0.32	0.35	0.56
a (calcd) ^b	-42	-28	-29	-47	-35	-37
a (obsd) ^c	-52	-32	-50	-52	-32	-50

^a Fraction of benzene in micellar pseudophase. ^b Equation 5. ^c Mean of AN and DMSO data.

as an index of the degree of restriction of solute (benzene) to a volume smaller than the nominal solution volume. The benzene chemical shift moves relatively rapidly (and linearly) to higher field with increasing benzene concentration in nonaromatic solvents²² (anomalous aromatic solvent-solute shift). The large negative a in aqueous surfactants relative to that in, e.g., cyclohexane results from the intramicellar benzene concentration being much higher than the nominal solution concentration. We have tested this model quantitatively, taking the $\delta_{mic}^{C_6H_6}$ vs. $M_{mic}^{C_6H_6}$ slope equal to that which we observed for benzene in cyclohexane (the anomalous aromatic shifts are approximately independent of the aliphatic solvent).²² From the micellar and aqueous-phase volumes, the values of $X_{aq}^{C_6H_6}$ and $X_{mic}^{C_6H_6}$ used previously, and eq 5

$$\delta^{C_6H_6} = \delta_0^{C_6H_6} + (X_{aq}^{C_6H_6} R_{aq}^{C_6H_6} + X_{mic}^{C_6H_6} R_{mic}^{C_6H_6})(-2.20)M^{C_6H_6} \quad (5)$$

one computes for sodium decanoate the slopes given in Table III. $R_i^{C_6H_6}$ is the ratio of benzene concentration in phase i to the nominal benzene concentration, $M^{C_6H_6}$. The calculated slopes are of the correct magnitude but are consistently low because the entire micellar volume is not available to the solubilizate; the head-group volume should be excluded. When this is done approximately by reducing the micellar volume by $3/12 = (\text{head group C} + \text{O atoms})/(\text{total C} + \text{O atoms})$ the values on the right of Table III are obtained, and agreement with the experimental values is reasonably good in the absence of added electrolyte. The fairly large positive slope observed in aqueous polyoxyethylene(23) lauryl ether implies a unique structural situation for benzene in these solutions.

Symmetrical Quaternary Ammonium Salts. Organic nonelectrolytes are salted in (γ decreased, solubility increased) by simple organic salts in aqueous solution. While this has been attributed to salt-induced medium effects,^{14,23} other evidence has been interpreted in terms of direct organic salt-nonelectrolyte interactions.^{4,24} Most of the salts are nonsurfactant-like, e.g., $(C_2H_5)_4N^+Br^-$, in lacking polar and nonpolar ends. However, cmc behavior (at 0.039 M) has been reported for $(n-C_4H_9)_4N^+Br^-$,²⁵ and the partial molal

volume data have been interpreted in terms of aggregation of groups of several R_4N^+ and Br^- in overlapping clathrate-like water cages²⁶ and in terms of micelle formation.²⁷ Exaltation of salting in by $R_4N^+Br^-$ is produced by addition of inorganic salt; this is reminiscent of enhanced solubilization in micellar system.⁴

We attempted to get some information on the medium experienced by benzene salted in by the lower $R_4N^+Br^-$ using the Z -value approach; results for several systems are shown in Table I. The results are characterized by small Z values, by relatively poor agreement between the data vs. the two references, and by some enhanced slopes. Only in the case of 1 M $(n-C_4H_9)_4N^+Br^-$ 1 M NaCl does the Z value indicate an environment convincingly more hydrocarbon-like than water, but the enhanced slopes do imply segregation of benzene in the presence of inorganic salt. We hope to test more stringently these indications of direct R_4N^+ -benzene interactions by measurements employing external referencing and ¹⁹F shifts.

Acknowledgment. This work was supported in part by National Science Foundation Grant GA 1261 and in part by a Kent State University faculty summer research fellowship to J. E. G.

(22) A. A. Bothner-By and F. E. Glick, *J. Chem. Phys.*, **26**, 1651 (1957).

(23) N. C. Deno and C. H. Spink, *J. Phys. Chem.*, **67**, 1347 (1963).

(24) E. F. J. Duynstee and E. Grunwald, *Tetrahedron*, **21**, 2401 (1965).

(25) S. Lindenbaum and G. E. Boyd, *J. Phys. Chem.*, **68**, 911 (1964).

(26) W.-Y. Wen and S. Saito, *ibid.*, **68**, 2639 (1964).

(27) H. E. Wirth, *ibid.*, **71**, 2322 (1967).

A Convenient Method for Obtaining Free Energies of Activation by the Coalescence Temperature of an Unequal Doublet

by H. Shanan-Atidi and K. H. Bar-Eli

Department of Chemistry, Tel-Aviv University, Tel-Aviv, Israel
(Received July 21, 1969)

A well-known method of obtaining information about free energy of activation by nmr is that using the coales-

cence temperature. (The coalescence temperature is the temperature at which the two peaks of the doublet merge into one, *i.e.*, the "valley" between the two separate peaks disappears.) Usually, one deals with coalescence of an equal doublet. The case of an unequal doublet occurs less often and the literature does not describe a simple formula to use in this case. We present here a simple graph which may be used easily and conveniently in order to find out the free energies of activation of any two exchanging species. Using the coalescence method, one finds the temperature T_c in which the two signals coalesce into one. In case of an equal doublet, this occurs when the condition $\delta\nu\tau = \sqrt{2}/2\pi$ is satisfied,¹ where $\delta\nu$ is the shift between the lines at very slow exchange in cps and τ is defined by the relation $1/\tau = (1/\tau_A) + (1/\tau_B)$ when τ_A and τ_B are the lifetimes of species A and B, respectively. The above condition is true only when $\tau_A = \tau_B$ and thus the exchange rate is $k = 1/2\tau$.

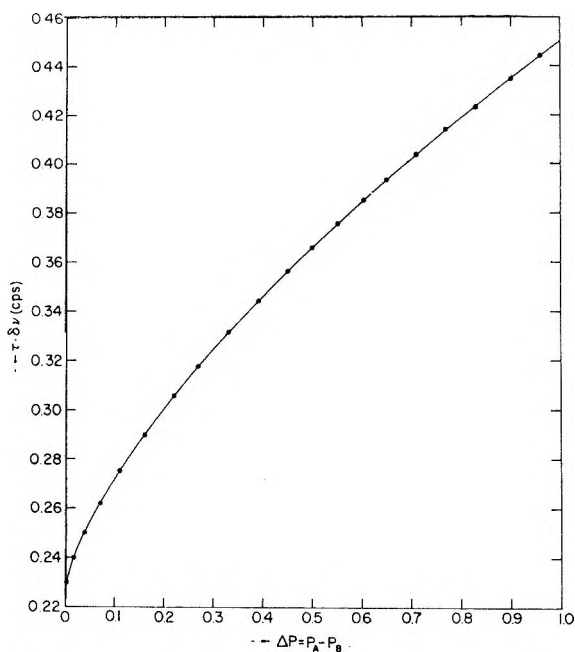


Figure 1. Calculated values of $\tau\delta\nu$ vs. ΔP from eq 1.

The method of Lynden-Bell² gives a simple way to find the coalescence condition for any values of P_A and P_B —the relative concentration of species A and B, respectively, when $\tau_A \neq \tau_B$.

Equation 33 of the above-mentioned paper reads

$$f(\omega) = (\omega_A - \omega)(\omega_B - \omega)(2\omega - \omega_A - \omega_B) + \tau^{-2}(\omega - \bar{\omega})$$

where ω_A and ω_B are the frequencies of species A and B with no exchange, and $\bar{\omega}$ is their weighted average: $\bar{\omega} = P_A\omega_A + P_B\omega_B$. The solutions of the equation $f(\omega) = 0$ give us the frequencies of the maxima and minima of the line shape; for instance, when there is no

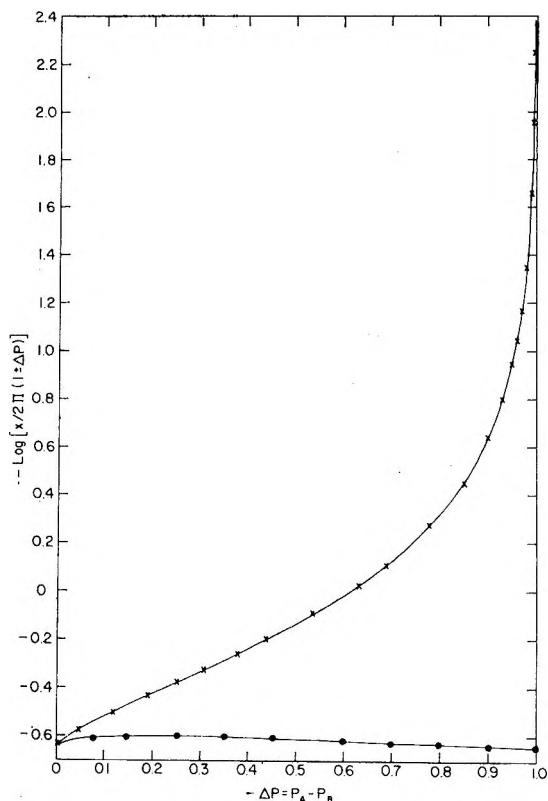


Figure 2. $\text{Log} [X/2\pi(1 \pm \Delta P)]$ vs. ΔP (eq 6 and 7): \times , $\text{log} [X/2\pi(1 - \Delta P)]$; \bullet , $\text{log} [X/2\pi(1 + \Delta P)]$.

exchange, *i.e.*, τ is very long, the solutions are $\omega = \omega_A$ and $\omega = \omega_B$; that is, the resonance peaks fall at ω_A and ω_B . The third solution is the minimum between the peaks. When the exchange is very fast, *i.e.*, τ is very short, the solution is $\omega = \bar{\omega}$, *i.e.*, a single peak which falls at the weighted average of A and B. Between these two extreme situations, there will be a value of τ which will cause $f'(\omega) = f(\omega) = 0$, *i.e.*, which will make two of the roots of $f(\omega) = 0$ to coincide. This, therefore, must be the coalescence criterion and it leads to the result³

$$P_A - P_B = \Delta P = \left(\frac{X^2 - 2}{3} \right)^{3/2} \frac{1}{X} \quad (1)$$

where $X = 2\pi\delta\nu\tau$. Figure 1 shows the graph of $X/2\pi$ vs. ΔP computed for all possible values of the parameters.

(1) J. A. Pople, W. G. Schneider, and H. J. Bernstein, "High-Resolution Nuclear Magnetic Resonance," McGraw-Hill Book Co., Inc., New York, N. Y., 1959, p 223.

(2) R. M. Lynden-Bell, "Progress in NMR Spectroscopy," Vol. 2, J. W. Emsley, J. Feeney, and L. H. Sutcliffe, Ed., Pergamon Press, New York, N. Y., 1967, p 163.

(3) It should be noted that the result given in the above-mentioned paper eq 34 is incorrect, since it does not extrapolate to the correct equation when $\tau_A = \tau_B$. The reason for this discrepancy is that the author used only the first term, *i.e.*, $g(\omega) = (\omega_A - \omega)(\omega_B - \omega)(2\omega - \omega_A - \omega_B)$, and found the criterion for which $g'(\omega) = f(\omega) = 0$.

The reaction rates are k_A and k_B which obey $k_A P_A = k_B P_B$ and since $k_A = \tau_A^{-1}$ and $k_B = \tau_B^{-1}$, one readily finds

$$k_A = \frac{1}{2\tau}(1 - \Delta P); \quad k_B = \frac{1}{2\tau}(1 + \Delta P) \quad (2)$$

The value of the free energy of activation can be deduced using Eyring's⁴ expressions, *i.e.*

$$\Delta G_A^\ddagger = RT_c \ln \left[\frac{k(T_c)}{h\pi(\delta\nu)} \left(\frac{X}{1 - \Delta P} \right) \right] \quad (3)$$

$$\Delta G_B^\ddagger = RT_c \ln \left[\frac{k(T_c)}{h\pi(\delta\nu)} \left(\frac{X}{1 + \Delta P} \right) \right] \quad (4)$$

The difference between eq 3 and 4 being obviously the free energy difference between the two species, *i.e.*

$$\Delta G = RT_c \ln \frac{P_A}{P_B} = RT_c \ln \frac{1 + \Delta P}{1 - \Delta P} \quad (5)$$

When the values of the constants are introduced, one obtains the following free energies in calories per mole

$$\Delta G_A^\ddagger = 4.57T_c \left[10.62 + \log \frac{X}{2\pi(1 - \Delta P)} + \log \frac{T_c}{\delta\nu} \right] \quad (6)$$

$$\Delta G_B^\ddagger = 4.57T_c \left[10.62 + \log \frac{X}{2\pi(1 + \Delta P)} + \log \frac{T_c}{\delta\nu} \right] \quad (7)$$

The values of $\log [(X/2\pi(1 \pm \Delta P))]$ are plotted against ΔP in Figure 2 and can be used directly with the measured values of T_c and $\delta\nu$ in order to calculate the free energies of activation.

It should be noted that this, as well as the regular formula when one has equal populations, gives only the value of ΔG^\ddagger at one particular temperature, and therefore no information is obtained about ΔH^\ddagger or ΔS^\ddagger separately without a detailed analysis of the lines shapes.

A detailed line-shape analysis will obviously give a more accurate result. However, since it is more time consuming, there is a considerable advantage of using the above short-cut method. A detailed analysis is also required when the lines are wide compared to their separation.

Conductance Measurements of Thallium Perchlorate and Fluoroborate in Acetonitrile

by Howard L. Yeager and Byron Kratochvil

Department of Chemistry, University of Alberta, Edmonton, Alberta, Canada (Received September 18, 1969)

Conductance measurements of several copper(I) and silver(I) salts in acetonitrile have been reported previously.¹ The stabilization of these metal ions by acetonitrile is indicated by their tetrafluoroborate and perchlorate salts being essentially unassociated. In contrast, the alkali metal perchlorates have association constants in the range of 10–20 in this solvent.² To extend the study of solvation of univalent metal ions by acetonitrile, a conductance investigation of thallium(I) perchlorate and tetrafluoroborate was made. Conductance results also are reported for potassium thiocyanate this salt was included to obtain the single-ion conductivity of the thiocyanate anion, which resembles the solvent molecule in size and shape.

Experimental Section

Thallium(I) perchlorate was prepared by the procedure of Coetzee and Champion³ from thallium nitrate (Fisher Purified reagent) and 72% perchloric acid (G. F. Smith Co.). The product was recrystallized three times from water and dried at 120° for 12 hr.

Thallium(I) tetrafluoroborate was prepared by slowly adding 40% fluoroboric acid (Baker and Adamson) to thallium carbonate (Alfa Inorganics, Inc.), collecting the resulting solid, and washing several times with absolute ethanol to remove excess acid. The salt partially decomposes during recrystallization from water, or upon heating the wet material. It was dried under vacuum at room temperature for 1 hr, then at 50° for 3 hr, and finally at 105° for 7 hr. Potassium thiocyanate (Fisher Certified reagent) was dried under vacuum at 50° for 2 hr.

The method of acetonitrile purification, the apparatus, and the experimental procedure are described in ref 1. All solutions were prepared by weight and vacuum corrected, and molar concentrations calculated by use of solution densities determined from the equation $d = d_0 + A\bar{m}$, where d_0 is the solvent density, d the solution density, and \bar{m} the concentration in moles of solute per kilogram of solution. The A values, determined by measuring the densities of 0.01 *M* solutions in acetonitrile with a capillary pycnometer, were 0.22, 0.22, and 0.06 for TlBF₄, TlClO₄, and KSCN. Values

(1) H. L. Yeager and B. Kratochvil, *J. Phys. Chem.*, **73**, 1963 (1969).

(2) R. L. Kay, B. J. Hales, and G. P. Cunningham, *ibid.*, **71**, 3925 (1967).

(3) J. F. Coetzee and J. J. Champion, *J. Amer. Chem. Soc.*, **89**, 2513 (1967).

(4) W. F. K. Wynne-Jones and H. Eyring, *J. Chem. Phys.*, **3**, 492 (1935).

Table I: Measured Conductances in Acetonitrile at 25°

10°C	Λ	$\Delta\Lambda$	10°C	Λ	$\Delta\Lambda$
	TIBF ₄ 10 ³ κ = 2.2			TIClO ₄ 10 ³ κ = 9.8	
5.187	189.02	0.03	5.626	183.02	0.00
8.500	185.75	-0.06	9.134	179.10	0.00
12.366	182.76	0.00	12.082	176.31	0.00
16.482	180.02	0.02	15.034	173.85	0.01
19.659	178.12	0.02	18.472	171.24	0.00
23.865	175.78	-0.05	22.121	168.72	-0.02
27.626	174.02	0.04	25.461	166.66	0.01
31.595	172.16	-0.02	29.416	164.38	0.00
	TIBF ₄ 10 ³ κ = 8.3			TIClO ₄ 10 ³ κ = 4.6	
5.249	188.64	-0.01	6.318	182.23	0.00
8.122	185.88	0.00	8.484	179.82	0.00
11.364	183.30	0.02	12.014	176.40	0.00
14.088	181.38	0.02	15.243	173.70	0.01
18.701	178.51	-0.01	17.647	171.84	-0.01
22.625	176.36	-0.01	20.898	169.55	-0.01
25.977	174.67	-0.03	25.088	166.89	0.01
30.282	172.74	0.02	30.032	164.02	0.00
	TIBF ₄ 10 ³ κ = 5.6			KSCN 10 ³ κ = 6.0	
3.995	190.14	0.00	8.053	182.66	0.00
6.647	187.29	0.01	12.288	178.79	0.00
9.354	184.88	0.00	16.504	175.54	0.00
12.118	182.74	-0.01	19.943	173.20	0.01
15.529	180.44	0.01	22.559	171.55	0.00
19.197	178.22	0.00	25.868	169.60	-0.01
23.732	175.79	0.00	30.232	167.27	0.00
				KSCN 10 ³ κ = 18.1	
			6.920	183.78	-0.01
			9.442	181.25	0.00
			12.172	178.85	0.02
			15.751	176.04	0.00
			18.658	173.98	-0.02
			22.621	171.46	-0.01
			25.594	169.74	0.01

Table II: Conductance Parameters and Averaged Conductance Values

Salt	Λ_0	d	K_A	σ_A	Λ_{av}	λ_0^+	λ_0^-
TIBF ₄	199.3 ± 0.1	3.0 ± 0.5	14 ± 2	0.04	199.1	90.7	108.4 ^a
TIBF ₄	198.95 ± 0.05	3.1 ± 0.3	14 ± 1	0.02			
TIBF ₄	199.08 ± 0.01	3.3 ± 0.1	15.4 ± 0.5	0.006			
TIClO ₄	195.12 ± 0.04	3.1 ± 0.2	32.1 ± 0.9	0.01	195.2	91.5	103.7 ^b
TIClO ₄	195.21 ± 0.03	3.1 ± 0.1	32.4 ± 0.7	0.01			
KSCN	197.00 ± 0.03	3.1 ± 0.1	26.3 ± 0.6	0.007	197.0	83.6 ^b	113.4
KSCN	196.93 ± 0.06	3.1 ± 0.4	26 ± 2	0.02			

^a Reference 1. ^b Reference 6.

used for the physical properties of acetonitrile were: density, 0.7767 g/ml;¹ viscosity, 0.003412 P;¹ and dielectric constant, 35.95.³

Results

The molar concentrations, measured equivalent conductances, and solvent specific conductances are given in Table I. Analysis of the data was by the Fuoss-Onsager theory,⁴ using their conductance equation in the form

$$\Lambda = \Lambda_0 - S(C\gamma)^{1/2} + EC\gamma \log C\gamma + JC\gamma - K_A C\gamma \Lambda f^2$$

The calculations were performed by the least-squares computer program of Kay⁵ modified for an IBM 360/67 computer.¹ The coefficients have their usual meaning.

(4) R. M. Fuoss and F. Accascina, "Electrolytic Conductance," Interscience Publishers, Inc., New York, N. Y., 1959.

(5) J. L. Hawes and R. L. Kay, *J. Phys. Chem.*, **69**, 2420 (1965).

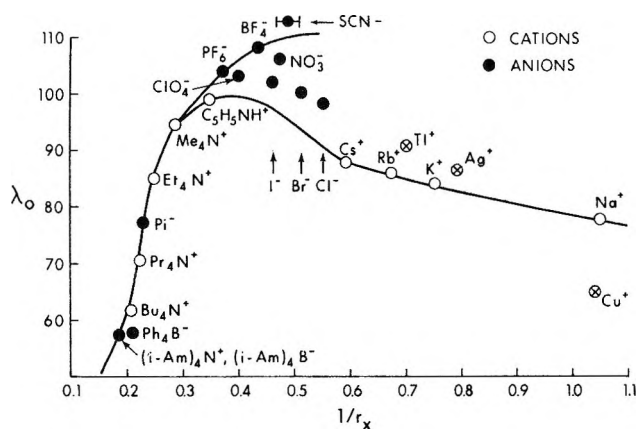


Figure 1. Single-ion conductivities in acetonitrile *vs.* reciprocal crystallographic radii.

The iterated \bar{a} obtained from the J coefficient was used in the calculation of the mean ion activity coefficient f in eq 1. The values of Λ were unweighted. Corrections for viscosity were not made. The $\Delta\Lambda$ values in Table I are the differences between the measured equivalent conductances and the values calculated from eq 1. The conductance parameters are presented in Table II, along with their standard deviations. The $\sigma\Lambda$ values are the standard deviations of the data points. Also tabulated are averaged limiting equivalent conductances and single-ion conductivities obtained from these values.

Discussion

In Figure 1 single-ion conductivities in acetonitrile are plotted *vs.* the reciprocal of estimated crystallographic radii. Included are several other ions in addition to those studied here.^{1,6} The low mobility of copper(I) relative to the alkali metal ions has been interpreted in terms of extensive solvation of this ion by acetonitrile;¹ the high mobility of silver(I), which also interacts strongly with acetonitrile,⁷ is not so readily explained. The mobility of thallium(I) also is high, but apparently thallium is not extensively solvated by acetonitrile. The standard reduction potential of the thallium(I-0) couple in acetonitrile, referred to the normal hydrogen electrode in water, is 0.191 V more positive in acetonitrile than in water.³ This shift, which is larger than that of the potassium or rubidium couples, is attributed to strong hydration of thallium(I). Therefore the high mobilities of silver and thallium are not related in a simple way to the extent of ionic solvation.

Association of the thallium and silver salts appears to

correlate with relative stabilization of these ions by acetonitrile. Silver tetrafluoroborate and perchlorate are unassociated, whereas the corresponding thallium(I) salts have association constants of 14 and 32. If ion pairing in these salts is attributed solely to electrostatic attraction, the smaller tetrafluoroborate ion would be expected to associate to a greater extent than the perchlorate. For example, preliminary conductance measurements on alkali metal tetrafluoroborates in acetonitrile indicate association constants of approximately 40, roughly twice the values found for the corresponding perchlorate salts.⁸ A possible explanation for the reverse relation of the thallium salts is that specific interaction occurs between thallium(I) and perchlorate.

To obtain more information about solvation in acetonitrile, we considered other univalent cations. Gold(I) perchlorate has been reported to be stable in acetonitrile,^{9,10} but our attempts to isolate the salt in sufficient purity to permit high-precision conductance measurements were not successful. Indium(I) undergoes partial disproportionation in acetonitrile,¹¹ and mercury(I) apparently forms a dimer in this solvent just as it does in water.⁷ Therefore extension of this study to other univalent metal ions was not possible.

As shown in Figure 1, thiocyanate has a higher single-ion conductivity than even tetrafluoroborate. Most salts of polarizable anions, such as thiocyanate and iodide, have relatively high solubilities in acetonitrile because a polarizable ion interacts more strongly with the solvent. The mobility of iodide appears to indicate such interaction, for it falls well below a line drawn through the points for the relatively ideal tetrafluoroborate and hexafluorophosphate ions in Figure 1. The association constant of 11 reported for potassium iodide in acetonitrile¹² is close to that found here for potassium thiocyanate. The anion mobilities of these salts, however, are quite different. Again it is seen that although association constants generally reflect the degree of stabilization of ions by acetonitrile, mobilities are more difficult to interpret on this basis.

(6) C. H. Springer, J. F. Coetzee, and R. L. Kay, *J. Phys. Chem.*, **73**, 471 (1969).

(7) I. M. Kolthoff and J. F. Coetzee, *J. Amer. Chem. Soc.*, **79**, 1852 (1957).

(8) H. Yeager, Ph.D. Thesis, University of Alberta, Edmonton, Alberta, 1969.

(9) A. D. Goolsby and D. T. Sawyer, *Anal. Chem.*, **40**, 1978 (1968).

(10) G. Bergerhoff, *Z. Anorg. Allgem. Chem.*, **327**, 139 (1964).

(11) J. B. Headridge and D. Pletcher, *Inorg. Nucl. Chem. Lett.*, **3**, 475 (1967).

(12) G. J. Janz, A. E. Marcinkowsky, and I. Ahmad, *Electrochim. Acta*, **9**, 1687 (1964).

COMMUNICATIONS TO THE EDITOR

Comments on "Onsager's Reciprocal Relation. An Examination of Its Application to a Simple Process"

Sir: Although the inaccuracies of the note by Bresler and Wendt¹ are very clear for anyone who has worked in this field, we feel it necessary to point out these inaccuracies, because the note may give rise to unjustified doubts about the general validity of the ORR for membrane processes.

The only limitation to the application of the ORR is the restriction to linear processes, that is to small forces and fluxes. If Bresler and Wendt consider that: "... a true diffusive flow will vanish for sufficiently rapid bulk flow across an open membrane" (p 265, column 2, section 2),¹ they implicitly admit that their argument breaks down for small bulk flow, which is the necessary condition for validity of the ORR.

However, it is our feeling that Bresler and Wendt have no intention or arguments to assume nonlinearity of forces and fluxes in open membranes. What they actually say is that L_p is very large in an open membrane, so in their eq 6

$$J_V = L_P \Delta P + L_{PD} \Delta \Pi \quad (6)$$

the second term of the right-hand side is already negligible for very small values of ΔP . Hence, they put $L_{PD} = 0$ (14). This is patently incorrect. The fact that $L_{PD} \Delta \Pi \ll L_P \Delta P$ means only that L_{PD} is very small, but does not imply that $L_{PD} = 0$ exactly. Moreover, a term can be very small compared to another term in (6) without being small in comparison to other terms in another equation like (7)

$$J_D = L_{DP} \Delta P + L_D \Delta \Pi \quad (7)$$

So the conclusion is that $L_{DP} \Delta P$ can be measurable without violating the ORR.

The failure of their reasoning can be illustrated with still more "quantitative arguments." By confronting their eq 11

$$J_D = (c_s^A/\bar{c}_s - 1)L_P \Delta P + (c_s^A/\bar{c}_s - 1)L_{PD} \Delta \Pi \quad (11)$$

with eq 7, the following expressions for the coefficients of ΔP and $\Delta \Pi$ result

$$\begin{aligned} L_{DP} &= (c_s^A/\bar{c}_s - 1)L_P \\ L_D &= (c_s^A/\bar{c}_s - 1)L_{PD} = 0 \end{aligned} \quad (12)$$

Now the combination of $L_D = 0$ and $L_{PD} = 0$ causes serious difficulties in a necessary condition which must

be satisfied in the case of a positive entropy production. This condition, easy to derive from eq 1 of the note and mentioned by de Groot and Mazur,² is given by the inequality

$$L_P L_D \geq 1/4(L_{PD} + L_{DP})^2$$

Insertion of $L_D = 0$ and $L_{PD} = 0$ into this condition leads to an absurdity.

Recently, we have tested the ORR in our laboratory for different sugar solutions in water, using rather open Vycor glass membranes.³ See Table I.

Table I

Membrane	Solute	$-L_{PD}/L_P$	$-L_{DP}/L_P$
2	Sucrose	0.198 ^a	0.204 ^a
1	Mannitol	0.124	0.130
3	Mannitol	0.112	0.106
1	Raffinose	0.28	0.30
3	Raffinose	0.25	0.24

^a Estimated limits of error: $-L_{PD}/L_P$, 1-3%; $-L_{DP}/L_P$, 3-5%.

These data are obtained by using an osmometer earlier described by Talen and Staverman.⁴ The reflection coefficients (last column of the table) are measured by an ultrafiltration procedure given by Talen⁴ with a permeability of about 30 mm³/hr atm, a pressure difference of 2.5 atm, and equal concentration of 5 g/l. for all solutes on both sides of the membrane.

The quantity $-L_{PD}/L_P$ has been determined by osmotic experiments, with various concentration differences, remaining nearly constant during the period of measuring. Varying ΔP in steps from about 0.2 till 1.0 atm, we can measure the corresponding J_V , running from 5 till 20 mm³/hr. A plot of J_V vs. ΔP yields a straight line and with $\Delta \Pi$ given, $-L_{PD}/L_P$ is calculated from the slope and intercept according to (6).

The average concentrations (in g/l.) during the osmotic experiments are given in Table II.

From our data, it is obvious that the ORR are not invalidated in the case $c^A \neq \bar{c}_s$, as intended by Bresler and

(1) E. H. Bresler and R. P. Wendt, *J. Phys. Chem.*, **73**, 264 (1969).

(2) S. R. de Groot and P. Mazur, "Non-Equilibrium Thermodynamics" North-Holland Publishing Co., Amsterdam, Chapter IV, Paragraph 1.

(3) J. A. M. Smit, thesis to be published.

(4) J. L. Talen and A. J. Staverman, *Trans. Faraday Soc.*, **61**, 2794 (1965).

Table II

	c_s^A	c_s^B	\bar{c}_s	$(c_s^A/\bar{c}_s - 1)$
Sucrose	15.71	0.81	5.03	2.12
	11.57	1.58	5.02	1.30
Mannitol	10.00	2.03	5.00	1.00
	9.64	2.17	5.01	0.92
	8.74	2.58	5.00	0.73
	8.21	2.76	5.05	0.64
Raffinose	10.03	2.02	5.00	1.01
	10.02	2.02	5.00	1.00
	9.24	2.31	5.00	0.85
	8.76	2.51	5.00	0.75

Wendt, but are quite reasonably valid. We conclude that there is no ground whatever for the assertion that the validity of the ORR should not be secured for open membranes. The limit of the linear region should be explored experimentally before the ORR may be applied rigorously. However, it is our impression that this region is rather wide for most membranes and certainly it is the region which should be and is the subject of most studies on permeabilities of membranes.

CHEMICAL LABORATORIES
UNIVERSITY OF LEIDEN
LEIDEN, HOLLAND

J. A. M. SMIT
A. J. STAVERMAN

RECEIVED JUNE 12, 1969

Reply to Communication of Smit and Staverman

Sir: Smit and Staverman¹ have pointed out no inaccuracies in our recent paper, although the data they present do help to clarify our original argument.

First, let us consider the alleged inaccuracies. Their inference that we had no intention of considering nonlinearities in the flow equations is unfounded, and their assumption concerning our definition of an open membrane is incorrect. An open membrane is defined in our paper by the sentence preceding eq 13 and by that equation: "An expression for L_{PD} can be inferred from the definition of an open membrane, *i.e.*, J_V does not depend on $\Delta\Pi$ but is directly proportional to ΔP ."

$$J_V = L_P \Delta P \quad (13)''$$

That nonlinearity, *i.e.*, dependence of transport coefficients on the forces, is a problem with the membrane transport equations is strongly implied by eq 12, derived by Smit and Staverman from our paper, which explicitly show coefficients L_{DP} and L_D to be strong functions of the concentrations c_s^A and c_s^B and hence the thermodynamic force $\Delta\Pi$. Finally, the fact that L_D and L_{PD} are zero for the open membrane under the experimental conditions specified in our paper does not lead to an absurdity. The inequality relating the four phenomenological coefficients was derived by deGroot

by assuming those coefficients to be independent of the thermodynamic forces; for the situation we discussed, the coefficients L_{DP} and L_D were shown to depend on the force $\Delta\Pi$, and hence the inequality could not be expected to hold.

Now let us consider the data presented by Smit and Staverman. Although the membrane they used is not open according to our definition, their values for $-L_{PD}/L_P = \sigma$ (the Staverman coefficient) are small and our criticism should be approximately applicable to their work. We specified no condition for the measurement of σ , since L_{PD} was defined to be zero, but in agreement with most workers in this field,² we consider σ and L_P , and hence L_{PD} , to be reasonably constant and independent of ΔP and $\Delta\Pi$. The osmotic experiments of Smit and Staverman for determining σ were performed at nonzero values for $\Delta\Pi$ and ΔP and violate none of the requirements for the validity of the Onsager relation specified in our paper. To obtain our theoretical expression for L_{DP}/L_P we described an experiment which involved bulk flow of solution A into B with $\Delta\Pi$ held constant at $RT(c_s^A - c_s^B)$; Smit and Staverman's ultrafiltration experiments for measuring L_{DP}/L_P involved bulk flow of A into B with $\Delta\Pi$ held vanishingly small, *i.e.*, with $c_s^A \simeq c_s^B$. For our experiment we stated that "... the Onsager relation will be satisfied only if $c_s^A = \bar{c}_s$. This condition is satisfied for the special case of bulk flow across an open membrane on either side of which $c_s^A = c_s^B = \bar{c}_s \dots$ " Thus the ultrafiltration experiments of Smit and Staverman satisfied our specified condition for the validity of the Onsager relation, and their osmotic experiments were performed under conditions which led to no nonlinearities in the flow equations such as those described in our paper.

Our criticism as originally stated is therefore not refuted by the results of Smit and Staverman, nor should our criticism be considered trivial or obvious, as implied by those authors, because of the supposed wide range of linearity of the transport equations for most membranes. In fact, when bulk flow exists, the coefficients L_D and L_{DP} are strong functions of $\Delta\Pi$ even for relatively small values for the bulk flow, J_V . We demonstrated this particular kind of nonlinearity by using a thought experiment and mathematics instead of making actual physical measurements to determine the region of linearity. The latter procedure would be required, for example, to determine when the hydraulic conductivity coefficient L_P becomes dependent on ΔP . The situation we discussed is quite analogous to the variation of ω , the coefficient of solute permeability, with J_V . In a recent paper,³ we showed that whenever

(1) J. A. M. Smit and A. J. Staverman, *J. Phys. Chem.*, **74**, 966 (1970).

(2) K. S. Spiegler and O. Kedem, *Desalination*, **1**, 311 (1966).

(3) E. H. Bresler and R. P. Wendt, *Science*, **163**, 944 (1969).

mass transport by convection is comparable with mass transported by diffusion, then ω is constant, and hence the flow equation in which it appears is linear, for vanishingly small concentration differences *only*.

For partially selective membranes, Spiegler and Kedem² and Patlak, *et al.*,⁴ showed that the local linear equations of irreversible thermodynamics must be integrated across the membrane subject to appropriate boundary conditions in order to obtain "overall" membrane transport equations which, although nonlinear, at least contain coefficients that do not depend on the forces ΔP or $\Delta \Pi$. According to eq 5b of ref 2 and eq 4 of ref 4, for the ultrafiltration experiments of Smit and Staverman the solute flow would be given by

$$J_s = (1 - \sigma)c_s J_v \quad (1)$$

where $c_s = c_s^A = c_s^B$ and the concentration gradient does not appear because $c_s = c_s^A = c_s^B$. The coefficient σ appears in eq 1 as a result of the application of the Onsager relation to the local linear flow equations before integration across the membrane. Letting $J_s/J_v = c_s^{\text{out}}$ and rearranging eq 1, we have

$$\sigma = 1 - (c_s^{\text{out}}/c_s^{\text{in}}) \quad (2)$$

where c_s^{out} and c_s^{in} are the concentrations of effluent and feed solutions, respectively, for an ultrafiltration experiment. Now, even without the application of irreversible thermodynamics, which contains in this case the rather restrictive requirement of membrane homogeneity in addition to the other usual assumptions, eq 2 sensibly seems to state an equivalence between the rejection (or reflection) coefficient of ultrafiltration experiments performed under conditions of negligible

transport by diffusion and the Staverman coefficient of osmotic experiments. For the experiments of Smit and Staverman, performed with $\Delta \Pi = 0$ and hence no appreciable diffusive transport, eq 7 of their communication simplifies to

$$J_D = (J_s/c_s) - \bar{V}_w J_w = L_{DP} \Delta P \quad (3)$$

Using $\Delta P = J_v/L_P$ and $\bar{V}_w J_w \simeq J_v$, eq 3 becomes after rearrangement

$$J_s = \left(1 + \frac{L_{DP}}{L_P}\right) c_s J_v \quad (4)$$

Comparing eq 1 and 4 we see that Smit and Staverman found $-L_{DP}/L_P = \sigma$, which serves to confirm for Vycor glass membranes what has been frequently observed for other partially selective membranes at high bulk flow rates,⁵ namely, the previously stated equivalence between σ and the rejection coefficient measured in the virtual absence of diffusion. For ultrafiltration experiments where diffusion is appreciable, we expect Smit and Staverman would find $-L_{DP}/L_P \neq \sigma$.

(4) C. S. Patlak, D. A. Coldstein, and J. F. Hoffman, *J. Theor. Biol.*, **5**, 426 (1963).

(5) J. S. Johnson, Jr., L. Dresner, and K. A. Kraus, "Principles of Desalination," Academic Press, New York, N. Y., 1966, Chapter 8.

DEPARTMENT OF CHEMISTRY
LOYOLA UNIVERSITY
NEW ORLEANS, LOUISIANA 70118

R. P. WENDT

VETERANS ADMINISTRATION HOSPITAL
AND DEPARTMENT OF MEDICINE
TULANE UNIVERSITY SCHOOL OF MEDICINE
NEW ORLEANS, LOUISIANA 70140

E. H. BRESLER

RECEIVED SEPTEMBER 16, 1969